ELEMENT PARTITIONING BETWEEN COEXISTING CARBONATE AND SILICATE LIQUIDS

Kevin Donald Fielding

A thesis submitted for the degree of Doctor of Philosophy

University of Edinburgh
1992

EX BIBL. UNIV. EDINBURGH.

Except where indicated otherwise, this thesis is entirely my own work

Abstract.

A number of experimental studies have shown that the first melt of carbonated mantle peridotite is carbonatitic in character. This first melt will contain a sizeable portion of the mantle budget for incompatible trace elements and, owing to its physical properties, it is likely to be very mobile. If no further melting occurs, the carbonatitic melt will migrate through the mantle, scavenging incompatible elements, before freezing in the lithosphere. Alternatively, melting can progress, resulting in the incorporation of this precursor melt in more voluminous silicate melt. In any case, carbonate melt - silicate mantle equilibria are likely to influence the trace-element characteristics of material produced.

One way of constraining the geochemical characteristics of mantle-derived carbonate melt is by investigation of the partitioning behaviour between coexisting carbonate and silicate liquids for trace elements of interest. This has been achieved by a series of experimental runs under a range of temperatures and pressures (0.2-2.0 GPa, 1100-1400°C), involving both natural rock compositions (phonolites, nephelinites and melilitites), and synthetic charges in the system SiO_2-Al_2O_3-CaO-Na_2O-CO_2. Whilst showing that carbonate and silicate melts are likely to be completely miscible under mantle conditions, these experiments have also shown that a wide range of Ca-Mg-Na-Fe carbonate liquids can be experimentally produced by liquid immiscibility at crustal pressures. This range incorporates the vast majority of carbonatite compositions seen at the Earth's surface. Coexisting carbonate and silicate liquids in the experimental charges produced were characterised by electron probe microanalysis. Melt compositions were found to be accurately reproducible, and subject to small but consistent variations with pressure and temperature. The charges were studied optically to ensure that the coexisting liquids were in equilibrium, to investigate quenching processes occurring in the liquids on cooling, and to analyse the two-liquid textures obtained.

Carbonate and silicate liquids produced in these experiments were analysed for a range of trace elements using ion microprobe techniques. The trace elements studied include examples of large-ion lithophile (LIL), high field-strength (HFS), and rare-earth elements (REE). The carbonate liquid was found to be enriched relative to the silicate liquid in LILE (e.g. Rb^{+}, Cs^{+}, Ba^{2+}, Sr^{2+}, Pb^{2+} and $LREE^{3+}$) and in extreme HFSE (e.g. Mo^{6+}, P^{5+}, V^{5+} and Nb^{5+}). The silicate liquid was most strongly enriched in ions of moderate size and charge (e.g. Ti^{4+}, Si^{4+} Al^{3+}, Th^{4+}, and Hf^{4+}). Variations in pressure, temperature, and composition have little effect on partitioning in the synthetic experiments, but seem to exert more influence on partitioning in experiments on natural rock compositions. The major chemical controls on partitioning are ionic size, and ionic charge. In general, partitioning of an ion can be predicted from these characteristics. Exceptions to this rule include the ion pairs U^{4+}-Th^{4+}, Zr^{4+}-Hf^{4+}, and Nb^{5+}-Ta^{5+} whose partitioning is significantly different despite their similar ionic radii.

Partition coefficients ($^{L_a/L_c}D_i$) obtained from these experimentally-produced liquids give an insight into the geochemical differences between carbonate and silicate melts, and the expected trace-element characteristics resulting from carbonate involvement. Mantle carbonate liquid is expected to have high ratios of LILE/HFSE, extreme LREE/HREE enrichment, low Th/U, high Zr/Hf, high Nb/Ta and high concentrations of P, V and Mo. With time, carbonate liquid, or material influenced by carbonate involvement, will also evolve distinctive Sr-, Nd-, and Pb-isotopic characteristics. These trace-element and isotopic predictions are tested against geochemical data from a wide variety of mantle-derived material in an attempt to constrain the role of carbonate liquid in mantle petrogenesis.

Acknowledgements.

There are many people whose help, interest, and expertise have improved both the presentation and content of this thesis. Mention must first go to my supervisors Dr's J.G. Fitton, C.E. Ford and R.W. Hinton for their encouragement and assistance throughout my stay at Edinburgh; my thanks to them all. I was first introduced to the joys of carbonatites and mantle processes by Prof. J.B. Dawson during my undergraduate course at Sheffield. I thank him for this, and for fostering my interest in these topics over these past three years.

Each and every success in this project has been achieved with guidance from both inside and outside the Grant Institute. The choice of experimental starting compositions employed in this study was based on the knowledge and collections of Dodie James, Godfrey Fitton, and Barry Dawson. Dodie's help was also essential in XRF preparation and analysis. It could easily have taken me the three years to "learn the ropes" of experimental petrology without the patience and humour of Steve Elphick. The experimental work was also aided by the experience of Nic Odling and the support of all those in the Experimental Petrology Unit. The precision and accuracy of the electron probe data quoted in this thesis could not have been achieved without the invaluable assistance of Stuart Cairns and Pete Hill. Likewise, the ion probe data could not have been obtained without the guidance of Richard Hinton and John Craven. Statistical analysis of the data was assisted by conversations with Dr. C.M. Theobald of the Department of Mathematics and Statistics. My thanks to Paul Beattie for his comments on experimental techniques, thermodynamics, and the workings of partition coefficients, and to the petrologists and geochemists in the Grant Institute for discussions on how and where the partitioning data obtained in this study should be applied.

Presentation of this thesis has been greatly improved by assistance from Shane Voss in the computing centre, and from Diana Baty and Yvonne Cooper in the photography office. Thanks also to Godfrey Fitton, Cliff Ford, Richard Hinton, and Barbara Page for their patience in reading draft copies of various chapters in this thesis, and for their useful comments.

Finally, I would like to thank all those who have put up with my geological ranting over the past three years, especially Barbara Page, Christine Kay, Ned Pegler, Jon Turner, Nicky Allison and Gordon Watt; they even listened at 3 a.m. in Sneaky Petes! Thanks also to my colleagues at the Centre for Leisure Research in RR IV, both past and present, and especially to Karen Dobbie and Gillie Hatton for the lunchtime gossips. Unfortunately, this is the last output from the Research Room IV production line; I hope that it does not disgrace its predecessors.

I gratefully acknowledge receipt of an NERC studentship.

Table of contents.

		Page
Title page.		i
Declaration.		ii
Abstract.		iii
Acknowledgements.		iv
Table of contents.		v
List of illustrations.		xiii
List of tables.		xviii
List of plates.		xxi
List of abbreviations.		xxii
Chapter 1:	**Carbonate liquids in mantle processes.**	**1**
1.1.	Introduction.	2
1.2.	The evidence for mantle carbon.	3
1.3.	Forms of carbon in an oxidised upper mantle.	5
1.4.	The oxidation state of the upper mantle.	7
1.5.	The effects of carbonate on mantle processes.	9
1.6.	Physical properties of carbonate liquids and their consequences.	12
1.7.	The fate of small-volume carbonatitic melts.	14
	1.7.1. Enrichment processes at the base of the lithosphere.	14
	1.7.2. Enrichment processes in the lithosphere at 60-80 km depth.	17
	1.7.3. The possibility of primary carbonatite melts.	17
	1.7.4. Incorporation in more voluminous mantle melting.	19
1.8.	The data to be collected.	24
1.9.	A summary of the theoretical basis for the study.	26
Chapter 2:	**Experiments on primary mantle melt compositions.**	**28**
2.1.	Introduction and background theory.	29
2.2.	Starting materials: preparation and composition.	34
2.3.	Experimental techniques.	35
2.4.	The experiments.	38
	2.4.1. Set 1. Experiments on TAS 3.	39
	2.4.2. Set 2. Experiments on TAS 3 and calcium-magnesium carbonate.	39
	2.4.3. Set 3. Addition of alkali carbonate to experimental charges.	42
	2.4.4. Set 4. Experiments in platinum capsules.	44
	2.4.5. Set 5. Experiments with various carbonate contents.	48
2.5.	Conclusions and Implications.	49
Chapter 3:	**Experiments in the system SiO_2-Al_2O_3-CaO-Na_2O-CO_2.**	**55**
3.1.	Introduction and background theory.	56
3.2.	Starting materials: preparation and composition.	59
3.3.	Experimental techniques.	61

3.4. The experiments. 64
3.4.1. Set 1. Experiments with SM1. 64
3.4.2. Set 2. P-T-t grid study of immiscibility in the system SiO_2-Al_2O_3-CaO-Na_2O-CO_2. 66
3.4.3. Set 3. Solid media experiments in the system SiO_2-Al_2O_3-CaO-Na_2O-CO_2. 72
3.4.4. Set 4. The effects of minor elements on immiscibility in the system SiO_2-Al_2O_3-CaO-Na_2O-CO_2. 74
3.4.5. Set 5. Experiments to produce "reversals" of $^{Ls/Lc}D_i$ values. 79
3.4.6. Set 6. Reproducibility of immiscibility. 81
3.5. Conclusions and implications. 83

Chapter 4: Experiments on natural rocks believed to be associated with immiscibility. 87

4.1. Introduction and background theory. 88
4.2. Starting materials: preparation and composition. 90
4.3. Experimental techniques. 92
4.4. The experiments. 94
4.4.1. Set 1. Experiments with silver oxalate. 94
4.4.2. Set 2. Experimental acquisition of a P-T-X grid of immiscible-liquid compositions. 94
4.4.3. Set 3. Variation of run duration. 110
4.4.4. Set 4. Solid-media experiments on natural rock compositions. 116
4.4.5. Set 5. Reproducibility of immiscibility. 119
4.5. Conclusions and implications. 121

Chapter 5: Experimental limitations and difficulties: a review. 127

5.1. Introduction. 128
5.2. Constraints imposed on the experimental data set by equipment and techniques. 128
5.2.1. Vertical quench furnaces for atmospheric pressure work. 128
5.2.2. Cold-seal vessels. 128
5.2.3. Internally heated gas-pressure vessels. 128
5.2.4. Solid-media piston cylinder apparatus. 128
5.3. Constraints due to the limits of carbonate-silicate immiscibility. 130
5.3.1. The effect of pressure. 130
5.3.2. The effect of temperature. 130
5.3.3. The effect of composition. 132
5.3.4. The effects of redox conditions. 133
5.4. Experimental problems. 134
5.4.1. Iron loss. 134
5.4.2. Crystallisation of experimental charges. 136
5.4.3. Boundary effects at the carbonate-silicate meniscus. 136
5.5. Conclusions. 142

Chapter 6: An analytical study of experimentally produced carbonate and silicate liquids. 143

6.1. Introduction. 144
6.2. Preparation of the experimentally produced charges for analytical work. 145
6.2.1. Introduction. 145
6.2.2. Mounting. 145
6.2.3. Grinding. 145
6.2.4. Polishing. 147
6.3. Optical analysis of textures and phase relationships. 148
6.3.1. Introduction. 148
6.3.2. Analytical techniques. 148
6.3.3. Analysis of the textural relationships between phases. 148
6.3.4. Analysis of quench textures in experimentally produced carbonate and silicate melts. 157
6.4. Electron probe microanalysis. 163
6.4.1. Introduction. 163
6.4.2. Sample preparation. 163
6.4.3. Analytical equipment and techniques. 164
6.4.4. Analyses undertaken. 166
6.4.5 Difficulties encountered during electron probe analysis. 167
6.5. Ion probe microanalysis. 183
6.5.1. Introduction. 183
6.5.2. Sample preparation. 183
6.5.3. Analytical equipment and techniques. 183
6.5.4. Analyses undertaken. 185
6.5.5. From count rates to concentrations. 187
6.5.6. Limitations of ion probe analysis. 198
6.5.7. Comparison of ion probe concentrations with starting materials and electron probe results. 200
6.6. A summary of the analytical work. 210
6.6.1. Sample preparation. 210
6.6.2. Optical analysis. 210
6.6.3. Electron probe analysis. 210
6.6.4. Ion probe analysis. 211
6.6.5. Conclusions. 212

Chapter 7: Element partitioning between coexisting carbonate and silicate liquids in the system SiO_2-Al_2O_3-CaO-Na_2O-CO_2. 223

7.1. The Data. 224
7.2. Group IA elements. 229
7.2.1. Sodium. 229
7.2.2. Potassium. 229
7.2.3. Rubidium. 229
7.2.4. Cesium. 231
7.2.5. The relationship of partitioning with ionic radius. 231

7.2.6. The effects of run duration on the partitioning of Group IA elements. 231
7.3. Group IIA elements. 234
7.3.1. Magnesium. 234
7.3.2. Calcium. 234
7.3.3. Strontium. 234
7.3.4. Barium. 234
7.3.5. The relationship of partitioning with ionic radius. 236
7.3.6. The effects of run duration on the partitioning of Group IIA elements. 236
7.4. Group III elements. 239
7.4.1. Aluminium. 239
7.4.2. Yttrium and the REE. 239
7.4.3. The relationship of partitioning with ionic radius. 241
7.4.4. The effects of run duration on the partitioning of Group IIIA elements. 241
7.5. Group IVA and IVB elements. 245
7.5.1. Silicon. 245
7.5.2. Titanium. 245
7.5.3. Zirconium. 245
7.5.4. Hafnium. 245
7.5.5. Partitioning with ionic radius. 247
7.5.6. The effects of run duration on the partitioning of Group IV elements. 247
7.6. Group VA and VB elements. 250
7.6.1. Phosphorus. 250
7.6.2. Vanadium. 250
7.6.3. Niobium. 250
7.6.4. Tantalum. 250
7.6.5. Partitioning of Group V elements with ionic radius. 252
7.6.6. The effects of run duration on the partitioning of Group V elements. 252
7.7. U, Th, and Pb. 255
7.7.1. Lead. 255
7.7.2. Thorium. 255
7.7.3. Uranium. 255
7.7.4. The effects of run duration on the partitioning of U, Th and Pb. 255
7.7.5. Partitioning of non-metals. 258
7.8. Physical controls on element partitioning. 260
7.8.1. The effect of pressure. 260
7.8.2. The effect of temperature. 262
7.9. Chemical controls on element partitioning. 264
7.9.1. Element partitioning as a function of ionic radius. 264
7.9.2. Element partitioning as a function of charge density. 266
7.10. The effects of minor elements on the partitioning between carbonate and silicate melts. 266
7.10.1. Fluorine. 266
7.10.2. Chlorine. 266

7.10.3. Sulphur. 266
7.10.4. Phosphorus. 271
7.11. Summary of partitioning between synthetic carbonate and silicate melts. 276

Chapter 8: Element partitioning between coexisting carbonate and silicate liquids of natural composition. 279

8.1. The Data. 280
8.2. Group IA elements. 281
8.2.1. Sodium. 281
8.2.2. Potassium. 281
8.2.3. Rubidium. 283
8.2.4. Cesium. 283
8.2.5. Partitioning of Group IA elements with temperature. 283
8.2.6. Partitioning of Group IA elements with pressure. 284
8.2.7. Compositional effects on Group IA element partition. 284
8.2.8. Partitioning of Group IA elements with ionic size. 287
8.3. Group IIA elements. 289
8.3.1. Magnesium. 289
8.3.2. Calcium. 291
8.3.3. Strontium. 291
8.3.4. Barium. 291
8.3.5. Partitioning of Group IIA elements with temperature. 293
8.3.6. Partitioning of Group IIA elements with pressure. 293
8.3.7. Compositional effects on Group IIA element partition. 293
8.3.8. Partitioning of Group IIA elements with ionic size. 293
8.4. Partitioning of transition elements. 295
8.4.1. Manganese. 295
8.4.2. Iron. 297
8.4.3. Chromium. 297
8.4.4. Copper. 297
8.4.5. Partitioning of Fe and Mn with temperature. 297
8.4.6. Partitioning of Fe and Mn with pressure. 299
8.4.7. Partitioning of transition elements as function of ionic radius. 299
8.5. Aluminium, Yttrium, and the REE. 301
8.5.1. Aluminium. 301
8.5.2. Yttrium. 301
8.5.3. The REE. 303
7.5.4. Partitioning of Yttrium and the REE at mantle pressures. 305
7.5.5. Partitioning of +3 ions as a function of ionic radius. 308
8.6. Group IVA and IVB elements. 310
8.6.1. Silicon. 310
8.6.2. Titanium. 310
8.6.3. Zirconium. 312
8.6.4. Hafnium. 312
8.6.5. Partitioning of Group IV elements as a function of pressure. 313
8.6.6. Partitioning of +4 elements as a function of ionic radius. 313
8.7. Group VA and VB elements. 316

8.7.1. Phosphorus. 316
8.7.2. Vanadium. 318
8.7.3. Niobium. 318
8.7.4. Tantalum. 318
8.7.5. Partitioning of Group V elements at mantle pressures. 320
8.7.6. Partitioning of +5 elements as a function of ionic size. 320
8.8. Other elements: U, Th, Pb and Mo. 323
8.8.1. Lead. 323
8.8.2. Thorium. 323
8.8.3. Uranium. 325
8.8.4. Molybdenum. 325
8.9. Controls on element partition in natural compositions. 326
8.9.1. Partitioning of elements in natural compositions as a function of time. 326
8.9.2. Partitioning of trace elements as a function of ionic radius. 326
8.9.3. Partitioning of trace elements as a function of charge density. 329
8.10. Carbonate-silicate partitioning under mantle conditions. 331
8.11. Comparison between partitioning in natural and synthetic systems. 332
8.11.1. Geochemical characteristics common to both natural and synthetic systems. 332
8.11.2. Differences between partitioning behaviour in natural and synthetic experiments. 333

Chapter 9: The geochemical characteristics of mantle carbonate melt. 339

9.1. Introduction. 340
9.2. Major-element characteristics. 341
9.2.1. The composition of carbonate liquid in equilibrium with mantle phases. 341
9.2.2. The possible effects of carbonate addition to primary silicate liquid. 342
9.2.3. Differences between carbonate liquid and other fugitive agents in the mantle. 344
9.3. Trace-element characteristics. 345
9.3.1. LILE enrichment in the carbonate liquid. 345
9.3.2. LREE/HREE enrichment. 346
9.3.3. Fractionation of U and Th. 349
9.3.4. Fractionation of Zr and Hf. 351
9.3.5. Fractionation of Nb from Ta. 352
9.3.6. Enrichment of extremely high charge density ions in the carbonate liquid. 353
9.4. Isotopic characteristics. 354
9.4.1. The effect of carbonate involvement on $^{87}Sr/^{86}Sr$ ratios. 354
9.4.2. The effect of carbonate liquid involvement on $^{144}Nd/^{143}Nd$. 355
9.4.3. The effect of carbonate addition on Pb-isotope ratios. 355
9.4.4. The effects of carbonate liquid involvement on U-series isotopic disequilibrium. 358
9.5. Conclusions. 361

Chapter 10: Implications of carbonate-silicate partitioning to carbonatite genesis and evolution. 362

10.1. The origins of carbonatites. 363
10.1.1. Petrological evidence for the origins of carbonatites. 363
10.1.2. Experimental evidence for the origins of carbonatites. 365
10.1.3. Geochemical evidence for the origins of carbonatites. 367
10.2. Evolution of carbonatites. 376
10.2.1. Element compatibility in the structure of a synthetic carbonate structure. 376
10.2.2. Trace-element chemistry of carbocernaite from the Samu carbonatite, India. 377
10.2.3. Trace-element chemistry of calcite from Kimsey Quarry carbonatite, Arkansas. 378
10.2.4. Trace-element chemistry of a dolomite standard. 379
10.2.5. Trace-element chemistry of strontianite NMNH R10065. 380
10.2.6. Separation of non-carbonate phases during carbonatite crystallisation. 381
10.3. Implications for the economic potential of carbonatites. 383
10.3.1. REE mineralisation. 383
10.3.2. Niobium (and tantalum). 383
10.3.3. Phosphorus. 383
10.3.4. Titanium. 384
10.3.5. Copper. 384
10.3.6. Fluorite. 384
10.3.7. Other elements that may have economic potential. 384
10.4. Conclusions. 385

Chapter 11: A wider role for carbonate liquid in mantle processes. 387

11.1. Diagnosing carbonate involvement in mantle processes. 388
11.2. Metasomatism by carbonate liquids. 389
11.2.1. Mineralogy and major-element chemistry of selected xenolith suites. 389
11.2.2. Trace-element and isotopic features of xenoliths from cratonic lithosphere. 390
11.2.3. Trace-element geochemistry and isotopic characteristics of lithosphere-derived melts. 394
11.3. Carbonate involvement in the formation of small-volume mantle melts. 400
11.3.1. Colorado minettes. 400
11.4. Carbonate liquid as a precursor to more voluminous silicate melting. 404
11.4.1. Geochemistry of the alkaline lavas of the Hessian depression, Germany. 404
11.4.2. The Nyiragongo volcanics, Virunga province, Zaire. 406
11.4.3. Hawaiian volcanism. 406
11.5. Is carbonate melt involved in MORB genesis? 413
11.6. Conclusions. 414

Chapter 12: Summary, conclusions, and implications for further research. 415

12.1. The experiments. 416
12.2. The data set. 417
12.3. Chemical controls on partitioning. 418
12.3.1. Ionic radius. 418
12.3.2. Charge density. 418
12.3.3. Complexing. 418
12.4. Physical controls on partitioning. 419
12.4.1. Structural and compositional control. 419
12.4.2. The effect of temperature. 419
12.4.3. The effect of pressure. 419
12.5. Geochemical characteristics of mantle-derived carbonate melt. 420
12.6. Application of carbonate-silicate partitioning to natural rocks. 421
12.6.1. Carbonatites. 421
12.6.2. Metasomatism in mantle xenoliths. 421
12.6.3. Source characteristics of lithosphere-derived melts. 421
12.6.4. Involvement in the generation of small-volume silicate melts. 422
12.6.5. Involvement as a precursor to voluminous silicate magmatism. 422
12.7. Avenues of further research. 423

References. 424

Appendices.

Appendix A: Electron probe analyses of coexisting carbonate and silicate liquids, and ion probe standards. 437
A.1. Carbonate and silicate liquids from experiments in the system SiO_2-Al_2O_3-CaO-Na_2O-CO_2. 438
A.2. Coexisting carbonate and silicate liquids from experiments on natural compositions. 448
A.3. Electron probe analyses of natural and synthetic carbonates for ion probe standardisation. 462

Appendix B: Ion orpbe analysis of coexisting carbonatie and silicate liquids, and carbonate standards. 466
B.1. Trace-element concentrations in coexisting carbonate and silicate liquids in the system SiO_2-Al_2O_3-CaO-Na_2O-CO_2. 467
B.2. Trace-element concentrations in carbonate and silicate melts of natural composition. 474
B.3. Carbonate and silicate standards for the ion probe, and the trace-element geochemistry of carbonate minerals. 486
Appendix C: Ion microprobe data; trace-element partition coefficients 496
C.1. Trace-element concentrations in coexisting carbonate and silicate liquids in the system SiO_2-Al_2O_3-CaO-Na_2O-CO_2. 497
C.2. Trace-element concentrations in coexisting carbonate and silicate liquids of natural composition. 504

List of illustrations.

		Page
1.1.	Forms of carbon in an oxidised upper mantle.	5
1.2.	Typical profiles of oxygen fugacities in the upper mantle.	8
1.3.	The peridotite-CO_2-H_2O solidus and near-solidus phase relations.	10
1.4.	The effect of small quantities of volatiles on mantle processes.	11
1.5.	The fate of small volume carbonatitic melts.	15
1.6.	Enrichment processes at the base of the lithosphere.	16
1.7.	Enrichment processes in the lithosphere at 60-80 km depth.	18
1.8.	Carbonate melt in petrogenetic processes in the sub-continental upper mantle.	20
1.9.	Carbonate involvement in intraplate volcanism.	21
1.10.	Carbonate involvement in decompression melting.	23
1.11.	Project rationale: why do we need carbonate melt-silicate melt partition coefficients?	25
2.1.	Compositional relationships between mantle-derived alkaline igneous rocks.	31
2.2.	Cell configuration for piston-cylinder apparatus runs.	37
2.3.	Quench products of Set 2 experiments.	41
2.4.	Quench products of Set 4 experiments.	46
2.5.	The extent of carbonate-silicate immiscibility at 2.5 GPa, 1250°C.	50
3.1.	Carbonate-silicate immiscibility in alkali-poor synthetic systems.	58
3.2.	Furnace configuration for experiments using internally heated gas-media vessels.	62
3.3.	Field of immiscibility in the soda-melilite-carbonate system.	65
3.4.	Field of immiscibility at 1300°C, 0.25, 0.5 and 0.8 GPa.	69
3.5.	The effect of temperature on immiscibility.	70
3.6.	Closure of the two-liquid solvus with temperature.	71
3.7.	The effects of run duration on immiscible liquids.	73
3.8.	The effect of pressure on immiscibility.	75
3.9.	The effect of minor elements on immiscibility.	77
3.10.	Compositions of coexisting liquids in reversal experiments.	80
3.11.	Reproducibility of coexisting immiscible liquids.	82
4.1.	Experiments on natural rocks from Oldoinyo Lengai, Tanzania.	89
4.2.	Starting materials employed in experiments involving natural rock compositions.	93
4.3.	Starting mixes for experimental charges involving natural rock compositions.	96
4.4.	Immiscibility between phonolite (BD50) and Ca-Na-carbonate.	98
4.5.	Immiscibility between phonolite (BD50) and Ca-carbonate.	100
4.6.	Immiscibility between olivine-free nephelinite (BD119) and Ca-Na-carbonate.	101

4.7.	Immiscibility between olivine-free nephelinite (BD119) and Ca-carbonate.	103
4.8.	Immiscibility between olivine nephelinite (SUN189) and Ca-Na-carbonate.	105
4.9.	Immiscibility between olivine nephelinite (SUN189) and Ca-carbonate.	107
4.10.	Immiscibility relationships in natural rock compositions at 0.25 GPa.	111
4.11.	Immiscibility relationships in natural rock compositions at 0.5 GPa.	112
4.12.	Immiscibility relationships in natural rock compositions at 0.8 GPa.	113
4.13.	Experiments of variable run duration.	117
4.14.	The effect of pressure on immiscibility in natural rock compositions.	118
4.15.	Reproducibility of immiscible liquids in natural rock compositions.	120
5.1.	Immiscibility as a thermodynamical consequence of non-ideality.	131
5.2.	Iron contents of charges with time.	135
5.3.	Variations in concentrations of Group IA elements in the silicate melt with distance from the carbonate-silicate meniscus.	137
5.4.	Variations in concentrations of Group IIA elements in the silicate melt with distance from the carbonate-silicate meniscus.	138
5.5.	Variations in concentrations of Mg, Fe, and Mn in the silicate melt with distance from the carbonate-silicate meniscus.	139
5.6.	Variations in concentrations of REE in the silicate melt with distance from the carbonate-silicate meniscus.	140
6.1.	Flow diagram illustrating sample preparation techniques.	146
6.2.	Quantification of textural relationships between immiscible liquids.	150
6.3.	Contact angles between coexisting phases, and resulting textural features. of Na-rich experimental charges.	152
6.4.	Contact angles between coexisting phases, and resulting textural features. of Ca-rich experimental charges.	154
6.5.	The variation of Ls-Lc-V contact angle with pressure and composition.	156
6.6.	The effects of slow quench rate on silicate liquid.	159
6.7.	The effects of slow quench rate on carbonate liquid.	161
6.8.	Variations in X-ray intensity with time during analysis of Na-rich carbonate quench. 20kV, 10nA.	170
6.9.	Variations in X-ray intensity with time during analysis of Na-rich carbonate quench. 15kV, 10nA.	171
6.10.	Variations in X-ray intensity with time during analysis of Na-rich carbonate quench. 20kV, 5nA.	172
6.11.	Variations in X-ray intensity with time during analysis of Na-rich carbonate quench. 20kV, 3nA.	173
6.12.	Variations in X-ray intensity with time during analysis of Na-rich silicate glass. 20kV, 5nA.	174
6.13.	The interference effects of 2nd order CaKβ on P Kα.	178
6.14.	Variations in composition across the carbonate quench of experiment G12.	179
6.15.	Simplified schematic diagram of the major features of the Cameca IMS-4f ion probe.	184
6.16.	REE partitioning using uncorrected data from a range of experiments.	196

6.17. REE partitioning using data corrected for relative ion yield effects in the carbonate liquid. 197
6.18. Comparison of starting materials and "mass-balance" estimates for G7.7. 205
6.19. Comparison of starting materials and "mass-balance" estimates for G2.1. 207
6.20. Comparison of starting materials and "mass-balance" estimates for G2.3. 208
6.21. Comparison of starting materials and "mass-balance" estimates for G2.6. 209

7.1. Sample population distributions for analyses of the carbonate quench of experiment G12: elements not seriously redistributed by quench processes. 227
7.2. Sample population distributions for analyses of the carbonate quench of experiment G12: elements seriously redistributed by quenching of the experiment. 228
7.3. Partitioning of Group IA elements between synthetic carbonate and silicate liquids. 230
7.4. Group IA partitioning with ionic radius. 232
7.5. Partitioning of Group IA elements as a function of run duration. 233
7.6. Partitioning of Group IIA elements between synthetic carbonate and silicate liquids. 235
7.7. Group IIA element partitioning with ionic radius. 237
7.8. Partitioning of Group IIA elements as a function of run duration. 238
7.9. Partitioning of Group IIIA elements between synthetic carbonate and silicate liquids. 240
7.10. Relative partitioning of the rare-earth elements. 242
7.11. Group IIIA partitioning with ionic radius. 243
7.12. Partitioning of the Group IIIA elements as a function of run duration. 244
7.13. Partitioning of Group IV elements between synthetic carbonate and silicate liquids. 246
7.14. Group IV partitioning with ionic radius. 248
7.15. Partitioning of Group IV elements as a function of run duration. 249
7.16. Partitioning of Group V elements between synthetic carbonate and silicate liquids. 251
7.17. Group V partitioning with ionic radius. 253
7.18. Partitioning of Group V elements as a function of run duration. 254
7.19. Partitioning of U, Th, and Pb between synthetic carbonate and silicate liquids. 256
7.20. Partitioning of U, Th, and Pb as a function of run duration. 257
7.21. Partitioning of highly electronegative elements F, Cl, and S. 259
7.22. Na partitioning in calcic compositions as a function of pressure. 261
7.23. The effect of temperature on partitioning in synthetic carbonate and silicate liquids. 263
7.24. Element partitioning as a function of ionic size in solid media experiments S42, S43. 265
7.25. Element partitioning as a function of charge density in solid media. experiments S42, S43. 265
7.26. The effect of fluorine on partitioning. 269
7.27. The effect of chlorine on partitioning. 270

7.28. The effect of phosphorus on partitioning of Group IA elements between synthetic carbonate and silicate liquids. 272
7.29. The effect of phosphorus on the partitioning of Group IIA elements between synthetic carbonate and silicate liquids. 273
7.30. The effect of phosphorus on the partitioning of Group IIIA elements between synthetic carbonate and silicate liquids. 274
7.31. The effect of phosphorus on the partitioning of Group IV elements between synthetic carbonate and silicate liquids. 275

8.1. Partitioning of Group IA elements in natural compositions. 282
8.2. The effect of pressure on the partitioning of Na and K in the calcic SUN189+CC composition. 285
8.3. The effect of pressure on the partitioning of Group IA elements. 286
8.4. Partitioning of +1 ions with ionic radius. 288
8.5. Partitioning of Group IIA elements in natural compositions. 290
8.6. The effect of temperature and pressure on partitioning of Group IIA elements in natural compositions. 292
8.7. Partitioning of Group IIA elements as a function of pressure. 294
8.8. Partitioning of Mn and Fe in natural compositions. 296
8.9. Partitioning of Mg, Mn, and Fe with pressure. 297
8.10. Partitioning of +2 ions as a function of ionic radius. 300
8.11. Partitioning of Group III elements in natural compositions. 302
8.12. Partitioning of the REE with changing ionic radius. 304
8.13. The effect of pressure and temperature on partitioning of the REE. 306
8.14. Partitioning of Yttrium and the REE as a function of pressure. 307
8.15. Partitioning of +3 ions as a function of ionic radius. 309
8.16. Partitioning of Group IV elements in natural compositions. 311
8.17. Partitioning of +4 elements as a function of pressure. 314
8.18. Partitioning of +4 elements as a function of ionic radius. 315
8.19. Partitioning of Group V elements in natural compositions. 317
8.20. The effect of pressure and temperature on partitioning of phosphorus. 319
8.21. Partitioning of Group V elements as a function of pressure. 321
8.22. Partitioning of +4 ions as a function of ionic size. 322
8.23. Partitioning of Pb, Th, U, and Mo in natural compositions. 324
8.24. Variations in partitioning behaviour as a function of run duration. 327
8.25. Partitioning as a function of ionic radius. 328
8.26. Partitioning behaviour as a function of charge density. 330
8.27. Variations in structure of the conjugate silicate liquid with pressure. 335
8.28. Partitioning of Yttrium and the REE with changing silicate melt structure. 336

9.1. Schematic diagram showing the likely geochemical effects of carbonate addition on ratios of LILE/HFSE. 347
9.2. The effect of addition of carbonate liquid on REE patterns. 348
9.3. Effects of carbonate liquid addition on Sr-Nd isotopic systematics. 356
9.4. Effects of carbonate addition on lead isotope systematics. 357
9.5. Effects of carbonate involvement on the uranium-series isotopic decay scheme. 360

10.1. Mechanisms of carbonatite formation. 364
10.2. The range of carbonatites that may be produced by immiscibility. 365
10.3. Evidence for immiscibility at Oldoinyo Lengai. 366
10.4. Modelling of LREE/HREE enrichment in carbonatites using inversion techniques (after McKenzie & O'Nions, 1991). 375

11.1. Normalised REE concentrations for melts calculated to be in equilibrium with the megacryst suite found at Loch Roag, Scotland. 391
11.2. Pb-isotopic systematics for the Loch Roag xenolith suite. 392
11.3. Sr-Nd isotope systematics for some cratonic lithosphere-derived mantle xenoliths and megacrysts. 393
11.4. REE distributions in lithosphere-derived mantle melts. 397
11.5. Sm-Nd isotope systematics for selected lamproites. 398
11.6. Pb-isotope systematics for selected lamproites. 399
11.7. LREE/HREE enrichment in kimberlites and melilitites. 401
11.8. REE modelling of minettes from NW Colorado (Thompson *et al.*, 1990). 403
11.9. Variations in trace-element ratios with undersaturation in the lavas of the Hessian trough, Germany. 405
11.10. U-series disequilibrium in oceanic and continental basalts. 407
11.12. Ba/Hf and Ba/Zr ratios of the Haleakala lavas of East Maui. 410
11.13. Ba/Hf and Ba/Zr ratios from the Honolulu volcanics, Oahu. 411
11.14. Variations in Zr/Hf and Nb/Ta in the alkaline lavas of Hawaii. 412

List of tables.

		Page
1.1.	Evidence for a mantle carbon component.	3
1.2.	Physical properties of carbonate liquids.	12
2.1.	Starting materials for experiments on primary mantle compositions.	34
2.2.	Experimental run data S1-S25.	38
2.3.	Electron probe analyses of mixed carbonate-silicate quench material suggesting an absence of immiscibility in alkali poor mantle melts.	40
2.4.	Selected electron probe results showing the problems associated with running volatile, sodium-rich charges in graphite capsules.	42
2.5.	Experimental run data S28-S38.	45
2.6.	Electron probe analyses of selected quenched liquids from experiments S8-S38.	47
3.1.	Starting materials for experiments in the system SiO_2-Al_2O_3-CaO-Na_2O-CO_2.	60
3.2.	Experiments using composition SM1: conditions and results.	64
3.3.	Compositions of coexisting carbonate and silicate liquids: SM1 experiments.	66
3.4.	P-T grid of experiments in the system SiO_2-Al_2O_3-CaO-Na_2O-CO_2.	67
3.5.	Solid-media experiments in the system SiO_2-Al_2O_3-CaO-Na_2O-CO_2.	72
3.6.	Experiments to investigate the effects of minor elements.	76
3.7.	Experiments using doped carbonate: reversal of the partitioning data.	79
3.8.	Reproducibility of immiscibility: experimental conditions and results.	81
4.1.	Major element analyses of rock compositions used in experiments on natural rocks.	90
4.2.	Trace-element contents of starting materials used in experiments on natural rocks.	91
4.3.	Experimental compositions, conditions, and results from experiments involving addition of $Ag_2C_2O_4$ to natural rocks.	94
4.4.	Experiments involving phonolite and calcium-sodium carbonate.	97
4.5.	Experiments involving phonolite and calcium carbonate.	99
4.6.	Experiments involving olivine-free nephelinite and Ca-Na carbonate.	99
4.7.	Experiments involving olivine-free nephelinite and Ca-carbonate.	102
4.8.	Experiments involving olivine nephelinite and Ca-Na-carbonate.	104
4.9.	Experiments involving olivine nephelinite and Ca-carbonate.	106
4.10.	Experiments involving ELG2 olivine-rich nephelinite.	108
4.11.	Experiments involving BD105 olivine-melilite-nephelinite.	109
4.12.	Experiments to investigate the effects of varied run duration on immiscibility in natural rock compositions.	115
4.13.	Solid-media experiments on natural rock carbonate-silicate immiscibility.	116
4.14.	Repeated experiments on natural rock carbonate-silicate immiscibility.	119

5.1.	FeO contents of conjugate silicate liquids at 0.8 GPa, 1300°C.	134
6.1.	Contact angles between coexisting phases in experimental charges.	153
6.2.	A study of quench effects in the carbonate and silicate melts: G6.7.	160
6.3.	Major elements analysed on the electron probe: conditions of analysis and standards used.	165
6.4.	Minor and trace elements analysed on the electron probe: conditions of analysis and standards used.	165
6.5.	Spectrometer set-up and count times for electron probe analysis.	166
6.6.	Acceptable analysis times for silicate and carbonate materials under differing analytical conditions.	175
6.7.	Apparent phosphorus contents of phosphorus-free materials: the relationship between Ca-content and phosphorus correction.	176
6.8.	Mass-balance estimates of bulk composition G6.7.	180
6.9.	Mass-balance estimates of bulk composition G2.1.	181
6.10.	Mass-balance estimates of bulk composition G2.6.	182
6.11.	Variations in RIY with respect to silicon between the first and second probe sessions.	189
6.12.	Trace-element concentrations in the calcium carbonate standard.	190
6.13.	Differences in RIY between carbonate and silicate structures from experimentally produced carbonate standards.	192
6.14.	Ion probe standards for carbonates: natural carbonate materials.	193
6.15.	Comparison of electron and ion probe analyses of major-element concentrations. Phonolitic rock compositions at 1200°C, 0.5 GPa.	201
6.16.	Comparison of electron and ion probe analyses of major-element concentrations. Nephelinitic rock compositions at 1200°C, 0.5 GPa.	202
6.17.	Comparison of electron and ion probe analyses of major-element concentrations. Olivine nephelinitic compositions at 1200°C, 0.5 GPa.	203
7.1.	Mean partition coefficients from SM2+CNC compositions.	276
8.1.	Partitioning of the Group IA elements in natural compositions.	281
8.2.	Partitioning of the Group IIA elements in natural compositions.	289
8.3.	Partitioning of manganese and iron in natural compositions.	295
8.4.	Partitioning of aluminium and yttrium in natural compositions.	301
8.5.	Partitioning of the REE in natural compositions.	303
8.6.	Partitioning of the Group IV elements in natural compositions.	310
8.7.	Partitioning of the Group V elements in natural compositions.	316
8.8.	Partitioning of U, Th, Pb, and Mo in natural compositions.	323
8.9.	Partitioning between carbonate and silicate liquids under mantle conditions; an estimate.	331
9.1.	The chemical composition of primary carbonate melt.	341
9.2.	Possible major-element effects of carbonate addition to primary silicate melt.	343
9.3.	Incompatible trace-element ratios in coexisting carbonate and silicate liquids.	345
9.4.	La/Y and La/Lu ratios in coexisting carbonate and silicate liquids.	349

9.5.	Th/U ratios of coexisting carbonate and silicate liquids.	350
9.6.	Th/U ratios in carbonatites and associated igneous rocks.	351
9.7.	Zr/Hf ratios of coexisting carbonate and silicate liquids.	351
9.8.	Nb/Ta ratios in coexisting carbonate and silicate liquids.	353
9.9.	Ti/V ratios in coexisting carbonate and silicate liquids.	353
9.10.	Rb/Sr ratios in coexisting carbonate and silicate liquids.	354
9.11.	U/Pb and Th/Pb ratios in coexisting carbonate and silicate liquids.	358
10.1.	Evidence for carbonate-silicate immiscibility at Oldoinyo Lengai.	368
10.2.	Compositional data for phonolites and carbonatites at Kaiserstuhl, Germany.	371
10.3.	Selected trace-element concentrations from Gardar dikes.	372
10.4.	Compatibility of elements in synthetic calcium carbonate.	377
10.5.	Compatibility of elements in carbocernaite from the Samu carbonatite, India.	378
10.6.	Compatibility of elements in calcite from the Kimsey Quarry carbonatite, Arkansas.	379
10.7.	Compatibility of elements in dolomite.	380
10.8.	Compatibility of elements in strontianite.	380
10.9.	The density of carbonate liquid in relation to phases which are believed to crystallise from carbonatite melt.	382
11.1.	Geochemical characteristics of selected lamproites, and the expected effects of enrichment by carbonate liquids.	395
11.2.	Trace-element characteristics of NW Colorado minettes.	403
11.3.	Geochemical features of the Koloa volcanic suite, Kauai, Hawaii.	408

List of plates.

		Page
2.1.	Experiments on sodium-free mantle compositions.	52
2.2.	Experiments on sodium-bearing mantle compositions.	53
2.3.	Experiments to determine $^{Cpx/Lc}D_i$ values.	54
3.1.	Immiscibility in synthetic soda-melilite compositions.	85
3.2.	Variation in quench textures resulting from cooling of the carbonate liquid.	86
4.1.	Immiscibility textures in experiments on natural melt compositions.	144
4.2.	Variations in two-liquid textures seen in natural compositions.	145
4.3.	Liquid separation in action; experiments of short run duration.	146
6.1.	Ls-Lc textures in sodium-rich charges.	216
6.2.	Ls-Lc textures in sodium-poor charges.	217
6.3.	Ls-Lc-V textures in sodium-rich charges.	218
6.4.	Ls-Lc-V textures in sodium-poor charges.	219
6.5.	Ls-Lc-Xtl textures from sub-liquidus experiments.	220
6.6.	Quench textures produced on cooling of the silicate liquid.	221
6.7.	Textures produced on quenching of the carbonate liquid.	222

List of Abbreviations.

Geochemical:

BE	Bulk Earth value for isotopic ratios.
DM	Depleted Mantle component
MORB	Mid-Ocean Ridge Basalt
OIB	Ocean Island Basalt
NHRL	Northern Hemisphere reference line.
FeO*	Total iron calculated as Fe^{2+}
REE	Rare-Earth Elements
LREE	Light Rare-Earth Elements
HREE	Heavy Rare-Earth Elements
HFSE	High Field-Strength Elements
LILE	Large-Ion Lithophile Elements
$^{\alpha/\beta}D_i$	A partition coefficient. The simple concentration ratio of element i between phases α and β
$^{\alpha/\beta}K_{Di/j}$	An exchange coefficient. A partition coefficient normalised to the value of another partition coefficient; an indication of the relative partitioning of two elements
γ_{ij}	The interfacial energy of the boundary between phases *i* and *j*
θ_{ij}	The interfacial angle between phases *i* and *j* at a three phase interface

Thermodynamical:

ΔG_i	Gibbs free energy change for a reaction for component *i*.
ΔS_i	Entropy change for a reaction for component *i*.
ΔH_i	Enthalpy change for a reaction for component *i*.
ΔV_i	Volume change for a reaction for component *i*.
C_i	The concentration of element *i* in a phase.
γ_i	The activity coefficient for element *i* in an phase
P	Pressure in bars
T	Temperature in degrees Kelvin
R	The gas constant
fO_2	The fugacity of oxygen (also for H_2 and H_2O)

Statistical:

μ	mean
σ	standard deviation
n	The number of measurements in population *i*
x_i	Estimate of the mean value of population *i*
SE_i	The standard error of the estimates of the mean value of population *i*
Σ	Sum of.....

Units:

°C	Degrees centigrade
kb	Kilobars
Pa	Pascals
GPa	Gigapascals

hr	Hours
min	Minutes
s	Seconds
cm	Centimetres
m	Metres
km	Kilometres
mm	milimetres
µm	micrometres
pm	picometres
kg	Kilogrammes
J	Joules

Elements:

Aluminium	Al	Oxygen	O
Argon	Ar	Paladium	Pd
Barium	Ba	Phosphorus	P
Berylium	Be	Platinum	Pt
Calcium	Ca	Potassium	K
Carbon	C	Radium	Ra
Cerium	Ce	Rubidium	Rb
Chlorine	Cl	Samarium	Sm
Chromium	Cr	Scandium	Sc
Copper	Cu	Silicon	Si
Dysprosium	Dy	Silver	Ag
Fluorine	F	Sodium	Na
Gold	Au	Strontium	Sr
Hafnium	Hf	Sulphur	S
Holmium	Ho	Tantalum	Ta
Hydrogen	H	Thorium	Th
Iron	Fe	Thulium	Tm
Lanthanum	La	Titanium	Ti
Lead	Pb	Uranium	U
Lithium	Li	Vanadium	V
Lutetium	Lu	Ytterbium	Yt
Magnesium	Mg	Yttrium	Y
Manganese	Mn	Zinc	Zn
Neodymium	Nd	Zirconium	Zr
Niobium	Nb	Nitrogen	N

CHAPTER 1

CARBONATE LIQUIDS IN MANTLE PROCESSES

1.1. Introduction.

There is substantial evidence that carbon exists as a minor constituent of both lithospheric and asthenospheric mantle. From this simple starting point, a line of reasoning can be established which leads to some significant conclusions as to the effects this component has on mantle processes. These conclusions are an *inevitable* consequence of the existence of mantle carbon. The aim of this chapter is to show the reader that carbonate melt exists in the upper mantle, and that it must, as a consequence, be involved in the following petrogenetic processes:

(a) Metasomatism of lithospheric mantle.

(b) Production of small-degree melts (kimberlites, lamprophyres, melilitites etc.).

(c) As a precursor melt to more voluminous silicate magmatism.

(d) The genesis of carbonatites.

Because of the belief that carbonate melt is involved in the above processes, it is important for us to gain an understanding of the geochemical properties of carbonate liquids, and how they differ from those of other fugitive agents which may be present in the upper mantle. This can only be done by undertaking experiments to obtain partitioning data between carbonate liquids and other phases. Such experiments form the basis of this study.

1.2. The evidence for mantle carbon.

There is now little doubt that the mantle contains a significant carbon component; current estimates of the actual carbon concentration by weight vary from 0.1% (McKenzie, 1985) to < 0.2 % (Turner *et al.*, 1990). Evidence for this mantle carbon comes from three main sources: Mantle xenoliths and xenocrysts, mantle-derived magma, and fluid inclusion studies.

Table 1.1. Some of the evidence for a mantle carbon component. Evidence has been accumulated from mantle-derived xenoliths, xenocrysts and melts.

Material	**Observation/interpretation**	**Reference**
Brucite-calcite intergrowths in xenoliths	Interpreted as primary mantle dolomite	Berg (1986)
Inclusions in diamonds	Carbonate -rich melts CO_2-H_2O rich fluid	Navon *et al.* (1988) Turner *et al.* (1990)
Inclusions in mantle-derived garnets	Carbonate-rich	McGetchin & Besançon (1973) Smith (1987)
Diamonds and their origin	Magnesite in xenoliths causes break-up; diamonds deposited by CO_2-rich fluid or melt	Richardson *et al.* (1984)
Carbonatites	Mantle carbon and oxygen isotope signatures Sr-isotope signatures Pb-isotope signatures	Deines & Gold (1983) Huberten *et al.* (1988) Allègre *et al.* (1973) Lancelot & Allègre (1974)
Breakdown of carbonate on ascent	Carbonate will not reach surface in xenoliths	Canil (1990)

Despite the frequency of CO_2-rich fluid inclusions in mantle-derived xenoliths (e.g. Jones *et al.*, 1983), carbonate is rare in mantle xenoliths. One of the few examples of xenoliths believed to contain evidence for primary carbonate are given in Berg (1986). Here, brucite-calcite intergrowths were interpreted as resulting from the breakdown of primary dolomite. Recent experiments by Canil (1990) have suggested that the scarcity of carbonate in mantle xenoliths should be expected; mantle carbonate is unstable in the presence of a mantle assemblage at depths less than 70 km, and will breakdown before eruption in even the most rapidly ascending kimberlitic melts. Carbonatites escape from such breakdown by isolation from silicate mantle phases.

Mantle-derived melts are commonly associated with CO_2 vapour. Degassing at ridges led McKenzie (1985) to estimate the carbon content of the asthenospheric mantle to be in the order of 0.1% by weight. Kimberlites are ubiquitously associated with CO_2, their explosive eruption and emplacement being attributed to exsolution of large quantities of CO_2. The most compelling evidence for carbonate involvement in mantle-derived melts are carbonatites themselves. The trace-element geochemistry, carbon-, oxygen-, strontium-, and lead-isotope signatures of carbonatites are all indicative of a mantle origin (e.g. Deines & Gold ,1983; Huberten *et al.*, 1988; Allèrge *et al.*, 1973; Lancelot & Allègre, 1974).

Apart from those produced in the vicinity of subduction zones, mantle-derived fluid inclusions are consistently carbon-rich. Inclusions in mantle garnets were studied first by McGetchin & Besançon (1973), and later by Smith (1987); the majority contain significant modal carbonate. Inclusions in diamonds are dominated by CO_2-H_2O fluids (Navon *et al.*, 1988; Turner *et al.*, 1990). Of course, the diamonds themselves are evidence for carbon in the mantle!

1.3. Forms of carbon in an oxidised upper mantle.

Carbonates are stable to extremely high pressures (e.g. Biellman *et al.*, 1992), and are thus potential constituents of both the upper and lower mantle. Many authors (e.g. Newton & Sharp, 1975; Eggler *et al.*, 1975; Brey *et al.*, 1983) have show that a variety of reactions occur between carbonates and peridotitic mantle. The two reactions considered most petrogenetically significant are given below for magnesium end-member components:

$$2Mg_2SiO_4 + CaMgSi_2O_6 + 2CO_2 = 4Mg_2SiO_6 + CaMg(CO_3)_2 \qquad (1.1)$$
Forsterite Diopside Vapour Enstatite Dolomite

$$Mg_2SiO_6 + CaMg(CO_3)_2 = CaMgSi_2O_6 + MgCO_3 \qquad (1.2)$$
Enstatite Dolomite Diopside Magnesite

Reaction (1.1) is both pressure and temperature dependent. The assemblage En + Dol is stable at low temperature, high pressure, Fo + Di + CO_2 is stable at low pressure and high temperature. Using typical mantle geotherms, the reaction should take place at *ca.* 70 km depth in oceanic mantle, and at *ca.* 80 km depth under the continents (see Figure 1.1). Reaction (1.2) is almost parallel to (1.1) but occurs at higher pressure (*ca.* 110 km in oceanic mantle, *ca.* 130 km under the continents). The assemblage Di +Magn is stable on the high pressure side of the reaction. In summary, in an oxidised upper mantle, CO_2 is the stable form of carbon at less than *ca.* 75 km, $CaMg(CO_3)_2$ is stable from *ca.* 75-120 km, and $MgCO_3$ at depths greater than 120 km.

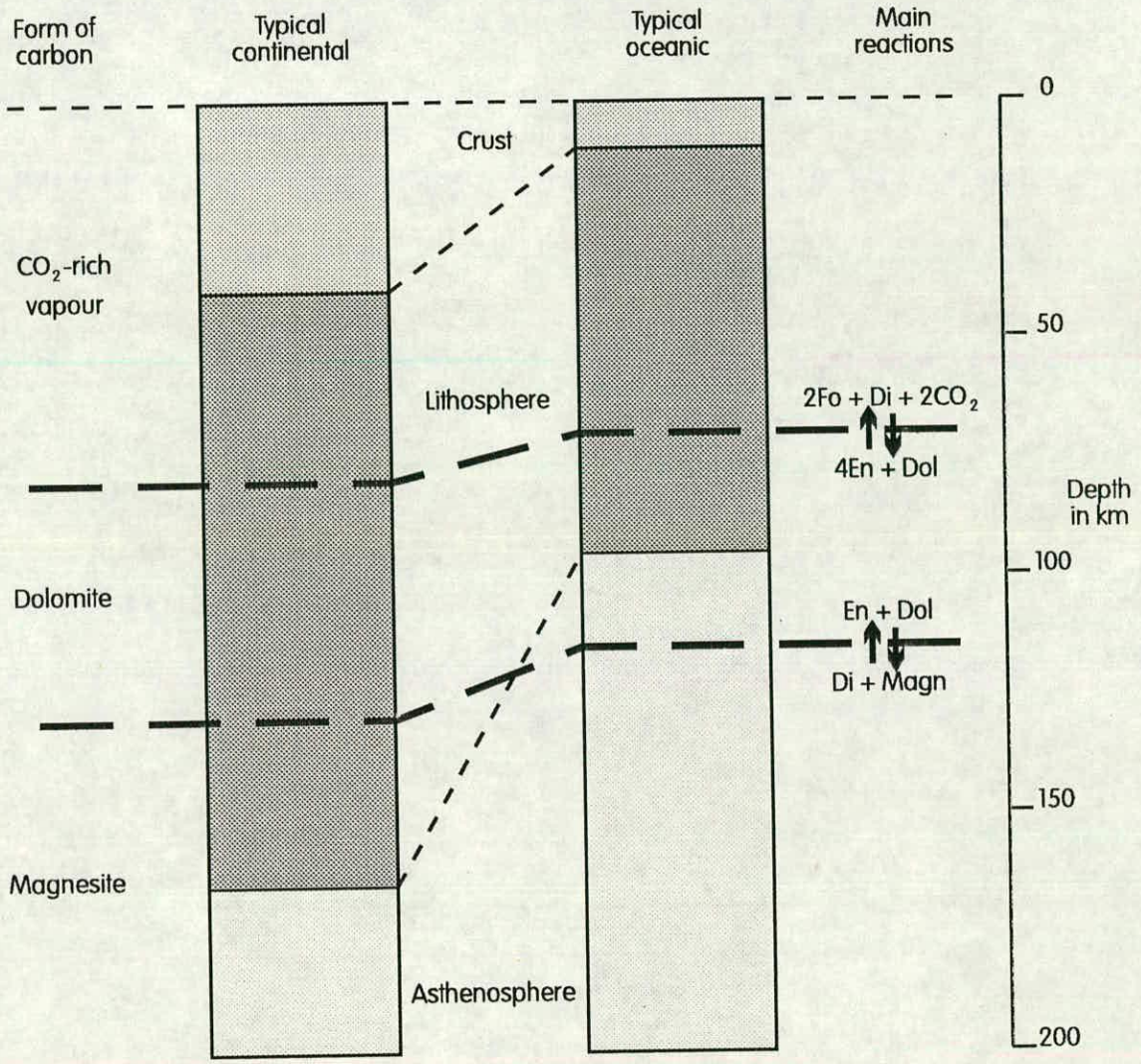

Figure 1.1. Forms of carbon in an oxidised upper mantle. At depths less than ca. 70 km, carbonate will not coexist with mantle phases. Instead, there will be a coexisting CO_2-rich vapour phase. At depths greater than 70 km this vapour will react to form first dolomite (from 70-120 km), and then magnesite (> 120 km). Magnesite is then stable throughout the upper mantle. (Data from Newton & Sharp, 1975; Brey et al., 1983; Falloon & Green, 1990; Biellman et al., 1992).

1.4. The oxidation state of the upper mantle.

There is still much controversy as to the oxidation state of the upper mantle (e.g. Ulmer *et al.*, 1987). This is clearly of importance when considering volatile systems such as those involving CO_2. CO_2 is only stable at oxygen fugacities substantially above the iron-wüstite (IW) reference buffer. Under more reduced conditions carbon exists as CO, C (graphite and diamond) and CH_4 (as mixed methane-water fluids). Eggler *et al.* (1976) showed that CO is unlikely to be the dominant species of carbon in the mantle, rarely making up more than 5-20% of any vapour phase. However, the presence of diamond in xenoliths, and experimental investigations of melting in the presence of CH_4 (e.g. Foley, 1988) have shown that a substantial part of the lithospheric mantle, at least, is under reduced conditions. Figure 1.2 is adapted from Haggerty & Tompkins (1983) and shows typical profiles of oxygen fugacities through sub-cratonic, sub-continental, and sub-oceanic mantle. Many authors would disagree with aspects of this diagram (see Arculus & Delano, 1987; Bryndzia & Wood, 1990; Daniels & Gurney, 1991; Darby Dyar *et al.*, 1989), but the following features are generally accepted:

(a) Lithospheric mantle suffers from extremely variable fO_2, ranging from relatively oxidised conditions near the fayalite-magnetite-quartz (FMQ) reference buffer in the source areas for lamprophyres and perhaps kimberlites, to reduced conditions approaching the IW reference buffer in the source areas for lamproites. Carbonates are therefore only likely to be stable in certain parts of the lithosphere.

(b) The fO_2 at the lithosphere-asthenosphere boundary and in the top part of the asthenosphere is believed to be high (near FMQ). Carbonate will be stable under these conditions. This is of importance as it is at this level in the mantle that melting is most likely to occur.

(c) The deep asthenosphere is believed to have a reduced nature with fO_2 near IW. Carbon is most likely to be present as CH_4 fluid under these conditions. Reduced fluids may rise from this source and oxidise in the upper asthenosphere or in the lithosphere:

$$CH_4 + O_2 = C + 2H_2O \qquad (1.3)$$

Methane Diamond

This oxidation of methane will lead to the production of diamonds, and to water-induced melting at the oxidation boundary (termed "redox melting" by Foley, 1988).

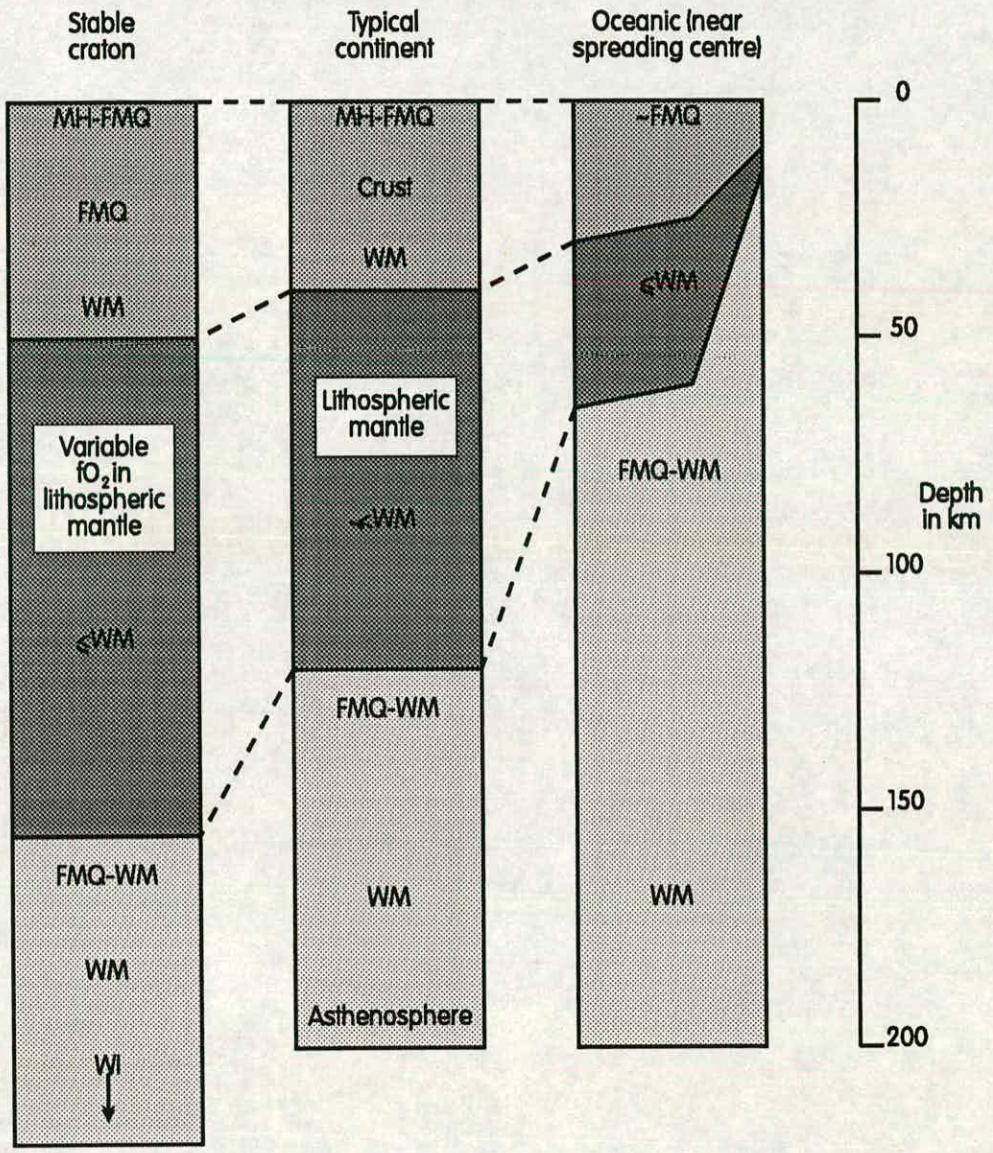

Figure 1.2. Typical profiles of oxygen fugacities in the crust and upper mantle (after Haggerty & Tompkins, 1983). Upper asthenospheric oxygen fugacities are thought to lie between the fayalite-magnetite-quartz (FMQ) and wustite-magnetite (WM) reference buffers. Here, carbon will exist in oxidised form (i.e. carbonate or CO_2). In contrast, the deep mantle is thought to be relatively reduced (below the Iron-Wustite (IW) reference buffer). Here carbon will exist as C or CH_4. The lithosphere is believed to have variable oxygen fugacity, with carbonate or CO_2 present at some levels (e.g. source areas for kimberlites, lamprophyres), and reduced CH_4-H_2O fluid present at others (e.g. source areas for lamproites).

1.5. The effects of carbonate on mantle processes.

The previous section has shown that carbonate is likely to be the stable form of carbon in much of the lithosphere, in the upper part of the asthenosphere, and at the lithosphere-asthenosphere boundary. Many authors have realised that the presence of carbonate will have an important influence on mantle behaviour. The most important effect of carbonate is to lower the dry peridotite solidus by *ca.* 200°C at pressures greater than 2.0 GPa. This produces a kink in the peridotite-CO_2 solidus, the importance of which was first noted by Wyllie & Huang (1975). The main features of the peridotite-CO_2 solidus were first outlined in experiments by Eggler (1978). Since then, a number of workers have produced modified solidi, most notably Olaffson & Eggler (1983) for amphibole-dolomite peridotite and phlogopite-dolomite peridotite, and Falloon & Green (1989, 1990) for "Hawaiian pyrolite"+CO_2. Olaffson & Eggler's solidus is plotted in Figure 1.3 together with near-solidus phase relations and the position of the main carbonate-mantle reactions. The major feature of this solidus is the presence of a ledge at *ca.* 2.0 GPa implying an almost isobaric increase in solidus temperature from near 1000°C to >1150°C. Wyllie (1987) and others have realised the importance of this ledge in terms of magma generation and ascent.

This lowering of the dry mantle solidus by *ca.* 200°C at depths greater than 70 km means that the solidus is very close to the mantle temperature at the base of the lithosphere assuming typical continental geotherms. Even slight perturbations in the thermal regime will, therefore, lead to the production of small quantities of near-solidus melt. With oceanic geotherms, it seems likely that there will always be melting at the base of the lithosphere if carbonate is present (Figure 1.4). Many workers have looked at the composition of these near-solidus melts. The first evidence that these melts were actually carbonatitic in character came from Koster van Groos (1975) who documented an experimentally produced carbonate melt from a peridotite-CO_2 source. Carbonatitic first melts have also been reported by Wendlandt & Eggler (1980), Wendlandt & Mysen (1980), and Olaffson & Eggler (1983). Most recently, the compositions of primary carbonatitic melts from mantle peridotite have been estimated by Wallace & Green (1988) and Thibault *et al.* (1992).

In summary, there is now firm evidence that initial melts produced from carbonated peridotite are carbonate liquids. These melts can be produced at any depth greater than 70 km, but are most likely at, or near, the lithosphere-asthenosphere boundary, where the solidus of amphibole-dolomite peridotite and phlogopite-dolomite peridotite approaches the stable mantle geotherm.

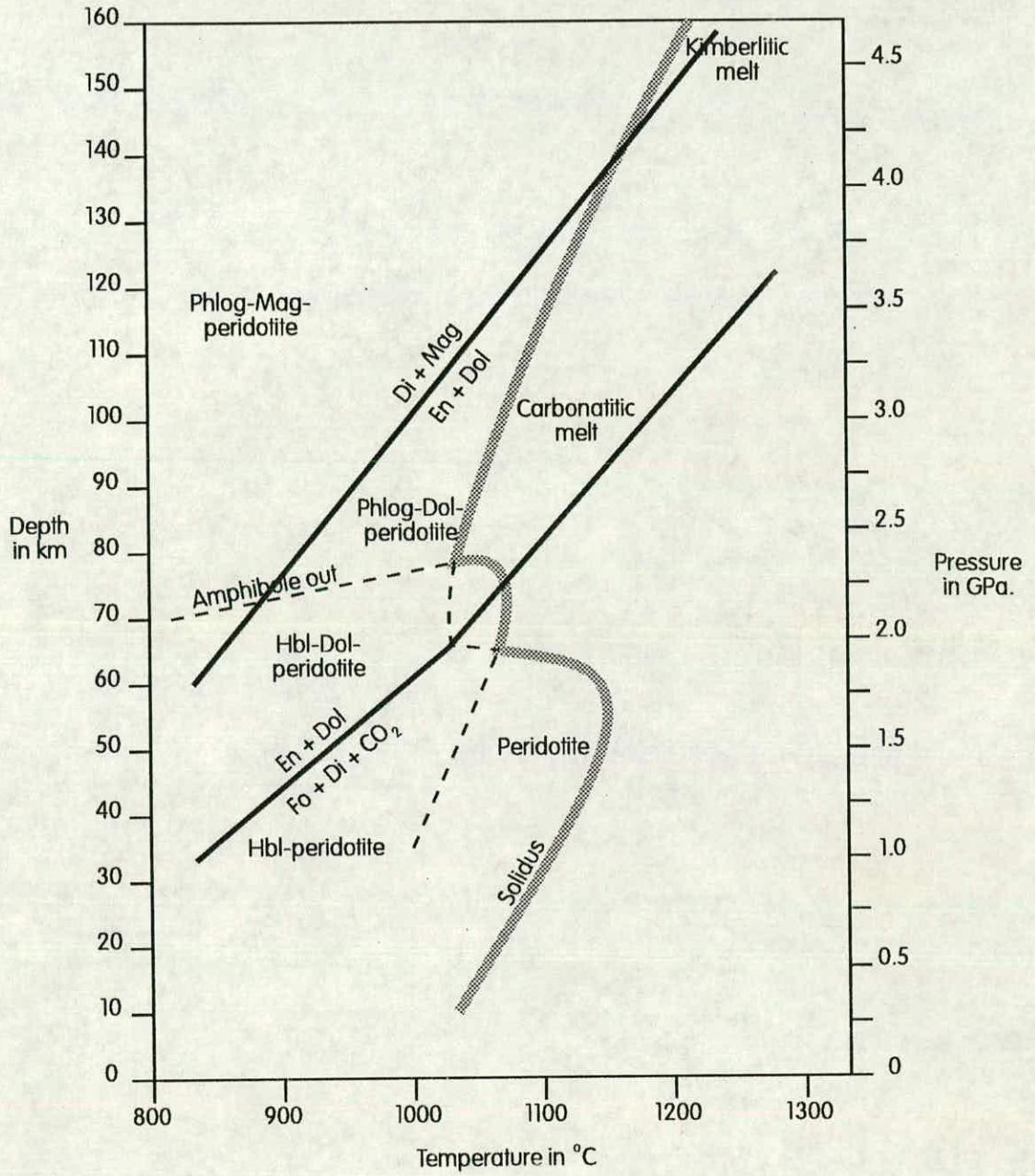

Figure 1.3. The peridotite-CO_2-H_2O solidus and near-solidus phase relations (after Olafsson & Eggler, 1983; Falloon & Green, 1990). The presence of small quantites of volatiles has a profound effect on the phase relations of mantle peridotite. Most notably, the peridotite solidus is lowered by over 100°C at pressures greater than ~2.1 GPa. Near-solidus melts produced at these pressures have been found to be carbonatitic in character. En, enstatite; Di, diopside; Fo, forsterite, Phlog, phlogopite; Hbl, hornblende; Dol, dolomite; Mag, magnesite.

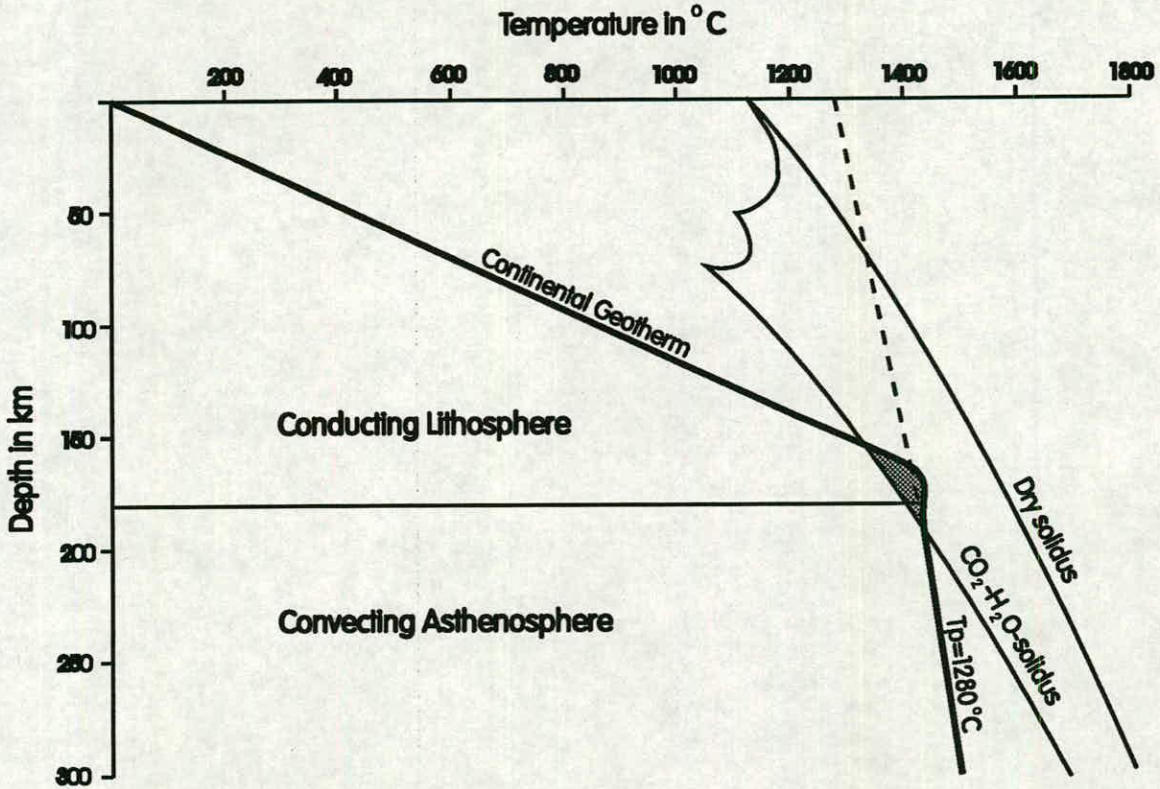

Figure 1.4. The effect of small quantities of volatiles on mantle processes. The presence of carbonate in the mantle assemblage brings the solidus down to temperatures close to those expected at the base of the lithosphere. This means that even very slight perturbation of the thermal regime will result in the production of melts at the lithosphere-asthenosphere boundary. These melts will be carbonatitic in character. (Lithospheric potential temperature from McKenzie & Bickle 1988).

1.6. Physical properties of carbonate liquids and their consequences.

Having established the stability and likely existence of carbonate liquids in the upper mantle, we now have to prove that these liquids will be mobile. If the melt does not escape from its source, it cannot be an agent of chemical mobility. Models of melt segregation and source compaction (e.g. Richter & McKenzie, 1984; McKenzie, 1984) have shown that the ability of a fluid to move depends on its physical characteristics. Table 1.2 shows some of the physical characteristics of carbonate liquids, and compares them to those of mantle silicate melt.

Table 1.2. Physical properties of carbonate liquids. Recent studies have shown that many of the physical properties of carbonate liquid are significantly different from those of mantle-derived silicate liquids. These differences have profound implications for the role of carbonate liquid in the mantle (see text).

Property	Value	Reference	Silicate melt
Density	2.2 gcm^{-3}	Treiman & Schedl (1983)	> 2.6 gcm^{-3}
Viscosity	5.10^{-3} Pas 0.3 Pas	Treiman & Schedl (1983) Dawson *et al.* (1990)	> 1 Pas
Heat of fusion	175 Jg^{-1}	Treiman & Schedl (1983)	*ca.* a factor of 2 more
Diffusion rate	fast	Minarik & Watson (1991)	Order of magnitude slower
Dihedral angle with mantle phases (ol-ol-melt)	28°	Hunter & McKenzie (1989)	Also low for silicate melt but > 60° for H_2O-CO_2 vapour (Watson & Brennan, 1987)

Carbonate liquids have very low density compared to silicate melt and mantle silicate phases (Treiman & Schedl, 1983). This provides a driving force for upward migration of carbonate liquid through the mantle.

Hunter & McKenzie showed that carbonate liquid has a low dihedral angle with silicate phases ($\theta_{ol\text{-}ol\text{-}Lc} = 28°$). This is much less than the value of 60° which is the maximum interfacial angle required to produce an interconnected network of fluid along grain edges; carbonate liquid will therefore produce an interconnected melt network, even at extremely low melt fractions.

The geometry of carbonate melt suggests that mobility is possible, but the rate of melt segregation and melt movement depends upon the viscosity of the carbonate melt. Estimates of carbonate melt viscosity vary (see Table 1.2) but it is clear that carbonate melt viscosities are lower than those of corresponding silicate liquids. Carbonate melt will therefore segregate rapidly from its source.

One final property which may enhance the ability of carbonate melt to effect chemical mobility is its diffusion properties. Diffusion rates in carbonate liquids are an order of magnitude faster than in their silicate counterparts (Minarik & Watson, 1991; Peterson, 1990). This should enhance the ability of carbonate liquid to scavenge incompatible elements from the grain edges of mantle phases. This scavenging ability of carbonate melt has been commented on by Jones (1989).

In short, all the physical properties point towards carbonate liquid as an efficient fugitive agent in mantle systems. McKenzie (1985, 1989) quantified these properties in his models of melt extraction, and showed that at 0.1% melting, carbonate liquid could move through more than 100 km of mantle in just a few million years.

1.7. The fate of small-volume carbonatitic melts.

We have shown that carbonate liquids produced near the lithosphere-asthenosphere boundary will be extremely mobile. Where will they move to? Reference to the carbonated peridotite solidus mentioned earlier presents us with three obvious possibilities (Figure 1.5):

(a) Solidification at the base of the lithosphere.

(b) Ascent to the solidus ledge at *ca.* 70 km depth followed by decarbonation.

(c) Rapid ascent of melt and escape to the surface.

1.7.1. Enrichment processes at the base of the lithosphere.

One further property of carbonate liquid is its low heat of fusion, and also high thermal diffusivity (Treiman & Schedl, 1983). This, combined with the likelihood that small-degree carbonate melt fractions will be of very low volume, leads to the conclusion that these melts will not be able to transport heat as they move. This concept was put forwards by McKenzie (1989) who suggested that small volume carbonate liquids would quickly equilibrate with the ambient mantle temperature, and would therefore rise up the mantle geotherm and solidify where the geotherm again crosses the solidus (Figure 1.6). There would thus be a continuous process of melt movement from the top of the asthenosphere into the base of the lithosphere. If solidification of this carbonatitic liquid takes place in the thermal boundary layer, any enrichment or metasomatism caused by addition of carbonate liquid to the mantle would be short-lived as the material would be quickly returned to the asthenosphere by convection. Carbonate liquids solidifying in the mechanical boundary layer would, however, produce permanent enrichment of lithospheric mantle, and thus cause mantle metasomatism. This process should produce a layer of metasomatised mantle at the base of the lithosphere which could then be re-melted in any thermal or rifting event. It must be stated that this process can only take place if the mechanical boundary layer of the lithosphere is substantially more than 70 km thick (i.e. continental lithosphere, and old oceanic lithosphere). This may explain why carbonatites are only found on continental crust; build up of carbonate melt at the base of the lithosphere is not possible if the lithosphere is not approaching 100 km thick. This may also explain why carbonatites are found on the Canary and Cape Verde islands, as they are known to lie on very old and thick oceanic lithosphere.

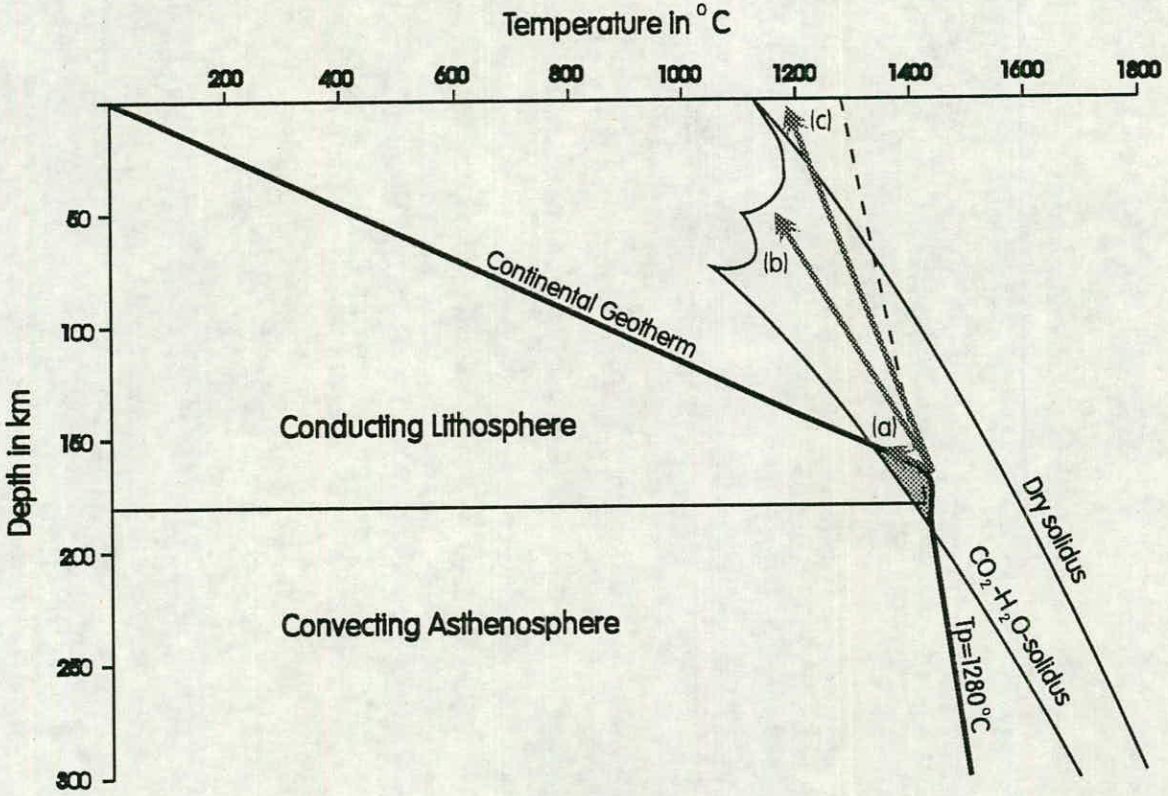

Figure 1.5. The fate of small volume carbonatitic melts. The physical properties of carbonate liquid suggests that carbonatitic melt produced at the base of the lithosphere will be highly mobile. Three likely destinations for this melt are proposed:
(a) Solidification at the base of the lithosphere.
(b) Ascent to the solidus cusp at ca. 70 km depth followed by decarbonation.
(c) Rapid ascent of melt, and escape to the surface.

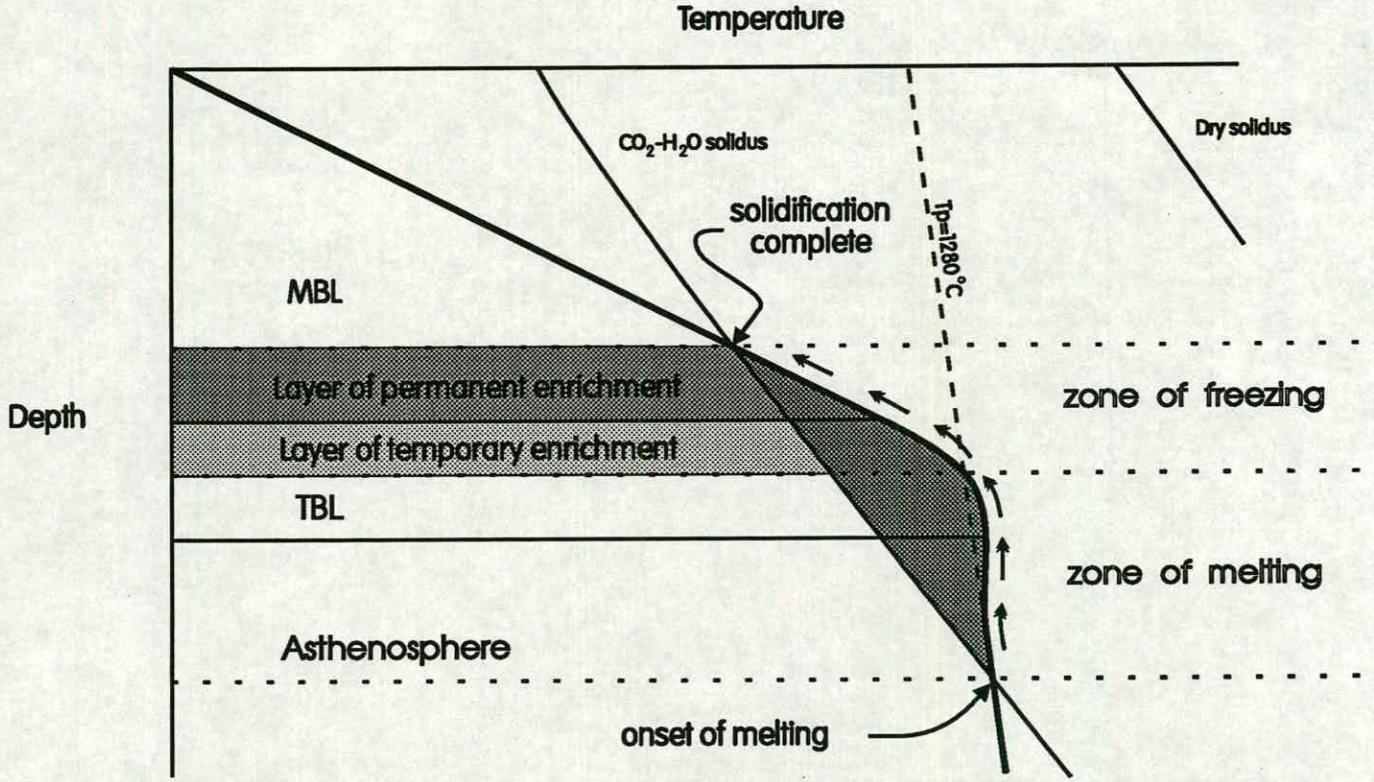

Figure 1.6. Enrichment processes at the base of the lithosphere. The most likely destination for carbonate melt formed at the lithosphere-asthenosphere boundary is the base of the lithosphere. The carbonate melts are of small volume, and have low heat of fusion. They will thus be unable to sustain their own temperature, and will instead follow the ambient temperature of the mantle. This will result in freezing of the carbonate melt where the mantle geotherm re-crosses the solidus. If this is in the thermal boundary layer, the enrichment will be shortlived owing to convection. If, however, the carbonate melt freezes in the mechanical boundary layer, permanent mantle enrichment will occur.

1.7.2. Enrichment processes in the lithosphere at 60-80 km depth.

If, despite the reasoning discussed above, mantle carbonate melt manages to escape from its immediate surroundings, it still has a number of obstacles to overcome before reaching the surface. The most formidable of these is the solidus ledge at between 70 and 80 km depth (Figure 1.7). Molten carbonate rising rapidly towards the surface will intersect the solidus at either 75-80 km or at *ca.* 70 km. At this point it will decarbonate according to reaction (1.1) or will react with mantle in other ways (discussed in Chapter 11). A number of authors have produced intricate models of how carbonate melt will react with mantle under these conditions (e.g. Wyllie & Rutter, 1986; Wilshire, 1987; Meen 1987; Meen *et al.*, 1989), it is sufficient here to say that metasomatism of the mantle will occur, with greatest effects likely to be seen in the geochemistry of those elements which are concentrated in the carbonate melt. As well as the modal metasomatism caused by solidification and decarbonation of the melt there will also be the opportunity of cryptic metasomatism of the overlying mantle by infiltration of CO_2 fluid. On decarbonation, the reservoir containing the incompatible elements in the system is suddenly removed. Most of these elements will be deposited in the new minerals produced. However, it may be possible that a significant concentration of incompatible elements is carried off in the remaining CO_2-H_2O fluid. This saturated fluid will infiltrate the mantle above, and should rapidly equilibrate with mantle phases, so causing cryptic metasomatism. (enrichment of incompatible trace elements without change in modal mineralogy; Dawson, 1984).

1.7.3. The possibility of primary carbonatite melts.

If the rising carbonate melt is at high enough temperature (and comes from great enough depth), it may avoid decarbonation and solidification, and escape to the surface. This is obviously not the likely destination for carbonate melt given the thermal regime of melting and the physical properties of carbonate liquids. However, it is believed that near-primary carbonatites have been found. Two possible examples of primary mantle carbonate liquids which have reached the surface are the Igwisi Hills carbonatite-kimberlite eruptives (containing fragmented peridotite xenoliths in a primary carbonate-rich matrix; Reid *et al.*, 1973), and the Rufunsa carbonatite eruptives in Zambia (contain xenoliths, mantle-like magnesiochromite, and show evidence for high eruption speeds; Bailey, 1989)

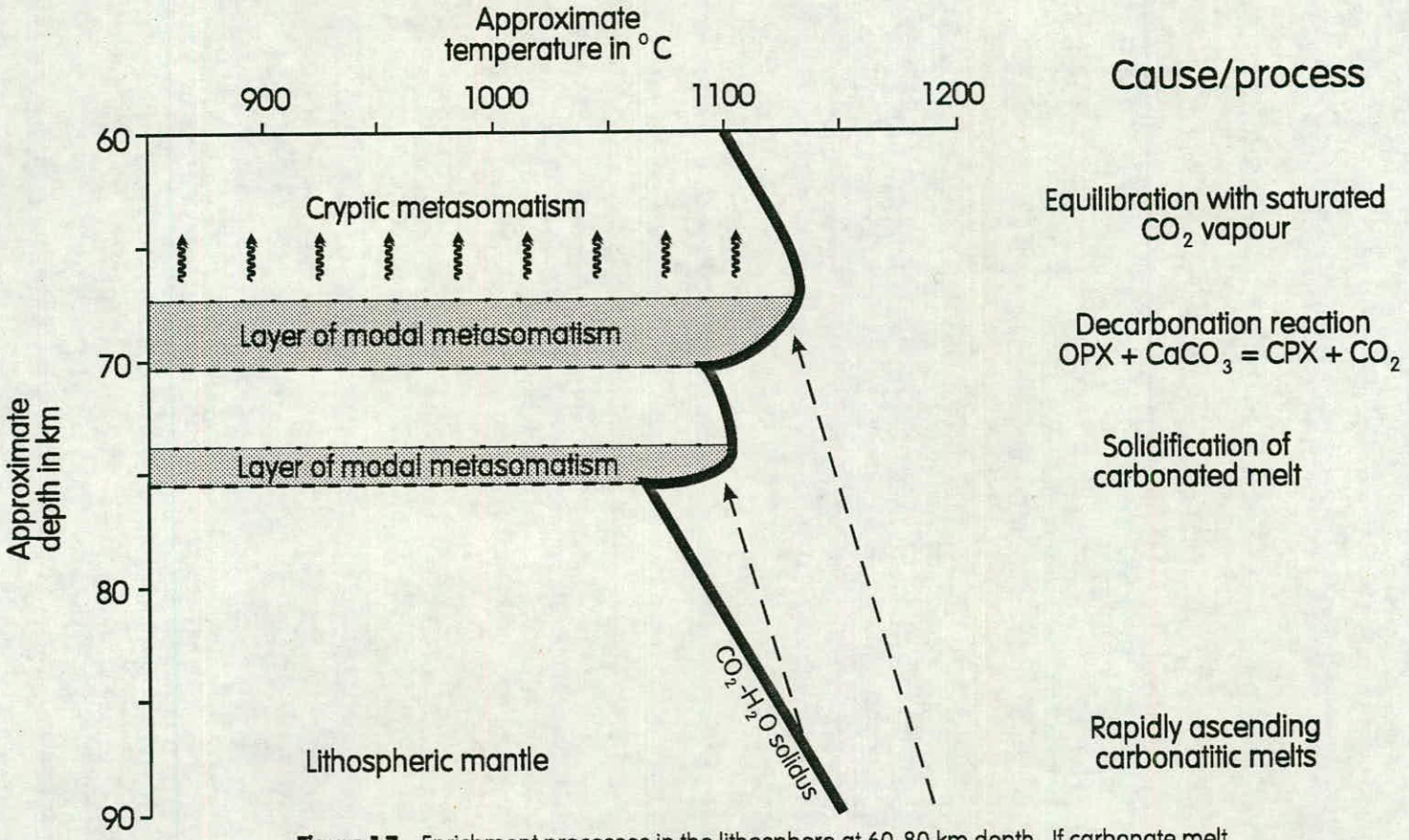

Figure 1.7. Enrichment processes in the lithosphere at 60-80 km depth. If carbonate melt produced at the base of the lithosphere can remain molten, it will rise rapidly towards the surface. At 70-80 km, these melts will intersect the solidus cusp, decarbonate, and thus metasomatise the host mantle. Some elements may be carried away by the CO_2 vapour produced during decarbonation. This fluid will then rapidly re-equilibrate with the mantle, causing cryptic metasomatism.

1.7.4. Incorporation in more voluminous mantle melting.

A further fate for mantle carbonate melt is also possible. If the thermal perturbation which produced the carbonate melt becomes more pronounced, more voluminous silicate melt may be produced. The carbonate melt is then likely to be incorporated in this material.

Figure 1.8. is a schematic diagram showing where, and in what rock-types carbonate melt may be involved in the genesis of mantle-derived melts. In particular it seems likely that low-degree partial melts from great depths (e.g. Kimberlites, lamprophyres and melilitites) will be greatly influenced by carbonate involvement. This is not to say that all low-degree partial melts have a carbonate component; for example, the silica-rich nature of lamproites suggests that they must be produced in the presence of ($H_2O + CH_4$) rather than carbonate (Mitchell & Bergman, 1991).

If we take this process further, it is likely that many silicate melting events were preceded by carbonate melting (or that carbonate melting takes place in the regions arround the melt zone). In this case the carbonate melt would act as a precursor to silicate magmatism, but will probably not be present in large enough quantities to affect the major-element concentrations of the mantle-derived melt. In contrast, the trace-element concentrations of the mantle-derived melt, and in particular ratios of incompatible trace-elements, may be quite significantly influenced by carbonate involvement.

Figure 1.9 shows an example of intraplate silicate magmatism. It is believed that most intraplate magmatism is caused by the presence of mantle plumes or "hotspots". The thermal regime involved with such a melting episode will result in only a relatively small volume of mantle being above the dry peridotite solidus temperature (e.g. Watson & McKenzie, 1991). In contrast, the corresponding volume of mantle which is at a temperature above that of the carbonated peridotite solidus is vast (probably an order of magnitude larger). If both the carbonate and silicate melts are then mixed together and erupted, the incompatible-element ratios of the resulting magma should be dominated by those in the carbonate liquid because of the volume of mantle from which the carbonate liquid has been produced.

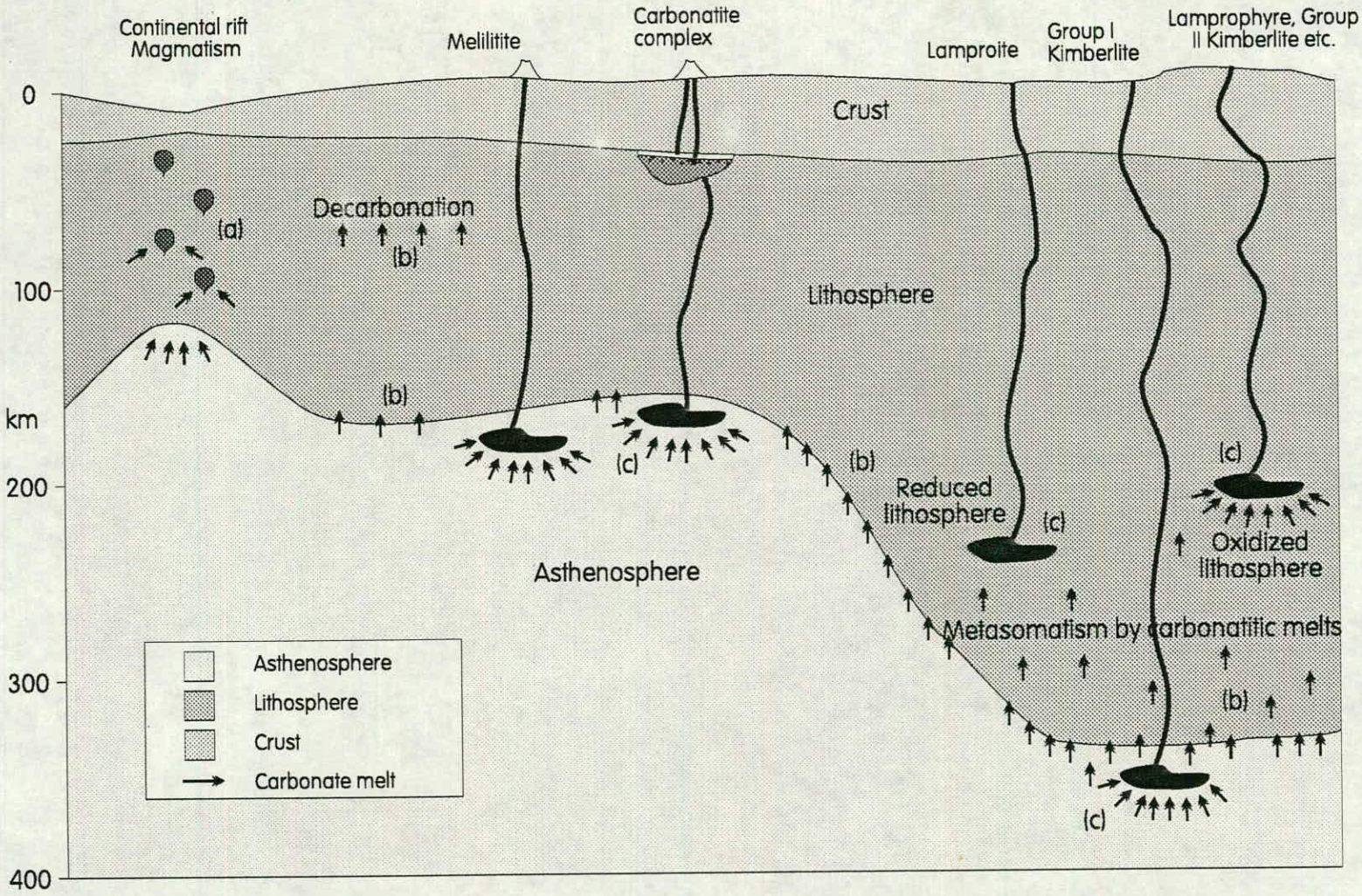

Figure 1.8. Carbonate melt in petrogenetic processes in the subcontinental upper mantle.
(a) In the first stages of continental rift magmatism.
(b) Metasomatism of lithospheric mantle.
(c) Production of small-volume asthenospheric and lithospheric melts.

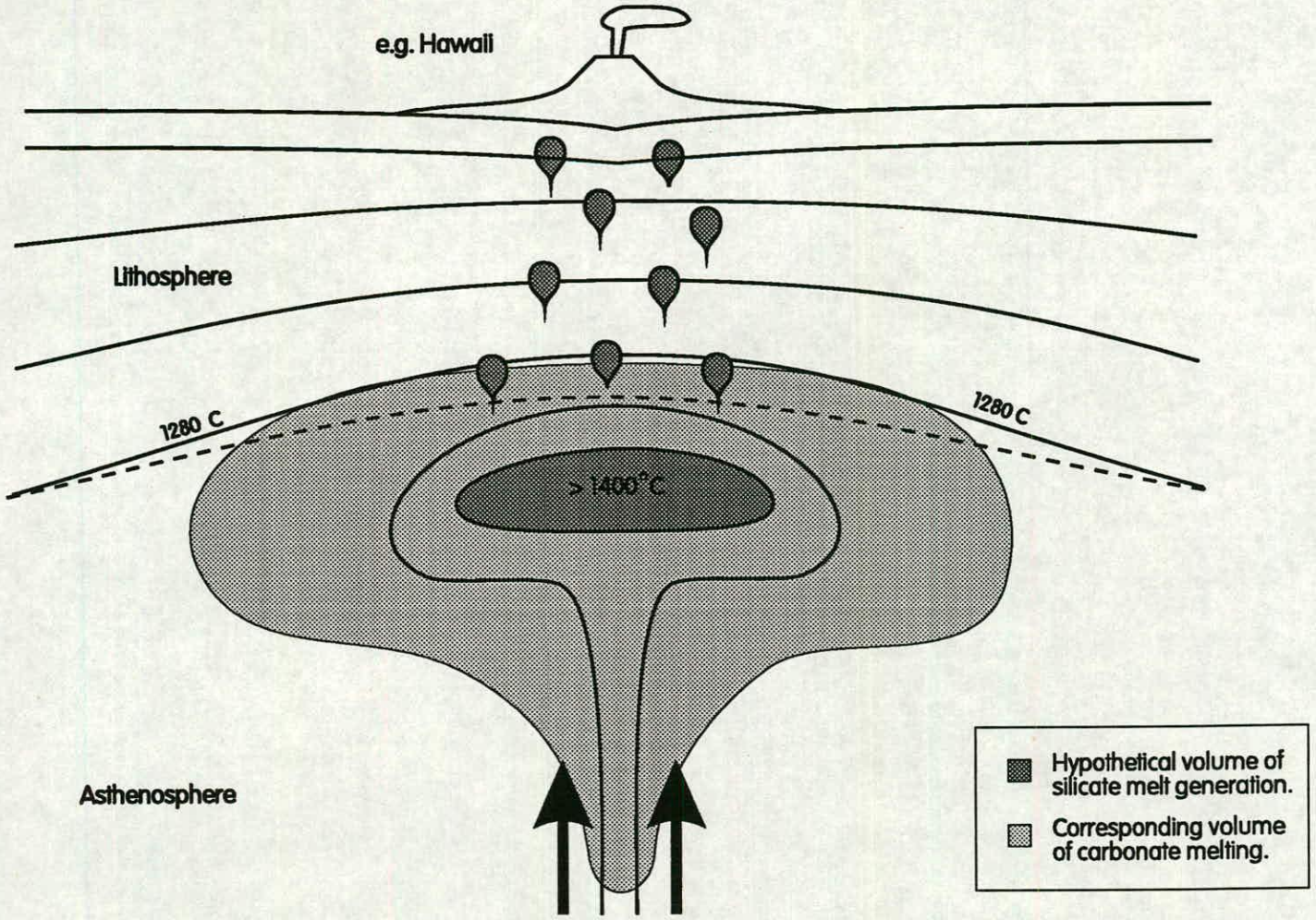

Figure 1.9. Carbonate involvement in intraplate volcanism. In melting events involving a plume or "hot spot", the volume of mantle subjected to silicate melt generation is insignificant compared to that producing carbonate liquid. Incompatible trace-element ratios will therefore be controlled by carbonate-melt equilibria.

A similar situation arises in magmatism at plate boundaries, represented in Figure 1.10 by melting under a mid-ocean ridge. Again, the volume of mantle melting to produce the silicate magma is much smaller than that which produces carbonate liquid, and will indeed already have been depleted by the removal of carbonate melt. In the case of MOR magmatism, however, the volumes of mantle producing carbonate and silicate melt are decoupled. With reference to equation (1.1), carbonated mantle can only exist at depths greater than *ca.* 75 km. Carbonate liquid will therefore only be produced from mantle below 75 km. In contrast, decompression melting of the mantle results in increasing degree of partial melting with decreasing pressure; the bulk of the silicate melt is produced from depths of less than 50 km (e.g. McKenzie & O'Nions, 1991). Despite their different origins, it is likely that these melts will combine in production of mantle-derived basaltic magma seen at mid-ocean ridges. This will again result in some of the features of the carbonate liquid being inherited by the more voluminous silicate material.

It must be stressed that, in both these cases, although the volume of mantle contributing to the production of carbonate melt is likely to be much larger than that producing silicate melt, the actual volume of carbonate melt produced is small compared to the total volume of silicate melt produced.

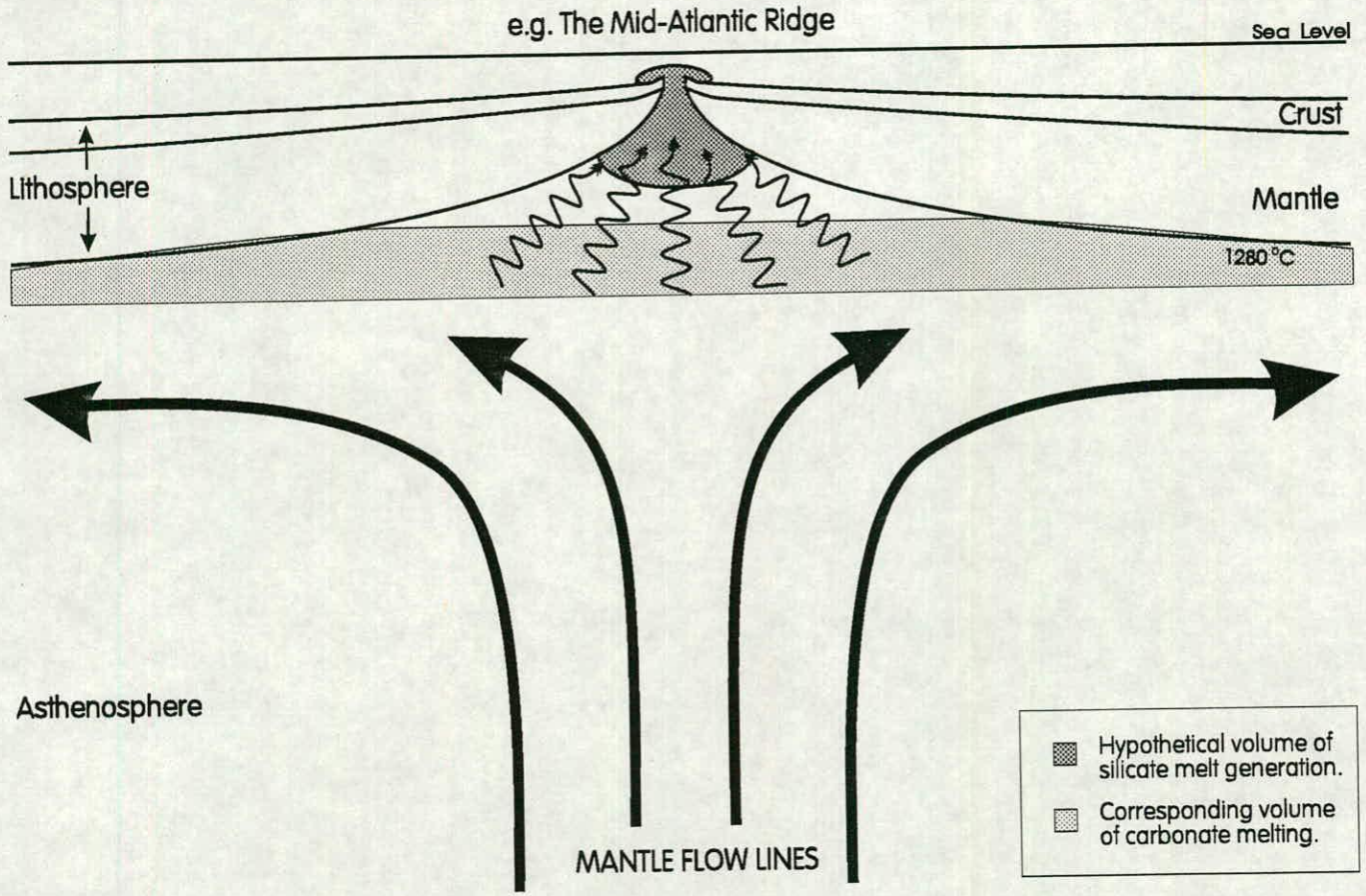

Figure 1.10. Carbonate involvement in decompression melting of upwelling mantle. As before, a much larger volume of mantle is susceptable to carbonate melting than silicate melting. In this case, the carbonate melt is only present below 70 km depth (due to mantle decarbonation reactions), whilst the main body of silicate melt is produced at much shallower depths (e.g. McKenzie & O'Nions, 1991).

1.8. The data to be collected.

In the above treatment, I have suggested that carbonate liquid is involved in many mantle processes; most notably small-volume melt generation, metasomatism, and carbonate-melt production as a precursor to silicate magmatism. In order to investigate the rôle of carbonate melt in these processes, we need to ascertain the geochemical characteristics of mantle-derived carbonate melt. This can only be done accurately by the experimental determination of partitioning behaviour between carbonate liquid and other phases present in the mantle.

Direct measurement of element partitioning between carbonate melt and crystalline mantle phases (olivine, orthopyroxene, clinopyroxene, garnet, etc.) was considered unlikely to produce unequivocal geochemical conclusions as:

(a) Experiments involving very low melt-fractions are difficult to perform:

(i) Temperature and pressure have to be extremely precisely constrained in order to produce the small fraction of melting required.

(ii) Quench modification of the interstitial carbonate liquid is likely to be a serious problem.

(b) Analytical difficulties will produce large uncertainties in the partitioning dataset. These will be mainly caused by:

(i) Quench problems in the carbonate melt.

(ii) Low concentrations of trace-elements in the silicate crystals due to the extremely low values of the partition coefficients being measured.

These difficulties can for the most part be circumvented by investigating partitioning behaviour between experimentally produced immiscible carbonate and silicate liquids. Here, the partitioning being investigated is unlikely to be as extreme as that between crystals and melt, and the composition of carbonate liquid in equilibrium with mantle silicate melts should be easy to measure. Experimental work has therefore concentrated on the immiscibility approach as a means of constraining the geochemical characteristics of mantle-derived carbonate liquids.

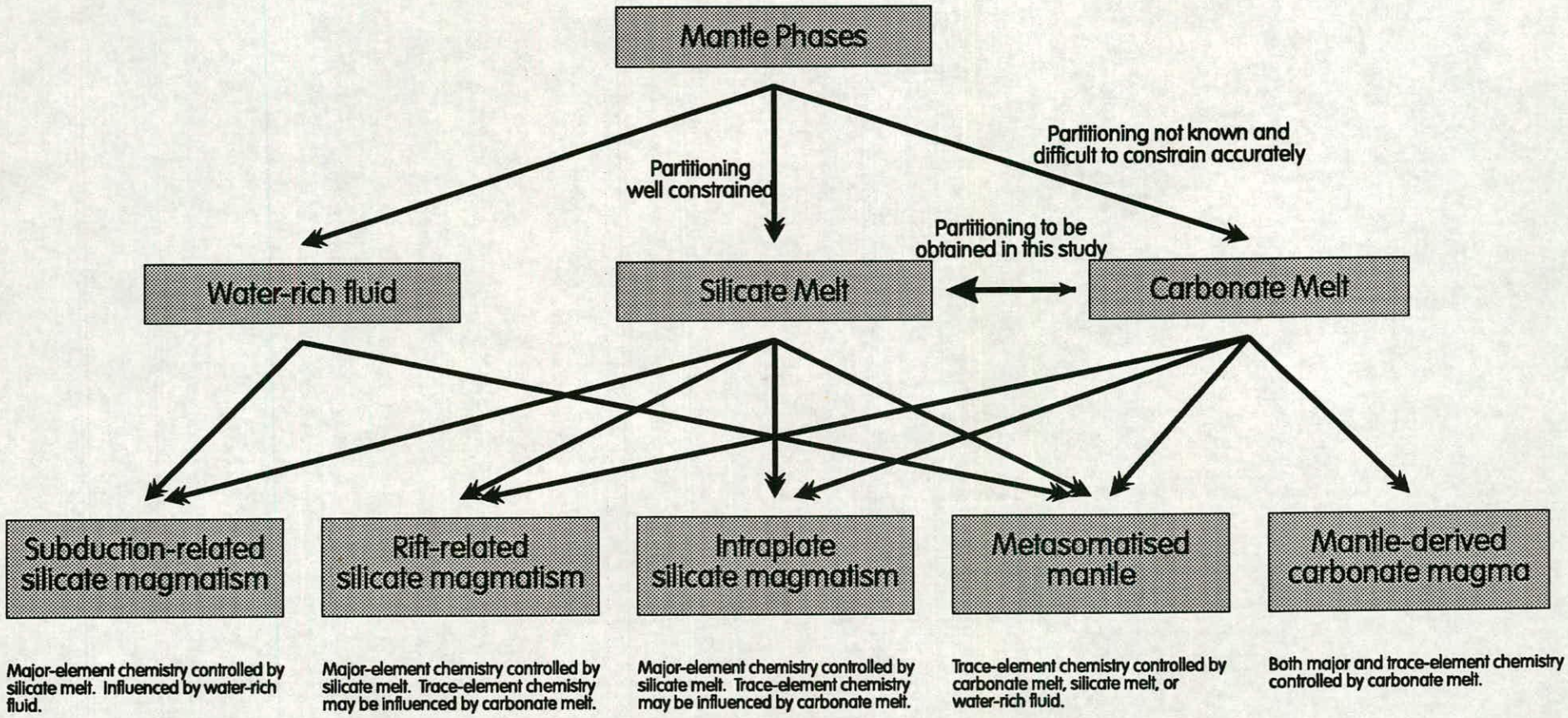

Figure 1.11. Project rationale: why do we need carbonate melt-silicate melt partition coefficients? In order to investigate the geochemical effects of carbonate involvement in mantle processes, element partitioning behaviour between mantle phases and mantle-derived carbonate melt must be constrained. Direct measurement of this partitioning by experiment is fraught with problems: these problems can be avoided by investigating the partitioning between immiscible carbonate and silicate liquids.

1.9. A summary of the theoretical basis for the study.

(a) There is a significant concentration of carbon in both lithospheric and asthenospheric upper mantle. Current estimates suggest that its concentration by weight approaches 0.1%.

(b) The upper asthenosphere, and much of the lithosphere, are at relatively high fO_2. Carbon will therefore exist in carbonates at depths greater than 75 km, and as CO_2 at depths less than 75 km.

(c) The presence of carbonate in the mantle assemblage has a profound effect on the peridotite solidus, resulting in the production of melt at *ca.* 200°C lower than in carbonate-absent melting events. These low temperature melts are carbonatitic in character.

(d) The physical properties of carbonate liquids suggest that these melts will be highly mobile, and will segregate rapidly from their source. They are thus excellent agents of chemical mobility in the upper mantle.

(e) These small-volume carbonate melts are most likely to be produced at or near the lithosphere-asthenosphere boundary. From here they may:

(i) Follow the mantle geotherm, and solidify at the base of the lithosphere. This will result in a layer of metasomatised, carbonated mantle at or near the base of the lithosphere.

(ii) Rise rapidly until they intersect the carbonated peridotite solidus at *ca.* 75 km depth where they will decarbonate. This will result in a layer of modal metasomatism at 70-80 km. CO_2 evolved in this reaction may result in cryptic metasomatism of the mantle above.

(iii) Escape to the surface to be extruded as primary carbonatites. This is thought to be the least likely destination for mantle carbonate liquids due to their physical properties, and the thermal regime under which they are produced. The majority of carbonatites are not believed to have been produced in this way, but are instead thought to be produced by immiscibile separation from evolved, carbonated silicate liquid at lower pressure.

(f) A fourth destination for mantle carbonate liquid involves further melting of the mantle to produce more voluminous silicate melt. In this case the carbonate liquid would be engulfed in silicate material, resulting in inheritance of the trace-element characteristics of the carbonate liquid by the resulting mantle-derived melt.

In order to constrain the rôle of carbonate liquids in the processes outlined above, we need an understanding of the geochemical features of mantle-derived carbonate melt. This understanding can only be achieved by experimental determination of partitioning behaviour between carbonate liquids and other phases. At present such partitioning data are not available, or are at least poorly constrained. This study aims to remedy this situation.

CHAPTER 2

EXPERIMENTS ON PRIMARY MANTLE MELT COMPOSITIONS

2.1 Introduction and background theory.

This experimental project was undertaken with a view to obtaining partition coefficients of relevance to mantle-carbonate systems. Ideally, the experiments would produce coexisting liquid compositions similar in composition to primary mantle carbonate melt and primary mantle silicate melt. The $^{Ls/Lc}D_i$ partitioning data obtained could then be related directly to $^{mantle/Lc}D_i$ equilibria through known $^{mantle/Ls}D_i$ values.

Primary silicate melt compositions produced from volatile-free peridotite are now reasonably well constrained (e.g. Takahashi & Kushiro, 1985). However, liquid compositions produced by low-degree melting of volatile-rich peridotite are more difficult to quantify and are strongly dependent upon pressure, temperature and fluid compositions (Wyllie, 1987). This said, a consensus view emerged in the 1970s (e.g. Eggler, 1972, 1973, 1975; Eggler & Mysen, 1976) that low-degree silicate partial melts of peridotite in the presence of CO_2-rich fluid are compositionally similar to olivine melilitite lavas. In addition to this compositional constraint, lavas which are taken to representa primary melt composition must have a number of geochemical and textural features including:

(a) Nickel contents of *ca.* 300 p.p.m. or more, in order to be in equilibrium with mantle olivine containing 0.3% NiO.

(b) Mg-numbers (i.e. Mg/(Mg+Fe)) of greater than 70, to be in equilibrium with forsteritic mantle olivine.

(c) Evidence of rapid quench from liquid (e.g. fine quench intergrowths, skeletal crystals etc.) indicating little time for modification to occur.

(d) Evidence for rapid ascent from source (e.g. mantle xenoliths and xenocrysts).

Olivine melilitites fulfilling these criteria are found all over the world, on oceanic islands (e.g. Hawaii, Gran Canaria; Brey, 1978), and in continental settings (e.g. E. Africa; Dawson *et al.*, 1985).

There were a number of lines of evidence that suggested that carbonate-silicate immiscibility under mantle conditions was possible:

(a) Bimodality of mantle-derived igneous rock compositions.

Mantle-derived igneous rocks seen at The Earth's surface are noticeably bimodal in composition, either silicate-rich or carbonate-rich. Very few mixed silicate-carbonate rocks have been reported, and most of these are thought to be late differentiates (e.g. Benfontein sill, South Africa; Dawson & Hawthorn, 1973). Rare exceptions do exist, including the rocks of the Igwisi Hills, Kenya (Reid *et al.*, 1973), and silicate-carbonate dikes in East Greenland (Larsen & Rex, 1992). This bimodality has been represented on a triangular diagram with apices (Na_2O+K_2O), (CaO+MgO+FeO), and ($SiO_2+Al_2O_3+TiO_2$), projected from CO_2 (Figure 3.1). This form of compositional representation will be used frequently throughout the chapter.

(b) Field relations.

Primary mantle silicate melts (e.g. olivine melilitites, olivine nephelinites, kimberlites etc.) are often associated with carbonatitic intrusions. For example, the olivine melilitites and nephelinites of East Africa are closely associated in space and time with the carbonatite-nephelinite volcanism in the East African rift (Dawson *et al.*, 1985).

(c) CO_2-solubility data for mantle-derived silicate melts.

Although controversial, the limited solubility of CO_2 in silicate melt up to 2.0 GPa suggested that immiscibility was possible (Eggler & Mysen, 1976; Eggler & Rosenhauer, 1978; Spera & Bergman, 1980; Fine & Stolper, 1985).

(d) Experimental evidence.

Amundsen (1987) reported the presence of carbonate-silicate immiscibility in trapped, quenched liquids in spinel lherzolite xenoliths from NW Spitsbergen. Basaltic and carbonatitic melts were seen to coexist with volatile-rich ultramafic liquids.

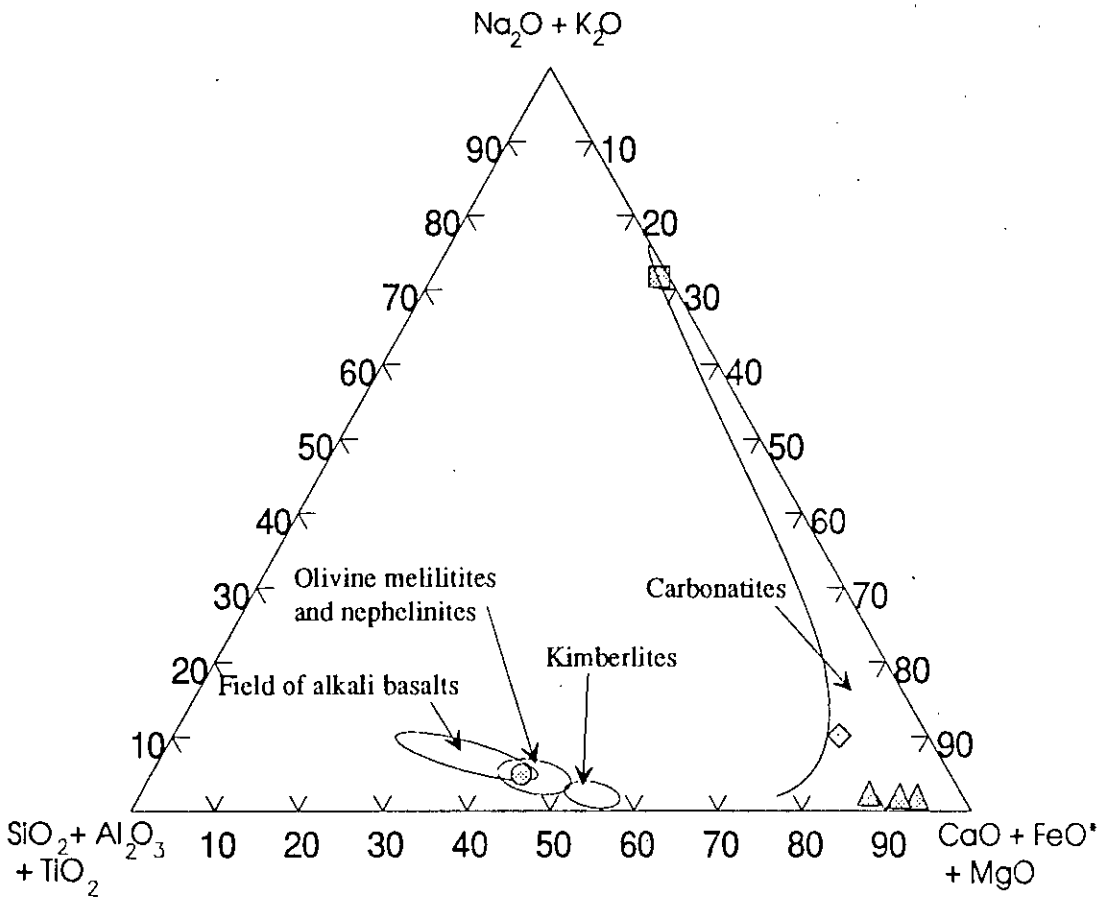

Figure 2.1. Compositional relationships (wt. %) between mantle-derived alkaline igneous rocks. Note the compositional bimodality between silicate and carbonate rock types. Circled areas represent typical compositions of rock types. Triangles are average calciocarbonatite, magnesiocarbonatite and Ferrocarbonatite (Woolley & Kempe, 1989). Square is approximate position of lengaiite (Dawson, *et al.*, 1992). Circle is TAS 3 olivine melilitite (Brey & Green, 1976). Diamond is Wallace & Green's (1988) estimate of primary carbonate melt.

It was decided that there was a possibility that immiscibility existed between carbonate and silicate melt in mantle systems, and that experiments using olivine melilitite as starting material were warranted.

Previous experimental work, of a similar nature to that in prospect, had been accomplished on an olivine melilitite (OM2927) from Laughing Jack Marsh, Tasmania (Brey, 1976; Brey & Green, 1976). This is a pristine lava showing many of the above features, although possibly containing a small number of inherited olivine xenocrysts.

In his PhD thesis Brey (1976) investigated the phase relations of OM2927 from 0-40kb, volatile free, in the presence of H_2O, and in the presence of CO_2. He decided that the presence of CO_2-vapour was essential in order for orthopyroxene and garnet to be brought towards the liquidus, and since these are believed to be residual phases in the generation of melilitites, CO_2 must also have been present in the source area of the melt. Brey (1976) also recorded carbonate-silicate immiscibility textures at 2 and 3 GPa on addition of $Ag_2C_2O_4$ which produces pure-CO_2 vapour on heating to 140° C, according to the breakdown reaction:

$$Ag_2C_2O_{4(s)} = 2Ag_{(s)} + 2CO_{2(vap)} \qquad (2.1)$$

However, as these textures were absent when he tried to enhance them by adding Ca-Mg-carbonate to the melilitite, he concluded that there was no immiscibility between olivine melilitite and carbonate melt at mantle pressures and temperatures. A number of workers since (e.g. Freestone and Hamilton, 1980) have argued that immiscibility is dependent on bulk sodium content, and that addition of Ca-Mg-carbonate diluted the Na content of the charge and therefore removed it from the two-liquid field. A sample of the Laughing Jack Marsh olivine melilitite (TAS 3, D. James) was obtained to be used as the silicate portion of the starting compositions.

Unlike silicate melts, our knowledge about the possible compositions of primary mantle carbonate melt is very restricted. Carbonatites seen at the Earth's surface, even if originally of primary mantle origin, are invariably altered by crustal and surface processes including crystal fractionation, carbonate-silicate immiscibility, contamination, metasomatism, devolatilization, leaching, and weathering. It is widely believed that we have yet to find an unmodified mantle-derived carbonatite in nature, although the rapidly erupted Rufunsa carbonatites from Zambia, containing mantle-like magnesiochromites and peridotite xenoliths, are probably only slightly modified (Bailey, 1989).

Perhaps the best constraint on the composition of primary carbonate melt is from the experimental work of Wallace & Green (1988), who determined that the carbonate melt in equilibrium with amphibole-carbonate-peridotite at 2.1 to 3.0 GPa was a sodic dolomitic carbonatite (Table 2.1), with a minor dissolved silicate component. This composition was therefore used as a basis for the synthetic carbonate mixes employed in the experiments.

2.2. Starting materials: preparation and composition.

Table 2.1 shows the compositions of the starting materials which were combined to produce the charges run in this set of experiments.

Table 2.1. Starting materials for experiments on primary mantle compositions.
1 is TAS 3, olivine melilitite from Laughing Jack Marsh (D. James).
2 is Primary carbonate melt in equilibrium with amphibole-carbonate-peridotite (Wallace & Green, 1988).
3 is CMC, Eutectic dolomitic carbonate at 3.0GPa. (Irving & Wyllie, 1975)
4 is CMN_5C, Eutectic carbonate with 5% added Na_2CO_3.
5 is $CMN_{10}C$, Eutectic carbonate with 10% added Na_2CO_3.
6 is $CMN_{20}C$, Eutectic carbonate with 20% added Na_2CO_3.
*Oxide components of carbonate starting materials are given on a CO_2-free basis.

Oxides	1	2	3	4	5	6
SiO_2	37.51	2.94	-	-	-	-
Al_2O_3	9.56	1.95	-	-	-	-
FeO*	14.22	4.61	-	-	-	-
MgO	15.68	14.19	34.09	32.13	30.23	26.46
CaO	13.09	21.29	65.91	62.34	58.70	51.39
Na_2O	3.69	4.99	-	5.53	11.07	22.15
K_2O	1.31	0.35	-	-	-	-
TiO_2	2.64	0.45	-	-	-	-
MnO	0.22	-	-	-	-	-
P_2O_5	1.31	0.48	-	-	-	-
Total	99.23	51.49	100*	100*	100*	100*

A xenocryst-free portion of TAS 3 was crushed, and ground in a Glen Creston Gy-Ro Mill to produce a fine powder. The powder was then pelleted and sintered at 1 atmosphere, under a gas mixture equivalent to an oxygen fugacity near the nickel-nickel oxide (NNO) reference buffer at 1000°C for >24 hr. The sintered pellets were then reground and mixed with the carbonate component.

The carbonate mixes consisted of Johnson Matthey analytical reagent grade calcium, magnesium and sodium carbonates, ground together in an agate mortar under acetone for 1 hr, and then stored at 110°C.

All starting mixes were ground together under acetone, for 1 hr to ensure homogeneity. The whole assembly was heated to 300°C+ for 24 hrs in order to remove any possible water sources. Assembly and sample were stored in an oven before runs.

2.3. Experimental techniques.

Apart from preliminary experiments at atmospheric pressure, using vertical quench furnaces, all runs were carried out using piston-cylinder, solid-media apparatus (Boyd & England, 1960) at 1.5-3.0 GPa. A similar cell configuration to that of Mirwald *et al.* (1975) was employed, contained within a 1/2" diameter tungsten carbide bomb (Figure 2.2). The sample was sealed within a 2 mm outside diameter graphite pot, with lid, and surrounded in crushable alumina. The capsule was placed in the hot spot of a 3 mm internal diameter graphite heater. The solid pressure-medium was provided by a Pyrex sheath, followed by a ring of talc. The Pyrex was employed as it is established as an efficient water-sink in short-term experiments. In order to lower friction effects and allow easy post-run removal of the sample assembly, the talc was surrounded by a thin sheet of lead foil, coated in molybdenum grease. The top-piece was machined from hardened steel, surrounded by a pyrophylite sleeve.

As was mentioned above, the oxygen fugacity of the staring materials was set at near NNO. A piston cylinder apparatus employing a graphite heater is also thought to buffer systems to near NNO reference buffer conditions (Allen *et al.*, 1972; Boettcher *et al.*, 1973). In any case, with pyrex in the assembly to act as a sink for H_2O, fH_2 is likely to be low, and diffusion of H_2 through the Pt capsule slow. Any change in redox conditions are therefore likely to be slow (e.g. run durations of >24 hrs did not consume small quantities of NNO (nickel-nickel oxide) and WM (wustite-magnetite) buffers; Boettcher *et al.*, 1973). The redox state of these experiments is therefore near NNO reference conditions.

Temperature was measured adjacent to the top of the sample capsule by means of a $Pt/Pt^{87}Rh^{13}$ thermocouple, protected by a ceramic sheath. The e.m.f. of the thermocouple was monitored by a Eurotherm electronic controller which limited variations in the recorded temperature to less than 1°C. Realistically, however, the actual experimental temperatures are believed accurate to ± 10°C. No correction was made for the effect of pressure on the thermocouple e.m.f., and no evidence was found for progressive poisoning of the thermocouple bead with time.

In order to avoid the need for a systematic pressure correction, the piston-out technique was employed. Piston-in under-pressures are believed to be in the region of 10% of the full value. An over-pressure of 10% was therefore applied before returning the charge to run conditions. In initial experiments, cold-pressing to near run pressure before turning the power on led to a high proportion of failures. As a result. a more complex experimental procedure was applied in later runs. The apparatus was pressed to a confining pressure of 7000 p.s.i. (equivalent to 170 tons). The piston ram was then engaged as slowly as possible and the pressure increased to 0.5 GPa. The power was then switched on, and the temperature raised to *ca.* 750°C (approximating the Pyrex softening temperature, Holloway &Wood, 1988) before final pressure was applied. Adjustments to the pressure were then made when run temperature was achieved. Quenching of the experiment was achieved at the end of the run time, by isolating the controller from the circuit by means of a fuse switch (in effect cutting of the power whilst allowing water to continue flowing around the cooling system). The quench rate was extremely rapid, the thermocouple reading being less than 200°C after just 5 seconds.

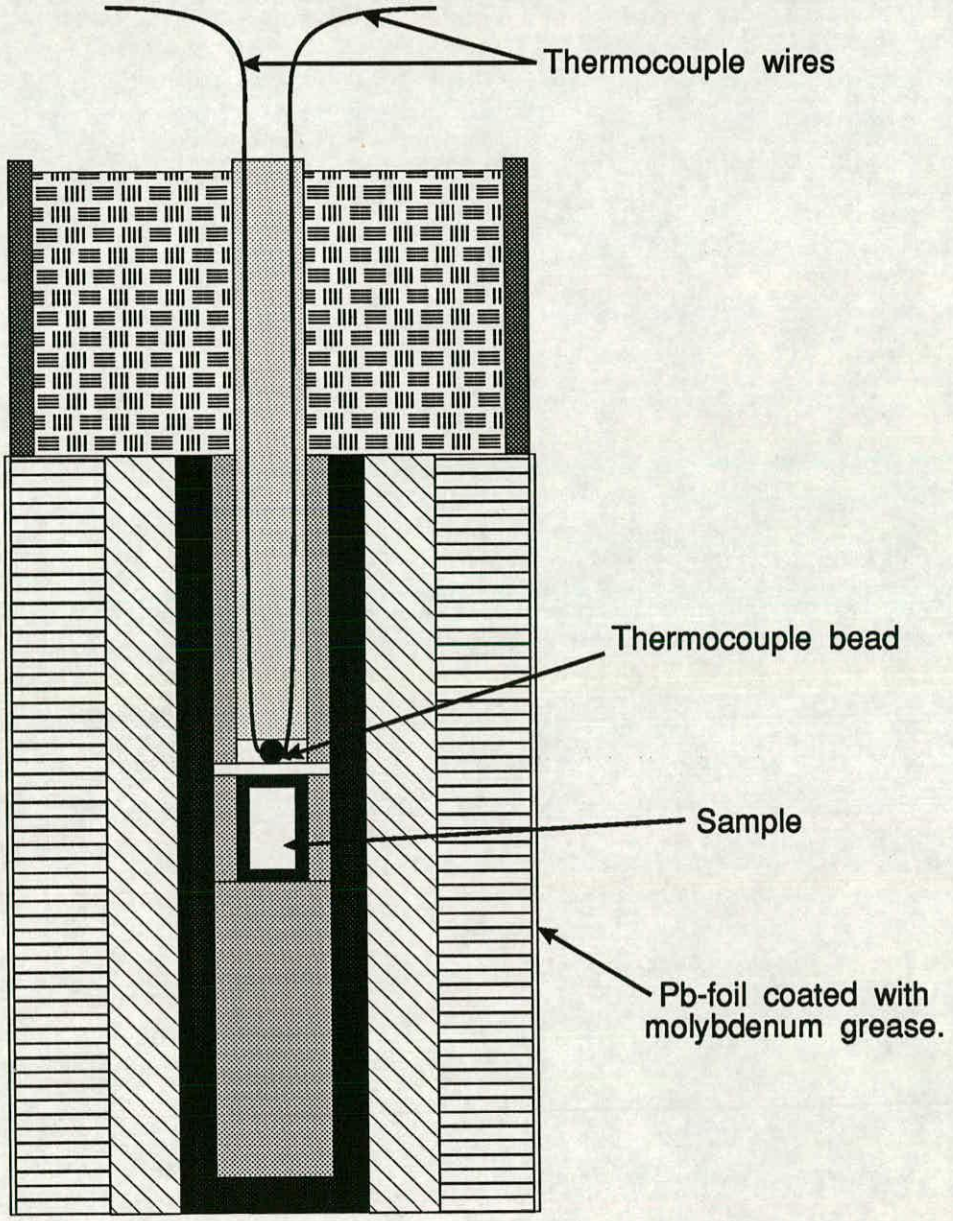

Figure 2.2. Cell configuration for piston-cylinder apparatus runs, S1-S38. S28-S38 used a sealed Pt capsule (designated furnace assembly B) instead of the graphite pictured here.

KEY

Talc } pressure medium
Pyrex

Graphite furnace and capsule

Pyrophylite slieve

Hardened steel

Crushable alumina cell parts

Ceramic thermocouple sheath

2.4. The experiments.

Thirty-eight experimental charges, containing a variety of primary melt compositions, were run over a range of conditions. The experimental run data are given for reference in Table 2.2 (Furnace assembly A), and Table 2.5 (Furnace assembly B).

Table 2.2. Experimental run data S1-S25 (Furnace assembly A, Graphite capsules).
Ol = olivine, Opx = orthopyroxene, Cpx = clinopyroxene, Gt = garnet, Sp = spinel, Per = periclase, Mont = monticellite, Q = quench inter growth, Ls = silicate glass, Lp = pyrex glass
* Contamination by influx of Pyrex from assembly
** Contamination by influx of Alumina from assembly
# CO_2-loss from charge

Run ident	Compositions (Wt. %)	Pressure (GPa.)	Temperature (°C)	Time (Mins)	Assemblage
S1	100% TAS3	3.0	1500	120	Ls
S2	100% TAS3	3.0	1300	120	Ol+Cpx+Opx+Ls
S3	100% TAS3	3.0	1400	120	Ol+Cpx+Opx+Ls
S4	50% TAS3, 50% CMC	3.0	1500	120	Ol+Per+Q
S5	50% TAS3, 50% CMC	3.0	1400	120	Ol+Sp+Q
S6	50% TAS3, 50% CMC	3.0	1300	120	Ol+Sp+Q
S7	50% TAS3, 50% CMN_5C	3.0	1500	135	Ls #
S8	50% TAS3, 50% CMN_5C	3.0	1400	120	Ls #
S9	50% TAS3, 50% CMN_5C	3.0	1300	125	Gt+Al +Ls #**
S10	50% TAS3, 50% $CMN_{10}C$	3.0	1300	122	Ls #
S11	50% TAS3, 50% $CMN_{10}C$	3.0	1400	120	Opx+Ls +Lp #*
S12	50% TAS3, 50% $CMN_{10}C$	3.0	1500	120	Ls #
S13	50% TAS3, 50% $CMN_{20}C$	3.0	1300	122	Opx+Ls #*
S14	50% TAS3, 50% $CMN_{20}C$	3.0	1400	123	Opx+Ls #*
S15	50% TAS3, 50% $CMN_{20}C$	3.0	1500	121	Ls #
S17	50% TAS3, 50% $CMN_{10}C$	3.0	1200	240	Ol+Cpx+Gt +Q
S18	50% TAS3, 50% $CMN_{20}C$	3.0	1200	243	Ol+Mont+Q
S20	50% TAS3, 50% $CMN_{10}C$	3.0	1100	240	Ol+Px+Mont+Q
S21	50% TAS3, 50% $CMN_{20}C$	3.0	1100	240	Ol+Cpx+Gt +Q
S24	100% $CMN_{10}C$	3.0	1350	180	Contaminated *
S25	100% $CMN_{10}C$	2.0	1350	120	Q+Per

2.4.1. Set 1. Experiments on TAS 3 (S1-3).

A brief investigation of the phase relations of TAS 3 were made, both at atmospheric pressure, and at 3.0 GPa., equivalent to *ca.* 90 km depth in the mantle. These experiments were undertaken for two main reasons:

(a) To constrain the liquidus temperature of TAS 3 at atmospheric pressure, and at 3.0 GPa., essential for setting the P-T conditions of future runs.

(b) To see if TAS 3 could be a primary, or near-primary mantle melt at *ca.* 90 km depth.

Experiments at 1 atmosphere showed that TAS 3 has a liquidus temperature of 1400-1450°C, and that, below this, there is a long crystallisation interval of olivine alone. This high liquidus temperature suggests that TAS 3 contains at least some cumulus olivine (mantle melt liquidus temperatures would be expected to be in the range 1250-1300°C).

The first experiment at 3.0 GPa, run at 1500°C, was above the liquidus, producing a charge of 100% glass. Subsequent experiments at 1300°C and 1400°C produced charges with the assemblage Ol+Cpx+Opx+Liquid. The liquidus for TAS 3 therefore lies between 1400°C and 1500°C at 3.0 GPa. As the three-phase mantle assemblage Ol+Cpx+Opx is stable to within a maximum of 100°C of the liquidus, and there is no long temperature interval of olivine crystallisation alone, it can be assumed that the TAS 3 composition is near to a primary melt at 90 km depth. However, as Brey (1976) pointed out, garnet is thought to be a residual phase in the genesis of olivine melilitites, and therefore should be near the liquidus. He showed that this only occurs in the presence of CO_2, again suggesting a link between CO_2 and olivine melilitite genesis.

2.4.2. Set 2. Experiments on TAS 3 and calcium-magnesium carbonate (S4-6).

50/50 mixtures of sintered TAS 3 and eutectic dolomitic carbonate ($\{Ca_{58}Mg_{42}\}CO_3$) were run at 3.0 GPa and 1500°C, 1400°C, and 1300°C in an attempt to obtain immiscibility between primary silicate melt and sodium-free carbonate. As with Brey's (1976) experiments, immiscibility was not confirmed, with mixed carbonate-silicate quench intergrowths being identified (see Table 2.3 for electron probe

analyses). Despite the extremely fast quench rates, no carbonate-silicate glasses were found, perhaps not surprising considering the reputation of carbonate melt for rapid quench-growth. The quench intergrowth was accompanied, in the 1300°C, and 1400 °C runs by olivine and spinel. In the 1500°C run, however, spinel no longer coexists with olivine and melt, although small, high-relief crystals of periclase were identified (Plate 2.1). It is believed that these could have formed as a result of a decarbonation reaction of the form;

$$CaMg(CO_3)_2 = CaCO_3 + MgO + CO_2 \qquad (2.2)$$

This could have either occurred under run conditions, or during heating and quenching.

Table 2.3. Electron probe analyses of mixed carbonate-silicate quench material (3.0 GPa, 1300-1500°C) suggesting an absence of immiscibility in alkali-poor mantle melts.

Oxide	S4H	S4K	S502	S605	S606
SiO_2	15.10	15.84	16.20	15.80	15.58
Al_2O_3	1.29	1.20	2.15	3.29	3.26
FeO*	2.87	2.75	3.84	4.81	4.01
MgO	19.32	20.15	18.46	16.02	18.16
CaO	34.68	34.23	31.06	28.34	28.54
Na_2O	0.41	0.43	0.84	1.26	1.18
K_2O	0.05	0.04	0.26	0.41	0.52
TiO_2	1.02	0.86	1.05	1.33	1.37
MnO	0.07	0.07	0.08	0.10	0.08
NiO	0.04	0.04	0.04	0.03	0.05
Total	74.87	75.60	73.98	71.40	72.77

The presence of mixed carbonate-silicate quenches in these experiments has some important implications. The compositions of the quench material given in Table 2.3 have been plotted on a triangular diagram in Figure 2.3. It can be seen that the quenches occupy the compositional space that was expected to contain carbonate-silicate immiscibility. This, combined with other evidence, points to the likelyhood of complete miscibility between carbonate and silicate melts under alkali-poor mantle conditions.

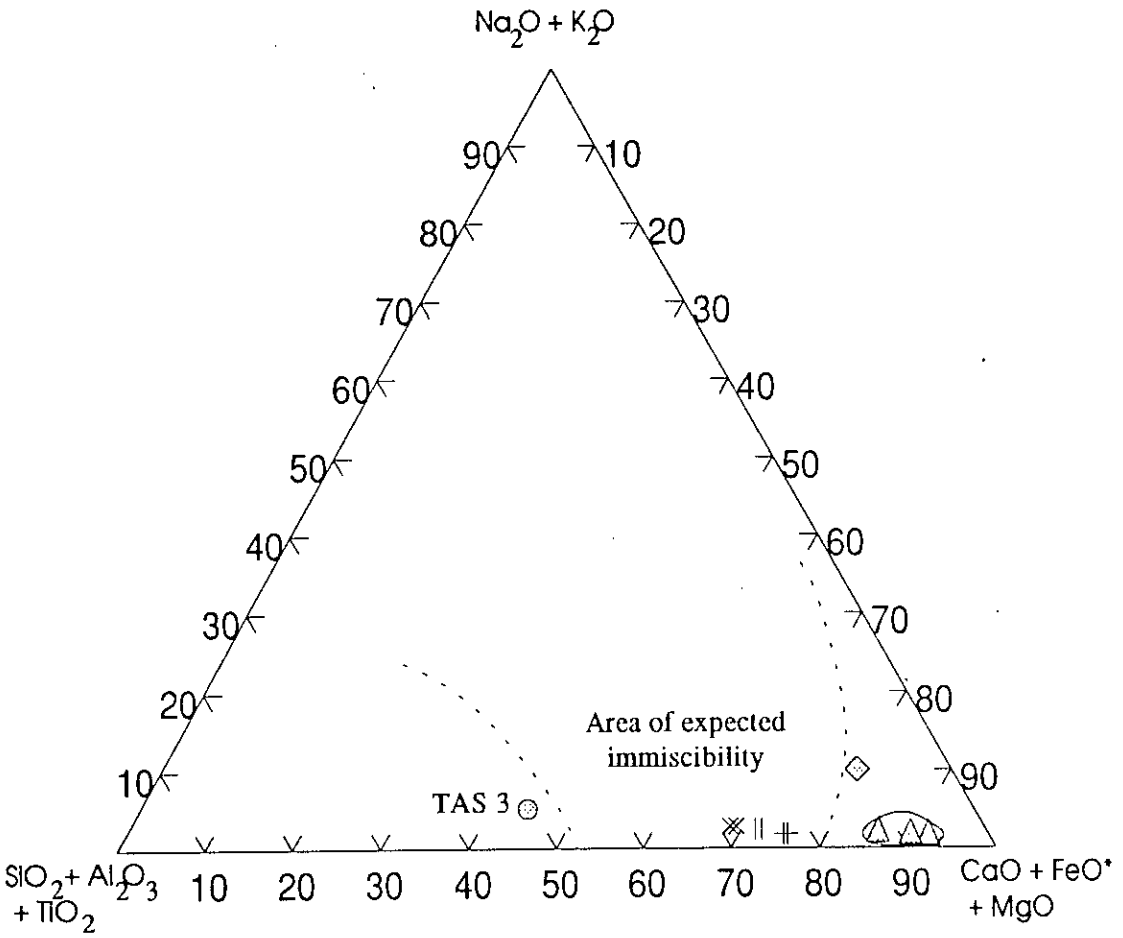

Figure 2.3. Quench products of Set 2 experiments: Evidence for lack of carbonate-silicate immiscibility in alkali-poor mantle systems. +, S4 mixed carbonate-silicate quench; ll, S5 mixed carbonate-silicate quench; X, S6 mixed carbonate-silicate quench. Triangles are average calciocarbonatite, magnesiocarbonatite and ferrocarbonatite (Woolley & Kempe, 1989). Diamond is Wallace & Green's estimate of primary carbonate melt (1988).

2.4.3. Set 3. Addition of alkali carbonate to experimental charges (S7-S21).

As a result of the failure to obtain immiscibility in the alkali-poor system, and following the work of Freestone & Hamilton (1980), sodium was progressively added to the charges in the form of anhydrous Na_2CO_3. This was deemed more likely to exhibit a two-liquid field, whilst still being within the range of mantle compositions. The alkali carbonate formed 5, 10, and 20 wt. % of the carbonate starting materials, which were then ground, together with the silicate portion of the composition, in an agate mortar, under acetone. Grinding was continued for a period of *ca.* 1 hr in order to ensure homogeneity. Due to the hydrophilic nature of sodium carbonate it was necessary to bake the whole assembly, including the sample charge, for at least 24 hrs before the run, and ensure rapid transfer of the furnace assembly from oven to bomb. The samples were again run at 3.0 GPa.

Far from enhancing the chances of obtaining immiscibility, however, the addition of Na_2CO_3 to the charges acted as a flux, causing a lowering in viscosity of the resulting molten charge. This allowed migration of sodium-rich melt away from the sample, through cracks and fissures in the graphite capsule (Plate 2.2). Ultimately the melt reached the alumina and Pyrex of the furnace assembly, causing melting and contamination of the charge (see Table 2.4).

Table 2.4. Selected electron probe results showing the experimental problems associated with running volatile, sodium-rich charges in graphite capsules.
S12B, S12E: Undersaturated silicate glass. Although still volatile rich (low totals), CO_2 appears to have been lost from the charge.
S11A, S11H: Immiscible pyrex globules (H) in melilititic glass (A).
S9B: Alumina-rich crystal in contaminated glass.
S4A, S4B: Disequilibrium olivine crystal with Mg-rich rim surrounding an Fe-rich core.

Oxides	S12B	S12E	S11A	S11H	S9B	S4A	S4B
SiO_2	30.57	30.60	54.71	92.46	6.22	41.29	40.42
Al_2O_3	9.12	9.21	8.46	0.47	77.44	0.30	0.17
FeO*	6.74	6.81	3.31	0.15	1.48	3.05	7.29
MgO	19.37	19.58	15.23	0.34	1.42	53.40	49.87
CaO	19.13	19.18	5.39	0.19	4.10	1.08	0.89
Na_2O	2.04	2.02	5.65	0.32	0.88	0.17	0.16
K_2O	0.44	0.42	0.10	0.01	0.20	0.03	0.01
TiO_2	1.53	1.57	0.43	0.02	0.42	0.08	0.08
MnO	0.11	0.13	0.07	0.05	0.05	0.06	0.14
NiO	0.03	0.03	0.03	0.01	0	0.01	0.03
Total	89.15	89.60	93.43	93.97	92.41	99.40	99.00

In summary, attempts to obtain immiscibility between olivine melilitite and sodium-rich carbonate, using graphite capsules, produced a number of difficulties:

(a) Fluidity of charges.

The low viscosity of the melt phase allowed migration of melt away from the crystalline portion of the sample and through cracks in the graphite capsule and furnace assembly(e.g. S10, Plate 2.2a).

(b) Loss of CO_2.

A number of the charges produced Ca-Mg-rich silica-undersaturated glasses (e.g. S12), with reasonably high totals (*ca.* 90%). These charges must have lost at least some of their carbonate component, either on the P-T path to run conditions, or actually during the run. This occurred in the high temperature runs (1500°C).

(c) Contamination by alumina from furnace assembly.

After the run, the graphite capsule in which the sample was contained was found to be shattered and veined with melt. The capsule was surrounded by alumina in the furnace assembly. The crushable alumina used in this design should not begin melting below 1800°C. There was however, evidence that the alumina had indeed melted, presumably due to fluxing by sodium carbonate, resulting in contamination of the charge by alumina-rich melt and crystals (e.g. S21, Plate 2.2c).

(d) Contamination by pyrex glass from the furnace assembly.

Surrounding the graphite heater in the furnace assembly is a pyrex sheath. Pyrex softens at *ca.* 700°C, but is known to have relatively high viscosity to well above 1500°C. In order for contamination to have occurred, therefore, it seems likely that the sodium again acted as a flux, resulting in increased fluidity and mixing with the charge. In one instance (S11), immiscible pyrex globules were found actually within the sample melt (Plate 2.2b).

(e) Disequilibrium olivines.

In those charges containing crystals, marked disequilibrium could be seen between magnesium-rich overgrowths (e.g. S4A), and iron-rich cores (e.g. S4B, see Table 2.4). One explanation for this phenomenon is that the olivine cores are relics from the original TAS 3 powder that were never melted during the experiment (*ca.* Fo_{87}). These fragments then acted as nucleii for growth of olivine in equilibrium with the charge (Fo_{94}) to produce the magnesian rims.

It was decided, as a result of these problems, that a new experimental design, and new techniques were required in order to confirm the presence or absence of immiscibility in these sodium-bearing charges.

2.4.4. Set 4. Experiments in Platinum capsules (S28-S34).

The previous set of experiments had shown that it was not possible to run volatile-rich sodium-bearing experimental charges in graphite capsules without exchange of material with the charge's surroundings. Sealed, welded platinum capsules were therefore preferred (Furnace assembly B). Also, in order to avoid any residual olivine crystals remaining unmelted under run conditions, it was deemed necessary to heat the charges to >1500°C (above the liquidus) for 20 mins before cooling slowly (20°C per hour) to run pressure and temperature. This produced very different crystal-melt relationships to the earlier charges, with large, often acicular crystals of olivine and pyroxene in quenched liquid. Experiments were performed at 1250 and 1350°C, at 1.5, 2.0, and 3.0 GPa. Compositions were 50/50 mixes of TAS 3 and $CMN_{10}C$.

This new experimental set-up managed to avoid all the difficulties encountered in the Set 3 experiments. However, immiscible carbonate and silicate liquids were again not identified in the run products (see Table 2.5 for assemblages found). Indeed, the resulting mixed carbonate-silicate quenches shown in Table 2.6 suggest that even with sodium contents higher than is realistic for a mantle assemblage, primary carbonate and silicate melts are unlikely to be immiscible in the pressure range studied (1.5-3.0 GPa).

Table 2.5. Experimental Run data S28-S38 (Furnace assembly B, platinum capsules).
* Was run without pre-heat to 1500°C, contains olivine relics.
Abbreviations as for Table 2.2.

Run ident.	Composition (Wt. %)	Pressure (GPa)	Temperature (°C)	Time (Mins)	Assemblage
S28*	50% TAS 3, 50% $CMN_{10}C$	3.0	1350	150	Ol+Q
S29	50% TAS 3, 50% $CMN_{10}C$	2.0	1350	180	Q
S30	50% TAS 3, 50% $CMN_{10}C$	1.5	1350	180	Q
S31	50% TAS 3, 50% $CMN_{10}C$	3.0	1350	180	Q
S32	50% TAS 3, 50% $CMN_{10}C$	3.0	1250	180	Ol+Px+Q
S33	50% TAS 3, 50% $CMN_{10}C$	2.0	1250	180	Q
S34	50% TAS 3, 50% $CMN_{10}C$	1.5	1250	180	Ol+Sp+Q
S35	60% TAS 3, 40% $CMN_{10}C$	3.0	1250	180	Ol+Px+Q
S36	70% TAS 3, 30% $CMN_{10}C$	3.0	1250	180	Ol+Px+Q
S37	80% TAS 3, 20% $CMN_{10}C$	3.0	1250	180	Ol+Px+Sp+Q
S38	90% TAS 3, 10% $CMN_{10}C$	3.0	1250	180	Ol+Px+Q

Table 2.6. Electron probe analyses of selected quenched liquids from experiments S28-S38.
All the above quench products, despite their varied compositions, show lack of immiscibility between carbonate and silicate components.

Oxides	S28I	S28J	S30D	S30E	S32D	S32E	S33C	S33D	S35H	S35I	S38A
SiO_2	16.18	13.23	25.49	27.10	26.88	26.66	20.42	19.90	7.10	7.35	11.32
Al_2O_3	3.63	1.53	7.53	7.91	7.09	7.14	5.24	5.11	0.42	0.37	1.27
FeO*	0.77	0.98	0.08	0.07	0.39	0.44	0.27	0.25	2.45	2.29	5.47
MgO	17.68	20.43	20.36	20.25	18.69	18.97	15.14	15.30	6.41	7.04	9.76
CaO	29.65	28.23	21.83	22.35	20.11	20.10	25.81	25.60	36.14	35.93	24.45
Na_2O	1.85	1.75	1.53	1.51	3.39	3.17	3.98	4.10	9.77	10.10	11.40
K_2O	0.18	0.24	0.51	0.49	0.69	0.65	0.77	0.76	2.05	2.04	3.04
TiO_2	1.55	1.52	1.89	1.81	1.67	1.74	1.54	1.52	1.00	0.92	3.34
MnO	0.08	0.15	0.12	0.07	0.18	0.08	0.10	0.11	0.17	0.20	0.30
NiO	0.04	0.00	0.03	0.00	0.01	0.00	0.00	0.01	0.00	0.00	0.04
P_2O_5	0.30	0.40	0.23	0.26	0.58	0.67	1.03	0.94	3.19	3.00	4.46
Totals	70.43	68.47	79.59	81.81	79.74	79.66	74.29	73.57	68.72	69.25	73.86

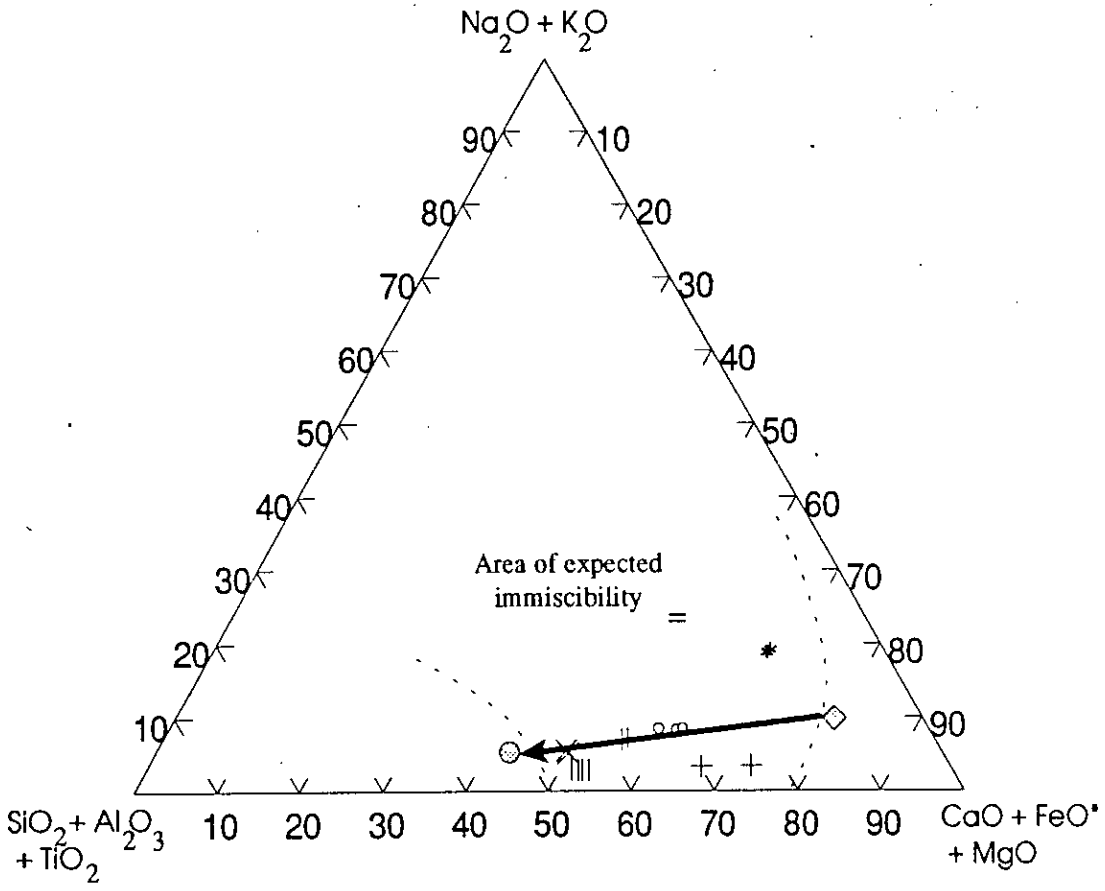

Figure 2.4. Quench products of Set 4. experiments: Evidence for lack of immiscibility in the mantle for geologically reasonable compositions. +, S28 quench; II, S30 quench; X, S32 quench; I, S33 quench; *, S35 quench; =, S38 quench. Circle is olivine melilitite TAS3. Diamond is Wallace & Green's estimate of primary carbonate melt (1988). The thick arrow represents a possible compositional melting path in the mantle.

Figure 2.4 shows a possible compositional melting path in alkali-rich peridotite assemblages. It can be seen that mixed carbonate-silicate quenches of various compositions have been obtained, both along this line, and with higher sodium contents. The idea of a compositional range over which immiscibility occurs is therefore suspect under realistic mantle conditions.

2.4.5. Set 5. Experiments with various carbonate contents (S35-S38).

Set 4. experiments were designed to be under conditions which were most likely to produce immiscibility in the compositions studied at mantle pressures and temperatures. Since no immiscibility was obtained in any of these charges, and $^{Ls/Lc}D_i$ values were clearly unobtainable, it was decided that another approach to the problem had to be attempted. The Set 4 experiments had shown that clinopyroxene crystals could be produced in equilibrium with carbonate-rich melts. If a wide range of melt compositions could be obtained in equilibrium with pyroxene, from silica-rich to carbonate-rich, it would be possible to obtain $^{Cpx/L}D_i$ partition coefficients. Systematic variations in $^{Cpx/L}D_i$ from carbonate-rich to silicate-rich would then indicate the geochemical effects of carbonate on $^{mantle/L}D_i$. In addition to the 50/50 mix run in Set 4, charges of 60/40, 70/30, 80/20, and 90/10 ratio of silicate to carbonate were made up, and run at 3.0 GPa., and 1250°C.

All these charges produced assemblages containing olivine, pyroxene, and quench intergrowth (Plate 2.3). S37 also contained some small crystals of spinel. In all cases, the pyroxene crystals were greater than 25 μm across, and therefore large enough to analyse. The quenched liquids were, however, very variable chemically, even when in large pockets and crystal-free areas. They were found to consist of coarse aggregates of quench crystals. These quenches were found to be laterally heterogenous with respect to major elements (see Table 3.6), and were therefore unlikely to produce consistent values for trace-element concentrations when presented to the ion probe. In addition, large uncertainties would be produced due to the extreme partitioning behaviour expected between silicate crystals and carbonate melt. Therefore it was concluded that this line of research would not result in data accurate enough to distinguish between carbonate and silicate equilibria.

This conclusion has been recently supported by Brenan & Watson (1991). They attempted similar experiments to those outlined above, in order to produce $^{Cpx/Lc}D_i$ and $^{Ol/Lc}D_i$ partitioning data. In this paper, Brenan & Watson showed that it was difficult to distinguish between crystal/carbonate melt, and crystal/silicate melt partitioning behaviour, and suggested that melting in the mantle, producing compositions ranging from carbonatites to nephelinites and basalts could be modelled with a single set of D values. Although, as Brenan & Watson suggest, it is likely that silicate melt/carbonate melt partitioning is likely to be less extreme than crystal/melt partitioning, it does not follow that these differences will be insignificant. It was therefore deemed necessary to continue with the concept of carbonate-silicate immiscibility as a method for determining the geochemical differences between carbonate and silicate melts.

2.5. Conclusions and Implications.

The experiments carried out on compositions believed to represent primary mantle melts were unsuccessful in producing coexisting immiscible carbonate and silicate liquids, and were therefore not of use in the quest for $^{Ls/Lc}D_i$ partitioning data. However, a number of useful conclusions can be drawn from this work:

(a) The mixed carbonate-silicate quench products produced from compositions of TAS 3 mixed with Ca-Mg-carbonate at 3.0 GPa confirm the experiments of Brey (1976). This leads to the conclusion that, at least under alkali-poor conditions, melting in the mantle at depths of *ca.* 90km will produce completely miscible carbonate and silicate melts, and combinations thereof. This is also consistent with the only other published experimental study on mixed carbonate-silicate mantle systems (Hunter & McKenzie, 1989), where again no immiscibility was observed.

(b) Results of the sodium-bearing experimental charges extend the conclusion reached in (a), as immiscibility textures were not produced, even for relatively sodium-rich compositions. Experimental evidence therefore points towards a continuous evolution of liquid composition, from carbonatite to melilitite and nephelinite, for melting involving all geologically realistic mantle compositions. Subsequent experimental work has confirmed this result (Baker & Wyllie, 1990), suggesting that the field of coexisting carbonate and silicate melts at 2.5 GPa, and 1050-1300°C is far removed from mantle compositions, and only exists at very elevated sodium contents (Figure 2.5). These melts are very different structurally from primary mantle melts, and it is believed that it is this structural control (in effect the polymerisation state of the silicate melt) that limits the extent of immiscibility.

(c) Experimental attempts to produce crystal-liquid D values in carbonate- silicate systems at present seem unlikely to produce unequivocal geochemical conclusions. The errors involved in the analysis of the carbonate quench, and the extreme nature of the D values under study are expected to make the analytical uncertainties in the results larger than the actual geochemical differences between carbonate and silicate melt.

In summary, it was concluded that a different experimental approach was required, and that any further work should be undertaken in systems where carbonate-silicate immiscibility is well documented and its extent known. A detailed study of the effects of pressure, temperature and composition on these melts could then be undertaken, in order to extrapolate the results to conditions appropriate to the mantle.

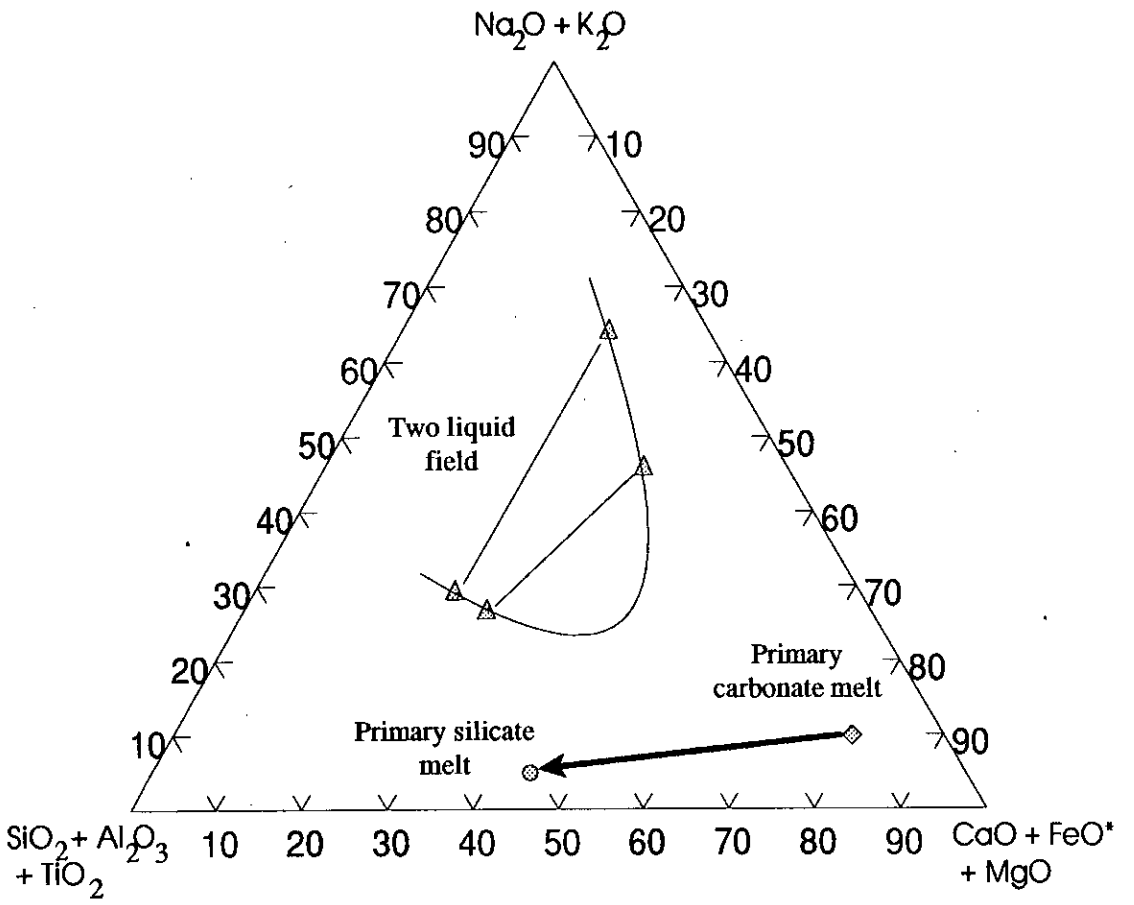

Figure 2.5. The extent of carbonate-silicate immiscibility at 2.5 GPa, 1250 °C (Baker & Wyllie, 1990), and the probable melting path in the mantle (thick line). Note that the two-liquid field is far removed from mantle melt compositions.

Plate captions: Chapter 2.

Plate 2.1. Experiments on sodium-free mantle compositions (S4-S6).

A. The charge from experiment S4, showing crystals of clinopyroxene (C) and olivine in a matrix of carbonate-silicate quench (Q). Scale bar is 100 μm.

B. A vertical section through the charge from experiment S4, showing gravity settling of olivines (Ol) and pyroxenes (C) through the carbonate quench (Q). This experiment was run for just 60 minutes, suggesting that crystal settling is rapid in these compositions. Scale bar is 100 μm.

C. The whole charge from experiment S6, showing crystals and carbonate-silicate quench. The small, rounded and high-reflectivity crystals are of periclase. Scale bar is 100 μm.

Plate 2.2. Experiments on sodium-bearing mantle compositions (S7-S28).

A. Sample mobility: the charge from experiment S10. At run P and T, the sample was molten and highly fluid. Much of the sample material (Ls) escaped from the graphite capsule (G) through cracks and fissures. Scale bar is 100 μm.

B. Contamination by SiO_2 from the experimental assembly. In this extreme example of contamination (S11), blebs of near-pure silica (P) are seen within the glass of the charge (Ls). This is thought to be meta-stable immiscibility between the two glass compositions. The only possible source for such a large quantity of silica is the Pyrex sheath which surrounds the furnace in the experimental assembly used. Scale bar is 50 μm.

C. Contamination by Al_2O_3 from the experimental assembly. The charge from experiment S21 contains many large crystals of garnet (GNT). The interstitial liquid is also alumina-rich. It is concluded that the charge has been contaminated by alumina from the sample assembly. Scale bar is 100 μm.

Plate 2.3. Experiments to determine $^{Cpx/Lc}D_i$ values (S28-S38).

A. Clinopyroxene crystals (C) within a quench (Q) of *ca.* 50% carbonate, 50% silicate (S32). The quench shows marked compositional heterogeneity. Scale bar is 50 μm.

B. Clinopyroxene crystals (C) within a silicate-rich quench (Q) from experiment S35. Scale bar is 50 μm.

C. Clinopyroxene crystals (C) surrounded by carbonate-rich quench (Q) from experiment S37. Again the interstitial quench material shows marked heterogeneity. Scale bar is 50 μm.

EX BIBL. UNIV. EDINBURGENSIS

A
G
O
C

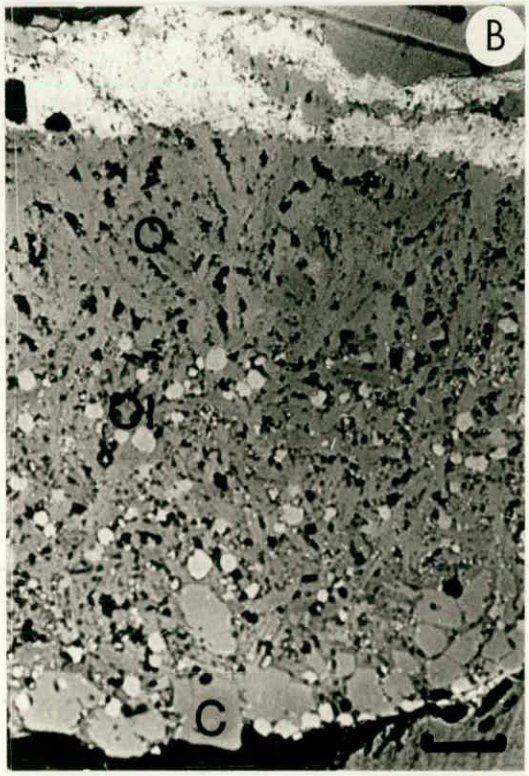
B
O
OI
C

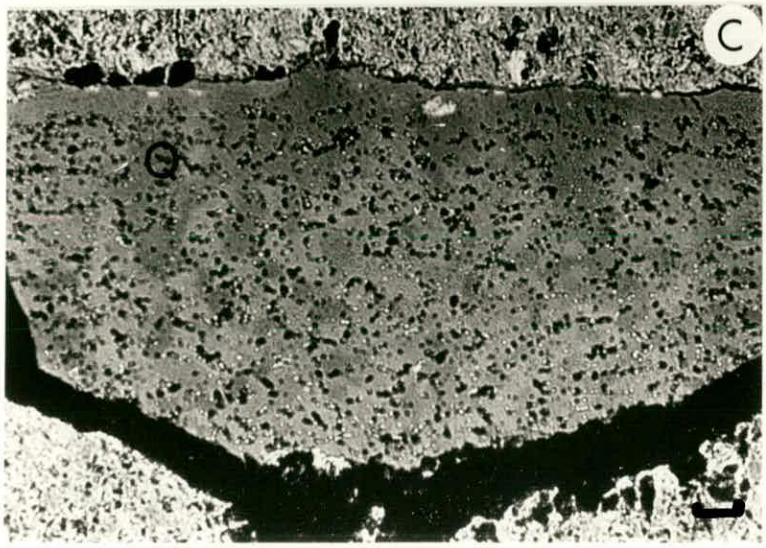
C
O

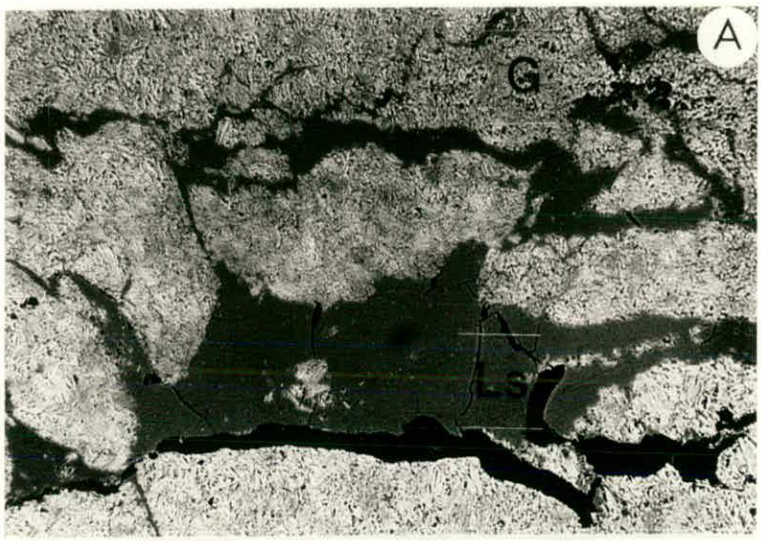
A
G
Ls

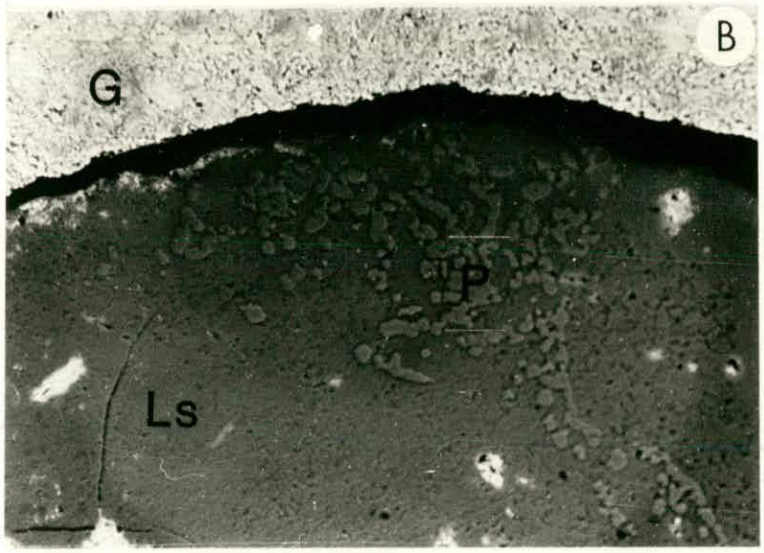
B
G
P
Ls

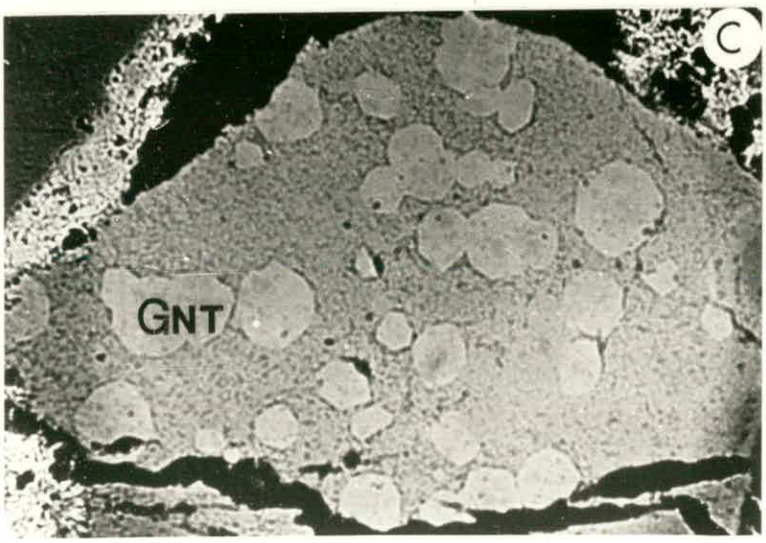
C
GNT

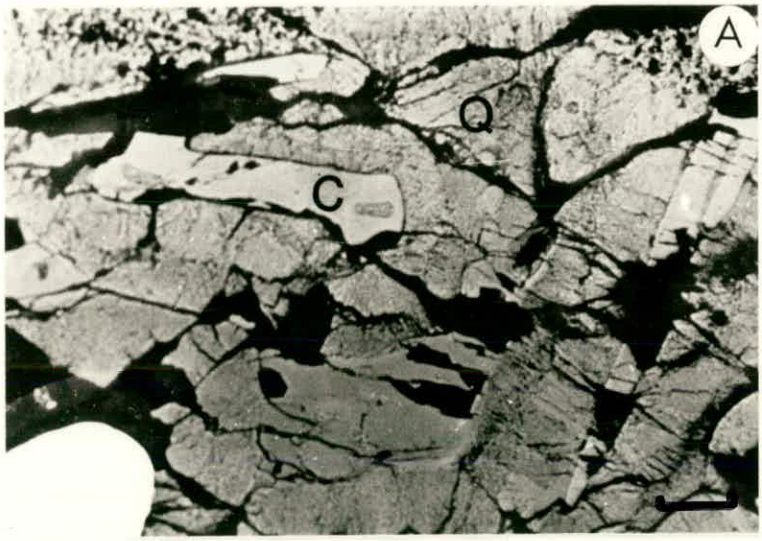
A
Q
C

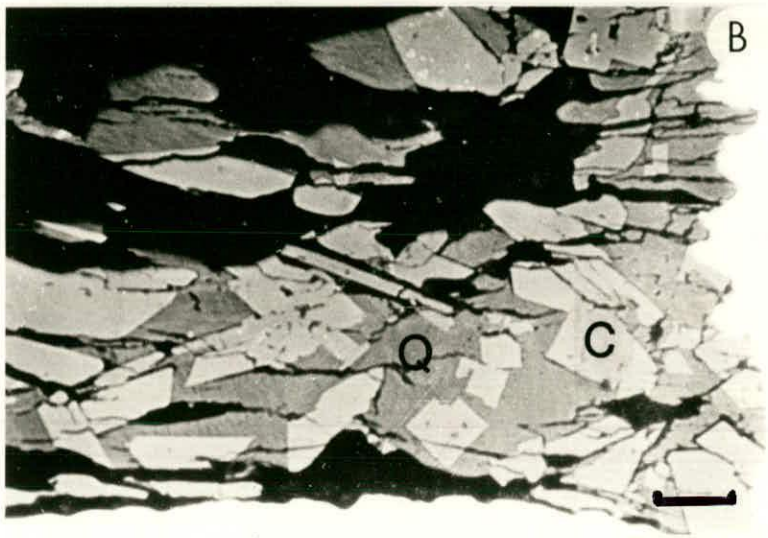
B
Q
C

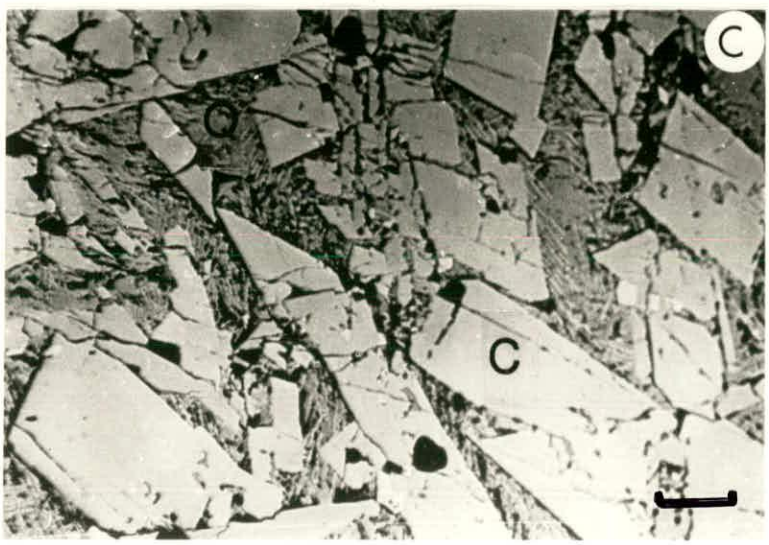
C
Q
C

CHAPTER 3

EXPERIMENTS IN THE SYSTEM SiO_2-Al_2O_3-CaO-Na_2O-CO_2.

3.1. Introduction and background theory.

After the failure to produce immiscibility in "natural" mantle systems, it was decided that the investigation would continue in systems where carbonate-silicate immiscibility was already well constrained. Work on synthetic compositions was considered preferable; with fewer components, synthetic systems are simple to operate, less subject to uncertainty, and are affected by fewer variables than their natural counterparts. One problem with synthetic systems, however, is that it is never clear how closely applicable the results are to naturally occurring processes, and a parallel study on natural rocks was considered essential.

Carbonate-silicate immiscibility has been documented in a wide range of synthetic compositions:

(a) Albite-sodium carbonate join.

Coexisting immiscible carbonate and silicate liquids were found in this extremely sodium-rich system at 0.1 GPa total pressure, and over a wide range of temperatures (870°C to >1000°C) by Koster van Groos & Wyllie (1966). Water was found to have little effect on the compositional extent of immiscibility, although, with large water contents, the coexisting liquids were found to be stable down to lower temperatures (Koster van Groos & Wyllie, 1968). Koster van Groos (1975) later went on to study more complex analogues of natural systems. Sodium-rich plagioclase compositions were also found to be immiscible with carbonate melt at 0.1 and 2.0 GPa. by Zyryanov & Volchkova (1987).

(b) Sanidine-potassium carbonate join.

Wendlandt & Harrison (1977) recorded immiscible carbonate and silicate liquids coexisting with CO_2-rich vapour at 0.5 GPa. and 2.0 GPa. in the system K_2O-Al_2O_3-SiO_2-CO_2. This was achieved by the addition of silver oxalate, $Ag_2C_2O_4$ (which breaks down to CO_2 on heating) and carefully dried K_2CO_3 to high sanidine powder. The compositions were spiked with REE in order to obtain partitioning data between the two melts and the CO_2-vapour (Wendlandt & Harrison, 1979). Two-liquid textures were confirmed between 1000°C and 1300°C.

(c) Synthetic ijolitic systems.

Work by Verwoerd (1977) on the join $Fe^{3+}Si_2O_6$-$CaCO_3$ confirmed a sizeable two-liquid field, but again suggested that high alkali contents were necessary for immiscibility to occur. Verwoerd also recorded problems associated with quench-produced immiscibility textures in these systems.

(d) The joins albite-calcite and anorthite-calcite.

A study at 0.5 GPa, and 1100-1250°C showed a continuation of immiscibility to alkali-poor and even alkali-free compositions (Kjarsgaard & Hamilton, 1988). This study was later extended to 1.5 GPa, and 1300°C (Kjarsgaard & Hamilton, 1989). The results of this study are plotted in Figure 3.1. They show that the compositional range over which immiscibility occurs is much larger than was previously thought.

(e) Soda-melilite-carbonate experiments.

An investigation into the carbon isotopic fractionation between soda-melilite melt ($NaCaAlSi_2O_7$) and CO_2-vapour by Mattey *et al.* (1990) produced immiscible carbonate and silicate melts at 2.0 and 3.0 GPa. This was achieved by simply adding CO_2 (in the form of silver oxalate) to the soda-melilite.

Soda-melilite is known to be a realistic simple analogue for basaltic melts (Yoder, 1964) both in terms of its chemical composition, and its melt structure. It is also readily quenched to a homogeneous glass. Work by Mysen & Virgo (1980) also showed that sodamelilite has similar CO_2 solubility and solubility mechanisms to those seen in natural basaltic melts.

Its simple chemistry, and its applicability to natural basaltic systems, led to the soda-melilite-carbonate system (SiO_2-Al_2O_3-CaO-Na_2O-CO_2) being chosen for the next phase of experimentation.

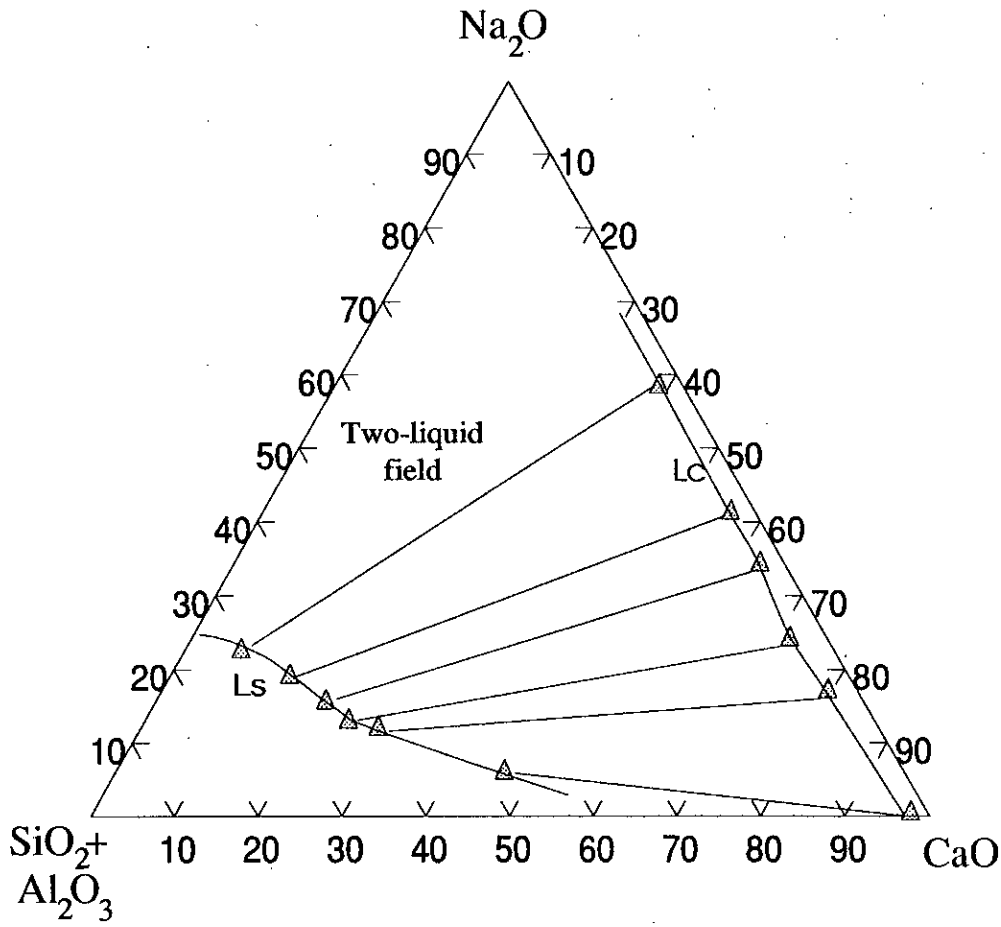

Figure 3.1. Carbonate-silicate immiscibility in alkali-poor synthetic systems (Kjarsgaard & Hamilton, 1988). In synthetic materials, carbonate-silicate immiscibility extends to sodium-poor compositions, producing carbonate melts applicable to geological processes.

3.2. Starting materials: preparation and composition.

Table 3.1 shows the starting materials used in experiments in the synthetic system SiO_2-Al_2O_3-CaO-Na_2O-CO_2. Two silicate compositions were made up from carefully dried Johnson Matthey analytical grade, anhydrous Na_2CO_3 and $CaCO_3$, and pure Al_2O_3 and SiO_2 gels (Ping Shi, 1987). The alumina and silica gels were used so as to avoid the problem of unmelted corundum and quartz fragments in the final prepared glass. The components were dried at >110°C for a week before being carefully weighed out on a five-place electronic balance, and then ground together under acetone for approximately 1.5 hrs. The powders were then stored in the oven until they were vitrified at 1350°C for 30 mins. Calculated weight loss on vitrification was slightly more than expected from stoichiometric loss of CO_2 from the carbonates (an extra 0.008 gms in 5 gms of sodamelilite). This is believed to have been due to volatilisation of sodium during the vitrification process, although no significant deviation from the initial compositions was discovered. An alternative possibility is that a few liquid droplets were lost as a spray during melting due to violent degassing of the carbonate components. The two compositions represented an accurate stoichiometric sodamelilite (SM2), and a sodium-rich equivalent (SM1). After vitrification, the glasses were re-ground under acetone before remelting to ensure homogeneity. No significant loss of weight was recorded on the second vitrification. The powdered sodamelilite glasses were then returned to the oven.

Two carbonates were also synthesised. One was a pure calcium carbonate powder (CC), whilst the other was an equal-weight mixture of powdered calcium carbonate and sodium carbonate, ground together in an agate mortar under acetone for *ca.* 1 1/2 hrs. 2 gms of each of these carbonates were stored in the oven at 110°C.

Table 3.1. Starting materials for experiments in the system CaO-Na_2O-Al_2O_3-SiO_2-CO_2.
A. Major element analyses. * are recalculated CO_2-free.
B. Trace-element concentrations added to SM2. Believed accurate to ±10 p.p.m.

A.

Oxides	SM1	SM2	CC	CNC
SiO_2	45.79	46.73	-	-
Al_2O_3	19.43	19.13	-	-
CaO	16.62	21.89	100	48.9
Na_2O	18.47	12.14	-	51.1
Total	99.31	99.89	100*	100*

B.

Element	SM2 conc. (p.p.m.)	Element	SM2 conc. (p.p.m.)
Mg	60	La	102
K	170	Ce	103
Ti	78	Nd	94
V	62	Sm	86
Rb	96	Tm	96
Sr	65	Lu	105
Y	95	Hf	224
Zr	82	Ta	214
Nb	84	Pb	78
Cs	103	Th	88
Ba	77	U	102

In addition, a wide selection of trace elements were added to a portion of the SM2 composition in order to allow investigation of trace-element partitioning behaviour. In all, 24 trace elements were added, representing HFSE, LILE, and LREE and HREE (see Table 3.1.B). All were added at concentration levels of *ca.* 100 p.p.m. apart from tantalum and hafnium which were added at higher concentrations to avoid any possible interference effects on the ion probe with the LREE-oxides. Trace elements were also added to a portion of the carbonate starting materials to allow reversals to be performed, with the partitioning equilibria being kinetically approached from the other direction.

3.3. Experimental techniques.

The majority of experiments in this section were undertaken at pressures of less than 1.0 GPa in internally heated gas-media vessels. Experiments at pressures greater than 1.0 GPa, however, can not be safely carried out in gas-media vessels of this type, and were therefore run in solid-media piston-cylinder apparatus. Techniques employed were similar to those mentioned in Section 2.3, using the furnace assembly B (platinum capsules).

The furnace configuration used for the gas-media vessels is detailed in Figure 3.2. The samples were sealed within platinum capsules, and placed centrally in a molybdenum container, kept in place by glass wool. The container was then placed in the central hotspot of a horizontally placed cylindrical furnace with molybdenum windings, and held in place by ceramic spacers. A second molybdenum can was also placed in the furnace, somewhat away from the sample container. This was filled with tantalum metal fragments to inhibit the build up of high fO_2, and therefore prevent oxidation of the molybdenum windings of the furnaces at high temperatures; furnaces are expensive and difficult to produce, failures must therefore be kept to a minimum, and furnace-life prolonged. The large size of the molybdenum sample container (*ca.* 3 ml) allowed a number of charges to be run simultaneously.

Pressure was provided by the surrounding argon gas which was compressed by a two-stage process. First the argon gas was pressurised up to 0.15-0.2 GPa by a hydraulic piston pump. The pump was then isolated from a 1.0 GPa pressure line, where the pressure was raised to that required in the run by an oil-driven intensifier. Since the samples were surrounded by a gas pressure-medium, the pressure they received was true hydrostatic pressure and was easily and precisely measured by means of an accurately calibrated gauge. Quoted pressures are therefore believed accurate to better than ± 0.01 GPa.

Temperatures were measured by two $Pt/Pt^{87}Rh^{13}$ thermocouples. One was situated towards the base of the sample container (designated thermocouple A), and the other towards the top (thermocouple B). Samples were always placed between these two thermocouples. The e.m.f. of thermocouple A was kept constant at the required value (within ± 1°C) by a Eurotherm controller. After reaching run conditions the e.m.f.s of the thermocouples were equalised by tilting the bomb, changing the temperature distribution in the gas. In this way, temperature gradients could be kept very low, and the quoted temperatures are therefore believed accurate to better than ± 5°C.

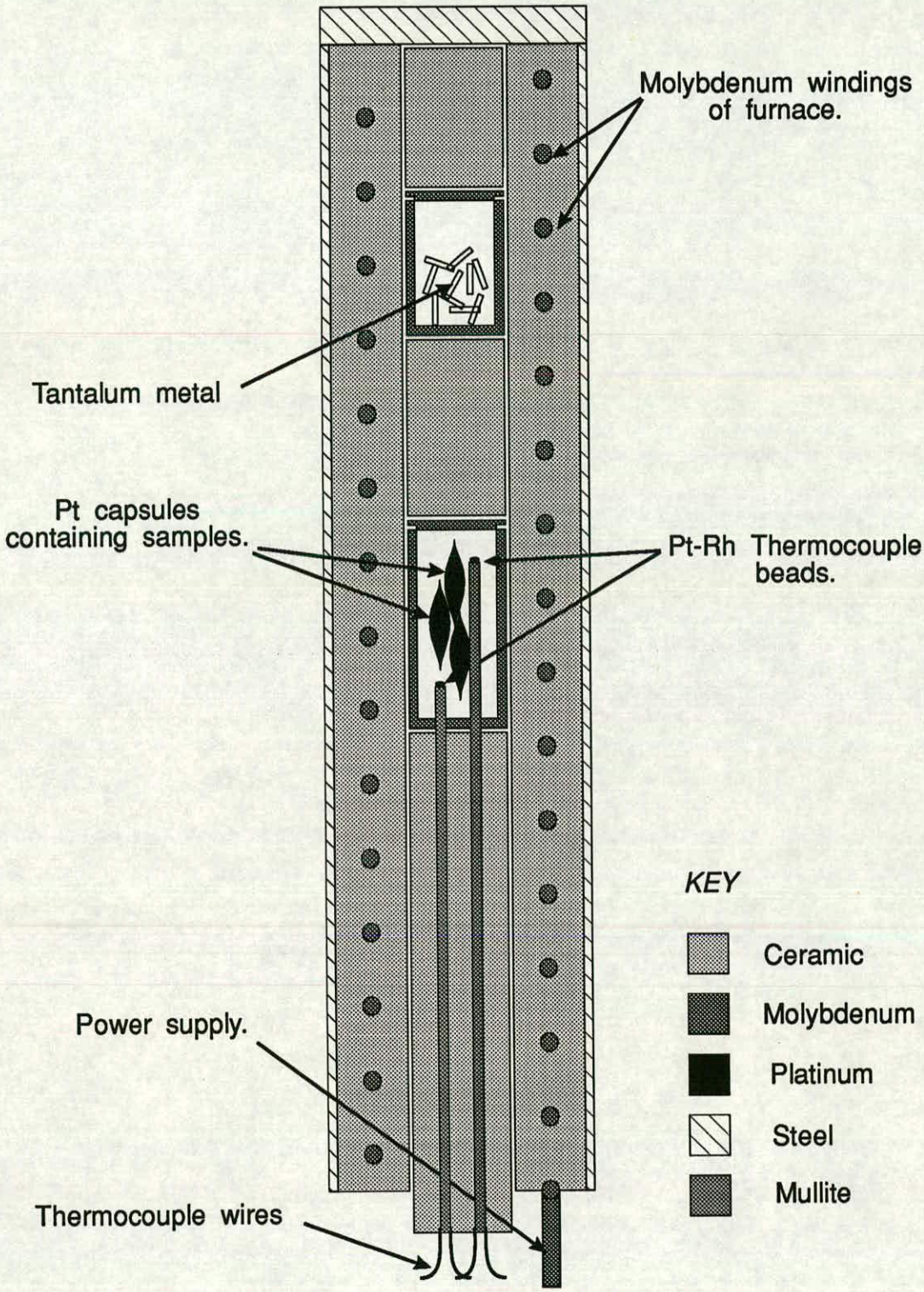

Figure 3.2. Furnace configuration for experiments using internally-heated gas-media vessels. The furnace is run horizontally in a pressurized argon gas-medium.

The soda-melilite system does not contain a multivalent cation (e.g. Fe). The oxygen fugacity under which these experiments were run was therefore controlled by external factors. Invariably, experiments involving soda-melilite compositions were run in tandem with charges containing natural rock compositions. These charges do contain multivalent cations, and their redox state was pre-experimentally set by sintering in a regulated gas mixture. These charges were initially under an fO_2 equivalent to the nickel-nickel oxide (NNO) reference buffer. Mature gas-media pressure vessels are believed to buffer experiments to relatively oxidised conditions, between the magnetite-hematite (MH) and nickel-nickel oxide (NNO) reference buffers. There is a dependence on the redox conditions of the preceding experimental run; however, this is considered insignificant in this case as the immiscibility experiments were generally run sequentially. In addition to the above evidence of oxidised conditions, the hydrogen concentrations in the bomb were kept low by flushing the bomb with compressed argon gas at least three times before the experiments, and by using hydrogen-free argon. This procedure is likely to keep fH_2 low so that changes in the pre-experimentally constrained oxygen fugacities will be slow. Further evidence for relatively oxidised conditions within the gas bombs was obtained by experiments where buffer assemblages were run. No change was noted in charges of magnetite, Nickel oxide or nickel metal, whilst iron metal was partially oxidised to iron oxide in just 1 hr. The oxygen fugacities in these experiments is therefore believed to approximate that of the NNO reference buffer.

One problem with internally heated gas-pressure vessels is their relatively slow quench rate. Quenching is achieved by isolating the controller, effectively turning off the power. Due to the large volume of heated material, cooling is slow, with as much as 30 seconds elapsing before the temperature has dropped 500°C. As will be mentioned later, this led to a number of analytical problems.

3.4. The experiments.

3.4.1. Set 1. Experiments with SM1.

In order to check that immiscibility was easily attainable with these starting materials, the sodium-rich silicate composition (SM1) was run with calcium-sodium-carbonate (CNC), calcium carbonate (CC), and silver oxalate ($Ag_2C_2O_4$). The proportions used were 75% silicate, 25% carbonate, or in the case of silver oxalate, enough to produce 25 Wt.% CO_2. The liquidus of sodamelilite is at *ca.* 1200°C. It was therefore decided that the runs would be carried out at 1300°C to ensure super-liquidus assemblages. 0.5 GPa was chosen as a preliminary pressure. The run conditions and results are shown in Table 3.2.

Table 3.2. Experiments using composition SM1: conditions and results.
Ls: Silicate liquid.
Lc: Carbonate liquid.
V: CO_2 vapour.
* CO_2 added as $Ag_2C_2O_4$, which breaks down to produce CO_2 at 140°C (Boettcher *et al.*, 1973).

Run ident.	Compositions (Wt %)	Pressure (GPa.)	Temperature (°C)	Time (Mins)	Assemblage
G1.11	75% SM1, 25% CNC	0.5	1300	60	Ls+Lc
G1.12	75% SM1, 25% CC	0.5	1300	60	Ls+Lc
G1.18	75% SM1, 25% CO_2*	0.5	1300	60	Ls+V

Both the SM1-CNC and SM1-CC experiments produced two-liquid textures, with a central silicate glass slug surrounded by a carbonate rind (Plate 3.1a). The two liquids were separated by a sharp, sub-micron meniscus (Plate 3.1b), indicating equilibrium coexistence. Compositions of these coexisting liquids are given in Table 3.3. In the sodium-rich composition, a silicate melt with *ca.* 7% dissolved CO_2 is in equilibrium with a more sodic carbonate melt with *ca.* 1.5% dissolved silica. Slightly more mixing of these two components can be seen in the more calcic composition, with the silicate containing *ca.* 9% carbonate component, and the carbonate containing *ca.* 4.5% silicate. These compositions are plotted on the pseudo-ternary diagram CaO-Na_2O-(SiO_2+Al_2O_3) (C-N-SA), projected from the CO_2 apex, along with the approximate extent of the two-liquid field (Figure 3.3).

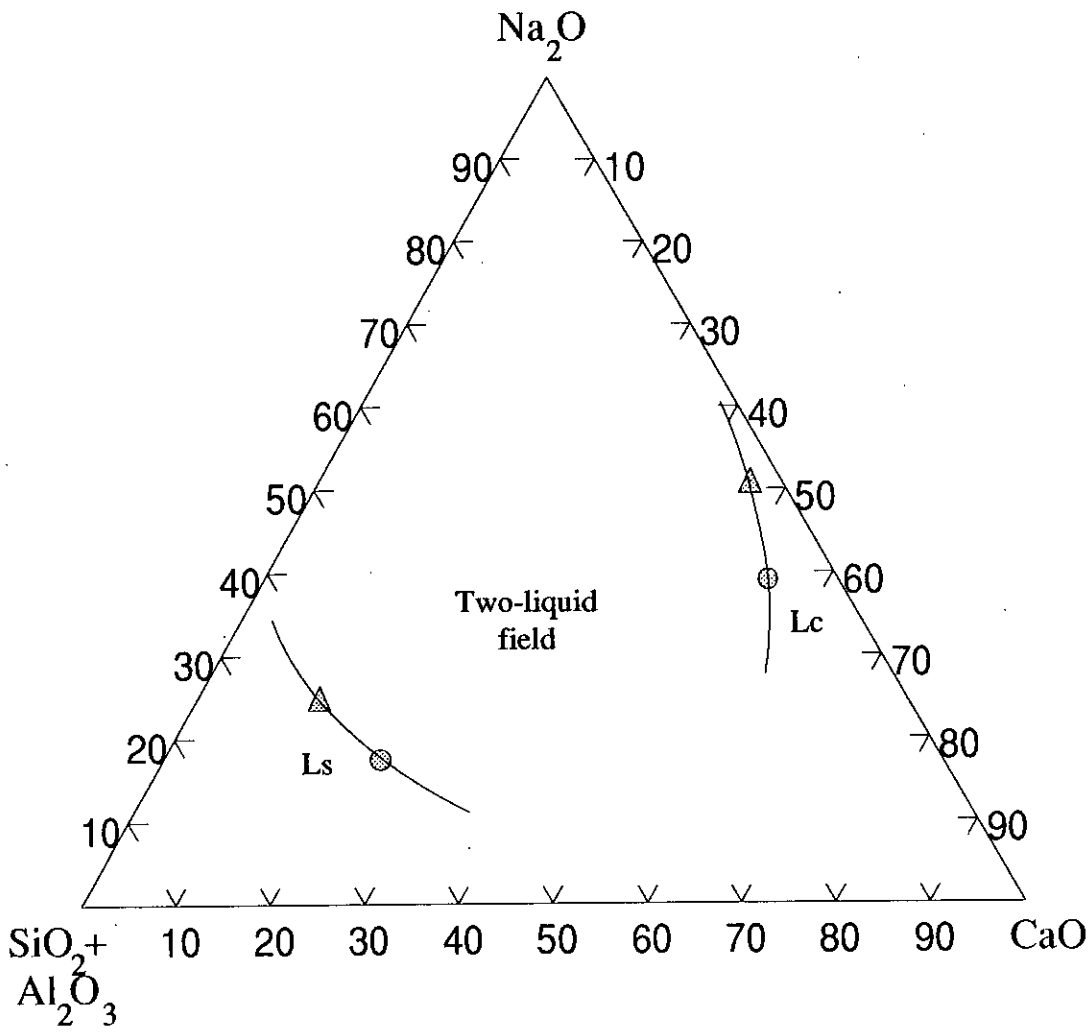

Figure 3.3. Field of two-liquid immiscibility in the soda-melilite-carbonate system. Triangles are SM1 + CNC, Circles are SM1 + CC. As observed by Freestone & Hamilton (1980) in natural rock systems, the two-liquid field of immiscibility seems to close towards sodium-poor compositions.

Table 3.3. Compositions of coexisting carbonate and silicate liquids: SM1 experiments. Shortfall in probe totals due to CO_2 component in both carbonate and silicate materials.

	G1.11				G1.12			
	Ls	σ	Lc	σ	Ls	σ	Lc	σ
No.	10		10		10		10	
SiO2	39.67	0.42	1.74	0.32	38.69	1.63	4.45	0.23
Al2O3	14.94	0.17	0.17	0.06	15.74	0.49	22.90	0.03
CaO	17.87	0.19	25.09	0.43	21.17	0.38	32.06	0.25
Na2O	22.78	0.31	27.45	0.51	15.68	0.21	23.08	0.28
Total	92.56		54.45		91.28		59.81	

The equilibrium coexistance of carbonate and silicate liquids, and the large scale, simple two-liquid textures, made the SM1-CNC and SM2-CC compositions ideal candidates for the experimental determination of carbonate-silicate partition coefficients.

The SM1-$Ag_2C_2O_4$ composition was, however, unsuccessful in terms of producing immiscible liquids. The resulting experimental charge contained only carbonated silicate melt and numerous bubbles of CO_2 vapour, within a silver-platinum alloy capsule. This, when combined with the studies of Brey (1976) and Mattey *et al.* (1990), suggests that the assemblage silicate melt-CO_2 vapour is stable at these relatively low pressures, and that it is only above 2.0 GPa that CO_2 will react with silicate melts to produce coexisting carbonate liquid (Mattey *et al.*, 1990). Any further experiments involving $Ag_2C_2O_4$ should therefore be attempted at high pressures (>2.0 GPa).

3.4.2. Set 2. P-T-t grid study of immiscibility in the system SiO_2-Al_2O_3-CaO-Na_2O-CO_2.

Since immiscibility had been confirmed in the soda-melilite-carbonate system by the Set 1. experiments, it was decided that the effects of pressure, temperature, time, and composition on the field of immiscibility would be studied by a systematic sequence of experiments. The SM2 composition, doped with the range of trace elements shown in Table 3.1.B, was combined with both the CNC and CC powders. The proportions 75% silicate, 25% carbonate were again used. Experiments were undertaken from 0.25-0.8 GPa, 1200-1300°C, and from 15 min to 16 hr (Table 3.4).

Table 3.4. Pressure-Temperature grid of experiments in the system SiO_2-Al_2O_3-CaO-Na_2O-CO_2. Abbreviations as Table 3.2. but with sM: soda-melilite crystals.

Run ident.	Composition (Wt %)	Pressure (GPa)	Temperature (°C)	Time (Mins.)	Assemblage
G6.7	75% SM2, 25% CNC	0.25	1200	60	Ls + Lc
G5.7	75% SM2, 25% CNC	0.5	1200	60	Ls + Lc
G27	75% SM2, 25% CNC	0.5	1200	90	Ls + Lc
G7.7	75% SM2, 25% CNC	0.8	1200	60	Ls + Lc
G9.11	75% SM2, 25% CNC	0.25	1300	60	Ls + Lc
G28	75% SM2, 25% CNC	0.5	1300	65	Ls + Lc
G8.11	75% SM2, 25% CNC	0.8	1300	15	Ls + Lc
G10.11	75% SM2, 25% CNC	0.8	1300	60	Ls + Lc
G25.6	75% SM2, 25% CNC	0.8	1300	240	Ls + Lc + V
G24.6	75% SM2, 25% CNC	0.8	1300	960	Ls + Lc
G6.8	75% SM2, 25% CC	0.25	1200	60	Ls + V
G5.8	75% SM2, 25% CC	0.5	1200	60	sM + Ls + V
G7.8	75% SM2, 25% CC	0.8	1200	60	sM + Ls + V
G9.12	75% SM2, 25% CC	0.25	1300	60	Ls + V
G11.2	75% SM2, 25% CC	0.5	1300	60	Ls + Lc
G8.12	75% SM2, 25% CC	0.8	1300	15	Ls + Lc
G10.12	75% SM2, 25% CC	0.8	1300	60	Ls + Lc
G25.7	75% SM2, 25% CC	0.8	1300	240	Ls + Lc
G24.7	75% SM2, 25% CC	0.8	1300	960	Ls + Lc

All the charges with the CNC carbonate produced immiscible two-liquid textures, over the whole range of pressures and temperatures studied. Runs of 1 hour duration showed exactly the same assemblage, and textural features, as those of 16 hour duration with a central silicate glass slug surrounded by a quench-carbonate rind. The 15 minute duration experiment also showed similar two-liquid textures, although a number of isolated spheres of both carbonate in silicate, and silicate in carbonate were also identified, suggesting that textural equilibrium was yet to be reached in the shortest duration runs. The compositions of coexisting carbonate and silicate liquids in these experimental charges are presented, togethor with partitioning data derived from them, in Appendix A.1. Both the carbonate and silicate liquids are remarkably constant in composition over the whole P-T range, although small variations can be seen with both temperature and pressure.

The charges involving the CC carbonate component were less successful. Immiscibility was only obtained in some of the experimental charges, the rest containing just silicate melt and vapour. However, this does not necessarily imply that the two-liquid field has closed in these compositions, as the silicate melts obtained only contain a few wt.% dissolved carbonate. There must therefore have been a breakdown reaction of the calcium carbonate, releasing CO_2 and adding CaO to the soda-melilite composition:

$$NaCaAlSi_2O_7 + CaCO_3 \Leftrightarrow NaAlSiO_4 + Ca_2SiO_4 + CO_2. \qquad (3.1)$$

(Components in melt) (Vapour)

This reaction only seems to occur in the 1200°C runs, and thus perhaps reflects different P-T heating loops rather than the run conditions themselves.

"Successful" runs using SM2+CC starting compositions produced two-liquid textures very similar to those obtained with SM2+CNC, although the quench structures in the carbonate were very different due to the much more calcic compositions (Plate 3.2).

Figure 3.4. shows the compositions of coexisting liquids at 1200°C, 0.25, 0.5, and 0.8 GPa on the C-N-SA diagram for both the SM2+CNC and SM2+CC starting compositions. As has been mentioned before, both the silicate melt compositions, and the sodium-rich carbonate melt compositions, are remarkably constant over this pressure range. However, the coexisting carbonate melt with the SM2+CC starting composition varies quite substantially, from nearly pure $CaCO_3$ with *ca.* 2.5 wt % SiO_2 at 0.25, and 0.5 GPa, to a mixed Ca-Na-carbonate with *ca.* 10 wt % SiO_2 at 0.8 GPa. This change in melt composition is also seen in natural silicate rocks (Chapter 4) and could have implications for both the primary composition, and depth of immiscible separation of carbonatite melts (Chapter 8).

The temperature effects on the compositions of coexisting liquids are small (Figure 3.5). Immiscibility relies on repulsive molecular interactions within a mixed-ion liquid, which produce extreme non-ideal behaviour. This allows two coexisting liquid compositions to be more stable energetically than a fully mixed solution. However, with increasing temperature, ideality should be more nearly approached (using the ideal gas model) and immiscibility less likely. Thus, thermodynamics suggests that the two-liquid field should close in compositional space as temperature is increased from 1200-1300°C. There is some evidence for this at 0.25, and 0.8 GPa (Figure 3.5), but the effect is small suggesting that the solvus limbs are near-vertical at these temperatures (Figure 3.6).

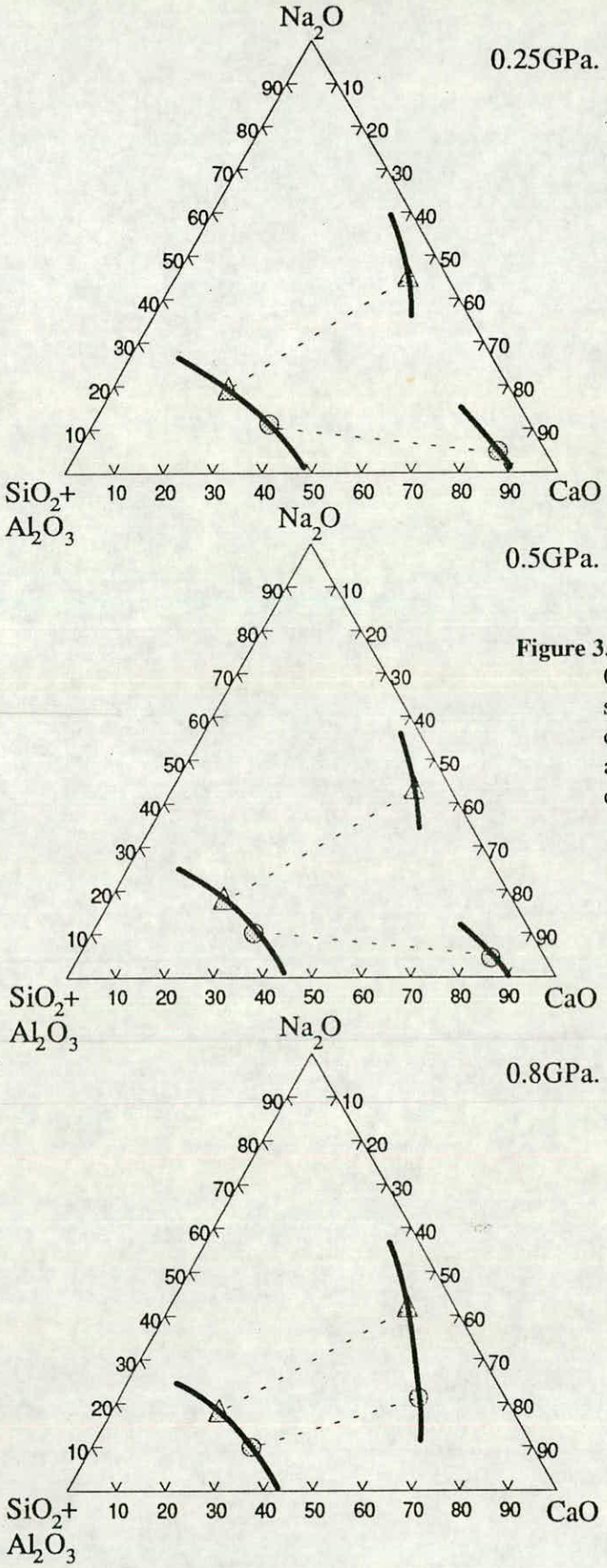

Figure 3.4. Field of liquid immiscibility at 1300 ℃, 0.25, 0.5, and 0.8 GPa in the soda-melilite-carbonate system. Calcium carbonate rich melts are produced at 0.25, and 0.5 GPa. Triangles are SM2+CNC, circles are SM2+CC

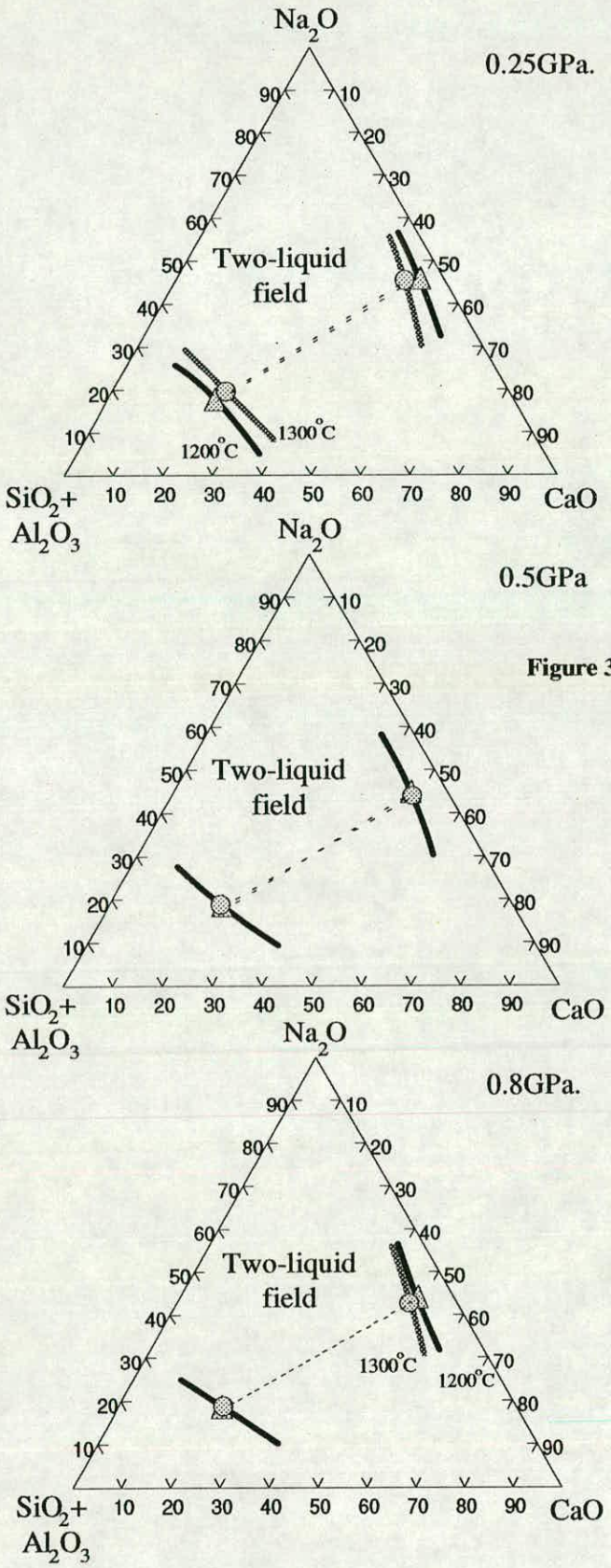

Figure 3.5. The effect of temperature on immiscibility in the soda-melilite -carbonate system. Evidence for closure of the two-liquid solvus with increasing temperature at 0.25 GPa, and at 0.8GPa. Temperature does not affect liquid compositions at 0.5 GPa. Triangles are 1200°C, circles are 1300°C

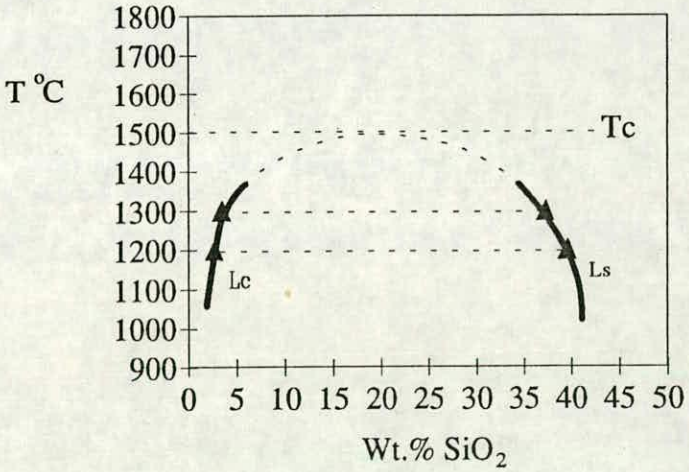

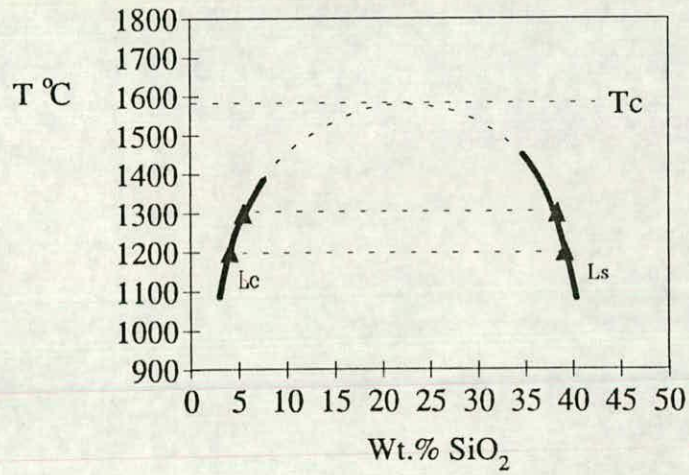

Figure 3.6. Closure of the two-liquid solvus with temperature. No evidence for closure was found at 0.5 GPa. Tc is a hypothetical critical temperature for immiscibility in the soda-melilite-carbonate system. Data from SM2+CNC under conditions stated.

As has already been mentioned, two-liquid textures seen in 1 hr runs were identical to those seen in 16 hr runs, implying that textural equilibrium had been reached. The compositions of these coexisting melts are plotted in Figure 3. for both the SM2+CNC and SM2+CC compositions. The close groupings of these liquid compositions in compositional space suggests that equilibrium coexistence was reached very quickly; even the 15 min runs are within analytical uncertainty of the longer runs. Having said this, there is a wide compositional spread in the calcium-rich carbonate melts. No systematic trend can be seen, so the variation has been ascribed to either the analytical difficulties involved in analysing the coarse quenches resulting from cooling of the calcite-rich liquids, or to extreme sensitivity to slight variations in run conditions.

3.4.3. Set 3. Solid-media experiments in the system SiO_2-Al_2O_3-CaO-Na_2O-CO_2.

In order to continue the investigation of immiscibility to higher pressures, it was necessary to carry out a series of solid-media runs in piston-cylinder apparatus at 1.1, 1.5, and 2.0 GPa. The SM2+CNC starting composition was used, and the experiments were at 1300°C to ensure completely molten charges at these high pressures (see Table 3.5 for run conditions and products).

Table 3.5. Solid-media experiments in the system SiO_2-Al_2O_3-CaO-Na_2O-CO_2.
* Failure of run after 15-20 mins. On failure the run quenches as normal, allowing inclusion in results.
** Lack of Lc could be due to polishing difficulties resulting from decompression fracturing rather than lack of presence under run conditions.

Run ident.	Composition (Wt. %)	Pressure (GPa)	Temperature (°C)	Time (Mins.)	Assemblage
S42*	75% SM2, 25% CNC	1.5	1300	15	Ls + Lc
S43	75% SM2, 25% CNC	1.5	1300	75	Ls + Lc
S44	75% SM2, 25% CNC	2.0	1300	75	Ls**
S45	75% SM2, 25% CNC	1.1	1300	60	Ls**

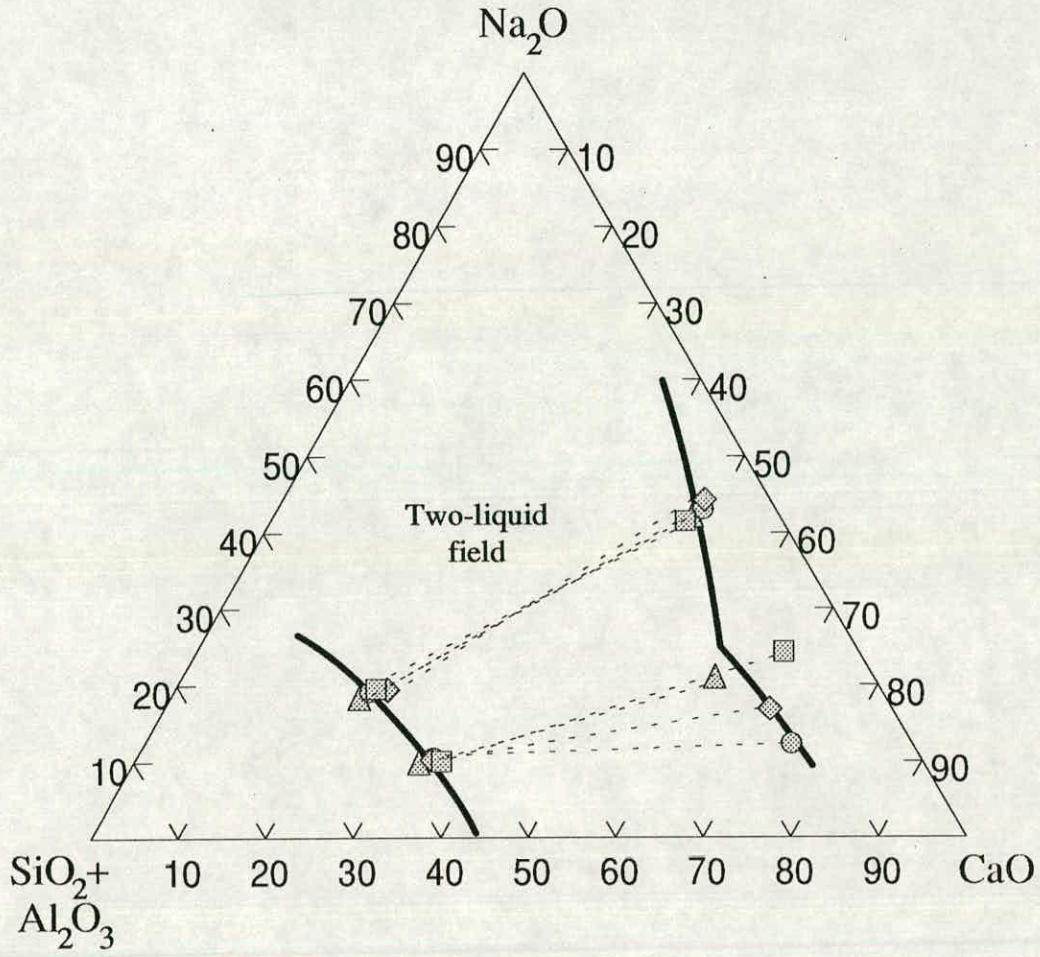

Figure 3.7. The effects of run duration on immiscible liquids in the soda-melilite-carbonate system. Close grouping of experimentally produced melt compositions suggests that equilibrium has been reached. The spread of data for the calcium-rich carbonate melts is either due to analytical difficulties (coarse quenches), or to extreme sensitivity to slight differences in run conditions. Triangles, 15 mins duration; circles 1 hr duration; diamonds, 4 hrs duration; squares 16 hrs duration.

Immiscibility textures, although on a smaller scale due to the smaller charge volume, were confirmed in two charges at 1.5 GPa. Due to the fast quench-rates in the solid-media apparatus, the carbonate melt was quenched to a much finer, although still heterogenous, intergrowth. It is possible that the charges run at 1.1 GPa and 2.0 GPa did actually produce two liquids under run conditions, but that the carbonate melt was lost during the polishing process (parallel decompression cracks could have caused the softer carbonate to be plucked out).

The liquid compositions of SM2+CNC melts over the whole pressure range (0.25-2.0 GPa) are plotted on the C-N-SA triangular diagram (Figure 3.8). Although the effects of pressure are small, two trends from low to high pressure can be delineated:

(a) On the silicate side of the solvus, a small but gradual expansion of the two-liquid field can be discerned with increasing pressure. This is as would be expected from thermodynamics. At higher pressures (using the ideal gas model) liquids tend to deviate from ideality more significantly, with more pronounced repulsive interactions between the closely packed ions. This increase in non-ideality would be expected to increase the compositional extent of immiscibility with increasing pressure.

(b) On the carbonate side of the solvus, melts become progressively more calcic with increased pressure. As yet, no explanation has been found for this feature.

It must be stated that these are very subtle changes and, although they are larger than the analytical errors quoted from the electron probe work, it is possible that they could be due to variations in analytical technique and conditions. It is only the systematic nature of these effects, and their agreement with data from other systems (e.g. Watson & Naslund, 1976; Freestone & Hamilton, 1980) that suggests these variations are real.

3.4.4. Set 4. The effects of minor elements on immiscibility in the system SiO_2-Al_2O_3-CaO-Na_2O-CO_2.

Synthetic systems, although advantageous from the experimental and analytical viewpoints, lack the full range of components present in natural systems. In order to study the effects of these components, they must be added independently to the charge, and the results compared with the reference sample run under the same conditions. In this way, the synthetic system gives us an opportunity to study the

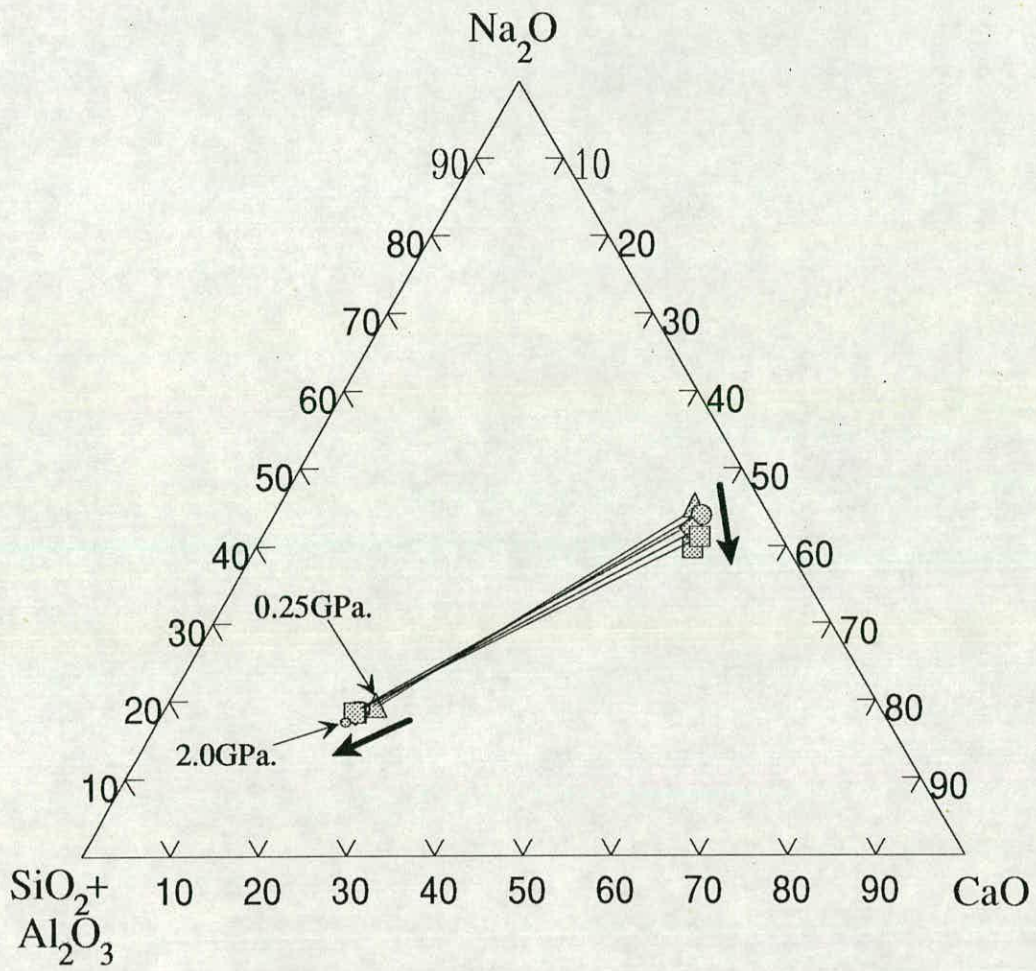

Figure 3.8. The effect of pressure on immiscibility in the sodamelilite-carbonate system. A small increase in the size of the two-liquid field with pressure can be seen on the silicate side of the solvus. Melts become more calcic with pressure on the carbonate side of the solvus. Triangles, 0.25 GPa; circles, 0.5 GPa; diamonds, 0.8 GPa; squares, 1.5 GPa; dots, 2.0 GPa.

effects of minor elements on immiscibility and partitioning in isolation, a prospect not possible in natural systems. Carbonatites from nature contain significant quantities of a number of elements in excess of calcium, sodium, silicon and aluminium. For example, lengaiite (alkali-carbonatite from Oldoinyo Lengai, Tanzania) contains *ca.* 8% K_2O (represented in this system by Na_2O), and *ca.* 1.5% BaO and SrO (represented by CaO). Four other components present in carbonatites which are not represented in the system, but which are believed to have a profound effect on structure and behaviour, are fluorine, chlorine, phosphorus, and sulphur. These are all present at *ca.* 1% or more in fresh lengaiite lava (Dawson, in press). Charges were prepared which contained minor, but analysable quantities of these elements. Fluorine was added as CaF_2, chlorine as NaCl, Sulphur as S, and phosphorus as P_2O_5. Phosphorus-rich carbonate melts are believed to be important in the mantle, so a further charge with >10% P_2O_5 was produced. Table 3.6 gives compositions, conditions, and results for these experiments.

Table 3.6. Experiments to investigate the effects of minor elements on immiscibility and partitioning behaviour.

Run ident.	Composition (Wt. %)	Added elements	Pressure (GPa)	Temperature (°C)	Time (Mins.)	Assemblage
G29.1	75% SM2, 25% CNC	2.5% F	0.5	1300	60	Ls + Lc
G29.2	75% SM2, 25% CNC	2.5% Cl	0.5	1300	60	Ls + Lc
G29.3	75% SM2, 25% CNC	2.5% SO_3	0.5	1300	60	Ls + Lc
G29.4	75% SM2, 25% CNC	2.5% P_2O_5	0.5	1300	60	Ls + Lc
G29.5	75% SM2, 25% CNC	10% P_2O_5	0.5	1300	60	Ls + Lc + V

As before, with this simple composition (SM2+CNC), clear two-liquid textures were obtained in all these runs, showing that none of these elements completely inhibits carbonate-silicate immiscibility at these low concentrations. Compared to the influences of pressure and temperature, the presence of these elements has a pronounced effect on the coexisting melt compositions, and on the extent of immiscibility.

The above data are plotted in Figure 3.9, again using the C-N-SA triangular diagram as a method of representing liquid compositions. Each spiked charge, containing either F, Cl, P, and S , is compared with the unspiked control, previously run under the same conditions (1300°C, 0.5 GPa).

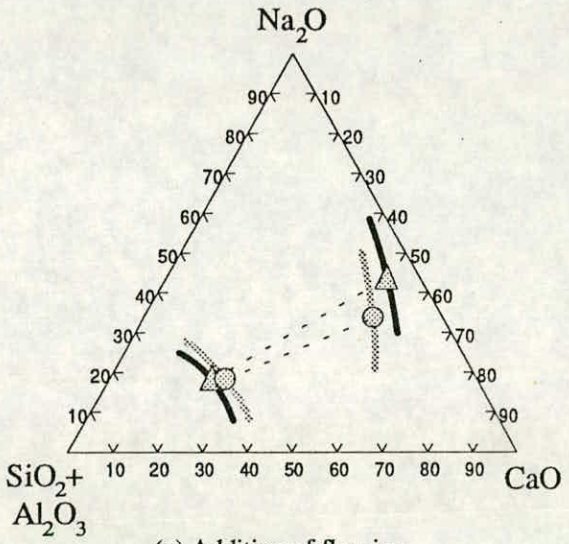

(a) Addition of fluorine.

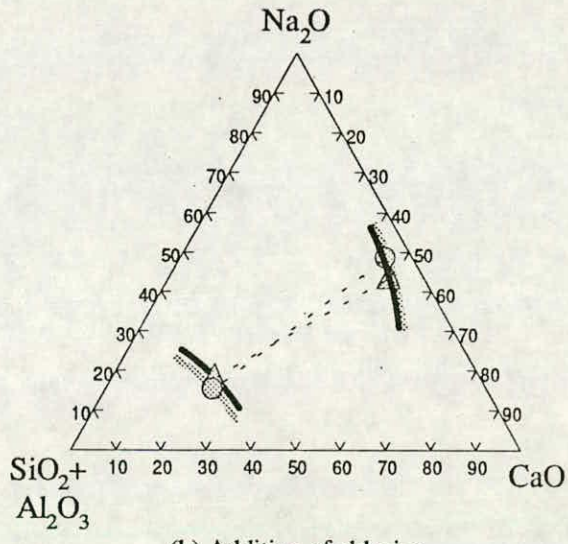

(b) Addition of chlorine.

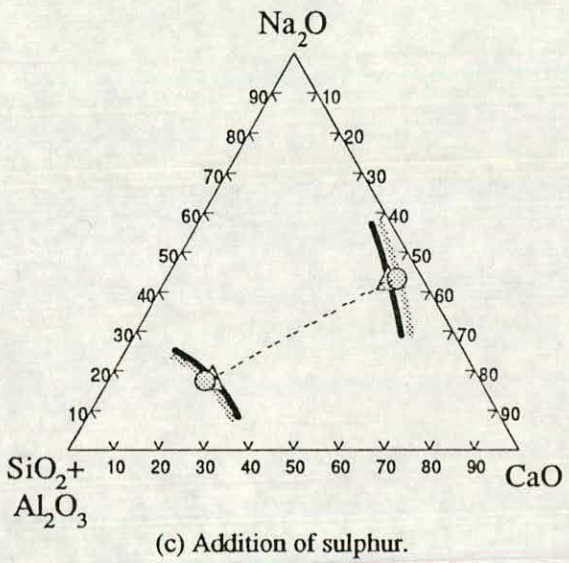

(c) Addition of sulphur.

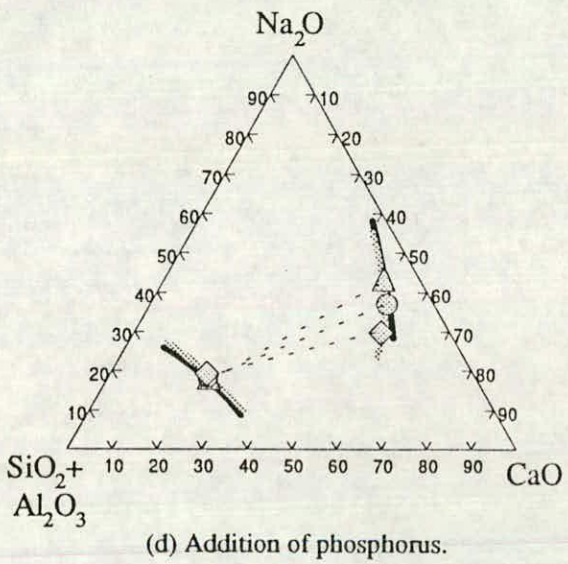

(d) Addition of phosphorus.

Figure 3.9. The effect of minor elements (F, Cl, S, P) on immiscibility in the sodamelilite-carbonate system.
(a) Addition of fluorine causes a marked contraction in the size of the two-liquid field.
(b) Chlorine has little effect on the size of the two-liquid field (perhaps slight expansion), but causes tie-line rotation.
(c) The addition of sulphur slightly expands the compositional extent of immiscibility.
(d) Phosphorus does not greatly effect the extent of immiscibility. Tie-lines are however rotated, with the production of more calcic carbonate melts when phosphorus is added. Triangles, minor-element free control experiment; circles, 2.5% added component; diamonds, 10% added component (only for P)

The effects have been summarised below:

(a) Addition of fluorine to the charge causes a marked closure of the two-liquid field in compositional space. It is believed that this is probably due to the depolymerising effect fluorine has on silicate melts (Allman & Koritnig, 1971; Dingwell & Mysen, 1985; Richardson, 1974) by breaking bridging oxygens in the silicate network according to the equation:

$$\equiv Si\text{-}O\text{-}Si\equiv + F^- \Leftrightarrow \equiv Si\text{-}O^- + F\text{-}Si\equiv. \qquad (3.2)$$

This depolymerisation effect will result in less pronounced structural differences between the carbonate and silicate melts, and consequently less pronounced immiscibility. Both the silicate and carbonate melts in the fluorine run are at slightly lower sodium contents due to the addition of fluorine as CaF_2.

(b) Addition of chlorine to the charge does not produce the same effect; indeed there is some evidence that chlorine actually expands the two-liquid field. This should not, however, be surprising as chlorine and fluorine are known to behave very differently in silicate melts. Fuge (1977) showed that chlorine has a high affinity for water and other volatiles, preferring a fluid phase to silicate melt. Henderson (1982) states that this makes it very unlikely that chlorine will have any depolymerising effect on silicate melt. Because of chlorine's affinity with depolymerising agents, it could actually produce a net polymerising effect. There is also a noticeable rotation of the tie-lines between the liquid compositions, resulting in a more calcic carbonate melt. No explanation for this phenomenon has been found.

(c) Addition of sulphur seems to produce a similar effect to chlorine, that is, a slight expansion of the two-liquid field. Haughton et al. (1974) showed that sulphur in silicate melts is likely to co-ordinate with metal cations (network modifiers), rather than influence the silicate network. This could again lead to a slight polymerising effect (Henderson, 1982).

(d) Addition of phosphorus, even in large quantities, seems to have no effect on the size of the two-liquid field. Ryerson & Hess (1980) suggested that P_2O_5 has a dual effect on silicate melt structure, depolymerising pure or near-pure silicate glasses, but polymerising mixed-cation silicate glasses. No evidence for either process is seen here. As with chlorine, there is a rotation of the tie-lines, leading to more calcium-rich carbonate melts at high phosphorus contents. Addition of phosphorus and chlorine must influence the relative stabilities of Ca^{2+} and Na^+ in the two melts.

3.4.5. Set 5. Experiments to produce "reversals" of $^{Ls/Lc}D_i$ values.

One way of proving that partition coefficients represent truly equilibrium conditions is to approach equilibrium from both directions. In the majority of experiments, the trace elements are present initially within the soda-melilite glass, and therefore $^{Ls/Lc}D_i$ move from infinity towards their true value. In this set of experiments, however, the trace elements are added to the carbonate powders before mixing the run compositions. Trace element $^{Ls/Lc}D_i$ values will therefore approach equilibrium from $^{Ls/Lc}D_i = 1$. Although not strictly a reversal, as the carbonate cannot be glassed before the run, if similar to the main body of data, these results will give reassurance as to the applicability of the conclusions made.

Table 3.7. Experiments using doped carbonate: Reversal of the partitioning data.
CC*: Calcium carbonate doped with trace elements.
NC*: Sodium carbonate doped with trace elements.

Run ident.	Composition (Wt. %)	Pressure (GPa)	Temperature (°C)	Time (Mins.)	Assemblage
REV1 (G22.1)	75% SM1, 25% NC*	0.5	1200	60	Ls + Lc
REV2 (G22.2)	75% SM1, 25% CC*	0.5	1200	60	Ls + Lc
REV3 (G22.3)	75% SM2, 25% NC*	0.5	1200	60	Ls + Lc + V
REV4 (G22.4)	75% SM2, 25% CC*	0.5	1200	60	Ls + V

Four compositions were run, representing mixtures of SM1 and SM2 with calcium carbonate and sodium carbonate. The carbonates in each experiment were doped with *ca.* 100 p.p.m. of the same range of trace elements as listed previously (Table 3.1.B), but without lutetium. Starting compositions, conditions and resulting assemblages are shown in Table 3.8. All four compositions produced immiscible carbonate and silicate liquids. The extents of immiscibility and liquid compositions are plotted on C-N-SA triangular diagrams in Figure 3.10. As will be discussed in Chapter 6, although minor variations were seen between forward and reverse values, the sense and degree of partitioning was the same, indicating that equilibrium was closely approached. The small differences seen (e.g. for Ca) may be accounted for by the slightly different compositions used.

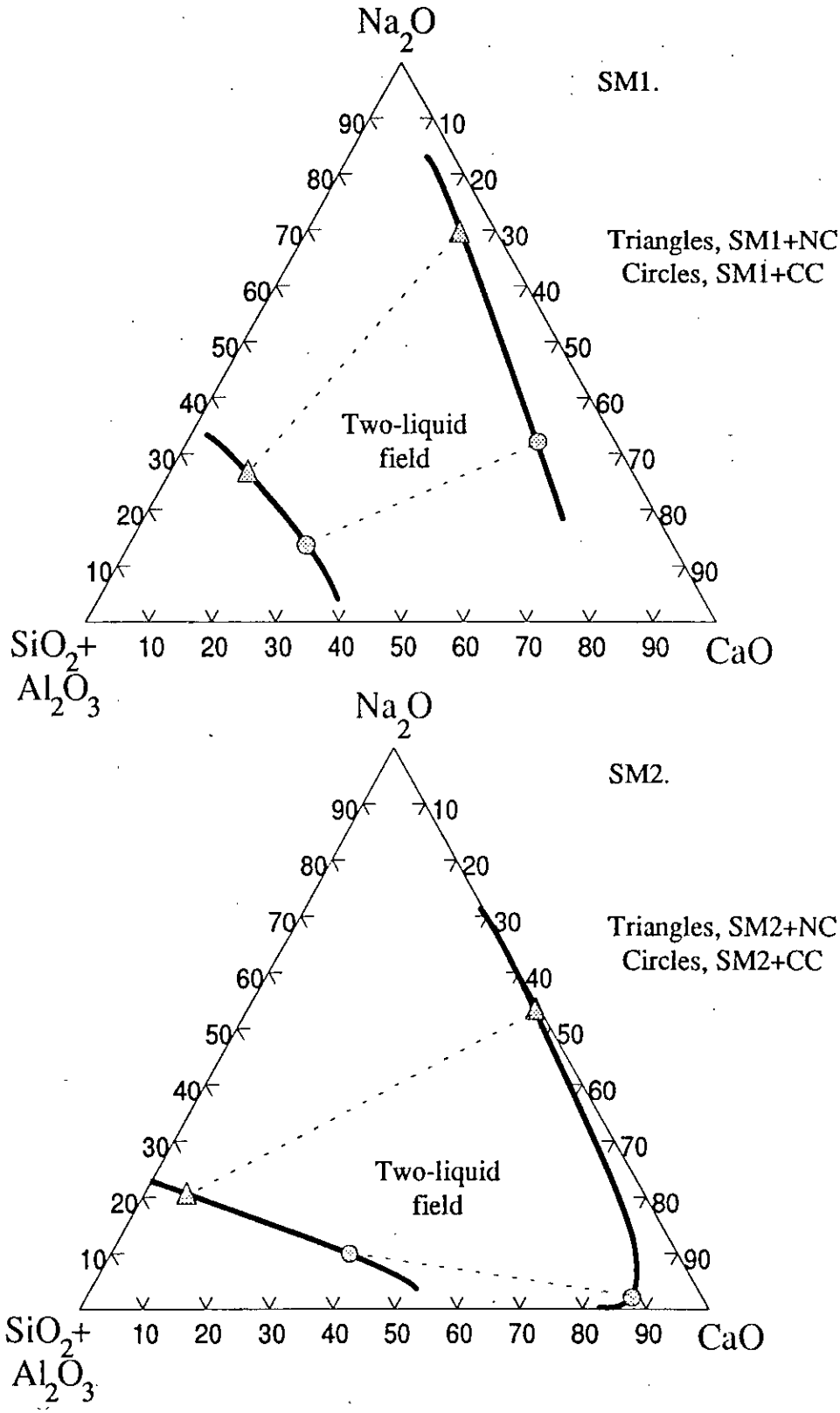

Figure 3.10. Compositions of coexisting liquids in reversal experiments in the sodamelilite-carbonate system at 0.5 GPa, 1200 °C.

3.4.6. Set 6. Reproducibility of immiscibility.

Reproducing experiments involving immiscibility is notoriously difficult (e.g. Brey, 1976). In order to dispel doubt as to the reproducibility of immiscibility and liquid compositions in this system, a number of repeated experiments were performed under the same conditions. Three charges of 75% SM2 + 25%CNC were run at 1200°C, 0.5 GPa (see Table 3.8. for results), and compared with the previous experiments G5.7, and G28. All the experimental charges run at these P-T conditions showed identical carbonate-silicate immiscibility textures, and very similar liquid compositions.

Table 3.8. Reproducibility of immiscibility: conditions and results of repeated experiments.

Run ident.	Composition	Pressure	Temperature	Time	Assemblage
	(Wt. %)	(GPa)	(°C)	(Mins.)	
R4 (G23.4)	75% SM2, 25% CNC	0.5	1200	60	Ls + Lc
R5 (G23.5)	75% SM2, 25% CNC	0.5	1200	60	Ls + Lc
R6 (G23.6)	75% SM2, 25% CNC	0.5	1200	60	Ls + Lc

Figure 3.11 shows that the compositions of all the silicate, and carbonate melts are closely grouped (within ± 2% of each of the components C, N, and SA). Immiscible melt compositions in the system SiO_2-Al_2O_3-CaO-Na_2O-CO_2 can therefore be accurately reproduced.

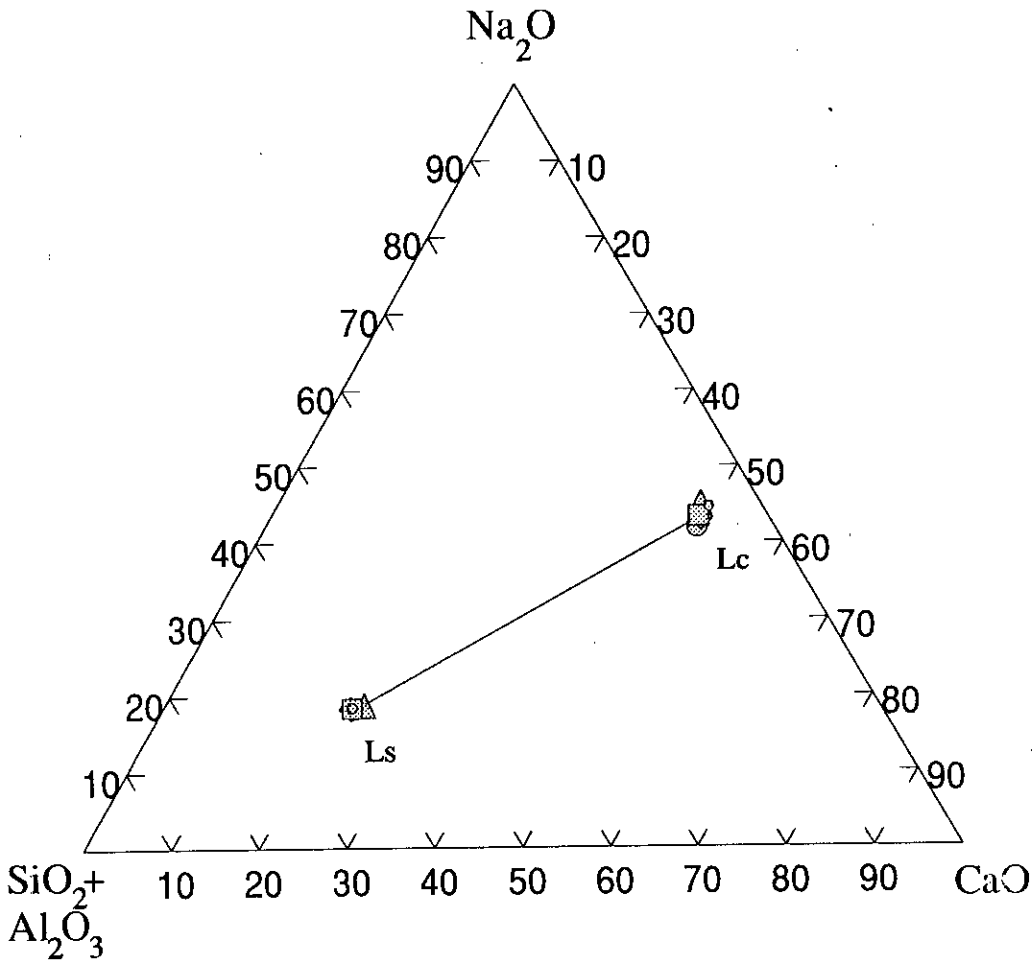

Figure 3.11. Reproducibility of coexisting immiscible liquids in the soda-melilite-carbonate system. Close grouping of the experimental liquid compositions shows that these immiscibility experiments can be reproduced accurately. Triangles, coexisting liquids in G5.7; circles, coexisting liquids in G27; diamonds, coexisting liquids in R4; squares, coexisting liquids in R5; dots, coexisting liquids in R6. All experiments at 0.5 GPa, 1200°C

3.5. Conclusions and implications.

Experiments in the system SiO_2-Al_2O_3-CaO-Na_2O-CO_2 were extremely successful in producing carbonate-silicate immiscibility over the whole P-T-X range studied. In all, 35 charges were run, 5 did not produce immiscibility textures and assemblages. These experimentally produced liquid compositions were studied further, with the aim of obtaining well constrained $^{Ls/Lc}D_i$ values for major, minor, and trace-elements. The results of these studies will be presented in subsequent chapters. Other conclusions may be drawn from this work; those of significance to this study are listed below.

(a) Carbonate melts with very low sodium contents (*ca.* 2.5% Na_2O) coexist with silicate melts with *ca.* 10% Na_2O at pressures of 0.25, and 0.5 GPa. These carbonate melts are compositionally similar to carbonatites seen at the Earth's surface. At higher pressures, sodium-rich carbonate melts become coexistent with silicate melts of the same composition.

(b) With increasing temperature, the two-liquid solvus begins to contract at 0.25, and 0.8 GPa. The effect is small, implying that both the carbonate and silicate limbs of the solvus are steep at these temperatures. The critical temperature (that is, the temperature above which no mixture of the components will produce immiscibility) for these compositions is therefore likely to be substantially higher than 1300°C.

(c) Runs of between 15 mins and 16 hrs all produce similar melt compositions, implying that equilibrium was attained rapidly.

(d) The effect of pressure on the melt compositions, although possibly significant, is very small over the range 0.25-2.0 GPa. Experimental evidence points towards a slight expansion of the two-liquid field with pressure.

(e) The effects of individual elements of the field of immiscibility can be studied using this synthetic system. This has been done for those minor elements thought to be important to carbonatite petrogenesis (F,Cl,P,S). Resulting changes in the field of immiscibility produced have been attributed to the effects of these elements on silicate melt structure. Carbonate melt, being an ionic liquid, is thought unlikely to be affected structurally.

(f) These experimentally-produced melt compositions can be easily reproduced, giving identical assemblages, textures, and melt compositions.

Plate captions: Chapter 3.

Plate 3.1. Immiscibility in synthetic soda-melilite compositions.

A. A typical two-liquid texture (G7.7). Usually, a central silicate slug (Ls) is surrounded by a carbonate rind (Lc). Scale bar is 1 mm.

B. The contact between the two liquids is a sharp, sub-micron meniscus indicating equilibrium coexistance (experiment G1.12). Scale bar is 50 μm.

C. A close up of the two liquids reveals quench textures in the carbonate and silicate liquids (experiment G1.12). The silicate liquid (Ls) quenches to a silicate glass containing small spheres of lower reflectivity carbonate material. The carbonate liquid (Lc) quenches to an intergrowth of calcite crystals in a matrix with composition approximating nyerereite. The carbonate liquid also contains quench spheres of silicate material. Scale bar is 10 μm.

Plate 3.2. Variation in quench textures resulting from cooling of the carbonate liquid. The carbonate liquid quenches to an almost infinite variety of textures depending on the composition, on the P-T conditions of production, and on the quench rate.

A. Sodium-rich carbonate quench at low pressure. Thin accicular crystals of calcite with roughly parallel orientation (light in colour) surrounded by darker areas of nyerereite. Scale bar is 10 μm.

B. Sodium-rich carbonate quench at higher pressure. A similar texture is produced to that shown in (a) but at a finer scale. This suggests faster quench rates at higher pressures. Scale bar is 10 μm.

C. Textures in quenched carbonate-rich liquids (experiment G5.8). Texturally more chaotic than those quenches shown previously, with more calcite and a larger silicate component. Scale bar is 10 μm.

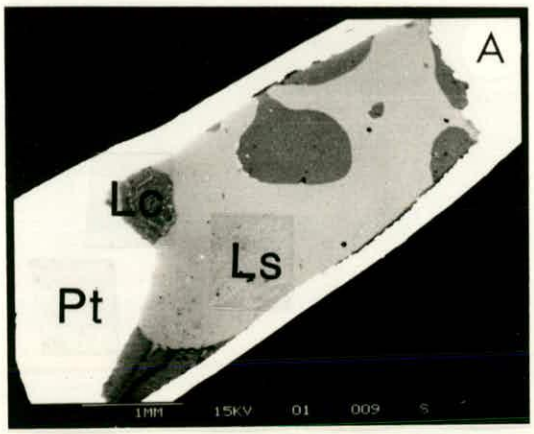
A
Lc
Ls
Pt
1MM 15KV 01 009 S

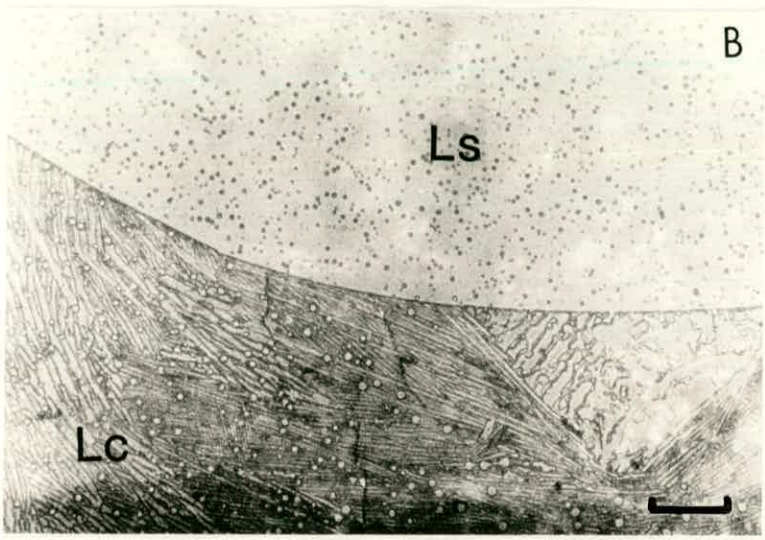
B
Ls
Lc

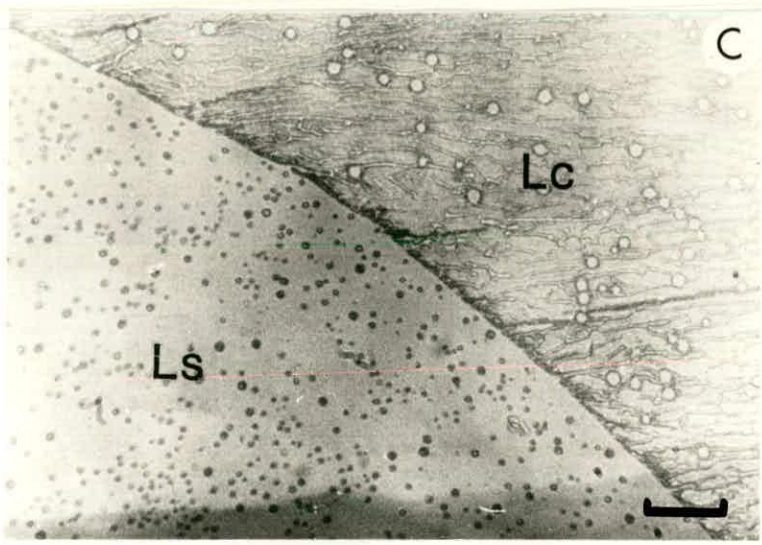
C
Lc
Ls

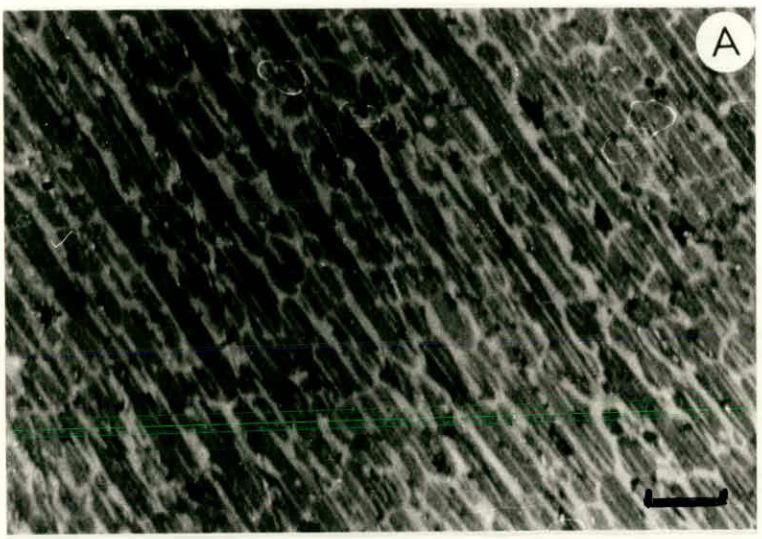
A

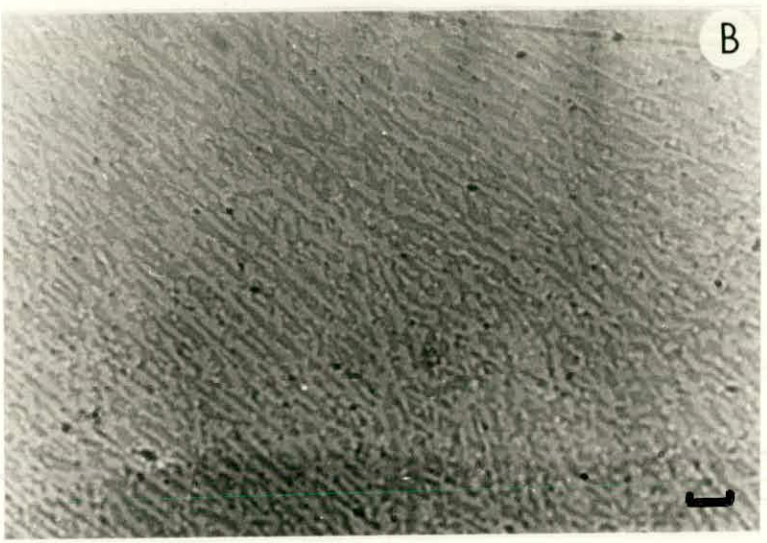
B

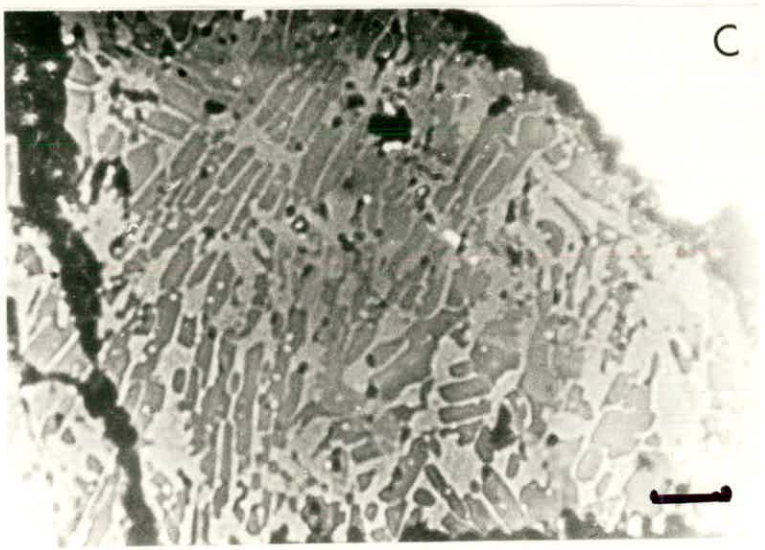
C

CHAPTER 4

EXPERIMENTS ON NATURAL ROCKS BELIEVED TO BE ASSOCIATED WITH IMMISCIBILITY.

4.1. Introduction and background theory.

If representation in the literature is a good indication, the favoured theory for the origin of the majority of carbonatites involves immiscible separation from a carbonated silicate melt. One of the most persuasive arguments for this theory is the close association in space and time of carbonatites and alkali-rich silicate rocks (e.g. phonolites, nephelinites, syenites and ijolites). Carbonate-silicate immiscibility experiments should therefore, at least in the first instance, be based on these rock types.

There have been two major experimental investigations of carbonate silicate immiscibility using natural rock compositions. The study of Baker & Wyllie (1990) on magnesian nephelinites at 2.5 GPa. has already been discussed in the section on primary mantle melt compositions (see Figure 2.5). The other relevant studies are those of Hamilton *et al.* (1979) and Freestone & Hamilton (1980). Their pioneering experiments proved the existence of carbonate-silicate immiscibility in natural rock compositions. Phonolite and phonolitic nephelinite from Oldoinyo Lengai, Tanzania, were mixed with a synthetic sodium-rich carbonate (similar to the lengaiite lavas), and also a more calcic carbonate powder. A stable two-liquid field was confirmed between 0.07-0.76 GPa and 950-1250°C for both compositions (Figure 4.1).

The experimental approach adopted in this section was to expand on the experimens of Freestone & Hamilton, where immiscibility is well documented, to obtain carbonate melts coexistent with phonolitic compositions. Further experiments involved more mafic silicate melt compositions (nephelinites, olivine nephelinites and olivine melanephelinites), more calcic carbonate liquids, and higher pressures.

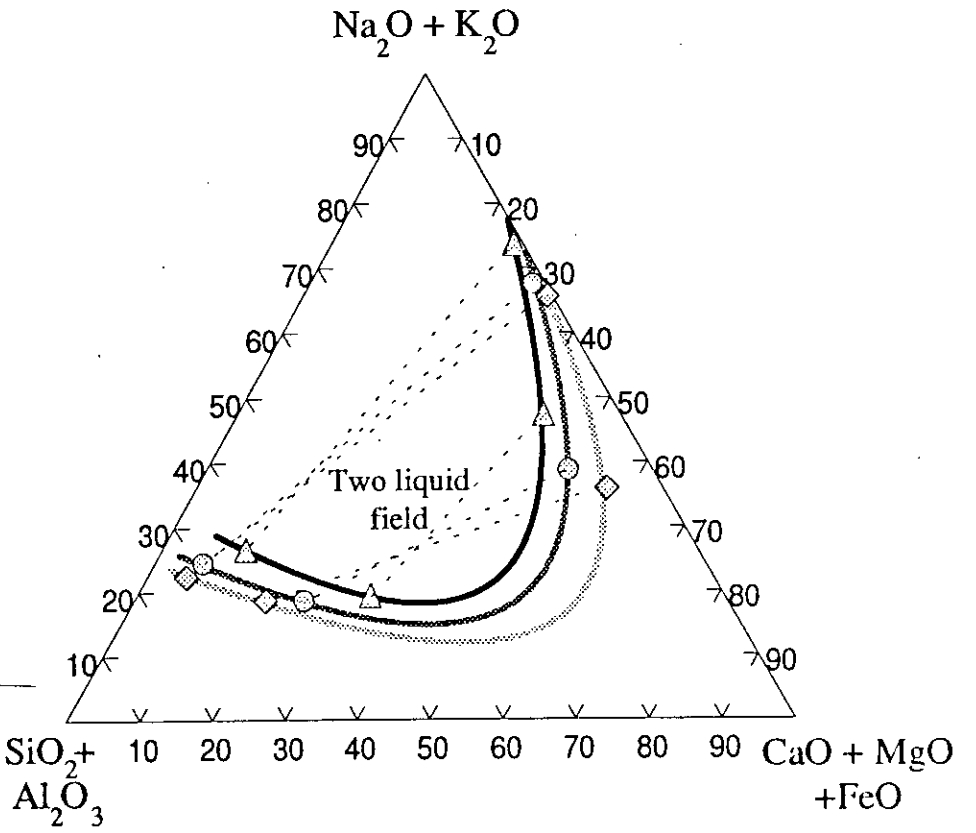

Figure 4.1. Experiments on natural rocks from Oldoinyo Lengai, Tanzania. 0.07-0.76 GPa, 1100° C (Freestone & Hamilton, 1980). — 0.07 GPa. ····· 0.29 GPa. ≈≈≈ 0.76 GPa.

4.2. Starting materials: preparation and composition.

XRF analyses of the five silicate rock compositions evaluated for use in these experiments are given in Table 4.1. They span a wide range in melt composition, and therefore also in melt structure. All were clean, unaltered lavas or hypabyssal rocks, and thus thought to be representative of liquid compositions.

Table 4.1. Major element analyses of rock compositions used in experimental charges.

Oxides	1	2	3	4	5
SiO_2	52.88	41.93	40.42	41.27	38.37
Al_2O_3	19.89	15.55	14.40	9.13	7.17
FeO*	5.65	8.69	12.04	14.09	14.62
MgO	0.45	1.28	5.22	8.77	15.67
CaO	2.67	10.89	13.22	14.93	12.53
Na_2O	10.63	10.26	6.24	2.75	2.26
K_2O	4.91	4.95	2.20	2.05	1.48
TiO_2	0.93	0.92	2.38	2.54	3.87
MnO_2	0.03	0.24	0.19	0.23	0.21
P_2O_5	0.11	0.54	0.75	0.63	0.83
Total	100.07	99.68	97.05	97.08	99.52

XRF analyses at the University of Edinburgh: analyst D.James.
1: BD50, phonolite from Oldoinyo Lengai, Tanzania.
2: BD119, olivine-free nephelinite from Oldoinyo Lengai, Tanzania.
3: SUN189, olivine nephelinite from Napak, Uganda.
4: ELG2, olivine nephelinite from Elgon, Uganda.
5: BD105, olivine melilite nephelinite from central rift, Tanzania.

The most evolved of these compositions was a silica-rich phonolite from the Oldoinyo Lengai volcano (BD50), as used by Freestone & Hamilton (1980). An olivine nephelinite was also obtained from this volcano (BD119). Although no more-primitive lavas were available from the Oldoinyo Lengai volcano itself, an olivine melilite nephelinite (BD105) was obtained from a flow just to the north, in the central rift valley (Dawson *et al.*, 1985). This, however, left a large compositional gap in terms of MgO content, and therefore also melt structure. The gap was filled by rocks from other carbonatite complexes: SUN189 from the Napak complex, and ELG2 from the Elgon complex, on the Kenya-Uganda border in the rift valley. Both are olivine nephelinites.

Being naturally occurring rock-types, all the silicate starting materials in this section of experimental work have their own inventory of trace-element concentrations (Table 4.2). The same is, to some extent, true of the carbonate powders (significant Sr and Ba was indicated by Neutron-Activation Analysis).

Table 4.2. Trace-element contents of starting materials in experiments on natural rocks.

Element	BD50	BD119	SUN189	ELG2	BD105
V	80	211	290	299	275
Cr	<10	5	7	266	685
Rb	101	119	49	85	44
Sr	1655	2288	752	1033	964
Y	31	48	24	24	29
Zr	555	869	180	186	404
Nb	160	324	84	79	98
Cs	-	-	-	-	-
Ba	1653	1720	546	949	806
La	100	155	72	69	77
Ce	180	249	151	130	151
Nd	59	81	60	-	67
Sm	9	13	-	-	-
Hf	Est.5*	-	-	-	-
Ta	Est.5*	-	-	-	-
Pb	41	43	8	9	6
Th	23	20	10	10	11
U	6	10	1.5	-	-

* estimated by Hamilton *et al.* (1989).
\- concentration unknown.

It was decided that doping was therefore unnecessary, as these concentrations were generally adequate for ion probe analysis. However, there were two exceptions.

(a) All the rock compositions studied are strongly LREE enriched. This makes ion probe analysis of the low contents of HREE very difficult due to interferences from the LREE oxides during mass-spectrometry. This problem was overcome by analysing for yttrium, traditionally regarded as a trustworthy analogue for HREE behaviour (e.g. Hinton & Upton, 1991).

(b) Due to the extremely low ion yields associated with analysis for Pb, contents of >50 p.p.m. are required to give reasonable precision. All these rock types contain less than 50 p.p.m. of Pb. At the time of experimental preparation it was believed, that, whatever its initial concentration, Pb would be lost from the melts, preferentially alloying with the Pt capsule. It was therefore decided that spiking the experimental charges with Pb would not be worthwhile. With hindsight, it can be seen that although significant loss of Pb to the Pt capsule did occur, artificially enriched Pb concentrations would probably have provided more accurate partitioning data.

All these rock-types were ground to a fine powder using a Glen Creston Gy-Ro mill, and then 3 gms of each were pelleted under a pressure of 8 tonnes before being placed in a furnace at 900°C+ for 48 hrs under an atmosphere of 3% H_2 in 97% CO_2. This is recognised as representing oxygen fugacity conditions approaching those of the NNO reference buffer. The pellets were then crushed between sheets of molybdenum and, as soon as cool enough to handle, ground under acetone in an agate mortar until finely powdered. They were then transferred to an oven, and kept at 110 °C until required for the experiments. The carbonate components of these charges were the same as those used in the soda-melilite experiments (CNC and CC). The carbonate and silicate starting materials employed in the experiments are shown in Figure 4.2, togethor with tie-lines between compositional end-members.

4.3. Experimental techniques.

Experimental techniques employed in these experiments were identical to those employed in Chapter 3. The majority of experimental charges were run in internally-heated gas-media vessels. As before, experiments requiring pressures exceeding 1.0 GPa were carried out in solid-media apparatus, using platinum capsules (Furnace assembly B). Oxygen fugacities in these experiments are thought to approach NNO conditions. Temperatures are believed to be accurate to ± 5°C in the gas pressure vessels, and ± 10°C in the solid-media apparatus. Corresponding pressures are believed accurate to 0.01 GPa (gas bombs) and 0.02 GPa (solid-media).

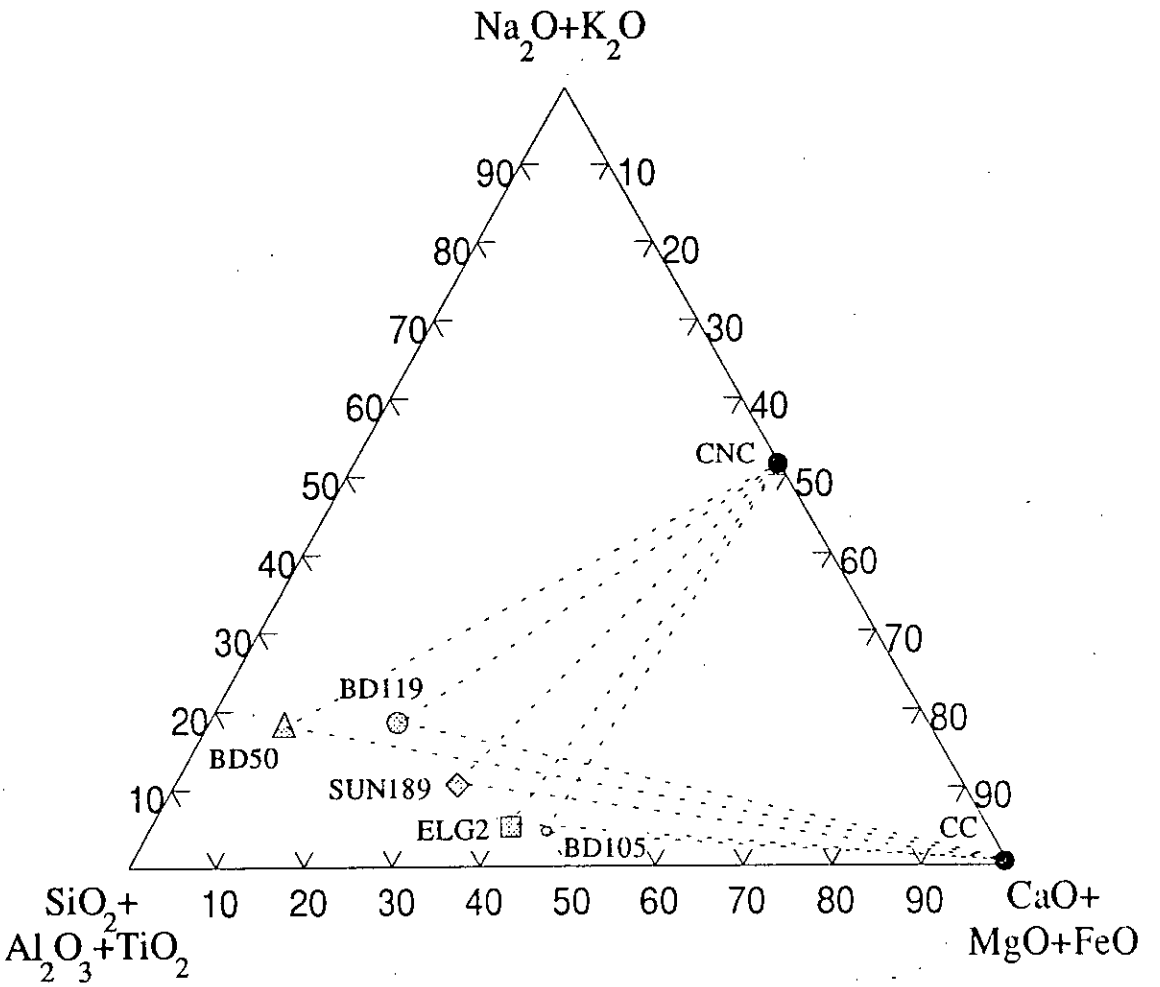

Figure 4.2. Starting materials employed in experiments involving natural rock compositions.

4.4. The experiments.

4.4.1. Set 1. Experiments with silver oxalate.

As with the soda-melilite starting material, an initial study was made into the possibility of obtaining immiscible carbonate and silicate melts by addition of CO_2 to silicate liquids. The CO_2 was again added in the form of silver oxalate ($Ag_2C_2O_4$). The experiments were run at 0.5 GPa, 1300°C with all five rock-types represented (Table 4.3).

Table 4.3. Experimental compositions, conditions and results for charges involving addition of $Ag_2C_2O_4$ to natural rocks.

Run ident.	Composition (Wt. %)	Pressure (GPa)	Temperature (°C)	Time (Mins)	Assemblage
G1.13	75% BD50, 25% CO_2	0.5	1300	60	Ls + V
G1.14	75% BD119, 25% CO_2	0.5	1300	60	Ls + V
G1.15	75% SUN189, 25% CO_2	0.5	1300	60	Ls + V
G1.16	75% ELG2, 25% CO_2	0.5	1300	60	Ls + Xtls + V
G1.17	75% BD105, 25% CO_2	0.5	1300	60	Ls + Xtls + V

These experiments were unsuccessful in obtaining immiscibility. The charges produced were pumice-like foams with numerous large vapour bubbles in silicate glass, either with or without crystals. As with the soda-melilite glass-$Ag_2C_2O_4$ experiment, it was decided that further experiments on natural rocks using this technique were not warranted: immiscibility was easily obtainable by addition of powdered carbonate to the silicate rocks.

4.4.1. Set 2. Experimental acquisition of a P-T-X grid of immiscible-liquid compositions.

This section represents the main body of experiments on natural melt compositions, and was designed to produce coexisting immiscible carbonate and silicate melts over a wide range of pressures, temperatures, and compositions. The effects of these variables on both immiscibility and trace-element partitioning between the equilibrium melts could then be investigated. Experiments were carried out over the P-T range 0.25-0.8 GPa, 1100-1300°C, and were of *ca.* 1 hr duration. All the starting compositions in Table 4.2 were used. As the experimentally produced melts were to

be representative of natural systems, mixtures were employed which were just inside the silicate limb of the compositional extent of immiscibility (Figure 4.3). Mixtures were also made up which lay to the calcium-poor side of the Freestone & Hamilton solvus in an attempt to produce more calcic immiscible carbonate melts than those produced by Freestone & Hamilton (1980). Owing to the size of the data set, each composition has had to be considered separately. Major-element analyses of coexisting liquids produced have been presented in Appendix A.2.

BD50 + CNC.

A powdered mix of 75% BD50, 25% CNC was made up and ground under acetone for *ca.* 1 hr to insure homogeneity. Samples of this mix were run under the conditions stated in Table 4.4. Apart from experiment G3.1, at 0.25 GPa, and 1100° C, all charges produced immiscible carbonate and silicate melts, either with coexisting vapour, or vapour absent (Figure 4.1a). The capsule of G3.1 was found to have failed when investigated after quenching, and it is believed that this failure resulted in CO_2-loss from the charge. The assemblage left was therefore Ls+V, Lc having been destabilized. When this experiment was repeated (G13.1), coexisting carbonate and silicate melts were produced with similiar textures to those at other pressures and temperatures.

Table 4.4. Starting compositions, conditions, and resulting assemblages for experiments involving phonolite and calcium-sodium-carbonate.

Run ident.	Composition (Wt.%)	Pressure (GPa)	Temperature (°C)	Time (Mins)	Assemblage
G3.1	75% BD50, 25% CNC	0.25	1100	60	Ls + V
G2.1	75% BD50, 25% CNC	0.5	1100	60	Ls + Lc
G4.1	75% BD50, 25% CNC	0.8	1100	60	Ls + Lc
G6.1	75% BD50, 25% CNC	0.25	1200	60	Ls + Lc
G5.1	75% BD50, 25% CNC	0.5	1200	60	Ls + Lc
G7.1	75% BD50, 25% CNC	0.8	1200	60	Ls + Lc
G9.1	75% BD50, 25% CNC	0.25	1300	60	Ls + Lc
G1.1	75% BD50, 25% CNC	0.5	1300	60	Ls + Lc
G10.1	75% BD50, 25% CNC	0.8	1300	60	Ls + Lc
G13.1	75% BD50, 25% CNC	0.25	1100	60	Ls + Lc + V
G16.1	75% BD50, 25% CNC	0.25	1200	60	Ls + Lc + V

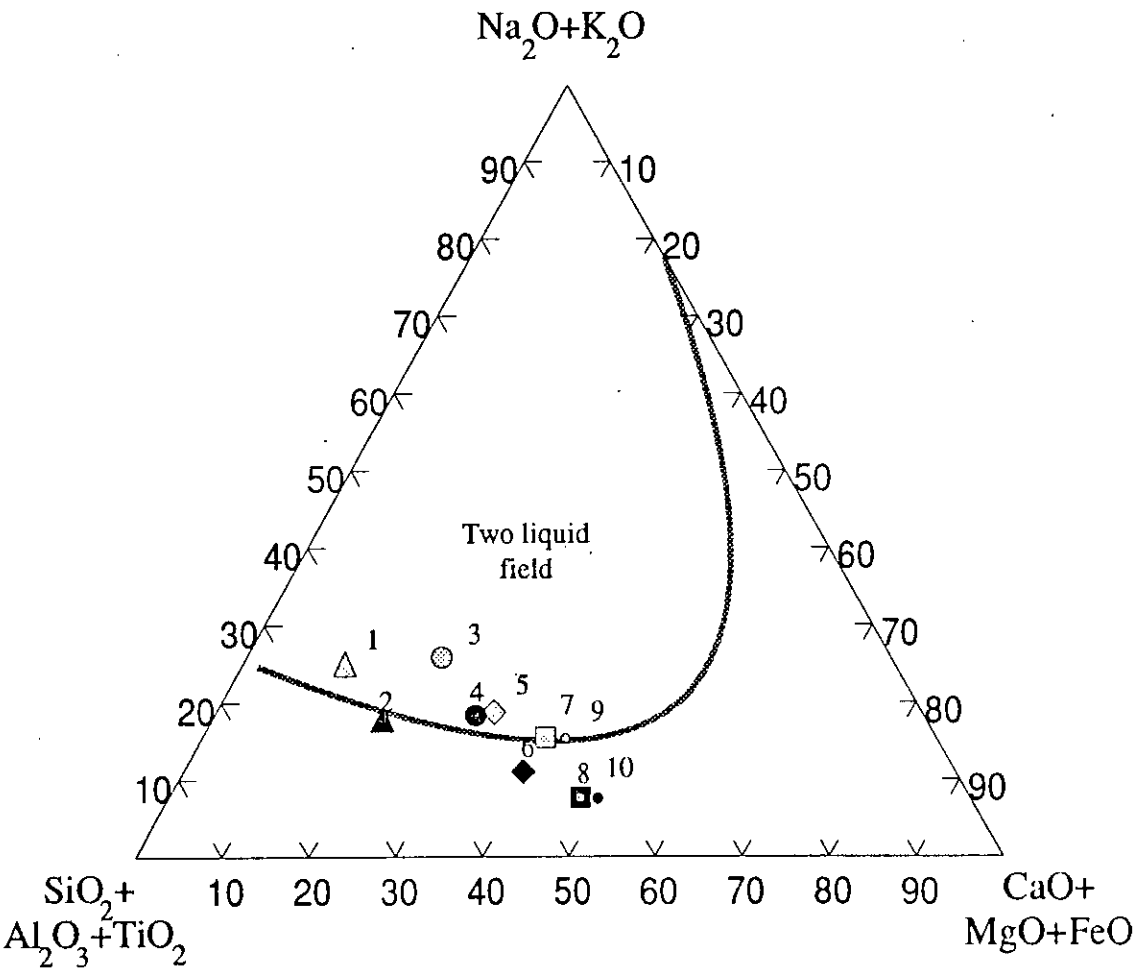

Figure 4.3. Starting mixes for experimental charges involving natural rock compositions. Also shown is the estimated field of immiscibility at 0.5 GPa, 1100°C (Freestone & Hamilton, 1980). Starting materials were employed outside this two-liquid field in order to produce more calcic carbonate liquid compositions, realistic of natural melts. 1, BD50+CNC; 2, BD50+CC; 3, BD119+CNC; 4, BD119+CC; 5, SUN189+CNC; 6, SUN189+CC; 7, ELG2+CNC; 8, ELG2+CC; 9, BD105+CNC; 10, BD105+CC.

The compositions of coexisting carbonate and silicate melts have been plotted in Figure 4.4. The melt compositions are reasonably similar over the whole P-T range. A silica-rich phonolitic melt coexists with a Na-Ca-carbonate melt with a maximum of 2 wt. % silicate component. Variation in the carbonate melt composition is restricted to changes in Na/Ca ratio (of only a few wt. %), whilst variation in the silicate is due to the amount of dissolved carbonate under differing P-T conditions.

BD50+CC.

A powder composition of 75% BD50, 25% CC was produced, and run under the conditions shown in Table 4.5.

Table 4.5. Starting compositions, conditions, and resulting assemblages for experiments involving phonolite and calcium carbonate.

Run ident.	Composition (Wt.%)	Pressure (GPa)	Temperature (°C)	Time (Mins)	Assemblage
G3.2	75% BD50, 25% CC	0.25	1100	60	Ls + Lc + V
G2.2	75% BD50, 25% CC	0.5	1100	60	Ls + Lc + Xtls + V
G4.2	75% BD50, 25% CC	0.8	1100	60	Ls + V
G6.2	75% BD50, 25% CC	0.25	1200	60	Ls + V
G5.2	75% BD50, 25% CC	0.5	1200	60	Ls + Lc + V
G7.2	75% BD50, 25% CC	0.8	1200	60	Ls + V
G9.2	75% BD50, 25% CC	0.25	1300	60	Ls + V
G1.	75% BD50, 25% CC	0.5	1300	60	Ls + Lc + V
G8.2	75% BD50, 25% CC	0.8	1300	15	Ls + Lc + V

Many of the charges did not produce immiscible melts, giving assemblages of Ls+V. Even those experiments that did show immiscibility (e.g. G3.2.) contained only very small wedges of carbonate melt, "wetting" the corners of contacts between silicate melt and CO_2-rich vapour bubbles. Although suitable for analysis for major element composition on the electron probe, these areas would not have been large enough for representative analysis on the ion probe. In any case, owing to their proximity to the Ls-Lc meniscus, their trace-element contents would probably be unrepresentative due to boundary effects (Chapter 5). The exception to this was G5.2, run at 0.5 GPa, 1200°C, which contained a sizable sphere of carbonate surrounding vapour. G5.2 is therefore the only example of this composition to be studied in terms of trace-element partitioning.

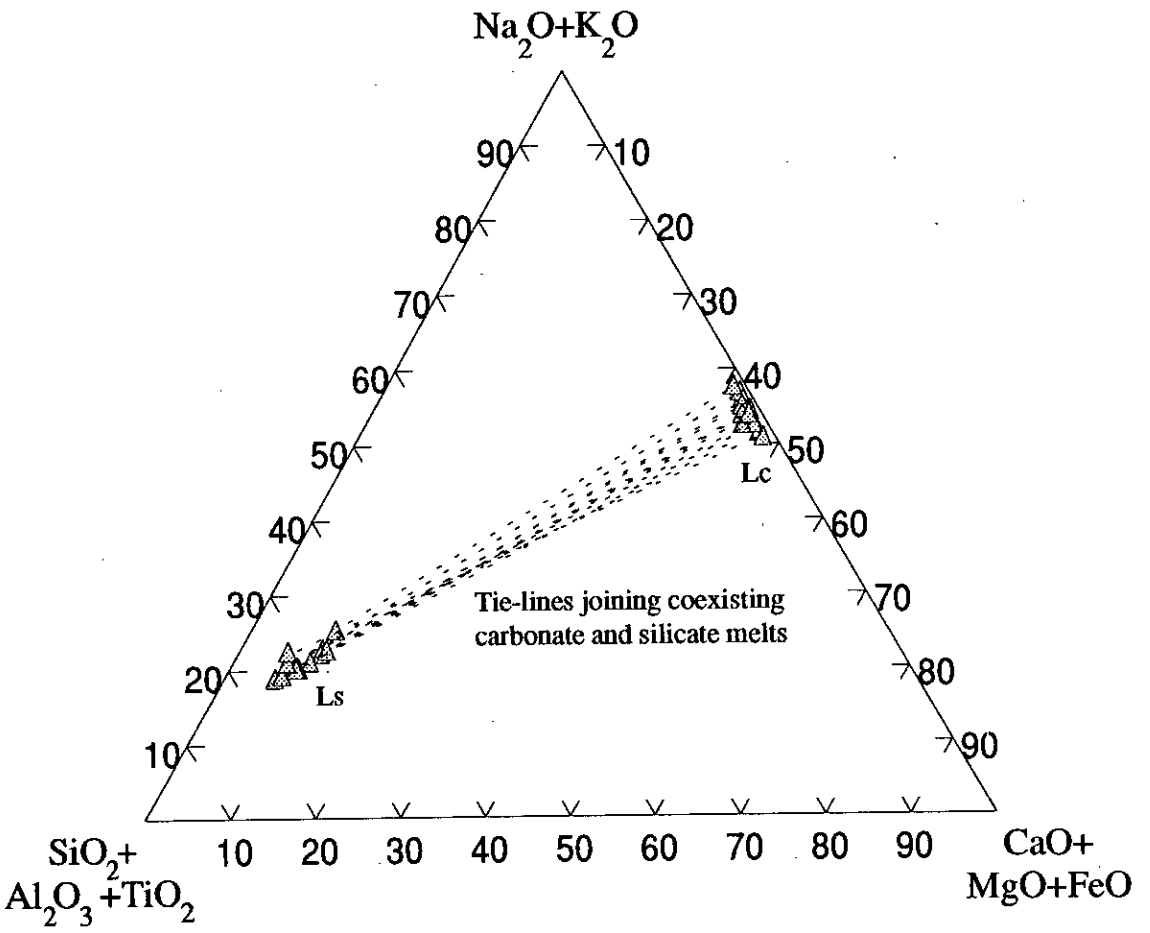

Figure 4.4. Immiscibility between phonolite (BD50) and Ca-Na-carbonate, 0.2-0.8 GPa, 1100-1300°C. Note the low solubility of silicate component in the sodium-rich carbonate liquids.

The compositional relationships of the coexisting liquids obtained in successful runs are plotted in Figure 4.5. The silicate melt compositions are closely grouped over the P-T range studied, whilst considerable variation can be seen in the carbonate melt. The carbonate melts contain variations in both silica contents and Na/Ca ratios. Some of this variation is likely to be due to difficulties in analysing the small areas of carbonate melt produced.

BD119+CNC.

The olivine-free nephelinite BD119 was combined with CNC, again in a 75/25 mix, and run over the P-T range used previously. All charges run using this starting mixture produced coexisting carbonate and silicate melts either with or without CO_2 vapour. The presence of vapour was identified in all the charges at low pressure (0.25 GPa), but only in those charges run at 1300°C at higher pressures.

Table 4.6. Starting compositions, conditions, and resulting assemblages for experiments involving olivine-free nephelinite and calcium-sodium-carbonate.

Run ident.	Composition (Wt.%)	Pressure (GPa)	Temperature (°C)	Time (Mins)	Assemblage
G3.3	75% BD119, 25% CNC	0.25	1100	60	Ls + Lc + V
G2.3	75% BD119, 25% CNC	0.5	1100	60	Ls + Lc
G4.3	75% BD119, 25% CNC	0.8	1100	60	Ls + Lc
G6.3	75% BD119, 25% CNC	0.25	1200	60	Ls + Lc + V
G5.3	75% BD119, 25% CNC	0.5	1200	60	Ls + Lc
G7.3	75% BD119, 25% CNC	0.8	1200	60	Ls + Lc
G9.3	75% BD119, 25% CNC	0.25	1300	60	Ls + Lc + V
G1.3	75% BD119, 25% CNC	0.5	1300	60	Ls + Lc + V
G10.3	75% BD119, 25% CNC	0.8	1300	60	Ls + Lc + V

The compositions of coexisting liquids produced from this starting mix are plotted in Figure 4.6. As with the BD50+CNC starting mix, both the carbonate and silicate melt compositions are similar over the whole P-T range. The nephelinitic melts differ from the phonolitic melts in that they contain a larger CO_2 component (up to 10 wt. %), and coexist with carbonate melts with higher silica contents. There seems to be more mixing of carbonate and silicate end-members in silica-poor nephelinitic compositions than in their phonolitic counterparts.

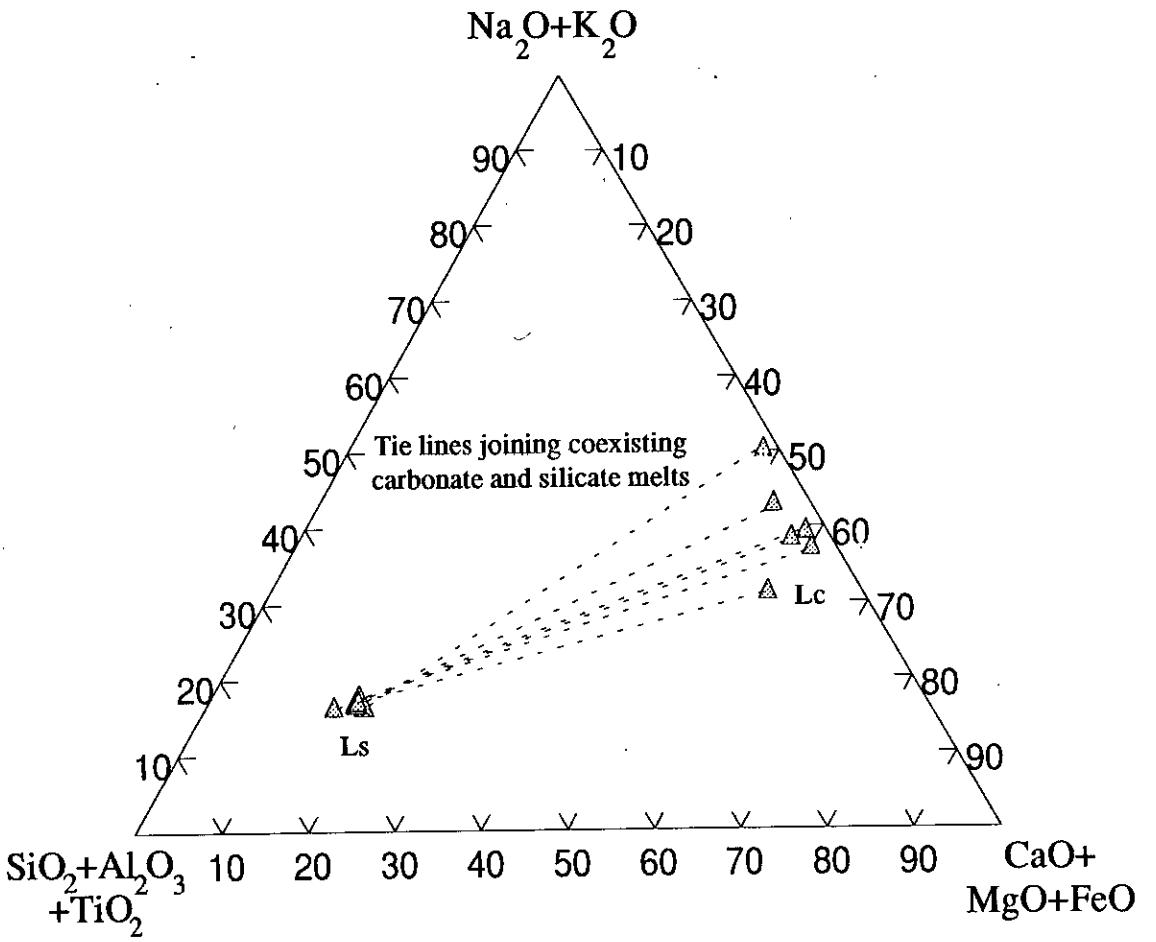

Figure 4.5. Immiscibility between phonolite (BD50) and Ca-carbonate, 0.2-0.8 GPa, 1100-1300°C. Note the variable nature of carbonate melts, both in terms of silicate component, and Na/Ca ratios.

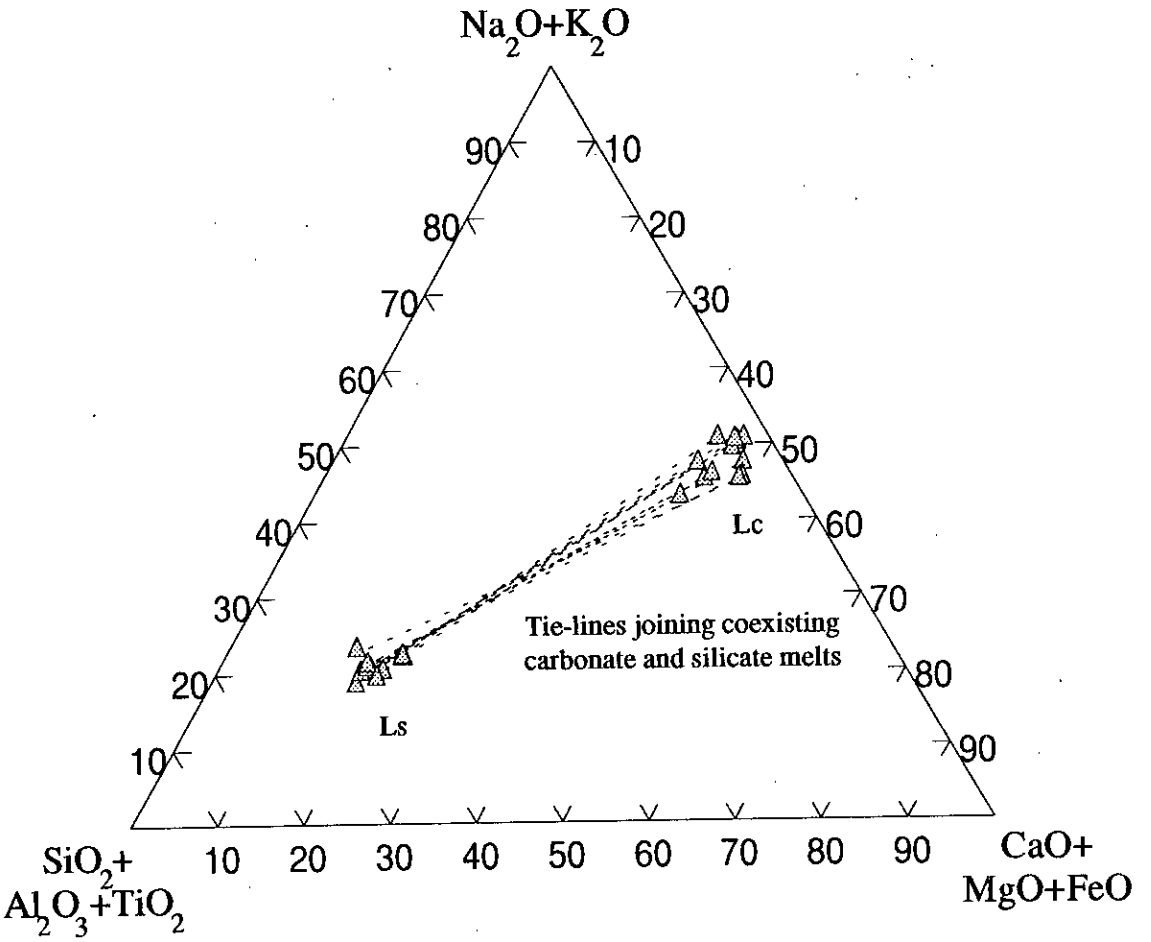

Figure 4.6. Immiscibility between olivine-free nephelinite (BD119) and Ca-Na-carbonate, 0.2-0.8 GPa, 1100-1300°C. It can be seen that there is significant mixing of carbonate and silicate components in these compositions.

BD119+CC.

A 75/25 mixture of olivine-free nephelinite and calcium carbonate was made up as previously, and run over the range 1100-1300°C, 0.25-0.5 GPa (Table 4.7). The majority of these experiments were successful in producing coexisting carbonate and silicate melts, many also with associated CO_2 vapour (Figure 4.1c). A few of the charges produced textures which made the carbonate melt unsuitable for trace-element microanalysis. These were repeated if analysis was considered essential.

Table 4.7. Starting compositions, conditions, and resulting assemblages for experiments involving olivine-free nephelinite and calcium carbonate.

Run ident.	Composition (Wt.%)	Pressure (GPa)	Temperature (°C)	Time (Mins)	Assemblage
G3.4	75% BD119, 25% CC	0.25	1100	60	Ls + Lc + V
G2.4	75% BD119, 25% CC	0.5	1100	60	Ls + Lc + V
G4.4	75% BD119, 25% CC	0.8	1100	60	Ls + Lc
G6.4	75% BD119, 25% CC	0.25	1200	60	Ls + Lc + V
G5.4	75% BD119, 25% CC	0.5	1200	60	Ls + Lc + V
G7.4	75% BD119, 25% CC	0.8	1200	60	Ls + Lc
G9.4	75% BD119, 25% CC	0.25	1300	60	Ls + V
G1.4	75% BD119, 25% CC	0.5	1300	60	Ls + Lc + V
G10.4	75% BD119, 25% CC	0.8	1300	60	Ls + Lc
G11.2	75% BD119, 25% CC	0.5	1300	60	Ls + Lc + V
G12	75% BD119, 25% CC	0.5	1100	60	Ls + Lc + V
G16.2	75% BD119, 25% CC	0.25	1200	60	Ls + Lc + V

The experimentally-produced immiscible melts are plotted in compositional space in Figure 4.7. The silicate melt compositions produced at all pressures and temperatures are remarkably similar, suggesting only minor compositional control by physical conditions. There is some evidence for variations in carbonate content of these silicate glasses, perhaps due to variations in the amount of mixing of the Ls and Lc components. The carbonate melt compositions are, by contrast, much more dispersed, with considerable variation in both silica content (2-8.5%), and Ca/Na ratio. Although some of this variation may be due to analytical uncertainty, it seems that these calcic compositions are more susceptible to changes in physical conditions, perhaps because they are near the closure of the two-liquid solvus in P-T-X space.

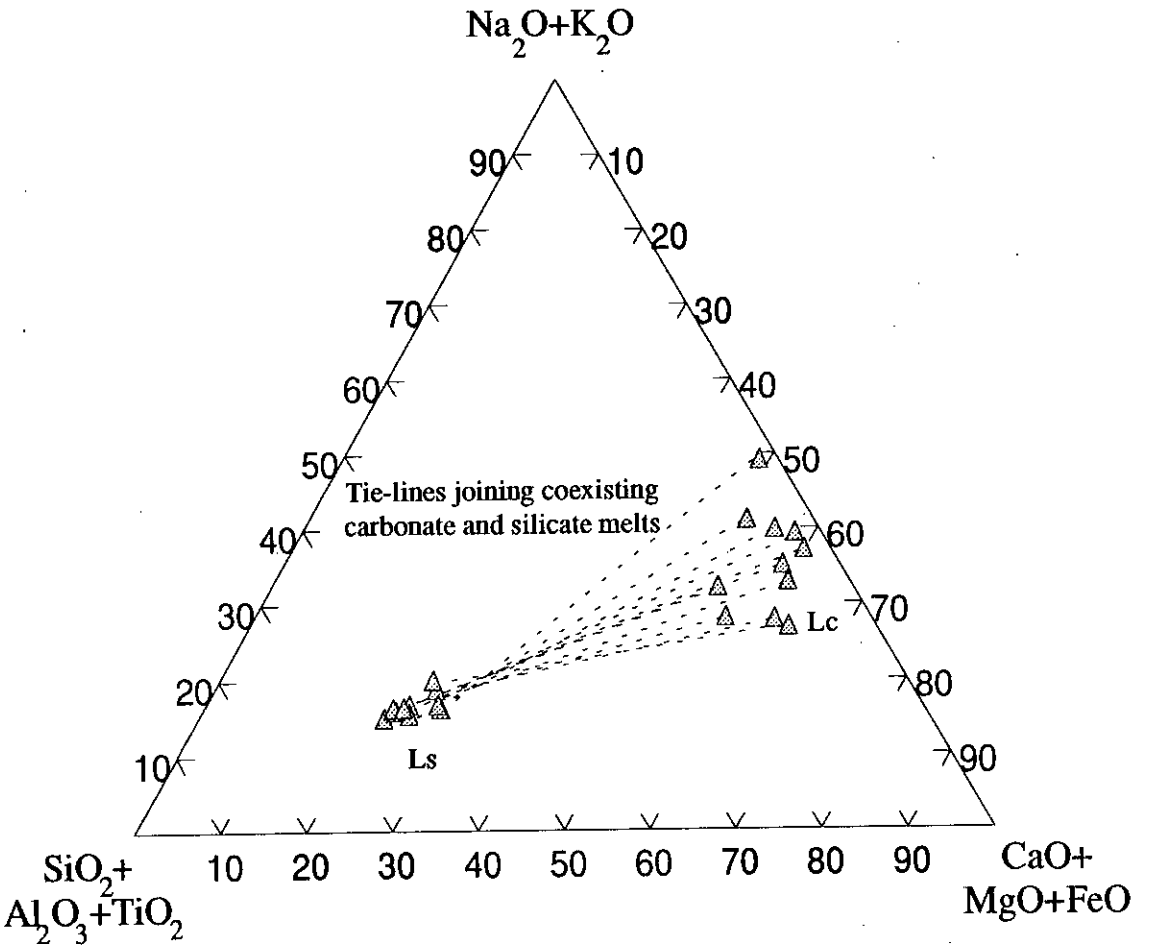

Figure 4.7. Immiscibility between olivine-free nephelinite (BD119) and Ca-carbonate, 0.2-0.8 GPa, 1100-1300°C. As with {BD50 + CC} starting compositions, there is significant variation in both the amount of silicate component, and the Na/Ca ratios of the carbonate liquid with changing P and T.

SUN189+CNC.

Olivine nephelinite powder and CNC were mixed togethor under acetone, and run at 1100-1300°C, 0.2-0.8 GPa (Table 4.8).

Table 4.8. Starting compositions, conditions, and resulting assemblages for experiments involving olivine nephelinite and calcium-sodium-carbonate.

Run ident.	Composition (Wt.%)	Pressure (GPa)	Temperature (°C)	Time (Mins)	Assemblage
G3.5	75% SUN189, 25% CNC	0.25	1100	60	Ls + Lc + V
G2.5	75% SUN189, 25% CNC	0.5	1100	60	Ls + Lc
G4.5	75% SUN189, 25% CNC	0.8	1100	60	Ls + Lc + Xtls
G6.5	75% SUN189, 25% CNC	0.25	1200	60	Ls + Lc + V
G5.5	75% SUN189, 25% CNC	0.5	1200	60	Ls + Lc
G7.5	75% SUN189, 25% CNC	0.8	1200	60	Ls + Lc
G9.5	75% SUN189, 25% CNC	0.25	1300	60	Ls + Lc + V
G1.5	75% SUN189, 25% CNC	0.5	1300	60	Ls + Lc + V
G10.5	75% SUN189, 25% CNC	0.8	1300	60	Ls + Lc
G16.3	75% SUN189, 25% CNC	0.25	1200	60	Ls + Lc + V

All experiments produced charges containing dominant silicate melt, with minor carbonate melt as spheres. Melts produced at 0.25 GPa coexisted with CO_2-rich vapour; those at higher pressures were vapour-absent. G4.5, run at 1100°C, 0.8 GPa, also contained a few olivine crystals (>5%), showing that the 0.8 GPa liquidus for this compositional mix is slightly above 1100°C. By using tie lines, it was established that these crystals were unlikely to have a significant effect on the compositions of coexisting liquids; certainly, due to the very small partition coefficients for olivine/melt, trace-element concentrations were unlikely to be greatly affected. The results were therefore included. All other charges contained assemblages produced at temperatures above the liquidus. G6.5 was repeated due to some difficulty in obtaining Lc in polished section.

Compositions of coexisting liquids are plotted in Figure 4.8. Again, close grouping of the silicate melt compositions suggests that pressure and temperature effects are small in the range 0.2-0.8 GPa and 1100-1300°C. The carbonate melt compositions, although quite calcic, are reasonably consistent in terms of Na/Ca ratio, but vary in terms of dissolved silica component contained under different P-T conditions.

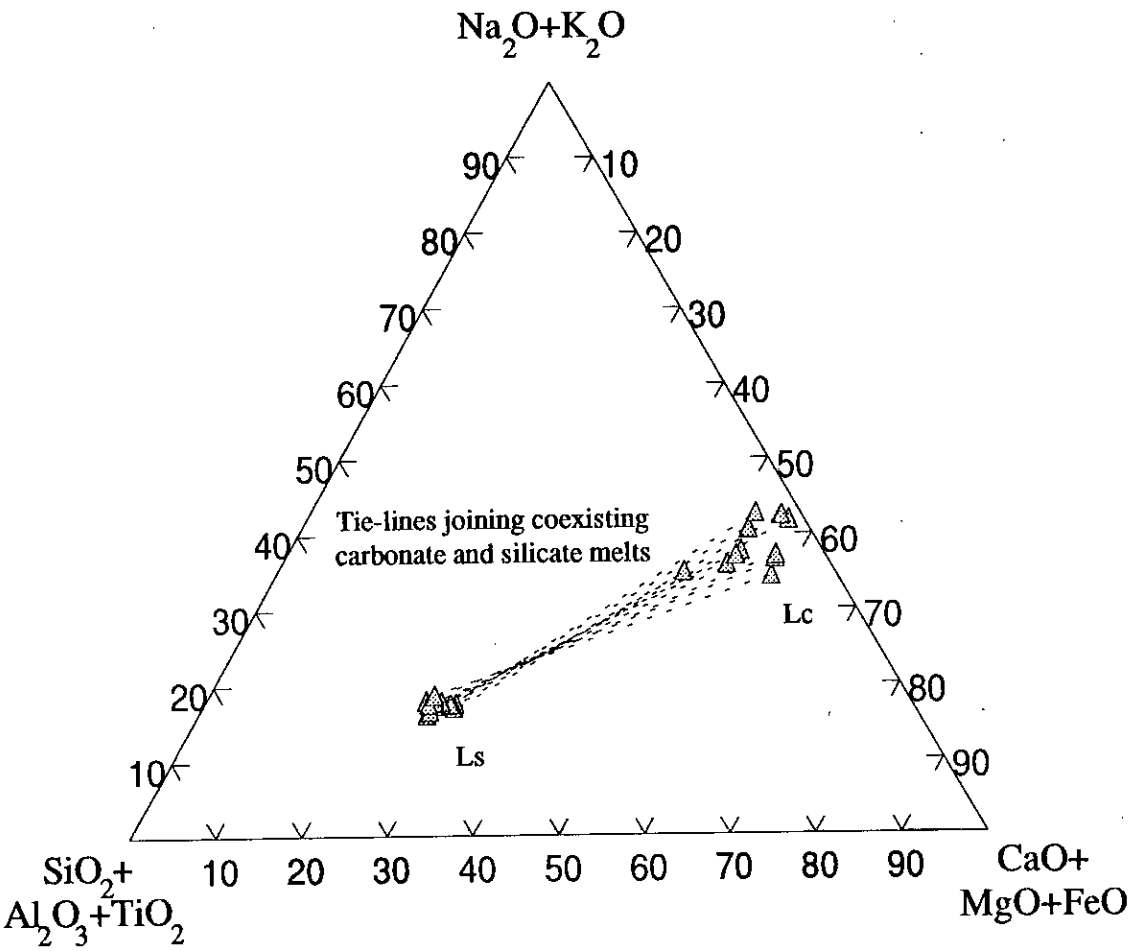

Figure 4.8. Immiscibility between olivine nephelinite (SUN189) and Ca-Na-carbonate, 0.2-0.8 GPa, 1100-1300°C . Again, there is substantial mixing of the carbonate and silicate components, but little change in Na/Ca ratios in either silicate or carbonate.

SUN189+CC.

The most "primitive" and sodium-poor of the compositions studied in detail was a starting mix of 75% olivine nephelinite (SUN189), and 25% calcium carbonate. This composition was run under conditions of 1100-1300°C, 0.2-0.8 GPa (Table 4.9).

Table 4.9. Starting compositions, conditions, and resulting assemblages for experiments involving olivine nephelinite and calcium carbonate.

Run ident.	Composition (Wt.%)	Pressure (GPa)	Temperature (°C)	Time (Mins)	Assemblage
G3.6	75% SUN189, 25% CC	0.25	1100	60	Ls + V
G2.6	75% SUN189, 25% CC	0.5	1100	60	Ls + Lc
G4.6	75% SUN189, 25% CC	0.8	1100	60	Ls + Lc + Xtls
G6.6	75% SUN189, 25% CC	0.25	1200	60	Ls + Lc + V
G5.6	75% SUN189, 25% CC	0.5	1200	60	Ls + V
G7.6	75% SUN189, 25% CC	0.8	1200	60	Ls + Lc + V
G9.6	75% SUN189, 25% CC	0.25	1300	60	Ls + Lc + V
G1.6	75% SUN189, 25% CC	0.5	1300	60	Ls + Lc + V
G10.6	75% SUN189, 25% CC	0.8	1300	60	Ls + Lc + V
G13.2	75% SUN189, 25% CC	0.25	1100	60	Ls + Lc + V
G15	75% SUN189, 25% CC	0.5	1200	60	Ls + Lc + V

Apart from two charges where it is believed that burst capsules allowed the escape of CO_2, all charges contained assemblages dominated by Ls, with small spheres of Lc and CO_2-rich vapour, often in association (Plate 4.1d). As with the SUN189+CNC composition, the 1100°C, 0.8 GPa charge was found to contain a few isolated crystals of olivine, and was therefore below its liquidus temperature. It was again decided that these crystals would have little effect on element partitioning between the coexisting carbonate and silicate melts, and that the liquids produced from this charge could be studied further.

Liquid compositions from these charges are plotted in Figure 4.9. Some variation can be seen in the compositions of conjugate silicate melts, attributed to varying amounts of dissolved carbonate component. However, the major feature of this diagram is that the carbonate melt compositions plot into two distinct populations. At low pressure, the carbonate melt produced in equilibrium with olivine nephelinite is

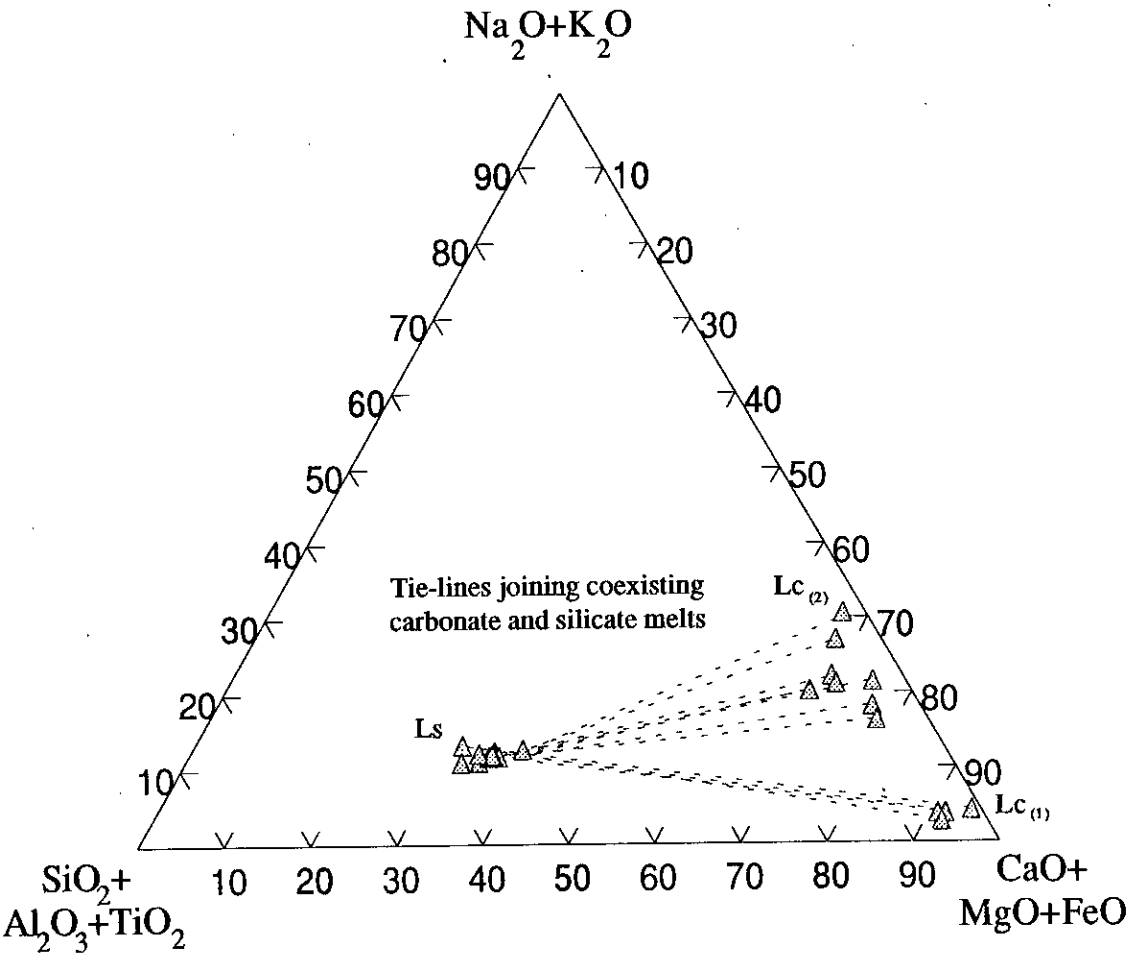

Figure 4.9. Immiscibility between olivine nephelinite (SUN189) and Ca-carbonate, 0.2-0.8 GPa, 1100-1300°C. Two distinct populations of carbonate melt can be seen; a nearly pure Ca-carbonate is produced at low pressure ($Lc_{(1)}$) and a more mixed Ca-Na-carbonate melt ($Lc_{(2)}$) at higher pressures.

nearly pure $CaCO_3$ ($Lc_{(1)}$), with just 1-2 wt. % of SiO_2 and Na_2O. At pressures higher than 0.5 GPa, this melt becomes suddenly more sodic ($Lc_{(2)}$), with as much as 15 Wt. % Na_2O. Olivine nephelinite melt can therefore coexist with two very different carbonate melts, depending on the P-T conditions.

Experiments involving ELG2.

The olivine nephelinite ELG2 was mixed with both CNC and CC in the proportions 75/25. It was realized that, owing to the high liquidus temperature of ELG2, these mixes were only likely to be approaching their liquidus at 1300°C or above. Unfortunately, 1300°C is approaching the practical temperature limit for experiments in gas-media vessels at Edinburgh. Therefore experiments on ELG2 compositions were restricted to 1300°C, 0.25, 0.5, and 0.8 GPa (Table 4.10).

Table 4.10. Starting compositions, conditions, and resulting assemblages for experiments involving ELG2 olivine-rich nephelinite.

Run ident.	Composition (Wt.%)	Pressure (GPa)	Temperature (°C)	Time (Mins)	Assemblage
G9.7	75% ELG2, 25% CNC	0.25	1300	60	Ls + Lc + Xtls + V
G9.8	75% ELG2, 25% CC	0.25	1300	60	Ls + Lc + Xtls + V
G1.7	75% ELG2, 25% CNC	0.5	1300	60	Ls + Lc + Xtls + V
G1.8	75% ELG2, 25% CC	0.5	1300	60	Ls + Lc + Xtls + V
G10.7	75% ELG2, 25% CNC	0.8	1300	60	Ls + Lc + Xtls + V
G10.8	75% ELG2, 25% CC	0.8	1300	60	Ls + Lc + Xtls + V
G8.7	75% ELG2, 25% CNC	0.8	1300	15	Xtls + Qc + V
G8.8	75% ELG2, 25% CC	0.8	1300	15	Ls + Xtls + V

Unfortunately, even at these high temperatures, the charges were extensively crystallized. This made identification of coexisting liquids difficult, although, at high magnification, small immiscible spheres of carbonate melt could be seen associated with silicate crystals in most of the charges studied. Immiscibility is present in these charges, but has only been confirmed in the presence of numerous crystals (Plate 4.1e).

Coexisting liquids produced in experiments involving ELG2 were not investigated further for two reasons:

1. Carbonate spheres seen were in the order of 10-100 μm in diameter. They were therefore unsuitable for ion probe trace-element analysis.

2. As the charges were extensively crystallized, the interstitial melt compositions would be far removed from initial liquidus compositions.

Experiments involving BD105.

Olivine melilite nephelinite BD105, was mixed with CNC and CC and run at 1300°C, 0.25-0.8 GPa. Resultant charges, despite the presence of Na_2CO_3, were virtually completely crystalline aggregates, with only small patches of melt remaining. This melt was often quenched to a carbonate intergrowth. Immiscible carbonate and silicate liquids were identified in at least one charge but, owing to their interstitial nature, were not studied further.

Table 4.11. Starting compositions, conditions, and resulting assemblages for experiments involving BD105, olivine-meliltie-nephelinite.

Run ident.	Composition (Wt.%)	Pressure (GPa)	Temperature (°C)	Time (Mins)	Assemblage
G9.9	75% BD105, 25% CNC	0.25	1300	60	Ls + Lc + Xtls + V
G9.10	75% BD105, 25% CC	0.25	1300	60	Ls + Xtls + V
G1.9	75% BD105, 25% CNC	0.5	1300	60	Ls + Lc? + Xtls + V
G1.10	75% BD105, 25% CC	0.5	1300	60	Ls + Lc? + Xtls + V
G10.9	75% BD105, 25% CNC	0.8	1300	60	Ls + Xtls + V
G10.10	75% BD105, 25% CC	0.8	1300	60	Ls + Xtls + V
G8.9	75% BD105, 25% CNC	0.8	1300	15	Xtls of silicate and carbonate
G8.10	75% BD105, 25% CC	0.8	1300	15	Ls + Xtls + V

Coexisting liquids from experiments involving BD50, BD119, and SUN189.

Figure 4.10 shows experimental conjugate liquids produced at 0.25 GPa. The approximate compositional extent of immiscibility is shown at 1100, 1200, and 1300° C. It must be made clear that these are natural rock compositions, containing appreciable quantities of minor components, and variable ratios of major elements; they cannot be expected to have the same phase relations. The size of the two-liquid field shown in these diagrams is an average of that seen in natural materials, under the P-T conditions stated, and does not suggest that all rock compositions will conform to this behaviour.

It can be seen from these diagrams that carbonate-silicate liquid immiscibility extends to sodium-poor compositions in natural rock-types at 0.25 GPa. Carbonate liquids with similar compositions to carbonatites seen at the Earth's surface would, if existing together, be in equilibrium with olivine nephelinite melt. This does not *prove* that carbonatites are produced by liquid immiscibility, but does confirm that they *could* be formed in this way.

Figure 4.11 shows the extent of carbonate-silicate immiscibility at 0.5 GPa, and Figure 4.12 at 0.8 GPa. With increasing pressure, the sudden change in carbonate-melt composition from sodium-rich to sodium-poor seen at 0.25 GPa becomes more gradual, with a continuum of carbonate melt compositions being produced at 0.8 GPa.

The effects of temperature on immiscibility are small; if there is closure of the two-liquid field with increasing temperature, this effect is small enough to be masked by experimental and analytical uncertainties.

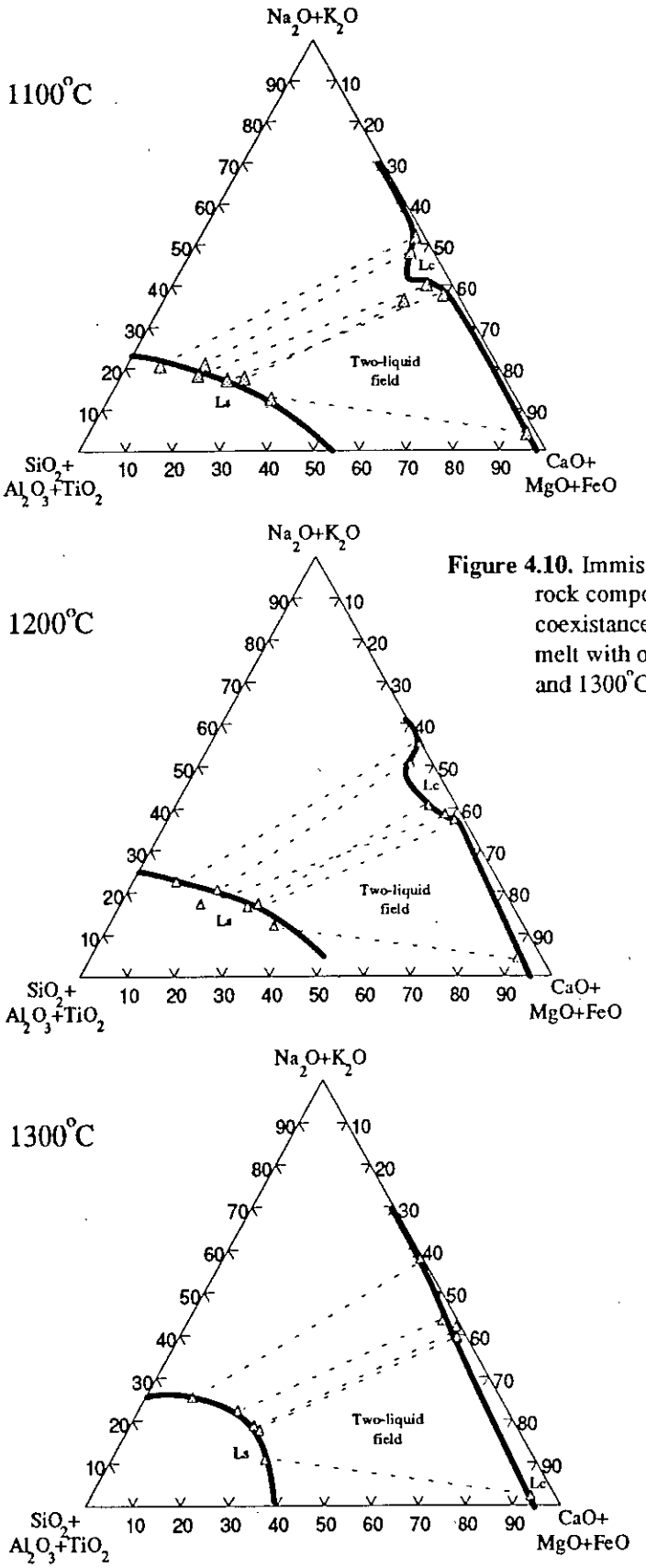

Figure 4.10. Immiscibility relationships in natural rock compositions at 0.25 GPa. Note the coexistance of near-pure calcium carbonate melt with olivine nephelinite at 1100, 1200, and 1300°C

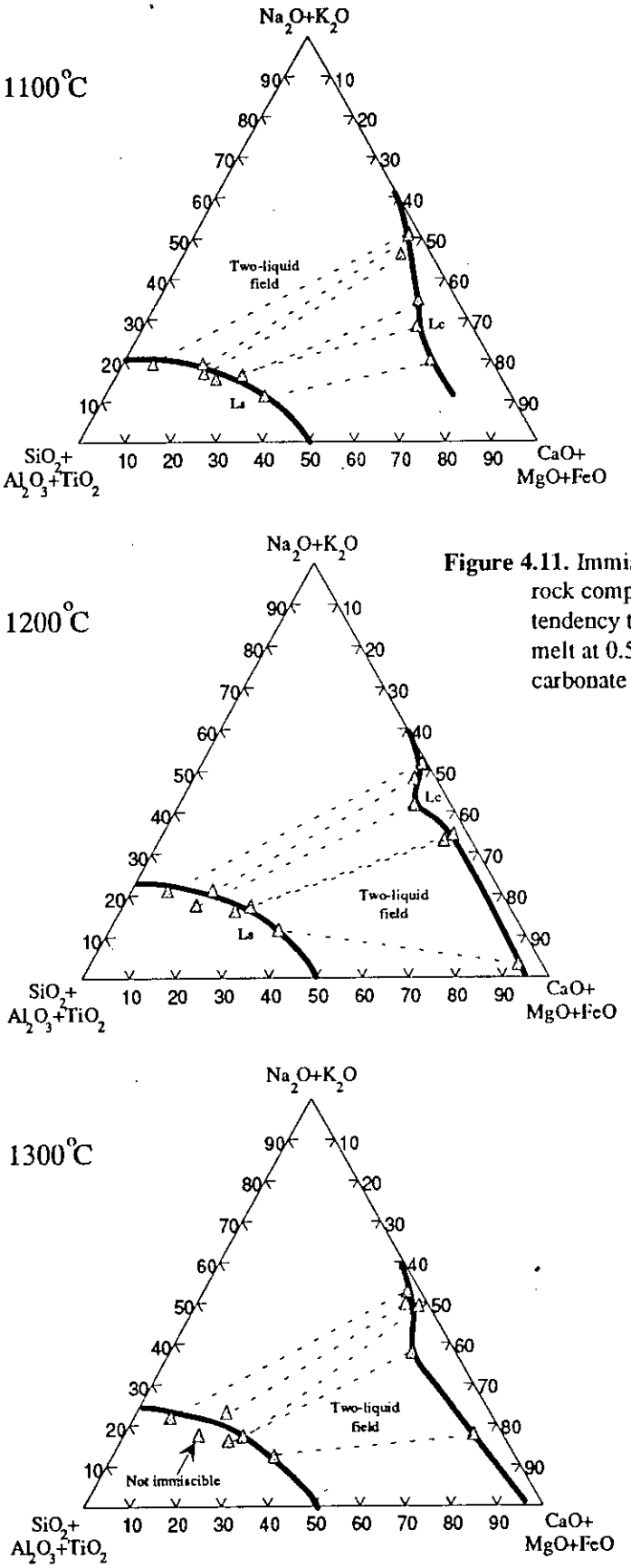

Figure 4.11. Immiscibility relationships in natural rock compositions at 0.5 GPa. There is a tendency towards calcium-rich carbonate melt at 0.5 GPa, but no pure calcium carbonate melts were produced.

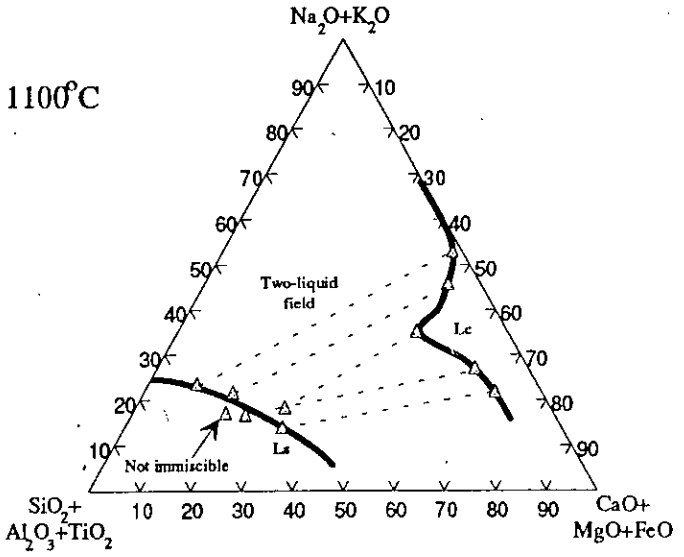

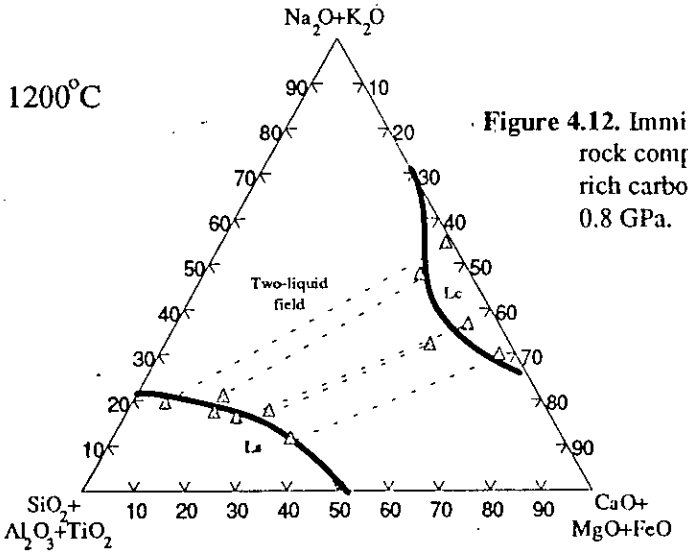

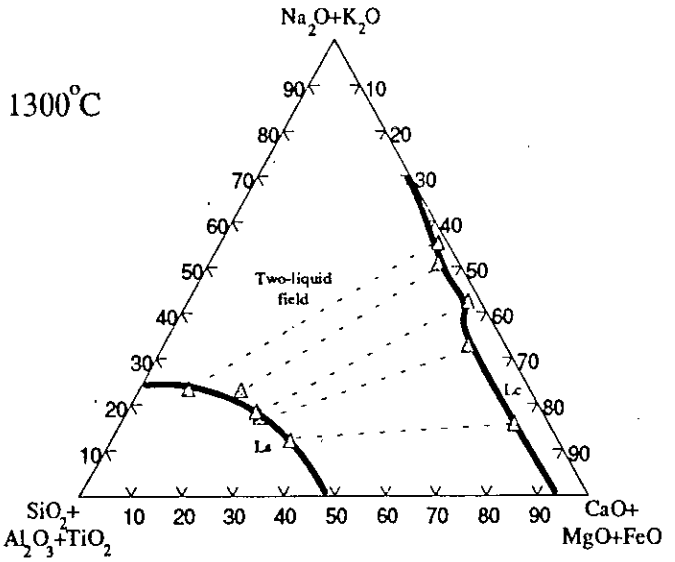

Figure 4.12. Immiscibility relationships in natural rock compositions at 0.8 GPa. No calcium-rich carbonate melts were produced at 0.8 GPa.

4.4.3. Set 3. Variation of run duration.

A series of experiments of various run duration were undertaken in order to address a number of questions:

(a) The effect of iron-loss.

Iron-bearing systems have long been a problem in experimental work. The noble metal capsules, which must be used to contain charges in high temperature experiments, are known to alloy with significant amounts of iron under run conditions. This results in iron depletion in the sample, the rate of depletion depending on the pressure, temperature, oxygen fugacity, initial concentration of iron, and the type of metal capsule used. Pre-saturated Fe-Pt alloy capsules have been prepared but have been found to be brittle and although Fe loss can be reduced, it is difficult to avoid some exchange of iron between sample and container (Ford, 1978a,b). It was decided that this feature of Fe-loss could be put to advantage, by allowing the effects of variable Fe contents on immiscibility and partitioning to be studied using order of magnitude variations in run duration times.

(b) Equilibration times.

Variations in run duration allowed investigation of the times required to obtain chemical and textural equilibrium in these natural compositions.

(c) Possible change in run conditions.

Three possible sources of variation during experimental runs are: oisoning of the thermocouple (leading to steadily increasing temperature), leakage of gas from the bombs (leading to decreasing pressure), and external buffering of fO_2 (leading to change in redox conditions). If such variations were occurring, they would manifest themselves as systematic changes in the compositions of coexisting melts produced from runs of different lengths.

Experiments were run, as before, in the gas-media vessels, using compositions of 75% silicate 25% carbonate. Run durations were of 15, 60, 360 and 960 mins. Conditions, compositions, and resulting assemblages are given in Table 4.12 overleaf.

Table 4.12. Experiments to investigate the effects of varied run duration on immiscibility in natural rock compositions: Starting compositions, conditions, and resulting assemblages.

Run ident.	Composition (Wt.%)	Pressure (GPa)	Temperature (°C)	Time (Mins)	Assemblage
G8.1	75% BD50, 25% CNC	0.8	1300	15	Ls + Lc + V
G10.1	75% BD50, 25% CNC	0.8	1300	60	Ls + Lc + V
G25.1	75% BD50, 25% CNC	0.8	1300	360	Ls + Lc + V
G24.1	75% BD50, 25% CNC	0.8	1300	960	Ls + Lc + V
G8.3	75% BD119, 25% CNC	0.8	1300	15	Ls + Lc
G10.3	75% BD119, 25% CNC	0.8	1300	60	Ls + Lc + V
G25.2	75% BD119, 25% CNC	0.8	1300	360	Ls + Lc
G24.2	75% BD119, 25% CNC	0.8	1300	960	Ls + Lc
G8.4	75% BD119, 25% CC	0.8	1300	15	Ls + Lc
G10.4	75% BD119, 25% CC	0.8	1300	60	Ls + Lc + V
G25.3	75% BD119, 25% CC	0.8	1300	360	Ls + Lc + V
G24.3	75% BD119, 25% CC	0.8	1300	960	Ls + Lc + V
G8.5*	75% SUN189, 25% CNC	0.8	1300	15	Ls + Lc + V
G10.5	75% SUN189, 25% CNC	0.8	1300	60	Ls + Lc + V + Xtls
G25.4	75% SUN189, 25% CNC	0.8	1300	360	Ls + Lc + V
G24.4	75% SUN189, 25% CNC	0.8	1300	960	Ls + Lc + V
G8.6*	75% SUN189, 25% CC	0.8	1300	15	Ls + Lc + V + Xtls
G10.6	75% SUN189, 25% CC	0.8	1300	60	Ls + Lc + V
G25.5	75% SUN189, 25% CC	0.8	1300	360	Ls + Lc + V
G24.5	75% SUN189, 25% CC	0.8	1300	960	Ls + Lc + V

* Contain a few small olivine crystals, believed to be relics of unmelted powder, due to insufficient time at run conditions

All the experiments produced charges containing immiscible carbonate and silicate liquids. Textures from experiments taking 15 mins were essentially identical to those of 960 mins duration. Generally two-liquid relationships were such that there was the lowest possible surface area of Ls-Lc boundary. This usually consisted of a central sphere of silicate surrounded by a carbonate rind, although this was sometimes distorted by vapour bubbles. This is assumed to be the lowest possible energy state for the two liquids, that is they are in textural equilibrium. Those charges run for just 15 mins were of slightly different appearance, consisting of a number of smaller carbonate spheres distributed throughout the silicate melt, along with the beginings of

a carbonate rind surrounding the central silicate slug. This texture has a higher surface area of Ls-Lc boundary, and is therefore considered to be at a higher energy state and not in textural equilibrium. Textural equilibrium was therefore obtained in *ca.* 1 hr.

The coexisting liquid compositions are plotted in Figure 4.13. Although there is considerable scattering of the data, no systematic trends can be identified. The scattering is best explained by analytical variations of *ca.* ± 2 wt. % of the components (Na_2O+K_2O), ($SiO_2+Al_2O_3+TiO_2$), and (CaO+MgO+FeO). This is probably due to the inhomogeneity of quenched melt in these charges.

4.4.4. Set 4. Solid-media experiments on natural rock compositions.

As with the soda-melilite experiments, it was decided that it was necessary to undertake experiments at pressures exceeding 1.0 GPa in order to have a good understanding of the effects of pressure on immiscibility and partitioning. These experiments were run in solid-media piston-cylinder apparatus, using furnace assembly B (Pt capsules) at 1.1, 1.5, and 2.0 GPa. The BD119+CNC composition was used (Table 4.13).

Table 4.13. Starting compositions, conditions, and resulting assemlages from solid-media experiments on natural rock carbonate-silicate immiscibility.

Run ident.	Composition (Wt.%)	Pressure (GPa)	Temperature (°C)	Time (Mins)	Assemblage
S40	75% BD119, 25% CNC	1.1	1300	75	Ls + Lc
S39	75% BD119, 25% CNC	1.5	1300	75	Ls + Lc
S41	75% BD119, 25% CNC	2.0	1300	75	Ls + Lc

All three experimental charges contained the quenched results of immiscible carbonate and silicate liquids. Immiscibility in natural systems is therefore stable to at least 2.0 GPa. Experimental liquids produced from the BD119+CNC composition over the whole pressure range are plotted in Figure 4.14. As with the soda-melilite experiments, systematic trends in composition with increasing pressure can be seen in both the carbonate and silicate melts.

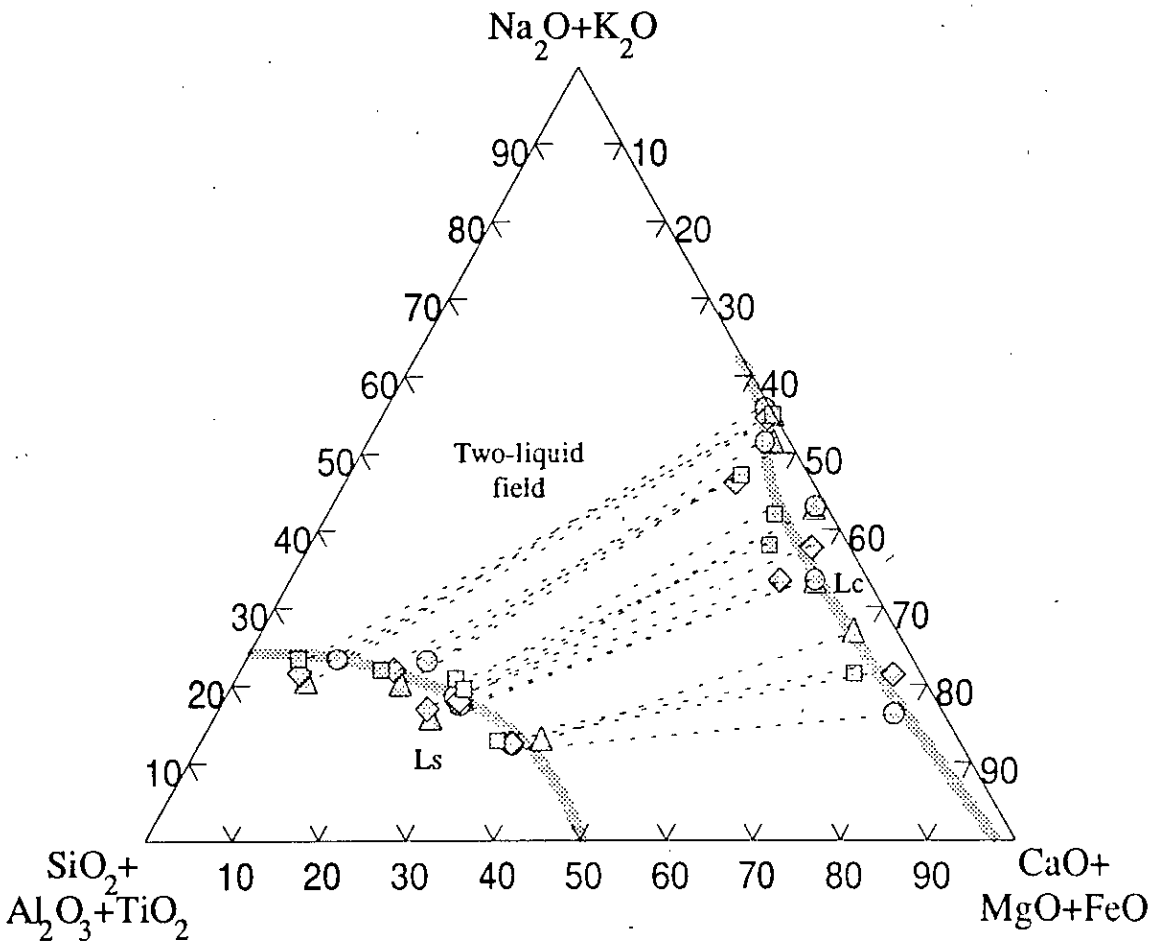

Figure 4.13. Experiments of variable run duration to assess the effects of time on immiscibility. Although there is considerable scatter in the data, no coherent trends in either the carbonate- or silicate-liquid compositions can be seen. The degree of variation is therefore probably attributable to analytical uncertainty, or slight differences in run conditions. Triangles, 15 mins duration; circles, 60 mins duration; diamonds, 240 mins duration; squares, 960 mins duration.

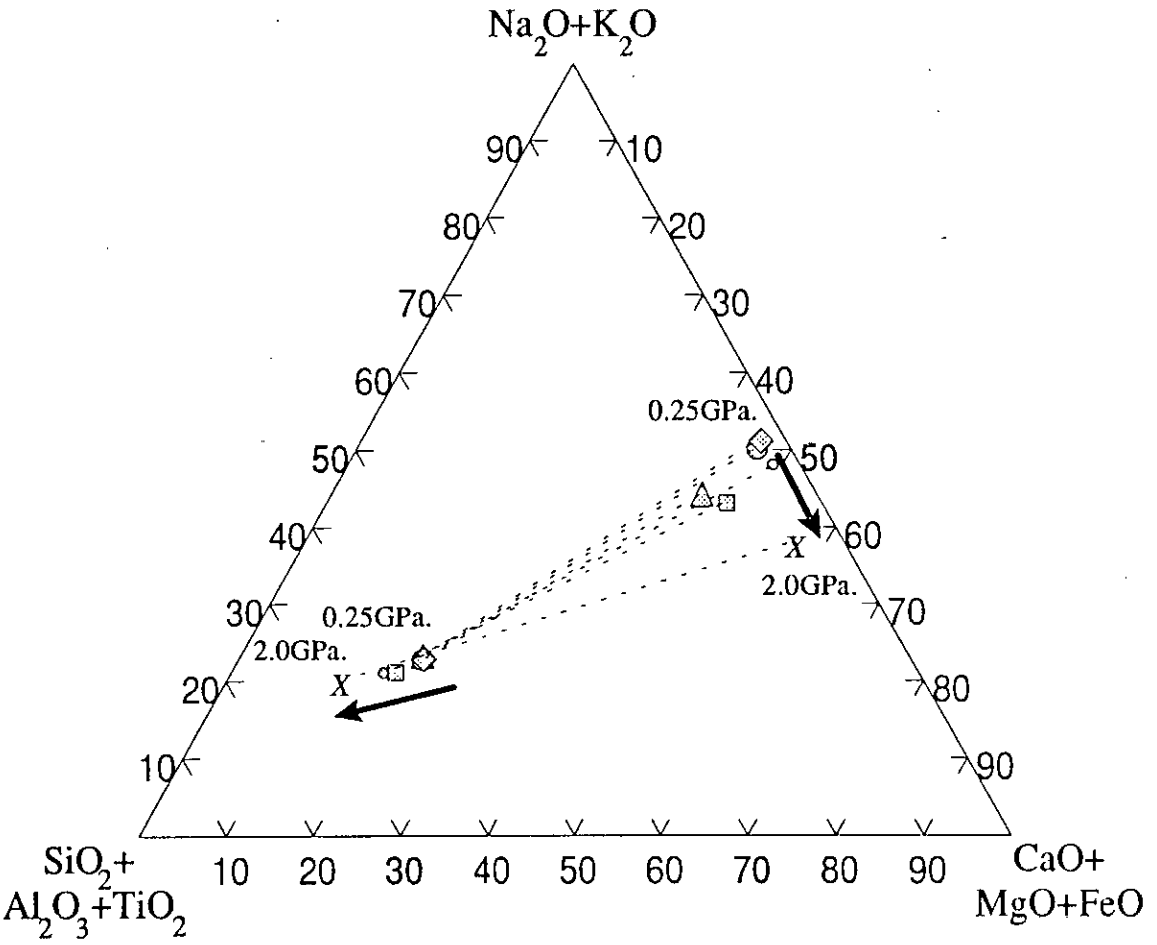

Figure 4.14. The effect of pressure on immiscibility in natural rock compositions. BD119+CNC at 1300°C, 0.2-2.0 GPa. Although partially obscured by scatter, coherent trends with pressure can be seen in both the carbonate and silicate melts. These are in agreement with the effects seen in the synthetic soda-melilite system (Figure 3.8).

The silicate melt compositions migrate towards the (SiO_2+Al_2O_3+TiO_2) apex of the triangular diagram with increasing pressure. This is interpreted as an increase in the compositional extent of immiscibility at high pressure. The same trend was seen in the synthetic compositions. In both systems, this has been attributed to the effects of pressure on interparticle interferences, leading to more extreme non-ideality, and thus making immiscibility more likely.

There is considerable scatter in the compositions of the carbonate melts. However, there is a general trend towards more calcic composition with increased pressure, as is seen in the synthetic system.

4.4.5. Set 5. Reproducibility of immiscibility.

As a check on the reproducibility of these experimentally produced liquids, three charges of BD119+CNC were run under identical conditions (Table 4.14). Conjugate liquids produced can then be compared with those of G5.3, already analysed.

Table 4.14. Starting compositions, conditions, and resulting assemlages from repeated experiments on natural rock carbonate-silicate immiscibility.

Run ident.	Composition (Wt.%)	Pressure (GPa)	Temperature (°C)	Time (Mins)	Assemblage
R1	75% BD119, 25% CNC	0.5	1200	60	Ls + Lc
R2	75% BD119, 25% CNC	0.5	1200	60	Ls + Lc
R3	75% BD119, 25% CNC	0.5	1200	60	Ls + Lc

All three experiments produced coexisting carbonate and silicate melts with identical textural relationships and quench characteristics. The compositions of these melts have been plotted in Figure 4.15 along with those of G5.3. They are consistent to within 1% error on both the silicate and carbonate limbs of the solvus. The small variations that are seen are attributed to analytical errors, and are in fact smaller than the maximum allowable variations due to quoted standard deviations of analyses. Experimentally-produced carbonate and silicate melts in natural systems can therefore be reproduced accurately.

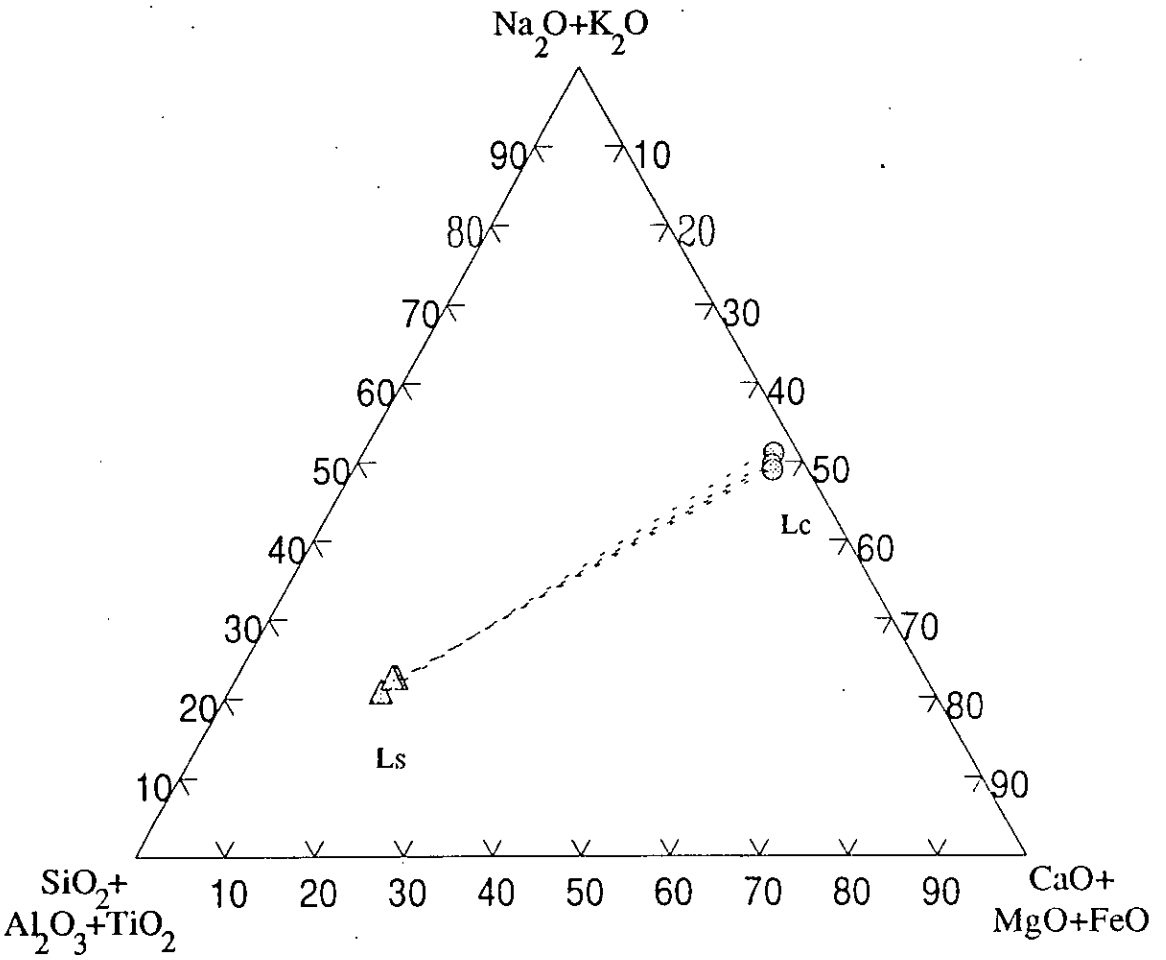

Figure 4.15. Reproducibility of coexisting immiscible liquids in natural rock compositions: nephelinite BD119+CNC at 0.5 GPa, 1200°C. Close grouping of the experimental liquid compositions shows that immiscibility experiments can be accurately reproduced.

4.5. Conclusions and implications.

Immiscible carbonate liquids have been produced in equilibrium with a wide range of natural silicate rock compositions (from silica-rich phonolite to olivine nephelinite). Coexisting liquids have been produced at 1100-1300°C, and 0.2-2.0 GPa. Immiscibility in melts with very high liquidus temperatures (e.g. BD105) could only be obtained as a small-scale phenomenon in the interstitial melt pools of mainly crystalline charges. This was due to mechanical constraints (the temperature limits of the available equipment) rather than chemical considerations. Overall, approximately 90 charges using natural silicate materials were run, of which *ca.* 60 produced super-liquidus assemblages containing coexisting carbonate and silicate quenches. Of these, 40 were deemed suitable for ion-probe study, on the basis of textural constraints over the size and position of representative sample areas. The experiments on natural rocks believed to be associated with immiscibility were successful in producing coexisting carbonate and silicate liquids for trace-element analysis on the ion probe.

More specific conclusions from this section include:

(a) Naturally occuring rocks of phonolitic, nephelinitic, and olivine nephelinitic compositions are in equilibrium with coexisting Ca-Na-Mg-carbonate melts of various compositions in the pressure range 0.2-2.0 GPa. Immiscibility extends from liquidus temperatures to at least 1300°C for all the compositions studied.

(b) Carbonate melts nearest in composition to the commonest carbonatites seen at the Earth's surface (i.e. Ca-Mg carbonatites with low Na-contents) were produced in equilibrium with an olivine nephelinite with *ca.* 8 wt. % Na_2O and 6 wt. % MgO at pressures of 0.25 and 0.5 GPa. These pressures represent depths of 7-15 km. Changing pressures, and changing conjugate silicate melt composition allows a whole spectrum of carbonate melt compositions to be produced by immiscibility.

(c) There is no evidence of closure of the two-liquid solvus with increasing temperature. Scatter of the data is considerable, so a small temperature effect is possible. In any case, both the carbonate and silicate limbs of the solvus are steep in the range 1100-1300°C, implying that the critical temperature for carbonate-silicate immiscibility in natural phonolites and nephelinites is substantially above 1300°C.

(d) As with the soda-melilite-carbonate experiments, no systematic changes in assemblage or liquid compositions were noted with increasing run durations in the range 15-960 mins. This implies that equilibrium in these super-liquidus assemblages was attained very rapidly, and that no systematic variations in physical conditions of the runs (i.e. P, T, and fO_2) were occurring over time. This also implies (because of exponential Fe-loss to the Pt capsules), that the effect of iron content on immiscibility is small.

(e) Pressure effects, although small, are consistent with those seen in the synthetic materials. Increased pressure produces a slight expansion in the compositional extent of immiscibility on the silicate limb of the solvus, whilst carbonate melt compositions become slightly more calcic with increased pressure.

(f) Experimentally-produced carbonate and silicate melt compositions in natural systems can be reproduced accurately.

Plate captions: Chapter 4.

Plate 4.1. Immiscibility textures in experiments on natural melt compositions.

A. Immiscibility in phonolitic charges. Clean separation of the two liquids occurs, with a central silicate slug (Ls) surrounded by a rind of carbonate (Lc). Charge from experiment G4.3. Scale bar is 1 mm.

B. The carbonate-silicate boundary (G4.3). The two quenched liquids (Ls is silicate quench, Lc is carbonate quench) are separated by a sharp, sub-micron meniscus indicating equilibrium coexistance. Scale bar is 20 μm.

C. Textures in nephelinitic charges (G2.5). There is a reversal of the relative roles of carbonate and silicate liquids in these charges, with spheres of carbonate quench (Lc) contained within silicate glass (Ls). Scale bar is 1 mm.

D. Textures in sodium-poor olivine nephelinitic charges (G2.6). Due to high solubility of carbonate in olivine nephelinitic melts, only a few percent of carbonate liquid is produced in these charges. Small spheres of carbonate (Lc) are found associated with vapour bubbles (V). Scale bar is 20 μm.

E. Textures on experiments containing primitive olivine nephelinites (ELG2 and BD105). Carbonate liquid (Lc) is only found when associated with silicate crystals (C), in this case clinopyroxene (G1.9). Scale bar is 20 μm.

Plate 4.2. Variations in two-liquid textures seen in natural compositions.

A. The most common texture seen is that of a central silicate sphere (Ls) surrounded by carbonate quench (Lc). Scale bar is 100 μm.

B. This simple case can be complicated by the presence of vapour bubbles (V). These bubbles can occur in both the carbonate and silicate liquids, indicating equilibrium coexistance. Scale bar is 20 μm.

C. During separation, spheres of Lc can remain isolated in Ls, and vice versa. This often occurs at the edges of the charge, where spheres remain in contact with the platinum (Pt) capsule. Scale bar is 10 μm.

Plate 4.3. Liquid separation in action: experiments of short run duration.

A. Formation of the carbonate rind by migration of small carbonate spheres through the silicate liquid: experiment G8.3. Scale bar is 100 μm.

B. In more basic compositions separation is faster, but numerous spheres of carbonate are still seen in the silicate melt after 15 minutes: experiment G8.4. Scale bar is 50 μm

C. Coalescence of a small silicate sphere with the main silicate body. This is seen in a charge run for 60 minutes showing that separation has yet to reach absolute completion. Scale bar is 20 μm.

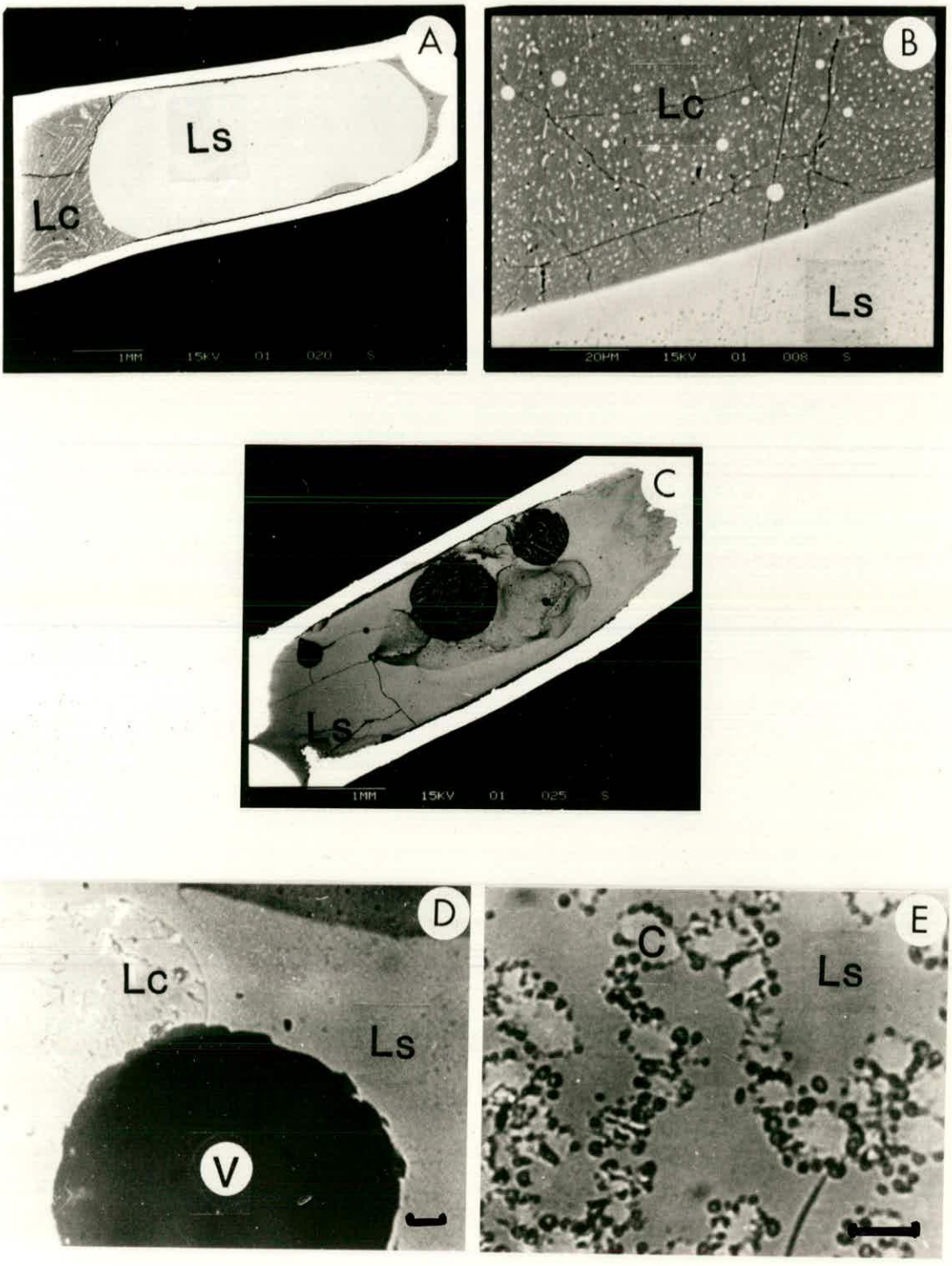
A
Ls
Lc
1MM 15kV 01 020 S
B
Lc
Ls
20PM 15kV 01 008 S
C
Ls
1MM 15kV 01 025 S
D
Lc
Ls
V
E
C
Ls

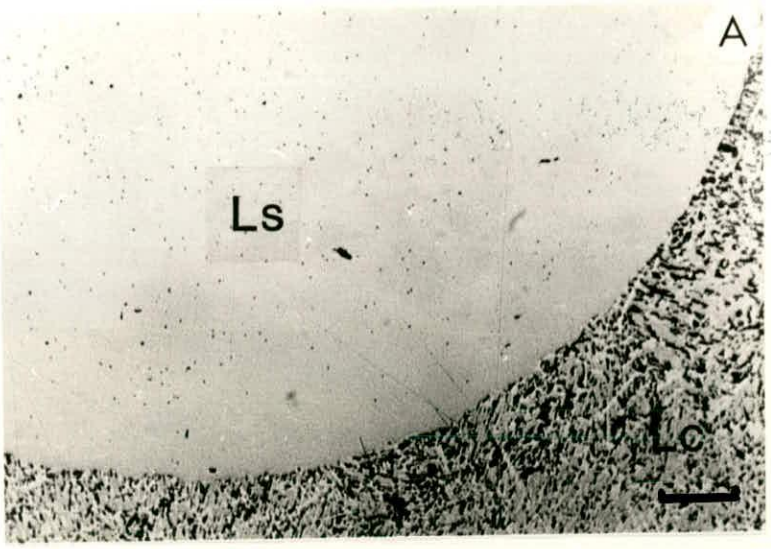
A
Ls
Lc

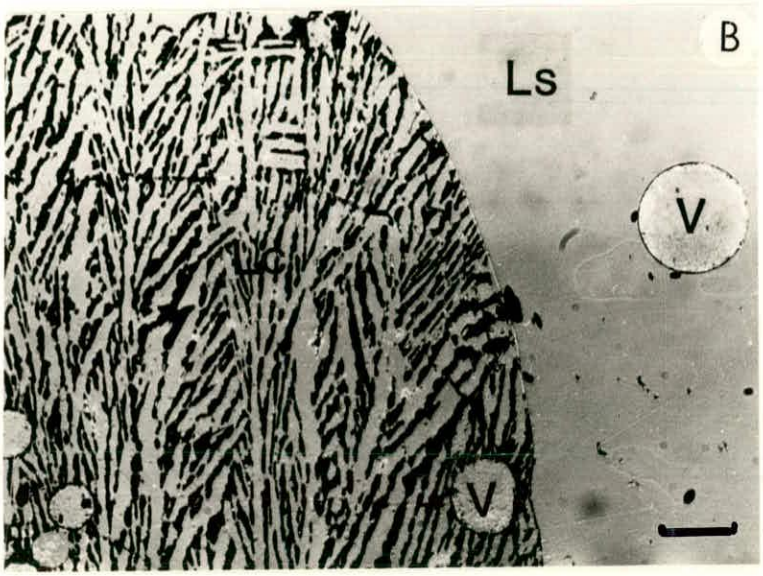
B
Ls
V
Lc
V

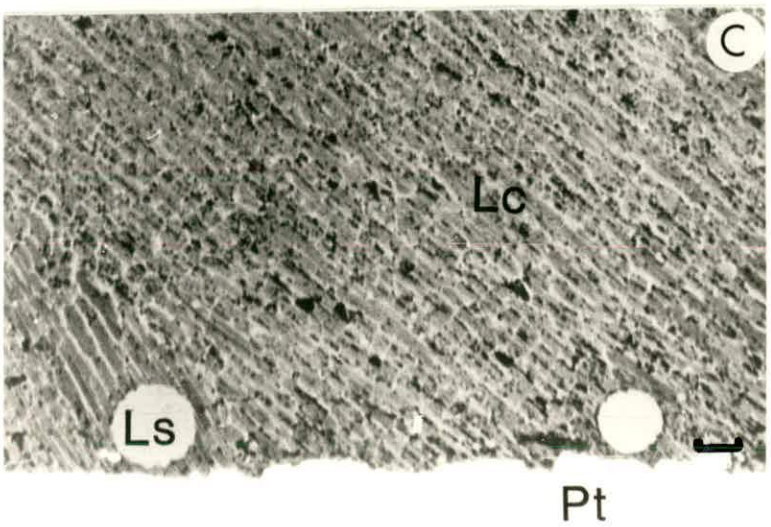
C
Lc
Ls
Pt

CHAPTER 5

EXPERIMENTAL LIMITATIONS AND DIFFICULTIES: A REVIEW.

5.1. Introduction.

As stated in the previous chapters, the aim of of these experiments was to obtain immiscible carbonate and silicate melts, over a range of pressures, temperatures, and melt compositions, with textural relationships that facilitated analysis of the two melts for trace-element concentrations on the ion probe. This aim has been achieved. However, there are a number of limitations in the experimental data-set produced which are likely to constrain the accuracy and applicability of the results. The major limitations, their cause, severity and resolution, will be discussed.

5.2. Constraints imposed on the experimental data-set by equipment and techniques.

The equipment available within the Experimental Petrology Unit at The University of Edinburgh comprises four major types:

5.2.1 Vertical quench furnaces for atmospheric pressure experiments.

Used in this study mainly to prepare starting materials under specific redox conditions, using controlled gas mixtures. Obviously of limited use in a study of high pressure phase-equilibria.

5.2.2. Cold-seal vessels.

Limited to moderately low temperatures (maximum *ca.* 1000°C), and low pressures (up to 0.15 GPa). External heating also means that highest temperatures can only be achieved at low pressure and *vice versa*. The resulting limitations on temperature made these vessels unsuitable for liquidus experiments on either natural rocks or synthetic analogues of relevance to this study.

5.2.3. Internally-heated gas-pressure vessels.

Although tested to 1.0 GPa, the safe practical limit for these vessels is nearer 0.8 GPa. Due to oxidation of the molybdenum furnaces, temperatures are limited to *ca.* 1300°C. This type of experimental equipment was employed for the bulk of the experimental work, limiting compositions under study to those with liquidus temperatures at or below 1300°C.

5.2.4. Solid-media piston-cylinder apparatus.

This equipment can operate up to 3.0 GPa with safety, and up to 1700°C. It was used for experiments on "primary mantle melt compositions", and experiments investigating the effects of pressure on immiscibility and partitioning in both natural and synthetic carbonate-silicate systems. Main constraints included small sample volume, pressure uncertainties, and poorly constrained fO_2.

To summarise, all experiments were limited to pressures of 3.0 GPa or less, with the best constrained experiments at <1.0 GPa, <1300°C.

5.3. Constraints due to the limits of carbonate-silicate immiscibility.

The presence of a field of immiscibility in any mixed component liquid implies extreme non-ideality of behaviour due to repulsive interactions between the components in the solution. The difference between the expected free energy of an ideal liquid (G_{ideal}) and the true free energy (G_{real}) is known as the excess free energy of mixing (G_{excess}) (see Figure 5.1). The size of G_{excess}, and therefore the likelihood of immiscibility, thus depends on the extent of repulsive interactions present in the solution. This in turn will depend on the physical and chemical conditions under which the solution exists. Pressure, temperature, composition, and redox condition are four variables in these experiments which can therefore exert control over the extent of immiscibility in carbonate-silicate systems.

5.3.1. The effect of pressure.

As pressure is increased, the particles in the mixed carbonate-silicate solution will be forced into closer proximity, resulting in an increase in mutual repulsive forces, and therfore an increase in G_{excess}. This would suggest that immiscibility should be more likely, and so more extensive compositionally, at higher pressure. An expansion in the size of the two-liquid field with pressure has been found both in this study (Figures 3.13., 3.30.), and in others (e.g. Freestone & Hamilton, 1980; Watson & Naslund, 1976). It is therefore possible that there will be a critical pressure (Pc) in carbonate-silicate systems below which immiscibility will not occur. It seems unlikely, from thermodynamical considerations, that an upper pressure limit to immiscibility will exist in carbonate-silicate systems. Pressure limitations on immiscibility are therefore not a serious constraint on the scope of this study.

5.3.2. The effect of Temperature.

As temperature is increased, the contribution of G_{excess} falls relative to G_{ideal} (G_{ideal} increases with temperature, G_{excess} is likely to remain constant), and thus immiscibility becomes less likely. We would therefore expect the field of immiscibility to contract with increasing temperature. This closure of the solvus has been noted in this study (Figure 3.6) and elsewhere (Freestone & Hamilton, 1980; Kjarsgaard & Peterson, 1991). There will therefore be a critical temperature (Tc) above which carbonate-silicate immiscibility will not occur. In this study Tc was not reached at 1300°C for natural rock and soda-melilite glass compositions; the temperature limits on immiscibility were thus also of little consequence to this study.

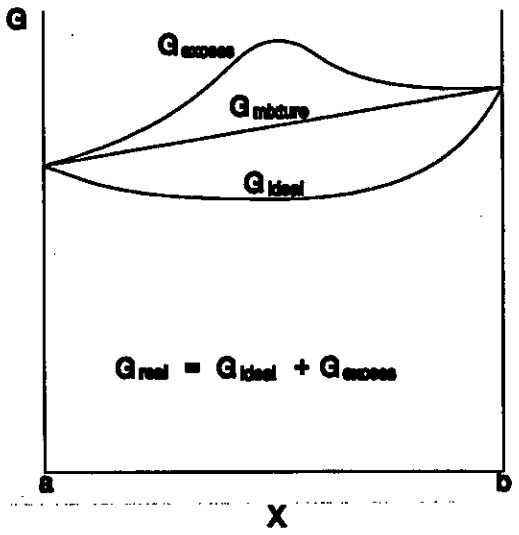

$G_{mixture}$ = Free energy of a mechanical mixture of components a and b.
G_{ideal} = Free energy of an ideal solution of a and b.
G_{excess} = Excess free energy caused by repulsive interactions of a and b. (A consequence of non-ideal behaviour).
G_{real} = Free energy of a real (non-ideal) solution.

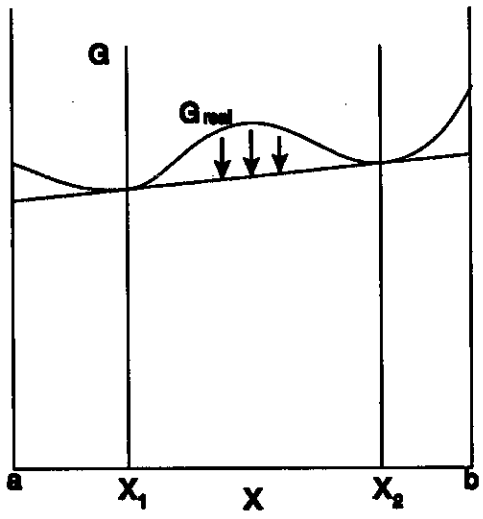

For any mixed composition between X_1 and X_2, the free energy of a homogeneous mixture is higher than the free energy of a mechanical mixture of liquid 1 and liquid 2.

Figure 5.1. Immiscibility as a thermodynamical consequence of non-ideality. A homogenous solution of bulk composition between X_1 and X_2 will spontaneously split into two immiscible phases, liquid 1 and liquid 2.

5.3.3. The effect of composition.

The size of repulsive interactions between particles in a solution is obviously going to depend on the nature of the particles present. Relating this concept to the carbonate-silicate system requires a knowledge of the structures, components and energetics involved in carbonate-silicate melts.

Silicate melt structures are now reasonably well understood (e.g. Mysen, 1990). They are believed to consist of silica-alumina anionic units in various states of polymerisation (called the "network") together with simple metal cations (known as "network modifiers"). The main variations in silicate melt structure are believed to be related to changes in the polymerisation state of the anionic units present; SiO4 and AlO4 can be present either as isolated tetrahedra, or combined as chains, rings, sheets etc. This characteristic of silicate melts has been quantified as the number of non-bridging oxygens per tetrahedrally coordinated metal cation (NBO/T). If NBO/T is high, the silicate melt is extensively depolymerised, whilst low NBO/T implies highly polymerised aluminosilicate units.

Carbonate melt structures have not been studied in as much detail. However, they are believed to approximate molten ionic salts and will thus consist of a mixture of positively and negatively charged ions. Variations in this structure are likely to be limited to differing complexing behaviour between the ions present.

It seems likely that the major sources of repulsive interactions caused by mixing of these two end member liquids will involve those molecules most extremely partitioned between the two phases. SiO_2 and Al_2O_3 are most strongly partitioned to the silicate melt, whilst CO_2 and P_2O_5 are most strongly partitioned to the carbonate. It is therefore suggested that the molecular interactions causing immiscibility in carbonate-silicate systems are dominantly between the polymerised aluminosilicate network and CO_3^{2-} and PO_4^{3-} ions. Breakdown of the polymerised aluminosilicate units, producing SiO_4^{4-} tetrahedra may therefore lead to a decrease in these repulsive interactions, and so to a decrease in G_{excess}. If this simple-minded approach is reasonable, immiscibility would be expected to become less likely as the silicate melt becomes more depolymerised. This may limit immiscibility to more evolved rock compositions with relatively high NBO/T, and could also explain why primary mantle silicate melt (consisting virtually completely of depolymerised SiO_4^{4-} tetrahedra) could not be made to coexist with carbonate melt. In the case of

depolymerised silicate melts, a carbonate-silicate mixture will be energetically more stable than coexisting immiscible liquids. This analysis of the effects of silicate melt structure on immiscibility seems more logical thermodynamically than the suggestion by some authors that sodium content is the primary control on the presence or absence of immiscibility (e.g. Freestone & Hamilton, 1980; Baker & Wyllie 1990).

There may well be a compositional limit to immiscibility which is related to the polymerisation state of the silicate liquid. It seems likely from these experiments, and those undertaken previously, that this compositional control constrains carbonate-silicate immiscibility to more evolved silicate compositions, and is therefore a major limiting factor on the applicability of this study to petrogenetic problems.

5.3.4. The effects of redox conditions.

Oxidation state is important in controlling the molecular species that are likely to be present in a solution, and therefore interactions between them. SiO_4^{4-}, AlO_4^{5-}, and more polymerised aluminosilicate units are stable over a very wide range of fO_2 conditions. They are the only forms of silicon and aluminium likely to be present in natural melt systems. The CO_3^{2-} ion is much more susceptable to changes in redox state, only being stable in relatively oxidising conditions. As conditions become more reduced the CO_3^{2-} ion is replaced by CO, C, and finally CH_4 (Eggler *et al.*, 1976). Study of carbonate-silicate immiscibility is therefore restricted to relatively oxidised conditions, and in order to ensure the presence of immiscibility, charge compositions were pre-set to fO_2 equivalent to NNO reference buffer, where CO_3^{2-} is known to be stable. The various experimental assemblies used are also thought to buffer to near NNO.

5.4. Experimental problems.

A number of experimental problems were encountered which need to be commented upon. In order, the problems addressed will be iron loss to the Pt capsules used, crystallisation of the experimental charges, presence of coexisting immiscible CO_2-rich vapour with the carbonate and silicate liquids, and some effects seen at the carbonate-silicate meniscus.

5.4.1. Fe-loss.

In systems containing FeO as a major component, substantial loss of Fe to the sample capsule can occur with time. Table 5.1 shows that for all the charge compositions studied in the experiments on natural rocks, significant fall in the FeO content of the coexisting silicate liquid can be seen with time at 1300°C, 0.8 GPa. It must be stated that these are the worst conditions used for Fe-Pt alloying to take place, and that those experiments run at lower pressures and temperatures will have suffered less Fe-depletion.

Table 5.1. FeO contents (wt. %) of conjugate silicate liquids at 0.8 GPa, 1300°C. Note the exponential fall in Fe-component of charge with time due to Fe-loss to the Pt sample container.

Duration in mins.	15	60	360	960
BD50+CNC	2.48	1.19	0.42	0.31
BD119+CNC	5.80	3.31	2.63	0.99
BD119+CC	5.28	3.57	2.69	1.11
SUN189+CNC	6.44	3.91	3.63	2.25
SUN189+CC	6.78	5.03	4.85	2.87

A graphical representation of the effects of Fe alloying with the Pt capsule is shown in Figure 5.2. It can be seen that the FeO component in the silicate melt is decreasing exponentially with run time. This process is not however seen as a major problem as it allows us to study the effect of variable FeO components on immiscibility and element partitioning behaviour. The soda-melilite glassses will represent FeO-free liquids, whilst those natural rock compositions that were at P and T for short periods of time still contain FeO concentrations appropriate to natural compositions.

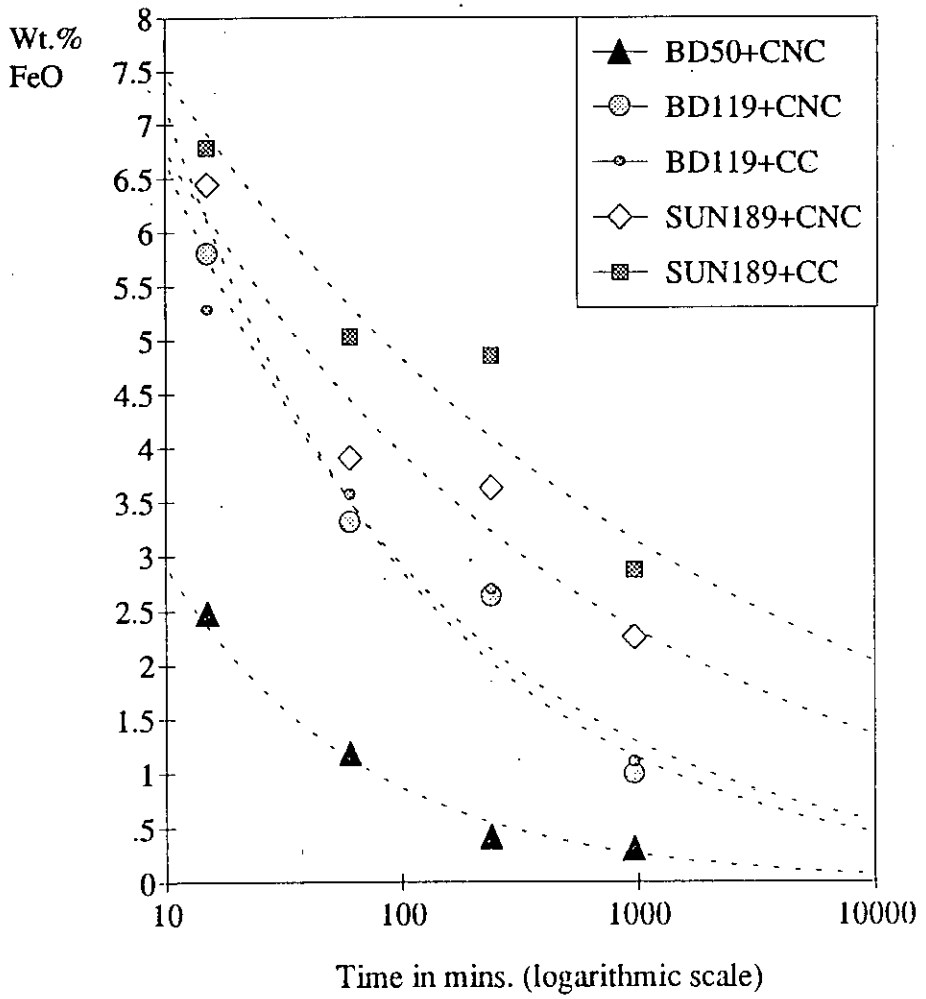

Figure 5.2. Iron contents of charges vs. time. Significant iron loss to the sample capsule occurred in all charges run at 0.8 GPa, 1300°C. After 60 mins (the run duration of most experiments) *ca.* 60% of the original iron content remains. Dotted lines are regressions through individual data series, showing exponential loss of FeO-component with time.

5.4.2. Crystallisation of experimental charges.

Crystallisation of charges was a major limitation on the rock compositions studied. If the run temperature is below the liquidus temperature of the starting materials, crystals will be present in the charge. This crystallisation will affect the compositions and structures of the coexisting carbonate and silicate melts produced, and therefore make comparative study difficult. It was decided that super-liquidus assemblages were preferable, and that any charge containing a significant proportion of crystals would be rejected. This severely limited the extent to which high-liquidus primitive melt compositions could be studied.

Although the experiments were designed to be vapour-absent (sintered starting materials, mixes scrupulously dried before runs, only stoichiometric CO_2 added), a number of the immiscible carbonate and silicate liquid pairs were seen to coexist with a CO_2-rich vapour phase. Quench spheres, produced by solute exsolving from the vapour on cooling, were not identified, and it is therefore believed that this CO_2-rich vapour contained only small amounts of dissolved oxides. This is in agreement with the studies of Meen (1989) and others, suggesting low solubilities in CO_2-rich vapour. It is possible, however, that the presence of fluid will affect the contents of certain elements in the coexisting liquids, most probably K, Rb, Cs, Na, F and Cl, all of which are believed to have a significant solubility in fluid. If we assume that the fluid, where present, is in equilibrium with the coexisting liquids, we can conclude that it should have no effect on carbonate-silicate partitioning equilibria. Charges containing coexisting vapour have therefore been included for further study.

5.4.3. Boundary effects at the carbonate-silicate meniscus.

Boundary effects have been discovered in a number of systems involving liquid immiscibility. A study was therfore undertaken to investigate the possibility of variations in liquid compositions on approaching the carbonate-silicate meniscus in these experimental charges. The carbonate melt could not be studied in this way due to heterogenous quenching, so analysis of compositions was limited to the silicate melt. Figures 5.3-5.6 shows that variations in major- and trace-element concentrations in the silicate liquid were seen as the Ls-Lc meniscus was approached. Concentrations of all the Group IA elements increased systematically towards the meniscus over a distance of *ca.* 20 μm. Group IIA elements were seen to display the opposite behaviour, with systematic decreases towards the Ls-Lc meniscus. This second trend was also seen in Mg, Fe, Mn, and the REEs.

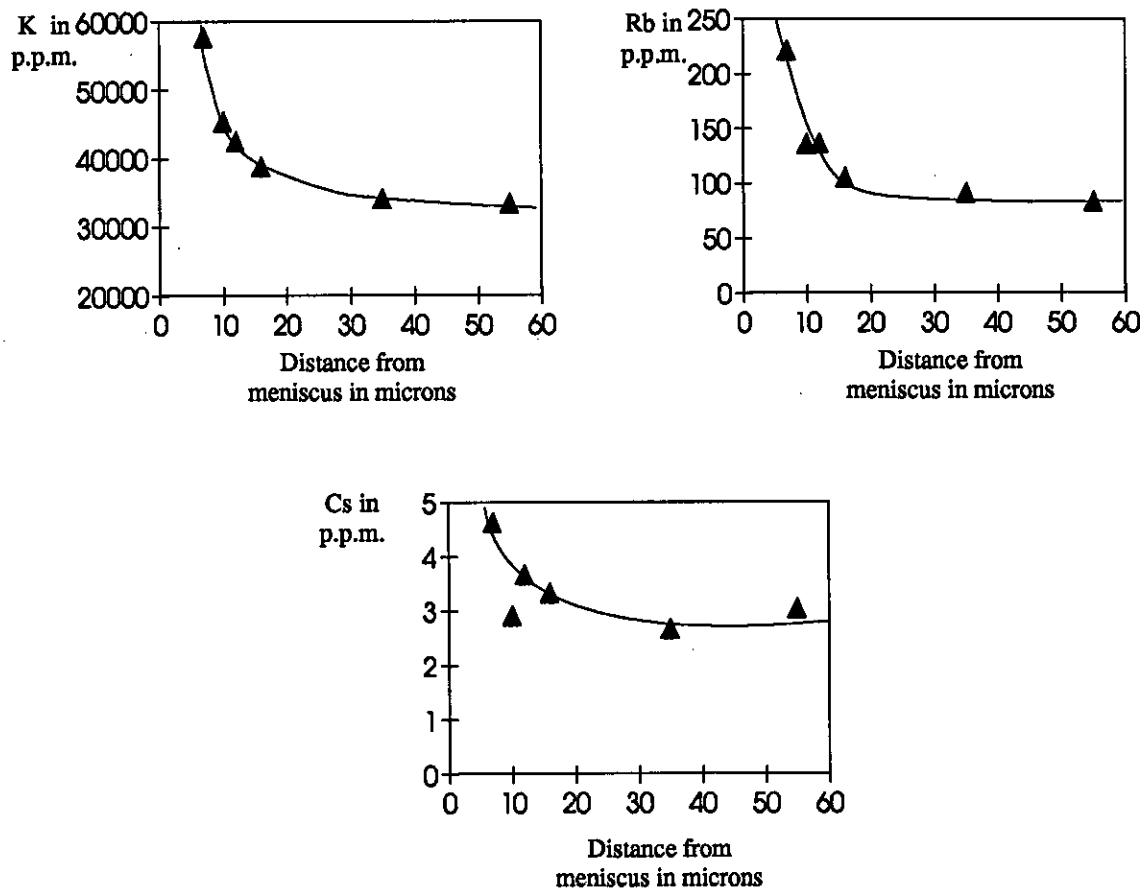

Figure 5.3. Variations in concentrations of group IA elements in silicate melt with distance from the carbonate-silicate meniscus. A systematic increase in concentrations is seen as the Ls-Lc boundary is approached. Analyses are from 25-micron diameter ion-probe pits in the silicate glass of BD119+CNC starting composition, run at 1200℃, 0.25 GPa.

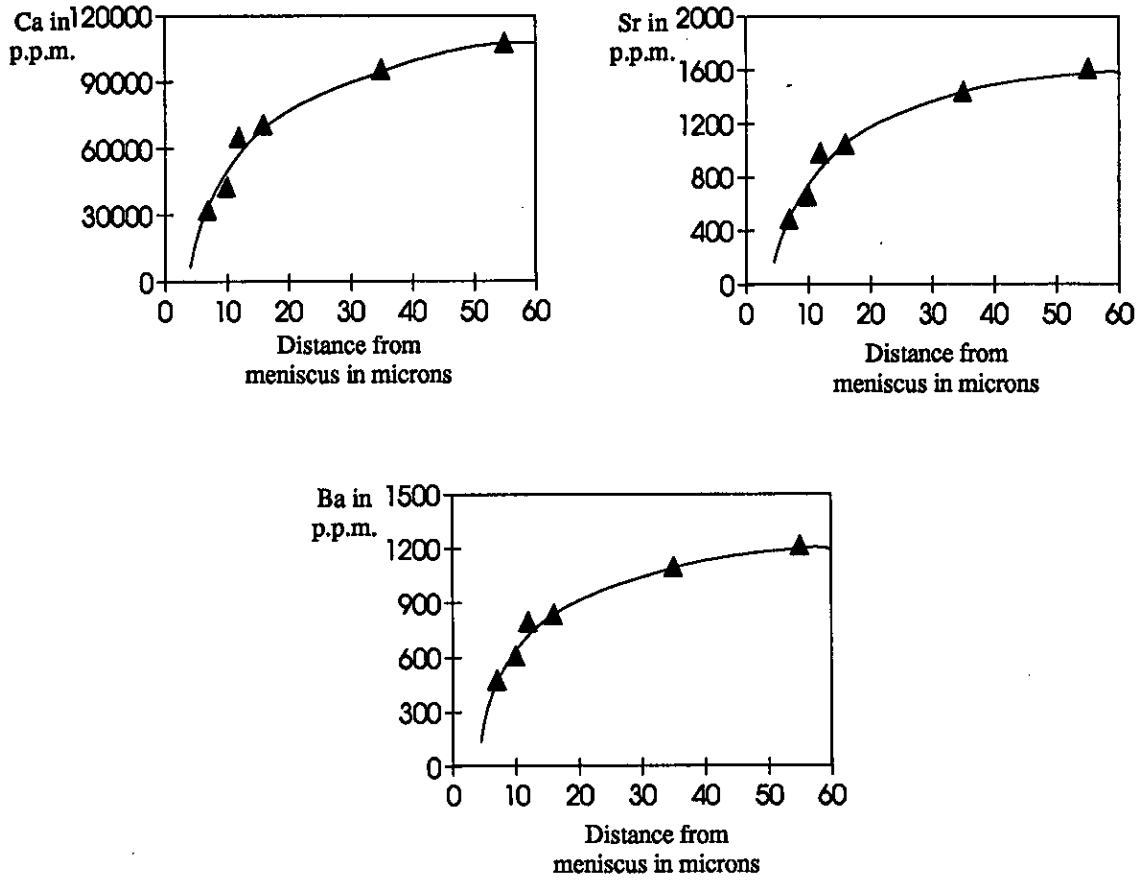

Figure 5.4. Variations in concentrations of group IIA elements in silicate melt with distance from the carbonate-silicate meniscus. A systematic decrease in concentrations is seen as the Ls-Lc boundary is approached. Analyses are from 25-micron diameter ion-probe pits in the silicate glass of BD119+CNC starting composition, run at 1200 ℃, 0.25 GPa.

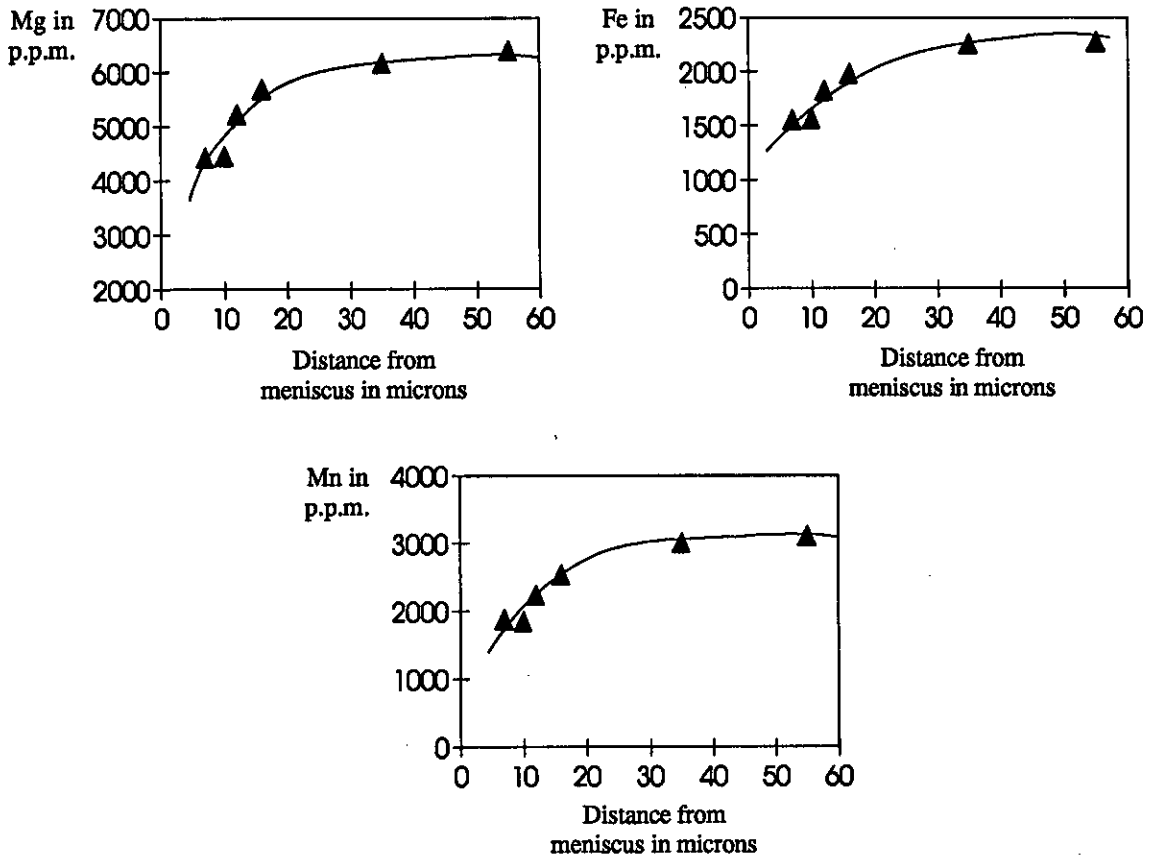

Figure 5.5. Variations in concentrations of Mg, Fe and Mn in silicate melt with distance from the carbonate-silicate meniscus. A systematic decrease in concentrations is seen as the Ls-Lc boundary is approached. Analyses are from 25-micron diameter ion-probe pits in the immiscible silicate glass of BD119+CNC starting composition, run at 1200°C, 0.25 GPa.

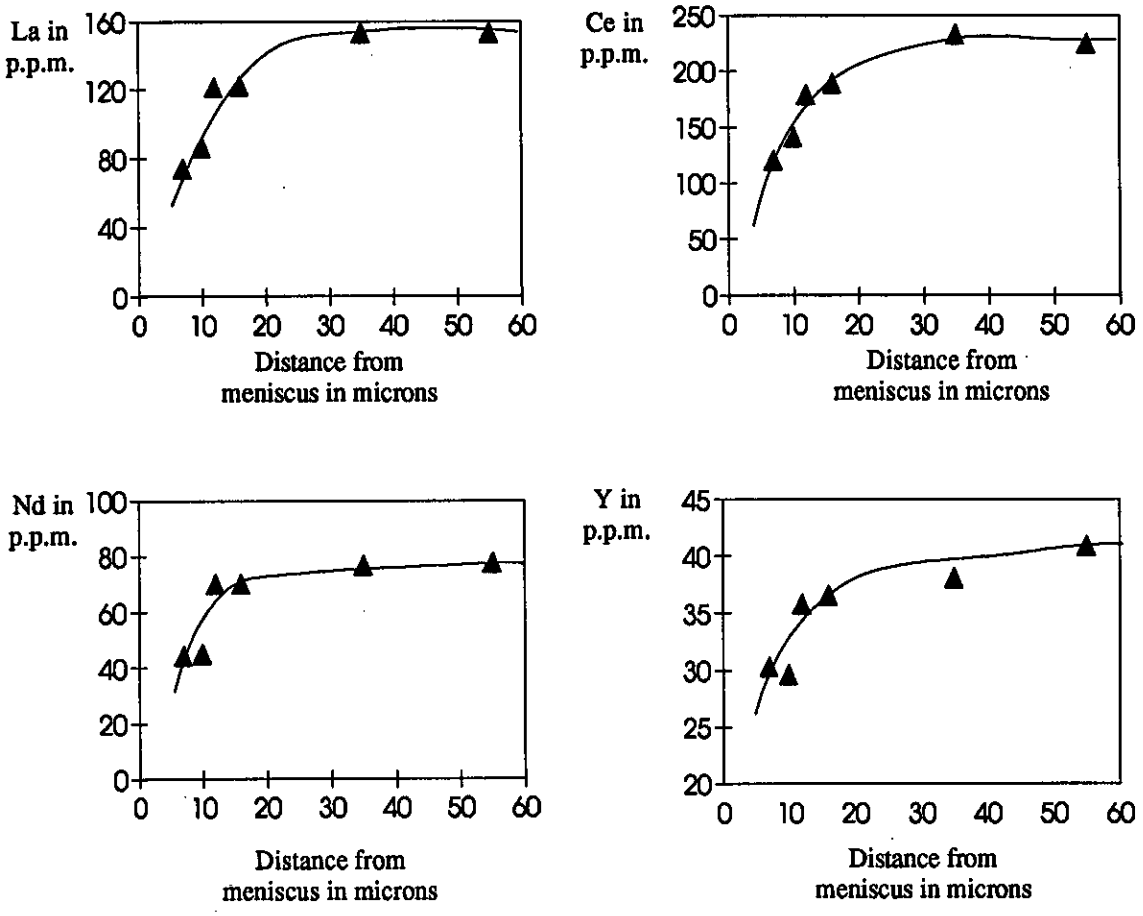

Figure 5.6. Variations in concentrations of REE in silicate melt with distance from the carbonate-silicate meniscus. A systematic decrease in concentrations is seen as the Ls-Lc boundary is approached. Analyses are from 25-micron diameter ion-probe pits in the silicate glass of BD119+CNC starting composition, run at 1200 ℃, 0.25 GPa.

It is difficult to reconcile this behaviour with that expected if these were simple quench effects. For example, both Cs and Ba are enriched in the carbonate melt, and would therefore be expected to behave similarly on quenching. They in fact behave in the opposite manner to each other. It is therefore suggested that these results may be due to the energetic influence of the Ls-Lc boundary on the relative activities and stabilities of elements in the silicate melt. The +1 charge cations seem to be attracted towards the Ls-Lc boundary, whilst the higher valency cations are repelled. This has been interpreted as adsorption of alkali metal cations on to the carbonate-silicate interface which presumably lowers the surface energy of the boundary, and therefore affects the two-liquid textures produced. If this is the correct interpretation of the patterns of concentration seen, then a similar distribution of elements would be expected to extend into the carbonate melt, again over a distance of *ca.* 20 μm. However, if this is a quench effect, then variations in concentrations in the carbonate intergrowth would be expected to extend much further due to faster diffusion rates. Peterson (1990) suggested that diffusion rates in carbonate melt were *ca.* 5 times as fast as in silicate melt, whilst work on iron diffusion under mantle conditions suggested that diffusion rates in carbonate liquid could be an order of magnitude faster than those in basaltic melt (Minarik & Watson, 1991). Boundary effects could extend up to 200 μm or more into the carbonate quench. In either case, bulk analysis of concentrations of trace elements will give erroneous results, and any spot analyses must be made well away from the Ls-Lc boundary.

5.4.4. Quenching of the run products.

The final part of any experiment is the "freezing" of phases produced under the run conditions so they can be studied in detail at room P and T. *In situ* study, although vastly preferable to the above proceedure, is at present limited to identification of a few simple properties. Trace-element concentrations are certainly not obtainable at P and T.

"Freezing" of phases produced at run conditions is achieved by rapid quenching of the charge. The temperature is lowered from run to room conditions as fast as possible by water-flow cooling systems. However, in the case of carbonate-bearing systems, this process is not fast enough to maintain the high temperature phases, and allows acicular quench crystals of carbonate minerals to form from the carbonate liquid. This heterogeneity in the run products has led to an increase in the analytical uncertainties associated with assessing liquid compositions. The nature of these quench products will be investigated in Chapter 6.

5.5. Conclusions.

The above experimental limitations have placed constraints on the form of carbonate-silicate immiscibility produced, as well as limiting the P-T-X range over which these melts can be studied. They do not however invalidate this approach as a means of studying carbonate-silicate equilibria. With hindsight, new and different experimental proceedures could perhaps have led to the eradication of some of the above constraints (e.g. vertical, rapid-quench gas-media vessels, control of fO_2 conditions with accurate redox sensors, Fe-presaturated capsules etc.). These experimental limitations should therefore be considered in advance of any further studies in carbonate-silicate systems.

CHAPTER 6

AN ANALYTICAL STUDY OF EXPERIMENTALLY PRODUCED CARBONATE AND SILICATE LIQUIDS

6.1. Introduction.

The coexisting carbonate and silicate melts produced in the experiments described in Chapters 3 and 4 have been analysed by a number of techniques. An optical and textural study was undertaken to investigate phase relationships. Major and trace-element chemistry of coexisting phases were determined by electron probe and ion probe. By combining textural and chemical information it was hoped to:

(a) obtain trace-element concentrations in the experimentally produced carbonate and silicate melts, and thus calculate $^{Ls/Lc}D_i$ partition coefficients.

(b) gain an understanding of the major-element compositions of the coexisting melts, and their relationship to each other. This will provide a context into which the partitioning data can be placed.

Since the final interpretation of the data requires detailed knowledge of the accuracy of the partitioning database, this chapter sets out the analytical techniques employed, and attempts to quantify the possible sources of error.

6.2. Preparation of the experimentally produced charges for analytical work.

6.2.1. Introduction.

The sample charges were recovered from the experimental assembly, after quenching from run conditions, still sealed inside their 2 mm or 3 mm Pt capsules. For electron and ion microprobe analysis, an even, well polished, flat surface is required. Difficulties were encountered in producing such surfaces on the experimental charges. A procedure was therefore established which could transform the samples from their post-run configuration into this analysable state without damaging the two-liquid textures, and without modifying the compositions of the phases present. After much trial and error, a strict sequence of actions was adopted for this sample preparation, the main points of which are discussed below. Figure 6.1 is a flow diagram illustrating the processes and procedures involved.

6.2.2. Mounting.

Immediately after retrieval from the experimental assembly, encapsulated samples were weighed to check for mass-loss during the run. Where significant mass-loss was found, it was usually associated with an obviously burst capsule. Such samples are believed to have lost at least some of their CO_2, and were therefore discarded. After weighing, the experimental charge, still sealed in its Pt capsule, was mounted in Araldite epoxy resin within a 1/2" diameter aluminium ring. The Araldite took up to 12 hours to harden, during which time the mounted capsule was kept at >50°C, on a heated plate. The sample was mounted whole as the two-liquid textures produced at high pressure would then be retained for study. The mounting was made with the sample capsule still sealed, as its removal was thought likely to damage the fragile carbonate part of the charge.

6.2.3. Grinding.

The mounted charge was then ground down using 180-600 grade carborundum laps until a flat surface showing Ls-Lc textures was thought to be exposed. During the grinding process, no water was allowed to come into contact with the samples as the quenched carbonate melt contains a sizable component of deliquescent Na_2CO_3 and K_2CO_3. It is certainly partially soluble in water. Paraffin was therefore used as the

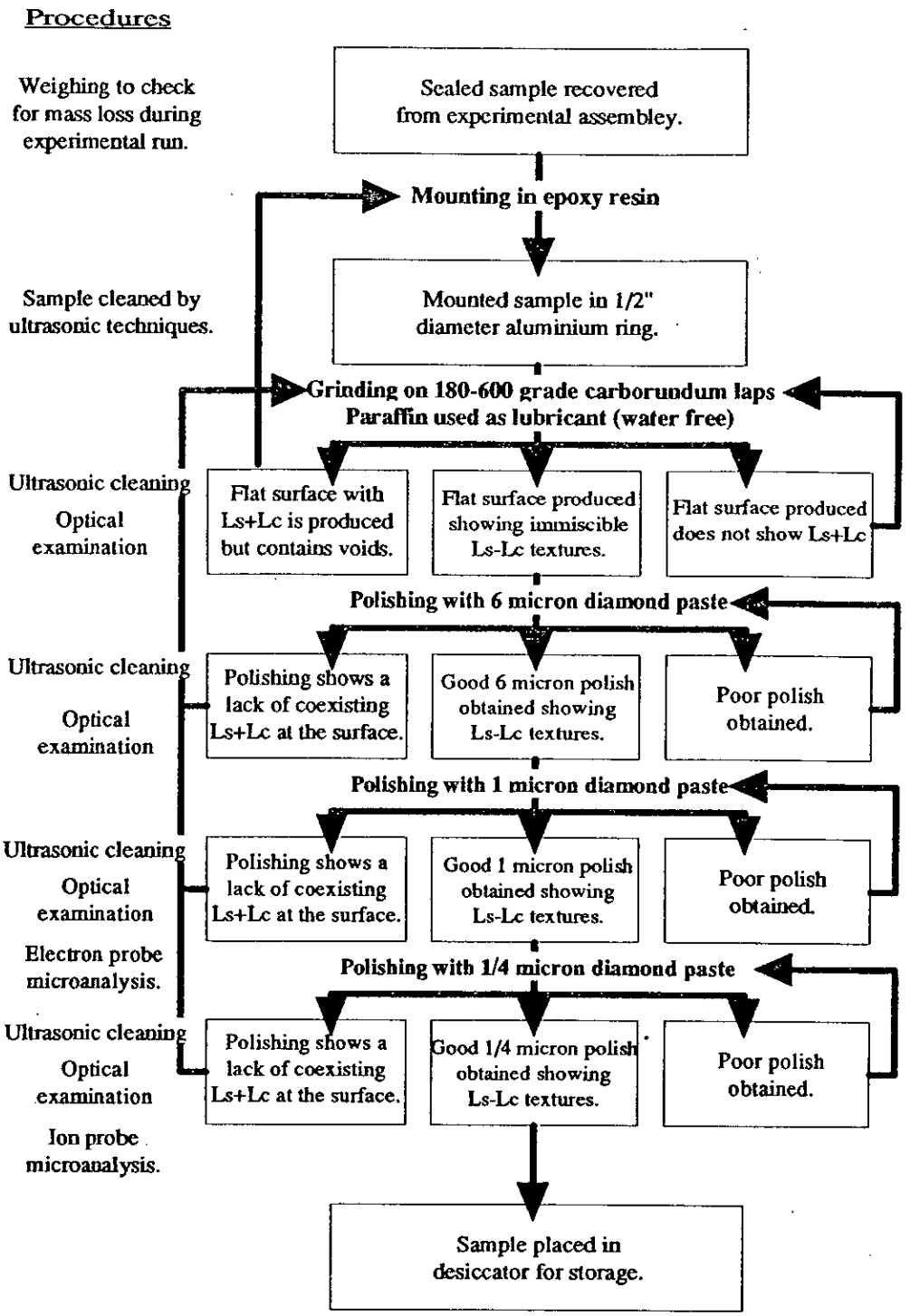

Figure 6.1. Flow diagram illustrating sample preparation techniques.

grinding lubricant. Despite using this effective lubricant, even grinding was difficult due to the very soft nature of the carbonate quench. Fragments of carbonate were often lost. If the sample contained voids, or areas of plucked-out material, a further layer of hot (and therefore very low viscosity) Araldite was poured slowly on to the sample surface. Due to the wetting characteristics of Araldite, any Ls-vapour or Lc-vapour surface was quickly engulfed, and voids therefore filled. This had a two-fold effect: firstly, it meant that a flat, smooth surface without voids was obtained, and secondly, it glued the carbonate material together, stopping any further plucking. In a few instances this process of remounting in Araldite had to be repeated a third time as further grinding had led to the uncovering of further vapour bubbles.

6.2.4. Polishing.

Once a smooth, flat surface was obtained, polishing could begin. Initial polishing was undertaken with 6 μm diamond paste on rotating cloth laps. Hy-prez[1] fluid was used as the polishing lubricant. Again water was avoided throughout the polishing process, and any washing/cleaning of samples or equipment was made in petroleum ether beakers, shaken by an ultrasonic bath. The carbonate quench was much softer than the silicate glass, and was noticeably recessed relative to the silicate on the ground-down surface. It therefore often required very long polishing times to produce a reasonable 6 μm polish over the whole charge. Initial identification of two-liquid textures on unpolished surfaces was difficult, and often incorrect; in a number of cases it was obvious after polishing that coexisting liquids were not exposed at the surface. These charges were therefore returned to grinding where a new surface was obtained.

Once a good 6 μm polish was produced, charges were cleaned thoroughly before polishing on a new lap with 1 μm diamond paste. These were then cleaned ultrasonically before analysis by optical methods, and characterisation by electron microprobe. Those samples analysed by ion microprobe, or S.E.M. techniques, were further polished with 1/4 μm paste. Polished samples were stored in a desiccator until analysis.

[1] a trade name for an organic, water-free fluid produced by Engis Ltd. Maidstone, Kent.

6.3. Optical analysis of textures and phase relationships.

6.3.1. Introduction.

Optical analysis of the experimental charges was undertaken to:

(a) identify the phases present in the experimental run products.

(b) investigate the two-liquid textures obtained in terms of both textural equilibrium, and surface behaviour.

(c) investigate the effects of quenching on the carbonate and silicate melts.

Phase identification, and phases present have already been discussed in Chapters 2-4. This section will therefore concentrate on textural relationships, and quench effects.

6.3.2. Analytical techniques.

All charges were studied and photographed at low magnification (X16) in reflected light, using a WILD Photomakroskop M400. Charges with good polish and clear textural features were studied at higher magnifications (up to X160) using a Carl Zeiss Ultraphot II. This instrument was also used in the measurement of contact angles discussed in 6.3.3.

A limited number of charges were prepared for analysis under a scanning electron microscope (S.E.M.). Back-scattered electron imagery of these charges concentrated on effects at the Ls-Lc meniscus. Those charges showing the coarsest quench textures were also studied, in an attempt to constrain quench processes.

6.3.3. Analysis of the textural relationships between phases.

The majority of experimental charges contained super-liquidus assemblages either of coexisting Ls+Lc, or of Ls+Lc+V. A number of charges were restricted to sub-liquidus conditions due to high liquidus temperatures; in these, Ls+Lc+Xtls textures could be investigated. A brief summary of the relationships between phases in each of the above assemblages is given below.

Ls-Lc textures.

In all the run products studied , a sharp, sub-micron meniscus separates the carbonate and silicate liquids. No signs of reaction or mixing could be seen, implying equilibrium coexistence. As would be expected for two relatively low-viscosity immiscible liquids, the Ls and Lc phases are arranged in such a way as to minimise the surface area of Ls-Lc interface. This can be interpreted as the lowest possible interfacial energy for the system, suggesting that textural equilibrium has been approached. The lowering of interfacial surface area manifests itself as the production of spherical masses of one liquid within the other. Smith (1948) stated that the liquid on the inside of the sphere (i.e. towards the centre of curvature) has a greater surface tension, and therefore stronger bonding forces within the liquid (See Figure 6.2a). In the case of carbonate-silicate immiscibility, the commonest texture consists of a central near-spherical slug of silicate, surrounded by a rind of carbonate (e.g. Plate 6.1). The silicate melt therefore has the stronger liquid bonding forces. This texture is clearly displayed between sodium-rich carbonate melt and phonolitic silicate melt. It is less obviously the case between calcic carbonate melt and nephelinitic melt. In this case isolated spheres of carbonate often occur within the silicate melt (e.g. Plate 6.2), implying a reversal of the relative surface tensions. It must be stated that in some charges both Lc spheres in Ls, and Ls spheres in Lc are identified. This is seen most commonly in those charges run for 15 mins, and can therefore be explained as a disequilibrium, or perhaps metastable, textural state.

Ls-Lc-V textures.

The presence of vapour inhibits the complete separation of Ls and Lc, often resulting in numerous areas of Lc and V within Ls (Plate 6.3). It is assumed that the addition of vapour results in the production of situations where metastable conditions are reached. In these situations, passage through a higher energy state than the one preserved would be required for textural equilibrium to be reached. An example of this would be where Lc completely surrounds a vapour sphere. Removal of the carbonate melt to the edge of the charge to produce complete liquid separation would result in an increased area of Ls-V boundary and thus, perhaps, higher overall surface energy.

2.a. Boundary between two immiscible liquids.

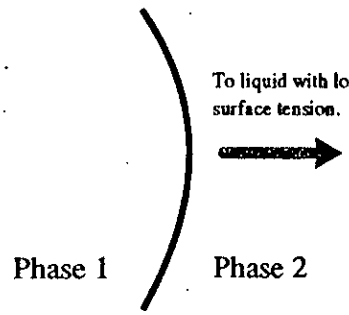

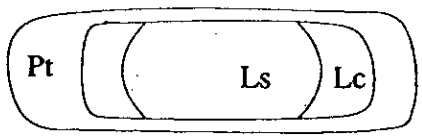

Stylized Ls-Lc immiscibility relationships in Na-rich charges.

2.b. Interfacial angle between three immiscible liquids.

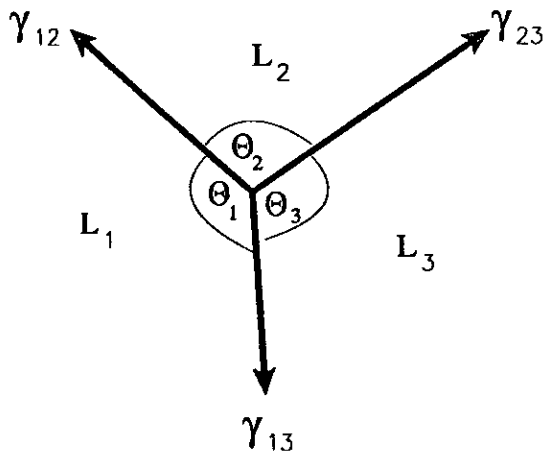

Figure 6.2. Quantification of textural relationships between immiscible liquids. (Smith, 1948).
(a) A two-liquid meniscus is convex towards the liquid with the lower surface tension. In Na-rich compositions showing carbonate-silicate immiscibility, the meniscus is convex to Lc, implying lower surface tension, and therefore weaker binding forces within the carbonate liquid.
(b) The sizes of the interfacial angles between three liquids will depend on the relative magnitudes of the three interfacial energies. Contact angles seen in Ls+Lc+V charges vary with composition and pressure, implying changes in relative size of Ls-V, Lc-V, and Ls-Lc boundary energies.

The presence of coexisting CO_2-vapour can be considered as equivalent to having a third immiscible fluid. The angles at which three fluid phases meet will give us an indication of their relative surface energies, and perhaps give an insight into controlling factors which influence liquid bonding behaviour.

In the case where three fluid phases intersect, the sizes of the three interfacial angles will depend upon the magnitude of the three conflicting interfacial energies. This is shown diagramatically in Figure 6.2.b, and can be quantified by trigonometry (Smith, 1948).

$$\gamma_{sc} / \mathrm{Sin}\theta_v = \gamma_{sv} / \mathrm{Sin}\theta_c = \gamma_{cv} / \mathrm{Sin}\theta_s \qquad (6.1)$$

Where γ_{sc} = Interfacial energy of the Ls-Lc boundary.
γ_{sv} = Interfacial energy of the Ls-V boundary.
γ_{cv} = Interfacial energy of the Lc-V boundary.
θ_v = Angle of Vapour at contact.
θ_c = Angle of Lc at contact.
θ_s = Angle of Ls at contact.

This equality has been used to investigate the relative sizes of γ_{sc},γ_{sv}, and γ_{cv} by obtaining contact angles at Lc-Ls-V triple junctions over a range of compositions and pressures. Coexisting vapour is commonest in the siliceous, Na-rich BD50+CNC charges, and the basic, Na-poor SUN189+CC charges. These compositions have therefore been studied in detail. *Ca.* 40 contact angles have been measured in each of these compositions. The results are given in Table 6.1, together with weighted averages, and the derived relative magnitudes of the interfacial energies.

In sodium-rich compositions, γ_{sv}, the interfacial energy of the silicate-vapour boundary, is much larger than γ_{cv} the corresponding energy of the carbonate-vapour boundary. This leads to a low angle of intersection of the Ls-Lc boundary with vapour spheres, and thus gives rise to textures seen in Figure 6.3, with carbonate melt surrounding the vapour bubbles, and "wetting" Ls-vapour junctions (Plate 6.3). The surface area of Ls-V contact has therefore been reduced to the lowest possible amount by this wetting process.

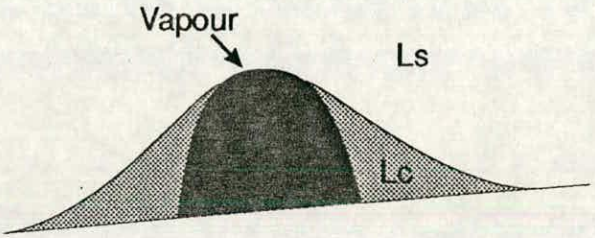

G1.3.

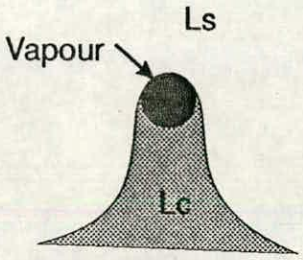

G13.1.

Approximate scale: x25

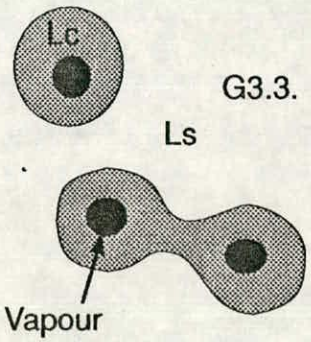

G3.3.

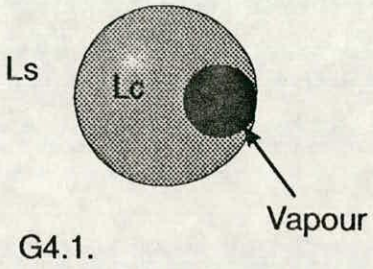

G4.1.

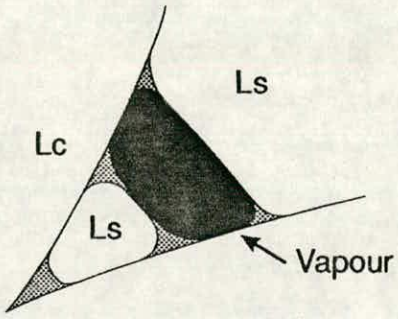

G9.1.

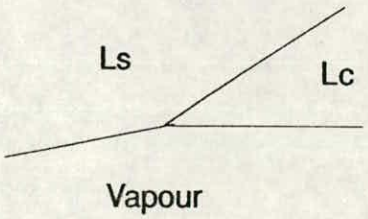

Schematic view of contact angles.

Figure 6.3. Contact angles between coexisting phases, and resulting textural features, of Na-rich experimental charges. The enwrapping of vapour with carbonate melt suggests that the Lc-vapour boundary has a lower surface energy than the Ls-vapour contact.
This leads to "wetting" the Lc-vapour junctions by carbonate melt.

Table 6.1. Average contact angles between coexisting phases in experimental charges: Ls-Lc-V triple points.

Sodium-poor charges: SUN189+CC

Run Ident.	Pressure (GPa)	No. of contacts	Contact angles in degrees θ_s	θ_c	θ_v
G9.6	0.25	26	85	108	167
G2.6	0.5	2	82	110	168
G25.5	0.8	2	65?	111	184
G10.6	0.8	4	88	107	165
G24.5	0.8	5	93	112	155
Weighted avg.		39	85	109	166

A. Sodium -poor charges. $\gamma cv >> \gamma sv > \gamma sc$. The Lc-vapour boundary has the highest surface energy.
1 : 0.95 : 0.23

Sodium-rich charges: BD50+CNC

Run Ident.	Pressure (GPa)	No. of contacts	Contact angles in degrees θ_s	θ_c	θ_v
G16.1	0.25	5	169	20	171
G13.1	0.25	6	179	23	158
G1.1	0.5	5	175	34	150
G2.1	0.5	1	179	42	139
G25.1	0.8	10	151	46	163
G24.1	0.8	6	152	43	165
Weighted avg.		39	168	34	162

B. Sodium -rich charges. $\gamma sv >> \gamma sc > \gamma cv$. The Lc-vapour boundary has the lowest surface energy.
1 : 0.55 : 0.37

In calcium-rich compositions, however, the situation is reversed, with γ_{cv} being at least as large as γ_{sv}. Here, the Ls-Lc meniscus has a large angle of intersection with vapour spheres (approaching 90°). This gives rise to textures displayed in Figure 6.4. and in Plate 6.4, where separated spheres of carbonate are seen associated with vapour bubbles. It is noticeable that, in these sodium-poor compositions, the shapes of the vapour bubbles are almost perfect spheres; they are not greatly affected by intersecting an Ls-Lc boundary. This implies that γ_{sc} is much smaller than either of the melt-vapour interfacial energies. It is therefore the overall surface area of melt-vapour interface that is minimised in these textures.

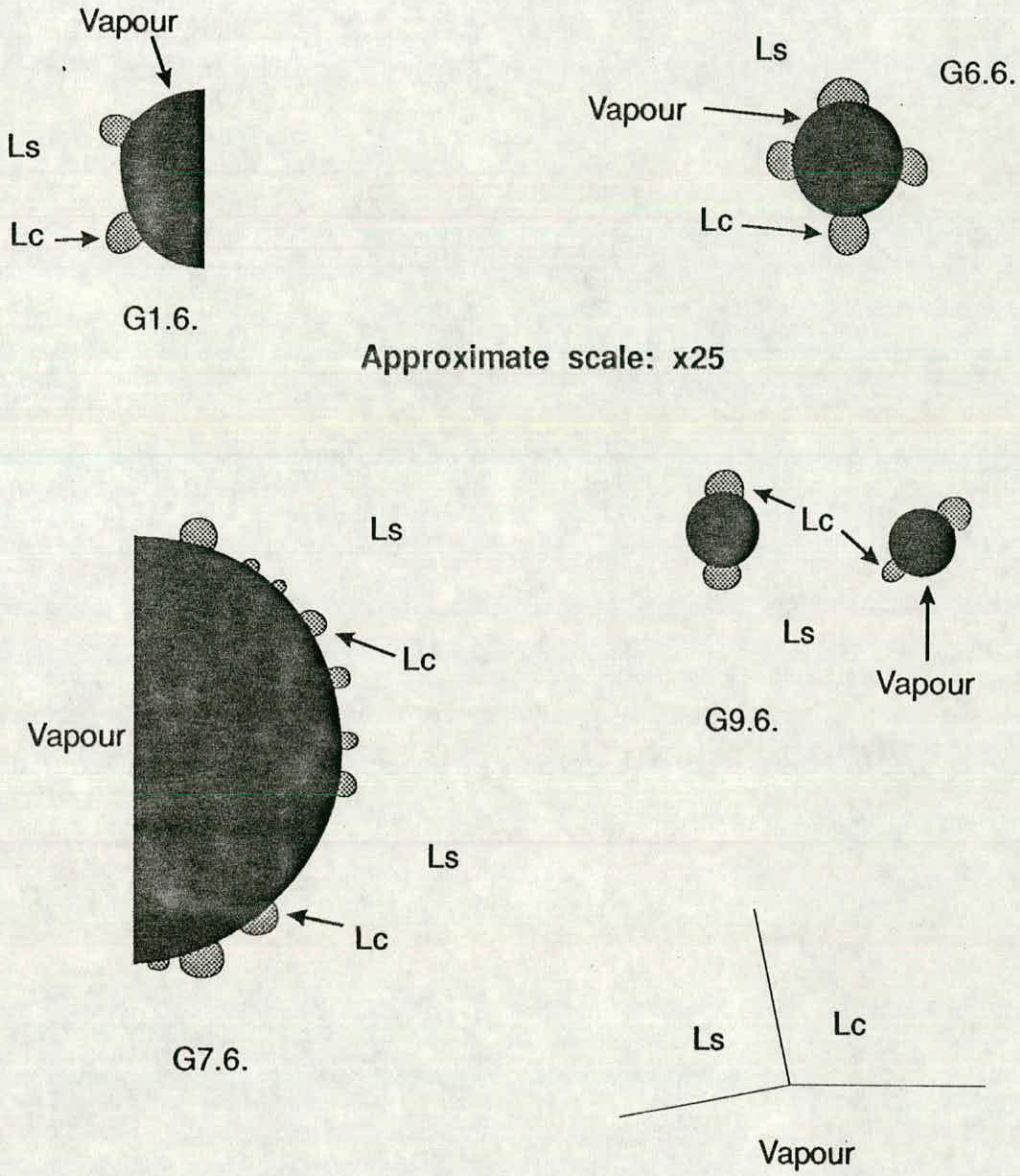

Figure 6.4. Contact angles between coexisting phases, and resulting textural features, in Ca-rich experimental charges. Since the angle of contact of the Ls-Lc meniscus with vapour is large, the Lc-V and Ls-V boundaries must be of similar surface energy.

The contact angles for both compositions are plotted in Figure 6.5. Pressure was chosen as the x-axis as it was deemed the most likely physical variable to affect interfacial energies (e.g. Holness, 1992). Contact angles are reasonably constant with pressure in the sodium-poor basic composition, with $\theta_v >> \theta_c > \theta_s$ always true. In Na-rich compositions, however, a correlation between variations in contact angle and pressure is observed. θ_c rises with pressure, with a corresponding fall in θ_s. This has been interpreted as a relative lowering in γ_{cv} with increased pressure.

It was thought that it might be possible to relate these textural features with the study of boundary effects seen in the silicate liquid as the Ls-Lc meniscus is approached (Section 5.4.3). There, an increase in alkali metal concentrations towards the meniscus was interpreted as adsorption of Na, K, and other alkalis on to the Ls-Lc boundary. This adsorption is likely to affect the interfacial energy of the boundary, and will therefore influence textural development. Unfortunately, constraints on the available data, and on time, have meant that this relationship could not be studied in greater detail.

Ls-Lc-Xtls textures.

These textures were only seen in charges of olivine nephelinitic composition. In all cases, Lc spheres in the silicate melt were seen in association with crystalline silicates. The crystals seemed to be very effective at stopping complete separation of the two liquid phases as seen in Plate 6.5. The resulting textures consisted of numerous small Lc spheres and silicate crystals within Ls glass. Contact angles at the three-phase intersection usually showed $\theta_c >> 90°$ (up to 140° or more) and $\theta_s < 90°$. θ_{xtl} is dominantly controlled by crystallography when surrounded by melt, and will therefore not be discussed. Equation 6.1 would predict that $\gamma_{s\text{-}xtl}$ will be larger than $\gamma_{c\text{-}xtl}$. It is therefore a surprise to find the ubiquitous association of Lc and crystals in these charges. This may imply that the origins of these two phases are related, i.e. formation of the carbonate spheres was triggered by crystallisation. This conclusion is in agreement with speculation on the origins of carbonatites, where it is believed that crystallisation of silicate phases from a carbonated nephelinite enriches the remaining melt in CO_3^{2-} component, resulting in spontaneous separation of immiscible carbonate (e.g. Kjarsgaard & Peterson, 1992).

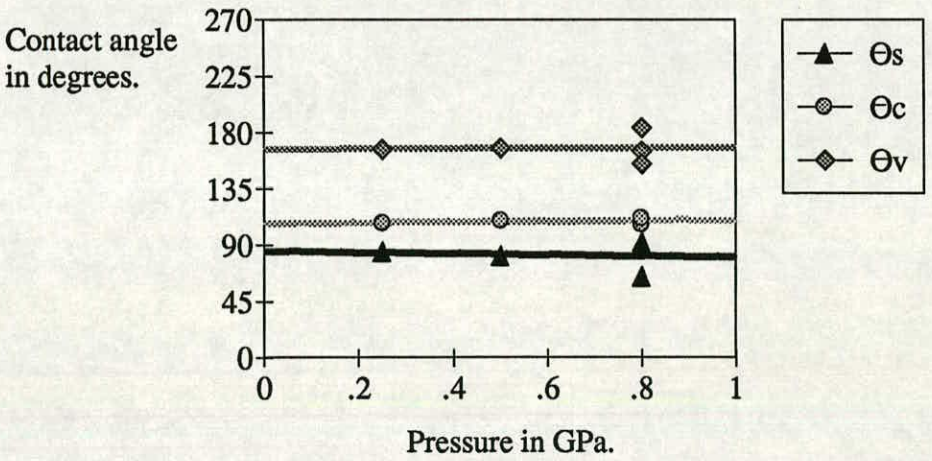

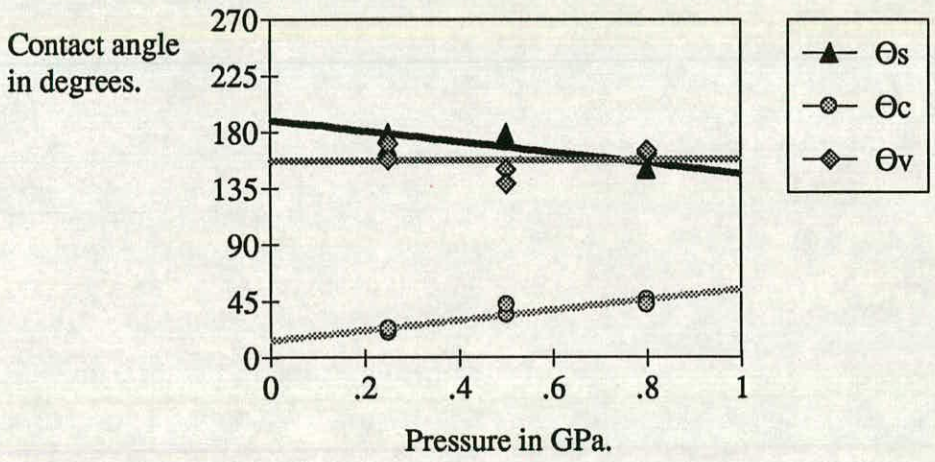

Figure 6.5. The variation of Ls-Lc-Vapour contact angles with pressure and composition.
(a) Contact angles in sodium poor charges (SUN189+CC) are unaffected by pressure.
(b) Contact angles in sodium-rich charges (BD50+CNC) vary with pressure. Θc increases with pressure from 20-45 degreees

Viscosity relationships.

The wetting characteristics of the carbonate melt, its rapid separation, and its inferred weaker liquid bonding forces, are strong evidence that measurements of very low viscosities for carbonate melts at atmospheric pressure are also valid for higher pressures. This is certainly the case for sodium-rich carbonate melt, although data for calcic carbonate melt is more equivocal.

Density relationships.

Samples in gas-media vessels are run horizontally, and are therefore cannot be used to discuss relative density. In contrast, vertically run, solid-media experiments (e.g. S39) showed that Na-rich carbonate melt rises rapidly towards the top of the capsule. Carbonate liquid therefore has a low density relative to silicate liquid even at reasonably high pressures (2.0 GPa). Again, however, the evidence is only for Na-rich carbonate melt compositions. Calcic carbonate melts are always associated with either CO_2 vapour, or silicate crystals. Individual density characteristics are difficult to isolate in these charges. No firm conclusion as to the relative densities of calcic carbonate and nephelinite can be drawn from these experiments.

6.3.4. Analysis of quench textures in experimentally produced carbonate and silicate melts.

On cooling, the coexisting carbonate and silicate liquids produced under experimental conditions undergo significant modifications before becoming frozen as the temperature drops. These effects are thought to occur mainly within the first 200°C of temperature fall, that is the first 4-5 seconds after quenching in the gas-media vessels (an order of magnitude faster in the solid-media experiments). In this time, a number of features are produced. These include the production of quench immiscibility, and the crystallisation of liquids into quench intergrowths.

Quench immiscibility was first identified in carbonate-silicate systems by Freestone & Hamilton (1980). As the temperature drops during quenching, the compositional extent of immiscibility expands (see section 4.3). This results in further unmixing of carbonate and silicate melts. That is, a silicate melt produced at 1300°C contains a sizable carbonate component. An equivalent melt at 1000°C contains much less carbonate. Therefore, on cooling, the 1300°C melt splits into a silicate melt with

lower carbonate content, containing coexisting carbonate spherules. The results of this process are seen in Plate 6.6. The carbonate spherules seen in this photograph, and in other charges, are considered to be a quench phenomenon rather than a disequilibrium feature present under run conditions for the following reasons:

(a) They are evenly distributed throughout the silicate glass.

(b) They are of uniform size in any particular area.

(c) They tend to be smaller at the ends of the charge, and at its edges. This is interpreted as being due to faster quench rates in these areas.

(d) Analyses of parts of the charge containing spherules (spherules included in analysis), and parts with small spherules or none at all, produce the same compositions.

(e) Silicate glasses from larger volume charges, which would be expected to retain heat longer, and therefore cool more slowly, contain larger carbonate spherules. This is compatible with their proposed slower quench rate.

The largest size of quench spheres of carbonate in the silicate glasses produced in 2 mm diameter Pt capsules was 1.5 μm. Silicate glasses from experiments run in 3 mm Pt capsules showed spheres up to 3 μm in diameter. Figure 6.6 shows the results from an electron probe study of the coarsest quench found (G6.7: a 3 mm capsule run at low pressure). Spot analyses were necessary to separate the quench spheres from the silicate glass, whilst the overall Ls composition was estimated by a 100 μm^2 rastered analysis. Although a low probe current was used, and the beam was on the sample for as short a time as possible, it is likely that the spot analyses will have led to Na-mobilisation within the charge (see analytical section). There are likely to be systematic errors in the compositions stated. A tie-line between compositions suggests that in this instance the silicate melt was quenched to produce *ca.* 93% silicate glass, and *ca.* 7% carbonate spherules. This agrees well with estimated modal proportions (Table 6.2). In one charge, a small area of silicate melt began crystallising during cooling. This produced a small patch of snowflake-like intergrowth, consisting of acicular olivine and pyroxene with interstitial carbonate. (Plate 6.6.B). Again, this charge was one of the few run in a 3 mm diameter capsule, and therefore suffered a slower quench rate.

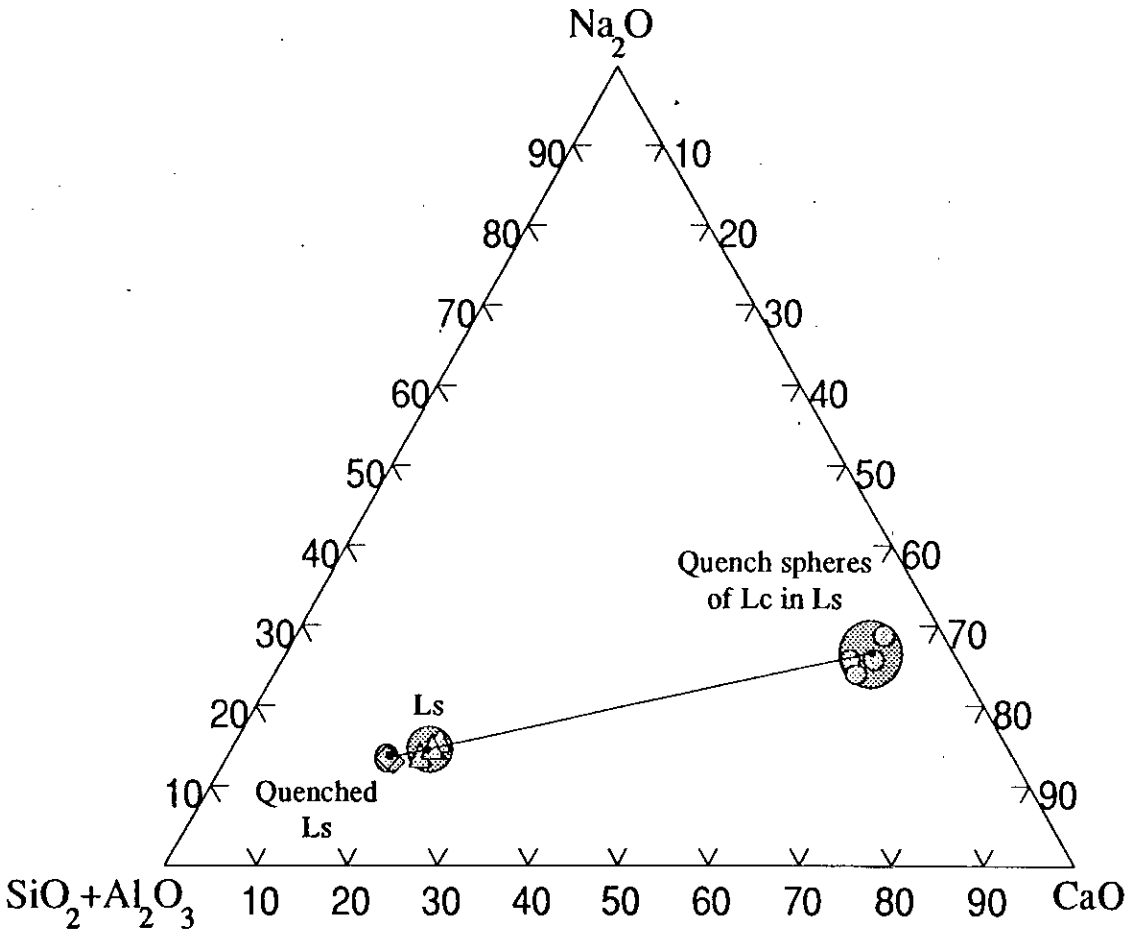

Figure 6.6. The effects of slow quench rate on silicate liquid and quench immiscibility. A study of immiscible silicate melt from SM2+CNC composition run at 1200°C, 0.25GPa. Analyses were obtained on a Cameca Camebax electron microprobe. Due to the small scale of the quench phenomenon, a rastered beam could not be employed. Quoted sodium contents are therefore likely to be unrealistically low because of sodium mobility away from the beam spot.

The carbonate melt was more profoundly affected by quench effects, with a wide variety of textures resulting (Plate 6.7). Four main phases have been identified in these carbonate quenches:

(a) Silicate spheres. Thought to be the equivalent of the quench immiscibility seen in the silicate melt. Quench spheres up to 5 μm across.

(b) Acicular calcite crystals. Interlocking needles of pure $CaCO_3$ composition.

(c) Irregular silicate material. Quench silicate blebs in the intergrowth.

(d) Background $(Na,K)_2Ca(CO_3)_2$.

The relative proportions of each of these components, and the characteristic textures produced, are dependant on the carbonate melt composition, and the quench rate. As an example, the quench of G6.7 was studied on the electron probe. Phase compositions are plotted on Figure 6.7.. The relative proportions of the phases have been assessed by joining compositions with tie lines. In the run featured in Figure 6.7, 68% is nyerereite background, 23% is acicular calcite crystals, and *ca.* 9% is silicate material. This again agrees well with the estimates of modal proportions (Table 6.2). As with the silicate quench analyses, Na-contents quoted should be treated with caution as spot analyses will lead to rapid and pronounced instability of the sodium carbonate materials, even at the low probe currents used.

Table 6.2. A study of the quench effects in carbonate and silicate melts: G6.7 as an example.

Equilibrium phase.	Quench phases.	Percentages present	
		By Lever rule from compositions	By modal proportions
Silicate melt	Silicate glass	93	95
	Carbonate spherules	7	5
Carbonate melt	Calcite	23	20
	Nyerereite	68	70
	Irregular silicate	9	5
	Silicate quench spheres	-	5

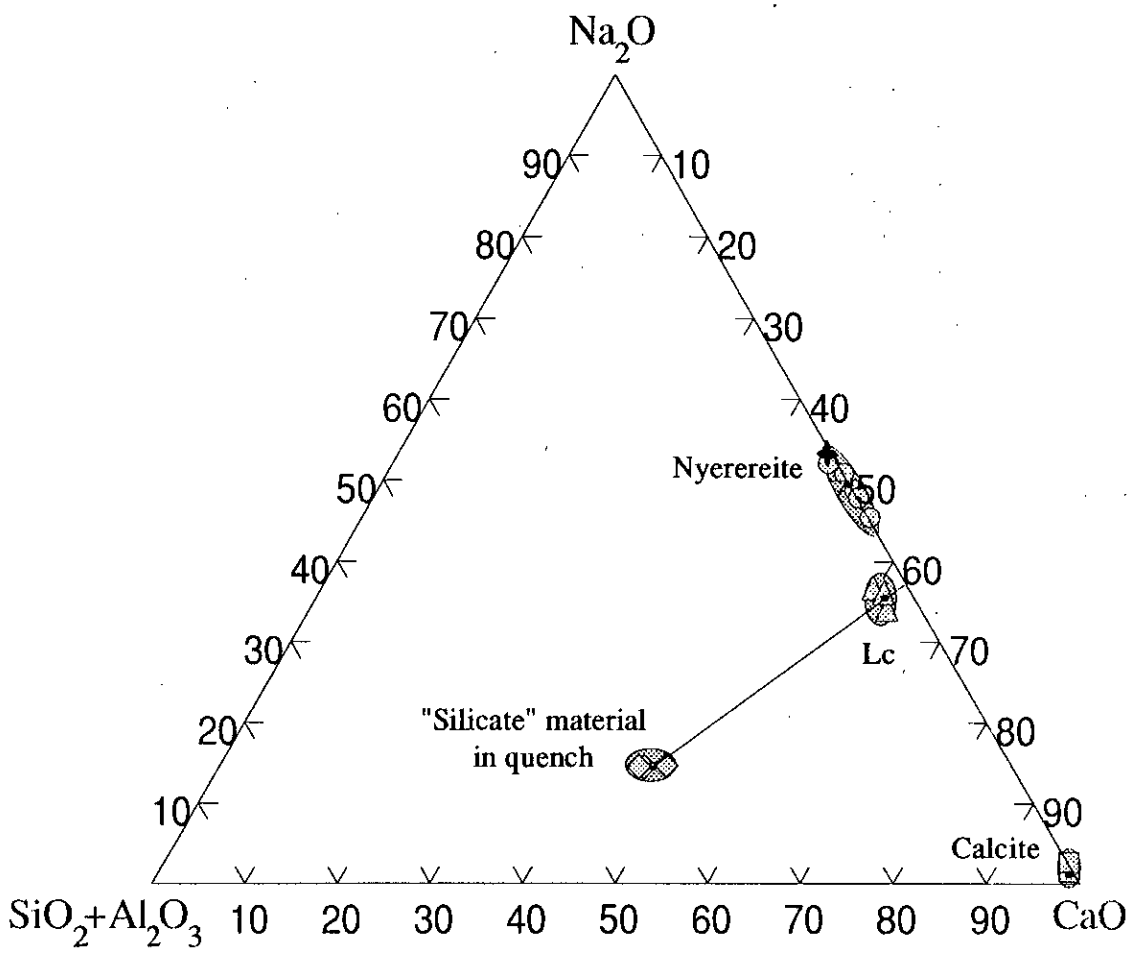

Figure 6.7. The effects of slow quench rate on carbonate liquid and production of quench carbonate intergrowth. A study of quenched immiscible carbonate melt from SM2+CNC starting composition run at 1200°C, 0.25GPa.

Analyses were obtained on a Cameca Camebax electron microprobe. Due to the small scale of the quench phenomenon, a rastered beam could not be employed. Quoted sodium contents are therefore likely to be unrealistically low because of sodium mobility away from the beam spot. The spread of Ca/Na ratio seen in the "nyerereite" quench material suggests that there is evidence for this process occurring. The stoichiometric position of nyerereite is marked +.

The presence of quench textures can cause significant errors in analysis. These are considerably greater than those expected from counting statistics and analytical matrix effects (see Appendices A and B). However, 100 μm^2 averages obtained in ion probe analysis, and by rastering the electron probe beam, are believed to give a reasonable approximation of the original liquid compositions, and should certainly not contain systematic errors.

6.4. Electron probe microanalysis.

6.4.1. Introduction.

Electron probe analytical techniques permitted:-

(a) Phase identification.

(b) Accurate determination of major-element concentrations in experimentally produced carbonate and silicate melts.

(c) Determination of trace-element concentrations within carbonate standard materials. These have then been used as the basis for standardisation of the ion probe results.

A brief summary of the equipment used, techniques employed, and analyses undertaken is presented below. This will be followed by a more detailed account of the analytical difficulties encountered. Finally, an estimate of the accuracy of this electron probe data has been made by comparison of mass-balance estimates of bulk composition with known starting compositions.

6.4.2. Sample preparation.

Once a flat, polished surface containing Ls+Lc textures had been obtained (Figure 6.1), the sample was coated with a thin film of carbon. This allows rapid charge dissipation away from the point of analysis. In this way, charge build-up on the sample, which can significantly affect the analytical results, is reduced. The possibility of sample charging was further reduced by the application of a colloidal, carbon-based dag (brand name Aquadag). This was applied in order to link the centre of the sample with the metallic probe-sample holder. After preparation in this manner, covered samples were stored in a desiccator until analysis.

6.4.3. Analytical equipment and techniques.

All electron probe analyses quoted were obtained on a Cameca Camebax Microbeam electron probe. This is a standard design probe, with four independently aligned spectrometers for wave-length dispersive spectral analysis. The probe is fitted with a back-scattered electron (BSE) imaging system which was used both as a means of beam positioning within the sample, and as an aid to textural analysis. A Link AN10000 image processor is also attached to the probe. This facility allows acquisition, display, and processing of BSE, secondary electron, and x-ray images. Energy dispersive x-ray spectra acquired on the Link analyser were also used for phase identification and qualitative analysis.

The primary electron beam (of between 2.5 and 20 nA) was accelerated towards the sample by a 20 kV directional voltage. The beam was focused optically to an area on the sample *ca.* 1 μm across. This spot-size was used for analysis of crystals, whilst glasses and quench intergrowths were analysed by rastering the beam over a 100 μm^2 area. Larger areas of analysis were not possible using wave-length dispersive analysis due to the resulting misalignment of the spectrometers. The actual conditions of analysis used for each type of material are given in the next section.

Wave-length dispersive analysis was employed, using PAP software to correct for matrix effects (developed by J.Pouchou, and F.Pichour, Dept. of Aerospace studies, Paris). Initial analyses (mainly those on experiments using primary melt compositions) used ZAF correction software, and could therefore vary systematically from the later results. These variations are, however, thought to be small for relatively low mean atomic number matrices. Data obtained were stored on the Electron Probe Unit's computer system before transfer to the departmental PC network where processing was undertaken. Original analysis files are retained on computer tape.

For brevity, a list of the analysed major elements is given in Table 6.3. Also given are the spectrometers and diffracting crystals employed, the approximate peak and background positions, and the standards used. Table 6.4. gives similar information for minor and trace-elements whose contents have been estimated by electron probe analysis.

Table 6.3. Major elements analysed on the electron probe: Conditions of analysis and standards used. Peak positions are sinθ values, background offsets are sinθ.10^5.

Element	Spectr. number	Diffract. crystal	Radiation	Theoretical peak posn.	Background offset	Standard Ident.	Standard Name
Na	1	TAP	Kα	.46363	+750	NaK2	Jadeite
Al	2	TAP	Kα	.32463	+750	AlK2	Corundum
K	3	PET	Kα	.42765	+750	K K2	Orthoclase
Fe	4	LIF	Kα	.48083	+1000	FeK1	Fe-metal
Mg	1	TAP	Kα	.38499	+1250	MgK3	Periclase
Si	2	TAP	Kα	.27737	+750	SiK3	Wollastonite
Ca	3	PET	Kα	.38387	+1000	CaK3	Wollastonite
Mn	4	LIF	Kα	.52200	+1000	MnK1	Mn-metal
P	2	TAP	Kα	.23968	-500	P K3	Apatite
Ti	3	PET	Kα	.31416	+1000	TiK2	Rutile

Table 6.4. Minor and trace elements analysed on the electron probe: Conditions of analysis and standards used. Peak positions are sinθ values, background offsets are sinθ.10^5 units.

Element	Spectr. number	Diffract. crystal	Radiation	Theoretical peak posn.	Background offset	Standard Ident.	Standard Name
F	1	TAP	Kα	.71315	-750	F K2	MgF_2
Cl	3	PET	Kα	.54040	-750	ClK2	Halite
P	4	PET	Kα	.70385	-500	P K3	Apatite
S	4	PET	Kα	.61405	+750	S K2	Pyrite
Sr	1	TAP	Lα	.26715	+750	SrL2	Celestite
Ba	3	LIF	Lα	.68943	+750	BaL2	Baryte
La	2	PET	Lα	.30470	+750	LaL5	Glass
Ce	3	LIF	Lβ	.58510	-700	CeL5	Glass
Nd	3	LIF	Lα	.58873	-750	NdL5	Glass
Pr	4	LIF	Lβ	.56087	+600	PrL5	Glass
Pb	4	LIF	Lα	.29182	+1000	PbL2	Galena

6.4.4. Analyses undertaken.

Electron probe analyses were principally made to determine the major element compositions of coexisting carbonate and silicate liquids. Owing to analytical difficulties associated with alkali-element mobility, analytical conditions used were different for carbonate and silicate melts, and for natural and synthetic materials. The elements analysed, and the analytical set-up are given in Table 6.5. Five oxides (Na_2O, CaO, Al_2O_3, SiO_2, and CO_2) made up >99% of both synthetic silicate and carbonate compositions. As carbon cannot be analysed accurately by electron probe techniques (owing to its low atomic number), a single pass to analyse for Na, Ca, Al, and Si was adopted. CO_2 contents were then estimated by shortfall in the total analysed oxides. A beam current of 3 nA was used for carbonates and 10 nA for silicates. Averages were obtained over the largest rastered area allowed for wave-length dispersive spectral analysis. The data produced is presented in Appendix A.1.

Table 6.5. Spectrometer set-up and count times for electron probe analyses.

Natural carbonates			I = 3 nA		V = 20 kV		Raster = 100 μm²	
Spectrometer	1	Count	2	Count	3	Count	4	Count
Crystal	TAP	Time	TAP	Time	PET	Time	LIF	Time
1st	Na	30	Si	20	K	20	Fe	30
2nd	Mg	30	Al	20	Ca	20	Mn	30
3rd			P	20	Ti	20		

Natural silicates			I = 10 nA		V = 20 kV		Raster = 100 μm²	
Spectrometer	1	Count	2	Count	3	Count	4	Count
Crystal	TAP	Time	TAP	Time	PET	Time	LIF	Time
1st	Na	10	Si	10	K	10	Fe	10
2nd	Mg	20	Al	10	Ca	10	Mn	20
3rd			P	10	Ti	10		

Synthetic carbonates			I = 3 nA		V = 20 kV		Raster = 100 μm²	
Spectrometer	1	Count	2	Count	3	Count	4	Count
Crystal	TAP	Time	TAP	Time	TAP	Time	PET	Time
1st	Na	30	Al	30	Si	30	Ca	30

Synthetic silicates			I = 10 nA		V = 20 kV		Raster = 100 μm²	
Spectrometer	1	Count	2	Count	3	Count	4	Count
Crystal	TAP	Time	TAP	Time	TAP	Time	PET	Time
1st	Na	30	Al	30	Si	30	Ca	30

The natural rock compositions have many more components than their synthetic counterparts, and it was necessary to analyse a total of 10 elements in three passes of the spectrometers. Due to the possibility of alkali mobilisation, sodium and potassium were always determined in the first pass. Other elements analysed were Si, Al, Ca, Mg, Fe, Mn, Ti, and P. Again, CO_2 contents were estimated by shortfalls in probe totals. A beam current of 3 nA was used for carbonate quenches, and 10 nA for silicate glasses. Average compositions were again obtained over the largest acceptable area of rastering (*ca.* 100 μm^2). The dataset produced from these analyses are given in Appendix A.2.

Other probe work was mainly concerned with finding adequate standards for carbonate analysis on the ion probe. Concentrations of Sr, Ba, Pb, Mg, and the REEs were measured in both natural and synthetic carbonate matrices. These attempts at ion probe standardisation will be commented on in Section 5.5. The electron probe data are presented in Appendix A.3.

6.4.5. Difficulties encountered during electron probe analysis.

Analysis of the CO_2 component of carbonate and silicate glasses.

Due to the mechanisms involved in x-ray formation, elements with low mean atomic numbers (Z) are difficult to analyse by electron probe techniques. This means that the CO_2 component present in both the carbonate and silicate liquids cannot be determined directly. Instead, CO_2 contents have been estimated by shortfalls in the sum of the oxides measured. In silicates, probe totals range from 88-98%, implying 1-10% dissolved CO_2. Carbonate quench totals range from *ca.* 56% in near-pure $CaCO_3$ melts, to 68% in quenches containing a sizable silicate component.

Instability of carbonate quench and silicate glass under the electron beam: Alkali mobility and oxygen outgassing.

Sodium-bearing silicate glasses have long been renowned for instability under probe beams (e.g. Varshneya *et al.*, 1966; Borom & Hanneman, 1967). This instability leads to compositional changes during probe analysis, and therefore will affect the measured glass compositions.

The effects observed during electron probe analysis of the carbonate and silicate melts produced in this study are similar to those recorded by Borom & Hanneman in FeO-Na_2O-SiO_2 glasses (1967). The Na X-ray intensity falls significantly with time. There is a corresponding increase in the X-ray intensities of the other elements present. This fall in X-ray intensity also occurs for K, although not in such an extreme manner. The processes controlling these changes in X-ray intensity with time are not fully understood. Autefage & Couderc (1973) explained this process in terms of alkali migration, by a two-stage process involving bond breaking and atom displacement. A more rigorous study into the controls on this process is warranted, although the underlying cause of alkali mobility may be related to mechanisms of oxygen outgassing seen during electron bombardment of glass (Lineweaver, 1963). Another explanation for the instability of the silicate glasses and carbonate quench may be outgassing of O_2 or CO_2. Even carbonates and glasses with insignificant alkali concentrations are known to suffer from instability at high probe currents due to this problem. Whatever the cause, instability was a significant problem during the analysis of both carbonates and silicates in these experimental charges. It was therefore necessary to undertake a study into the factors controlling instability, in order for stable analytical conditions to be found.

A criterion of acceptability was fixed before this study was undertaken: an analysis was considered to be "acceptable" if the average X-ray intensities measured over the whole of the period of analysis were within 2% relative of the initial intensity for all elements determined. A sequence of investigations into variations of X-ray intensities over time was undertaken, spanning various conditions and compositions. Initially, spot analyses were employed, using a beam with high current and accelerating voltage. Sodium X-ray intensities were found to fall off extremely rapidly in both silicate and carbonate compositions (*ca.* 30% loss in the first 5 seconds). In all further investigations, 100 μm^2 areas were analysed with a rastered beam in order to dissipate the beam heating effect. Even so, variations in X-ray intensities over time were significant for both the carbonate and silicate compositions.

Figure 6.8 shows instability in count rates for a carbonate quench analysed over a 100 μm^2 square at 20 kV, 10 nA. The fall-off in count-rate for sodium is rapid, and therefore an "acceptable" analysis is not possible under these conditions. Dropping the accelerating voltage to 15 kV (Figure 6.9) had only a very limited effect on stability, but significantly lowered the overall count-rates for heavier elements, leading to considerably reduced precision. It was therefore decided that analyses

should be at 20 kV. Decreasing the probe beam current was found to be a much more effective way of improving stability. Figure 6.10 shows the carbonate quench stability at 5 nA probe current. Stability is markedly improved, with a plateau of constant X-ray intensities for all elements for the first few seconds of analysis. Unfortunately, after *ca.* 5 seconds, sodium count rates begin to fall, so that only a very short analysis time would be acceptable under these conditions. The probe current was therefore dropped to 3 nA (Figure 6.11). The plateau of constant X-ray intensities was seen to extend for *ca.* 50 seconds, making acceptable analysis of carbonate quench possible. This plateau was also seen in X-ray intensities produced from the silicate glass at 5 nA and 10 nA (Figure 6.12). Taking the criterion of an acceptable analysis as being one with <2% relative variation from the starting X-ray intensities, analysis times can be calculated (Table 6.6). These times represent the longest possible duration of electron probe analysis under the conditions stated. To improve precision, times of >50 seconds are required.

The final decisions on the analytical conditions to be used for electron probe microanalysis were: 20 kV, 10 nA, 100 μm^2 raster, and 10 second count times for the silicate glass; 20 kV, 3 nA, 100 μm^2 raster, and 30 second count times for the carbonate quenches. Alkali mobility was not considered to be a significant problem under these conditions.

At low beam currents, counting errors increase due to the reduction in X-ray intensities. However, the counting errors on the analytical results were found to be less than 2% relative for most elements. A notable exception is manganese which, due to its low concentration in some materials, and low count-rates on the LIF diffracting crystal, suffers from considerable variability. Manganese data from some of the probed compositions should therefore be treated with caution.

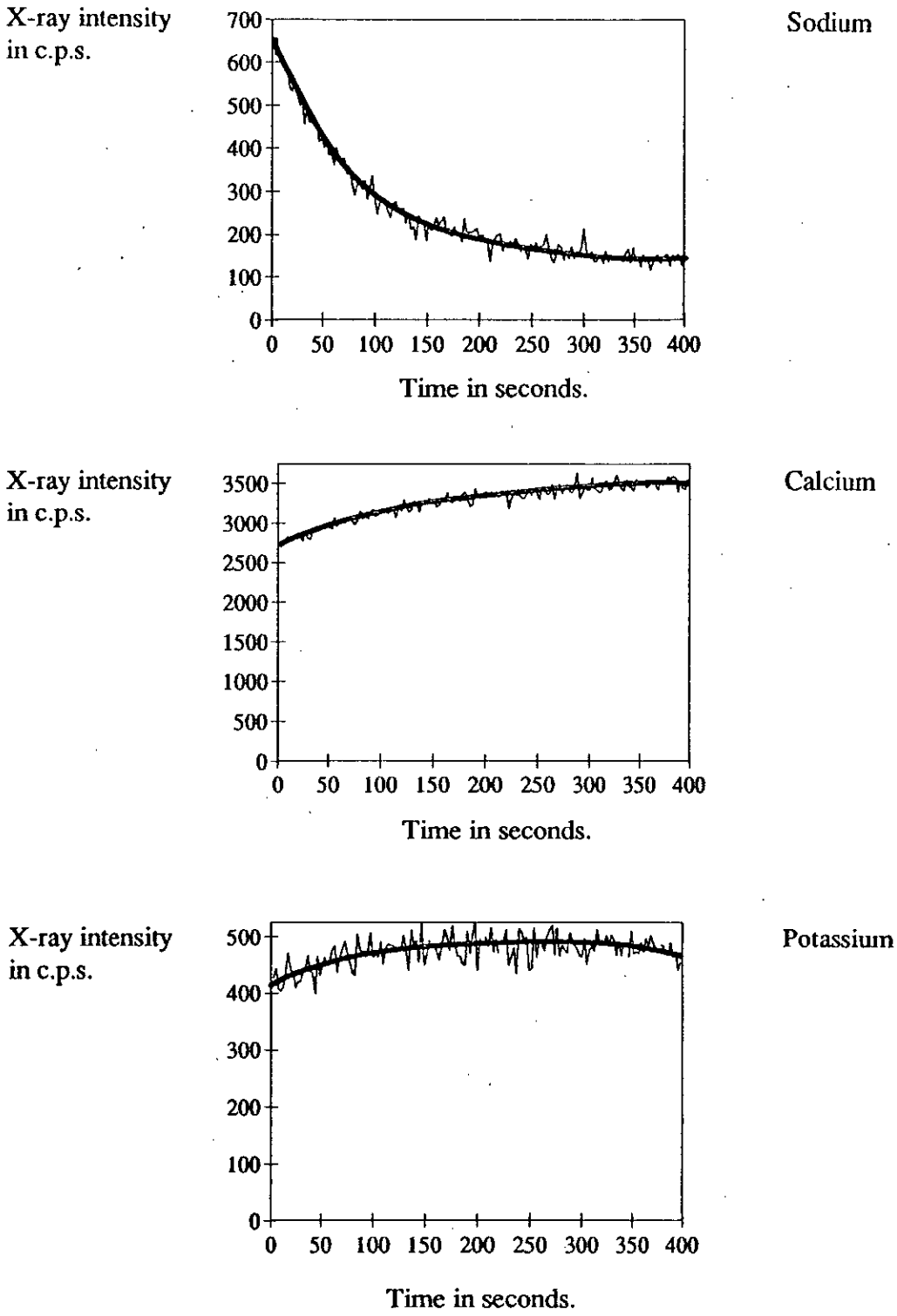

Figure 6.8. Variations in X-ray intensity with time during analysis of Na-rich carbonate quench. 20 kV, 10 nA. For sodium, there is >15% loss in intensity in the first five seconds. An acceptable analysis of carbonate material is therefore not possible using these conditions.

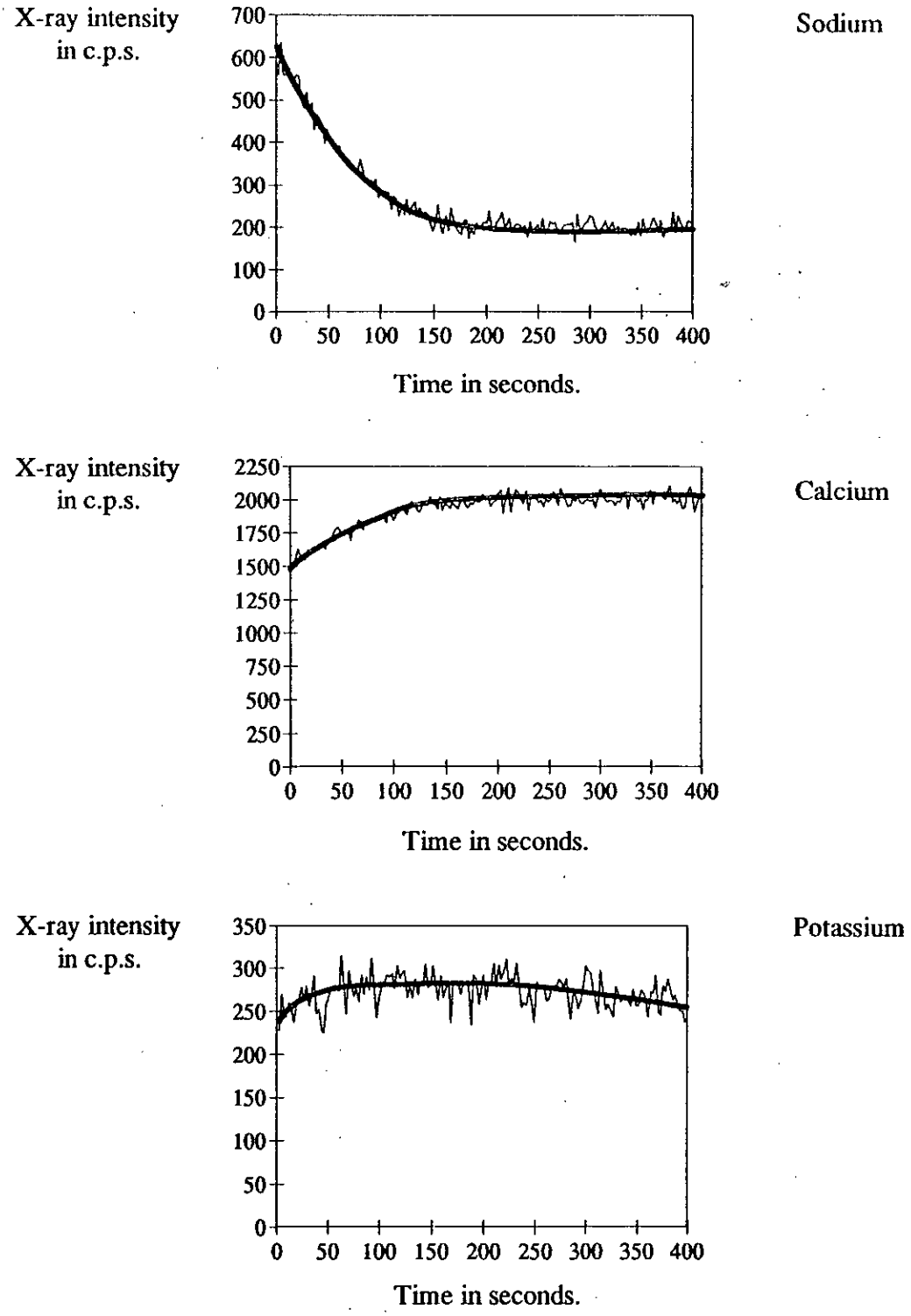

Figure 6.9. Variations in X-ray intensity with time during analysis of Na-rich carbonate quench. 15 kV, 10 nA. The 15 kV stability data shows little improvement on the data at 20 kV, the X-ray intensities are however much reduced. Lowering the accelerating voltage is therefore not a viable method of reducing probe instability.

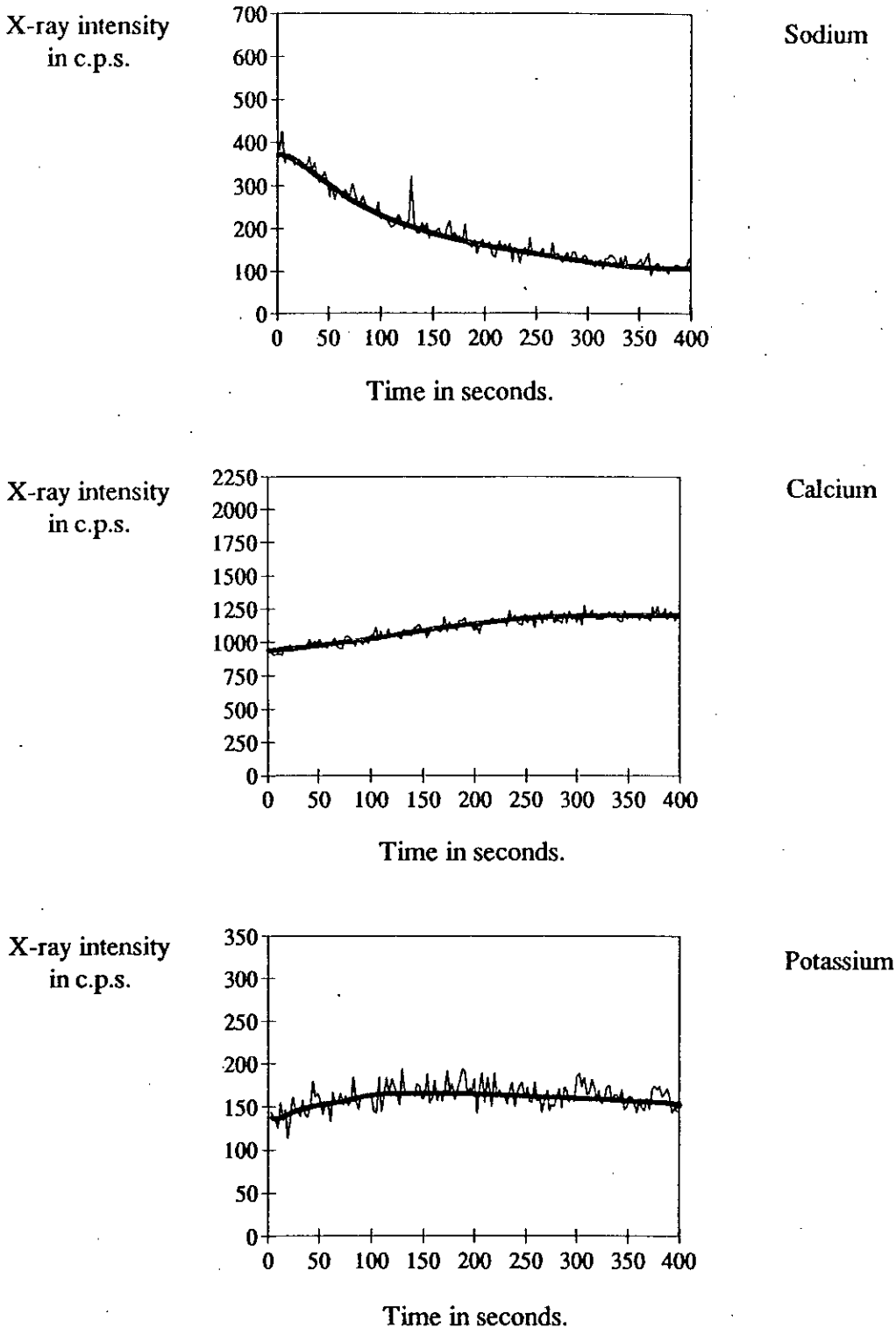

Figure 6.10. Variations in X-ray intensity with time during analysis of Na-rich carbonate quench. 20 kV, 5 nA. Although lowering the probe current leads to a significant improvement in Na-stability, conditions are still not acceptable for an analysis of reasonable duration.

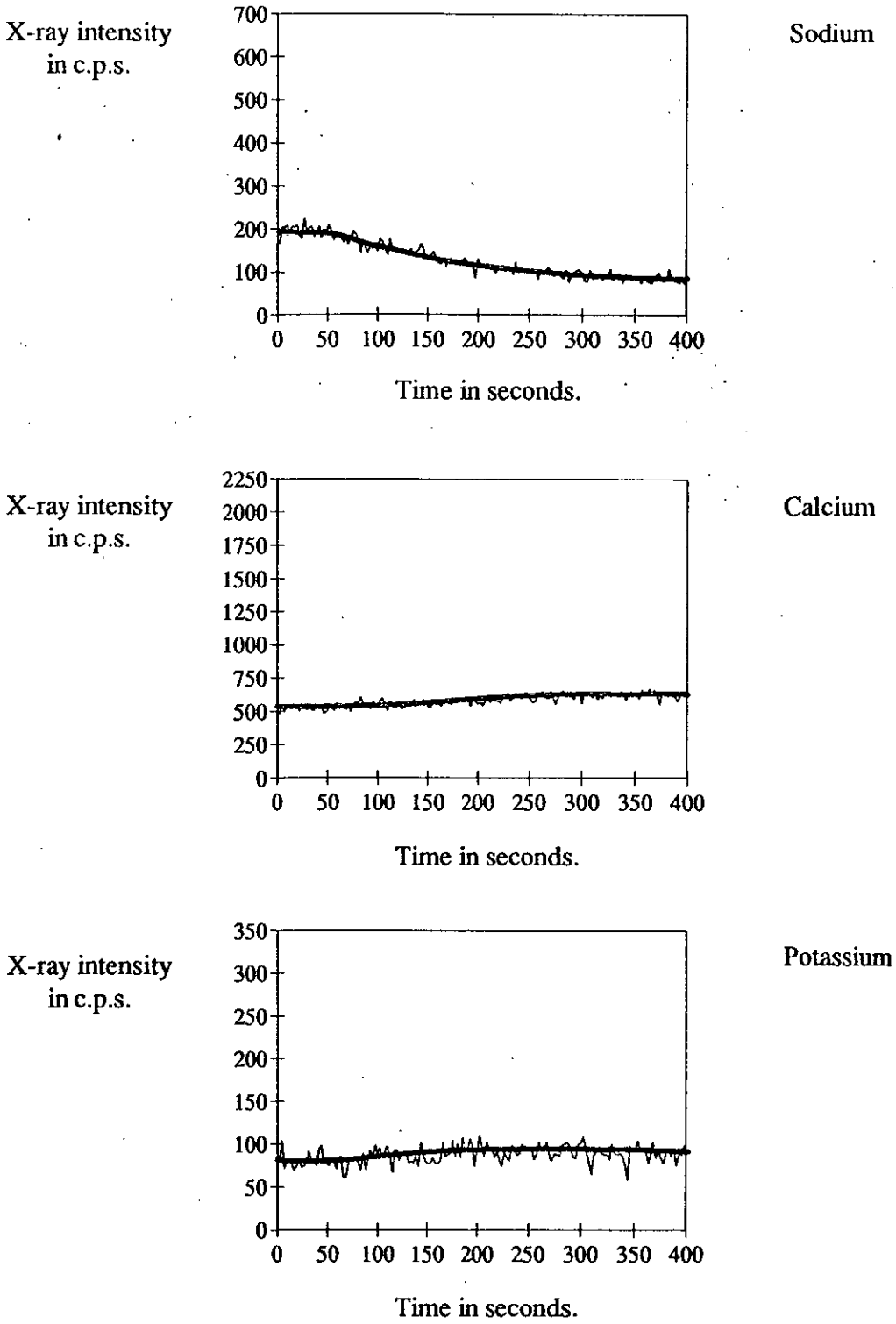

Figure 6.11. Variations in X-ray intensity with time during analysis of Na-rich carbonate quench. 20 kV, 3 nA. A plateau of X-ray intensity extends for *ca.* 50 seconds after analysis starts. Acceptable analysis of carbonate quench is therefore possible under these conditiitons.

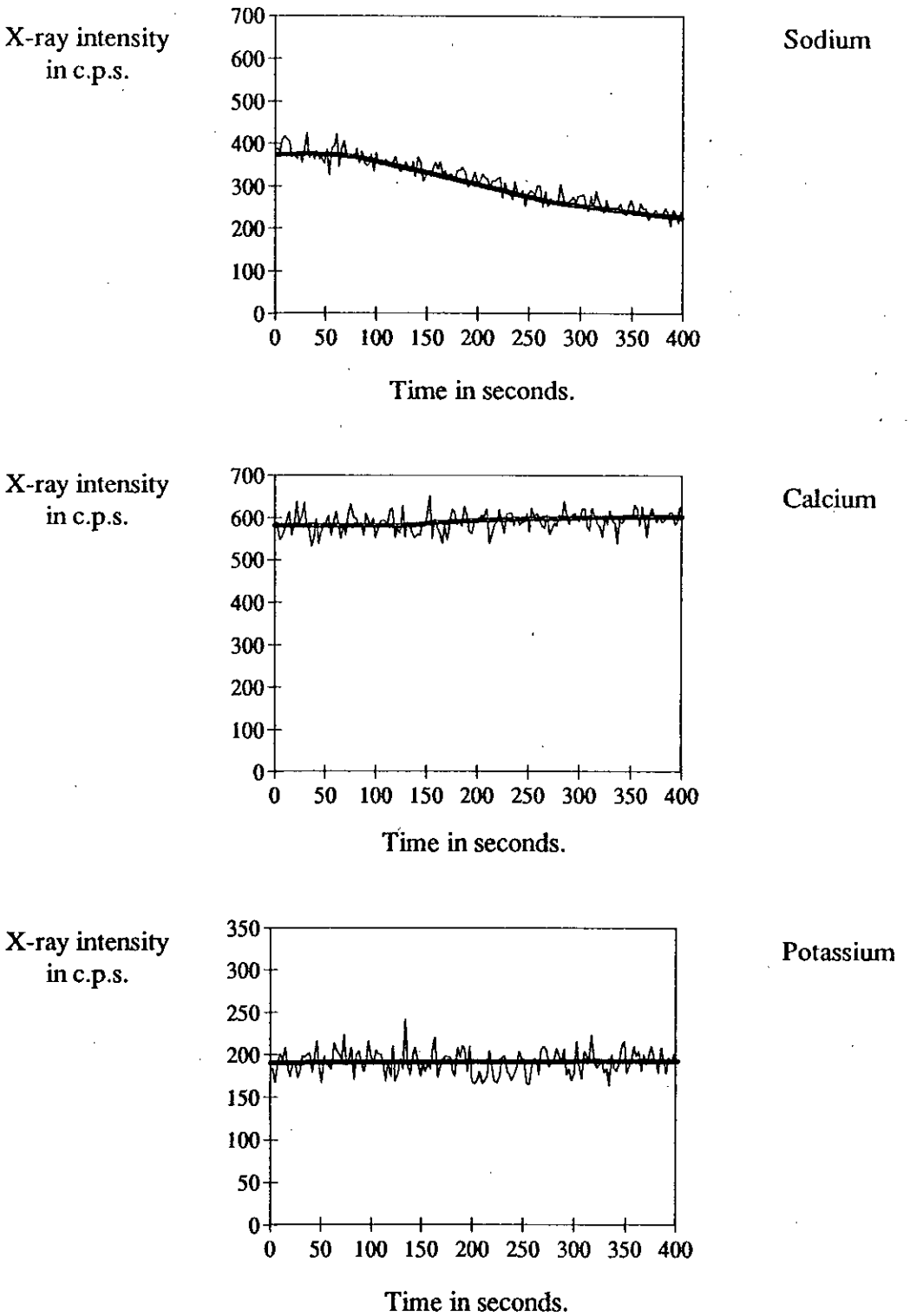

Figure 6.12. Variations in X-ray intensity with time during analysis of Na-rich silicate glass. 20 kV, 5 nA. No systematic changes can be seen in X-ray intensity for at least the first 50 seconds after analysis begins. An acceptable analysis of silicate glass is therefore possible under these conditions.

Table 6.6. Acceptable analysis times for silicate and carbonate materials under differing analytical conditions.

Carbonate quench				
Analytical conditions			Element	Acceptable
Voltage	Current	Raster area	studied	Count-times
20 kV	10 nA	Spot	Na	None
20 kV	10 nA	100 μm²	Na	6
			Ca	15
			K	35
15 kV	10 nA	100 μm²	Na	8
			Ca	12
			K	15
20 kV	5 nA	100 μm²	Na	20.6
			Ca	31.5
			K	22.2
15 kV	5 nA	100 μm²	Na	12
			Ca	20
			K	20
20 kV	3 nA	100 μm²	Na	40
			Ca	65
			K	65
15 kV	3 nA	100 μm²	Na	50
			Ca	79
			K	81
Silicate glass.				
Analytical conditions			Element	Acceptable
Voltage	Current	Raster area	studied	Count-times
20 kV	10 nA	Spot	Na	None
			Ca	None
			K	None
20 kV	10 nA	100 μm²	Na	60 secs
			Si	250 secs
20 kV	5 nA	100 μm²	Na	100 secs
			Ca	150+ secs
			K	>400 secs

Interference effects.

Interference effects can sometimes be a problem when analysing multi-component glasses by electron probe techniques. Problems occur when excitation of different elements produces X-rays of similar energy/wavelength. These can then not be resolved by the spectrometers. In this study, most interferences were avoided by careful choice of X-ray line and positioning of background. One interference was, however, unavoidable with the set-up used.

2nd order CaKβ radiation overlaps in energy with P Kα radiation. The overlap is considerable when using the poorer-resolution TAP diffracting crystal as used in this study. A correction factor to account for this interference must therefore be applied. The magnitude of the interference effect was estimated from apparent phosphorus contents of nominally phosphorus-free materials. In phosphorus-free materials, there can be no contribution to the measured X-ray intensity by P Kα radiation. The X-rays measured can therefore only be contributed by 2nd order CaKβ rays. In this way the relationship between Ca-contents and intensity of 2nd order CaKβ radiation could be isolated. Table 6.7 gives the apparent phosphorus contents of a number of available phosphorus-free materials.

Table 6.7. Apparent phosphorus contents of phosphorus-free materials: The relationship between Ca-content and phosphorus correction.

Material	Wt. % CaO	Wt. % P_2O_5
Andradite at 10 nA	32.5	0.57
Andradite at 3 nA	32.5	0.54
Calcites at 10 nA	53.1	0.67
	52.3	0.66
	51.6	0.64
	51.7	0.74
	50.1	0.76
	50.2	0.63
Soda-melilite glasses	20.2	0.29
	21.1	0.32
	21.6	0.33
	22.1	0.32
	22.4	0.31

These data have been plotted against calcium content of the materials in order to give an approximate relationship between Ca-content and phosphorus-correction (Figure 6.13). It has been assumed that the relationship between these two variables is approximately linear. This is a normal assumption to make in microprobe standardising processes (e.g. Ray & Hart, 1982).

The resulting equation is:

$$y = 0.007 + 0.015x \qquad (6.2)$$

where:

y = phosphorus correction to be applied,

x = CaO content of material analysed.

Although there is some evidence for non-linearity, and variation away from this relationship, the correction is believed to produce phosphorus values within 0.1% absolute of the true value. This correction has therefore been applied to all phosphorus determinations obtained from the electron probe.

Quench variation.

A study was made of the effects of the carbonate quench on analytical accuracy. Run G12 was selected for this study as:-

(a) It showed large-scale two-liquid textures, with large areas of carbonate quench available for analysis.

(b) It was a reasonably coarse quench intergrowth, giving a slightly pessimistic view of the variability likely in other charges.

(c) It had an extremely good polish, permitting an automated stepwise line of analyses to be performed in order to investigate quench heterogeneity.

42 100 μm^2 rastered areas were analysed in a straight line transect across the carbonate quench. Figure 6.14 shows the variability seen in concentrations of the ten major elements across the carbonate quench. Most elements are not seriously affected by quench redistribution. The Variability in concentration estimates for Na_2O, CaO, K_2O, FeO, P_2O_5, MnO and TiO_2 is only slightly larger than would be expected from counting statistics for this low beam current (3 nA). SiO_2, and Al_2O_3 are, however,

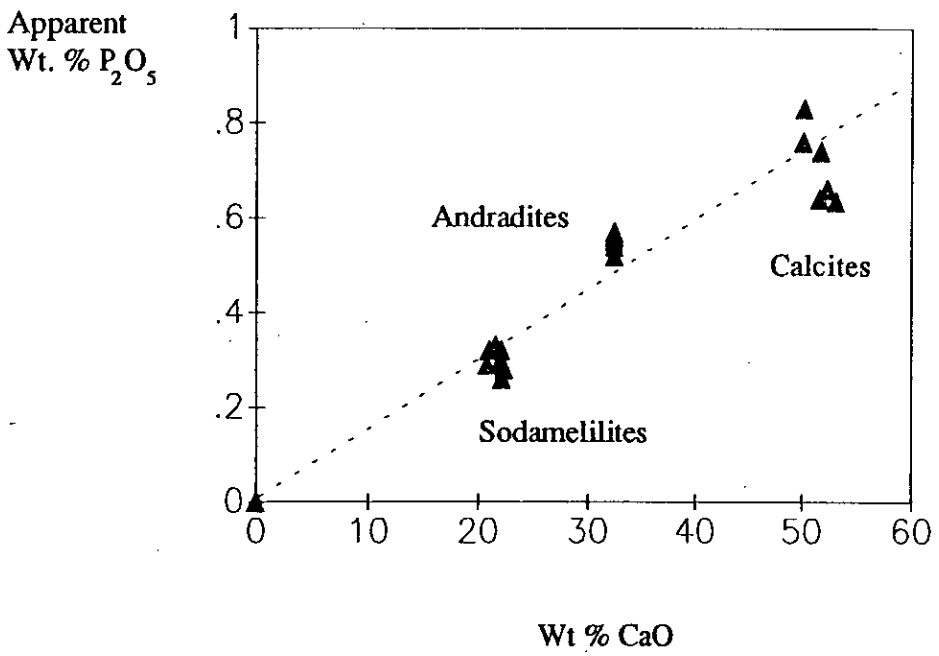

Figure 6.13. The interference effects of 2nd order CaKb on P Ka.

Apparent phosphorus cocentrations in materials known to be phosphorus free can be plotted against Ca content. Assuming linear behaviour, the relationship obtained can be used to remove the effects of Ca interference on phosphorus analyses.

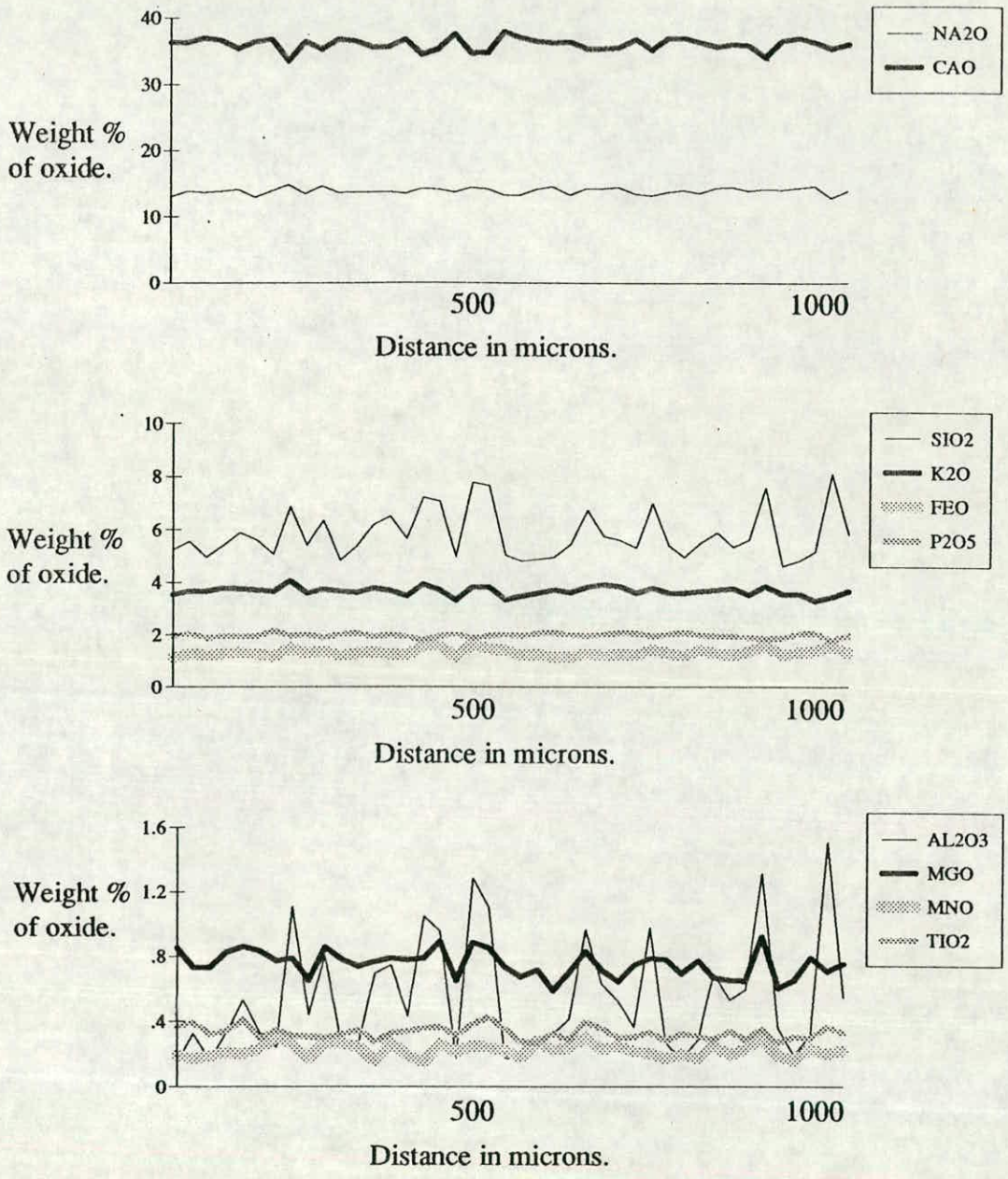

Figure 6.14. Variations in composition across the carbonate quench of experiment G12. A stepwise line of analyses were performed on the electron probe extending for *cc*. 1mm across the carbonate portion of the charge. As expected quenching problems causes greatest variations in the concentrations of silica and alumina. No systematic variations are seen accross the line, suggesting that the carbonate is homogenous on the scale of milimetres, but beterogenous on the scale of microns. Points are taken 25 microns apart.

greatly affected by quenching. Concentration estimates for SiO_2 show variations of up to 30% relative, whilst concentration estimates for Al_2O_3 can vary by over 200%. Statistical errors are therefore large for determinations of the SiO_2 and Al_2O_3 contents of carbonate quenches quoted in the Appendices.

6.4.6. Comparison with starting materials: mass-balance calculations.

Mass-balance estimates of the bulk compositions of experimental charges can be obtained from electron probe analyses of the carbonate and silicate components, combined with approximate modal proportions of the two phases in the charge. These mass-balance estimates of bulk composition can then be compared with the known starting compositions, and discrepancies noted. Confidence in the technique of electron probe analysis of the carbonate and silicate materials will be improved if there is general agreement between these values. Mass-balance estimates of bulk composition have been undertaken for one synthetic charge (G6.7: SM2+CNC) and two natural compositions (Na-rich G2.1 and Na-poor G2.6). The results are given in Tables 6.8, 6.9, and 6.10.

Table 6.8. Mass-balance estimates of bulk composition G6.7.
CO_2 is calculated from shortfall in probe totals (assuming 0.5% trace elements)

Oxides	Ls	Lc	Mass-balance estimate (12%Lc)	Starting composition
SiO_2	39.63	2.73	35.20	35.05
Al_2O_3	16.34	0.08	14.39	14.35
CaO	20.39	29.01	21.43	22.02
Na_2O	16.46	26.62	17.68	17.88
CO_2	6.68	41.06	10.80	10.625
Totals	92.82	58.44	99.50	99.93

The synthetic composition G6.7 (SM2+CNC) contains *ca.* 88% silicate glass and *ca.* 12% carbonate quench from modal analysis. The mass-balance estimate of bulk composition obtained using these proportions is within 5% of the starting composition for all elements.

This permits three major conclusions:

(a) Electron probe microanalysis of quenched carbonate and silicate melts gives a true representation of the liquid compositions.

(b) Instability and sodium-mobilisation are confirmed as being negligible under the chosen analytical conditions.

(c) Shortfall in the sum of measured oxides in electron probe analysis is a reasonably accurate representation of CO_2 content. This will only be true in the H_2O-free systems analysed in this study.

Table 6.9. Mass-balance estimates of bulk composition G2.1.
CO_2 is calculated from shortfall in probe totals (assuming 1.0% minor and trace elements)
* are discrepancies between calculated mass-balance bulk composition, and starting contents. See text for details.

Oxides	Ls	Lc	Mass-balance estimate (20%Lc)	Starting composition
SiO_2	51.26	0.28	41.06	39.66
Al_2O_3	18.51	0.03	14.82	14.92
FeO	2.00	1.08	1.82*	4.24
MgO	0.62	1.14	0.72*	0.34
CaO	3.53	25.67	7.96	7.60
Na_2O	14.55	26.44	16.93	16.75
K_2O	3.86	3.21	3.73	3.68
TiO_2	0.93	0.17	0.77	0.70
MnO	0.13	0.17	0.14*	0.02
P_2O_5	0.08	0.43	0.15	0.08
CO_2	3.09	40.00	10.47	10.63
Totals	95.91	59.00	99.00	100.05

Mass-balance estimates for the bulk composition of charge 2.1 (BD50+CNC) have been obtained using modal proportions of 20% Lc, and 80% Ls. There is more Lc present in this charge because of less mixing of carbonate and silicate components in this sodium-rich, high-silica charge. Estimated concentrations are in general within error of the starting contents. There are three exceptions: FeO, MgO and MnO. The FeO content of the mass-balance bulk composition is *ca.* 40% of the original value. This large discrepancy can be attributed to alloying of the iron in the charge with the Pt capsule (discussed elsewhere). The mass-balance estimate of MgO content is much higher than expected. This could be due to inhomogeneity of the starting material (silicate melts are notoriously heterogeneous with respect to MgO contents). Alternatively, the MgO could have been added as a component of the $CaCO_3$ powder. Finally MnO estimates in the bulk composition are imprecise. This is thought to be

due to large statistical errors in analysis resulting from a combination of very low concentrations, and low beam currents. Again, Na-loss during analysis does not appear to have been significant, and CO_2 contents are in agreement with the shortfall in probe analyses.

Table 6.10. Mass-balance estimates of bulk composition G2.6.
CO_2 is calculated from shortfall in probe totals (assuming 1.0% minor and trace elements)
* are discrepancies between calculated mass-balance bulk composition, and starting contents. See text for details.

Oxides	Ls	Lc	Mass-balance estimate (9%Lc)	Starting composition
SiO_2	33.71	5.89	31.20	30.32
Al_2O_3	12.23	0.75	11.13	10.80
FeO	6.79	3.14	6.46*	9.03
MgO	4.14	3.93	4.12	3.92
CaO	19.73	35.48	21.14	21.11
Na_2O	8.35	10.65	8.55	7.61
K_2O	1.73	1.86	1.74	1.65
TiO_2	1.97	0.66	1.85	1.79
MnO	0.16	0.14	0.15	0.14
P_2O_5	0.49	1.80	0.60	0.56
CO_2	9.40	34.17	11.62	10.875
Totals	89.60	64.83	99.00	97.75

Mass-balance estimates of the calcic bulk composition of G2.6 (SUN189+CNC) are also mainly within error of the starting contents. FeO is again an exception (*ca.* 70% of the starting value) due to Fe-loss to the Pt capsule. There is also a slight discrepancy in the Na_2O estimate. A low Na_2O estimate could be explained by sodium migration during probe analysis, resulting in a fall-off in X-ray intensity with time. However, the mass-balance estimate of Na_2O content is in fact *ca.* 12% high. No explanation has been found for this behaviour; the discrepancy is small and is thought not to be of great significance.

There is thus reasonable agreement between bulk compositions estimated by mass-balance calculations and the original starting compositions. This strongly supports the contention that electron probe analyses of 100 μm^2 rastered areas are representative of the Ls and Lc compositions.

6.5. Ion probe microanalysis.

6.5.1. Introduction.

Trace-element concentrations in coexisting carbonate and silicate melts were measured by ion probe analysis. These concentrations were then used to calculate $^{Ls/Lc}D_i$ partition coefficients. In order to obtain realistic estimates of concentrations using the ion probe, homogenous, well characterised standard materials must be obtained. A sizable proportion of the time spent on the ion probe was therefore dedicated to analysing natural and experimentally produced carbonates to form the basis of standardising the Lc analyses.

Topics covered in this section include a brief summary of the equipment used, the techniques of analysis, and the analyses undertaken. There will also be detailed explanations of the standardising procedures, the data processing, and the analytical difficulties encountered. Finally, an estimate of the accuracy of the ion probe concentrations has been made by comparison of mass-balance estimates of bulk composition with known starting concentrations.

6.5.2. Sample Preparation.

After polishing with 1/4 μm diamond paste, samples were sputter-coated with a thin, even-thickness gold coating. This, like the carbon coat used on the electron probe, inhibits charge build-up on the sample. The coated samples were then covered, and stored in a sealed desiccator. The IMS-4f has poor optical capability, and many textural features are hidden by the gold coat, therefore, a detailed photographic map of the sample presentation surface was often required. This was especially true where complex mixed-crystalline assemblages were present. Without these maps, accurate positioning of the primary beam on the sample would not have been possible.

6.5.3. Analytical equipment and techniques.

Analyses were made on a Cameca IMS-4f. A schematic diagram of the main features of the probe is given in Figure 6.15. This method of analysis employs the technique of Secondary Ion Mass Spectrometry (SIMS), where ions are sputtered from the surface of a sample, and accelerated into a mass spectrometer.

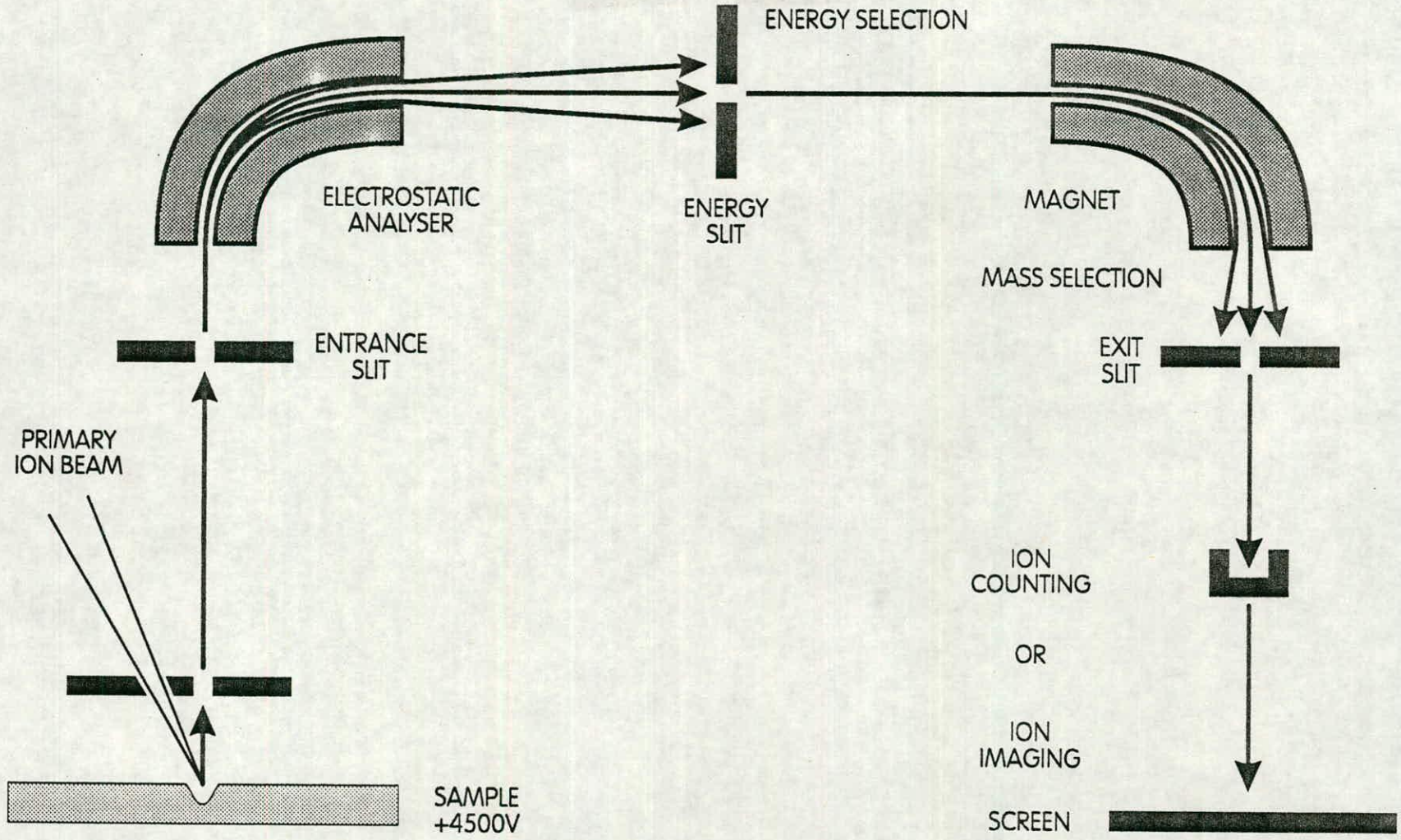

Figure 6.15. Simplified schematic diagram of the major features of the Cameca IMS-4f ion probe (after Hinton, in press).

Since this study was primarily concerned with obtaining concentrations for trace-elements with positive ions, a primary beam of $^{16}O^-$ ions was used to enhance cation formation. This primary beam was mass-filtered to avoid implanting Ni^+, Fe^+ and OH^- ions. The resulting pure beam was accelerated by a primary voltage of 10 keV. A further voltage was applied to the sample (+4.5 keV) giving a total accelerating voltage of 14.5keV. This beam was regulated to a current of *ca.* 5 nA, and focussed by a series of electrostatic lenses to a spot size of 25 μm. The primary beam was allowed to burn into the sample surface for *ca.* 3 mins before analysis commenced.

The sample was kept under a vacuum of between 2.10^{-8}, and 5.10^{-9}. This vacuum was maintained by a nitrogen cold-trap which freezes any water vapour in the vicinity of the sample. In this way interference problems are reduced, as any gas molecules arriving at the surface will be sputtered along with the matrix. The sputtered ions therefore consist of a variety of molecular and elemental species from both the primary beam and sample matrix (i.e. M^+, MO^+, MOH^+ M^{2+}, MSi^+ etc.). Molecular ions have narrower energy distributions than elemental ions. Molecular interferences have therefore been reduced by energy filtering (77 ± 19 eV). Although reduced, molecular ions are not always completely eliminated (Section 6.5.6.). Study of the high-energy tail of the energy distribution also reduces matrix effects (Hinton, 1990). Secondary ion count-rates were measured by sequential stepping of the magnetic field through a cycle of relative atomic mass. Ion counting was achieved by use of an electron multiplier. Some of the observed variations in ion yields for the NBS standard discussed later can be attributed to discrimination of the ion counting system (i.e. variations in efficiency of ion→electron conversion).

6.5.4. Analyses undertaken.

The analyses produced on the ion probe were in three categories, each with different set-up conditions:

(a) Determination of trace-element concentrations in quenched synthetic melts.

22 trace elements were added to the soda-melilite melts at *ca.* 100 p.p.m. levels (see Table 3.2). Concentration estimates were made on the ion probe for all these elements. Count-rate for a single isotope from each element was measured for 10 seconds in a cycle through the relative atomic masses (Z). Each analysis of carbonate and silicate was 5-25 cycles long, with statistics printed out every five passes. These

statistics (mean value and standard deviation) were transferred to microcomputer and processed to produce concentrations. The 5-cycle averages from all analyses of a single quenched liquid were then themselves averaged to produce estimates of liquid concentrations. 4-12 sets of 5 cycles were produced for each quenched silicate liquid with more on the carbonate compositions due to larger errors.

Fifteen samples were analysed. Where possible, samples were chosen that showed clear, well polished Ls-Lc textures. Data were produced to investigate the effects on partitioning of pressure, temperature, minor elements, composition, and run duration. One of the reversal experiments was also analysed to investigate the effects of approaching equilibrium from different starting conditions.

(b) Determination of trace element concentrations in quenched "natural" melts.

34 samples from experiments on natural rock samples were analysed on the ion probe, each with its own inventory of trace elements. The concentrations of 24 trace elements were determined in each sample. In some samples, analysis of Fe concentrations was replaced by analysis for Mo, as it was decided that Mo partitioning would be of interest geochemically. Again, each element was counted for either 4 or 10 seconds in each cycle of Z, usually with 10 cycles per analysis. The statistics from each 5-cycle printout were used to obtain mean concentrations in the quenched melts, and standard deviations from the mean.

Samples analysed on the ion probe included examples of each starting composition in which super-liquidus immiscibility was found. For each composition, samples were analysed so that the effects of pressure and temperature on partitioning could be investigated. For BD119+CNC, the pressure effect to 2.0 GPa, and the effects of run duration from 15-960 minutes were also investigated.

(c) Standardisation of carbonate and silicate melts.

A number of materials with known concentrations of certain trace elements were run as standards. For silicates, the NBS610 standard silicate glass was run every day on the first session, and three times in the second. Relative ion yield (RIY) values used for standardisation are given in the next section.

Carbonate standard materials were much more difficult to obtain, due to generally low concentrations of trace elements, and the presence of trace-element-rich inclusions in natural carbonates. A series of experiments were undertaken in an attempt to produce synthetic carbonate standards. However, these also tended to suffer from heterogeneity. Four synthetic, and seven natural carbonates were analysed to produce carbonate RIY values for at least some of the elements studied.

6.5.5. From count rates to concentrations.

The sputtering and ionisation process is poorly understood, and no physical model can adequately predict ion yields. Calculation of concentrations are therefore made relative to a standard of known composition. The following series of procedures have to be applied to the raw data:

(a) Normalisation of count rates to a species in the melt of known concentration.

This is done in order to remove variations and artefacts caused by the analytical conditions (machine type, beam density, spot-size, beam current, etc.).

The normalising species used in silicates is usually ^{30}Si. There is now some doubt as to the efficacy of normalisation to ^{30}Si (e.g. Hinton, 1990); it is believed that ratios to silicon are more susceptible to variations in operating conditions than other ratios (due to the broad energy distribution of Si compared to other elements). This suggestion is supported by the large variations seen in RIY for many elements in the NBS610 glass between the two major probe sessions (Table 6.11). However, variations within the probe sessions were small.

Despite this question mark as to the reliability of ^{30}Si as a normalising species, it was chosen in this study as Si was the only element well constrained by electron probe analysis which could also be counted on the electron multiplier.

^{42}Ca was used as the normalising species for carbonate quenches; the Ca concentration was well known from electron probe analysis, it can be measured on the electron multiplier, and it is regarded as a relatively stable element under different analytical conditions.

(b) Conversion of normalised $[^{n}i]/[^{30}Si]$ and $[^{n}i]/[^{42}Ca]$ ratios into concentrations.

This required a simple mathematical calculation according to the equations below.

For silicate:

$$X_i = \frac{[^{n}i]/[^{30}Si] \cdot IA_i \cdot X_{Si} \cdot RIY_i}{IA_{Si}}$$

Where:

X_i = Concentration of element i in the silicate liquid.

X_{Si} = Concentration of silicon in the silicate liquid.

$[^{n}i]/[^{30}Si]$ = Ratio of count-rates of ion ^{n}i and ^{30}Si.

IA_i = Percentage of element i which occurs as ^{n}i.

IA_{Si} = Percentage of silicon which occurs as ^{30}Si.

RIY_i = Ion yield of element i relative to that of silicon in standard.

For carbonate:

$$X_i = \frac{[^{n}i]/[^{42}Ca] \cdot IA_i \cdot X_{Ca} \cdot RIY_i}{IA_{Ca}}$$

Where:

X_i = Concentration of element i in the carbonate liquid.

X_{Ca} = Concentration of calcium in the carbonate liquid.

$[^{n}i]/[^{42}Ca]$ = Ratio of count-rates of ion ^{n}i and ^{42}Ca.

IA_i = Percentage of element i which occurs as ^{n}i.

IA_{Ca} = Percentage of calcium which occurs as ^{42}Ca.

RIY_i = Ion yield of element i relative to that of calcium in standard.

Therefore, in order to convert the normalised ratios into concentrations we need the concentration of the reference species (from the electron probe data), the isotopic proportions of the elements studied (known to better than four significant figures for most elements), and the RIY of the element being analysed.

RIYs for silicate glass were obtained by regular analysis of the NBS610 silicate standard. The mean values obtained from this standard for the analysed elements are given in Table 6.11. RIY data from KFNBS1 was used in the processing of data from the morning sessions 20/9/90-24/9/90, and from the main session 9/4/91-14/4/91. RIY values were found to have changed considerably before the final analytical session was obtained; the data from this session (4/5/92-10/5/92) were therefore processed with the KFNBS2 values.

Table 6.11. Variations in RIY with respect to silicon between the first and second probe sessions. Variations in RIY within probe sessions are small. Values are for a 25 μm spot size, 77 eV energy offset.

Element	RIY (KFNBS1)	RIY (KFNBS2)
Mg	1.88	1.98
K	1.14	1.05
Ca	3.26	3.09
Ti	2.56	2.36
V	1.70	1.61
Cr	1.22	1.16
Fe	1.05	-
Mn	0.83	1.05
Rb	0.98	0.80
Sr	2.90	2.51
Y	3.47	3.01
Zr	2.23	1.88
Nb	1.39	1.05
Mo	-	0.66
Cs	0.66	0.49
Ba	2.04	1.60
La	2.27	1.81
Ce	2.21	1.73
Nd	2.59	1.81
Sm	2.78	2.22
Hf	1.29	0.99
Ta	0.71	0.62
Pb	0.061	0.033
Th	1.36	1.09
U	1.34	1.05

On first processing, trace-element concentrations in the quenched carbonate melt were also estimated using NBS610 standard RIY values. These values are only an approximation, and for accurate quantitative analysis of the carbonate concentrations, standard values for RIYs in carbonate materials had to be measured. A number of carbonate samples, with known trace-element contents, were therefore run as standards for those elements within a carbonate matrix.

The experimental manufacture of a homogeneous carbonate standard was attempted. Calcium carbonate, and mixed calcium-sodium-carbonate powders were produced with *ca.* 100 p.p.m. of each of the elements analysed on the ion probe. A portion of

each was sealed inside a Pt capsule and run in gas media vessels for *ca.* 6 hours at 1300°C, 0.5 GPa. Unfortunately, the majority of elements added to the carbonates were not admitted into the calcite and nyerereite structures on quenching, and were instead left concentrated as interstitial material between six-sided, close-packed carbonate crystals. Ion imagery obtained from the Cameca probe, shows this effect clearly for the elements Cs and Rb. Although the imaging was performed before the gold coat was removed, the distribution of Rb and Cs reflects the actual alkali metal distribution in the sample. The estimated concentrations of the trace elements in the $CaCO_3$ material, together with its starting contents, is given in Table 6.12.

Table 6.12. Trace-element concentrations in calcium carbonate standard. Many elements do not enter the carbonate structure, and will be present in the silicate part of the quenched Lc.

	Calcite standard concentrations.	
Elements.	Added	In structure
Mg	*ca.* 700	458
K	100	17
Ti	100	1
V	100	3
Cr	100	9
Rb	100	13
Sr	169	105
Y	100	22
Zr	100	0.6
Nb	100	<0.1
Cs	100	2
Ba	72	60
La	100	35
Ce	100	32
Nd	100	36
Sm	100	45
Tm	100	24
Yb	100	11
Hf	100	<0.1
Ta	100	0.2
Pb	100	5
Th	100	<0.1
U	100	<0.1

In the $CaCO_3$ material the elements Ti, Zr, Nb, Hf, Ta, Th, and U were present at $<<1$ p.p.m. despite being added at 100 p.p.m. levels. Indeed, many are present at <0.1

p.p.m. implying extreme $^{calcite/sil}D_i$ values in excess of 10^{-3}. It can be assumed that this is also the case in the quenched carbonate liquid from the immiscibility experiments, and that the above elements are not present in significant quantities in the quench carbonates. They are therefore being sputtered from the exsolved silicate portion of the quench, and their concentrations are thus best estimated using silicate RIY values.

The majority of the other elements are present in the carbonate, but at concentrations much lower than originally added (e.g. K, Rb, Cs, Pb, and the REEs). A substantial proportion of these elements is likely to be contained within the carbonate component of the quenched carbonate melt. Appropriate RIY values are therefore required. Only three elements (Mg, Sr, and Ba) seem to have remained in the carbonate at approximately the added concentrations, but even for these elements, this standard must be considered suspect.

The second attempt at experimental production of carbonate standard materials met with more success. Calcium carbonate powders were doped with Mg, Sr, Ba, and Pb at sufficiently high concentrations to permit electron probe analysis. These mixtures were known to form homogenous subsolidus assemblages at the run conditions (Chang, 1971.a & b). The samples produced were in fact not completely homogenous, but nevertheless could be analysed for Mg, Sr, and Ba. The Pb standard had to be abandoned due to heterogeneity. The electron probe and ion probe concentrations are given in Table 6.13. Ion probe concentrations were obtained using the NBS610 RIY values, and the difference between these and the electron probe values therefore represents the difference in ion yield between silicate and carbonate. This "conversion factor" is also given in Table 6.13.

Table 6.13. Differences in RIY between carbonate and silicate structures from experimentally produced carbonate standards. The effect of carbonate structure on RIY can be assessed by comparison of ion probe concentrations obtained using NBS610 RIY values with electron probe concentrations. Magnesium RIY values are significantly different from 1, whilst no evidence is seen for variations in RIY for Sr or Ba

	Ion probe values.		Electron probe values.		Conversion factor
Sr-standard					
	Mean (2)	Std. Dev.	Mean (10)	Std. Dev.	(RIY_{car}/RIY_{sil})
Sr	9840	126	10238	2962	0.96
Mg	98	4	180	60	0.54
Ba-standard					
	Mean (2)	Std. Dev.	Mean (10)	Std. Dev.	(RIY_{car}/RIY_{sil})
Ba	10284	260	10029	2776	1.03
Mg	102	6	180	60	0.57

In conjunction with these experimentally produced standards, a number of natural carbonate materials were obtained and analysed on the ion probe. The standards included 4 calcites, a strontianite, a dolomite, and a REE-rich Ca-Sr carbonate called carbocernaite. These carbonates were also processed using the NBS610 RIY values, and the concentrations calculated were then compared with electron probe, INAA, and ICP-MS values. Table 5.14 shows the ion probe concentrations, the standard values, and the resulting conversion factor between RIY_{sil} and RIY_{car}. All ion probe data are obtained by standardisation to Ca concentrations. This is considered valid as absolute Ca count-rates per unit concentration for the Ls and Lc phases were found to be virtually identical.

Table 6.14. Ion probe standards for carbonates: natural carbonate materials. Standard values for Kimsey Quarry calcite and Samu carbocernaite from electron probe analyses (Appendix A.3). Other standard values from Ion Probe Unit standard sheets. Ion probe values calculated using NBS610 RIY values. The difference between ion probe concentration and standard content is ascribed to RIY differences between carbonate and silicate matrices.
* Standards with low concentrations. These values should be treated with caution.

	Ion probe values.		Standard values.		Conversion factor
Carbocernaite; Samu carbonatite, India.					
	Mean (9)	Std. Dev.	Mean (29)	Std. Dev.	(RIY_{car}/RIY_{sil})
Mn	1763	172	1317	624	1.34
Sr	161435	3460	170470	-	0.95
Ba	9907	510	7886	950	1.26
La	66568	2654	94072	22460	0.71
Ce	71522	2274	109850	2290	0.65
Nd	14712	551	16020	1220	0.92
Sm	532	44	509	68	1.04
Kimsey Quarry calcite, Arkansas, USA.					
	Mean (6)	Std. Dev.	Mean (5)	Std. Dev.	(RIY_{car}/RIY_{sil})
Mg	194	5	270*	120	0.72
Sr	6810	73	5630	110	1.20
Ba	678	14	780	500	0.87
Derbyshire Iceland Spar.					
	Mean (2)	Std. Dev.	Mean	-	(RIY_{car}/RIY_{sil})
Mg	409	12	662		0.62
Mn	701	1	802		0.87
Norman cross calcite.					
	Mean (2)	Std. Dev.	Mean	-	(RIY_{car}/RIY_{sil})
Mg	1652	41	2749		0.60
Mn	1295	14	1486		0.87
Sr	801	15	845		0.95
Departmental Iceland spar standard.					
	Mean (2)	Std. Dev.	Mean	-	(RIY_{car}/RIY_{sil})
Mn	22	0	53*		0.42
Sr	267	6	183*		1.46
Strontianite (USNM R10065).					
	Mean (2)	Std. Dev.	Mean	-	(RIY_{car}/RIY_{sil})
Sr	628802	2082	572210		1.09
Ba	98	2	100		0.98
Dolomite (USNM 1005).					
	Mean (2)	Std. Dev.	Mean	-	(RIY_{car}/RIY_{sil})
Mg	71049	281	132240		0.54

It should be noted from Tables 6.13 and 6.14 that none of the ion probe estimates vary from the standard values by as much as a factor of two. This implies that, for these elements at least, RIYs from a carbonate matrix are not different from NBS610 silicate values by as much as a factor of two. Due to the cumulative nature of the errors in both analyses, the uncertainties associated with the conversion factors are large. Indeed, most ion probe estimates are not significantly different from the standard values, giving no evidence for variations in RIY. In any case, RIY effects are certainly small compared to the order of magnitude variations seen in $^{Lc/Ls}D_i$ values determined in this study.

For Sr, values of (RIY_{car}/RIY_{sil}) vary between 0.95, and 1.46. The average value is *ca.* 1.08. The highest value is given by the standard with the lowest Sr concentration. If this value is ignored, the average (RIY_{car}/RIY_{sil}) is 1.05. This value is not sufficiently different to produce significant variations in calculated $^{Lc/Ls}D_i$ values. This fact, combined with lack of confidence in the higher Sr (RIY_{car}/RIY_{sil}) values, led to the decision that NBS610 RIY values were adequate for estimations of Sr contents in carbonates. For Ba, values of (RIY_{car}/RIY_{sil}) vary between 0.87 and 1.26. The average is not significantly different from 1, and therefore no correction to the NBS610 RIY values has been made. For Mn, values of (RIY_{car}/RIY_{sil}) range widely, from 0.42 to 1.34. An average of *ca.* 0.9 has been considered untrustworthy due to this spread. No correction has been applied. For Mg, values of (RIY_{car}/RIY_{sil}) vary from 0.54 to 0.72. The average is *ca.* 0.6. This value has been applied to all carbonate ion probe data. After corrections using a fixed RIY for all carbonate analyses, carbonate compositions more closely approximate electron probe analyses, and mass-balance estimates fit more closely to starting compositions. For the REE, only the (RIY_{car}/RIY_{sil}) value from the carbocernaite in the Samu carbonatite, India has been obtained. Because of the precision available on these values (due to the large concentrations of REE in carbocernaite), they have been applied to ion probe carbonate data where significantly different from 1. Values used were $(RIY_{car}/RIY_{sil})_{La} = 0.71$, $(RIY_{car}/RIY_{sil})_{Ce} = 0.65$, $(RIY_{car}/RIY_{sil})_{Nd} = 0.92$, $(RIY_{car}/RIY_{sil})_{Sm} = 1.04$.

Unlike the Mg data, the REE (RIY_{car}/RIY_{sil}) values have been obtained from just one carbonate structure. Employment of these values would therefore perhaps be unwarranted without further evidence as to their applicability to the carbonate quenches being analysed. This evidence comes from two observations. Firstly, during ion probe analysis of the quenched carbonate and silicate melts, an estimate of

the $REE^+/REE\text{-}O^+$ ratio was made for La, Ce and Nd. The element/oxide ratios were found to be significantly smaller from the carbonate matrix, and variations between individual $REE^+/REE\text{-}O^+$ significantly more extreme. The Ce/CeO ratio is particularly low, and may explain the lower relative ion yield for elemental Ce (0.65) in carbonates than those seen in NBS610.

The other observation can be seen in Figures 6.16 and 6.17, where the REE partitioning data with corrections applied are compared with uncorrected values. REEs are well known for coherent behaviour in geochemical processes. Any differences in behaviour between REEs is normally ascribed to the gradual decrease in ionic radius from LREE to HREE. Exceptions to this are Eu^{2+} and Ce^{4+}, neither of which is likely to be present in these experimental materials. A simple relationship of $^{Lc/Ls}D_{REE}$ with ionic radius was therefore expected. Figure 6.16 shows a selection of experimental $^{Lc/Ls}D_{REE}$ data produced before correcting the carbonate melt concentration estimates. A general decrease in $^{Lc/Ls}D_{REE}$ with increasing ionic radius is seen, but the correlation is poor, with kinked, incoherent behaviour between Sm, Nd, and Ce (i.e. $^{Lc/Ls}D_{Sm} < {}^{Lc/Ls}D_{Nd} < {}^{Lc/Ls}D_{Ce}$). This kinked pattern of REE behaviour is difficult to explain in terms of geochemical characteristics, and was considered likely to be a machine artefact. Figure 6.17 shows the $^{Lc/Ls}D_{REE}$ data obtained by using corrected RIY values. A much smoother trend with ionic radius now occurs, with correlation coefficients of 0.98 or better. This increased coherency of REE behaviour is taken as further evidence that adoption of the carbocernaite (RIY_{car}/RIY_{sil}) values produces a better estimate of carbonate REE concentrations. It must be stated that still only one RIY is being applied; this is obviously a source of error in charges where the carbonate quench has a significant silicate component.

For those elements where values of RIY_{car} are not known, NBS610 values have been used. As mentioned earlier, most of these elements are likely to have been sputtered from a silicate matrix, making the use of these RIY values valid. However, even if they are contained within carbonate, the standardising work done on other elements shows that variations in RIY are likely to be small, and are certainly unlikely to exceed a factor of 2. Where possible, conclusions are based on elements whose RIY_{car} is known, before extrapolation to data where assumptions about RIY have been made. The assumption that errors produced by ion yield effects are small is confirmed by the agreement between mass-balance calculations undertaken on various charges with the original starting compositions.

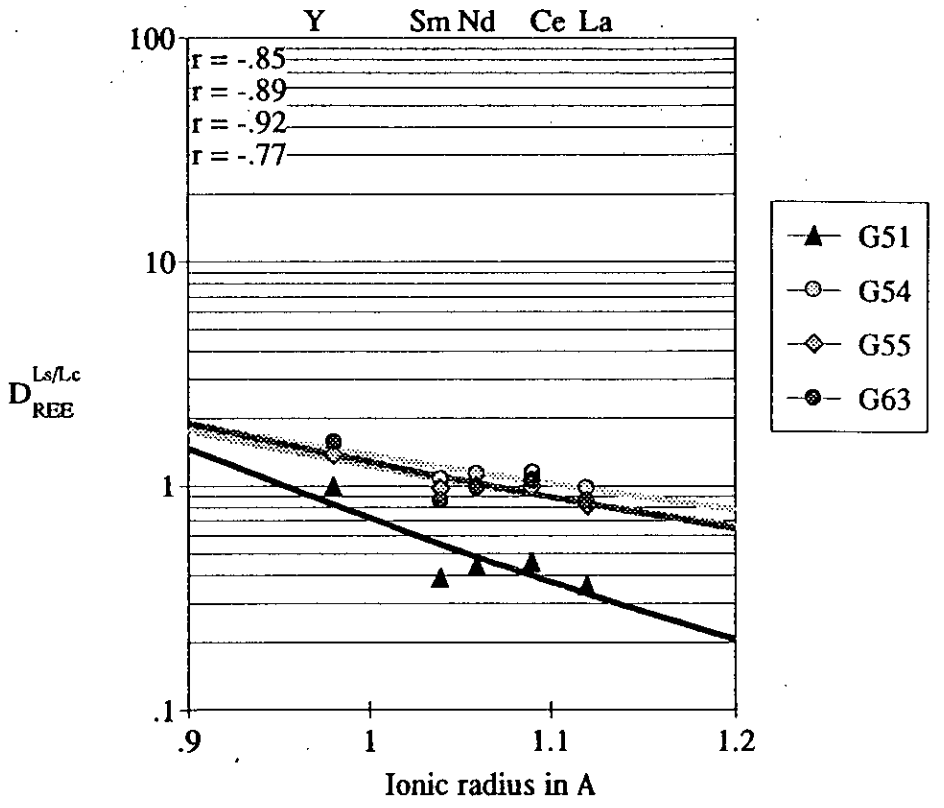

Figure 6.16. Rare earth element partitioning using uncorrected data from natural compositions from a range of experiments.
A relatively poor correlation of partitioning behaviour with ionic radius is seen. A reproducible pattern occurs with a general decrease in D with increasing ionic radius, but with a rise in D value from Sm to Ce. This is seen in all the experimental charges, and is therefore a systematic effect, and not just due to uncertainty. It is difficult to see how this pattern could be produced by magmatic processes, and was instead interpreted as an ion yield problem.

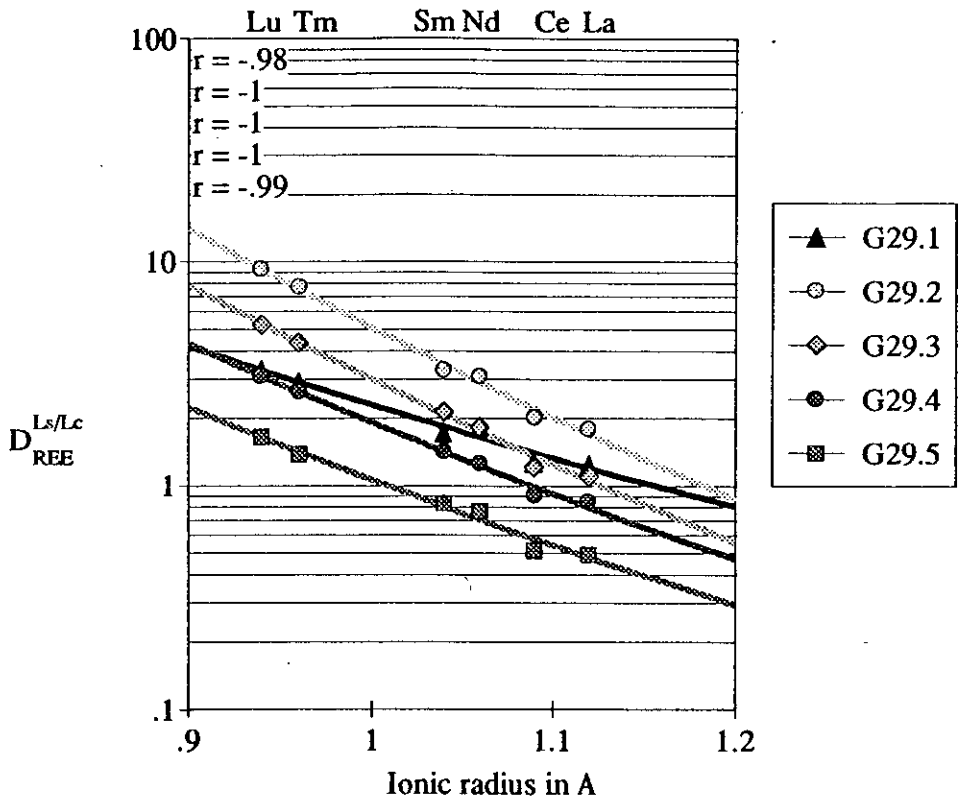

Figure 6.17. Rare earth element partitioning using data corrected for relative ion yield effects in the carbonate liquid: Coexisting melt data from run G29 (SM2+CNC). Very good correlation of partitioning behaviour with ionic radius is seen. A continuous, smooth decrease in D value occurs from HREE to LREE.

6.5.6. Limitations of ion probe analysis.

Four major limitations were encountered during ion probe analysis of the quenched carbonate and silicate melts:

(a) Ion yield effects and standardisation.

These have been discussed in some detail in the previous section, and, despite the improvements in carbonate standardisation achieved here, are still considered to be a source of uncertainty when analysing carbonate-bearing materials.

(b) Interference effects.

Interferences were in general avoided by careful consideration of the elements to be studied, and the isotopes of these elements to be counted. In the doped samples, elements were chosen to avoid possible molecular ion overlap. This was not the case for three elements in the natural rock compositions.

Rb has only two naturally occurring isotopes, ^{87}Rb, and ^{85}Rb. ^{87}Rb is often swamped by Sr peaks, and is therefore rarely used in ion probe analysis. ^{85}Rb also has an interference problem in iron-bearing silicates due to the presence of [Fe+Si] at mass 85. A correction (generally <<5%) was therefore made on the Rb data according to the equation;

$$^{85}Rb = {}^{85}Total-(^{84}[Fe+Si]*0.074)$$

Chromium data are also subject to interferences in silicate melts. ^{52}Cr consistently gave concentration estimates well in excess of those present in the starting materials. It was therefore concluded that Cr concentrations quoted, and the $^{Lc/Ls}D_{Cr}$ data derived from them are subject to sizable but unquantifiable interference effects.

Hafnium data have interference problems in the data for natural compositions due to interference from $Dy\text{-}O^+$. In glasses made from natural composition material, count rates at the Hf masses can be attributed to $HREE\text{-}O^+$ ions. In contrast, the synthetic experiments have both high hafnium concentrations, and no dysprosium; $^{Ls/Lc}D_{Hf}$ from these experiments will be well constrained.

A similar interference may occur to a lesser extent on tantalum concentrations in the natural experiments, this time due to the presence of Ho-O^+. Again, the data for synthetic compositions will be unaffected, due to both the high concentrations of tantalum in these charges, and the since no holmium was added to the starting materials.

Finally, in some charges, two values of Ti concentration have been determined, one based on ^{47}Ti count-rates, and the other on ^{50}Ti. The concentrations are different, and it is believed that this is due to interference on the ^{50}Ti peak by [Na+Al], both of which are present at high concentration in the silicate melt. Correcting this interference effect produces concentrations similar to those estimated by ^{47}Ti; however, it is better that the interference-free ^{47}Ti data be used. ([Na+Mg] interference will only be sizeable in the Mg-rich natural rocks where Ti is present at 1000s of p.p.m.).

(c) Poor counting statistics.

Counting errors on the Pb concentrations are large (up to 100% of the actual value in the charges with lowest concentrations!). This is due to a combination of very low concentrations, combined with very low Pb ion yields. The resulting $^{Lc/Ls}D_{Pb}$ data has large uncertainties attributable to counting statistics, but is still useful in qualitatively constraining Pb partitioning behaviour.

(d) Inability to study negative ions.

Although negative ion measurement is feasable, it was not possible to measure both positive and negative ions simultaneously. However, $^{Lc/Ls}D_F$, $^{Lc/Ls}D_{Cl}$, $^{Lc/Ls}D_S$, and $^{Lc/Ls}D_P$ values have been obtained on the electron probe, and it is hoped that these data will give an adequate indication of the basic features of non-metal carbonate-silicate partitioning.

(e) Quench heterogeneity.

On cooling, the carbonate melt undergoes quench crystallisation, forming an intergrowth of carbonate and silicate material. As seen in the failed synthetic carbonate standards, some elements are present in the carbonate melt that cannot be accommodated in crystalline carbonate structures. These are strongly segregated into

the exsolved silicate part of the quench, and are therefore heterogeneously distributed in the quenched melt. This leads to large analytical errors in the $^{Lc/Ls}D_i$ values for those elements strongly affected by quenching processes (Si, Ti, V, Zr, Nb, Ta, Hf, Th, U). The bulk of the elements analysed are little affected by the quench, and thus the partitioning data for many elements are well constrained. These elements include Mg, K, Mn, Rb, Sr, Y, Cs, Ba, La, Ce, Nd, Sm, Tm, Lu. Many of the conclusions drawn from $^{Lc/Ls}D_i$ values will be formulated on those elements with well constrained partitioning behaviour before incorporating the data from those elements which suffer extensively from quench heterogeneity.

6.5.7. Comparison of ion probe concentrations with starting materials and electron probe results.

A number of major elements in the natural immiscible melt compositions were analysed both on the electron probe and on the ion probe. This gives us the opportunity to compare the results of these two differing analytical techniques to check for inconsistencies and systematic differences. The elements analysed by both techniques were Mg, K, Ca, Ti, Fe, and Mn. Tables 6.15, 6.16, and 6.17 give the comparisons between the two values for each of the natural starting compositions.

The silicate concentrations measured by both instruments are in close agreement with each other, with the differences between analyses rarely exceeding 10%. The exceptions to this are Fe and Mn that give comparison values of 1.08 and 1.58, that is the ion probe tends to overestimate the Fe and Mn contents compared to the electron probe analyses.

As would be expected from quench heterogeneity, the carbonate analyses are considerably more variable. Electron and ion probe analyses are in general agreement within a factor of 2. However, this is not the case for the carbonate liquid G5.5, where the ion probe concentrations for Mg, Si, Ti, and Fe are all substantially higher than the electron probe estimates. This is probably due to the inadvertant inclusion of a silicate sphere during the carbonate analysis, resulting in low Ca count-rates, as well as high Si, Ti, and Fe count-rates. The effects on overall concentration estimates of this sphere are therefore large.

Table 6.15. Comparison of electron and ion probe analyses of major element concentrations. Phonolitic rock compositions at 1200 C, 0.5GPa.

	G5.1				
Silicate	Oxides		Elements		Comparison between electron
	E. probe	Ion probe	E. probe	Ion probe	and ion probe estimates.
Mg	0.69	0.63	0.41	0.38	0.92
K	3.81	3.62	3.16	3.00	0.95
Ca	4.83	4.89	3.45	3.49	1.01
Ti	0.85	0.80	0.51	0.48	0.94
Fe	2.68	2.91	2.09	2.26	1.09
Mn	0.13	0.14	0.10	0.11	1.08
Carbonate	Oxides		Elements		Comparison between electron
	E. probe	Ion probe	E. probe	Ion probe	and ion probe estimates.
Mg	0.95	0.64	0.57	0.38	0.67
Si	0.60	0.70	0.28	0.33	1.16
K	3.69	5.74	3.06	4.76	1.55
Ti	0.17	0.28	0.10	0.17	1.67
Fe	0.85	0.74	0.66	0.58	0.88
Mn	0.15	0.08	0.11	0.06	0.53
	G5.2				
Silicate	Oxides		Elements		Comparison between electron
	E. probe	Ion probe	E. probe	Ion probe	and ion probe estimates.
Mg	0.69	0.69	0.42	0.41	1.00
K	3.94	3.60	3.27	2.99	0.91
Ca	11.98	12.28	8.56	8.77	1.02
Ti	0.83	0.72	0.49	0.43	0.87
Fe	2.07	2.74	1.61	2.13	1.32
Mn	0.12	0.16	0.09	0.12	1.30
Carbonate	Oxides		Elements		Comparison between electron
	E. probe	Ion probe	E. probe	Ion probe	and ion probe estimates.
Mg	0.47	0.64	0.28	0.38	1.36
Si	0.72	0.70	0.34	0.33	0.97
K	3.32	5.74	2.76	4.76	1.73
Ti	0.18	0.28	0.11	0.17	1.55
Fe	0.72	0.74	0.56	0.58	1.03
Mn	0.10	0.08	0.08	0.06	0.79

Table 6.16. Comparison of electron and ion probe analyses of major element concentrations. Nephelinitic rock compositions at 1200 C, 0.5GPa.

	G5.3				
Silicate	Oxides		Elements		Comparison between electron
	E. probe	Ion probe	E. probe	Ion probe	and ion probe estimates.
Mg	0.91	0.96	0.55	0.58	1.06
K	3.66	3.55	3.04	2.95	0.97
Ca	10.91	12.53	7.79	8.95	1.15
Ti	0.99	0.91	0.59	0.54	0.92
Fe	4.26	5.27	3.31	4.10	1.24
Mn	0.28	0.36	0.22	0.28	1.27
Carbonate	Oxides		Elements		Comparison between electron
	E. probe	Ion probe	E. probe	Ion probe	and ion probe estimates.
Mg	0.68	1.40	0.41	0.84	2.07
Si	1.87	3.11	0.87	1.45	1.67
K	5.43	5.68	4.51	4.71	1.05
Ti	0.12	0.24	0.07	0.14	2.09
Fe	0.81	1.24	0.63	0.96	1.53
Mn	0.21	0.24	0.16	0.19	1.15
	G5.4				
Silicate	Oxides		Elements		Comparison between electron
	E. probe	Ion probe	E. probe	Ion probe	and ion probe estimates.
Mg	0.89	0.99	0.54	0.60	1.12
K	3.63	3.73	3.01	3.10	1.03
Ca	16.82	19.30	12.02	13.79	1.15
Ti	0.93	0.87	0.55	0.52	0.94
Fe	5.13	7.22	3.99	5.61	1.41
Mn	0.27	0.39	0.21	0.30	1.44
Carbonate	Oxides		Elements		Comparison between electron
	E. probe	Ion probe	E. probe	Ion probe	and ion probe estimates.
Mg	0.69	1.57	0.41	0.95	2.29
Si	3.38	6.60	1.58	3.09	1.96
K	5.51	6.56	4.57	5.44	1.19
Ti	0.19	0.55	0.11	0.33	2.95
Fe	1.52	3.32	1.18	2.59	2.19
Mn	0.21	0.28	0.16	0.22	1.36

Table 6.17. Comparison of electron and ion probe analyses of major element concentrations. Olivine nephelinitic rock compositions at 1200 C, 0.5GPa. * Ion probe data from just three analyses, at least one of which is believed to be contaminated by a silicate sphere.

		G5.5			
Silicate	Oxides		Elements		Comparison between electron
	E. probe	Ion probe	E. probe	Ion probe	and ion probe estimates.
Mg	4.22	4.93	2.55	2.98	1.17
K	1.71	1.94	1.42	1.61	1.14
Ca	13.68	16.70	9.77	11.93	1.22
Ti	2.08	2.17	1.25	1.30	1.04
Fe	7.13	11.23	5.54	8.73	1.58
Mn	0.16	0.23	0.12	0.18	1.44
Carbonate	Oxides		Elements		Comparison between electron
	E. probe	Ion probe	E. probe	Ion probe	and ion probe estimates.*
Mg	3.00	6.70	1.81	4.04	2.23
Si	2.37	4.37	1.11	2.04	1.84
K	2.91	3.23	2.41	2.68	1.11
Ti	0.31	0.65	0.19	0.39	2.10
Fe	1.92	4.19	1.49	3.26	2.18
Mn	0.09	0.10	0.07	0.08	1.15
		G5.6			
Silicate	Oxides		Elements		Comparison between electron
	E. probe	Ion probe	E. probe	Ion probe	and ion probe estimates.
Mg	4.08	4.44	2.46	2.68	1.09
K	1.80	1.75	1.49	1.45	0.97
Ca	21.92	23.83	15.66	17.02	1.09
Ti	2.01	2.03	1.21	1.22	1.01
Fe	6.24	7.51	4.85	5.84	1.20
Mn	0.16	0.19	0.12	0.15	1.21
Carbonate	Oxides		Elements		Comparison between electron
	E. probe	Ion probe	E. probe	Ion probe	and ion probe estimates.
Mg	3.38	3.34	2.04	2.01	0.99
Si	1.45	3.87	0.68	1.81	2.67
K	0.82	1.60	0.68	1.33	1.95
Ti	0.25	0.44	0.15	0.26	1.74
Fe	1.95	2.35	1.52	1.83	1.21
Mn	0.08	0.07	0.06	0.06	0.89

Trace-element comparisons of a similar nature cannot be made as electron probe analysis lacks the sensitivity to analyse elements at p.p.m. levels. An alternative method of looking at the reliability of the ion probe analyses was therefore required. As with the electron probe analyses, it was decided that mass-balance calculations were the best way of confirming analytical accuracy. The same charges were investigated by mass balance as were discussed in the electron probe section (alkali-rich G2.1, alkali-poor G2.6, and synthetic composition G7.7) with the same proportions of phases (20%, 9%, and 12% of Lc respectively, Tables 6.8-6.10). A third natural composition, BD119+CNC (G2.3), was also investigated as variations in major element compositions can lead to different interference and standardising problems. The modal proportions in this charge were estimated as 14% Lc, 86% Ls.

In the synthetic composition G7.7, the mass-balance estimate of bulk compositionproduced from the ion probe concentrations was compared to the initial trace-element concentrations added to the soda-melilite. These added concentrations are believed accurate to ± 10% weighing error. We therefore have an upper and lower boundary between which the mass-balance estimate should sit. This is in fact the case for the majority of trace-elements studied, as is shown by Figure 6.18. There are a number of exceptions, where the ion probe concentrations fall outside the weighing errors. K and Cs concentration estimates are too high, by *ca.* 20%. Zr and Y are too low by *ca.* 20%. These are small, but significant differences, and are probably due to variations in ion yield for these elements. Two elements have more pronounced departures from the original added concentrations. These are Pb and Rb. It is thought that these elements were actually lost during the experimental work, with Pb alloying with the Pt capsule, and Rb partitioning into the coexisting vapour phase. The other elements are within error of starting compositions.

With the natural rock compositions, the starting concentrations are much more closely constrained, with each rock composition having XRF determinations available for most elements, often augmented by INAA data. The concentrations of two elements, Ta and Hf, are unknown in these rocks, although an estimate of 5 p.p.m. of each was suggested by Hamilton *et al.* (1989). A rough estimate of Ta and Hf concentrations can be obtained from Nb and Zr contents by using average Nb/Ta and Zr/Hf ratios (*ca.* 16 and 35 respectively). Estimates produced in this way are in better agreement with the mass balance calculations shown here than those of Bedson & Hamilton (1988), giving concentrations of 18 p.p.m. Hf and 12 p.p.m. Ta. The mass-balance estimates of bulk composition based on ion probe averages of quenched silicate and

Figure 6.18. Comparison of starting materials and "mass-balance" estimates: ion probe accuracy. G7.7: A synthetic example.

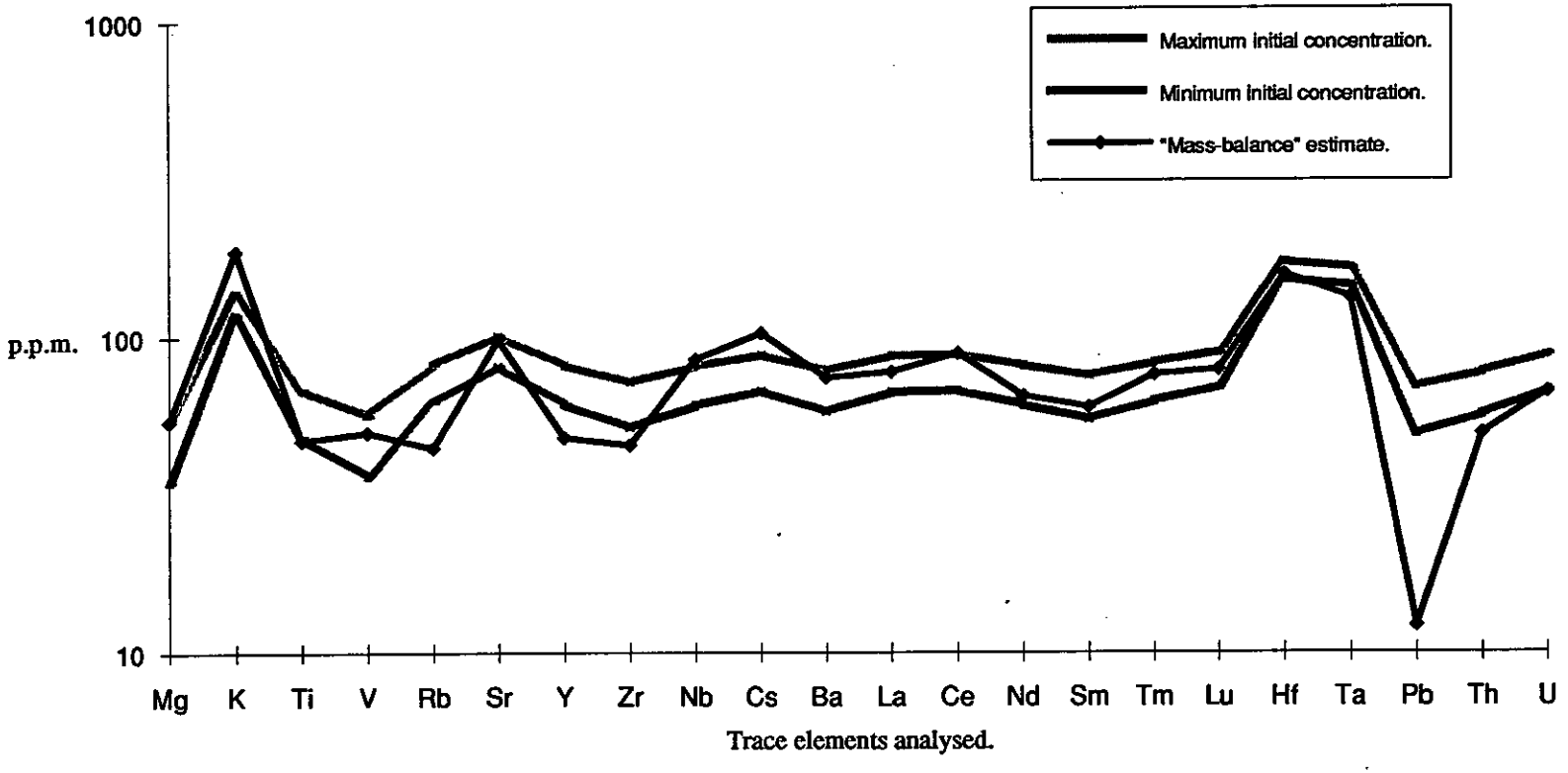

carbonate components agrees very closely with that based on XRF analyses of the starting materials for all elements except Cr and Pb (Figures 6.19, 6.20, and 6.21). Ion probe analysis of trace-element concentrations of quenched carbonate and silicate liquids is therefore considered an acceptable method for obtaining $^{Lc/Ls}D_i$ data.

The Pb estimates from mass-balance are always lower than the starting contents. This is perhaps best explained by Pb-loss to the Pt sample capsule, a process known to occur in conjunction with the iron-loss seen in these experiments. Although this lack of agreement between starting content and ion probe concentrations places some doubt on the $^{Lc/Ls}D_{Pb}$ data, there are grounds for accepting the partitioning results since the reason for this departure is well established.

Cr mass-balance concentration estimates are always significantly higher than the starting contents. This could be explained by contamination of the charge with chromium, or perhaps an extreme ion yield effect. However, the most likely explanation is that the quoted mass-balance values do not represent Cr contents at all, and that the peak at ^{52}Cr that was analysed is in fact an interference effect. Since this interference swamps the true Cr contents by a factor of *ca.* 10, there is no way of accurately determining the true Cr contents. The $^{Lc/Ls}D_{Cr}$ data will therefore not be considered further.

Figure 6.19. Comparison of starting materials and "mass-balance" estimates: A test for ion probe accuracy. G2.1, BD50+CNC.

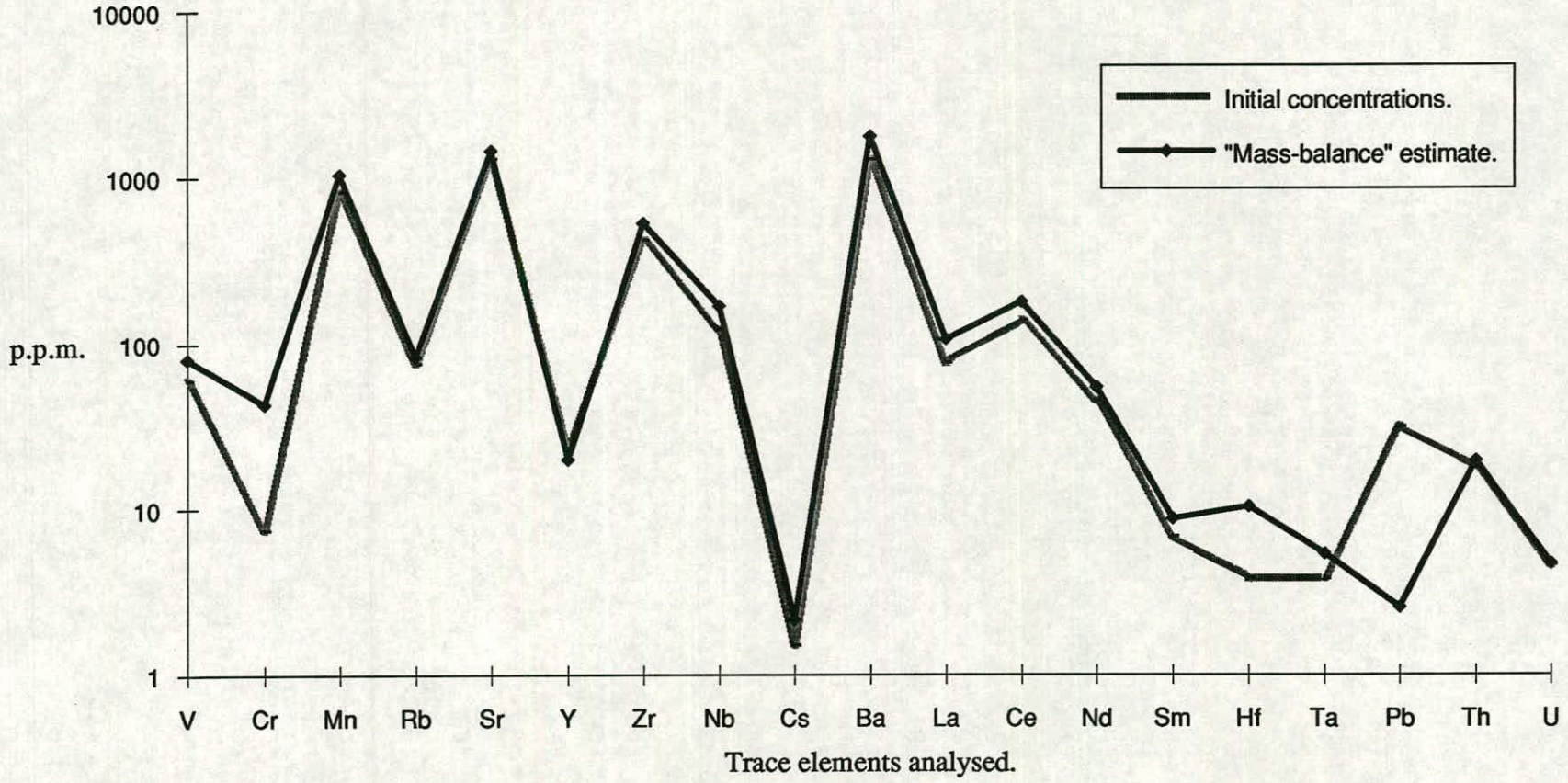

Figure 6.20. Comparison of starting materials and "mass-balance" estimates: A test for ion probe accuracy. G2.3, BD119+CNC.

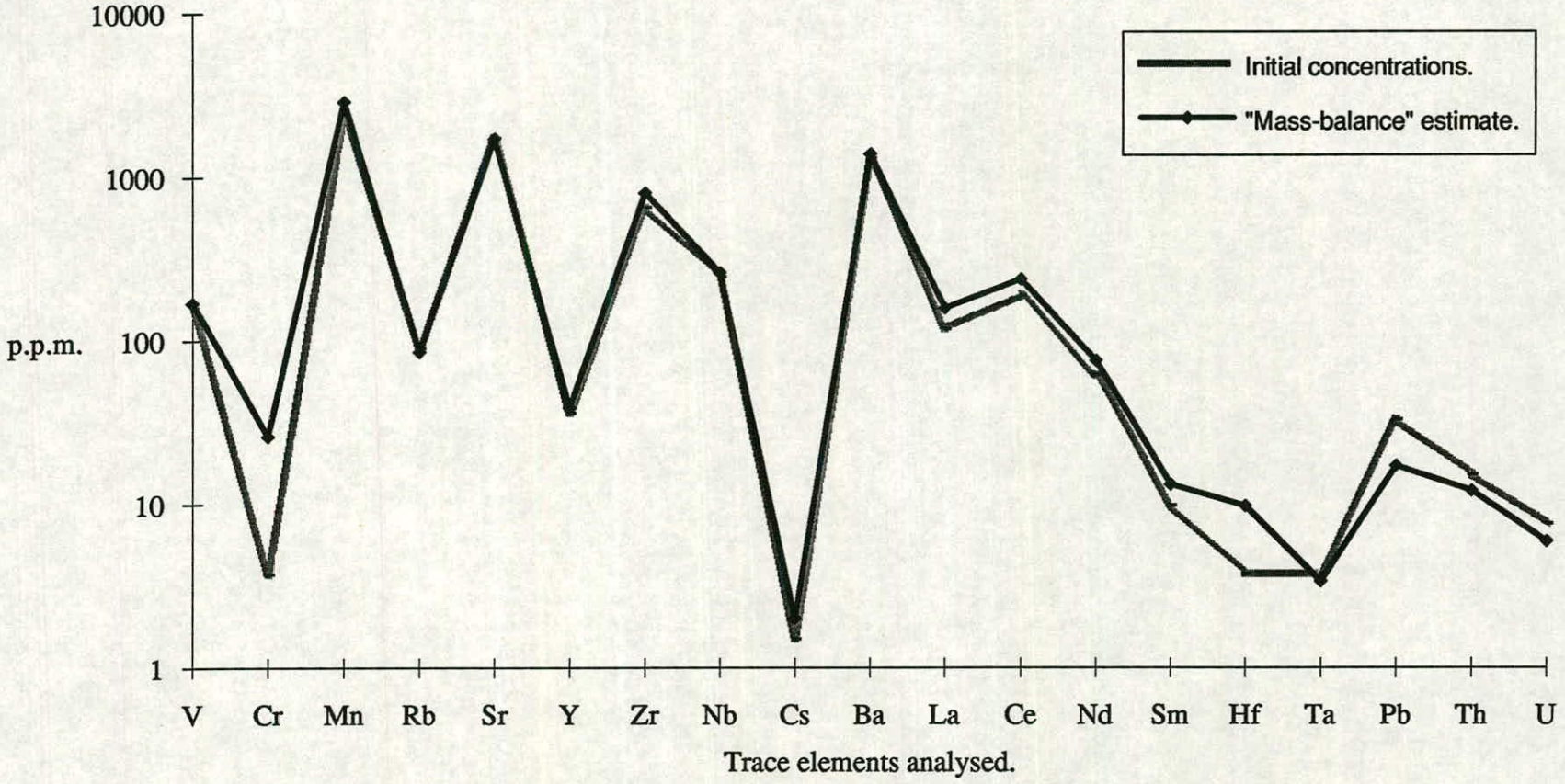

Figure 6.21. Comparison of starting materials and "mass-balance" estimates: A test for ion probe accuracy. G2.6, SUN189+CC.

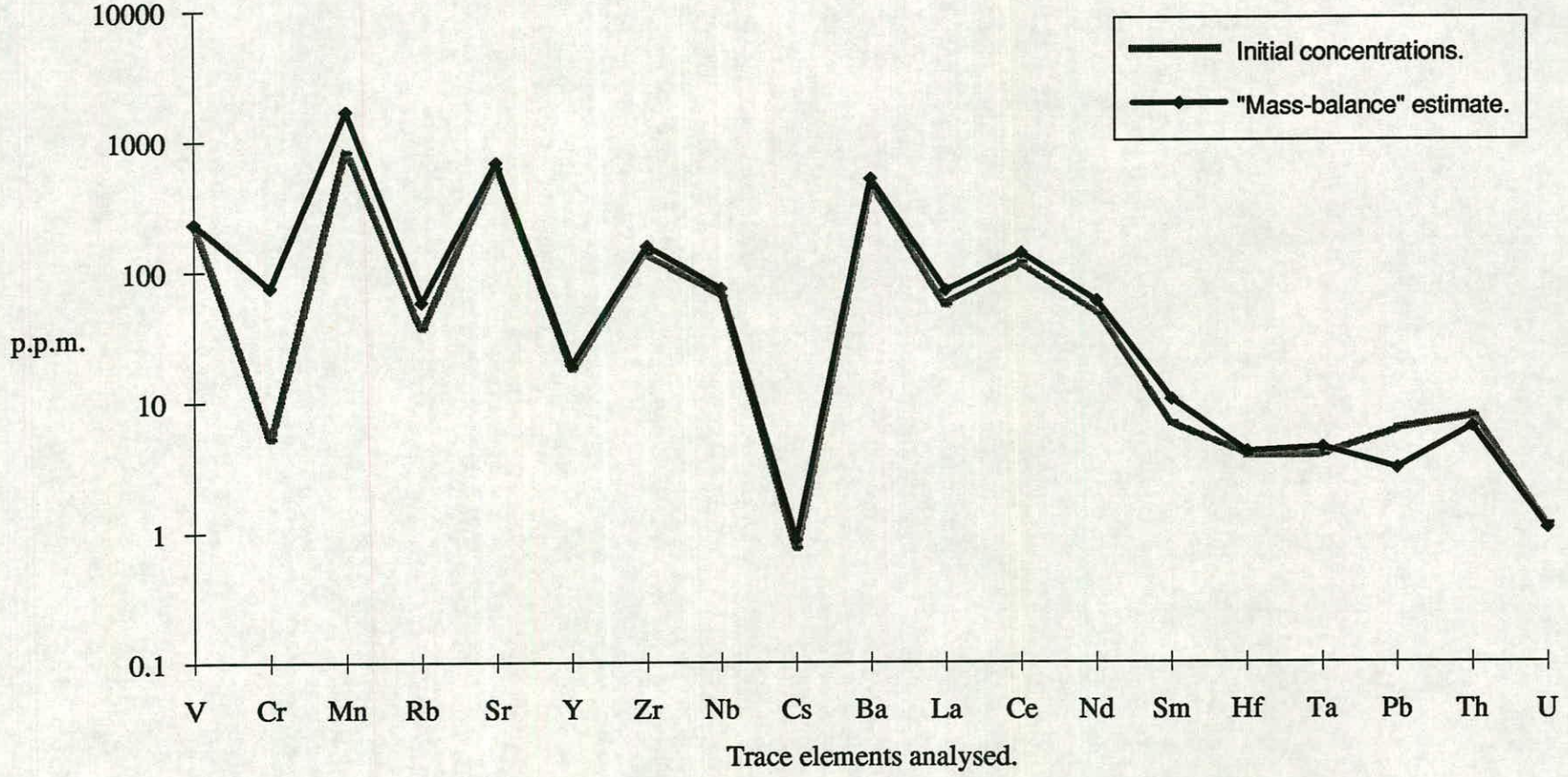

6.6. A summary of the analytical work.

6.6.1. Sample preparation.

Experimentally produced charges have been mounted, ground down, and polished to form a flat surface. This process was kept meticulously water-free in order to avoid modification of the carbonates. The juxtaposition of resistant silicate phases with soft carbonate quench led to polishing problems, and long polishing times.

6.6.2. Optical analysis.

Optical analysis of these prepared samples showed that the coexisting carbonate and silicate liquids were in textural equilibrium.

A more quantitative study of the textures seen was made by measuring interface curvatures, and contact angles at three-phase boundaries. Composition, and to a lesser effect pressure, are controlling factors on the textures seen, and thus on the boundary energies between phases.

Two-liquid textures imply that intra-liquid bonding forces are weaker in the carbonate melt. This, combined with the Lc wetting characteristics, and the rapid segregation of phases, implies that the low measured viscosities of Na-Ca-carbonate melt at atmospheric pressure apply to carbonate melts up to at least 2.0 GPa.

Na-rich carbonate melts are also seen to be significantly less dense than silicate to 2.0 GPa, although the density of Ca-carbonate melt relative to silicate melt is more difficult to ascertain in these experiments.

An S.E.M. study at high magnification showed that complex modifications occur in both the carbonate and silicate liquids during quenching of the experimental charges.

6.6.3. Electron probe analysis.

Mass-balance calculations confirm that electron probe analyses of 100 μm^2 of quenched carbonate and silicate liquids using a rastered low current beam gives accurate estimates of the equilibrium liquid compositions. These electron probe

analyses have been used both to calculate $^{Ls/Lc}D_i$ values for major elements, and to put these data, and the trace element partitioning behaviour into compositional context.

Interference effects in electron probe analysis can in general be avoided in these compositions by careful choice of analytical line, and background position. Even when interferences cannot be avoided, empirical relationships can be produced which allow the effects to be corrected.

Alkali mobility is a severe problem during spot electron probe analysis of both the carbonate and silicate quenches. Using a 100 μm^2 rastered area of analysis reduces this effect considerably, but still results in analyses at 20 nA which are systematically in error due to sodium mobility. Acceptable analyses which do not suffer from this systematic error can only be obtained using very weak beam currents (3-10 nA). This solution results in less precise concentration data due to increased counting errors.

6.6.4. Ion probe analysis.

For the majority of trace elements studied, ion probe analysis of quenched carbonate and silicate liquids gives an adequate estimate of trace-element concentrations. These concentrations have then been used to obtain $^{Ls/Lc}D_i$ data for the trace elements studied.

Problems of standardisation occur on the ion probe due to differences in relative ion yields when sputtering different matrices. These problems can be removed by obtaining RIY data for carbonate and silicate materials. The standards produced showed that RIY effects are relatively small for Sr, Ba, and Mn. Larger, and therefore significant effects were seen for Mg and REE. In none of these elements were RIY differences seen to exceed a factor of 2.

During quenching of the experimental carbonate liquids, many elements that were present in the melt could not be incorporated into crystalline carbonate structures, and were therefore expelled into the silicate part of the quench intergrowth. This heterogeneous distribution in the carbonate quench has led to large errors on the $^{Ls/Lc}D_i$ values for certain elements.

Mass-balance calculations showed that the ion probe concentration estimates agreed with XRF starting compositions for the majority of elements. The exceptions were

Pb and Cr. Pb concentrations in the charges were much less than starting contents. This can be explained by Pb loss to the Pt capsule during the experimental run. This process is well documented, and would be expected to occur in experiments where significant Fe loss by the same process is occurring. Ion probe estimates of Cr contents are much higher than the initial charge compositions. This could be due to contamination, but is more likely to be the result of a machine artefact due to interference on the ^{52}Cr peak by [Si+Mg]. $^{Ls/Lc}D_{Cr}$ values will therefore not be considered in further discussions on partitioning.

6.6.5. Conclusions.

Electron and ion probe analyses, although subject to various difficulties, have produced accurate concentration estimates for major, minor, and trace elements in quenched carbonate and silicate melts. These analyses have then been used to produce the $^{Ls/Lc}D_i$ data used in the following discussions.

Plate captions: Chapter 6.

Plate 6.1. Ls-Lc textures in sodium-rich charges.

In sodium-rich charges, the Ls-Lc meniscus shows marked curvature (from reproducibility experiments R1-R6). It is usually convex towards the carbonate liquid implying that the silicate liquid has higher surface tension, and therefore stronger liquid bonding forces than its carbonate counterpart. Scale bars are 50 μm.

Plate 6.2. Ls-Lc textures in sodium-poor charges.

In sodium poor charges, the most common texture is that of carbonate spheres surrounded by silicate material. In this case, the Ls-Lc meniscus is convex to the silicate liquid implying that the carbonate melt now has the stronger liquid bonding forces. This may have profound implications for the relative viscosities of calcic and sodic carbonate melts.

A. Charge G8.4. Scale bar is 20 μm.

B. Charge G2.4. Scale bar is 50 μm.

C. Charge G2.5. Scale bar is 50 μm.

Plate 6.3. Ls-Lc-V textures in sodium-rich charges.

The surface area of Ls-V boundary is minimized by wetting with carbonate melt. This results in partial or complete surrounding of the vapour spheres with carbonate liquid. It is suggested that this texture results from $\gamma_{cv} << \gamma_{sv}$. Examples from G2.1, G2.3, G4.1. Scale bar is 1 mm for A., 100 μm for B. and C., and 20 μm for D.

Plate 6.4. Ls-Lc-V textures in sodium-poor charges.

Lc spheres associated with vapour bubbles form contact angles approaching 90°. This suggests that $\gamma_{cv} \sim \gamma_{sv}$, and that both are much larger than the interfacial energy of the Ls-Lc meniscus. In this case, it is the total surface area of melt-vapour boundary that is being minimised in the production of these textures.

A. G9.6. Scale bar is 50 μm.

B. G2.6. Scale bar is 20 μm.

C. G5.6. Scale bar is 20 μm.

Plate 6.5. Ls-Lc-Xtls textures from sub-liquidus experiments (G1.9).

A. and B. show the most common liquid-crystal textures seen. In general small spheres of carbonate liquid are found surrounding crystals of silicate phases. It seems likely that the crystals are acting as nucleation sites for the production of immiscibility.

C. Occasionally, areas of melt without crystals can spontaneously produce immiscible carbonate blebs as is shown here from experiment G1.9.

All scale bars are 20 μm.

Plate 6.6. Quench textures produced on cooling the silicate liquid.

A. A high magnification back-scattered electron image of the silicate liquid showing the presence of sub-micron spherules of carbonate material within silicate glass. These are believed to be produced by quench immiscibility; as the temperature falls, the silicate liquid can no longer contain its carbonate component, and so exsolves spheres of carbonate melt. Charge from experiment G2.3. Scale bar is 2 μm.

B. A back-scattered electron image of the coarsest quench texture seen in Ls. Carbonate spherules up to 2 μm accross are seen in the silicate glass. Also shown is an area of silicate liquid which has quenched to an intergrowth of acicular silicate crystals (pale) surrounded by carbonate-rich background (dark). This charge is from experiment G3.5. This experiment was run at low pressure (0.25 GPa), and was in a large capsule (3mm diameter). The large sample volume, and the small volume of cool gas due to the low pressure, result in this experiment (G3) having the slowest quench rate of all experiments undertaken. In addition, the charge was a sodium-rich, basic composition (SUN189+CNC) which would therefore quench rapidly. It is therefore not surprising that the quench was coarsest in this sample. Scale bar is 20 μm.

C. Vapour spheres within the silicate liquid act as magnets for quench spheres of Lc on cooling. Scale bar is 50 μm.

Plate 6.7. Textures produced on quenching the carbonate liquid.

The textures produced in the carnbonate liquid on cooling are extremely variable, depending on the quench rate, the P-T conditions of formation, and on the liquid composition. Three components of the quench are seen: acicular calcite crystals, spheres or blebs of silicate material, and a background phase of nyerereitic composition.

A. Very fine-scale quenching of a small sphere of carbonate melt in experiment G2.3. Scale bar is 10 μm.

B. Slightly coarser quench of a sodium-rich carbonate liquid from experiment G4.3. The quench consists of irreguar calcite- and silicate-rich areas surrounded by nyerereitic material. Also visible are some small, isolated silicate spheres. Scale bar is 20 μm.

C. An equivalent, but coarser quench from experiment G2.3. Scale bar is 20 μm.

D. Coarse quench from experiment G4.3.

E. A coarse quench showing acicular calcite crystals (Cc) surrounded by nyerereite background (Nc). Experiment G2.5.

F. A close up of the quench from experiment G2.5 again showing calcite crystals in nyerereitic material.

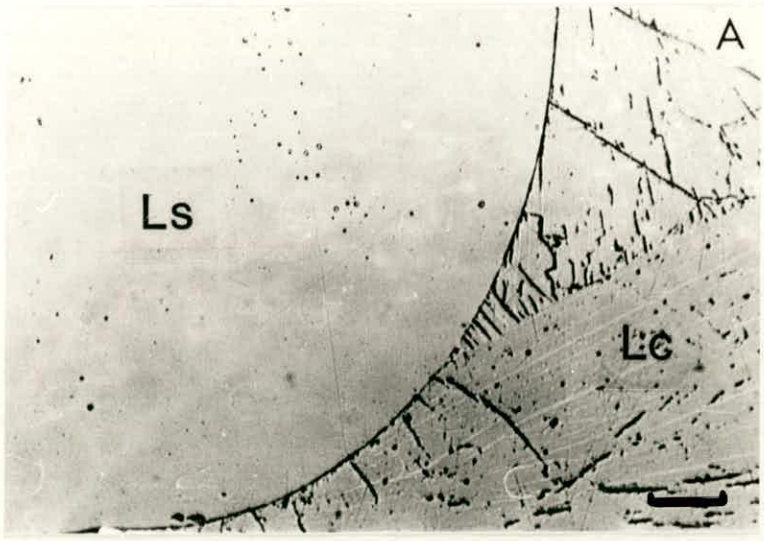
A
Ls
Lc

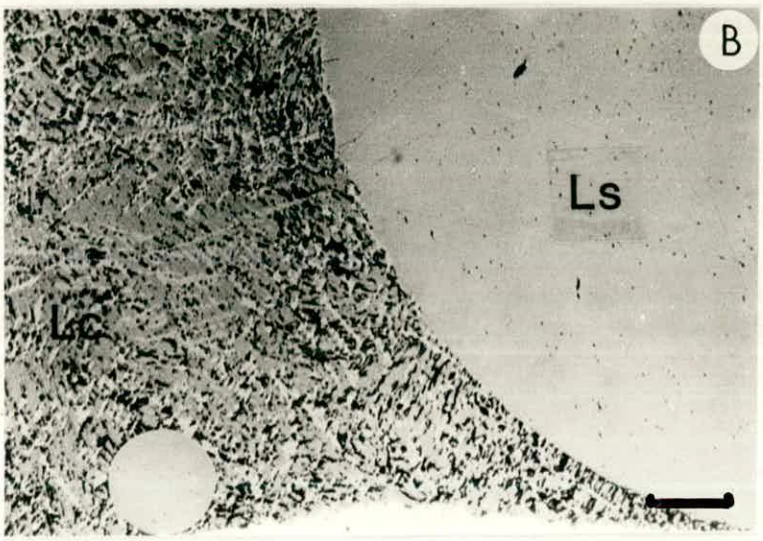
B
Ls
Lc

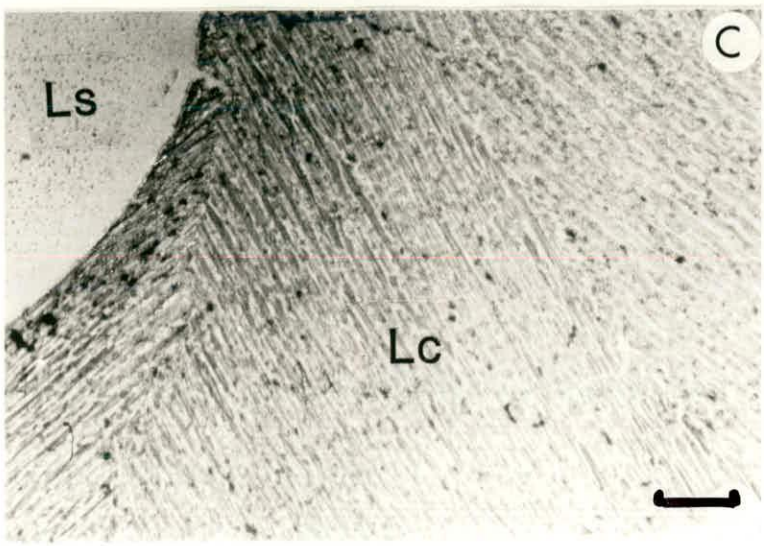
C
Ls
Lc

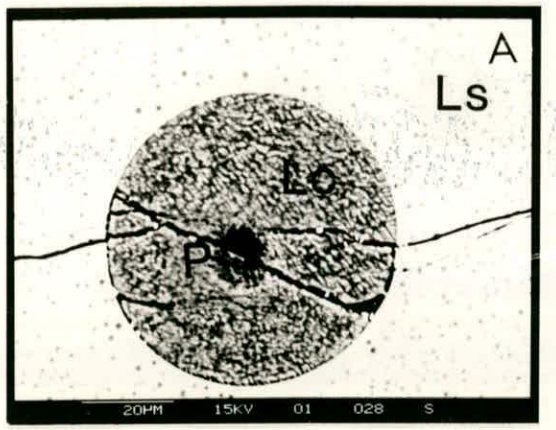
A
Ls
Lc
Pt
20MM 15KV 01 028 S

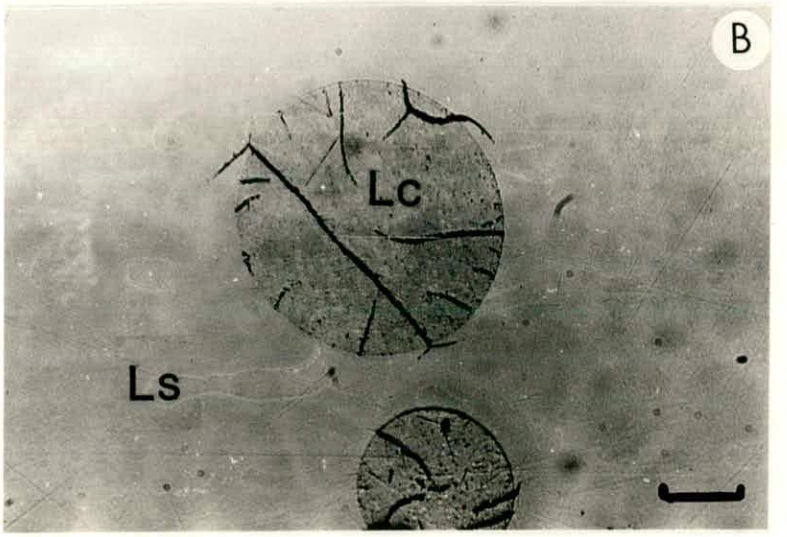
B
Lc
Ls

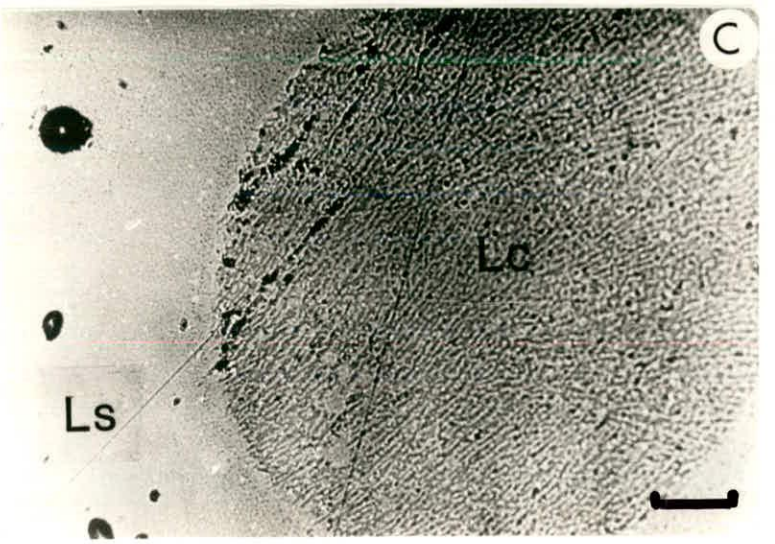
C
Lc
Ls

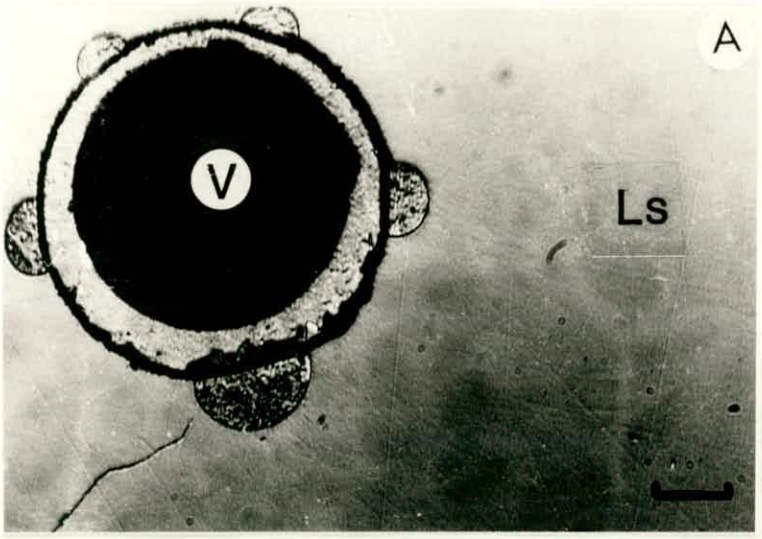
A
V
Ls

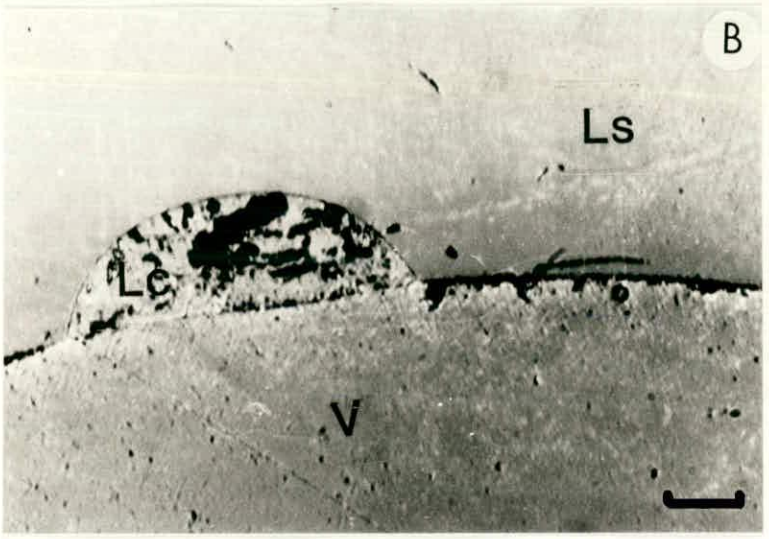
B
Ls
Lc
V

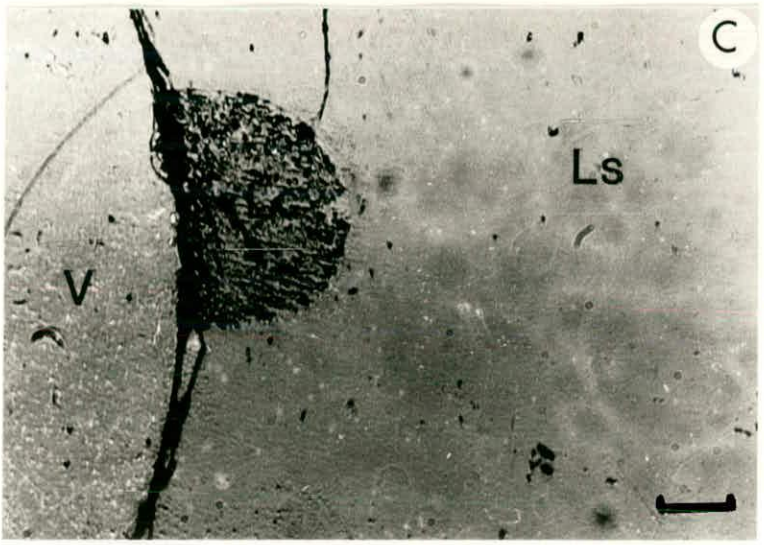
C
Ls
V

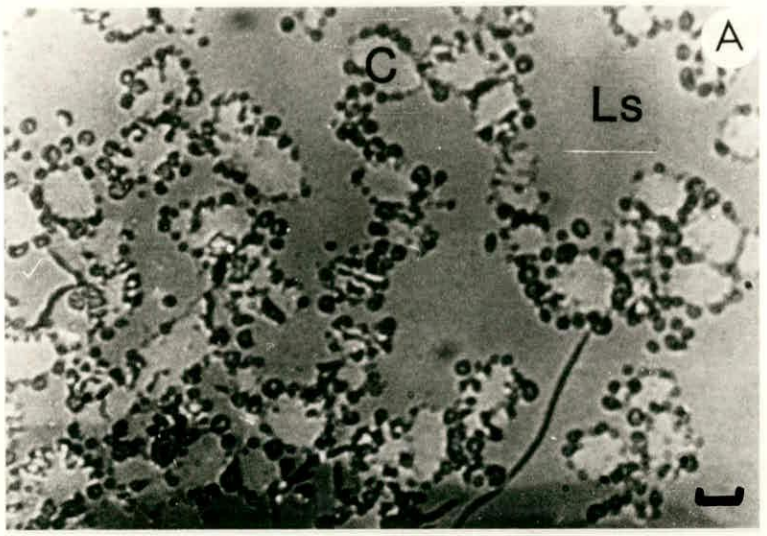
A
C
Ls

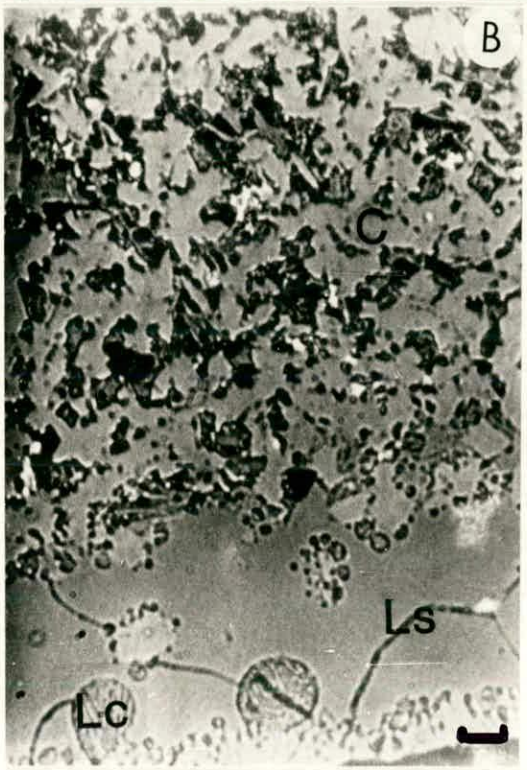
B
C
Ls
Lc

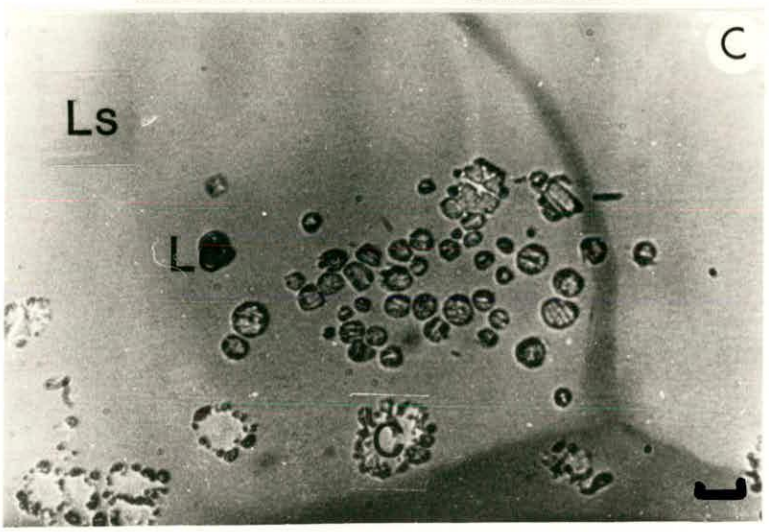
C
Ls
L
C

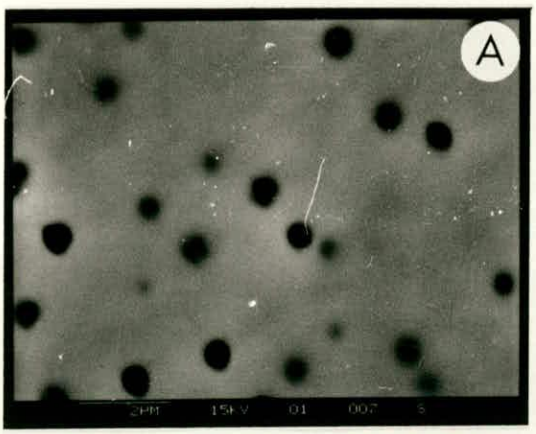
A
2MM 15kV 01 007 S

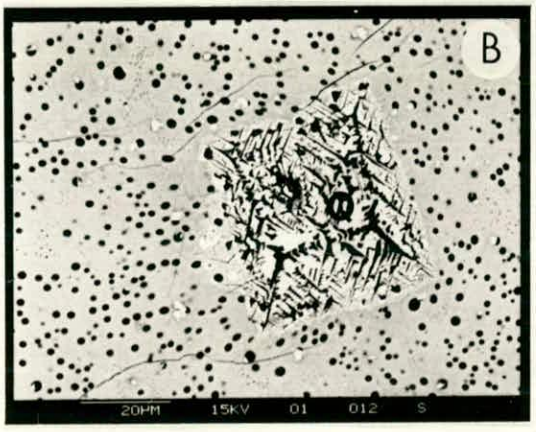
B
20MM 15KV 01 012 S

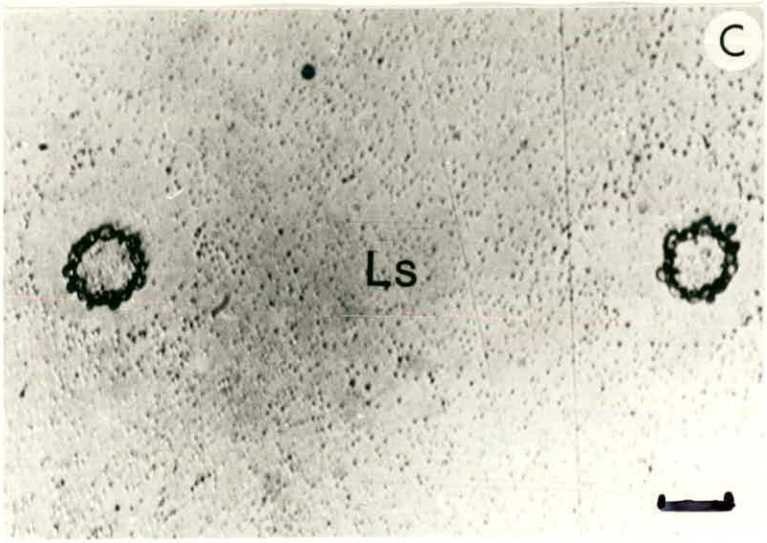
C
Ls

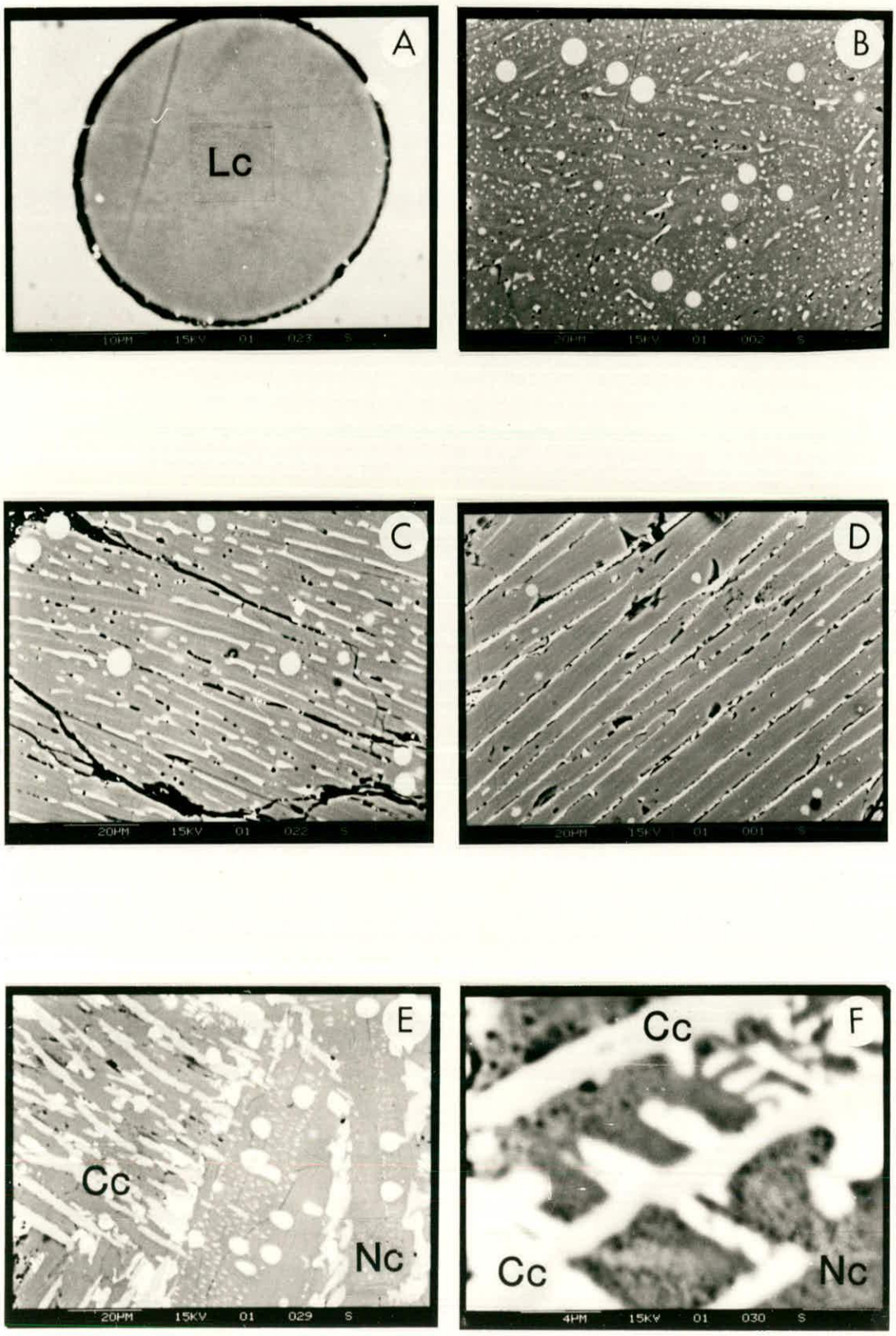
A
Lc
B
C
D
E
Cc
Nc
F
Cc
Cc
Nc

CHAPTER 7

ELEMENT PARTITIONING BETWEEN COEXISTING CARBONATE AND SILICATE LIQUIDS IN THE SYSTEM SiO_2-Al_2O_3-CaO-Na_2O-CO_2.

7.1. The Data.

$^{Ls/Lc}D_i$ partition coefficients have been obtained for 30 elements from the soda-melilite-carbonate experiments. Partitioning for each element will be discussed individually in the context of its chemical properties. An overview of the controlling factors on partitioning will then be presented, followed by a section on how the presence of certain minor components affect these carbonate-silicate equilibria.

Three compositions within this system were studied. The majority of the data were obtained using the SM2+CNC composition due to the ease with which immiscibility was produced experimentally, and the resulting simple two-liquid textures. As changing pressure and temperature have only limited effect on partitioning, the data have been collated, and the average value quoted, together with the maximum and minimum values of $^{Ls/Lc}D_i$. This mode of presentation, which has also been adopted for the SM2+CC composition, is used in order to give the reader an indication of the extent of variation in $^{Ls/Lc}D_i$ which is possible with changing pressure, temperature, and composition. Individual $^{Ls/Lc}D_i$ from each experiment are quoted in the appendices. The REV3 composition was only available for analysis in one sample, and therefore has been presented as a single value, with asymmetric errors based on 2 σ variations on the ion probe concentrations.

The errors quoted in the appendices, and presented in graphical form, are calculated in a two stage statistical process:

(a) Errors on the ion probe concentration estimates.

Mean concentrations of elements in the carbonate and silicate liquids have been quoted with 95% confidence limits based on $\pm$ 2 SE variations, where SE is the standard error on the sample mean ($SE = \sigma/[n]^{1/2}$ for a sample population with standard deviation σ, and sample size n). In order for calculations based on standard deviations to be an accurate estimation of confidence, the sample population must have a gaussian distribution. It has therefore been assumed that the distribution of concentration estimates produced on the ion probe is approximately gaussian. This is found to be the case for silicate glass analyses where the errors are mainly due to counting statistics on the relevant ions in the mass spectrometer. However, the carbonate quench suffers from significant spatial heterogeneity, and it is this that

produces a large proportion of the errors on concentration estimates. Figure 7.1 shows that, for the majority of elements, concentration estimates still approximate a gaussian distribution, and therefore errors based on standard error variations from the mean value are an accurate estimation of confidence interval. This is not the case for elements whose distributions are greatly affected by quench processes in the carbonate liquid (e.g. Si, Al, Ti etc.). The distributions of concentration estimates for these elements is distinctly non-gaussian (Figure 7.2). Estimates of confidence based on standard deviations from mean concentrations are therefore inaccurate. However, population sizes are not large enough for more rigorous statistical treatment, and these approximations of confidence levels have had to be employed for all elements.

(b) Errors on $^{Ls/Lc}D_i$ data.

$^{Ls/Lc}D_i$ values are calculated as being the concentration of element *i* in the silicate liquid divided by the concentration of element i in the carbonate liquid. Even if we assume that the distributions of concentration estimates form an approximate normal distribution (true for the majority of elements), the distribution of estimates of the quotient of these two values will not be normally distributed. Quoting $^{Ls/Lc}D_i$ values with $\pm 2\,\sigma$ errors would therefore be inappropriate. Instead, asymmetric 95% confidence limits can be calculated according to the following treatment.

$E(x_1) = \mu_1$ = Expected value of concentration in silicate liquid.
$E(x_2) = \mu_2$ = Expected value of concentration in carbonate liquid.
$S.D.(x_1) = \sigma_1$ = Standard deviation of silicate liquid concentrations.
$S.D.(x_2) = \sigma_2$ = Standard deviation of carbonate liquid concentrations.
n = number of analyses.

If we assume that distributions of both x_1 and x_2 are approximately normal, and that there is negligible covariance between x_1 and x_2, then the variable x_1-rx_2 is also normally distributed for any constant r.

Therefore, the distribution for x_1-rx_2 is: $(\mu_1-r\mu_2,\ \sigma_1^2+r^2\sigma_2^2)$
Mean variance

If $r = \mu_1/\mu_2$

distribution for x_1-rx_2 is: $(0,\ \sigma_1^2+r^2\sigma_2^2)$

Using the standard normal curve, we can calculate the 0.95 confidence limits as ± 1.96σ:

$$-1.96 < x_1 - rx_2 / (\sigma_1^2 + r^2\sigma_2^2)^{1/2} < 1.96$$

Or:

$$(x_1 - rx_2)^2 / (\sigma_1^2 + r^2\sigma_2^2) \leq 1.96^2$$

Multiplying through gives:

$$r^2x_2^2 - 2rx_1x_2 + x_1^2 \leq 1.96^2\sigma_1^2 + 1.96^2r^2\sigma_2^2$$

$$r^2(x_2^2 - 1.96^2\sigma_2^2) - 2rx_1x_2 + x_1^2 - 1.96^2\sigma_1^2 \leq 0$$

Simplified:

$$ar^2 + br + c = 0$$

Where: $a = (x_2^2 - 1.96^2\sigma_2^2)$

$b = -2x_1x_2 + x_1^2$

$c = -1.96^2\sigma_1^2$

This relationship can then be solved for r by simultaneous equations to produce upper and lower confidence intervals according to:

$$r = b \pm [(b^2 - 4ac)^{1/2}] / 2a.$$

The partitioning data will be discussed in the scheme of the periodic table (i.e. Group IA, Group IIA etc.), the exception being U, Th, and Pb which will be discussed separately.

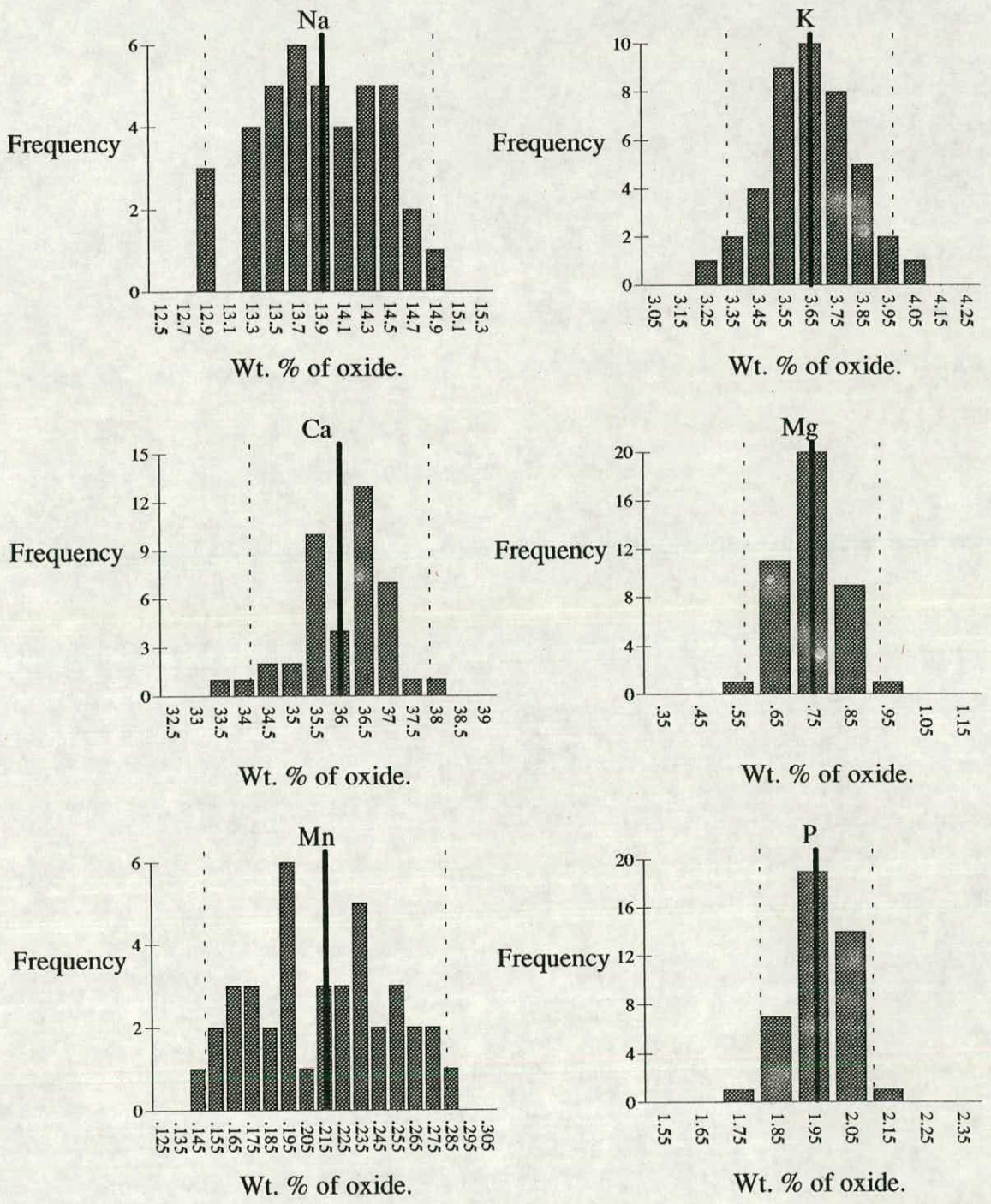

Figure 7.1. Distributions of sample populations of analyses of the carbonate quench of experiment G12: elements not seriously redistributed by quench processes. Sample populations of analyses for the majority of elements show near-gaussian distributions around the concentration mean. Error calculations based on standard error values are therefore accurate as estimates of confidence limits. Thick line is sample mean, dotted lines are 95% confidence limits.

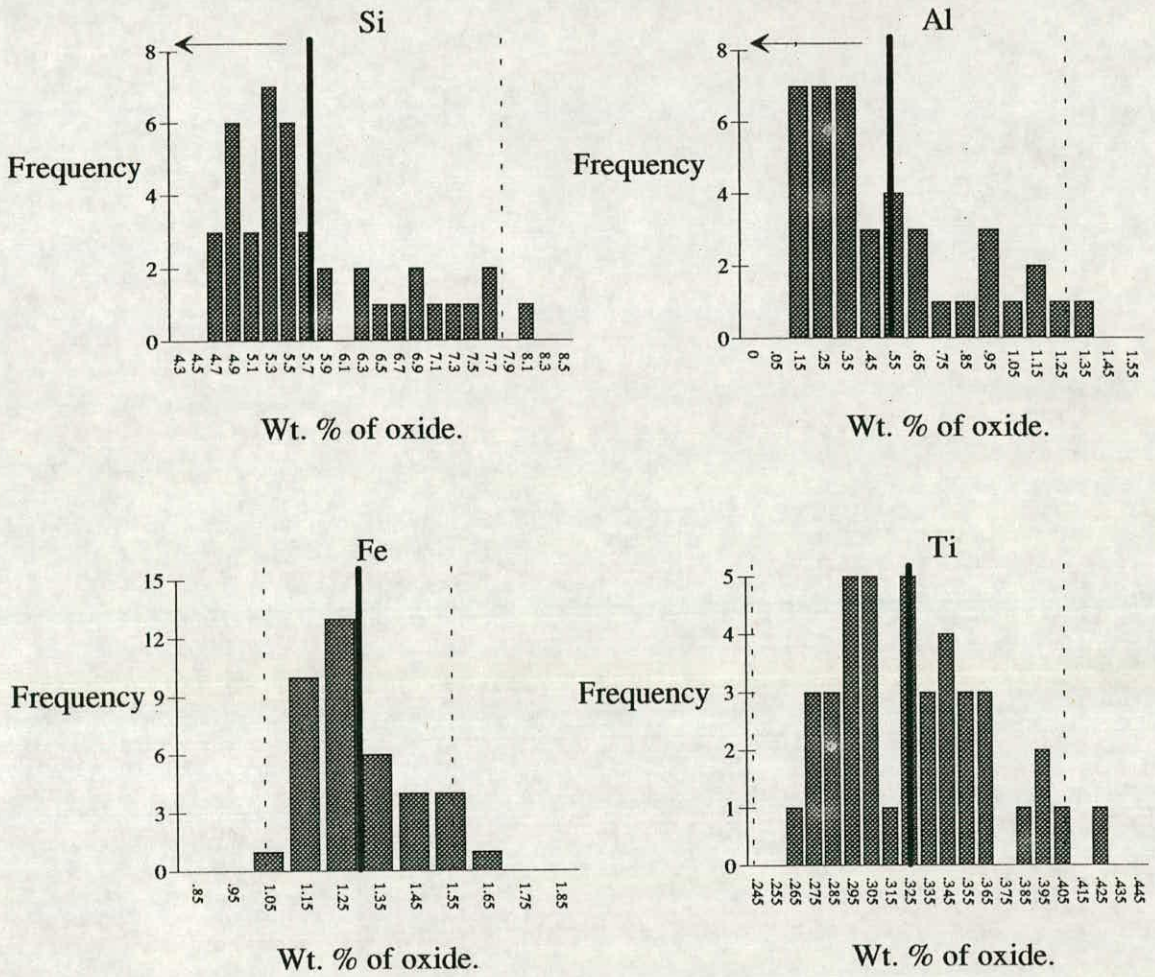

Figure 7.2. Distribution of sample population for analyses of carbonate quench of G12: elements seriously affected by quenching of experiment. The distributions of analyses for these elements is non-gaussian. The skewness of the silica and alumina concentration estimates is distinct, and therefore will affect statistical behaviour. For elements affected by quench in this way, the mean value (thick line) will still have relevance, as it is still a valid representation of the average concentration in the unmodified liquid phase. This will, however, no longer correspond to the peak of the distribution due to skewness of the distribution caused by quenching. Because of this skewness, the standard error is no longer an accurate representation of the confidence limits on the average. Errors quoted for Si, Al, etc. are therefore only approximations of the 95% confidence limits. Thick line is sample mean, dotted lines are estimates of 95% confidence limits assuming a gaussian distribution, arrows represent situations where confidence limits based on standard errors obviously lie outside the total population range.

7.2. Group IA elements.

Four elements in Group IA were studied: Na on the electron probe, K, Rb, and Cs on the ion probe. All were found to be enriched in the carbonate liquid (Figure 7.3), although the degree of this enrichment varied between elements, and with physical conditions.

7.2.1. Sodium.

$^{Ls/Lc}D_{Na}$ values for SM2+CNC compositions were found to be remarkably consistent. The average value was 0.66, with a maximum seen of 0.69, and a minimum of 0.62. Pressure and temperature therefore have little effect on sodium partitioning. The REV3 composition also produced a value of $^{Ls/Lc}D_{Na} = 0.66$.

For SM2+CC, the sodium partitioning was more varied, with $^{Ls/Lc}D_{Na}$ ranging from 0.6 in the high pressure runs, to 3.8 in a 0.25 GPa run. This pronounced pressure effect, also seen in other +1 elements, is discussed in section 7.8.1.

7.2.2. Potassium.

$^{Ls/Lc}D_{K}$ values are in general lower than $^{Ls/Lc}D_{Na}$. Potassium is therefore more strongly enriched in the carbonate melt than sodium. The mean value of $^{Ls/Lc}D_{K}$ for SM2+CNC compositions is 0.33, with a maximum value seen of 0.51, and a minimum of 0.18. The SM2+CC data are within this range, but the REV3 composition produced a value of $^{Ls/Lc}D_{K} = 0.61$, higher than any seen in the "forwards" experiments. The 1200°C values are lower than those at 1300°C, indicating more extreme partitioning at lower temperature (see Figure 7.23).

7.2.3. Rubidium.

$^{Ls/Lc}D_{Rb}$ are always lower than the corresponding $^{Ls/Lc}D_{K}$ values. The mean value is 0.29, with a range from 0.42-0.16. The SM2+CC composition gave a value of 0.29, whilst the REV3 composition was again significantly different with $^{Ls/Lc}D_{Rb} = 0.46$. Again, partitioning is more extreme at lower temperature.

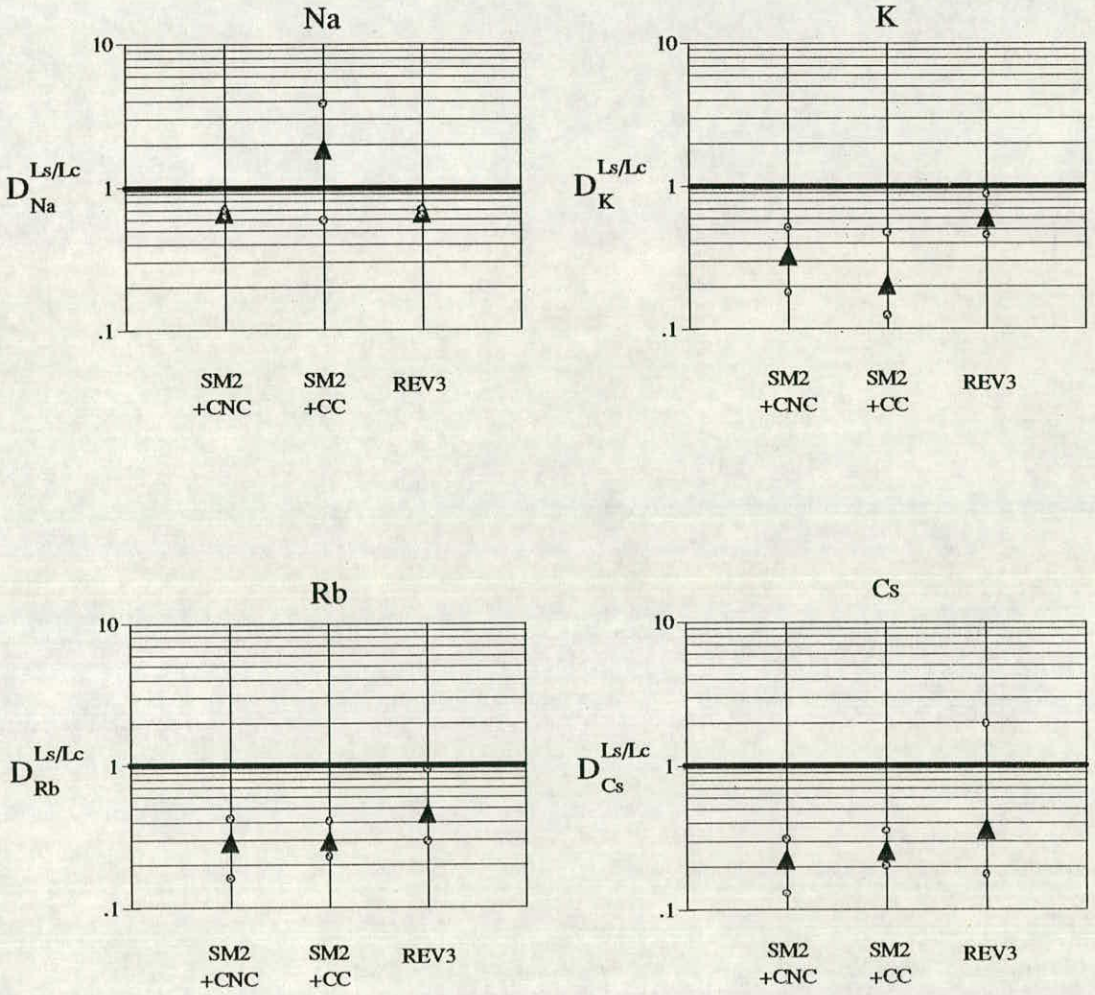

Figure 7.3. Partitioning of Group IA elements between synthetic carbonate and silicate melts. Upper and lower limits for the SM2+CNC and SM2+CC compositions represent the measured extremes. For the REV3 composition, upper and lower limits are the standard deviation from the mean value, as only one sample was analysed. The small ranges shown by the SM2 compositions suggest that changes in pressure and temperature have little effect on partitioning of +1 elements in this synthetic system. The exception to this is Na in SM2+CC compositions, where a wide variation is seen. This is due to a pressure effect on Na partitioning in calcic compositions.

7.2.4. Cesium.

$^{Ls/Lc}D_{Cs}$ are the most extreme of all those seen in Group IA, indicating that Cs is most strongly enriched in the carbonate melt. The SM2+CNC average was $^{Ls/Lc}D_{Cs} = 0.22$, with a range of 0.13-0.31. The SM2+CC composition gave a value of 0.26, and the REV3 value was again significantly higher at $^{Ls/Lc}D_{Cs} = 0.36$.

7.2.5. The relationship of partitioning with ionic radius.

The average SM2+CNC $^{Ls/Lc}D_i$ values have been plotted against ionic radius in Figure 7.4. A clear trend is seen with strong negative correlation (r = -.99). As ionic radius is increased, enrichment in the carbonate melt becomes more pronounced. This is also true for the data from each individual experiment. Using this relationship, we can predict that $^{Ls/Lc}D_{Li}$ should be near unity, assuming an ionic radius of *ca.* 82 pm. (Whittaker & Muntus, 1970). The high correlation coefficient seen suggests that ionic radius is the main influence on the relative partitioning of the Group IA elements.

7.2.6. The effect of run duration on partitioning of Group IA elements.

The products of experiments run for periods of between 15 and 960 minutes were analysed for trace-element concentrations. The data for Group IA elements are plotted in Figure 7.5. $^{Ls/Lc}D_{Na}$ from all the runs are virtually identical, and certainly within analytical error. This implies that sodium reached equilibrium partitioning rapidly. For K, Rb, and Cs, only $^{Ls/Lc}D_i$ values from the 60-, 360-, and 960-minute runs are within error. The products of the 15 minute duration experiment yield $^{Ls/Lc}D_i$ that are lower than the equilibrium values. This is surprising, as the trace elements were present in the silicate glass component of the starting material. $^{Ls/Lc}D_i$ would therefore be expected to be higher than the equilibrium values if equilibrium had yet to be reached, with residual enrichment still in the silicate melt. There must be a mechanism acting during immiscible separation which over-enriches the carbonate melt in Group IA elements, and so causes an "overshoot" of the equilibrium values. Data from the 15-minute charge is therefore suspect for Group IA elements.

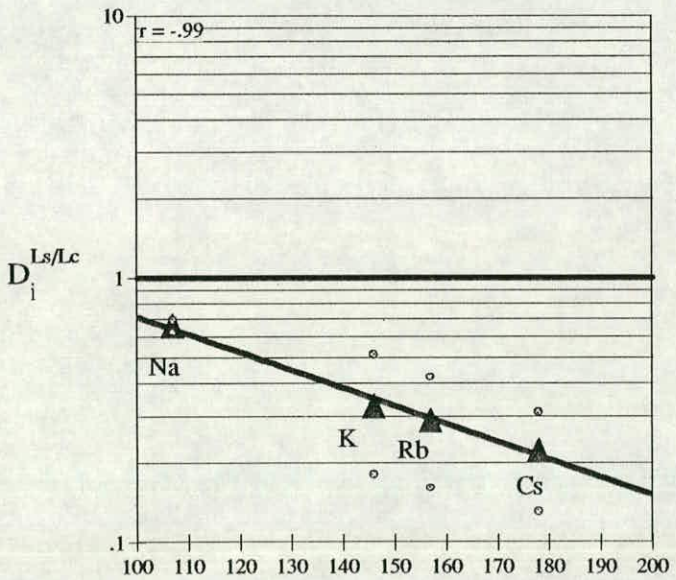

Figure 7.4. Group IA partitioning with ionic radius. Using data for the SM2+CNC composition, a simple relationship is seen between partitioning and ionic radius for all +1 elements studied. More extreme partitioning to the carbonate melt is seen as the ionic radius increases. All +1 elements are enriched in the carbonate melt. (Ionic radii from Whittaker & Muntus, 1970).

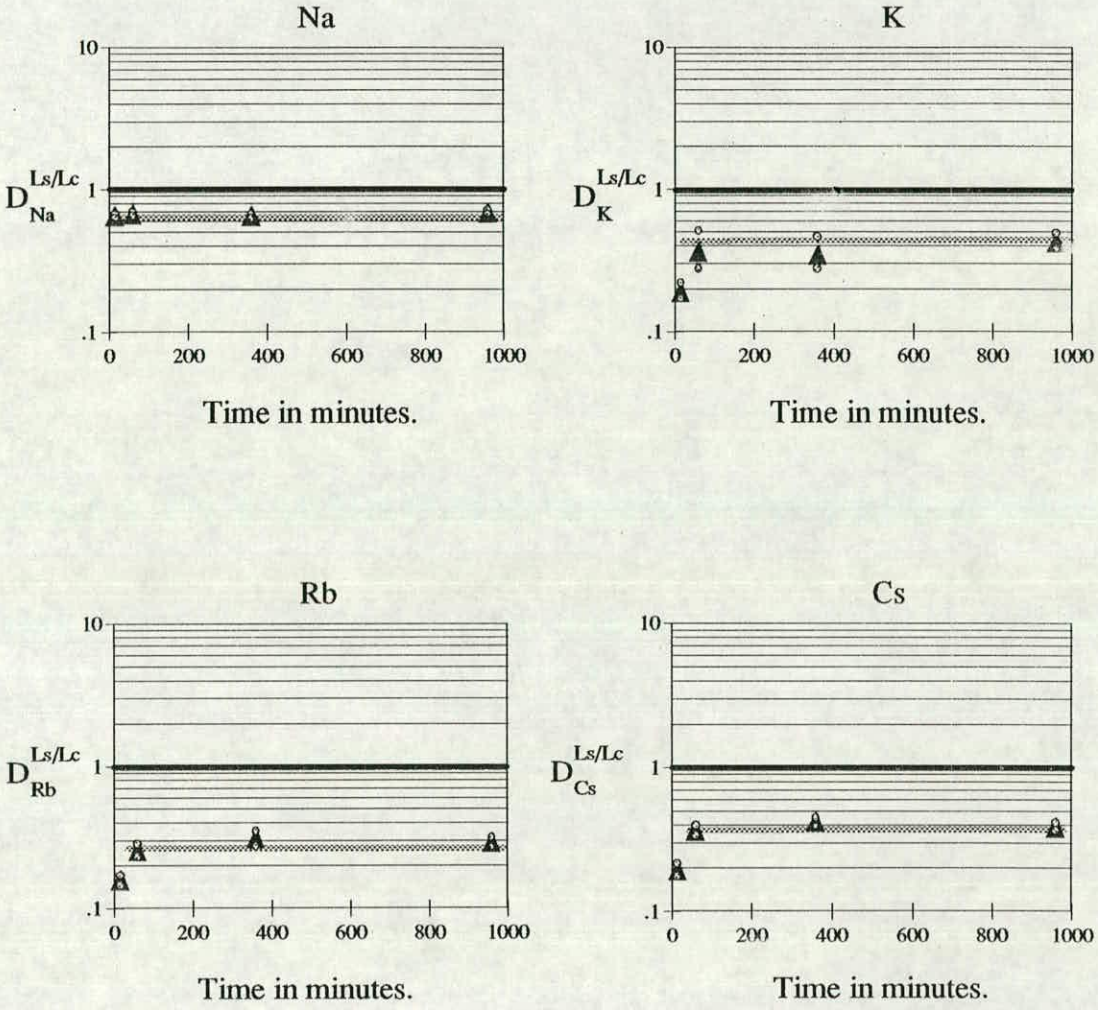

Figure 7.5. Partitioning of Group IA elements as a function of run duration in synthetic carbonate and silicate melts. All duration times produce D values which are within analytical error for sodium. Duration times of 60, 360 and 960 mins are within analytical error for the other +1 elements. The 15-minute duration runs produced more extreme partitioning results than the other experiments. This is surprising as, if equilibrium had not been reached, the D values should have been less extreme, or even greater than 1. The majority of the respective trace elements would still have been in the silicate portion of the charge. Some mechanism must therefore be invoked which causes an "overshoot" of the equilibrium D values for +1 elements.

7.3. Group IIA elements.

Four Group IIA elements were studied: Ca on the electron probe; Mg, Sr, and Ba on the ion probe. As with the Group IA elements, all were found to be enriched in the carbonate liquid (Figure 7.6).

7.3.1. Magnesium.

For the SM2+CNC composition, the average value of $^{Ls/Lc}D_{Mg}$ is 0.65, with a range from 0.45-0.85. The value for SM2+CC composition is 0.38, and for the REV3 composition, $^{Ls/Lc}D_{Mg} = 0.83 \pm 0.2$. Magnesium therefore seems to be more strongly partitioned to the carbonate liquid in the calcic starting compositions.

7.3.2. Calcium.

$^{Ls/Lc}D_{Ca}$ for SM2+CNC compositions is consistent at *ca.* 0.7, with a range of values seen from 0.65-0.77. The SM2+CC value fits in this range (0.72). However, the REV3 sample yielded $^{Ls/Lc}D_{Ca} = 0.24 \pm 0.01$. No explanation has been found for this rather large discrepancy between the forwards and reverse experiments. Calcium seems to be the only element to show such a pronounced difference.

7.3.3. Strontium.

As expected, strontium partitions in a similar manner to calcium. However, $^{Ls/Lc}D_{Sr}$ is always lower than $^{Ls/Lc}D_{Ca}$; strontium is always more strongly enriched in the carbonate melt than is calcium. Average $^{Ls/Lc}D_{Sr}$ for SM2+CNC compositions is 0.39, with a range of 0.23-0.56. Again, the REV3 composition produces more extreme partitioning ($^{Ls/Lc}D_{Sr} = 0.14 \pm 0.1$) than is seen in the main body of data.

7.3.4. Barium.

The most strongly partitioned Group IIA element, barium always shows pronounced enrichment in the carbonate melt. Mean $^{Ls/Lc}D_{Ba}$ for SM2+CNC is 0.30, with a range of 0.19-0.40. The SM2+CC composition gives $^{Ls/Lc}D_{Ba} = 0.22$, and the REV3 composition is again more extreme at $^{Ls/Lc}D_{Ba} = 0.16 \pm 0.02$.

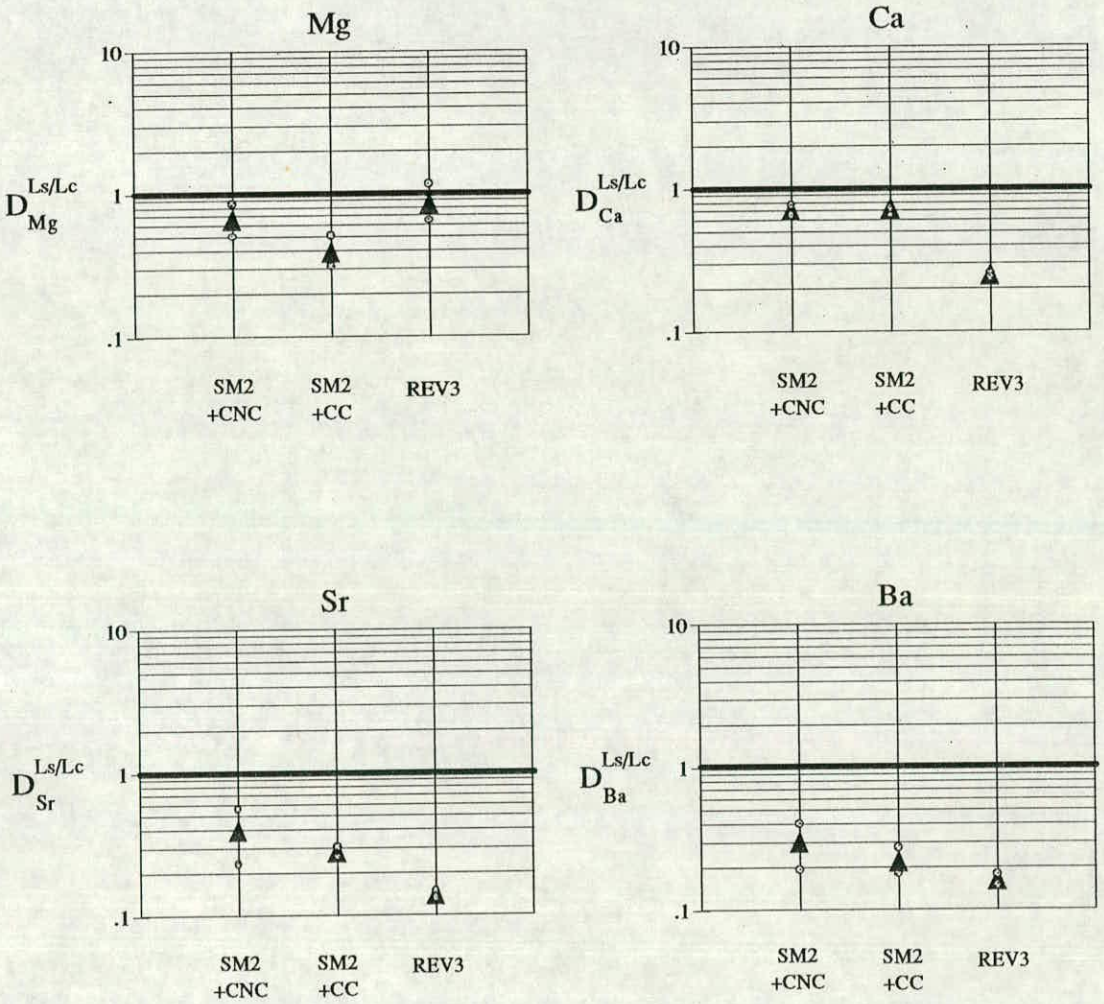

Figure 7.6. Partitioning of Group IIA elements between synthetic carbonate and silicate liquids. Upper and lower limits for SM2+CNC, and SM2+CC represent the measured extremes. For the REV3 composition, where only one sample was analysed, upper and lower limits reperesent the standard deviation from the mean value. The small ranges suggest that partitioning is little affected by changing pressure and temperature. However, composition seems to be a major factor, as shown by the significantly different partitioning in SM2+CNC, SM2+CC, and REV3. As the liquid compositions become more calcic, Ca, Sr, and Ba become more strongly partitioned to the carbonate liquid. Mg behaviour seems to be more varied. Under all conditions studied, Group IIA elements are partitioned to the carbonate liquid.

7.3.5. The relationship between partitioning and ionic radius.

$^{Ls/Lc}D_i$ for the Group IIA elements has been plotted against ionic radius in Figure 7.7. A simple relationship can be seen for Mg, Sr, and Ba. As ionic radius increases, partitioning becomes more extreme towards the carbonate melt. Calcium does not fit well into this trend, $^{Ls/Lc}D_{Ca}$ being higher than expected from its ionic charge and size. This is thought to be related to the high concentrations of calcium present in this system, taking $^{Ls/Lc}D_{Ca}$ out of the range of concentrations for which Henry's law behaviour applies.

Despite this inconsistency, it is clear that a relationship with ionic radius does exist. From this relationship, we can predict that radium, with an ionic radius of *ca.* 172 pm. (Whittaker & Muntus, 1970), would be expected to have a partition coefficient more extreme than that of barium. An estimate of $^{Ls/Lc}D_{Ra} = 0.10\text{-}0.20$ would be reasonable. The behaviour of beryllium, at the other end of Group IIA, would be more difficult to estimate due to the large difference in ionic radii. However it is suggested that $^{Ls/Lc}D_{Be}$ will exceed unity, and Be^{2+} will partition to the silicate melt in a similar manner to Al^{3+}.

7.3.6. The effects of run duration on the partitioning of Group IIA elements.

Figure 7.8 shows the change in $^{Ls/Lc}D_i$ with time for the Group IIA elements. All the elements show within error values of $^{Ls/Lc}D_i$ for partitioning in the 60, 360, and 960 mins duration runs. $^{Ls/Lc}D_i$ values from the 15 minute run are significantly different from these equilibrium values. In the case of Mg, Sr, and Ba, $^{Ls/Lc}D_i$ from the 15 minute run is substantially lower than from the longer runs. As mentioned before, partitioning would be expected to be less extreme if equilibrium was yet to be reached, so again there seems to be overshoot of the equilibrium D values. One possible explanation for this process is that immiscible separation actually took place at a substantially lower temperature than 1300°C (this composition would be expected to commence melting at *ca.* 1100°C) and that partitioning was therefore more extreme when immiscibility was first produced. After this initial partitioning, distances between carbonate and silicate blebs would be greatly increased, and thus the diffusion back towards equilibrium partitioning at 1300°C would take a correspondingly longer period of time. This could result in the time profiles seen in $^{Ls/Lc}D_i$ values for the Group IA and Group IIA elements.

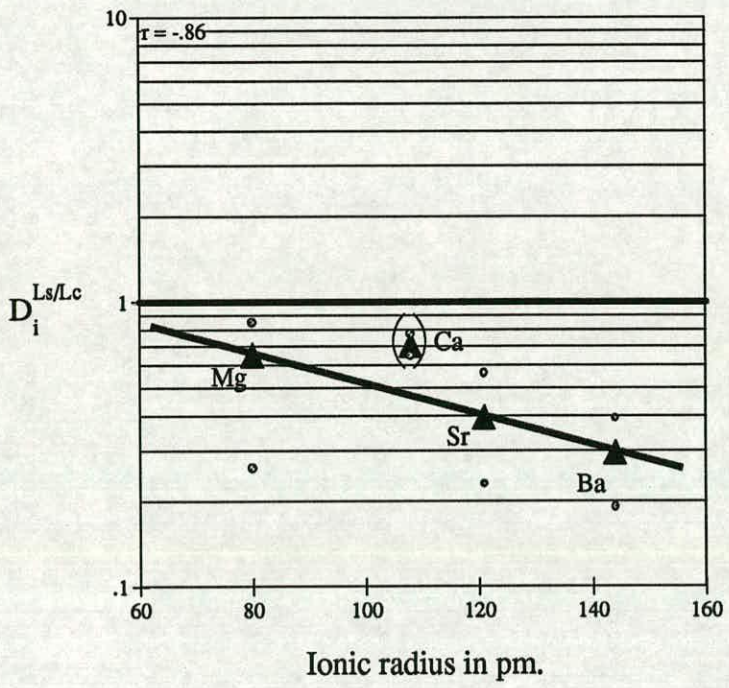

Figure 7.7. Group IIA partitioning with ionic radius. A simple relationship is seen for Mg, Sr, and Ba. More extreme partitioning to the carbonate melt is seen with increasing ionic radius. Ca does not fit this trend well, and has a larger D value than would be expected from its ionic size and charge (i.e. is less extremely partitioned). This is probably because of the high concentrations of Ca in this system, removing it from the range of concentrations for which Henry's law applies. Ca partitioning is therefore not simply controlled by its ionic radius. Despite this anomaly, it is still clear that all Group IIA elements partition into the carbonate melt.

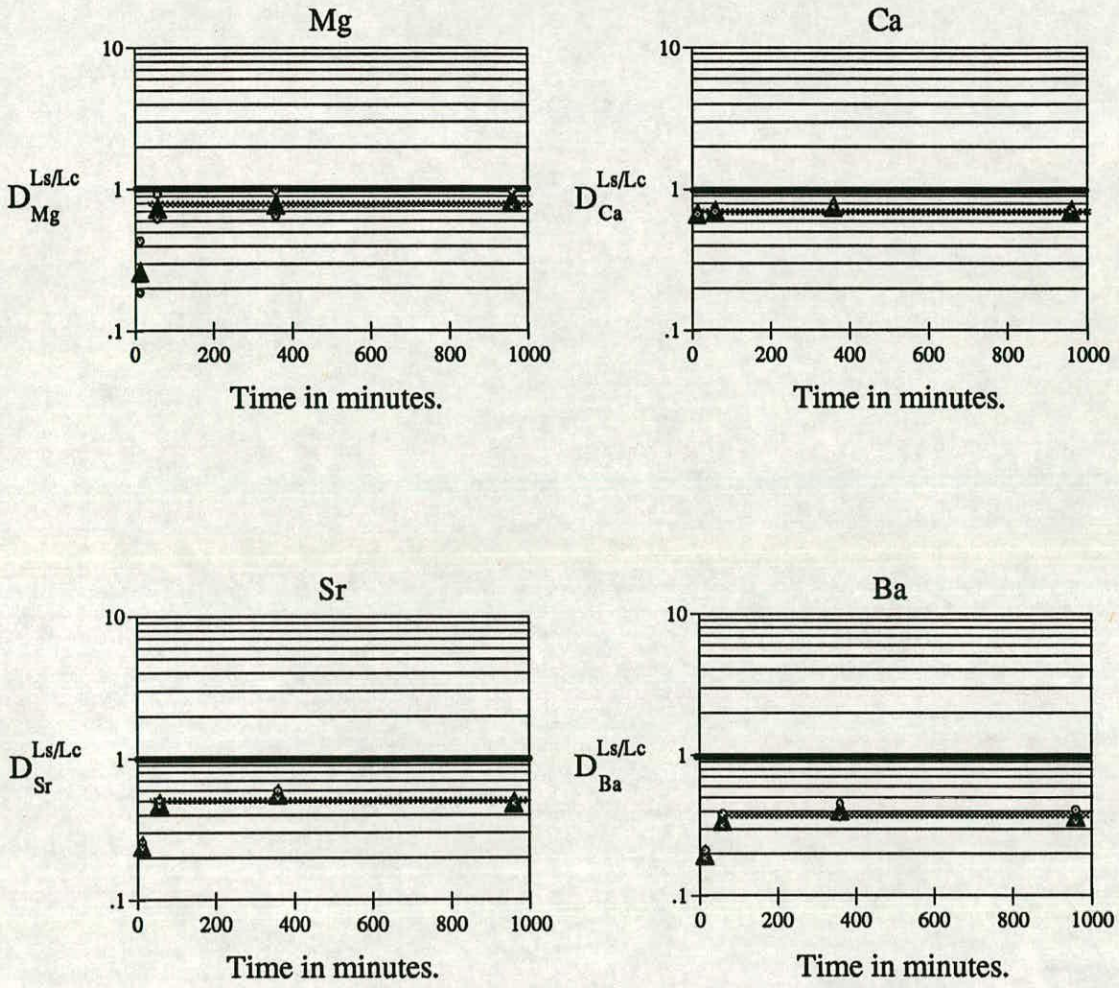

Figure 7.8. Partitioning of Group IIA elements as a function of run duration in synthetic carbonate and silicate liquids. All elements show D values within analytical error variations for runs of 60, 360, and 960 mins. The D values produced from experiments run for 15 minutes are lower than the equilibrium values.

7.4. Group III elements.

8 Group III elements were studied; Al was determined on the electron probe, Y and the 6 REE on the ion probe. The LREE were found to be enriched in the carbonate liquid, whilst the HREE, Y, and especially Al, were enriched in the silicate melt (Figure 7.9).

7.4.1. Aluminium.

Not surprisingly, aluminium partitions into the silicate liquid. $^{Ls/Lc}D_{Al}$ ranges between 204 and 19, with an average of 62.2. The large range of values is due to the problems of heterogeneous distribution within the carbonate quench. In any case, aluminium is always enriched in the silicate melt by at least a factor of 20 for the SM2+CNC composition. $^{Ls/Lc}D_{Al}$ for the SM2+CC charges are less extreme due to closure of the solvus towards more calcic compositions; they range from 8-44 with a mean of 17.20. The REV3 sample gave $^{Ls/Lc}D_{Al} = 96.76$. Aluminium is the most strongly partitioned element studied, and is always greatly enriched in the silicate liquid.

7.2. Yttrium and the REE.

Due to the generally coherent behaviour of the REE and Y, they will be considered together. Figure 7.9 shows some marked systematic trends within the group.

In all cases $^{Ls/Lc}D_{La}$ is the lowest value; La is always partitioned into the carbonate liquid. The range of partitioning is from 0.46-0.94 with an average of $^{Ls/Lc}D_{La} = 0.75$. The REV3 composition gives a significantly lower value ($^{Ls/Lc}D_{La} = 0.35$). The range for cerium is 0.64-1.11, with an average of 0.81. Again, the REV3 composition yielded a lower value ($^{Ls/Lc}D_{Ce} = 0.43$). $^{Ls/Lc}D_{Nd} = 1.17$ is the average for SM2+CNC, with a range of 0.72-1.57. The REV3 composition gave a D value for neodymium of 0.54. Neodymium is roughly equipartitioned between carbonate and silicate liquids. The range of $^{Ls/Lc}D_{Sm}$ in SM2+CNC compositions was from 0.95-1.76, with a mean value of 1.31. The REV3 composition gave $^{Ls/Lc}D_{Sm} = 0.54$. For yttrium, the range of D values was 1.42-2.89, with mean $^{Ls/Lc}D_{Y} = 2.07$. The REV3 composition gave $^{Ls/Lc}D_{Y} = 2.00$. Yttrium is always partitioned to the silicate liquid. Thulium was also partitioned to the silicate liquid, with a range of $^{Ls/Lc}D_{Tm}$ from 1.99-3.50, and an average value of 2.57. REV3 sample gave $^{Ls/Lc}D_{Tm} = 1.91$. Lutetium was the most

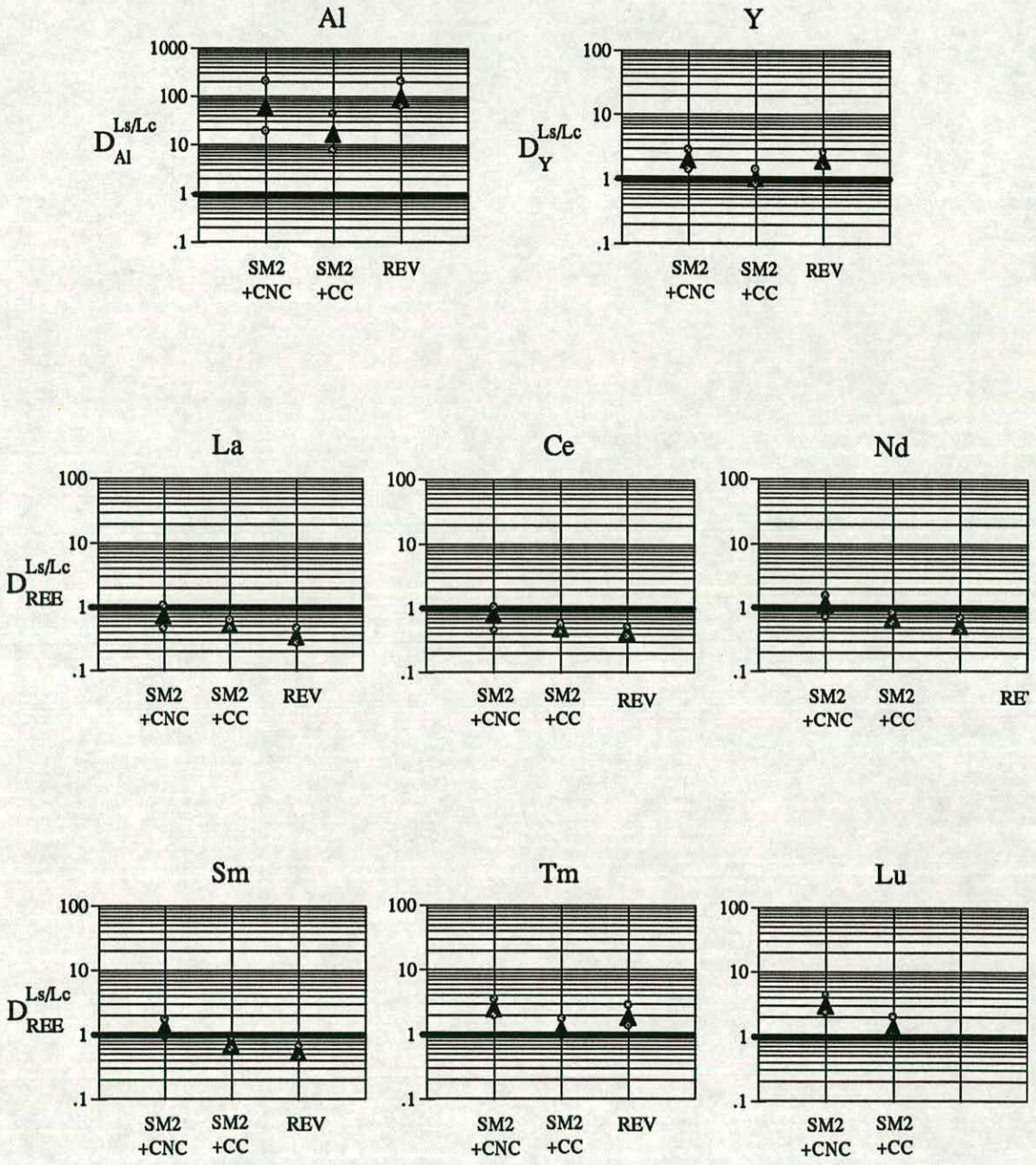

Figure 7.9. Partitioning of Group IIIA elements between synthetic carbonate and silicate melts. Upper and lower limits represent the maximum and minimum measured values of partitioning for each composition, or the standard deviation on the coefficient for the REV3 composition, where only one charge was analysed. Lu was not added to the REV3 composition. T he small ranges in the D values show that pressure and temperature have little effect on partitioning of +3 elements in this synthetic system.

strongly partitioned of the REE, being enriched in the silicate liquid by *ca.* a factor of 3. The average for SM2+CNC compositions was $^{Ls/Lc}D_{Lu} = 3.08$, with a range of 2.40-4.33. The REV3 composition did not contain lutetium.

Figure 7.10 shows the relative partitioning of the REE with respect to ionic radius. It can be seen that there is a trend in partitioning from LREE to HREE. The LREE (represented here by La, Ce, and Nd) partition to the carbonate liquid. This enrichment never greatly exceeds a factor of 2. The middle REE (represented by Sm) are roughly equipartitioned, whilst Y and the HREE (Tm and Lu) are enriched in the silicate component. Despite the scatter in the data, one feature is consistent: LREE/HREE ratio is always higher in the carbonate liquid: $^{Ls/Lc}K_{D_{La/Lu}}$ is always *ca.* 0.25. That is, the carbonate is LREE/HREE enriched by a factor of 4 over the silicate liquid.

7.4.3. Partitioning of +3 elements with ionic radius.

We have already seen that ionic radius exerts an influence on partitioning of the REE. Figure 7.11 shows that this effect extends to other +3 elements as well. Indeed, there is near perfect negative correlation between $^{Ls/Lc}D_i$ and ionic radius for +3 ions. +3 ions with radii >105 pm (e.g. LREE) partition to the carbonate liquid, whilst those with radii <105 pm partition to the silicate liquid. The position of the cross-over point seems only slightly affected by pressure and temperature.

7.4.4. The effect of run duration on the partitioning of Group III elements.

Figure 7.12 shows the variation in $^{Ls/Lc}D_i$ with time for Al, Y, and the REE. In all cases, the 60, 360, and 960 data are within analytical error. As with the Group IA and IIA elements, however, there are lower $^{Ls/Lc}D_i$ values in the 15 minute run. This is especially prominent for La and Ce. Run times of over 60 mins are therefore considered to have reached equilibrium.

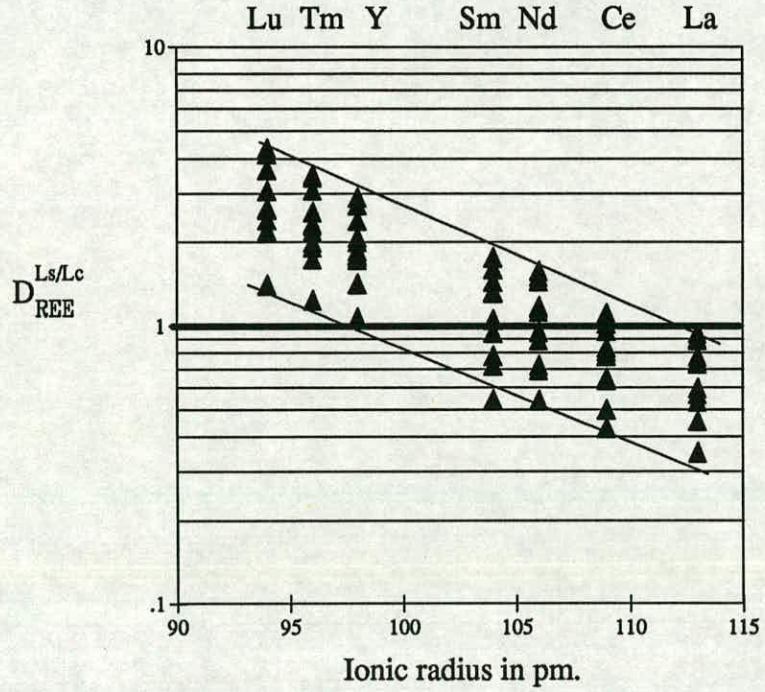

Figure 7.10. Relative partitioning of the rare-earth elements: data from all the synthetically-produced carbonate and silicate liquids analysed. Despite the variations in partitioning seen, there is a distinct trend in partitioning with ionic radius. The carbonate is always enriched in the LREE relative to HREE by a factor of *ca.* 4.

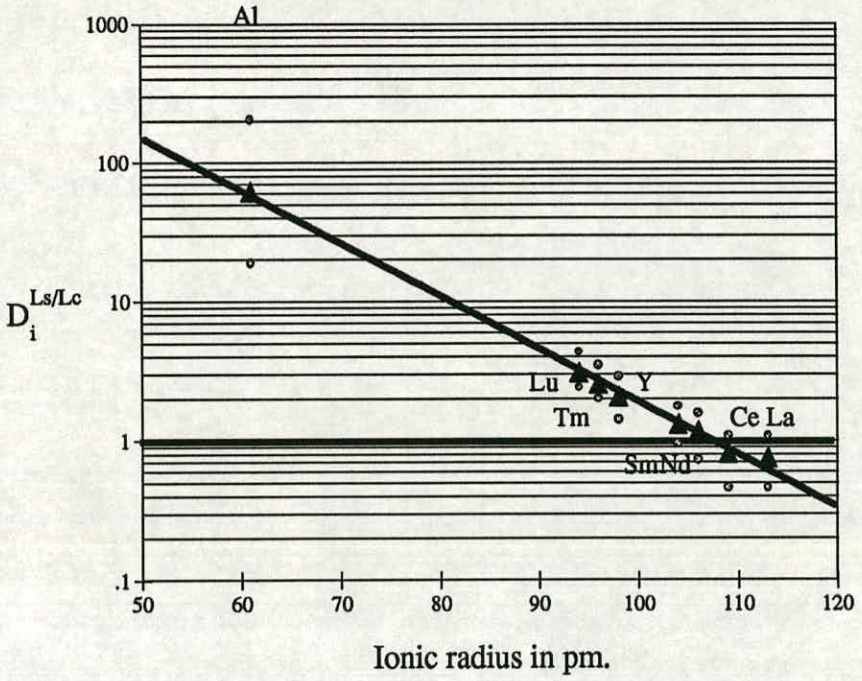

Figure 7.11. Group IIIA partitioning with ionic radius. Using SM2+CNC data, a simple relationship is seen for all +3 elements studied. With increasing ionic radius, partitioning to the silicate melt becomes less extreme until equipartitioning is reached at ca. 105 pm. Larger ions, for example those of the LREE, are preferentially enriched in the carbonate melt. The positioning of the cross-over point is little affected by P and T in these synthetic compositions.

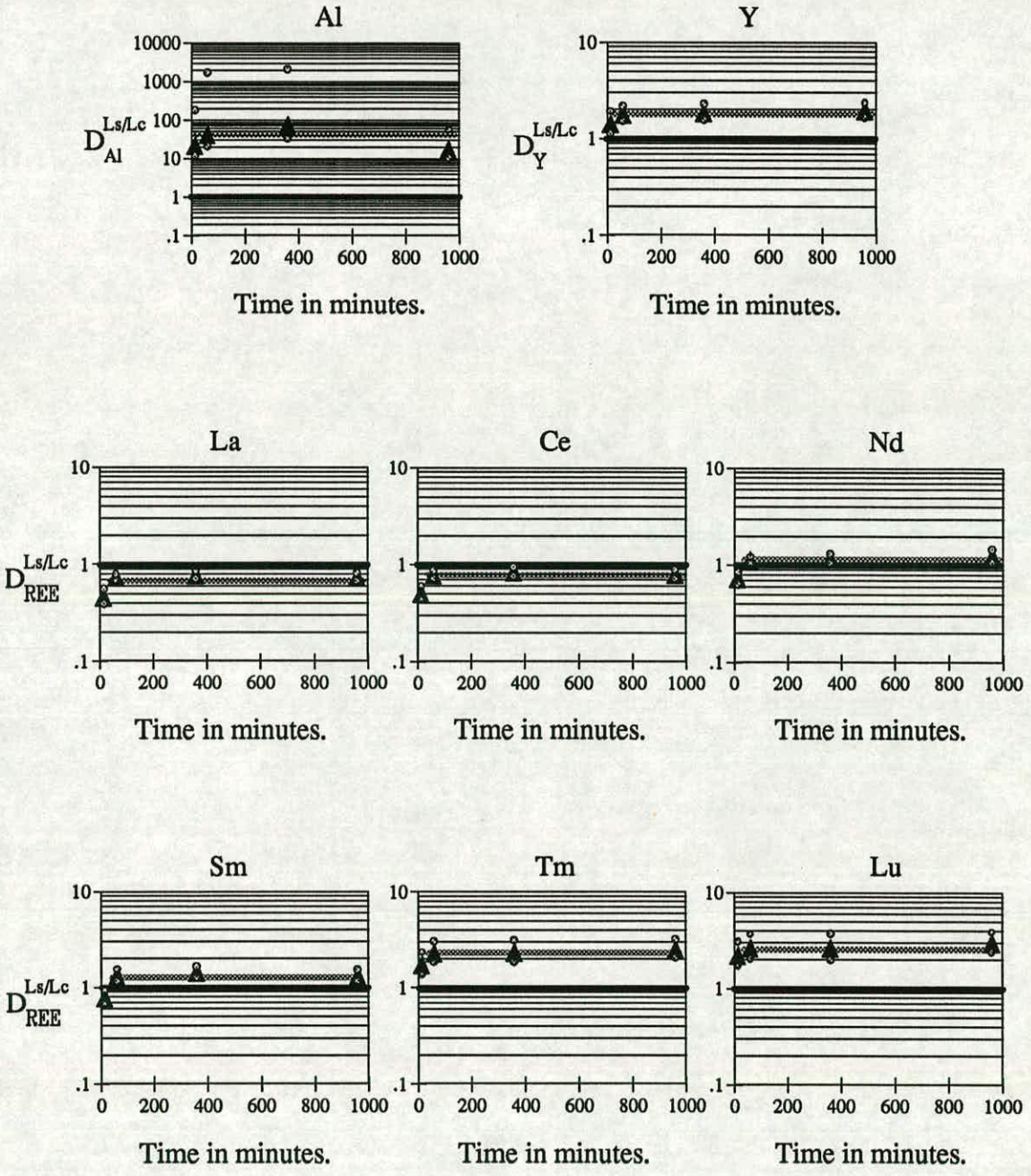

Figure 7.12. Partitioning of Group IIIA elements as a function of run duration in synthetic carbonate and silicate melts. D values for Al are variable due to quench problems, but are all within analytical error. For Y and the REE, duration times of 60, 360, and 960 mins are within analytical error. The 15-minute duration run produces D values lower than longer experiments. The reason for this is not clear. If the partitioning had not reached equilibrium, larger D values would have been expected.

7.5. Group IVA and IVB elements.

The three elements in Group IVA (Ti, Zr, and Hf) were all determined using the ion probe. Electron probe data for silicon is also presented, although it is realised that the $^{Ls/Lc}D_{Si}$ data obtained are likely to be distorted due to the high silicon concentrations present (as seen for Ca values). All the Group IV elements studied partition to the silicate melt, often by a factor of 10 or more (Figure 7.13).

7.5.1. Silicon.

For the SM2+CNC compositions, mean $^{Ls/Lc}D_{Si} = 8.79$, with a range from 6.00-14.50. As with aluminium, this large range of values is thought to be due to quench problems in the carbonate liquid. The SM2+CC compositions showed less pronounced partitioning, with $^{Ls/Lc}D_{Si} = 6.30$, and a range from 2.65-9.20. This is again thought to be due to closure of the solvus in calcic compositions. The REV3 composition gave a much more extreme $^{Ls/Lc}D_{Si}$ value of 119. Not surprisingly, silicon shows pronounced enrichment in the silicate liquid in all charges studied.

7.2.2. Titanium.

Titanium also partitions strongly to the silicate liquid. Mean $^{Ls/Lc}D_{Ti} = 9.83$, with a range from 8.21-13.33. The REV3 composition gave a value of 19.35.

7.5.3. Zirconium.

The average value of $^{Ls/Lc}D_{Zr}$ in SM2+CNC compositions is 10.26, with a range 7.50-12.30. The SM2+CC composition gave a much less extreme value of 2.95, whilst the REV3 composition gave $^{Ls/Lc}D_{Zr} = 14.97$.

7.5.4. Hafnium.

Hafnium is the most extremely partitioned of the Group IV elements. The mean SM2+CNC value of $^{Ls/Lc}D_{Hf}$ is 17.73, with a range from 11.60-24.70. The SM2+CC value is again less extreme at 5.0, and the REV3 value is 10.02.

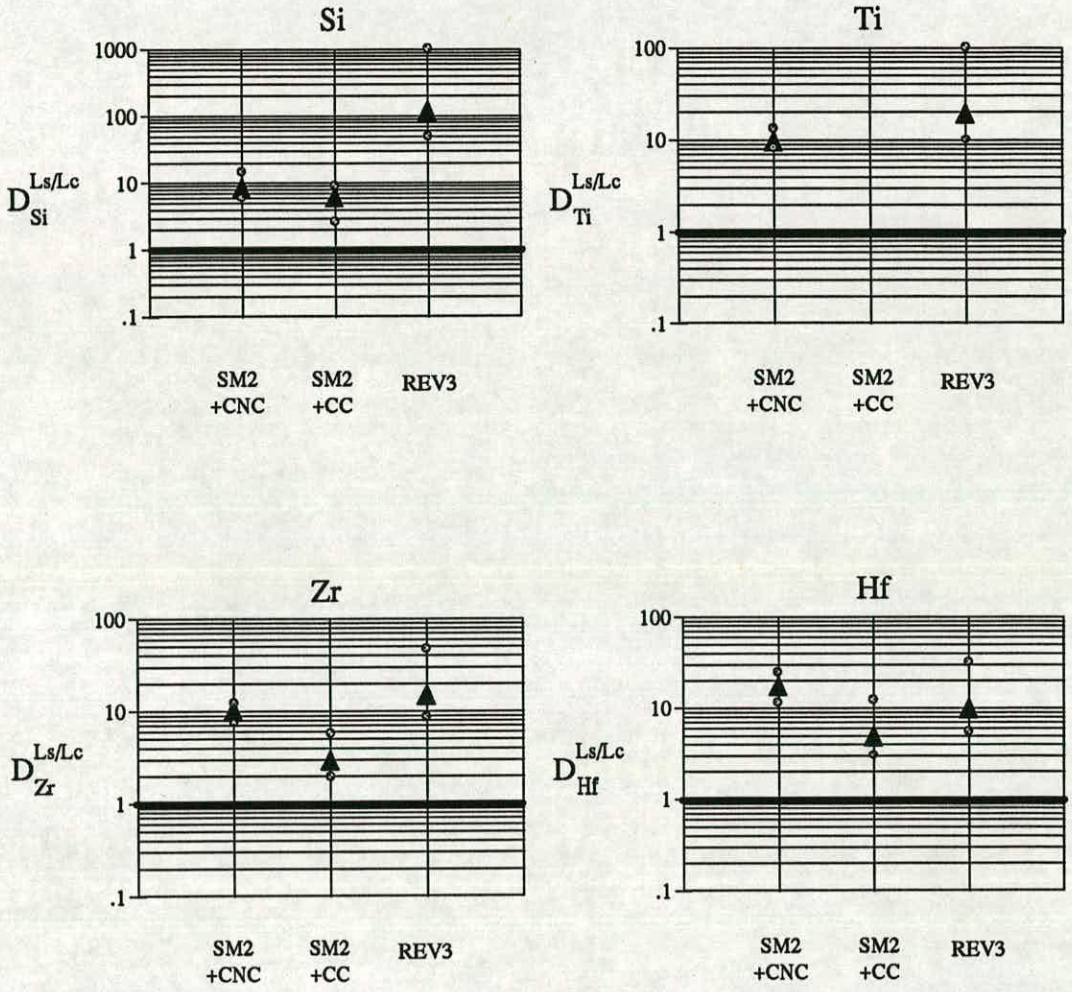

Figure 7.13. Partitioning of Group IV elements between synthetic carbonate and silicate melts. Upper and lower limits for SM2+CNC and SM2+CC represent the measured extremes. For REV3, where only one sample was analysed, the standard deviation on the analysis has been plotted. Data for the three compositions are within analytical error for Ti, Zr, and Hf. The D value for Si in the REV3 composition is significantly higher than in the other compositions. No reason for this difference has been found. All Group IV elements partition strongly into the silicate liquid.

7.5.5. Partitioning with ionic radius.

In the Group IA, IIA, and III elements, a clear relationship existed between ionic radius and relative partitioning. Figure 7.14 shows that this relationship is not well defined for the Group IV elements; indeed, all the $^{Ls/Lc}D_i$ values for the Group IV elements have some overlap at *ca.* 10-15. In individual runs, however, the general trend is $^{Ls/Lc}D_{Si} < ^{Ls/Lc}D_{Ti} < ^{Ls/Lc}D_{Zr} < ^{Ls/Lc}D_{Hf}$. The systematically more extreme partitioning of Hf compared to Zr is a surprise, as Zr^{4+} and Hf^{4+} ions are of identical charge and size. Zr and Hf are believed to behave similarly in most geochemical processes, and any fractionation effect produced by involvement of carbonate liquid could be of considerable diagnostic importance.

7.5.6. The effect of run duration on the partitioning of Group IV elements.

As before, the variations in $^{Ls/Lc}D_i$ with time for the Group IV elements has been plotted in Figure 7.15. All values are within error, regardless of the run duration. This is probably because of the large errors involved in analysing the Si, Ti, Zr, and Hf concentrations of the carbonate quench, disguising any trend in the data. Despite this, there is some evidence that the 15 minute $^{Ls/Lc}D_{Zr}$ and $^{Ls/Lc}D_{Hf}$ values are higher than the equilibrium values. This would fit in with the idea of initially more extreme partitioning at low temperature where immiscible separation first took place, before re-equilibration to the 1300°C run temperature.

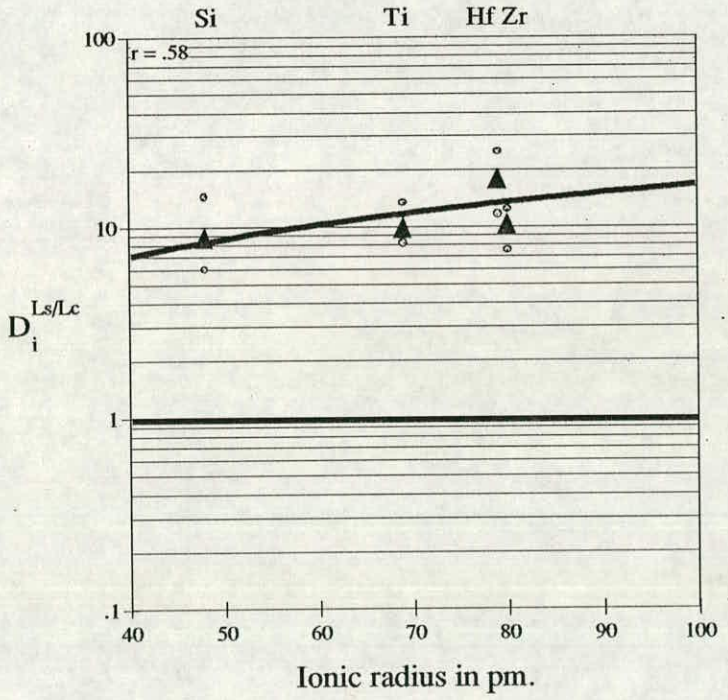

Figure 7.14. Group IV partitioning with ionic radius. There is little evidence of a relationship between partitioning and ionic size for Group IV elements. All the Group IV elements are partitioned to the silicate liquid by *ca.* a factor of 10. Despite being of similar ionic radius, zirconium and hafnium have significantly different partitioning behaviour in most of the experiments.

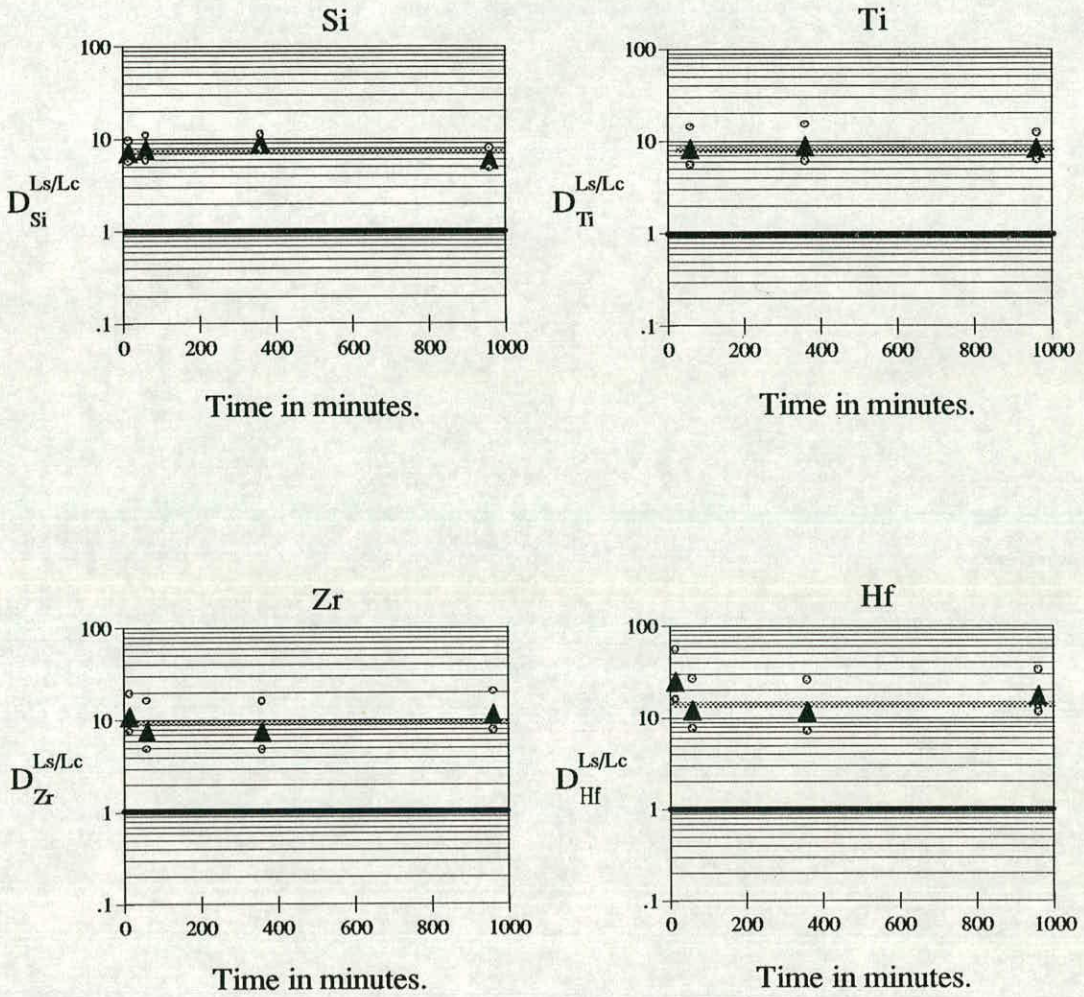

Figure 7.15. Partitioning of Group IV elements as a function of run duration in synthetic carbonate and silicate melts. The results from all experiments are within analytical error, indicating equilibrium values have been attained. Data for zirconium and hafnium in the 15 mins duration run are slightly, but not significantly, higher than the equilibrium values.

7.6. Group VA and VB elements.

All three of the Group VA elements (V, Nb, and Ta) were analysed on the ion probe in order to obtain $^{Ls/Lc}D_i$ data. In addition, phosphorus was analysed on the electron probe in the two doped experiments of G29. P, and V are enriched in the carbonate melt; Nb is approximately equipartitioned, and Ta is partitioned into the silicate liquid (Figure 7.16).

7.6.1. Phosphorus.

Phosphorus was analysed in just two charges , giving $^{Ls/Lc}D_P$ =0.23, and $^{Ls/Lc}D_P$ = 0.26. The errors on these values are unknown, although analytical errors are very small (± 0.02).

7.6.2. Vanadium.

$^{Ls/Lc}D_V$ for SM2+CNC compositions range from 0.32-1.33, with an average of 0.69. This large range is again due to quench problems in the carbonate liquid. For the SM2+CC composition, $^{Ls/Lc}D_V$ = 0.49, and for REV3, $^{Ls/Lc}D_V$ = 0.69.

7.6.3. Niobium.

$^{Ls/Lc}D_{Nb}$ for SM2+CNC compositions range from 0.66 to 1.83, with an average of 1.17. For the SM2+CC composition, $^{Ls/Lc}D_{Nb}$ = 0.72, and for the REV3 composition $^{Ls/Lc}D_{Nb}$ = 0.55. Uncertainty on the Nb values are therefore substantial, but it is clear that Nb is either slightly enriched in the carbonate liquid, or nearly equipartitioned.

7.6.4. Tantalum.

$^{Ls/Lc}D_{Ta}$ for SM2+CNC compositions ranges between 1.90 and 5.40, with a mean value of $^{Ls/Lc}D_{Ta}$ = 3.40. For SM2+CC and REV3, the values are less extreme (1.73 and 1.61 respectively). In the majority of runs, $^{Ls/Lc}K_{D_{Nb/Ta}}$ = 0.33, that is, carbonate liquid enriches niobium over tantalum by a factor of *ca.* 3.

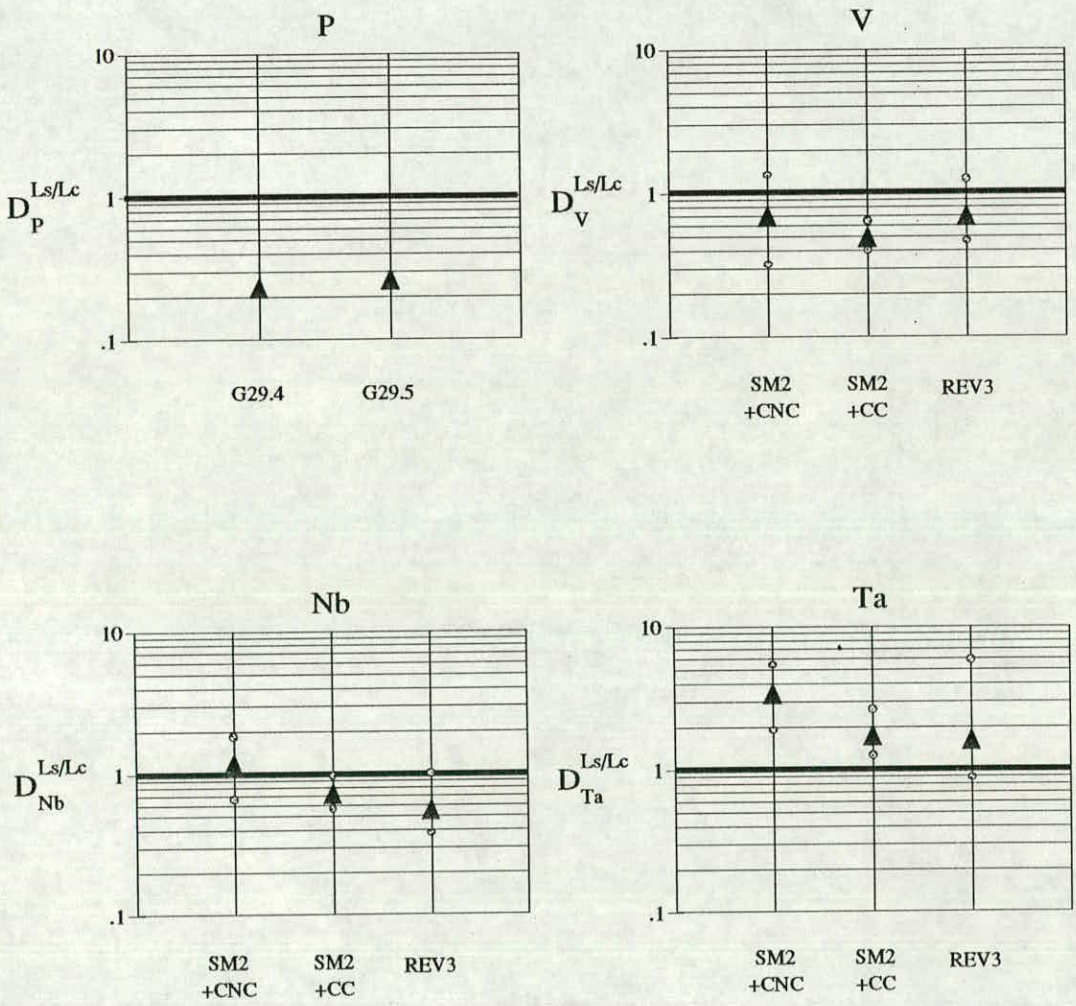

Figure 7.16. Partitioning of Group V elements between synthetic carbonate and silicate liquids. Phosphorus was only analysed by electron probe in the two charges doped to investigate the effects of phosphorus on immiscibility. The errors on the phosphorus data are thus indeterminate. Phosphorus and vanadium are strongly enriched in the carbonate liquid. Niobium is enriched in the carbonate or equipartitioned (depending on composition). Tantalum is enriched in the silicate liquid.

7.6.5. Partitioning of Group V elements with ionic radius.

As with the Group IA, IIA, and III elements, there is a strong correlation between relative partitioning of Group V elements and ionic radius (Figure 7.17). Unlike the other groups, however, with Group V this is a strong positive correlation. As ionic radius increases, $^{Ls/Lc}D_i$ increases, and elements change from being enriched in the carbonate melt to being enriched in the silicate melt. Although this correlation is well defined, there is one surprise: Nb and Ta have significantly different partitioning behaviour despite having the same ionic charge and ionic radius. As mentioned above, Nb/Ta ratio is *ca.* three times as high in the carbonate melt as in the coexisting silicate. Again, this fractionation between niobium and tantalum could be of great importance when diagnosing the involvement of carbonate liquid in mantle metasomatism.

7.6.6. The effect of run duration on the partitioning of Group V elements.

Figure 7.18 shows the variation in $^{Ls/Lc}D_i$ with time for the Group V elements. All the $^{Ls/Lc}D_{Ta}$ values are within error, regardless of run duration. There is considerable variability of the data for V, and Nb, with $^{Ls/Lc}D_i$ for both the 15 minute and 960 minute runs being outside the uncertainties of the other two values. The 15 minute run is believed to be out of equilibrium by comparison with the data for other elements, however, the 960 minute run ought to be consistent with the shorter runs. The discrepancies in this run are seen in the most poorly constrained data (Ta, Nb and V): this cannot be coincidence, and is implying that the statistical errors on the Group V data are probably in excess of those quoted. This is likely to be due to the non-gaussian distribution of concentration estimates for V, Nb, and Ta in the carbonate liquid, which in turn is due to redistribution of these elements in the carbonate liquid on quenching of the experiments. It is certainly unlikely that these differences represent disequilibrium after 960 mins in these superliquidus experiments, especially since $^{Ls/Lc}D_V$ is lower than expected, whilst $^{Ls/Lc}D_{Nb}$ is higher.

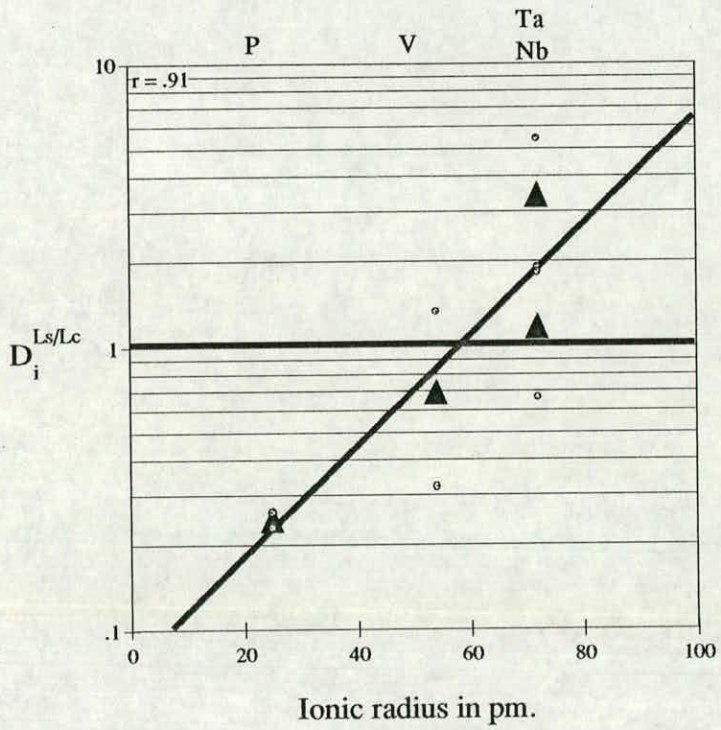

Figure 7.17. Group V partitioning with ionic radius. A strong positive correlation with D value is seen. As ionic size increases, Group V elements partitioning changes from being strongly to the carbonate melt, to being strongly to the silicate melt. Ta and Nb, despite being of similar ionic size, have significantly different D values.

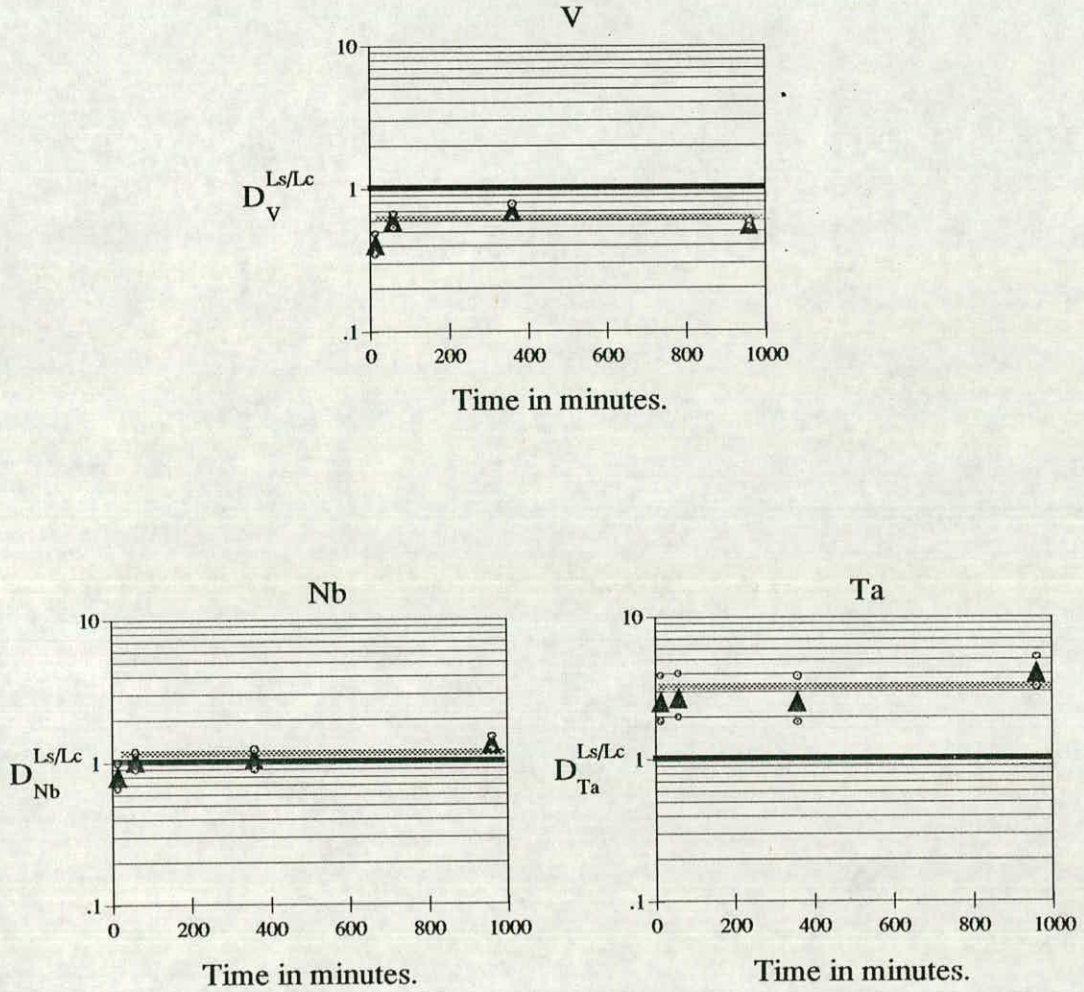

Figure 7.18. Partitioning of Group V elements as a function of run duration in synthetic carbonate and silicate liquids. For Ta, all run durations produce D values within analytical error. However, for both Nb and V, the 960 mins run duration D values are outside analytical error of the shorter run times. The V value is lower than the other runs, whilst the Nb value is higher. This could be a disequilibrium feature, but it is thought to be more likely that these variations are caused by analytical errors in excess of those quoted. No data are available for phosphorus.

7.7. U, Th, and Pb.

Partitioning data for lead, thorium and uranium are given in Figure 7.19.

7.7.1. Lead.

$^{Ls/Lc}D_{Pb}$ are the most poorly constrained due to counting errors on the ion probe. For the SM2+CNC composition they range from 0.61-2.46. The SM2+CC value is 1.03, and the REV3 value is 0.63. All that can be surmised from this data is that Pb is roughly equipartitioned in the synthetic system.

7.7.2. Thorium.

$^{Ls/Lc}D_{Th}$ values range from 5.28 to 20.70, with an average of $^{Ls/Lc}D_{Th} = 9.48$. The reversed composition gave a value of 4.90. Thorium is in general enriched in the silicate melt by a factor of *ca.* 10.

7.7.3. Uranium.

$^{Ls/Lc}D_{U}$ values for SM2+CNC compositions range from 2.14-4.68, with an average of 3.12. For SM2+CC, the value is 1.58, and for REV3, the value is 1.18. Uranium is only weakly partitioned to the silicate liquid. Carbonate liquid will therefore fractionate U from Th, and Pb from U and Th.

7.7.4. The effect of run duration on the partitioning of U, Th, and Pb.

$^{Ls/Lc}D_{U}$, $^{Ls/Lc}D_{Th}$, and $^{Ls/Lc}D_{Pb}$ data are all within error regardless of run duration (Figure 7.20). U and Th data are constant, whilst there does seem to be some variation in the Pb value, perhaps due to Pb loss to the Pt capsule during the actual experiment.

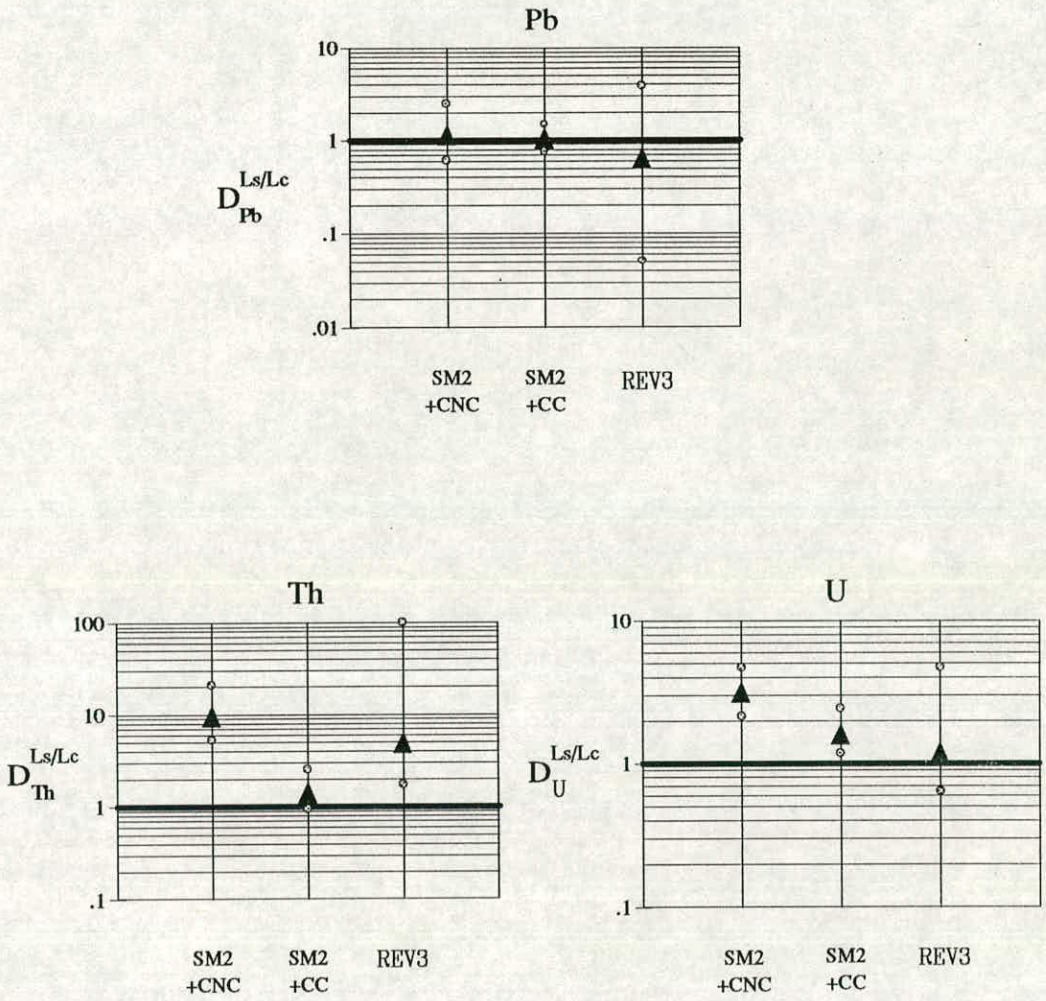

Figure 7.19. Partitioning of U, Th, and Pb between synthetic carbonate and silicate liquids. Upper and lower limits for SM2+CNC and SM2+CC represent the measured extremes. For REV3, the maximum and minimum D values are calculated from standard deviations on ion probe concentrations. The errors on REV3 are larger than those on SM2 compositions because uncertainty on a single result greatly exceeds variation between results. Thorium is strongly, and uranium weakly partitioned to the silicate liquid. Pb is roughly equipartitioned, although as mentioned in Chapter 6 the Pb data should be treated with caution. SM2+CC D values are less extreme due to closure of the solvus in the calcic composition.

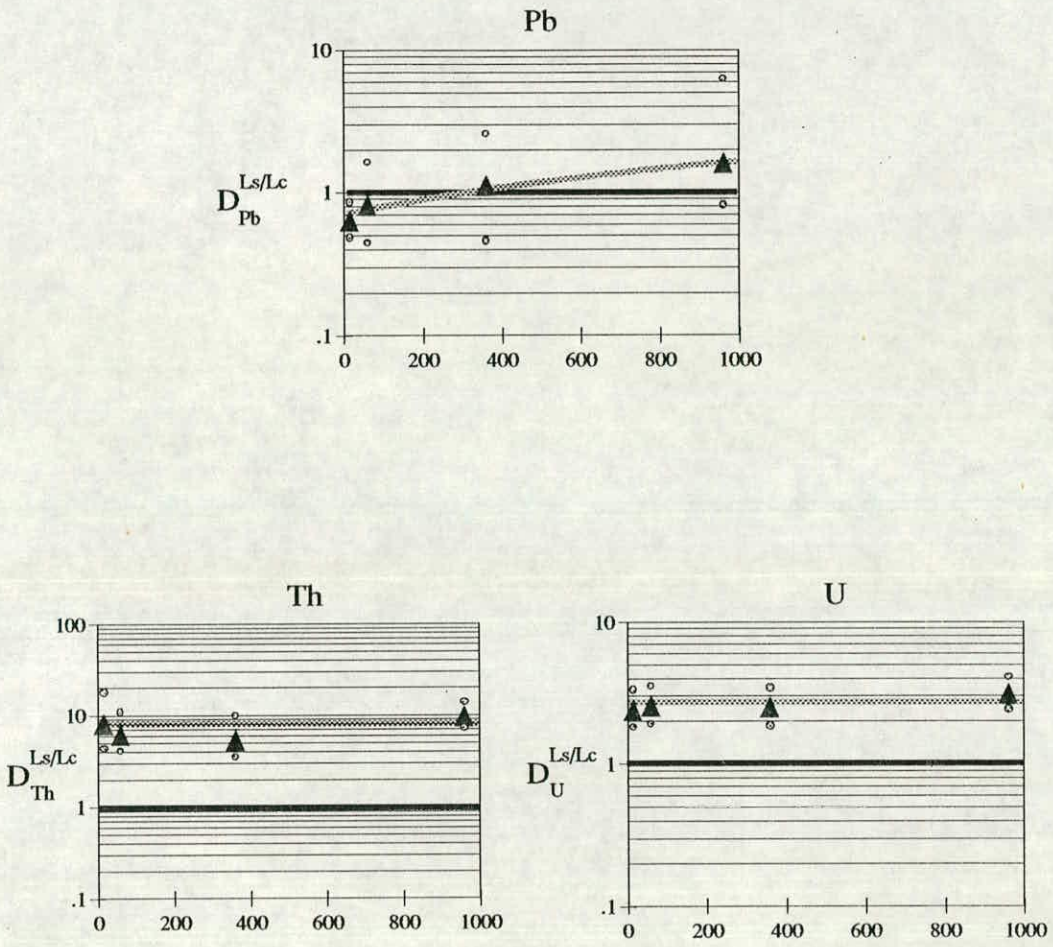

Figure 7.20. Partitioning of U, Th, and Pb as a funvction of run duration in synthetic carbonate and silicate liquids. U and Th values are constant with time (*ca.* 8 for Th, *ca.* 2.5 for U). However there is a distinct trend in D values for Pb, from partitioning to the carbonate after 15 mins, to partitioning to the silicate after 960 mins. This lack of equilibrium may be due to the loss of Pb to the platinum sample capsule during the run.

7.8. Partitioning of non-metals.

The ion probe cannot analyse for negative ions whilst in the configuration employed to analyse for trace cations. Therefore the only data on the partitioning of strongly electronegative ions is from electron probe analyses of the doped minor element runs (G29). The data are presented in Figure 7.21. $^{Ls/Lc}D_F = 0.39$. $^{Ls/Lc}D_{Cl} = 0.37$. $^{Ls/Lc}D_S = 0.09$. The halogens, and sulphur, are strongly partitioned into the carbonate melt.

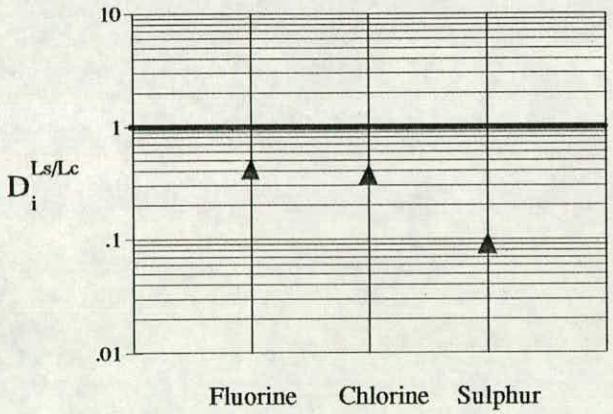

Figure 7.21. Partitioning of highly electronegative elements F, Cl, S. All partition strongly to the carbonate liquid, with the greatest enrichment for sulphur. The size of errors on these data is unknown, as only one experiment containing each of these elements was undertaken. Analytical errors are smaller than the symbols.

7.8. Physical controls on element partitioning.

7.8.1. The effect of pressure.

The results of Bedson (1983), and Bedson & Hamilton (1989) suggested that pressure was a major control on partitioning, and that not only the extent of partitioning, but also the sense of partitioning was changed for a number of elements with increasing pressure. This has not been found to be the case in this synthetic system. Indeed, in only two cases has a pronounced pressure effect been established:

At low pressure (0.25, and 0.5 GPa), carbonate liquids produced from the SM2+CC starting composition are virtually pure $CaCO_3$, with only a very minor sodium component. At 0.8 GPa, however, the same bulk composition produces a coexisting carbonate melt with *ca.* 15% Na_2O. This manifests itself in terms of partitioning as a pressure effect on $^{Ls/Lc}D_{Na}$. Figure 7.22 shows $^{Ls/Lc}D_{Na}$ vs. pressure for SM2+CC compositions. A strong negative correlation is seen, with sodium partitioning to the silicate melt at low pressure, and to the carbonate melt at high pressure. It must be stated that this effect is only present in the calcic composition; indeed, the pressure effect in more sodic carbonate liquids, although small, seems to indicate an increase in $^{Ls/Lc}D_{Na}$ with pressure. To a certain extent, this effect is mimicked by other Group IA elements.

The only other effect of pressure seen in these compositions is that of greater solubility of some elements in the carbonate liquid at high pressure, illustrated by the decrease in $^{Ls/Lc}D_{Al}$ with increasing pressure. This effect can be interpreted as a closure of the solvus, with more mixing of carbonate and silicate components leading to less pronounced partitioning. However, compositionally, there is no contraction of the two-liquid field, and for the majority of other elements $^{Ls/Lc}D_i$ are unaffected. It has therefore been suggested that this relationship represents a greater ability for the carbonate melt to accept Al and Si ions at higher pressure, rather than a general solvus effect.

No pressure effects were seen on other elements, including the REE. Bedson (1983) reported a strong and coherent pressure effect on $^{Ls/Lc}D_{REE}$ in his experiments on carbonate-silicate immiscibility. This effect has not been reproduced in the synthetic system, and may therefore be related to the compositional differences between the two systems (perhaps the presence of Fe or Mg).

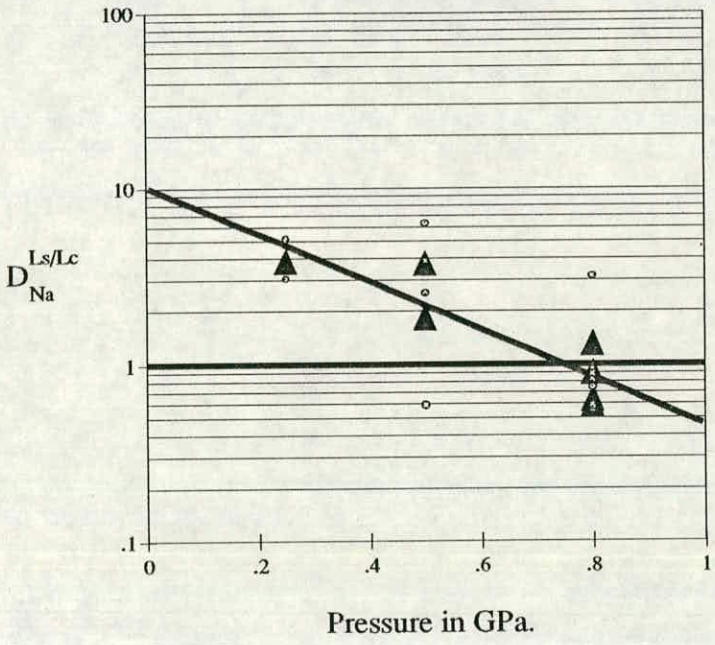

Figure 7.22. Na partitioning in calcic compositions as a function of pressure. A distinct negative correlation is seen. Calcic carbonate melts are therefore only produced at relatively low pressures (<0.8 GPa) in this synthetic system.

7.8.2. The effect of temperature.

Temperature effects were found to be very limited. No change in sense of partitioning was seen with increasing temperature, and in most elements, no significant change in extent of partitioning was seen. The exception to this rule is that the elements most extremely partitioned to either the carbonate or the silicate liquid show less extreme partitioning in the 1300°C runs than in their 1200°C counterparts. This effect is shown in Figure 7.23. $^{Ls/Lc}D_i$ has been plotted against temperature for the Group IA and Group IV elements. The less extreme values seen at 1300°C are attributed to closure of the solvus. Increased mixing of the carbonate and silicate components leads to less pronounced structural differences between the two liquids, and therefore less pronounced partitioning of the component elements. The partition coefficients are expected to approach unity in this system at between 1450°C and 1500°C.

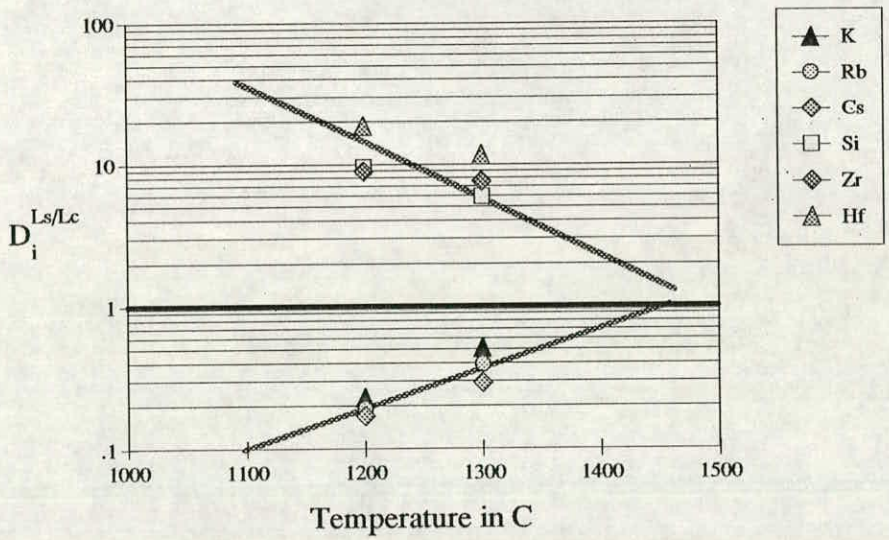

Figure 7.23. The effect of temperature on partitioning in synthetic carbonate and silicate liquids. The less extreme partitioning at 1300℃ suggests closure of the solvus with increasing temperature. An estimate for the critical temperature above which immiscibility would not occur would be between 1450 and 1500℃.

7.9. Chemical controls on element partitioning.

7.9.1. Element partitioning as a function of ionic radius.

Ionic radius has often been considered to be the most influential factor controlling element partitioning (e.g. Möller, 1988). When dealing with crystal-liquid systems, it is the crystal that exerts the control on element partitioning; those elements of specific ionic size and charge are accepted into the crystal lattice, others are expelled into the liquid. Liquid-liquid systems, such as the carbonate-silicate partitioning investigated here, are unconstrained by rigid lattices. It might therefore be expected that variations with ionic charge and size would be less specific, and more gradual in character.

In each individual periodic table group, we have seen a coherent relationship with ionic radius. Does this coherency extend to all elements studied? Figure 7.24 shows element partitioning plotted against ionic radius for all elements studied on the ion probe. Data have been displayed from the two solid-media experiments at 1300°C, 1.5 GPa. These have been used since the $^{Ls/Lc}D_i$ values from the solid-media experiments are slightly better constrained than the gas-media data due to higher quench rates.

Two areas can be delineated in this graph:

(a) Elements with ionic radius greater than 105 pm. are enriched in the carbonate liquid, and behave coherently with ionic radius. There is a clear negative correlation, with elements of larger ionic radius being more extremely partitioned to the carbonate liquid. It is believed that it is the carbonate liquid that controls this behaviour, with larger ions being energetically more stable in the carbonate melt.

(b) Elements with ionic radius less than 105 pm. are generally enriched in the silicate melt. However there is a large range of values, and little evidence of a relationship with ionic radius in these elements. Ionic size is therefore not the controlling factor on partitioning for the majority of trace elements.

This lack of coherency in partitioning with ionic radius led to the consideration of other factors which might exert control over element partitioning.

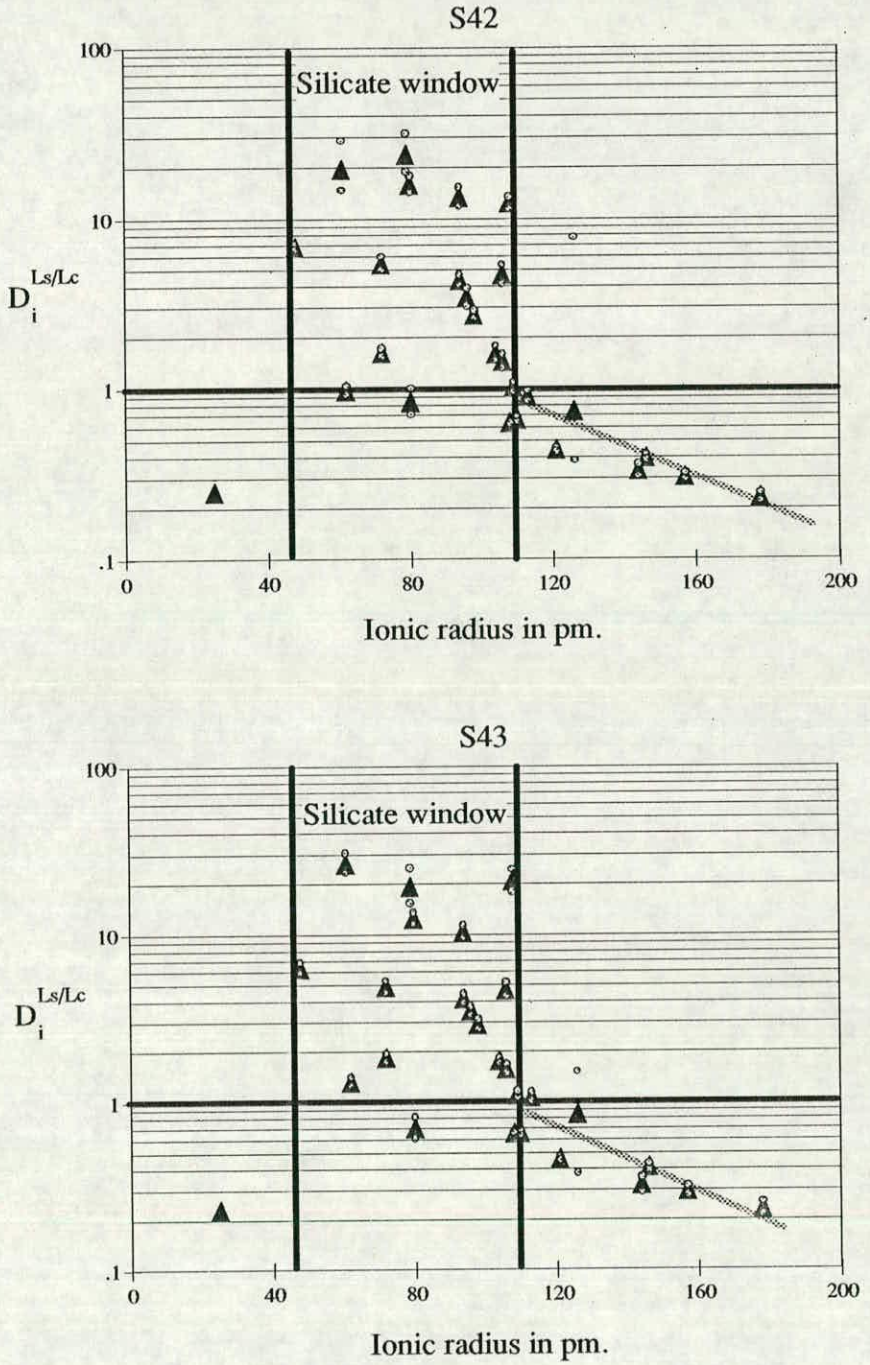

Figure 7.24. Element partitioning as a function of ionic size in solid media experiments S42, S43. A distinct relationship can be seen, with the carbonate melt generally prefering elements with large ionic radii. The trend is subject to considerable scatter, especially at the low ionic radius end.: There is clearly another controlling factor on partitioning.

7.9.2. Element partitioning as a function of charge density.

$^{Ls/Lc}D_i$ values for experiments S42 and S43 have been plotted against charge density in Figure 7.25. Charge density was estimated as the ionic charge (C) divided by the ionic radius (R). A clear relationship was seen between $^{Ls/Lc}D_i$ and C/R. Two relationships can be seen. The majority of elements have C/R < 0.05. These elements lie on a line of +ve correlation, with $^{Ls/Lc}D_i$ increasing with charge density as expected from the energetics of the ionic carbonate melt. However, a maximum value of $^{Ls/Lc}D_i$ is consistently reached at C/R = 0.05. Above this, a negative correlation of $^{Ls/Lc}D_i$ with C/R is seen, with elements of extremely high charge density (e.g. Nb, V, P) being again partitioned to the carbonate liquid.

There is still a considerable variability around these trends: for example charge density for Zr and Hf, and Nb and Ta, are identical, but their partitioning noticeably different: there is perhaps also a mass effect on partitioning (perhaps related to field strength).

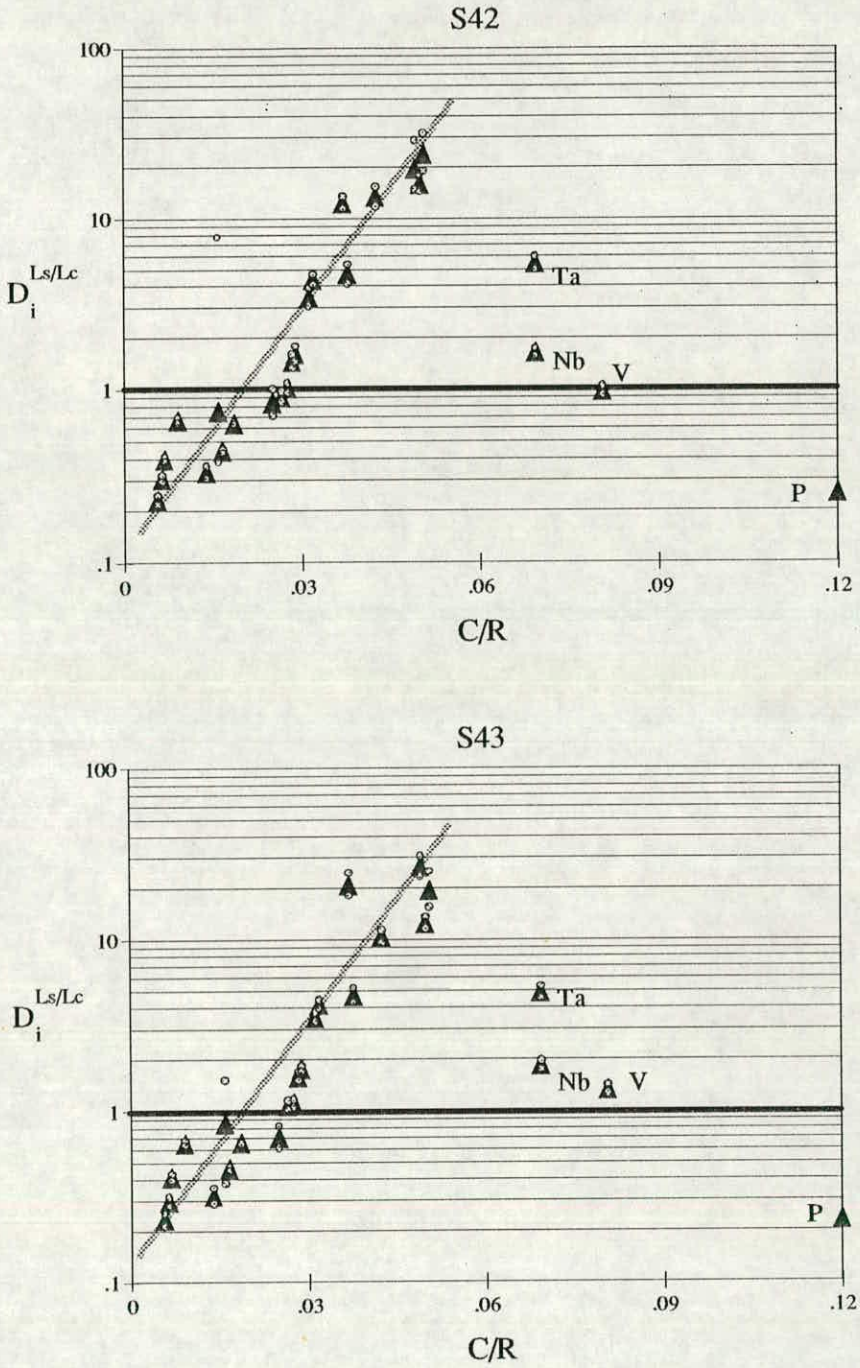

Figure 7.25. Element partitioning as a function of charge density (C/R) in solid media experiments S42, S43. The majority of elements fit on a line of positive correlation between charge density and partitioning. However, elements with C/R > 0.5 (e.g. Nb, Ta, V, P) do not adhere to this trend, but instead fall on a line of negative correlation. It is suggested that this duality can be explained by a discriminating silicate melt, whose ideal constituents would have C/R at ca. 0.05-0.06. Elements of lower charge density, or of much higher charge density, are preferentially incorporated into the carbonate melt.

7.10. The effects of minor elements on the partitioning between carbonate and silicate melts.

7.10.1. Fluorine.

The effect of fluorine on partitioning has been investigated for all elements studied on the ion probe. In all cases partitioning becomes less extreme in the presence of fluorine. This effect is significantly outside analytical error for the elements K, Rb, Cs, Sr, Ba, Al, Si, Ti, Zr, and Hf (Figure 7.26). Since the less extreme partitioning is seen in virtually all the elements studied, it is assumed that this represents a general closure of the solvus in the presence of fluorine, with more mixing of components, and correspondingly less extreme partitioning. This is attributed to the depolymerising effect of fluorine on silicate melts.

9.10.2. Chlorine.

In major element compositions, it was noticed that chlorine did not produce the same effect on immiscibility as fluorine. This is also true in trace-element partitioning. Although no effect can be seen in the Group IIA elements, all the other elements studied show more extreme partitioning in the presence of chlorine (Figure 7.27). It seems that chlorine actually results in less mixing of the carbonate and silicate liquids, and correspondingly more extreme partitioning. Chlorine therefore results in an expansion of the extent of immiscibility in carbonate-silicate systems.

It was expected that the presence of fluorine and chlorine would have affected the partitioning of the REE due to the formation of REE-fluoride and REE-chloride complexes (e.g. Choppin, 1971). There is no evidence that this process is taking place in these experiments.

7.10.3. Sulphur.

For the majority of trace-elements (e.g. Group IA, Group IIA...), sulphur has no significant effect on partitioning. There is some evidence from the Group III, and Group V elements that sulphur causes $^{Ls/Lc}D_i$ values to become slightly more extreme although the effect is not important. Sulphur has little effect on partitioning of trace elements between carbonate and silicate liquids.

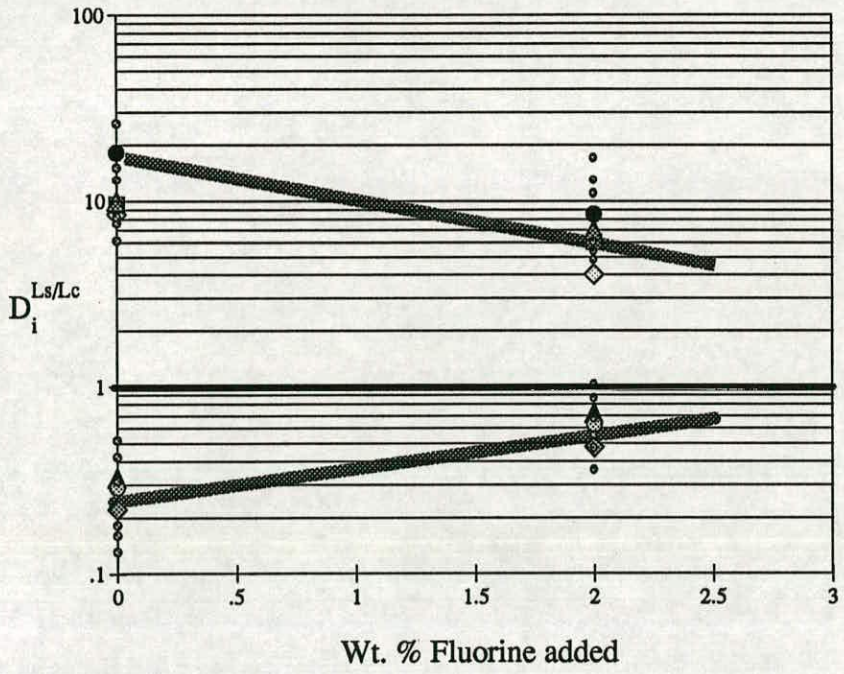

Figure 7.26. The effect of fluorine on the partitioning of +1 and +4 elements. It is clear that the presence of fluorine causes partitioning between carbonate and silicate liquids to become less extreme. This is believed to be caused by the depolymerising effect of fluorine on silicate liquids, resulting in less pronounced differences in structure between Ls and Lc, and therefore more mixing of carbonate and silicate components. This effect can be seen for other elements, although it is less obvious as partitioning is generally less extreme.

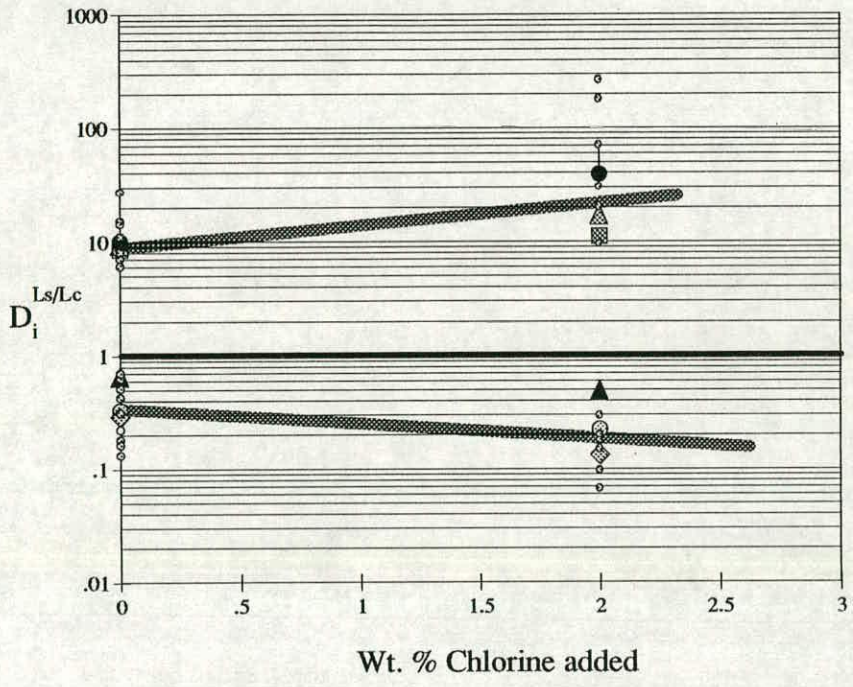

Figure 7.27. The effect of chlorine on the partitioning of +1 and +4 elements between synthetic carbonate and silicate melts. Chlorine seems to produce the opposite effect to that of fluorine, with partitioning between carbonate and silicate liquids becoming more extreme for most elements. Chlorine and fluorine are therefore behaving in very different ways in these experiments. This effect can be seen for other elements, although it is generally less obvious for less extremely partitioned elements.

7.10.4. Phosphorus.

Of the minor elements investigated, phosphorus is the only one to have clearly disparate effects on different elements, and can result in changes in the sense of partitioning as well as the severity. Figure 7.28 clearly shows that $^{Ls/Lc}D_i$ for Group IA elements increases with the addition of phosphorus (i.e. the presence of phosphorus leads to less pronounced enrichment of the Group IA elements in the carbonate liquid). If this were a solvus effect, we would expect the same process to occur in Group IIA elements. In fact, the opposite occurs (Figure 7.29), with decrease in $^{Ls/Lc}D_i$ for the Group IIA elements when phosphorus is added (i.e. addition of phosphorus leads to more pronounced enrichment of the Group IIA elements in the carbonate liquid). This effect is also seen in the Group III elements, with the REE and Y becoming progressively more enriched in the carbonate liquid with increasing phosphorus content (Figure 7. 30). For the Group IV elements, addition of phosphorus leads to less extreme partitioning (Figure 7.31).

It is therefore believed that phosphorus has a dual effect on partitioning. Whilst causing a closure of the solvus and therefore less pronounced partitioning for the majority of elements (e.g. Group IA and Group IV elements), phosphorus causes an increase of stability for the Group IIA elements, and more especially the REE, in the carbonate liquid. This is probably due to the formation of phosphate-carbonate complexes, which are known to exist for Ca and the REE under other geological conditions (e.g. Cantrell & Byrne, 1987; Byrne *et al.*, 1991). This phosphorus effect will again be discussed in the chapter on partitioning between natural carbonate and silicate liquids, which often contain 2% or more of P_2O_5.

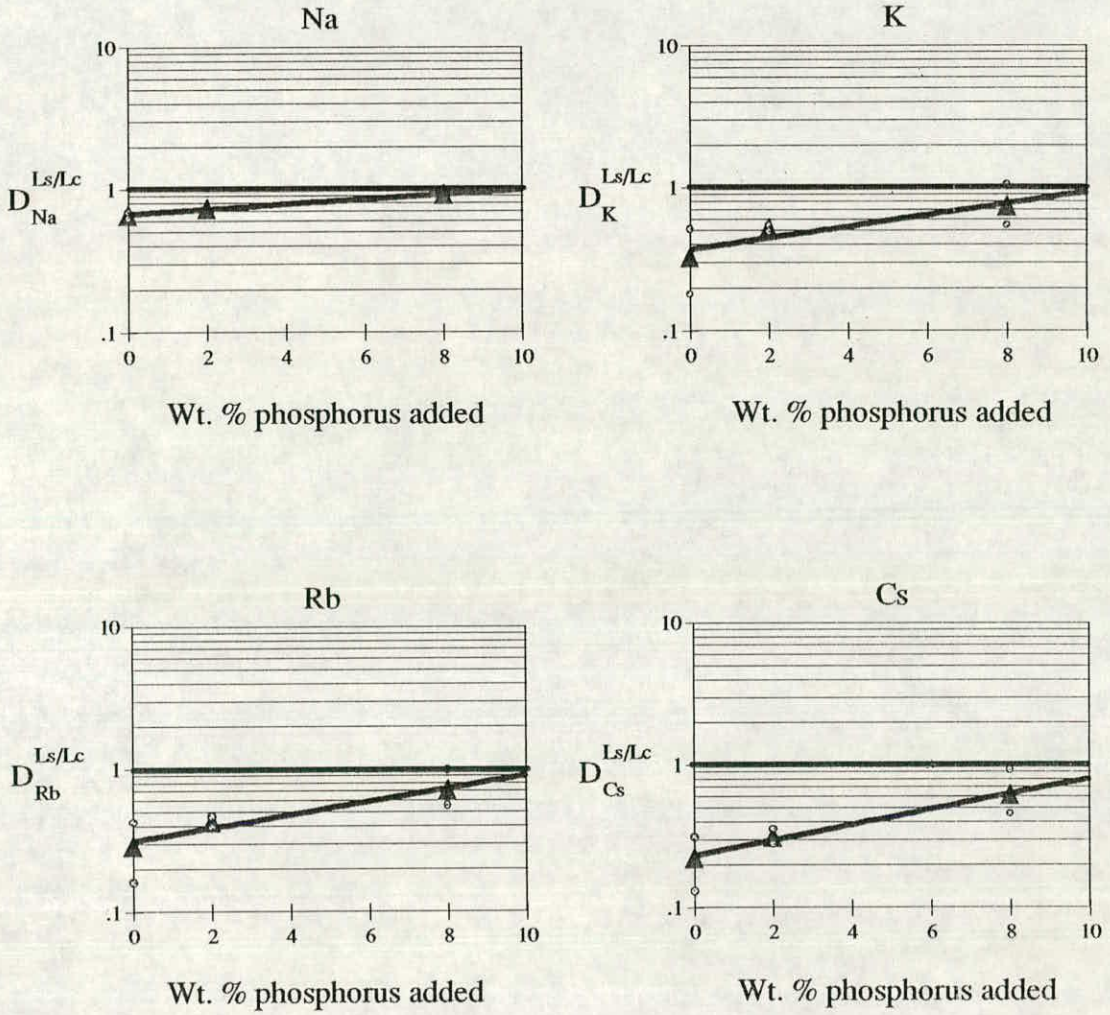

Figure 7.28. The effect of phosphorus on the partitioning of +1 elements between synthetic carbonate and silicate melts. On addition of phosphorus, partitioning of the +1 elements to the carbonate melt becomes significantly less pronounced. It is this effect that is believed to cause the less extreme alkali metal partitioning seen in natural systems.

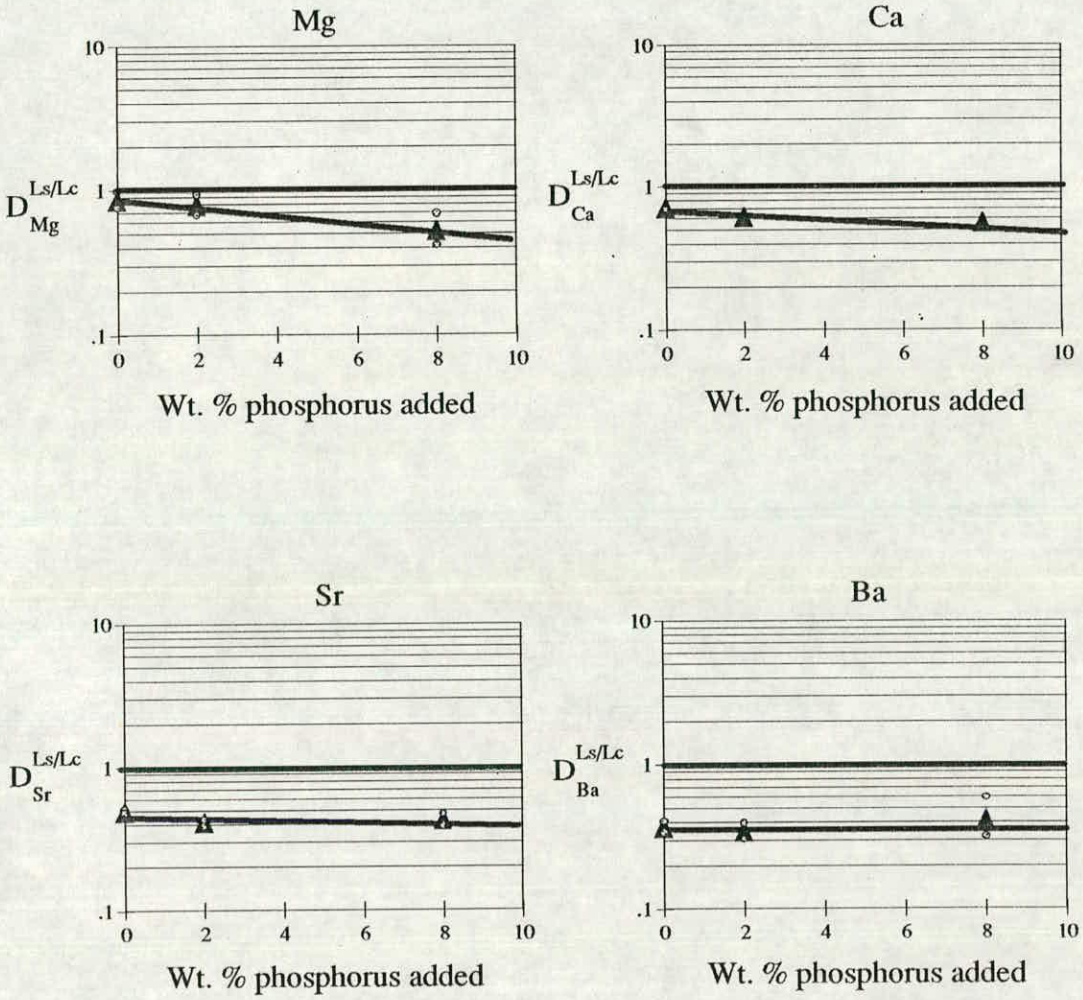

Figure 7.29. The effect of phosphorus on the partitioning of Group IIA elements between synthetic carbonate and silicate melts. The effect of phosphorus seems to be variable. A pronounced decrease in Mg D value is seen on addition of phosphorus. The effect is less pronounced for Ca, and very small for Sr. Phosphorus does not seem to effect Ba partitioning at all.

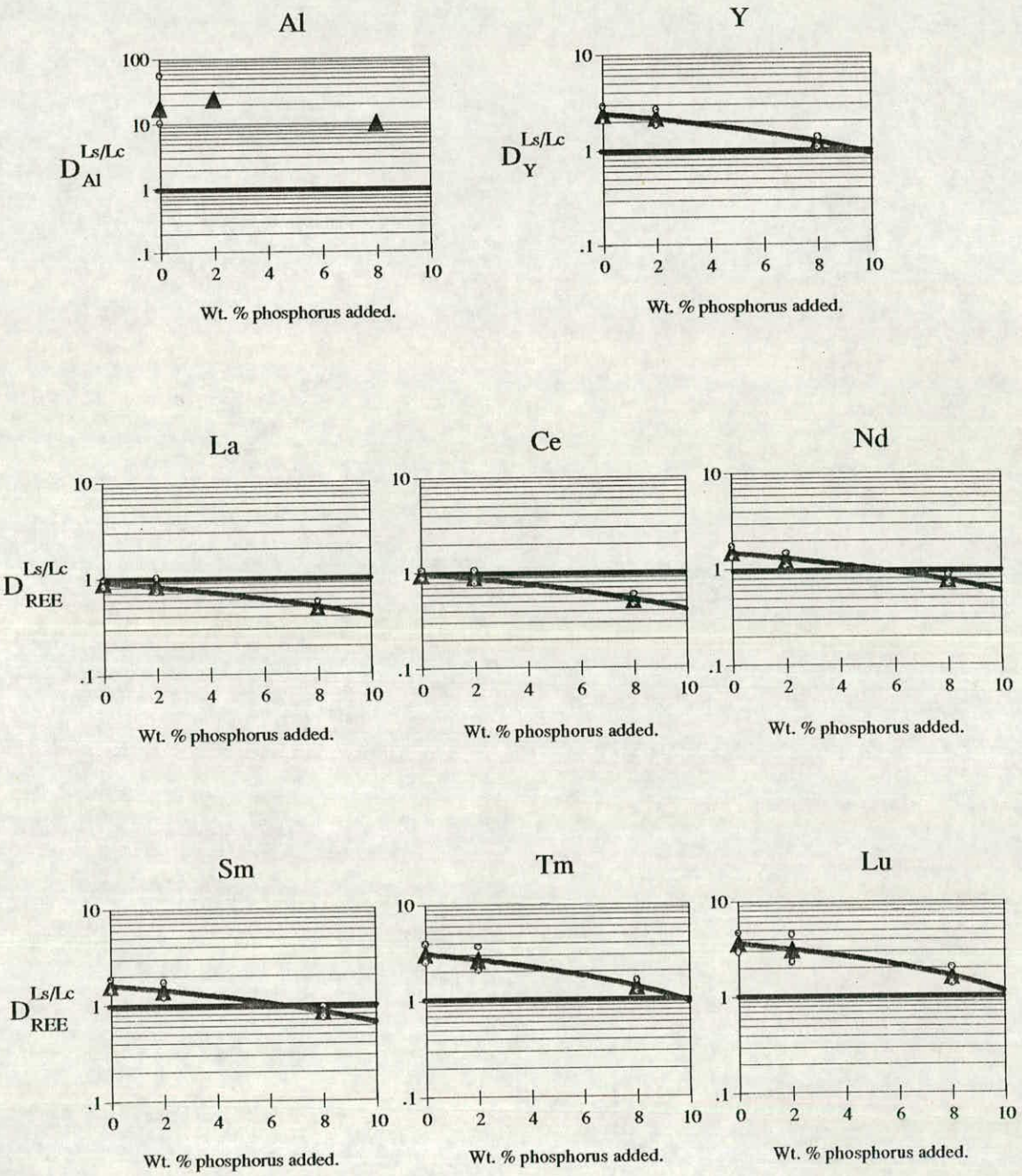

Figure 7.30. The effect of phosphorus on the partitioning of Group IIIA elements between synthetic carbonate and silicate liquids. Note that Y and the REEs all show an increased affinity for the carbonate melt when phosphorus is present. This is thought to be due to the stability of phosphato-carbonate complexes of these elements. The data for aluminium are more equivocal.

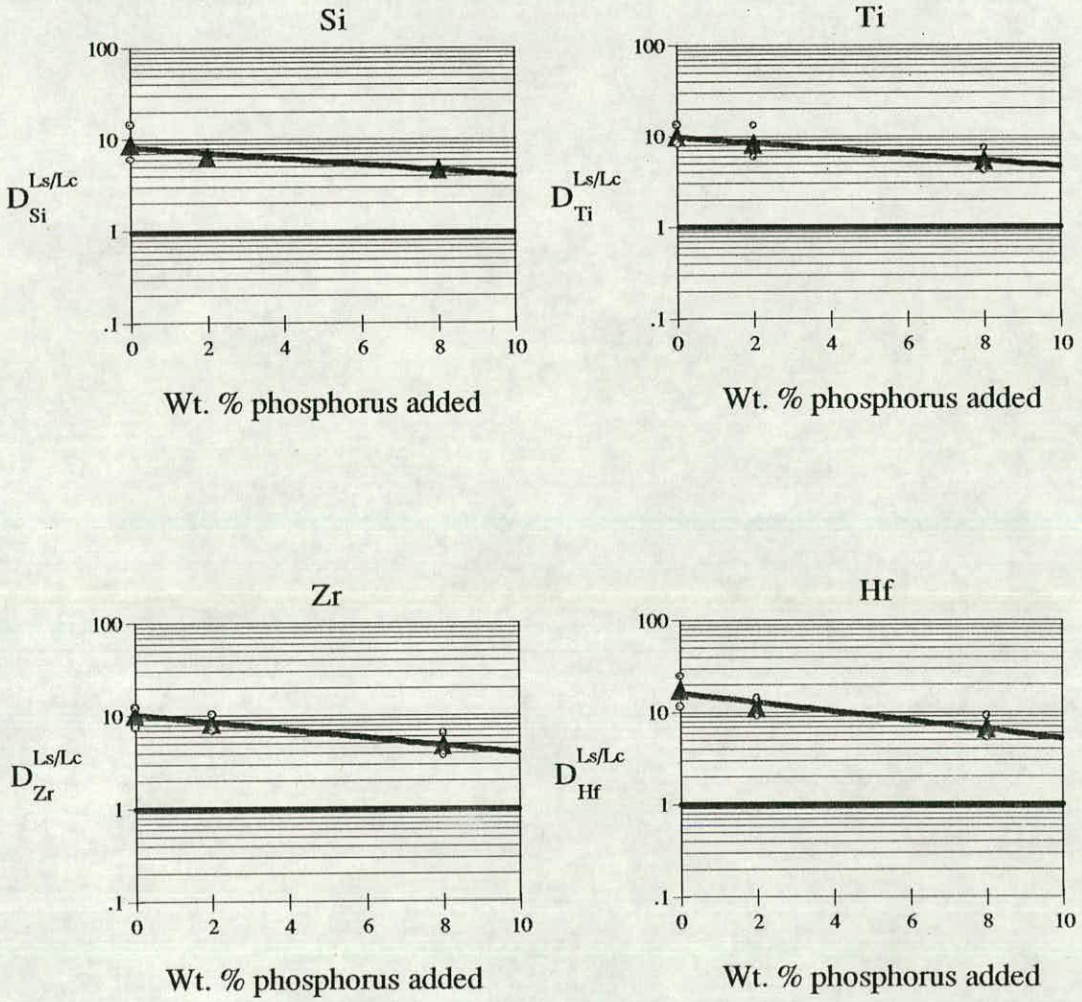

Figure 7.31. The effect of phosphorus on partitioning of Group IV elements between carbonate synthetic carbonate and silicate melts. D values for all elements in the presence of phosphorus are lower than those produced under phosphorus-absent conditions, Phosphorus causes partitioning of Group IV elements to the silicate liquid to become significantly less extreme.

7.11. Summary of partitioning between synthetic carbonate and silicate melts.

$^{Ls/Lc}D_i$ partition coefficients have been obtained for 30 elements in the synthetic system SiO_2-Al_2O_3-CaO-Na_2O-CO_2. Data have been obtained for three compositions over a range of pressures, temperatures and run duration. Mean values of partitioning for the main body of data (SM2+CNC composition) are given in Table 7.1.

Table 7.1. Mean partition coefficients from the SM2+CNC composition experiments.

Element	$^{Ls/Lc}D_i$	Element	$^{Ls/Lc}D_i$
Na	0.66	Si	8.79
K	0.33	Ti	9.83
Rb	0.29	Zr	10.26
Cs	0.22	Hf	17.73
Mg	0.65	P	0.25
Ca	0.70	V	0.69
Sr	0.39	Nb	1.17
Ba	0.30	Ta	3.40
Al	62.21	U	3.12
Y	2.07	Th	9.48
La	0.75	Pb	1.13
Ce	0.81		
Nd	1.17	S	0.09
Sm	1.31		
Tm	2.57	F	0.39
Lu	3.08	Cl	0.37

Some general conclusions can be made from these data:

(a) All Group IA elements partition to the carbonate melt. This enrichment becomes steadily more pronounced as ionic radius increases, giving $^{Ls/Lc}D_{Na} > {}^{Ls/Lc}D_{K} > {}^{Ls/Lc}D_{Rb} > {}^{Ls/Lc}D_{Cs}$.

(b) All Group IIA elements are partitioned to the carbonate melt. As with the alkali metals, this partitioning becomes more extreme with increasing ionic radius, giving: $^{Ls/Lc}D_{Mg} > {}^{Ls/Lc}D_{Ca} > {}^{Ls/Lc}D_{Sr} > {}^{Ls/Lc}D_{Ba}$. Calcium does not fit into this trend perfectly. This is thought to be due to its high concentrations in these melts, taking its partitioning behaviour out of the range of concentrations for which Henry's law applies.

(c) Partitioning of the Group III elements is variable. Aluminium is strongly partitioned to the silicate melt. Yttrium and the HREE are weakly partitioned to the silicate melt. The LREE are however partitioned to the carbonate melt. In all experiments $^{Ls/Lc}D_{Al} > {}^{Ls/Lc}D_{Lu} > {}^{Ls/Lc}D_{Tm} > {}^{Ls/Lc}D_{Y} > {}^{Ls/Lc}D_{Sm} > {}^{Ls/Lc}D_{Nd} > {}^{Ls/Lc}D_{Ce} > {}^{Ls/Lc}D_{La}$. This variation in partitioning is again related to ionic radius, with Group III elements with ionic radius less than *ca.* 100 pm. being partitioned to the silicate melt, and elements with ionic radius greater than *ca.* 100 pm. being partitioned to the carbonate.

(d) Group IV elements always partition strongly to the silicate melt, by a factor of *ca.* 10. There is little evidence of a relationship with ionic radius. Surprisingly, Zr and Hf partitioning is not identical.

(e) Group V element partitioning varies substantially. Phosphorus and vanadium are partitioned to the carbonate melt, niobium is roughly equipartitioned, and tantalum is partitioned to the silicate melt. Again, although caution must be applied when comparing these geochemically distinct elements, a relationship with ionic radius seems to exist. With the Group V elements, however, partitioning changes from enrichment in the carbonate to enrichment in the silicate with increasing ionic radius. As with Zr-Hf, tantalum and niobium do not show identical partitioning behaviour despite their chemical similarity.

(f) Carbonate-silicate immiscibility effectively separates U from Th. Thorium is strongly partitioned to the silicate melt, whilst uranium is only weakly partitioned or equipartitioned. $^{Ls/Lc}D_{Pb}$ data is poor but suggests partitioning to the carbonate, or equipartitioning.

(g) Fluorine, chlorine and sulphur all partition to the carbonate melt.

(h) A distinct correlation exists between $^{Ls/Lc}D_i$ and charge density (C/R). There is an optimum charge density of *ca.* 0.05 where the most extreme partitioning to the silicate liquid occurs. Ions with charge densities much higher (e.g. Nb, V, P) and much lower (e.g. Cs, Rb, Ba) than this value are partitioned to the carbonate melt.

(g) Although ionic radius and charge density seems to explain adequately most of the partitioning seen, some anomalies persist. These include the disparate behaviour of Zr-Hf, Ta-Nb, and U-Th.

CHAPTER 8

ELEMENT PARTITIONING BETWEEN COEXISTING CARBONATE AND SILICATE LIQUIDS OF NATURAL COMPOSITION.

8.1. The Data.

For immiscible liquids of natural rock compositions, $^{Ls/Lc}D_i$ partitioning data has been obtained for a total of 27 elements. Ten of these were present in both liquids at high enough concentrations to be measured by electron probe analysis. Concentration estimates for the other 17 elements were estimated on the ion probe. For K, Ti, Mg, and Mn, $^{Ls/Lc}D_i$ were obtained by both analytical methods.

Run products from experiments using each of the six successful starting compositions (BD50+CNC, BD50+CC, BD119+CNC, BD119+CC, SUN189+CNC, SUN189+CC) were analysed, allowing the variations in partitioning due to compositional control to be investigated. Also, for each composition, charges run at 1100-1300°C, and 0.2-0.8 GPa were analysed, allowing investigation of the effects of pressure and temperature. For the BD119+CNC nephelinitic composition, the study of pressure effects was extended to 2.0 GPa in order to simulate partitioning behaviour under mantle conditions. An investigation into the effects of run duration on partitioning was performed on this composition. The data treatment used here is identical to that outlined in Chapter 7. Data tables are presented in Appendix B.2.

The $^{Ls/Lc}D_i$ data for each element has been studied graphically with respect to variations with pressure, temperature, and time. Inclusion of this extensive graphical material was considered unnecessary, and it is only where coherent trends with pressure and temperature are seen that example graphs have been included. The elements have been considered separately, and then in the context of their position in the periodic table. Previous determinations of partitioning (e.g. Bedson, 1983) will also be discussed.

8.2. Group IA elements.

As with the synthetic compositions, $^{Ls/Lc}D_i$ values were obtained for four alkali metals: Na, K, Rb, and Cs (Table 8.1). In general, all four were relatively enriched in the carbonate liquid ($^{Ls/Lc}D_i < 1$), although in very calcic compositions at low pressure, Na, K, and Rb were seen to partition to the silicate liquid (Figure 8.1).

Table 8.1. Partitioning of the Group IA elements in natural compositions.
n is the number of determinations, μ is the mean value obtained. Max and Min are the most extreme partitioning seen for that composition.

	Sodium				Potassium				Rubidium				Cesium			
Composition	n	μ	Max	Min	n	μ	Max	Min	n	μ	Max	Min	n	μ	Max	Min
BD50+CNC	9	**0.63**	0.77	0.55	9	**1.00**	1.22	0.82	5	**0.60**	0.68	0.41	5	**0.51**	0.68	0.32
BD50+CC	9	**0.64**	0.78	0.47	9	**1.11**	1.42	0.86	1	**0.78**	0.87	0.70	1	**0.68**	0.99	0.47
BD119+CNC	9	**0.65**	0.74	0.57	9	**0.80**	0.98	0.57	14	**0.61**	0.85	0.44	14	**0.46**	0.83	0.16
BD119+CC	9	**0.68**	0.82	0.50	9	**0.90**	1.35	0.59	7	**0.74**	1.01	0.56	7	**0.67**	1.12	0.48
SUN189+CNC	9	**0.66**	0.72	0.58	9	**0.77**	1.04	0.59	6	**0.45**	0.55	0.39	6	**0.41**	0.56	0.27
SUN189+CC	9	**2.84**	8.29	0.59	9	**2.94**	9.61	0.70	3	**1.07**	1.96	0.49	3	**0.74**	0.98	0.52

8.2.1. Sodium.

Sodium partitioning across the majority of compositions is extremely constant at $^{Ls/Lc}D_{Na} \sim 0.65$. This does not hold for the most calcic composition studied (SUN189+CC) where there is a strong dependence of $^{Ls/Lc}D_{Na}$ on pressure, ranging up to $^{Ls/Lc}D_{Na} = 8.29$ at 0.25 GPa. There thus seems to be constant partitioning of sodium between liquids with $Na_2O > 8\%$, but extremely variable partitioning in less sodic compositions. Bedson (1983) found a range in $^{Ls/Lc}D_{Na}$ from 0.4-1.5 in sodium-rich phonolitic charges.

8.2.2. Potassium.

Potassium is not strongly partitioned, with $^{Ls/Lc}D_K$ usually close to 1. Again the exception is in low-sodium charges at low pressures, where potassium becomes incompatible with the calcic carbonate liquid, and is enriched in the silicate. $^{Ls/Lc}D_K$ ranges up to a maximum of 9.61 at 0.25 GPa for the SUN189+CC composition.

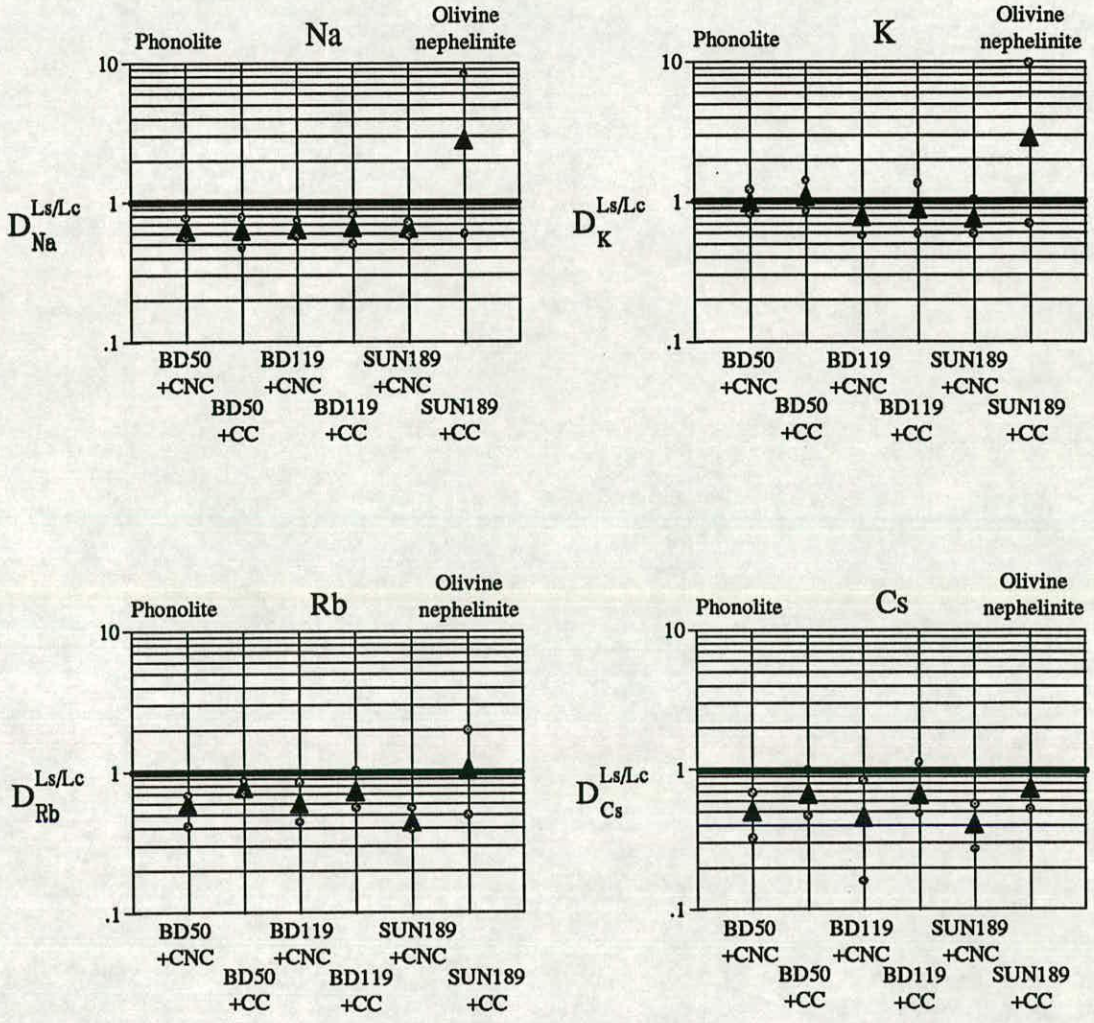

Figure 8.1. Partitioning of the Group IA elements in natural compositions. Mean values of partitioning are plotted with upper and lower limits representing the measured extremes. The closeness of these ranges shows that P and T have little effect on partitioning of the Group IA elements. The exception to this is the SUN189+CC composition, where a pronounced pressure effect can be seen for Na, K, and Rb.

Bedson's experiments on the sodic compositions are in good agreement with our values in sodic liquids, with $^{Ls/Lc}D_K \sim 1$.

8.2.3. Rubidium.

$^{Ls/Lc}D_{Rb} < {}^{Ls/Lc}D_K$ in all compositions studied, with rubidium being moderately enriched in the carbonate melt ($^{Ls/Lc}D_{Rb} = 0.4\text{-}1.0$). Again, there is some evidence for rejection of rubidium by the most calcic carbonate liquids produced (see Table 8.1). Rubidium enrichment in the carbonate liquid seems to be enhanced by two compositional factors:

(a) High sodium contents in the carbonate liquid ($^{Ls/Lc}D_{Rb}$ is lower in the CNC compositions than in the corresponding CC mixes).

(b) Low degrees of polymerisation in the silicate melt ($^{Ls/Lc}D_{Rb}$ is lower in the nephelinites than in the phonolites).

These features are also seen in cesium partitioning, and to a lesser extent in potassium partitioning.

8.2.4. Cesium.

$^{Ls/Lc}D_{Cs} < {}^{Ls/Lc}D_{Rb}$ for all compositions studied. Cesium is always enriched in the carbonate liquid, the most extreme enrichment seen being $^{Ls/Lc}D_{Cs} = 0.16$ in the BD119+CNC composition at 1100°C, 0.25 GPa. Cesium partitioning follows the same compositional controls as rubidium.

8.2.5. Partitioning of Group IA elements with temperature.

Temperature has no effect on the partitioning of the Group IA elements. In a few experiments, $^{Ls/Lc}D_i$ are outside the confidence limits of experiments at other temperatures; however, these variations are small, and no coherent trend with temperature is seen.

8.2.6. Partitioning of Group IA elements with pressure.

In the SUN189+CC composition, a distinct negative correlation of $^{Ls/Lc}D_i$ with pressure can be seen for sodium and potassium (Figure 8.2). This is related to the formation of low-alkali calcic carbonate liquids at low pressures discussed previously.

No significant variations in $^{Ls/Lc}D_i$ for Group IA elements is seen in the main dataset for sodic compositions. However, extension of the study of pressure effect to 2.0 GPa in the BD119+CNC composition revealed that +1 elements partition to the carbonate liquid at low pressure, and are gradually partitioned more towards the silicate melt at higher pressure (Figure 8.3). This trend is compensated for by the reverse effect in +2 and +3 elements (see Figures 8.7, 8.9, and 8.14). Carbonate liquids produced at mantle pressures are therefore unlikely to be enriched in potassium, rubidium, and cesium.

8.2.7. Compositional effects on Group IA element partition.

As discussed in the section on rubidium partitioning, two compositional factors seem to affect alkali metal partitioning:

(a) Partitioning to the carbonate liquid is enhanced by high sodium content in the carbonate liquid. This is as expected chemically, as K, Rb, and Cs will more easily replace sodium in a structure than calcium due to both ionic size, and valency considerations. Therefore, a lack of sodium sites in the carbonate melt should lead to less pronounced partitioning of the other +1 elements.

(b) Partitioning to the carbonate liquid is enhanced by decreased polymerisation of the silicate liquid. This is also an expected result, as rubidium and cesium are known to be enriched in polymerised silicate melt over basic melt (Ottonello, 1983).

These factors have an important implication for mantle carbonate liquids. Due to the low sodium contents of mantle systems, it seems unlikely that carbonate liquid will be greatly enriched in K, Rb and Cs.

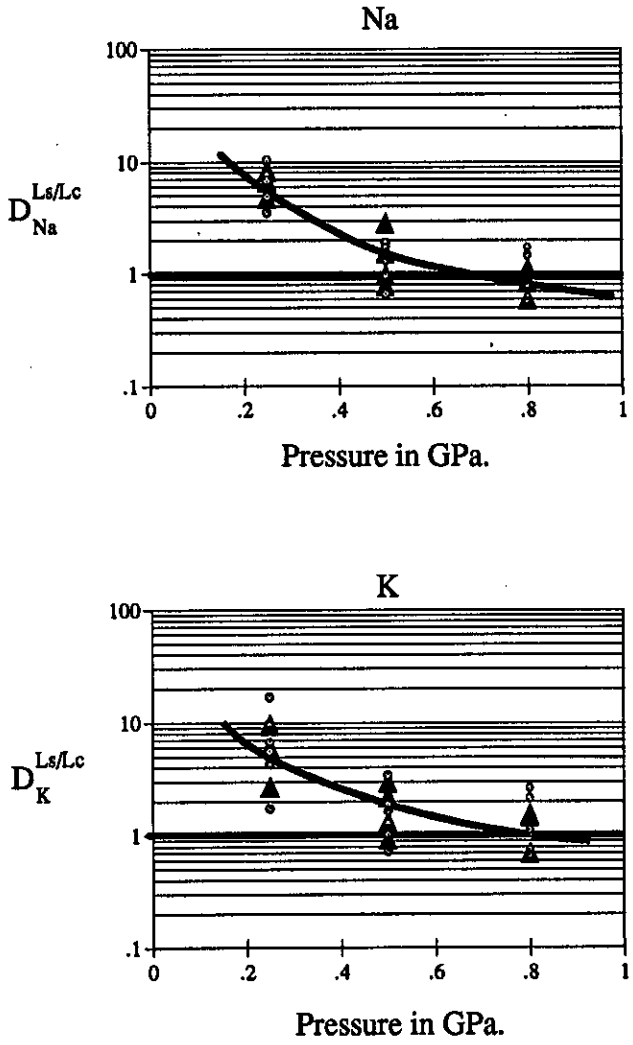

Figure 8.2. The effect of pressure on partitioning of sodium and potassium in the calcic SUN189+CC composition. A strong negative correlation of D with pressure can be seen. This feature was also prominent in the calcic mixtures studied in the synthetic system.

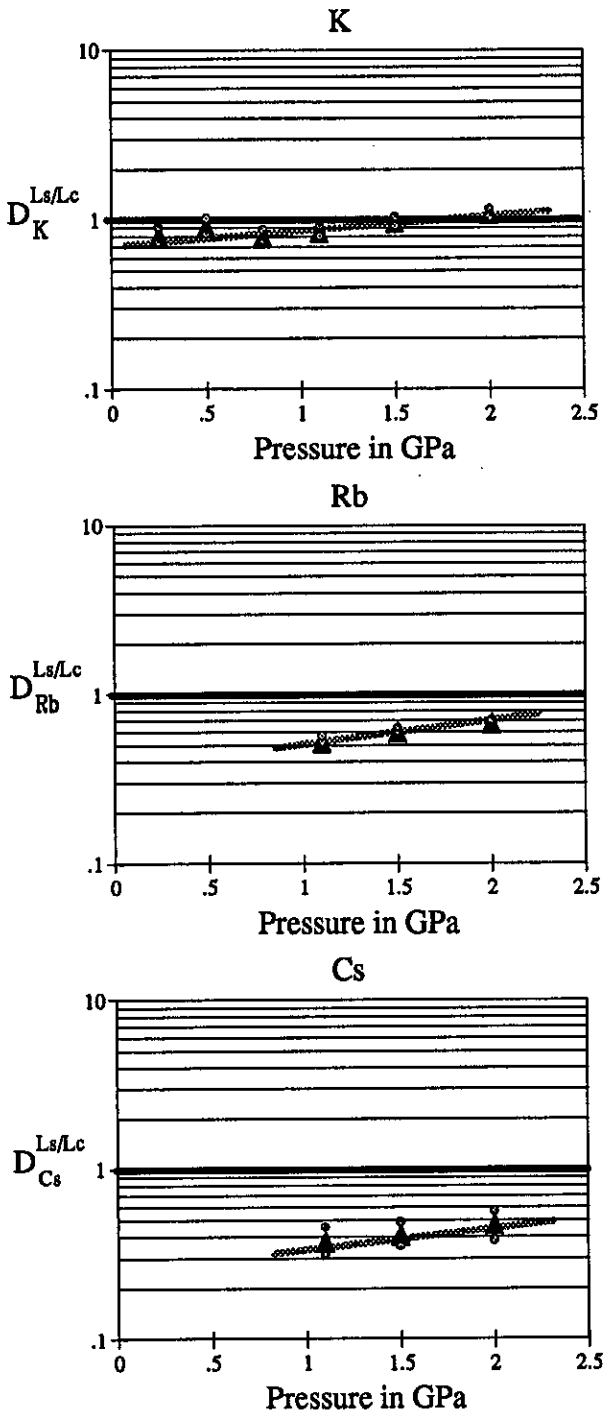

Figure 8.3. The effect of pressure on the partitioning of Group IA elements in BD119+CNC compositions at 1300°C. Increasing pressure causes less extreme enrichment of the +1 elements in the carbonate melt.

8.2.8. Partitioning of Group IA elements with ionic size.

As with the synthetic compositions, $^{Ls/Lc}D_K > {}^{Ls/Lc}D_{Rb} > {}^{Ls/Lc}D_{Cs}$ (i.e. the larger ions are partitioned more strongly into the carbonate liquid). This is displayed in Figure 8.4. Unfortunately, this trend is not continued by sodium. This is believed to be due to the high sodium contents of these melts, causing sodium partitioning to be controlled by its concentration. Sodium partitioning seen in these charges is therefore not a good indication of its likely behaviour as a trace element (i.e. Henry's law does not apply). This suggestion is backed up by the calcic experimental charges studied, where $^{Ls/Lc}D_{Na} > {}^{Ls/Lc}D_K > {}^{Ls/Lc}D_{Rb} > {}^{Ls/Lc}D_{Cs}$. The influence of ionic size on partitioning is believed to be related to the relative energy states of the ions in the carbonate liquid; larger +1 ions have a lower charge density, and are therefore more stable energetically in an ionic melt. If this trend with ionic size can be extrapolated, it would be expected that $^{Ls/Lc}D_{Li}$ would be larger than $^{Ls/Lc}D_K$. In that case, lithium would be enriched in the silicate liquid over the carbonate liquid in most situations. Carbonate liquids are therefore unlikely to contain significant concentrations of lithium.

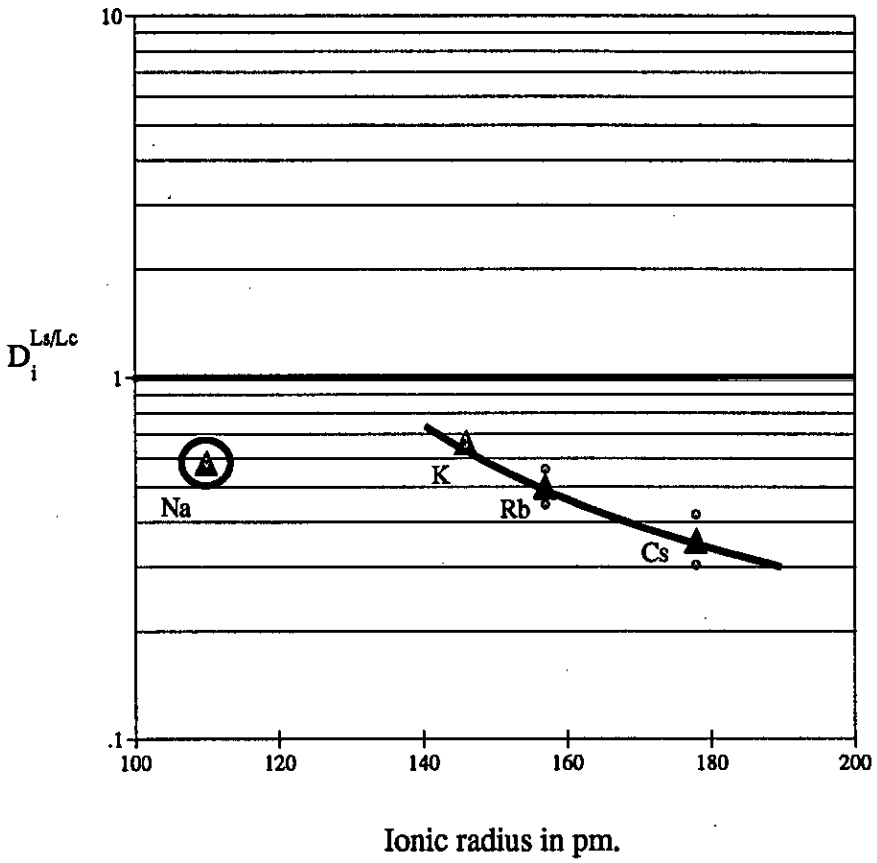

Figure 8.4. Partitioning of +1 ions with ionic radius. K, Rb, and Cs show a coherent trend in partitioning with ionic size. Enrichment in the carbonate liquid is more extreme for the larger ions. This trend of $D_K > D_{Rb} > D_{Cs}$ is seen in all analysed charges. Sodium fails to fit into this trend and is always more strongly partitioned to the carbonate liquid than would be expected from its ionic size. This is believed to be due to its high concentration in these charges, resulting in non-Henry's law behaviour.

8.3. Group IIA elements.

$^{Ls/Lc}D_i$ values were obtained for Mg, Ca, Sr, and Ba. Magnesium was found to be approximately equipartitioned, whilst calcium, strontium, and barium were all enriched in the carbonate liquid. Table 8.2 gives mean $^{Ls/Lc}D_i$ values for each composition studied, along with the measured extreme values. The data are plotted in Figure 8.5.

Table 8.2. Partitioning of the Group IIA elements in natural compositions.
n is the number of determinations, μ is the mean value obtained. Max and Min are the measured extreme values for that composition.

	Magnesium				Calcium				Strontium				Barium			
Composition	n	μ	Max	Min	n	μ	Max	Min	n	μ	Max	Min	n	μ	Max	Min
BD50+CNC	9	**0.89**	1.23	0.54	9	**0.25**	0.36	0.14	5	**0.18**	0.22	0.12	5	**0.17**	0.21	0.14
BD50+CC	9	**1.52**	1.96	1.08	9	**0.42**	0.51	0.35	1	**0.28**	0.29	0.27	1	**0.28**	0.31	0.25
BD119+CNC	9	**1.50**	2.39	1.22	9	**0.46**	0.60	0.39	14	**0.37**	0.57	0.22	14	**0.32**	0.47	0.25
BD119+CC	9	**1.56**	2.46	0.98	9	**0.53**	0.62	0.42	7	**0.44**	0.53	0.35	7	**0.29**	0.59	0.29
SUN189+CNC	9	**1.28**	1.52	1.00	9	**0.53**	0.60	0.47	6	**0.48**	0.54	0.40	6	**0.39**	0.51	0.29
SUN189+CC	9	**1.32**	1.57	1.05	9	**0.53**	0.62	0.46	3	**0.50**	0.53	0.48	3	**0.43**	0.48	0.36

8.3.1. Magnesium.

In all compositions studied, magnesium was approximately equipartitioned. Over the whole range of pressure, temperature and composition, $0.54 < {}^{Ls/Lc}D_{Mg} < 2.46$. Magnesium was more enriched in the carbonate liquid in the BD50+CNC composition. As with all the Group IIA elements, pressure and temperature have small, but significant effects on partitioning; partitioning to the carbonate liquid is preferred at lower temperature and higher pressure.

Bedson (1983) found much more variable $^{Ls/Lc}D_{Mg}$ than found in this study, with values ranging from 0.3-100. It is considered unlikely that the slightly different compositions used by Bedson could result in such disparate partitioning behaviour for magnesium. The variability in Bedson's magnesium data is therefore considered to be due to experimental or analytical problems.

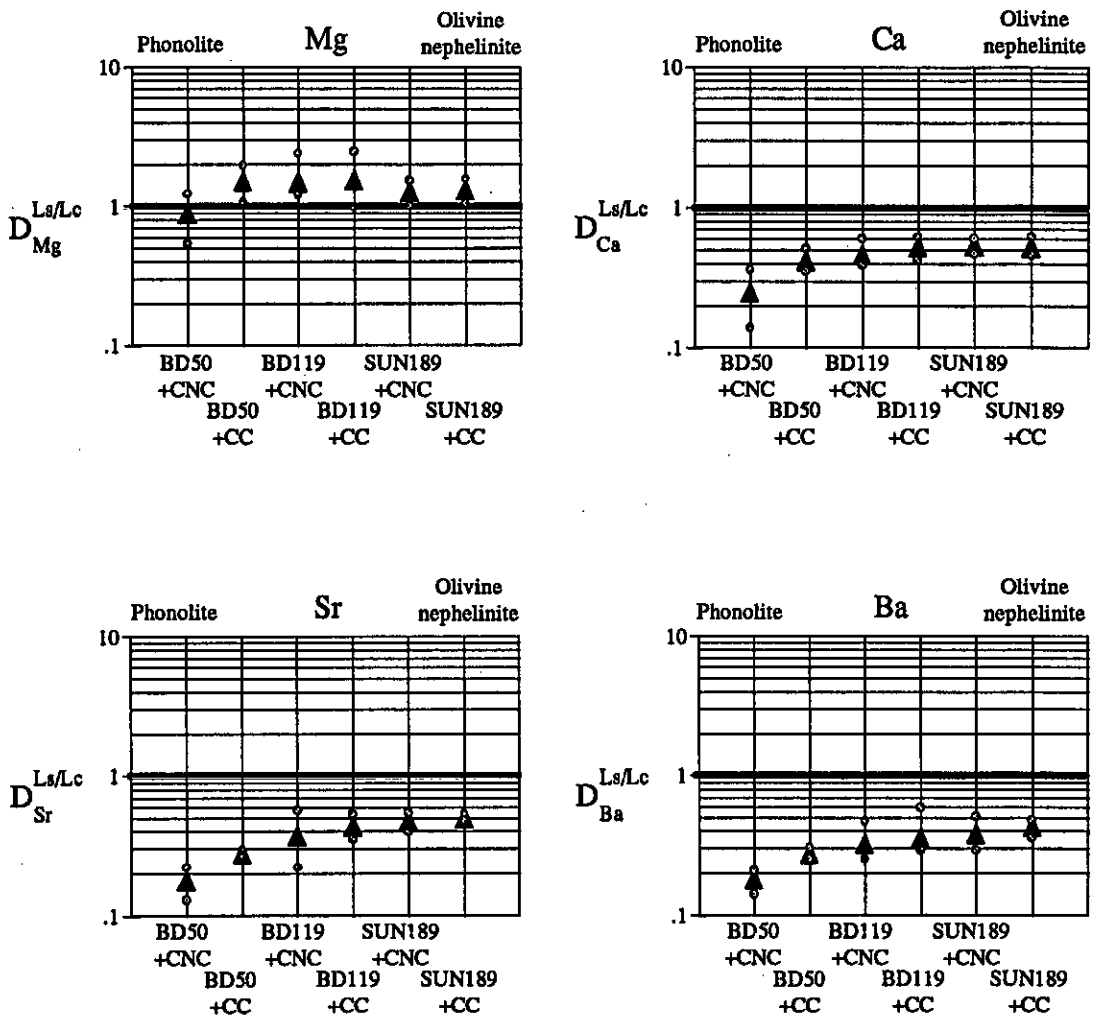

Figure 8.5. Partitioning of the Group IIA elements in natural compositions. All compositions are quoted, with upper and lower limits representing the maximum and minimum values of partitioning seen. The closeness of these ranges shows that P and T have only minor effect on partitioning of the Group IIA elements. The range is larger for BD119+CNC compositions because of a pressure effect up to 2.0 GPa. A smooth trend to less extreme partitioning in more basic compositions is seen for Ca, Sr and Ba. The behaviour of Mg seems little affected by changing composition.

8.3.2. Calcium.

Calcium is always partitioned into the carbonate liquid. $0.62 > {}^{Ls/Lc}D_{Ca} > 0.14$. Partitioning is more extreme in the phonolitic compositions, and becomes less pronounced as the silicate liquid becomes more basic (see Figure 8.5). As with magnesium, enrichment in the carbonate melt is more pronounced at low temperature and high pressure (see Figure 8.6).

These values, and the trends with pressure and temperature, are in close agreement with those reported by Bedson (1983).

8.3.3. Strontium.

Strontium is always strongly partitioned into the carbonate melt, and ${}^{Ls/Lc}D_{Ca} > {}^{Ls/Lc}D_{Sr}$ for all experiments studied. $0.57 > {}^{Ls/Lc}D_{Sr} > 0.12$. Enrichment of strontium in the carbonate liquid is most extreme in the phonolitic compositions, and becomes progressively less pronounced as the silicate melt becomes more basic. Partitioning is more extreme at low temperatures and high pressures.

8.3.4. Barium.

In all experiments ${}^{Ls/Lc}D_{Ba} > {}^{Ls/Lc}D_{Sr}$. Barium is one of the most extremely partitioned elements studied. It is always preferentially enriched in the carbonate liquid. As with other Group IIA elements (Figure 8.6), partitioning is more extreme at low temperature and high pressure, and is accentuated in the phonolitic compositions (Figure 8.5).

This data is in agreement with most of that produced by Bedson (1983). Bedson did however produce more variable ${}^{Ls/Lc}D_{Ba}$, ranging from 0.15-5. Bedson (1983) suggested that partitioning of barium to the carbonate liquid was accentuated by increasing pressure, as seen in this study.

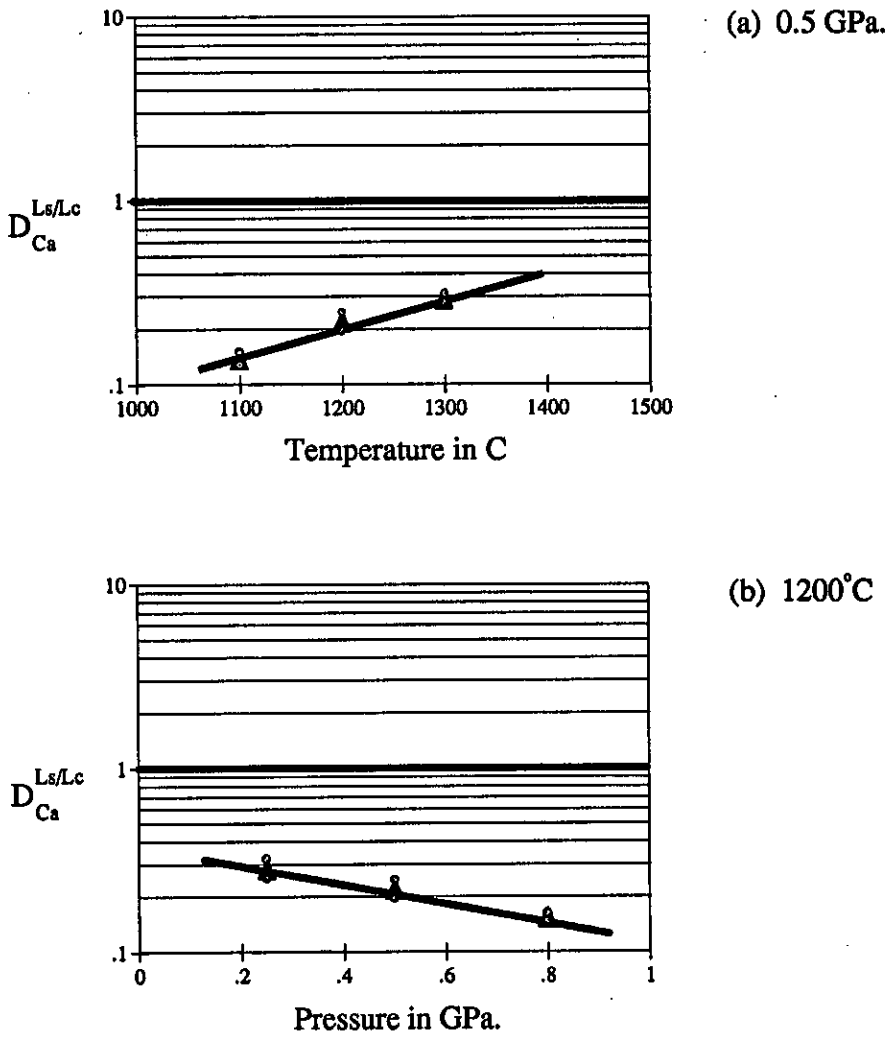

Figure 8.6. The effect of temperature and pressure on Group II partitioning in natural compositions; calcium partitioning in BD50 +CNC is used as an example. (a) For all Group IIA elements, partitioning to the carbonate liquid becomes less extreme with increasing temperature, (b) For all Group IIA elements, partitioning to the carbonate liquid becomes more extreme with increasing pressure.

8.3.5. Partitioning of Group IIA elements with temperature.

For all the Group IIA elements, partitioning becomes more extreme at low temperature (e.g. Figure 8.6a). This can possibly be ascribed to a widening of the solvus at low temperatures, although the effect is considerable, and similar effects are not seen in other groups.

8.3.6. Partitioning of Group IIA elements with pressure.

A considerable pressure effect on partitioning can also be seen for the Group IIA elements (e.g. Figure 8.6b). Enrichment in the carbonate liquid over the silicate liquid becomes more extreme in the range 0.2-0.8 GPa. This trend was seen to continue to at least 2.0 GPa in the BD119+CNC composition (Figure 8.7). Enrichment of Sr and Ba in the carbonate melt at mantle pressures will therefore be extreme (a factor of *ca.* 10 over silicate).

8.3.7. Compositional controls on Group IIA element partition.

As Figure 8.5 shows, calcium, strontium and barium all become less extremely enriched in the carbonate liquid as the coexisting silicate liquid becomes more basic. This effect is not seen for magnesium, which is little effected by changes in composition, and if anything seems to prefer the evolved phonolitic compositions.

8.3.8. Partitioning of the Group IIA elements with ionic radius.

In all experiments $^{Ls/Lc}D_{Mg} > {}^{Ls/Lc}D_{Ca} > {}^{Ls/Lc}D_{Sr} > {}^{Ls/Lc}D_{Ba}$. These data have been plotted with other +2 elements in Figure 8.10. As ionic radius increases, partitioning of the Group IIA elements becomes more extreme, resulting in more pronounced enrichment in the carbonate liquid. From this trend, it would be expected that radium (ionic radius 156 pm in eight-fold co-ordination, Whittaker & Muntus, 1970) would be even more extremely enriched in the carbonate than barium. This could have profound implications for studies of U-series isotope disequilibrium studies since Ra is produced during the decay of U.

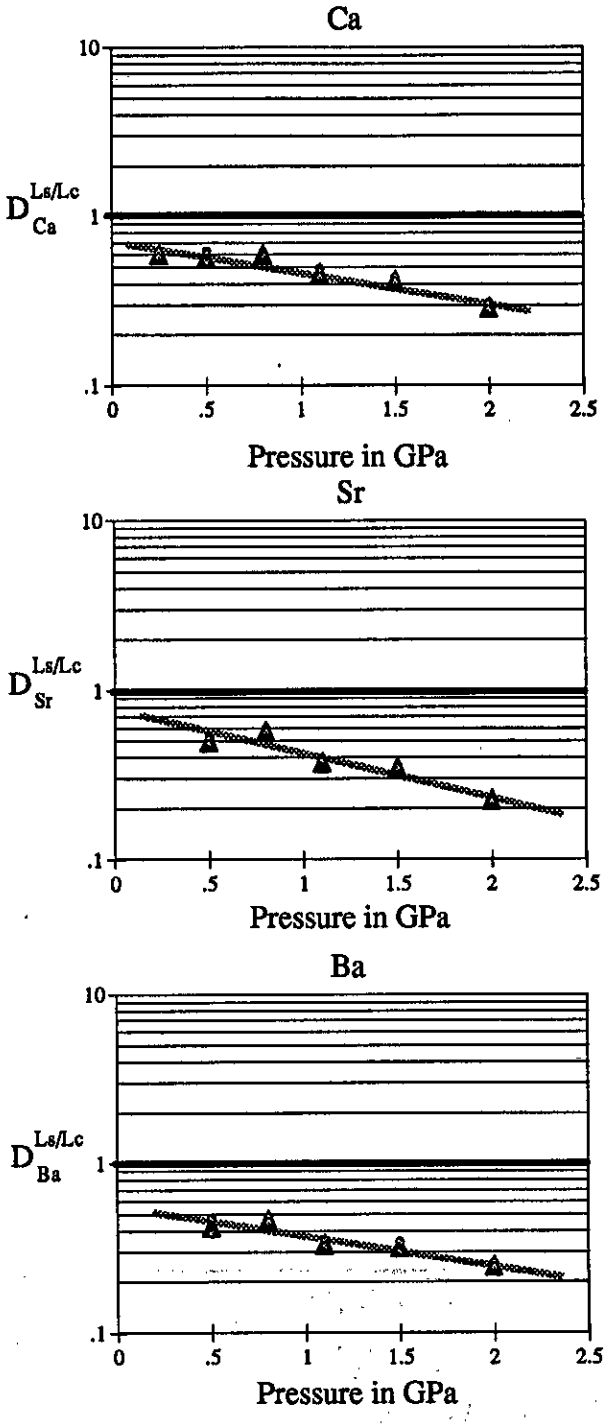

Figure 8.7. Partitioning of the Group IIA elements as a function of pressure in BD119+CNC compositions at 1300°C. More pronounced enrichments of Group IIA elements in the carbonate liquid occur at higher pressures.

8.4. Partitioning of transition elements.

The majority of transition elements are infrequently used in geochemical studies. This, combined with the fact that analysis of transition elements by ion probe is fraught with difficulties, led to only iron and manganese being studied in detail (Table 8.3). Chromium was also analysed in all charges, but will not be discussed in detail as there are questions as to the accuracy of $^{Ls/Lc}D_{Cr}$ data, due to interference problems. Molybdenum was also studied in later charges, and will be considered separately. Another transition element of interest is copper, which is often enriched in carbonatite complexes. As $^{Ls/Lc}D_{Cu}$ data has not been obtained here, the data of Bedson (1983) will be reviewed.

Table 8.3. Partitioning of manganese and iron in natural compositions.
n is the number of determinations, μ is the mean value obtained. Max and Min are the measured extreme values for that composition.

	Manganese				Iron			
Composition	n	μ	Max	Min	n	μ	Max	Min
BD50+CNC	9	1.06	1.45	0.63	9	4.54	10.21	1.85
BD50+CC	9	1.96	3.28	0.83	9	7.31	16.71	1.75
BD119+CNC	9	1.68	2.33	1.20	9	5.39	9.85	2.76
BD119+CC	9	1.58	2.20	0.72	9	3.88	7.12	1.75
SUN189+CNC	9	1.61	2.13	1.14	9	3.57	6.04	2.68
SUN189+CC	9	1.51	2.05	1.14	9	3.62	5.30	2.17

8.4.1. Manganese.

In the vast majority of charges, manganese is weakly partitioned into the silicate liquid. $^{Ls/Lc}D_{Mn}$ is in general between 1 and 2 (Figure 8.8). Manganese seems to follow the behaviour of magnesium closely, although it is slightly more inclined to enter the silicate liquid, probably because of its slightly smaller ionic radius (75 pm for Mn^{2+} compared to 80 pm for Mg^{2+} in six-fold co-ordination; Whittaker & Muntus, 1970). There is little variation of manganese partitioning with composition. As with all the other +2 elements, the tendency for manganese to enter the carbonate liquid is increased by high pressure and low temperature. Bedson (1983) produced data in broad agreement with the above, although of a more variable nature. The same trends with pressure and temperature were outlined.

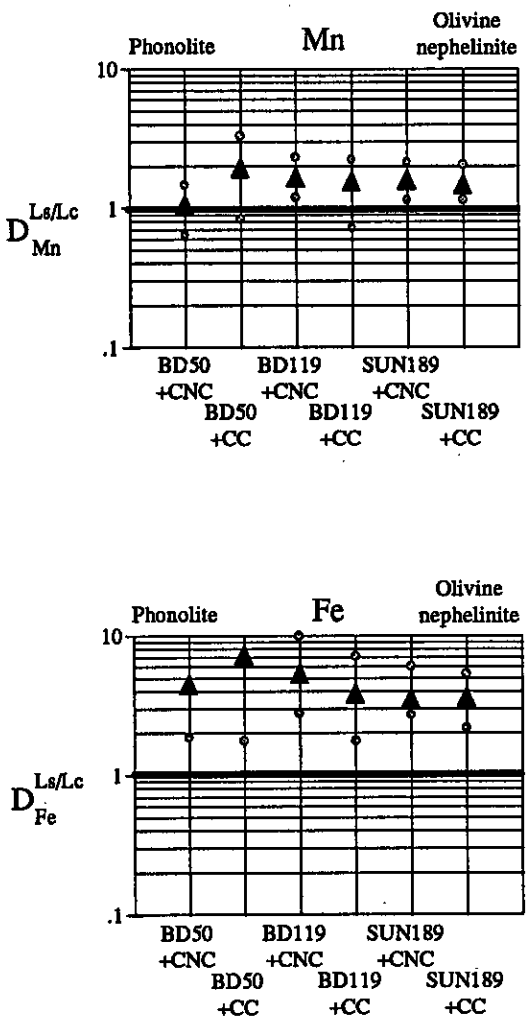

Figure 8.8. Partitioning of Mn and Fe in natural compositions. Mn partitioning is very similar to that of Mg. Fe partitions more strongly into the silicate liquid.

8.4.2. Iron.

In all charges $^{Ls/Lc}D_{Fe} > 1$. Iron is often substantially enriched in the silicate liquid. It is not clear whether this is due to the small ionic radius of Fe^{2+} in six-fold co-ordination (*ca.* 69 pm, Whittaker & Muntus, 1970), or to the presence of substantial Fe^{3+} in the charge. In either case, iron would be expected to be partitioned to the silicate liquid, and is indeed found to do so. The different partitioning behaviour of iron and magnesium should lead to a higher Mg/(Mg+Fe) ratio in the carbonate liquid.

8.4.3. Chromium.

Bedson found that chromium behaved in a similar manner to the other transition elements mentioned. Chromium was slightly enriched in the silicate liquid at low pressures, and in the carbonate at higher pressures. This would fit well with ionic radius and valency considerations.

8.4.4. Copper.

Bedson (1983) found that copper was enriched in the carbonate liquid in the majority of charges. This may imply that Cu had a +1 charge in Bedson's experiments, resulting in its enrichment in the carbonate melt.

8.4.5. Partitioning of Fe and Mn with temperature.

Both Fe and Mn behave in the same manner as Group IIA elements with temperature. Partitioning to the silicate liquid is accentuated by high temperature, affinity for the carbonate liquid is enhanced at low temperatures. This trend is seen for all +2 elements.

8.4.6. Partitioning of Fe and Mn with pressure.

Figure 8.9 shows the effect of pressure on partitioning for Mg, Mn, and Fe. All three partition to the silicate melt at low pressures. However, as pressure is increased, there is an increased tendency to enter the carbonate liquid for all three elements.

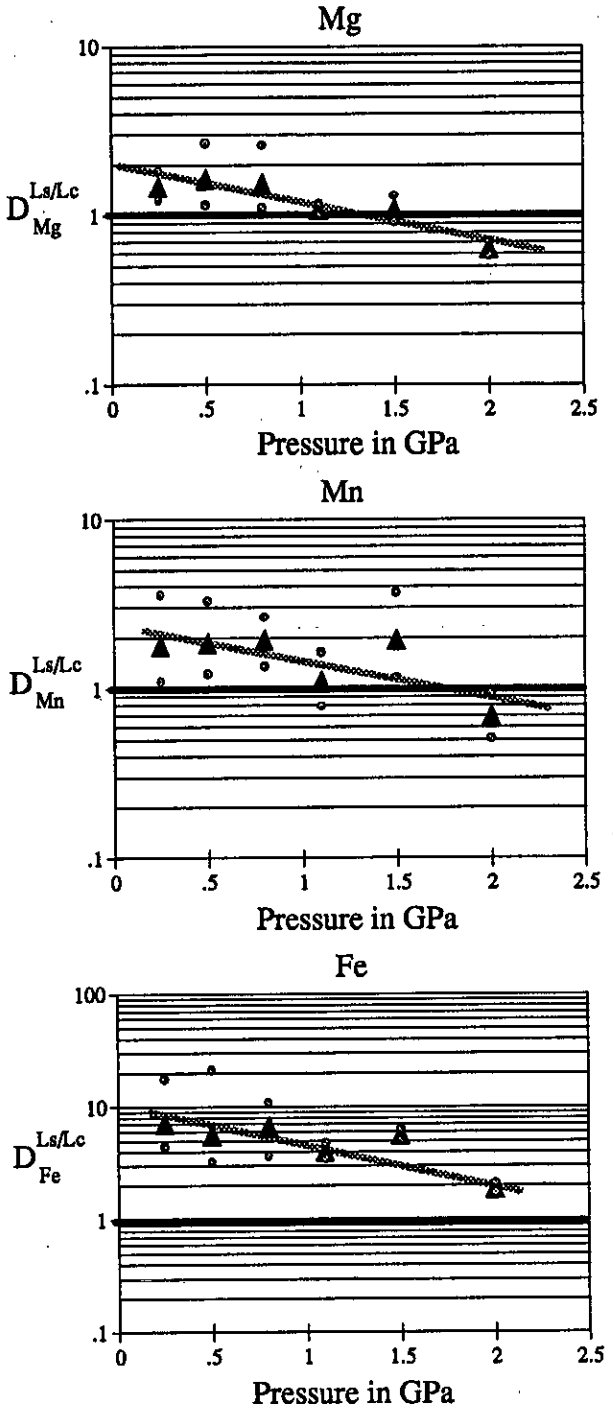

Figure 8.9. Partitioning of Mg, Mn, and Fe as a function of pressure for BD119+CNC compositions at 1300°C. As with the Group IIA elements, partitioning of Mg, Mn, and Fe trends more towards carbonate at higher pressure.

8.4.7. Partitioning of transition elements as a function of ionic radius.

Fe and Mn have been added to the data for Group IIA elements in Figure 8.10. A clear relationship between partitioning and ionic radius can be seen. Small ions (e.g. Fe^{2+}, Mn^{2+}) are enriched in the silicate liquid, large ions (e.g. Sr^{2+}, Ba^{2+}) are enriched in the carbonate liquid. This is the same general trend as was seen for +1 elements (see Figure 8.4).

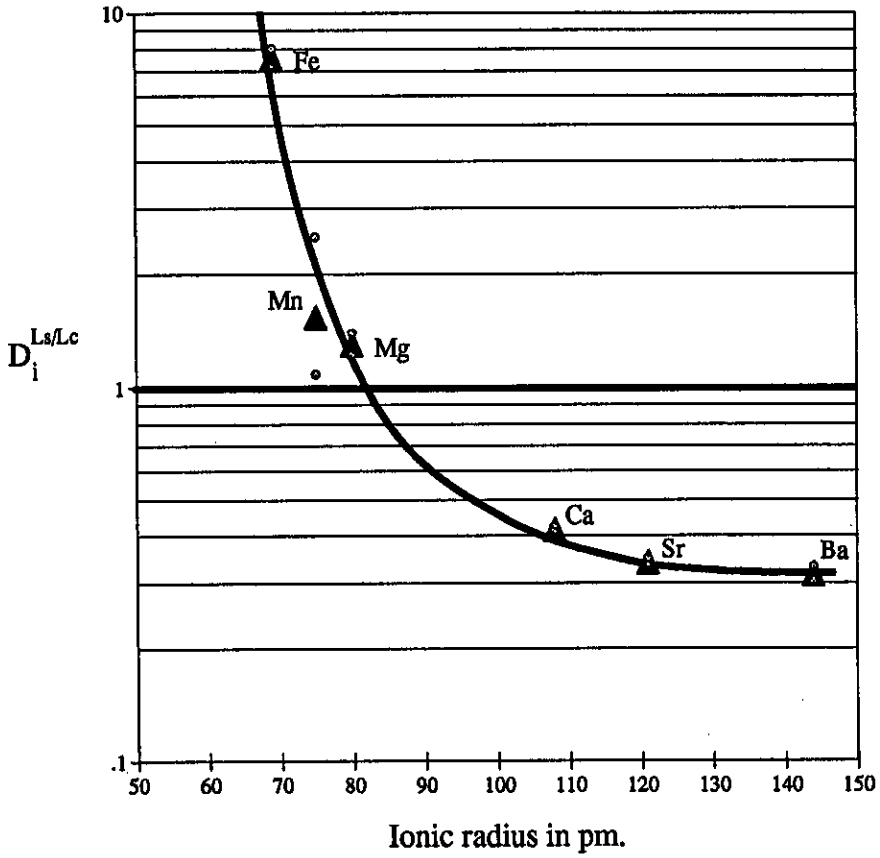

Figure 8.10. Partitioning of +2 ions as a function of ionic radius. Again a good negative correlation is seen between partition coefficient and ionic size. Larger +2 ions (e.g. Ba, Sr, Ca) are partitioned to the carbonate melt, whilst smaller ions are enriched in the silicate. It is realized that plotting both the Group IIA elements, and the geochemically very different transition elements on the same diagram could be misleading. However, this is considered justified as ionic radius seems to be the major control on partitioning for +2 elements.

8.5. Aluminium, Yttrium, and the REE.

Partitioning of +3 ions has been studied for six elements: Al, Y, La, Ce, Nd, and Sm. As in the majority of geochemical processes, the REE behaved as a coherent group, and will therefore be considered together. Although aluminium concentrations were heavily affected by quench processes, the data have been included as it is clear that aluminium is partitioned strongly to the silicate liquid. Indeed, in the majority of charges, aluminium is the most extremely partitioned element.

Table 8.4. Partitioning of aluminium and yttrium in natural compositions.
n is the number of determinations, μ is the mean value obtained. Max and Min are the measured extremes.

	Aluminium				Yttrium			
Composition	n	μ	Max	Min	n	μ	Max	Min
BD50+CNC	9	256	756	37	5	1.61	2.35	0.98
BD50+CC	9	213	575	28	1	1.27	1.62	1.04
BD119+CNC	9	120	417	13	14	1.83	2.78	0.86
BD119+CC	9	86	199	11	7	1.96	3.33	1.30
SUN189+CNC	9	85	376	13.5	6	2.18	3.98	1.37
SUN189+CC	9	68	252	16.2	3	2.57	2.94	1.84

8.5.1. Aluminium.

In all experiments $^{Ls/Lc}D_{Al} > 10$, ranging up to 756. In most charges, aluminium is the most strongly enriched element in the silicate liquid. Due to the large errors on $^{Ls/Lc}D_{Al}$ values, no pressure or temperature effects have been recorded. However, Figure 8.11 shows that partitioning of aluminium to the silicate liquid seems to become less extreme as the silicate liquid becomes more basic. This is probably a solvus effect.

8.5.2. Yttrium.

Yttrium is normally weakly partitioned to the silicate liquid with $^{Ls/Lc}D_{Y} \sim 1.5$. This value changes with pressure, temperature and composition. Partitioning to the silicate liquid is enhanced by low pressure, high temperature, and basic silicate liquid

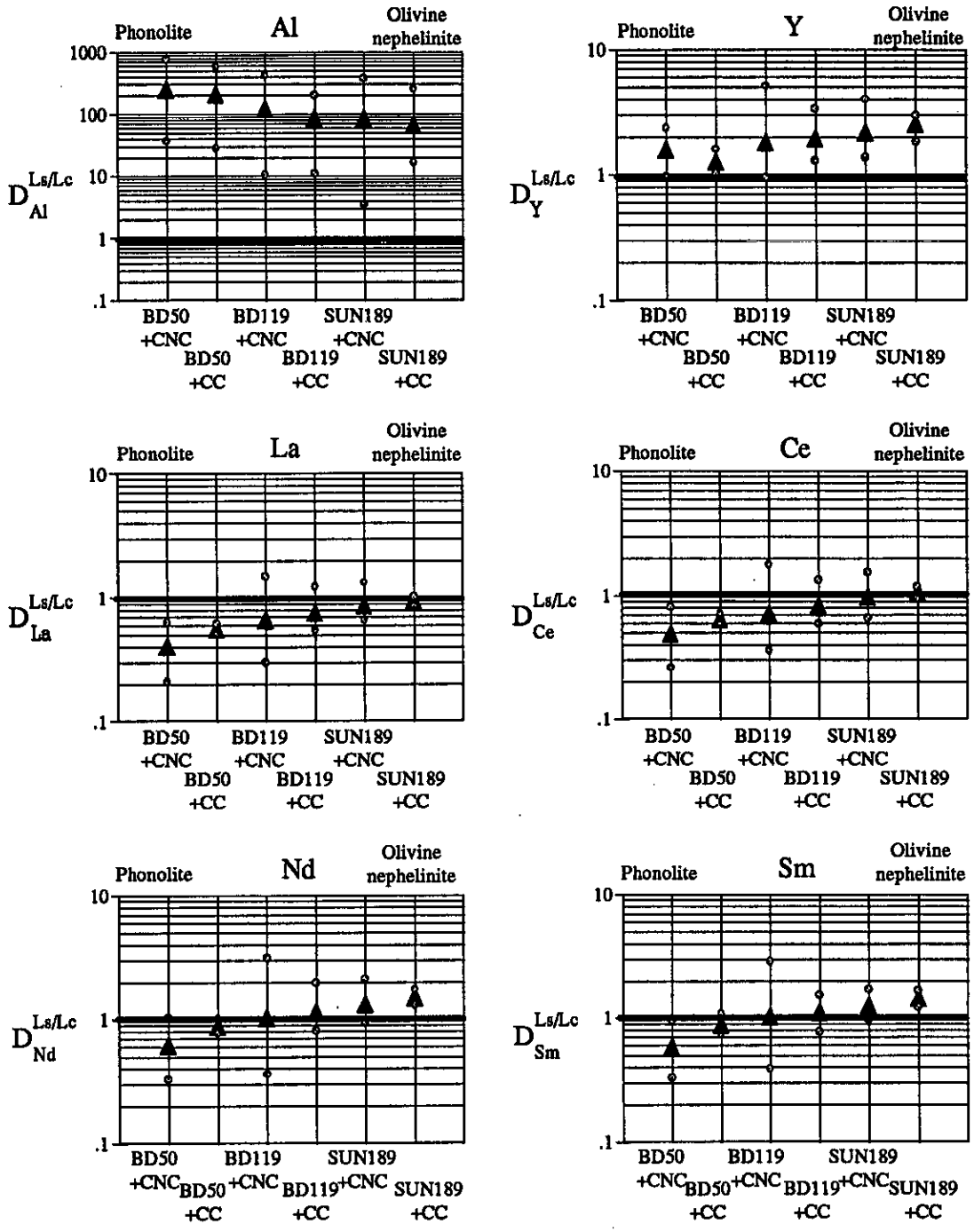

Figure 8.11. Partitioning of the Group III elements in natural compositions. Mean partitioning values are plotted, with upper and lower limits representing the maximum and minimum values of partitioning seen. A smooth trend is seen in Al partitioning, with less extreme partitioning in the more basic compositions. In Y and the REE there is another compositional effect, with REE partitioning to the carbonate melt in phonolitic compositions, and tending more towards the silicate in basic nephelinitic compositions. Note the much wider range in partitioning for the REE in the BD119+CNC composition. This is due to inclusion of data up to 2.0 GPa for this composition; there is a pronounced effect of pressure on REE partitioning

composition. Conversely partitioning to the carbonate is preferred at low temperature, high pressure and with polymerised silicate liquid. Variations in partitioning of yttrium closely match those of the REE, and the data have therefore been plotted together (Figures 8.12, and 8.13)

Table 8.5. Partitioning of the REE in natural compositions.
n is the number of determinations, μ is the mean value obtained. Max and Min are the measured extremes

	Lanthanum				Cerium				Neodymium				Samarium			
Composition	n	μ	Max	Min	n	μ	Max	Min	n	μ	Max	Min	n	μ	Max	Min
BD50+CNC	9	**0.41**	0.63	0.21	9	**0.50**	0.81	0.26	5	**0.62**	1.04	0.33	5	**0.59**	0.95	0.33
BD50+CC	9	**0.57**	0.62	0.52	9	**0.65**	0.71	0.60	1	**0.88**	1.01	0.78	1	**0.89**	1.07	0.74
BD119+CNC	9	**0.67**	1.02	0.30	9	**0.72**	1.19	0.36	14	**1.03**	1.50	0.36	14	**1.04**	1.49	0.39
BD119+CC	9	**0.77**	1.23	0.55	9	**0.84**	1.34	0.59	7	**1.14**	1.96	0.81	7	**1.12**	1.54	0.78
SUN189+CNC	9	**0.88**	1.33	0.66	9	**0.98**	1.54	0.66	6	**1.33**	2.12	0.93	6	**1.27**	1.70	0.98
SUN189+CC	9	**0.96**	1.03	0.86	9	**1.08**	1.17	0.93	3	**1.51**	1.75	1.29	3	**1.45**	1.68	1.23

8.5.3. The REE.

The REE show coherent partitioning behaviour. Variations in partitioning exist with pressure, temperature, composition, and ionic radius:

(a) Compositional effect (Figure 8.11).

Partitioning of the REE to the carbonate liquid is most extreme in the phonolitic BD50+CNC composition. As the silicate liquid becomes more basic, partitioning to the carbonate liquid becomes progressively less pronounced. In the most basic compositions, some of the REE are partitioned to the silicate liquid. This dependency of $^{Ls/Lc}D_{REE}$ on composition is similar to that recorded by Bedson (1983), who showed that REE partitioning was dependent on the polymerisation state of the silicate liquid.

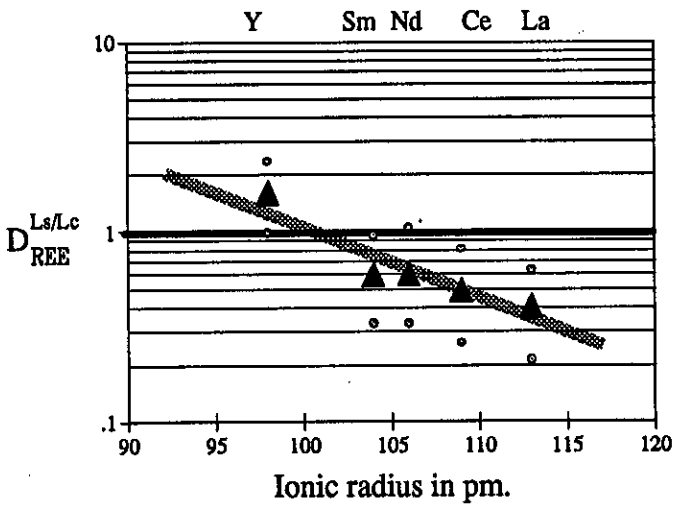

Figure 8.12. Partitioning of the REE with changing ionic radius. Average D values for REE from BD50+CNC charges vary from La to Y. Partitioning to the carbonate liquid becomes more pronounced with increasing ionic radius. One result of this behaviour is that, in all charges analysed, the carbonate liquid is more extremely enriched in LREE over HREE than its silicate counterpart.

(b) Ionic radius effect (Figure 8.12).

$^{Ls/Lc}D_Y > {}^{Ls/Lc}D_{Sm} > {}^{Ls/Lc}D_{Nd} > {}^{Ls/Lc}D_{Ce} > {}^{Ls/Lc}D_{La}$. This results in relative enrichment of LREE/HREE in the carbonate liquid. This feature was seen in all charges studied, and is present regardless of pressure, temperature, and composition.

(c) Pressure effect (Figure 8.13.a).

Partitioning of the REE is pressure dependent. Partitioning of REE to the silicate liquid is preferred at low pressure, partitioning to the carbonate liquid is preferred at high pressure.

(d) Temperature effect (Figure 8.13.b).

Partitioning of the REE to the carbonate liquid is preferred at lower temperature. Also noticeable on this diagram is that the relative difference in partitioning between LREE and HREE becomes less pronounced as temperature is increased. This is thought to represent less pronounced structural differences between silicate and carbonate liquids at higher temperature (i.e. closure of the solvus).

All the above features were observed by Bedson (1983) for phonolitic compositions at low pressure. This study confirms that the behaviour of REE noted by Bedson (1983) is valid for a wide range of compositions, and physical conditions.

8.5.4. Partitioning of yttrium and the REE at mantle pressures.

Experiments on BD119+CNC compositions were performed in solid media apparatus to extend the pressure range studied. The $^{Ls/Lc}D_i$ data produced for yttrium and the REE are plotted in Figure 8.14. The trend in partitioning seen at low pressures continues to at least 2.0 GPa. LREE are strongly partitioned into the carbonate melt at mantle pressures even at the relatively high temperatures of these experiments (1300°C). At the likely temperatures of carbonate melting in the mantle (*ca.* 1050-1150°C) partitioning to the carbonate melt would be expected to be even more extreme.

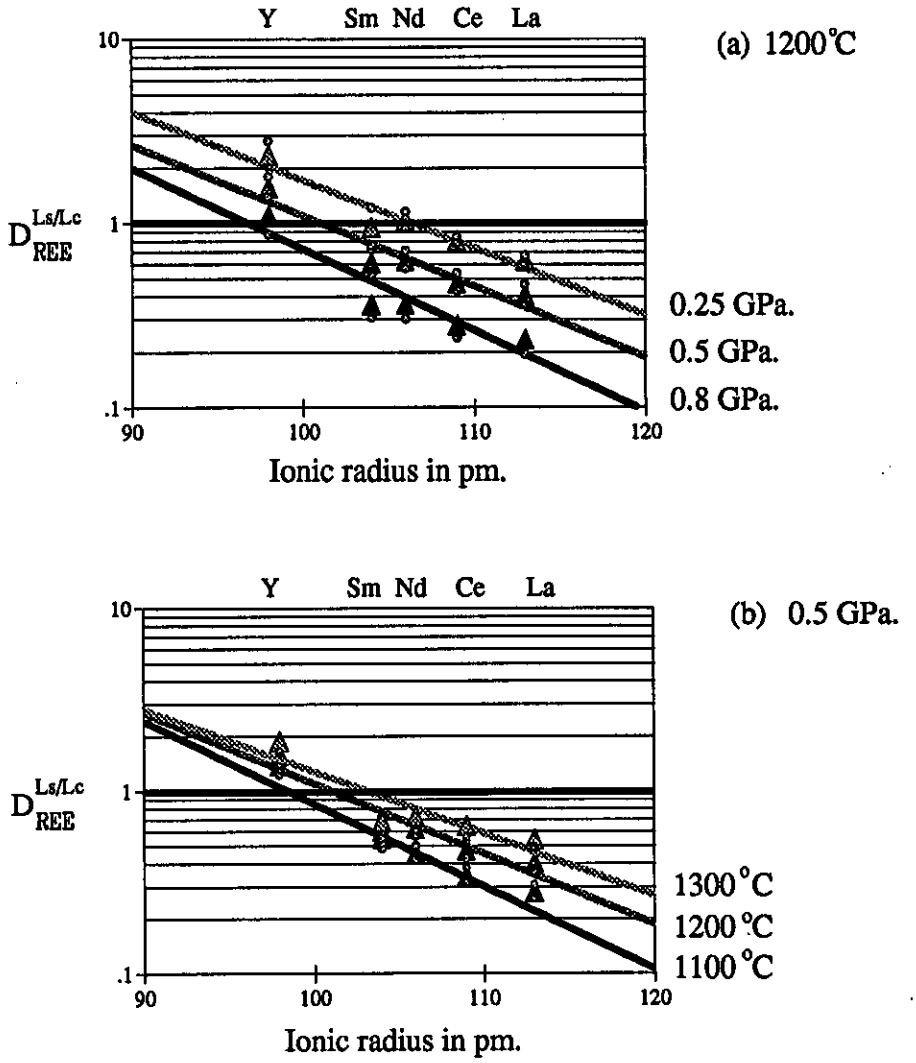

Figure 8.13. The effect of pressure and temperature on partitioning of the REE in BD50+CNC compositions. With increasing pressure, the REE increasingly prefer the carbonate liquid. With increasing temperature, the REE prefer the silicate liquid. There also seems to be less extreme relative enrichment of LREE/HREE in the carbonate liquid at higher temperature. This is attributed to closure of the solvus at these high temperatures.

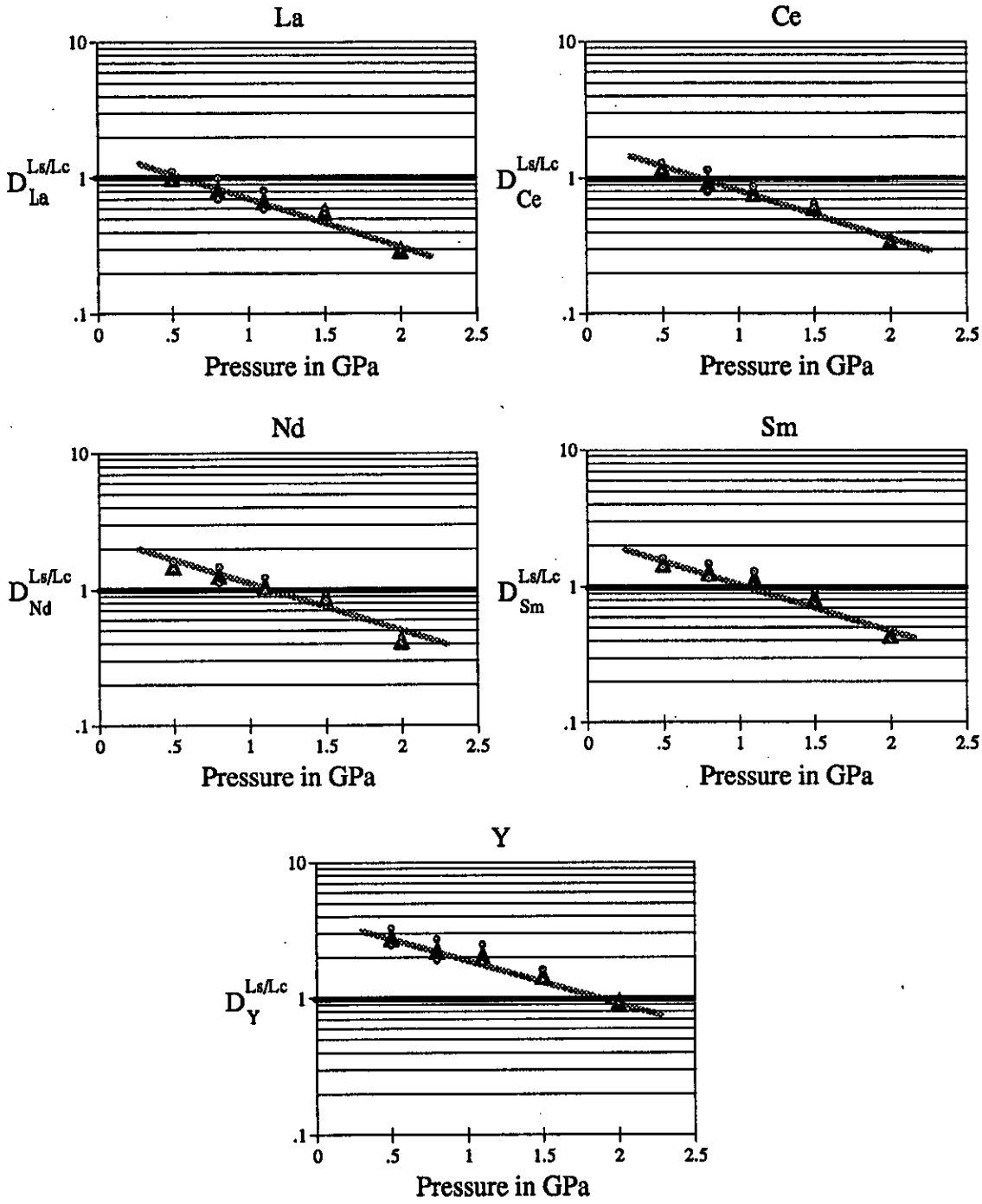

Figure 8.14. Partitioning of Yttrium and the REE as a function of pressure in the BD119+CNC compositions at 1300°C. The trend of increased tendancy to enter the carbonate liquid with increasing pressure which was seen from 0.25-0.8 GPa continues up to at least 2.0 GPa. Mantle carbonate melts will therefore have moderately high contents of REE as well as high LREE/HREE ratios.

8.5.5. Partitioning of +3 ions with ionic radius.

Figure 8.15 shows that, as with the synthetic experiments, partitioning of +3 ions between carbonate and silicate liquids is a simple function of ionic radius. Small ions are partitioned to the silicate liquid (e.g. Al^{3+}), large ions are partitioned to the carbonate liquid (e.g. La^{3+}, Ce^{3+}). This is the same trend as seen for +1, and +2 elements. From this relationship, we can predict the likely partitioning behaviour of other +3 ions. For example Sc^{3+}, with ionic radius 83 pm in six-co-ordination, would be expected to be enriched in the silicate over the carbonate by *ca.* a factor of 3.

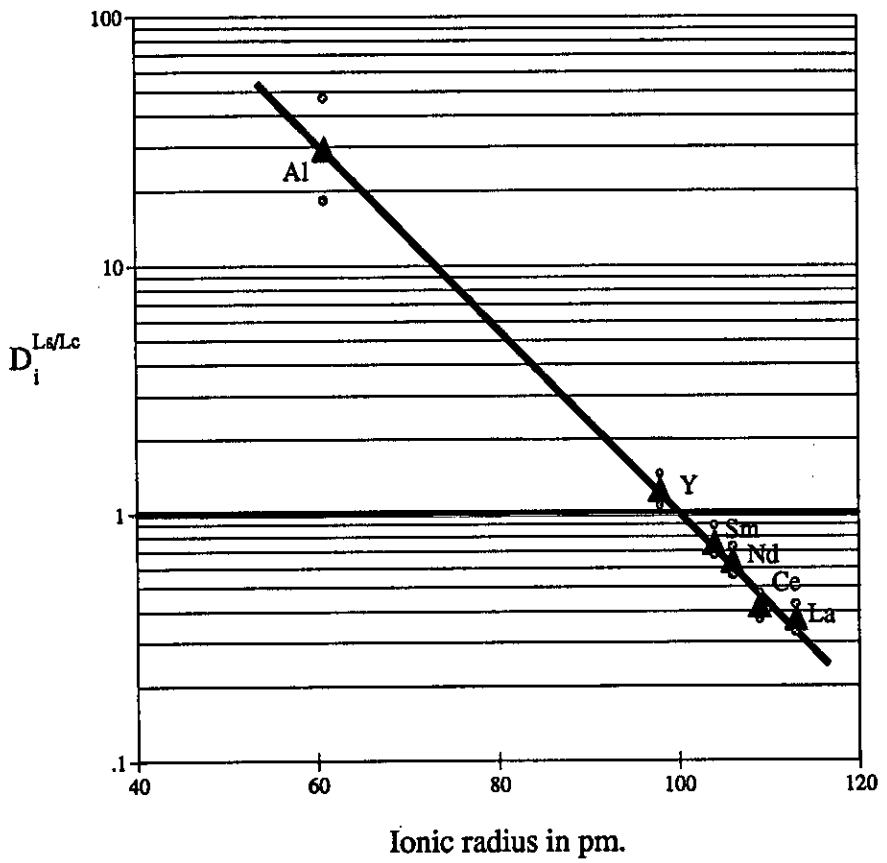

Figure 8.15. Partitioning of +3 ions as a function of ionic radius. A near-perfect exponential correlation is seen between partition coefficients and ionic size for the +3 ions. One result of this behaviour is that the carbonate melt always has a higher La/Y ratio than its silicate counterpart. This feature is believed to be one of the most diagnostic geochemical characteristics of carbonate melts.

8.6. Group IVA and IVB elements.

As with the synthetic system, partitioning data were obtained for Si, Ti, Zr and Hf. All were found to be strongly enriched in the silicate liquid (Table 8.6).

Table 8.6. Partitioning of the Group IV elements in natural compositions.
n is the number of determinations, μ is the mean value obtained. Max and Min are the measured extremes.
* Due to interference problems when measuring Hf concentrations in the carbonate liquid, only estimates of the approximate minimum value of $^{Ls/Lc}D_{Hf}$ could be obtained.

	Silicon				Titanium				Zirconium				Hafnium			
Composition	n	μ	Max	Min	n	μ	Max	Min	n	μ	Max	Min	n	μ	Max	Min
BD50+CNC	9	304	879	77	9	6.84	14.5	3.23	5	327	827	159	5	>10*		
BD50+CC	9	42	87	8.01	9	8.06	11.6	3.93	1	21	48	13	1	>10*		
BD119+CNC	9	16	28	5.43	9	7.88	26.4	3.28	14	21	53	4.27	14	>10*		
BD119+CC	9	19	50	4.78	9	7.07	19.7	3.10	7	12	19	7.34	7	>10*		
SUN189+CNC	9	20	70	4.55	9	8.44	22.1	3.14	6	5.47	9.06	2.62	6	>5*		
SUN189+CC	9	15	25	5.73	9	8.68	19.3	2.99	3	12	17	5.66	3	>10*		

8.6.1. Silicon.

Not surprisingly, silicon was found to be relatively enriched in the silicate liquid! This enrichment was usually in the order of a factor of 10-20 over the carbonate liquid. However, in the more evolved phonolitic compositions $^{Ls/Lc}D_{Si}$ averaged over 300. This more extreme partitioning in phonolitic compositions reflects less mixing of the carbonate and silicate components. Errors on $^{Ls/Lc}D_{Si}$ values are considerable, masking any pressure or temperature effects present in the main dataset.

8.6.2. Titanium.

Titanium is always enriched in the silicate liquid. Average values of $^{Ls/Lc}D_{Ti}$ for each composition studied cluster at between 7 or 8 (Table 8.6), although in some charges partitioning of titanium resulted in enrichment in the silicate liquid by a factor of 20 over carbonate.

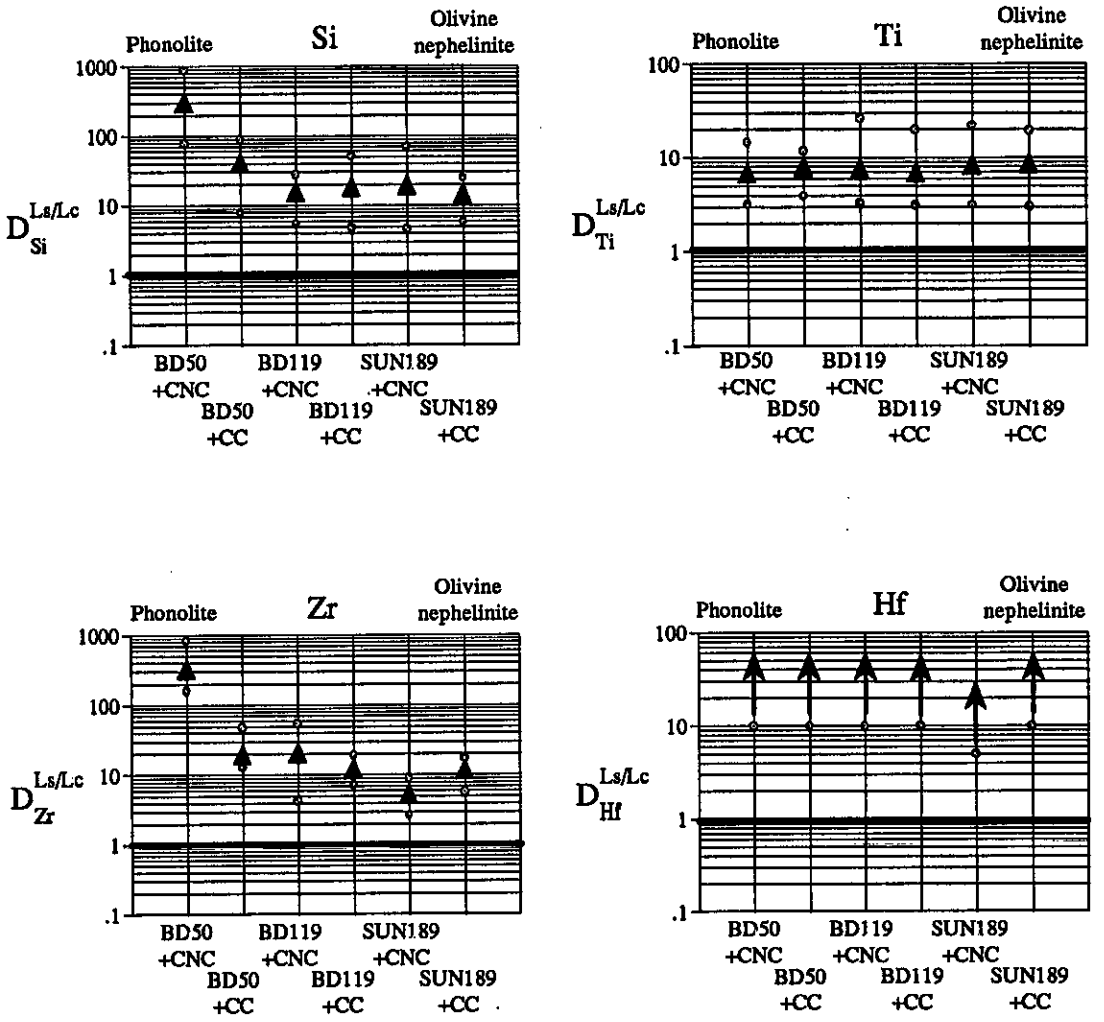

Figure 8.16. Partitioning of the Group IV elements in natural compositions. Mean values of partitioning are shown, togethor with measured extremes. Ti partitioning is identical for all compositions, whilst Si, and Zr show less extreme partitioning in the more basic compositions. This is thought to be due to closure of the solvus. Partitioning of Hf is poorly constrained due to low concentrations and interference problems. All that can be stated is that Hf is strongly partitioned to the silicate liquid (probably by more than a factor of 10 for most compositions).

8.6.3. Zirconium.

Zirconium is always enriched in the silicate liquid. Partitioning is extreme for phonolitic compositions, but becomes less pronounced as the silicate liquid becomes more basic. $^{Ls/Lc}D_{Zr}$ is always > 100 for the phonolites, and is generally between 10 and 20 for the nephelinites.

Bedson's (1983) experiments on sodium-rich phonolitic charges (1983) produced much less extreme partitioning of zirconium, with $^{Ls/Lc}D_{Zr}$ usually between 0.7 and 7. In a number of charges Bedson (1983) found that zirconium was partitioned into the carbonate liquid. Errors of this magnitude are most unlikely in ion probe analysis. The large discrepancy between the data produced in these experiments, and those of Bedson (1983), is thus thought to be due to differences between *in situ*, and bulk analytical methods in these quenched phases.

8.6.4. Hafnium.

Due to pronounced enrichment of hafnium in the silicate portion of the charge, analysis of the correspondingly low hafnium contents in the carbonate liquid was found to be difficult. ^{180}Hf and ^{177}Hf were thought to be the most likely isotopes to produce interference-free data. Unfortunately, in both cases the vast majority of the apparent hafnium counts recorded could be due to an interference effect. ^{180}Hf was found to have interference from $^{90}Zr^{2+}$, whilst ^{177}Hf was masked by Dy-O^+. Estimates of the interference caused by Dy-O^+ were made by analogy with known REE concentrations and element-oxide ratios; only a very small part of the apparent Hf is real. Since quantification of this interference effect is impossible without accurate dysprosium analysis, all that can be said about Hf partitioning is that it is extremely enriched in the silicate liquid. This enrichment is thought to exceed a factor of 10 in most charges. Bedson (1983) also found that hafnium was greatly enriched in the silicate liquid.

8.6.5. Partitioning of Group IV elements as a function of pressure.

As has been commented, no pressure effect on Group IV element partition could be seen in the main body of data. However, for the BD119+CNC composition where experiments were performed to 2.0 GPa, systematic variations with pressure may be present (Figure 8.17). Enrichment in the silicate liquid of Group IV elements seems to become more pronounced to 0.8 GPa. Thereafter partitioning becomes less extreme as pressure is increased. This would imply that the carbonate-silicate two-liquid solvus expands to *ca.* 0.8 GPa, and then begins to contract again. This conclusion is based on the least well constrained data produced in this study, and should therefore be treated with great caution.

8.6.6. Partitioning of +4 elements with ionic radius.

Partitioning data for all +4 ions has been plotted against ionic radius in Figure 8.18. No coherent trend with ionic radius can be seen. It is therefore concluded that relative stability of the ions in the carbonate liquid is not the dominant controlling factor in +4 ion partitioning. Instead, it seems likely that it is the ability of the ions to for complexes with silicate tetrahedra that is being distinguished by differing partitioning behaviour. Of special note is that, despite virtually identical ionic radii, the U^{4+} and Th^{4+} show significantly different partitioning behaviour. This is also thought to be the case for Zr^{4+} and Hf^{4+} (from synthetic experiments).

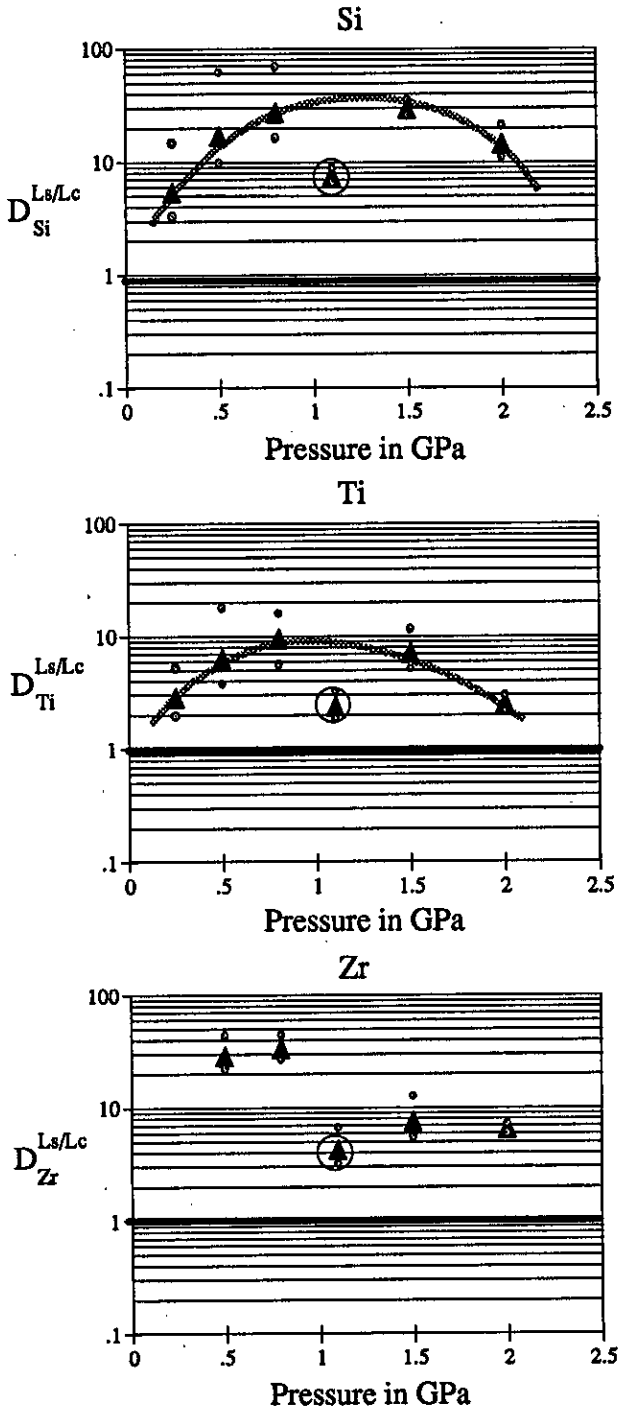

Figure 8.17. Partitioning of +4 elements as a function of pressure in BD119+CNC compositions at 1300°C. Variable partitioning is seen, although there is some evidence that partitioning of Group IV elements reflects the degree of mixing of carbonate and silicate components, becoming more extreme to *ca.* 0.8 GPa, and then gradually less extreme at higher pressures. The circled value is believed to have a biased carbonate analysis due to the presence of a large silicate sphere.

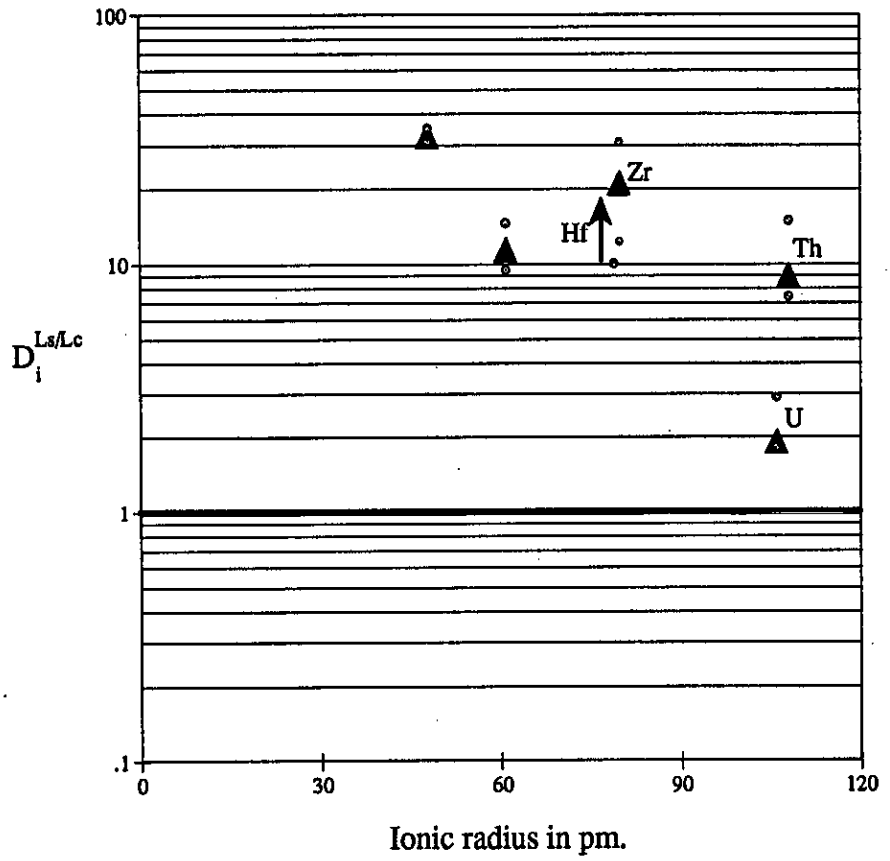

Figure 8.18. Partitioning of +4 ions as a function of ionic radius. No coherent variation in partitioning with ionic size is seen. Partitioning of the +4 ions must be mainly controlled by other factors. One possible controlling factor is the ease with which the ions form complexes with silicate and carbonate.

8.7. Group VA and VB elements.

Group V elements have widely varying chemical characteristics. It is therefore not surprising that their partitioning behaviour should also be variable across the group. Four elements were studied: P, V, Nb, and Ta (Table 8.7).

Table 8.7. Partitioning of the Group V elements in natural compositions.
n is the number of determinations, μ is the mean value obtained. Max and Min are the measured extremes.

	Phosphorus				Vanadium				Niobium				Tantalum			
Composition	n	μ	Max	Min	n	μ	Max	Min	n	μ	Max	Min	n	μ	Max	Min
BD50+CNC	9	0.17	0.29	0.07	5	0.69	1.33	0.19	5	1.48	2.02	1.00	5	7.44	9.91	4.35
BD50+CC	9	0.18	0.28	0.12	1	0.41	0.50	0.35	1	1.16	1.47	0.94	1	2.59	4.54	1.71
BD119+CNC	9	0.28	0.51	0.17	14	0.54	1.07	0.33	14	1.54	3.25	0.82	14	3.20	10.81	1.11
BD119+CC	9	0.35	0.64	0.14	7	0.48	0.78	0.27	7	1.31	2.01	0.83	7	2.85	4.05	1.45
SUN189+CNC	9	0.43	0.77	0.24	6	0.34	0.48	0.25	6	0.87	1.06	0.72	6	2.16	2.60	1.63
SUN189+CC	9	0.79	1.71	0.27	3	0.57	0.75	0.36	3	1.71	2.34	0.98	3	3.74	5.08	2.22

8.7.1. Phosphorus.

Phosphorus is, in general, strongly enriched in the carbonate liquid. $^{Ls/Lc}D_P$ ranges from 0.07 in phonolitic compositions, to nearly 1 in the most basic compositions studied. As the silicate liquid becomes more basic, enrichment of phosphorus in the carbonate liquid becomes less pronounced (Figure 8.19). As well as this compositional effect, phosphorus may also be affected by temperature and pressure. Figure 8.20a shows that phosphorus enrichment in the carbonate liquid may get less pronounced with increasing temperature. Figure 8.20b shows that phosphorus enrichment in the carbonate liquid may get more pronounced with increasing pressure. In its partitioning behaviour, and its trends with pressure, temperature, and composition, phosphorus behaves in a very similar manner to Ca and the other Group IIA elements studied in these experiments.

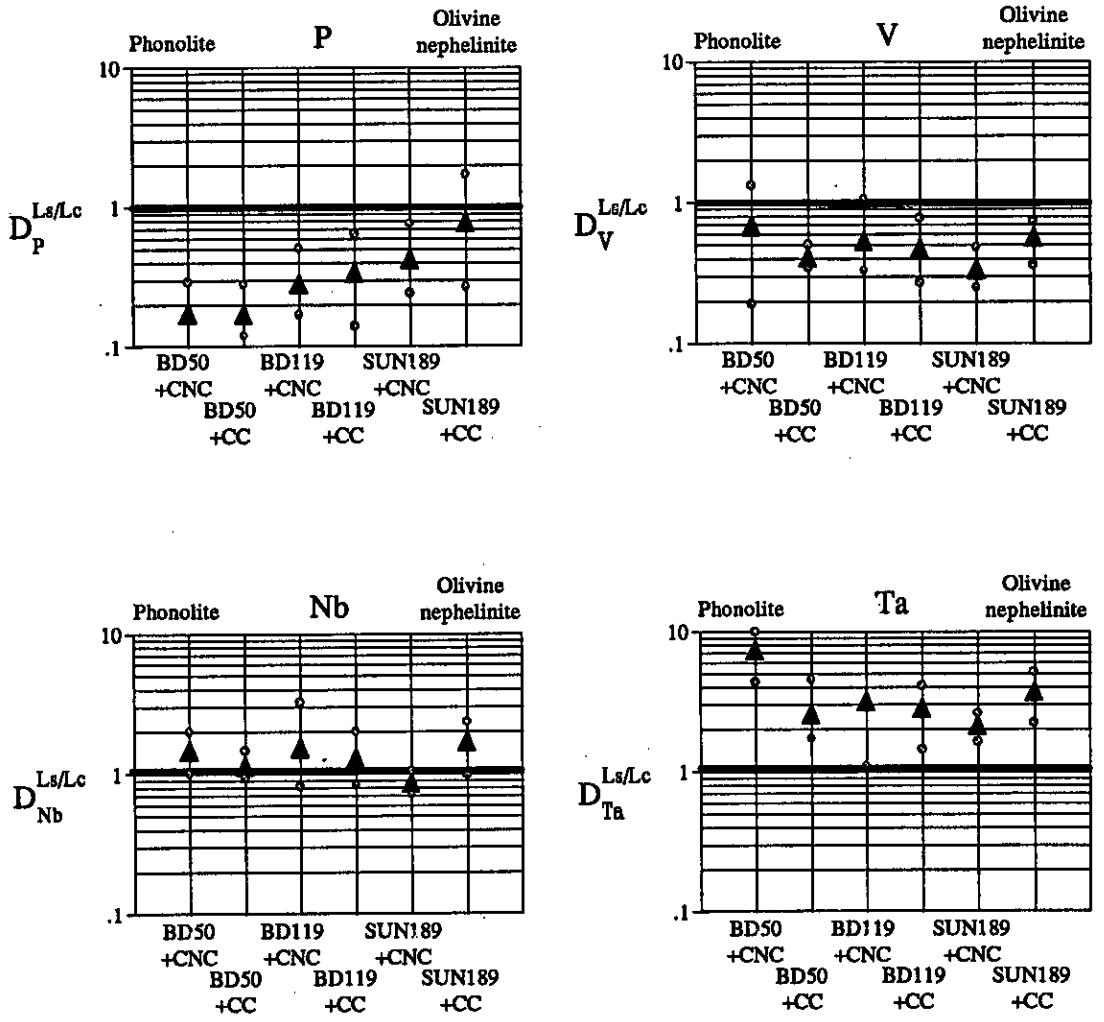

Figure 8.19. Partitioning of the Group V elements in natural compositions. Triangles are mean values for each composition, upper and lower limit are the most extreme values measured. V, and Nb show no change in partitioning with composition. Ta is more extremely enriched in the silicate melt in the phonolitic compositions (thought to be a solvus effect). Phosphorus is strongly enriched in the carbonate melt in silicic compositions, but becomes progressively less extremely partitioned as the compositions become more basic.

8.7.2. Vanadium.

Vanadium is always partitioned to the carbonate liquid. In all compositions the mean $^{Ls/Lc}D_V$ value is *ca.* 0.5. No significant variation in this value was seen with either composition, temperature or pressure in the main dataset.

8.7.3. Niobium.

In all compositions studied, niobium is roughly equipartitioned between carbonate and silicate liquids. $^{Ls/Lc}D_{Nb}$ ranges between 0.78 and 3.25, but is most commonly between 1 and 1.5. Niobium partitioning does not seem to be affected by pressure, temperature or composition.

8.7.4. Tantalum.

Tantalum is always enriched in the silicate liquid. $^{Ls/Lc}D_{Ta}$ ranges between 1.11 and 10.81, with most charges between 3 and 5. In all experiments, regardless of pressure, temperature, and composition, $^{Ls/Lc}D_{Ta} > {}^{Ls/Lc}D_{Nb}$. Tantalum partitioning is unaffected by pressure and temperature, although enrichment in the silicate liquid does seem to be more extreme in the phonolitic compositions.

Apparent tantalum concentrations in the carbonate may be significantly affected by an interference from $Ho\text{-}O^+$. Holmium concentrations are not known in the experimental quenches, and could not be measured on the ion probe due to interference from $Nd\text{-}O^+$, so no correction could be applied. Holmium is believed to behave identically to yttrium in most geological processes; the severity of this interference effect was therefore estimated by using known yttrium concentrations to estimate holmium content. In the worst case studied, $Ho\text{-}O^+$ could be responsible for 20-25% of the apparent Ta concentration in the carbonate quench. In the majority of charges, however, $Ho\text{-}O^+$ could only be responsible for 5% of the apparent tantalum. In any case, the maximum effect on $^{Ls/Lc}D_{Ta}$ will be to increase it by 25%. This will not affect either of the main conclusions drawn from tantalum partitioning:

(a) Tantalum partitions to the silicate liquid.

(b) $^{Ls/Lc}D_{Ta} > {}^{Ls/Lc}D_{Nb}$ for all charges studied.

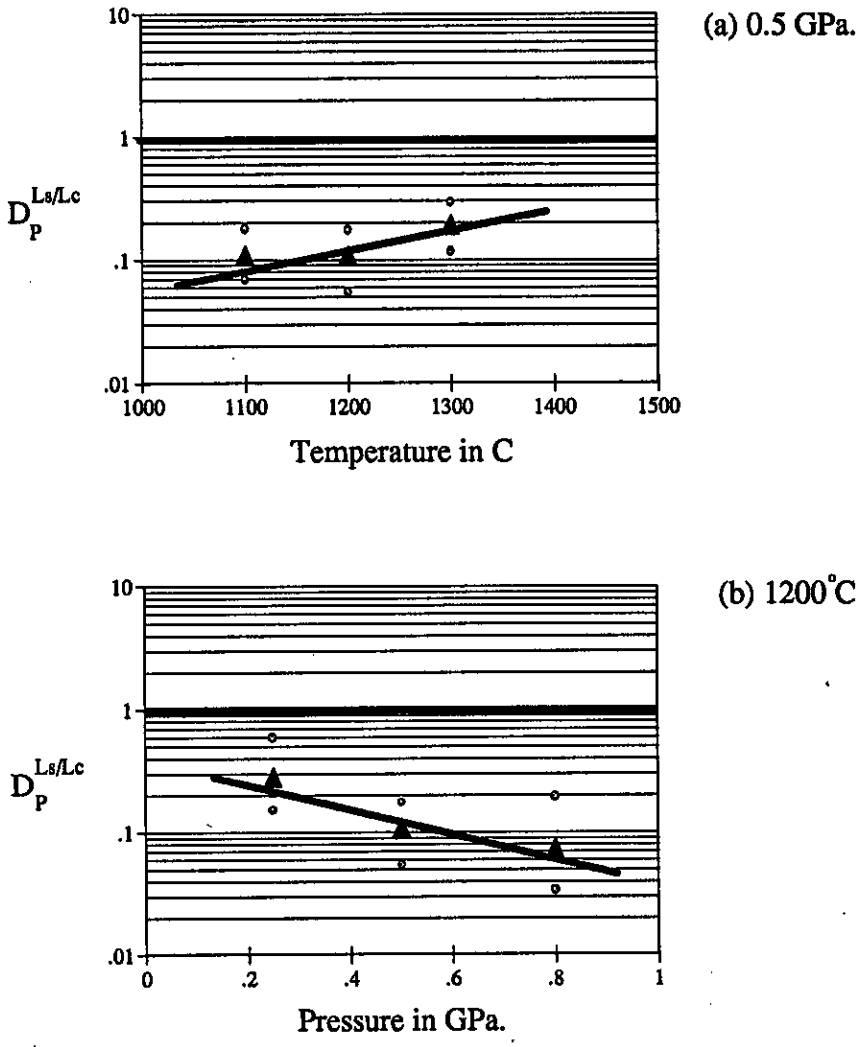

Figure 8.20. The effect of temperature and pressure on partitioning for phosphorus in BD50+CNC compositions Phosphorus behaves like calcium and other Group II elements. It is more strongly enriched in the carbonate liquid at lower temperature and higher pressure.

One possible effect of the Ho interference would be to mask the extent of Ta-Nb fractionation between carbonate and silicate liquids. Fractionation in the synthetic system, where Ho was absent and the interference can therefore not apply, was found to be a factor of *ca.* 2 or 3. This is in good agreement with data from natural compositions presented above.

8.7.5. Partitioning of Group V elements at mantle pressures.

Figure 8.21 shows partitioning of P, V, and Nb for the BD119+CNC composition at 1300°C, between 0.2 and 2.0 GPa. Phosphorus, like calcium and the other Group IIA elements, becomes more strongly enriched in the carbonate liquid with increasing pressure. Mantle carbonate liquids would therefore be expected to be very phosphorus-rich. By contrast, vanadium enrichment in the carbonate liquid becomes less pronounced with increasing pressure. Vanadium contents of mantle carbonate liquid would therefore be expected to approximate those of the corresponding silicate liquid. Partitioning of niobium (and also tantalum) is unaffected by pressure. Niobium is always roughly equipartitioned between carbonate and silicate liquids.

8.7.6. Partitioning of +5 elements as a function of ionic radius.

Unlike the negative correlation of $^{Ls/Lc}D_i$ and ionic size seen for +1, +2 and +3 ions, +5 ions show a distinct positive correlation with ionic radius (Figure 8.22). Larger ions are preferred by the silicate liquid, whist smaller ions enter the carbonate liquid. This is thought to be due to these +5 ions being too highly charged to enter the silicate environment; thus those smaller +5 ions will be even less able to enter the silicate due to their higher charge density. As with Zr-Hf, distinctly different partitioning behaviour of Nb and Ta is observed despite their identical charge and size. An additional control on partitioning must be responsible for the separation of these pairs.

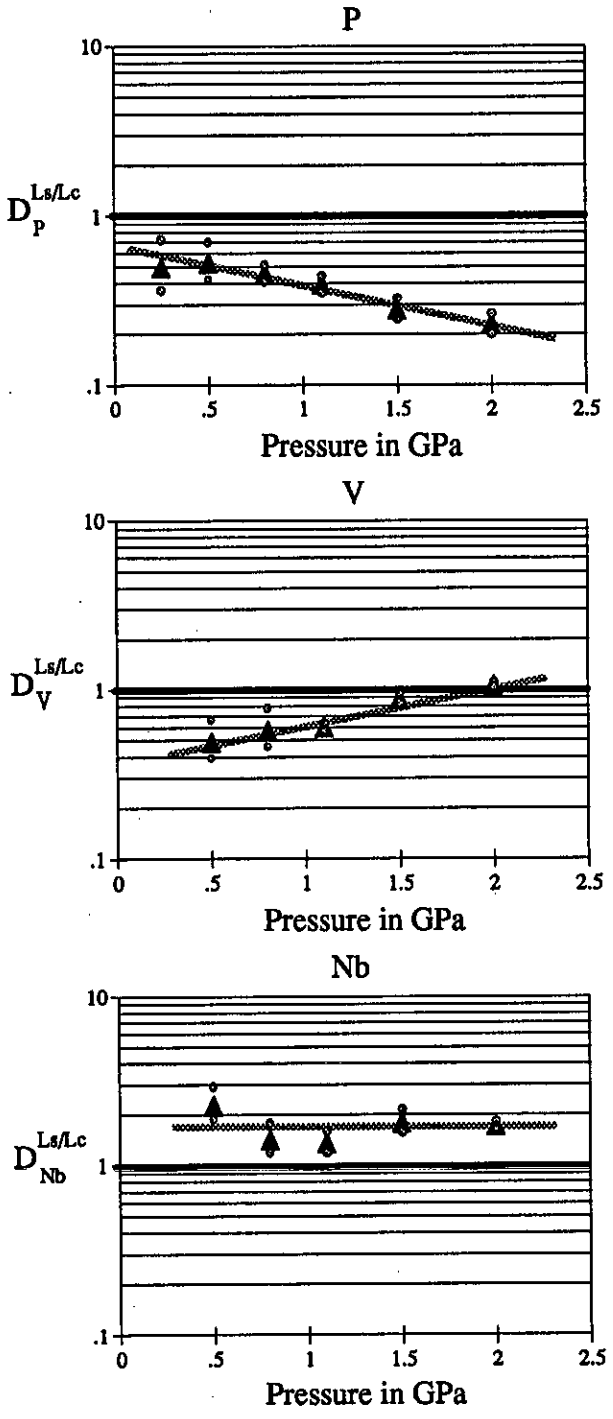

Figure 8.21. Partitioning of Group V elements as a function of pressure in BD119+CNC compositions at 1300°C Phosphorus becomes progressively more enriched in the carbonate liquid as pressure increases. Mantle carbonate melts are therefore likely to be phosphorus-rich. Vanadium shows the opposite tendancy, becoming less strongly partitioned to the carbonate melt with increasing pressure. Niobium (and tantalum) seem unaffected by pressure.

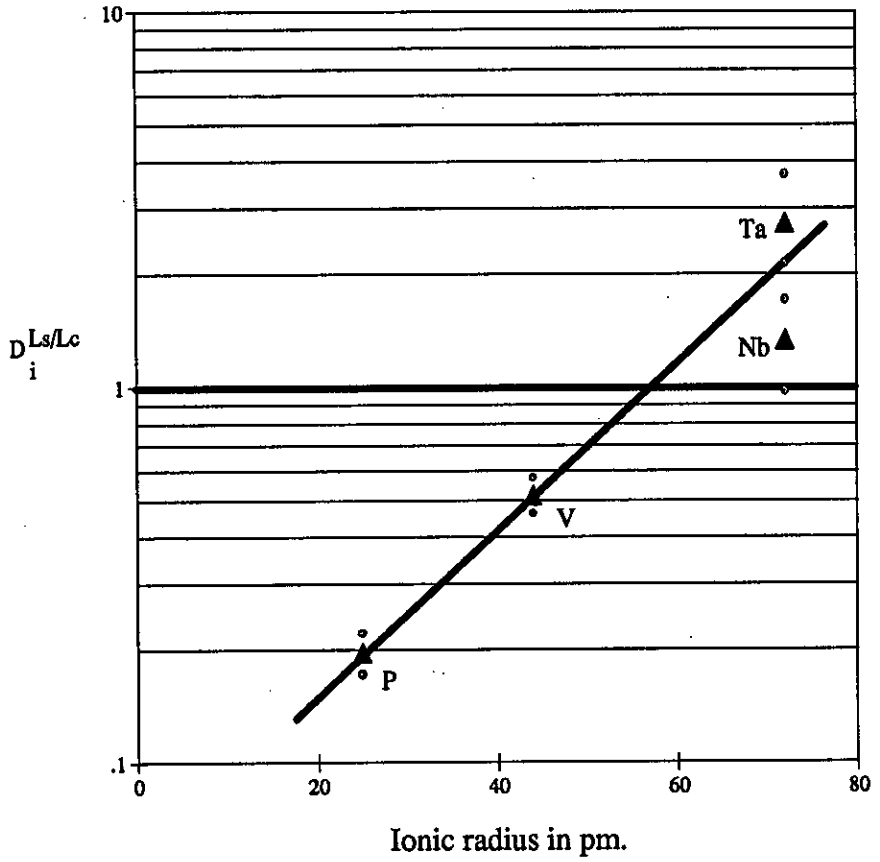

Figure 8.22. Partitioning of +5 ions as a function of ionic size. Unlike the strong negative correlations seen in the lower valency ions, partitioning of the +5 ions between silicate and carbonate liquids shows a distinct positive correlation. The extremely small and highly charged ions of phosphorus and vanadium are rejected from the silicate melt, and become enriched in the carbonate. Note that despite their identical valency and ionic sizes, niobium and tantalum show noticeably different partitioning behaviour. There must be an additional discriminating factor between these two ions.

8.8. Other elements: U, Th, Pb, and Mo.

Some elements were analysed which do not fit into the above chemical groupings. Data for these elements (U, Th, Pb, and Mo) are given in Table 8.8.

Table 8.8. Partitioning of U, Th, Pb, and Mo in natural compositions.
n is the number of determinations, μ is the mean value obtained. Max and Min are the measured extremes.

	Lead				Thorium				Uranium				Molybdenum			
Composition	n	μ	Max	Min	n	μ	Max	Min	n	μ	Max	Min	n	μ	Max	Min
BD50+CNC	9	0.22	0.46	0.07	9	20.4	39.4	11.5	5	3.48	6.28	1.94	1	0.13	0.19	0.08
BD50+CC	9	0.41	1.43	0.07	9	6.83	9.95	5.09	1	1.80	2.38	1.41	-	-	-	-
BD119+CNC	9	0.50	1.31	0.03	9	8.46	11.9	2.53	14	2.26	3.17	0.75	7	0.19	0.26	0.14
BD119+CC	9	0.77	1.07	0.42	9	6.38	11.4	4.33	7	2.39	3.38	1.66	3	0.28	0.58	0.16
SUN189+CNC	9	0.48	0.77	0.24	9	4.67	7.66	3.69	6	1.50	1.96	0.93	1	0.10	0.14	0.08
SUN189+CC	9	0.36	0.51	0.11	9	7.44	11.3	3.94	3	2.01	2.21	1.90	1	0.52	0.78	0.36

8.8.1. Lead.

As has been mentioned previously, errors on $^{Ls/Lc}D_{Pb}$ values are large due to the very low relative ion yield of Pb^+ in ion probe analysis. However, a number of observations on lead partitioning can be made. Lead is always partitioned into the carbonate liquid. This partitioning is strong in phonolitic compositions, but becomes less pronounced in the more basic starting compositions. No pressure or temperature effects on lead partitioning could be found.

8.8.2. Thorium.

Thorium is always enriched in the silicate liquid. In phonolitic compositions this enrichment is extreme (by a factor of 20 or more), whist in nephelinitic compositions thorium is only moderately enriched in the silicate (a factor of *ca.* 5). Pressure and temperature seem to have little effect on thorium partitioning.

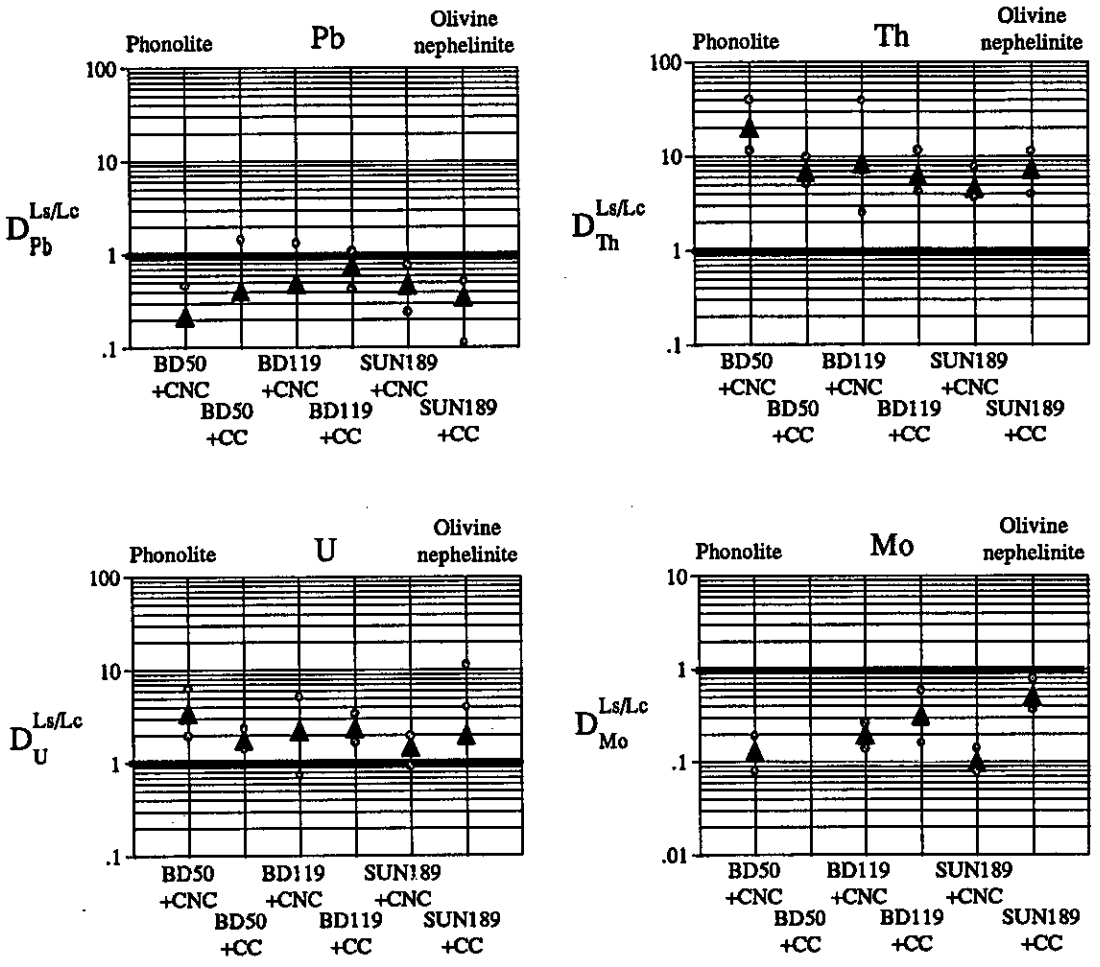

Figure 8.23. Partitioning of Pb, Th, U, and Mo in natural compositions. Lead shows an interesting relationship with composition in becoming less extremely enriched in the carbonate melt in intermediate compositions. Lead is always enriched in the carbonate melt. Thorium is more strongly enriched in the phonolitic compositions, but is enriched in the silicate melt by a factor of at least 5 in all compositions. Uranium seems unaffected by composition and is always equipartitioned, or slightly enriched in the silicate component. Molybdenum data are poorly constrained; however Mo is always enriched in the carbonate liquid by at least a factor of 2.

8.8.3. Uranium.

Uranium is usually weakly enriched in the silicate liquid. In the majority of experiments $^{Ls/Lc}D_U \sim 2$. Uranium partitioning is little effected by pressure, temperature, or composition. In all experiments, $^{Ls/Lc}D_{Th} > {}^{Ls/Lc}D_U > {}^{Ls/Lc}D_{Pb}$.

8.8.4. Molybdenum.

Molybdenum was only analysed in a few charges: it was a late addition to the analytical list. In those charges, molybdenum is partitioned strongly to the carbonate liquid ($^{Ls/Lc}D_{Mo} << 1$). Not enough data were obtained to investigate the effects of pressure and temperature in detail, although initial results suggests that the effects will be small.

8.8A. Comparison of results with Hamilton *et al.* (1989).

8.8A.1. Comparison of major element data.

As stated in Chapter 4, major-element partitioning behaviour between coexisting carbonate and silicate components of experimental charges produced in this study is in broad agreement with that recorded by Hamilton *et al.* (1989). In both studies aluminium, silicon and titanium are enriched in the silicate glass, whilst calcium and sodium are enriched in the carbonate quench. Potassium is approximately equipartitioned between the two phases. Hamilton *et al.* (1989) did, however, report very variable partitioning behaviour for iron ($1.0<{}^{Ls/Lc}D_{Fe}<60$), magnesium ($0.2<{}^{Ls/Lc}D_{Mg}<30$), and manganese ($0.6<{}^{Ls/Lc}D_{Mn}<3.2$). In this study, partition coefficients for these elements are better constrained, with iron strongly enriched in the silicate liquid ($3.57<{}^{Ls/Lc}D_{Fe}<60$), manganese weakly enriched in the silicate liquid ($1.06<{}^{Ls/Lc}D_{Mn}<1.96$), and magnesium roughly equipartitioned ($0.89<{}^{Ls/Lc}D_{Mg}<1.56$). In general, better constraints on the major-element compositions of the quenched coexisting liquids allowed more rigorous treatment of the effects of pressure, temperature, and composition on major-element distribution.

8.8A.2. Comparison of trace-element data.

With a few noticeable exceptions, there is good agreement between the trace-element partitioning data published by Hamilton *et al.* (1989) and those recorded in this study.

Both the sense, and degree of partitioning of the REE between carbonate and silicate liquids suggested by Hamilton *et al.* (1989) have been confirmed in this study. Also confirmed are the relationship of $^{Ls/Lc}D_{REE}$ with ionic radius, and the effects of pressure and temperature on REE partitioning. This study has extended the REE partitioning data set to higher pressures (2.0 GPa), and includes experiments on more-primitive bulk compositions.

The partitioning data of Hamilton *et al.* (1989) for hafnium and tantalum are also in agreement with behaviour seen here. In both studies, hafnium is always seen to be strongly enriched in the silicate portion of the charge ($^{Ls/Lc}D_{Hf}>>10$), whilst tantalum is only weakly partitioned to the silicate melt ($1<^{Ls/Lc}D_{Ta}<10$).

However, partitioning data for zirconium and barium obtained in this study are inconsistent with those of Hamilton *et al.* (1989). For both elements, the data of Hamilton *et al.* (1989) are extremely variable ($0.69<^{Ls/Lc}D_{Zr}<7.14$ and $0.16<^{Ls/Lc}D_{Ba}<5.47$), and no systematic partitioning behaviour can be discerned for either element. More coherent partitioning of these elements has been seen in this study, with zirconium **always** enriched in the silicate liquid ($^{Ls/Lc}D_{Zr}\sim10$), and barium **always** enriched in the carbonate quench ($^{Ls/Lc}D_{Ba}<0.5$). It is suggested that Hamilton *et al.* (1989) may have had difficulties with neutron activation analysis for these elements, although no simple explanation for such data variability could be found, as both zirconium and barium were reported to be at concentrations >1000 ppm in the experimental charges analysed.

In addition to the partitioning data collected for the elements above (previously determined by Hamilton *et al.*, 1989), this study has also presented data for 14 elements for which carbonate-silicate partitioning has been hitherto unstudied: rubidium, cesium, strontium, yttrium, phosphorus, vanadium, niobium, uranium, thorium, lead, molybdenum, sulphur, fluorine, and chlorine.

8.9. Controls on element partition in natural compositions.

8.9.1. Partitioning of elements in natural compositions as a function of run duration.

Figure 8.24 shows the effect of run duration on partitioning for a selection of trace elements. In general it can be seen that , as in the synthetic system, chemical equilibrium seems to have been obtained in a period of *ca.* 60 mins. Those runs of shortest duration give $^{Ls/Lc}D_i$ values that are significantly different from those of longer run duration. The 60 minute data for silicon is also distinctly different, as is that of Mg and P. It is thought that this is due to analytical problems for this experiment (G10.3) and is not related to equilibration.

8.9.2. Partitioning of trace elements as a function of ionic radius.

The discussions of partitioning within chemical groups showed that ionic radius influences partitioning between geochemically similar elements. In order to investigate a more general relationship of partitioning with ionic size, partition coefficients for all the elements studied have been plotted against ionic radius (R) for experiment G24.2 (Figure 8.25). It can be seen that elements with small ionic radii (< 50 pm) and very large ionic radii (> 110 pm) partition to the carbonate liquid, whilst ions with $50 < R < 110$ pm partition to the silicate liquid. This range of ionic size over which partitioning is to the silicate liquid has been named the "silicate window". This behaviour has been interpreted as being due to competition between a discriminating silicate liquid which can only accommodate ions of specific size and charge, and an indiscriminate carbonate liquid which can accommodate all ions, but with different degrees of ease. This difference in behaviour can be related to liquid structure. The silicate liquid consists of aluminosilicate chains and isolated SiO_4 tetrahedra. Ions which can substitute into these chains, or which can form stable chelate complexes with SiO_4 tetrahedra will be enriched in the silicate liquid. Ions too large or too small for this will be rejected by the silicate liquid. By contrast, the carbonate liquid is believed to approximate an ionic melt. Size considerations therefore become less important, and stability in the melt should be solely related to charge density considerations.

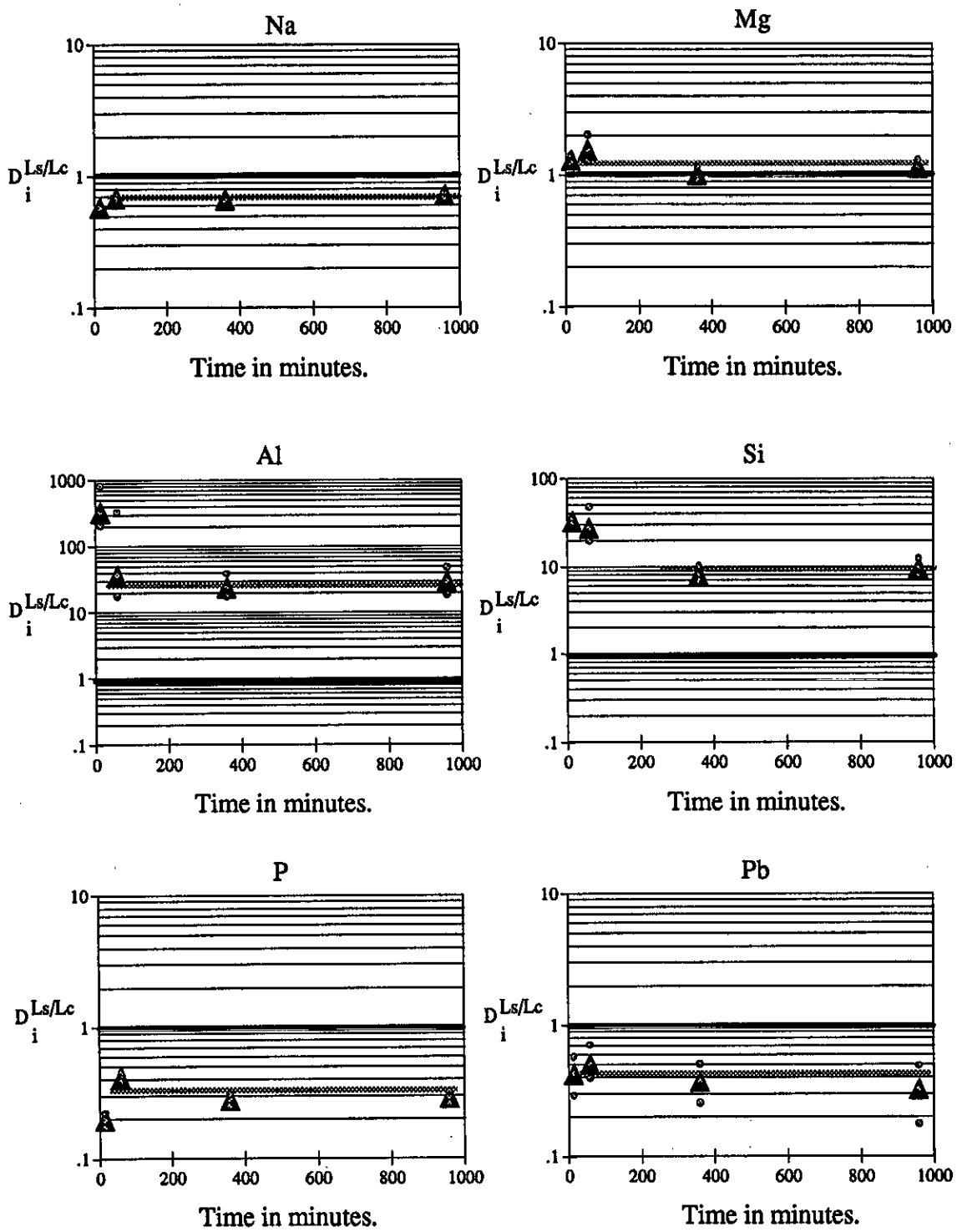

Figure 8.24. Variations in partitioning behaviour as a function of time for a selection of elements at 1300°C, 0.8 GPa. In a number of the graphs shown above, the 15 minute duration run gives D values which are considerably different from those produced in longer duration experiments. It seems likely, therefore, that the shortest runs do not represent equilibrium conditions.

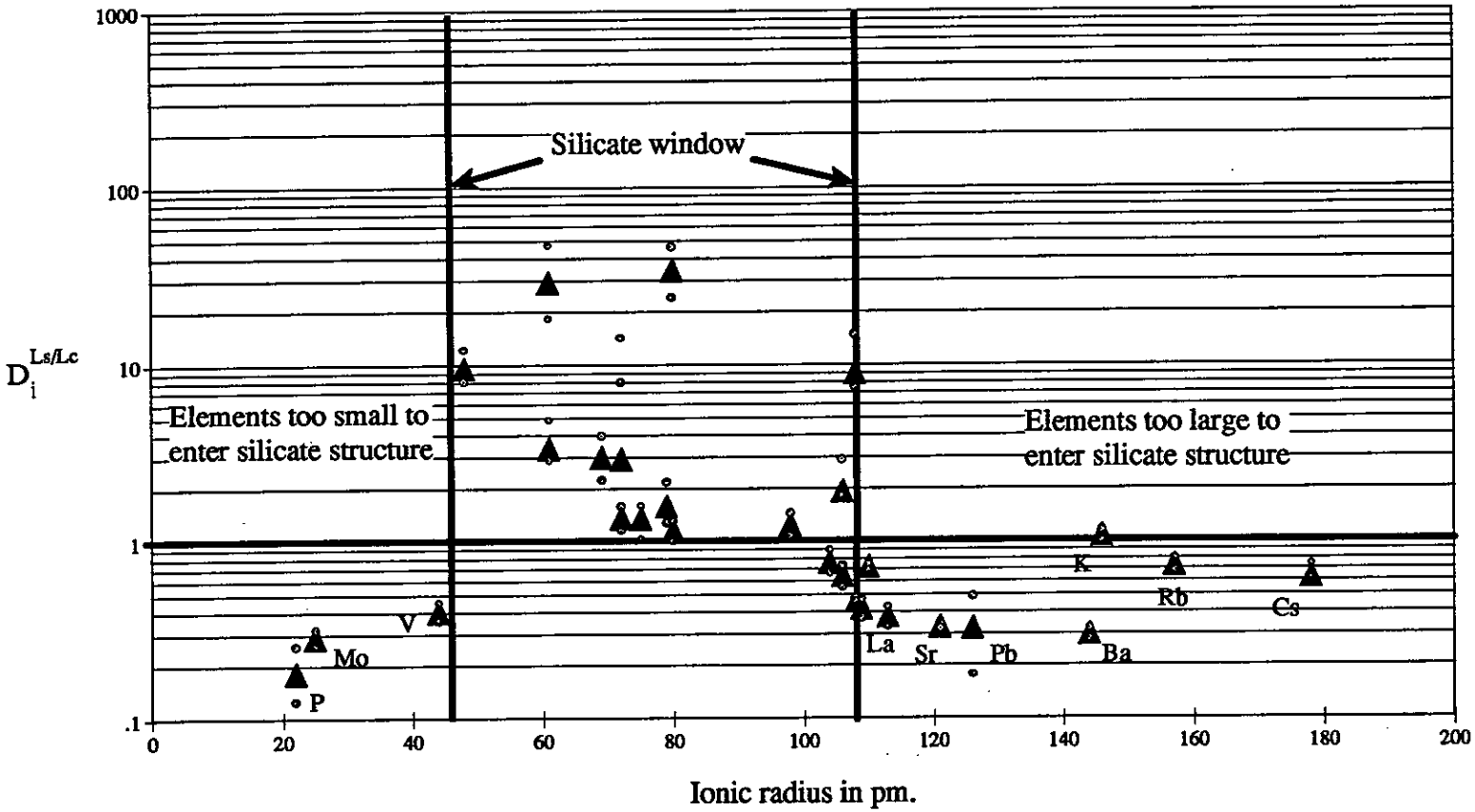

Figure 8.25. Partitioning as a function of ionic radius. As well as the relationships of partitioning with ionic radius seeen in individual groups, an overall picture of how ionic size controls partitioning can be outlined. Elements whose ions are of radius <50, or >110 pm are all partitioned to the carbonate melt. Elements with 50<R<110 are in general partitioned to the silicate melt. This behaviour has been interpreted as being the competition between a discriminating silicate melt, which only allows ions with specific size and charge into its structure, and an indiscriminate carbonate liquid, which in general just prefers ions of low charge density.

8.9.3. Partitioning as a function of charge density.

Charge density has been quantified as the ionic charge divided by the ionic radius. As suggested in the previous section, partition of elements into the carbonate liquid should be related to charge density considerations. A general relationship with charge density should be seen, although the influence of the silicate liquid should result in deviations from this trend. Figure 8.26 shows the relationship between $^{Ls/Lc}D_i$ and charge density for experiment G24.2. A positive correlation is seen for ions of low charge density (< 5). However, at C/R > 5 the trend reverses, and a diffuse negative correlation can be seen. There is therefore an optimum charge density for ions to enter the silicate liquid. Ions which are near this optimum value include Al^{3+}, Zr^{4+}, and Hf^{4+}.

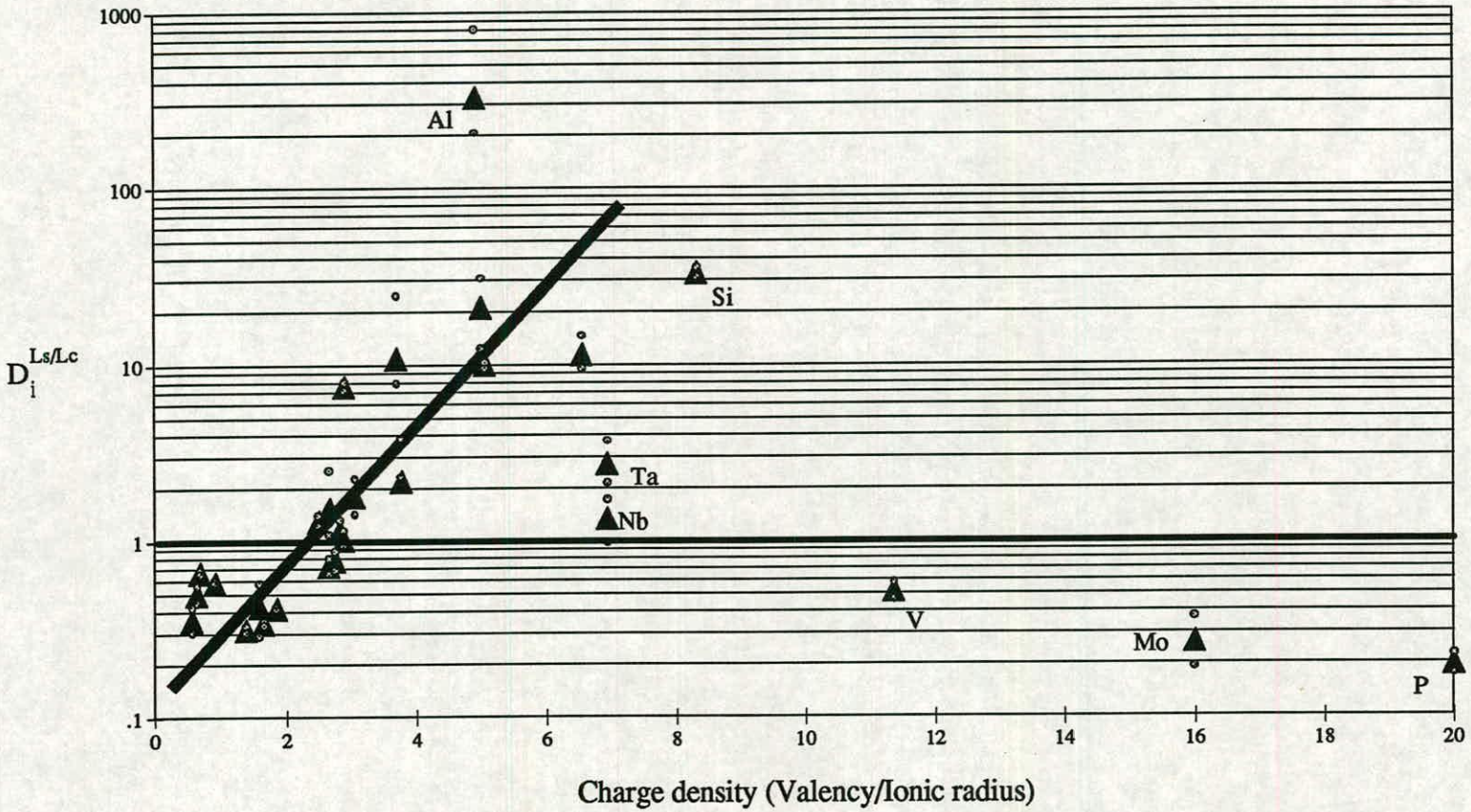

Figure 8.26. Partitioning behaviour as a function of charge density for all elements studied. Charge density is calculated as the ionic charge (C) divided by the ionic radius (R) (Whittaker & Muntus, 1970). A correlation between partitioning and charge density is seen for low values of C/R. However, a maximum D value is reached at C/R = 4-6. Above this value, ions are again partitioned more to the carbonate melt. Only elements with C/R of 3-10 are partitioned to the silicate melt.

8.10. Carbonate-silicate partitioning under mantle conditions.

The solidus for carbonated mantle peridotite has been investigated by a number of workers. (e.g. Olaffsson & Eggler, 1983; Falloon and Green, 1990). It is believed that melting will commence at between 950 and 1150°C at 2.5-3.0 GPa. It is therefore under these conditions that $^{Ls/Lc}D_i$ data will be required. Using trends shown in this chapter, partitioning behaviour between an olivine nephelinitic silicate liquid and a calcic carbonate liquid have been estimated for 2.5 GPa, and 1100°C. These values can only be estimates for two reasons:

(a) The olivine nephelinitic compositions studied here would not be liquids at temperatures much below 1300°C.

(b) Immiscibility between olivine nephelinite and calcic carbonate would not be expected to extend above 1.0-1.5 GPa.

Table 8.9. Partitioning between carbonate and silicate liquids under mantle conditions: an estimate.

Element (*i*)	$^{Ls/Lc}D_i$	Element (*i*)	$^{Ls/Lc}D_i$
Na	2	Si	10
K	1.5	Ti	5
Rb	1	Zr	10
Cs	0.8	Hf	18
Mg	0.5	P	0.2
Ca	0.15	V	1
Sr	0.1	Nb	1.2
Ba	< 0.1	Ta	3
Mn	0.6		
Fe	1	Pb	0.5
		Th	8
Al	50	U	2
Y	0.8		
La	0.2	Mo	0.2
Ce	0.25		
Nd	0.3		
Sm	0.35		

$^{Ls/Lc}D_i$ values applicable to mantle conditions are calculated from data for nephelinite BD119+CNC at 1300°C, 2.5 GPa, using relationships of partitioning with pressure, temperature, and composition.

8.11. Comparison between partitioning in natural and synthetic systems

8.11.1. Geochemical characteristics of partitioning common to both natural and synthetic partitioning experiments.

In general $^{Ls/Lc}D_i$ values obtained in the natural rock compositions are very similar to those obtained for synthetic liquids (Chapter 7). Some of the important characteristics common to both data sets are listed below.

(a) Enrichment of LILE in the carbonate liquid.

In both the natural and synthetic experiments, the carbonate liquid was found to contain higher concentrations of LILE than its silicate counterpart. In general, the larger the ion, the more extreme the enrichment of that ion in the carbonate liquid.

(b) Relative fractionation of REE between carbonate and silicate liquids.

In all experiments undertaken, relative fractionation of the rare earth elements was seen; the carbonate liquid was always relatively enriched in LREE over HREE compared to its silicate counterpart.

(c) Strong enrichment of +4 ions in the silicate liquid.

Although the extent of enrichment varies for different elements, all +4 ions are found to be enriched in the silicate over the carbonate liquid in both natural and synthetic compositions. This enrichment in the silicate liquid is extreme, and often exceeds a factor of 10.

(d) Very small, or very highly charged ions partition to the carbonate liquid.

In both natural and synthetic systems, elements like P, V, Mo, and to a certain extent Nb, are enriched in the carbonate liquid.

(e) Separation of elements with ions of similar charge and size.

In both natural and synthetic systems, the element pairs Zr-Hf, Nb-Ta, and U-Th are separated from each other. In virtually all experiments $^{Ls/Lc}D_{Hf} > {}^{Ls/Lc}D_{Zr}$, $^{Ls/Lc}D_{Ta} > {}^{Ls/Lc}D_{Nb}$, and $^{Ls/Lc}D_{Th} > {}^{Ls/Lc}D_{U}$.

8.11.2. Differences between partitioning behaviour in natural and synthetic experiments.

Differences between the natural and synthetic experiments have also been noted. The most significant of these are listed below.

(a) Relative partitioning of Group IA and Group IIA elements.

In the synthetic experiments, $^{Ls/Lc}D_i$ for the Group IA elements were generally lower than for their Group IIA counterparts (i.e. $^{Ls/Lc}D_{Rb} < {}^{Ls/Lc}D_{Sr}$, $^{Ls/Lc}D_{Cs} < {}^{Ls/Lc}D_{Ba}$ etc.). In the natural experiments, this behaviour was reversed, with Group IIA elements being much more extremely enriched in the carbonate liquid than the Group IA elements. This behaviour must be related to the compositional differences between the two systems (that is, the presence of Mg, Fe, Ti, and P as major components). The effect of phosphorus was investigated in Chapter 7. It was found to encourage partitioning of Group IIA elements into the silicate liquid, and discourage partitioning of Group IA elements to the carbonate liquid. It is therefore suggested that the presence of phosphorus is the cause of this discrepancy in partitioning between natural and synthetic liquids.

(b) Partitioning of the REE.

The REE show more affinity with the carbonate liquids in natural compositions than they do in the corresponding synthetic compositions under the same conditions. This is again thought to be due to the presence of phosphorus, as it was shown in Chapter 7 that the addition of phosphorus to synthetic liquids led to more extreme partitioning of the REE to the carbonate liquid.

(c) Variation in element partitioning with pressure.

Changing the physical conditions of the experiments was seen to have negligible effect on partitioning in synthetic compositions. By contrast, experiments on natural compositions have shown considerable variation in partitioning behaviour with temperature, and more importantly pressure. This pressure effect is most pronounced for phosphorus, Group IIA elements, and the REE. Again, this discrepancy in partitioning behaviour must be related to the compositional differences between the natural and synthetic systems. In order for partitioning to be affected in such a profound manner, the physical or structural properties of at least one of the liquids must be varying significantly with increasing pressure. The carbonate liquid approximates a molten ionic salt and is therefore considered unlikely to be susceptable to slight changes in pressure or composition. In contrast, the structural state of the Silicate liquid behaviour is strongly composition dependant with relatively small changes in composition resulting in significant variation in the polymerisation state of the liquid. The most widely accepted measure of polymerisation state in silicate liquids is the proportion of non-bridging oxygens per tetrahedrally coordinated cation (NBO/T). This melt characteristic can be calculated for known liquid compositions (e.g. Mysen, 1990). After charge compensation for tetrahedral PO_4^{3-}, Al^{3+}, and Fe^{3+}, the ratio can be calculated as:

$$NBO/T = 1/T \sum nM^{n+} \qquad (8.1)$$

Where: T is the molecular proportion of tetrahedral cations.
M is a network modifying cation (e.g. Na^+, Ca^{2+} etc.).
n is the charge of ion M.

This ratio has been calculated for selected conjugate silicate melts from both synthetic and natural compositions (see Mysen, 1990 for procedures). Figure 8.27 shows that significant structural changes are indeed occurring in the natural silicate melt compositions as pressure is increased. In melts from experiments involving nephelinite BD119, NBO/T systematically decreases from *ca.* 0.6 to *ca.* 0.35 as pressure increases from 0.25 to 2.0 GPa; this represents a polymerisation of the silicate melt with increasing pressure. In contrast, no change in polymerisation state occurs with pressure for the synthetic experiments, NBO/T remaining fixed at *ca.* 0.85. This variation in NBO/T with pressure is therefore suggested as the cause of pressure effects on partitioning seen in the natural system; although the calculation of NBO/T is subject to considerable uncertainty, a correlation with partitioning behaviour clearly exists for many elements (e.g. the REE in Figure 8.28).

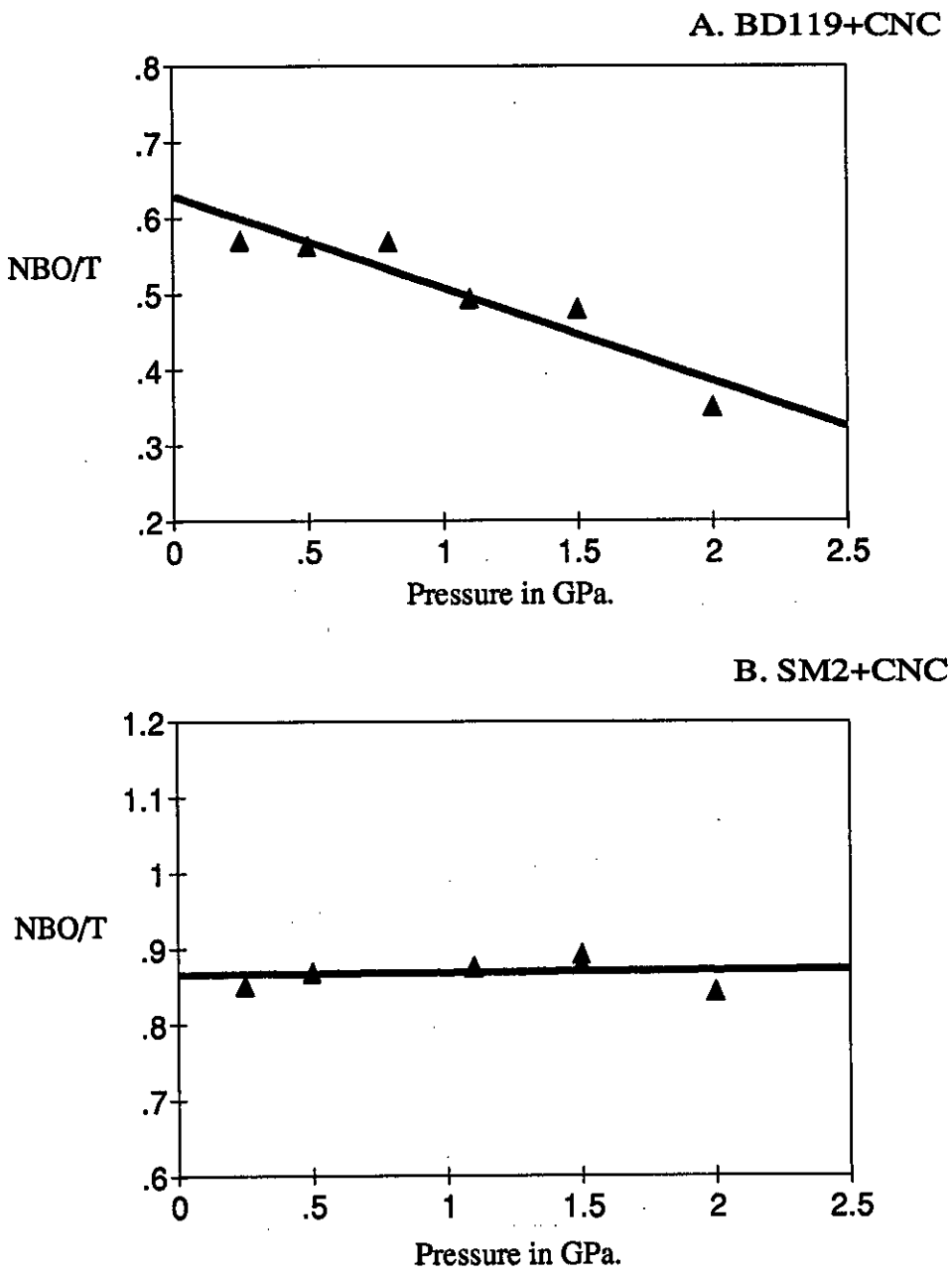

Figure 8.27. Variations in structure of the conjugate silicate liquids with pressure.
A. In Natural compositions, there is substantial decrease in NBO/T with increasing pressure. It is this structural variation that is believed to be responsible for the significant variations in partitioning with pressure seen for many trace elements.
B. In synthetic compositions, very little variation in NBO/T is seen with increasing pressure. This may explain the lack of variation seen in partitioning with pressure seen in these experiments.

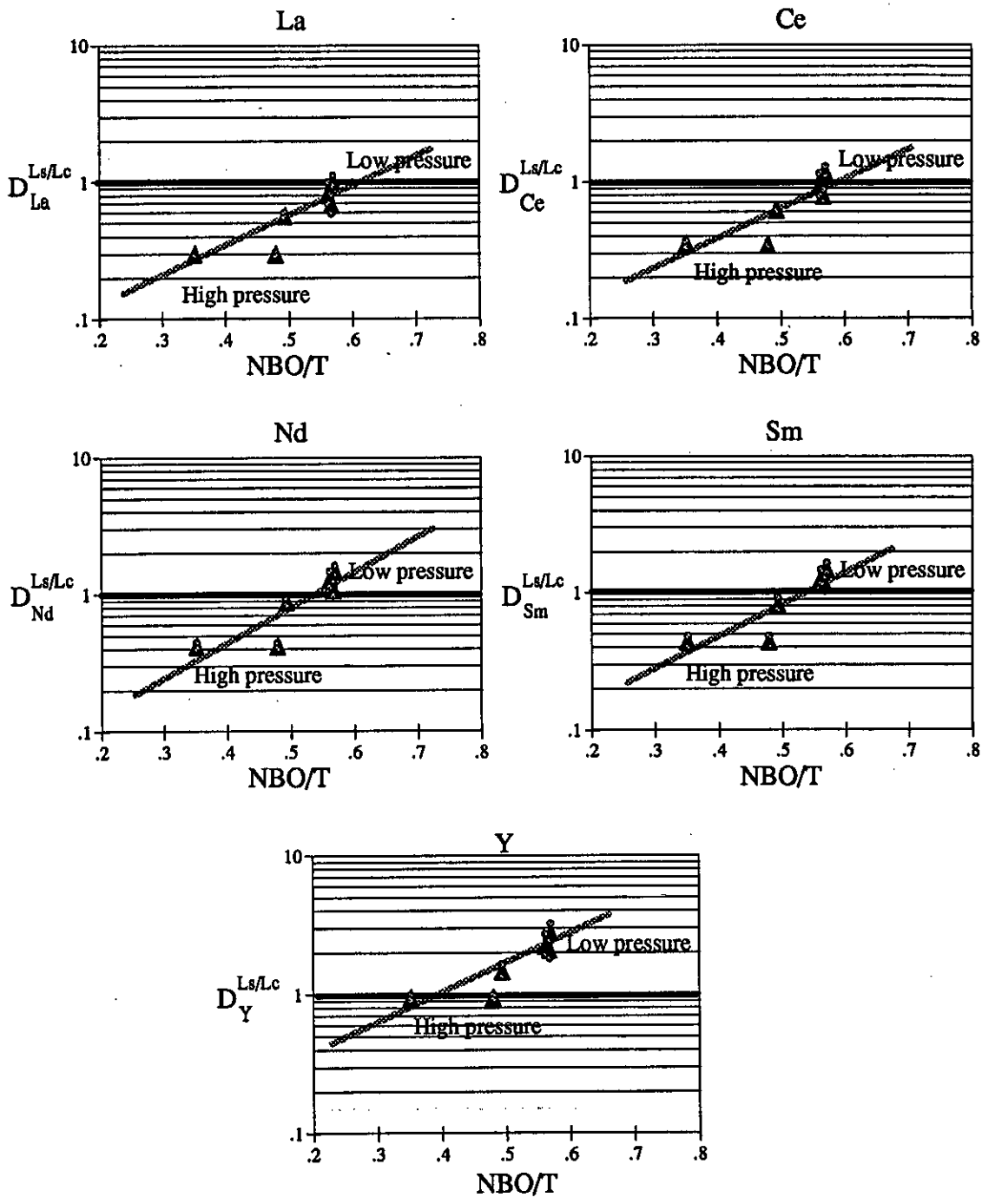

Figure 8.28. Partitioning of Yttrium and the REE with changing silicate melt structure, represented by NBO/T. The REE are more inclined to enter the carbonate liquid as the silicate melt becomes more polymerised (NBO/T decreases). It is this variation in melt structure with pressure that is believed to be responsible for pressure effects seen in the partitioning of many elements in experiments on natural compositions.

Does this, in itself, explain the pressure effects seen on partition coefficients? The answer is unfortunately *no*: the change in melt composition with pressure that results in polymerisation of the silicate melts must in itself be explained. The key to this problem is that the pressure effects on partitioning are not seen in the synthetic melts. The only significant difference in major-element composition between the natural and synthetic systems is the presence of Mg, Fe and Mn in the natural rock powders. The cause of the pressure variations seen must ultimately lie in the presence of these components.

For component i in the silicate melt:

$$G_{i_s} = H_{i_s} - TS_{i_s} + (P-1)V_{i_s} + RT\ln X_{i_s} + RT\ln\gamma_{i_s} \qquad (8.2)$$

And in the carbonate melt:

$$G_{i_c} = H_{i_c} - TS_{i_c} + (P-1)V_{i_c} + RT\ln X_{i_c} + RT\ln\gamma_{i_c} \qquad (8.3)$$

Subtracting (8.3) from (8.2) gives:

$$\Delta G_{i_{s/c}} = \Delta H_{i_{s/c}} - T\Delta S_{i_{s/c}} + (P-1)\Delta V_{i_{s/c}} + RT\ln(X_{i_s}/X_{i_c}) + RT\ln(\gamma_{i_s}/\gamma_{i_c})$$

At equilibrium, $G_{i_s} = G_{i_c}$:

$$\therefore \Delta G_{i_{s/c}} = 0 = \Delta H_{i_{s/c}} - T\Delta S_{i_{s/c}} + (P-1)\Delta V_{i_{s/c}} + RT\ln(X_{i_s}/X_{i_c}) + RT\ln(\gamma_{i_s}/\gamma_{i_c})$$

$(X_{i_s}/X_{i_c}) = D_{i_{s/c}}$, therefore:

$$-RT\ln D_i = \Delta H_{i_{s/c}} - T\Delta S_{i_{s/c}} + (P-1)\Delta V_{i_{s/c}} + RT\ln(\gamma_{i_s}/\gamma_{i_c})$$

$$\ln D_i = \Delta S_i/R - \Delta H_i/RT - (P-1)\Delta V_i/RT + \ln(\gamma_{i_s}/\gamma_{i_c}) \qquad (8.4)$$

Where: D_i is the partition coefficient of element i.
G_i is the Gibbs free energy of element i.
S_i is the entropy of element i.
H_i is the enthalpy of element i.
V_i is the molar volume of element i.
R is the gas constant.
T is the temperature in degrees Kelvin.
P is the pressure in bars.
subscript s refers to the silicate liquid.
subscript c refers to the carbonate liquid.
s/c refers to equilibrium between coexisting carbonate and silicate liquids.

It can be seen from equation (8.4) that pressure is only involved in the ΔV term. If changes in pressure are to cause the changing partitioning behaviour (and thus liquid compositions and structure), ΔV must vary substantially. In crystal-melt systems, the ΔH term is large (e.g. 90 000 J mol^{-1} for forsterite melting; Navrotsky *et al.*, 1989) compared to ΔV, and thus dominates the behaviour of D. This may explain why pressure effects on partition coefficients are not common in crystal-liquid systems (Beattie *et al.*, 1989). For liquid-liquid partitioning, however, it is likely that ΔH will be *much* smaller, perhaps by more than a factor of 10 (from strength of element partitioning). In this case, only small differences in molar volume for components between the carbonate and silicate liquids would be required to produce a significant effect on D.

If we assume a likely maximum value of $\Delta H_{i_{s/c}}$ of 10 000 J mol^{-1}, then for the pressure term to be significant (i.e. $\geq$ 10% of the enthalpy term):

$$(P-1)\Delta V_{i_{s/c}} \geq \Delta H_{i_{s/c}}/10$$

At 2.0 GPa (2.10^9 Pa):

$$\Delta V_{i_{s/c}} \geq 10\,000/2.10^{10}.$$

$$\Delta V_{i_{s/c}} \geq 5.10^{-7}\ m^3$$

$$\Delta V_{i_{s/c}} \geq 0.5\ cm^3$$

So, we require a volume change with pressure in the carbonate liquid of in excess of 0.5 cm^3 mol^{-1} in order to explain pressure effects on partitioning behaviour. An attempt to constrain $\Delta V_{i_{s/c}}$ for Mg, Mn, and Fe (the elements believed to be responsible for the presence of the pressure effect) proved unsuccessful due to the lack of molar volume data available for carbonate liquids. It is suggested, however, that there is likely to be a significantly smaller molar volume in the carbonate liquid for at least one of these components.

CHAPTER 9

THE GEOCHEMICAL CHARACTERISTICS OF MANTLE CARBONATE MELT.

9.1. Introduction.

The $^{Ls/Lc}D_i$ partition coefficients obtained in this study can be used to calculate partition coefficients for elements during carbonate melting events in the mantle by comparison with known silicate partition coefficients. This allows us to deduce the probable geochemical characteristics of carbonate liquids produced by melting of the mantle.

It was the initial intention of this study that $^{mantle/Lc}D_i$ values would be produced by combining $^{Ls/Lc}D_i$ data produced in this study with $^{mantle/Ls}D_i$ data from the literature. Considerable study of published mantle-silicate melt partitioning data has suggested that this intention was unrealistic; there are as many values of trace-element partition coefficients as there are determinations. For most elements, the variability in $^{mantle/Ls}D_i$ values used by different authors is large enough to encompass the order of magnitude (and more) differences in partitioning behaviour seen in this study. A more qualitative approach has therefore been applied, involving a study of the geochemical differences between carbonate and silicate liquids. It is left to the reader to apply his or her preferred $^{mantle/Ls}D_i$ values in order to make more quantitative estimates of carbonate involvement in specific circumstances.

This chapter will discuss the most prominent of the geochemical features of mantle carbonate liquids. It is split into three sections: major-element characteristics, trace-element characteristics, and implications for isotopic studies. The geochemical and isotopic predictions made in this chapter will be tested against geochemical data from naturally occurring mantle-derived material in Chapter 11.

9.2. Major-element characteristics.

9.2.1. The composition of carbonate liquid in equilibrium with mantle phases.

Major element compositions of experimentally produced mantle carbonate liquids have been estimated by Wallace & Green (1988), and Thibault *et al.* (1992). Due to the experimental problems involved in mantle-carbonate melting experiments, the uncertainties on these estimates are large, and caution has to be applied when referring to these results. In Table 9.1, the composition of a hypothetical carbonate liquid in equilibrium with the "primary magma" for Hawaiian alkali basalts (Clague & Frey, 1982) has been estimated using $^{Ls/Lc}D_i$ data from these experiments. Clague and Frey (1982) believe that this "primary magma" was at some time in equilibrium with a four phase mantle assemblage. It follows, from thermodynamics, that the carbonate liquid calculated to be in equilibrium with it could also be in equilibrium with mantle phases. Table 9.1 also contains analyses of primary carbonate melt compositions from the experiments of Wallace & Green (1988), and Thibault *et al.* (1992). There is a marked similarity between all these estimates of primary mantle carbonate melt composition.

Table 9.1. The chemical composition of primary carbonate melt. The chemical composition of a hypothetical carbonate liquid in equilibrium with primitive Hawaiian basalt has been estimated. A comparison of its major element chemistry with the experimental liquids of Wallace & Green (1988), and Thibault *et al.* (1992) allows us to predict some of the major element characteristics of primary carbonate liquid.
* High alumina content possibly due to contamination of analysis.
** Low phosphorus content of starting material.
*** Phlogopite-rich (and therefore K-rich) starting material.

Oxides	Primary Hawaiian basalt (Clague & Frey, 1982)	$^{La/Lc}$Di (SUN189+CC) (Fielding, this study)	Estimated primary carbonate melt	Primary carbonate melt (Wallace & Green, 1988)	Primary carbonate melt (Thibault *et al.* 1992)
SiO_2	44.50	15	2.97	2.94	2.57
TiO_2	2.15	7.0	0.31	0.45	0.72
Al_2O_3	14.01	25	0.56	1.95*	0.38
FeO	12.51	2.5	4.17	4.83	4.54
MnO	0.19	1.2	0.16	0.11	0.16
MgO	10.12	0.8	12.65	14.19	15.12
CaO	10.63	0.40	23.62	21.29	21.60
Na_2O	2.47	0.65	3.80	4.99	4.93
K_2O	0.53	1.0	0.53	0.35	7.01***
P_2O_5	0.42	0.2	2.10	0.5**	-

It is realised that the compositions of the quoted experimental liquids are strongly dependent on starting compositions, and on the pressure and temperature conditions of production. The composition of the estimated carbonate melt using $^{Ls/Lc}D_i$ data is dependent on the silicate liquid with which it is assumed to be in equilibrium. Despite the completely different origins of the three carbonate liquid compositions given in Table 9.1, it is clear that they have many geochemical features in common. It is therefore assumed that these features are characteristic of at least some mantle carbonate melts. These include:

(a) High calcium contents.

(b) High Mg/Fe ratios.

(c) Moderately high Na and K.

(d) High phosphorus content.

(e) Very low contents of SiO_2, Al_2O_3, and TiO_2.

Involvement of liquids of these compositions in melt production, or in metasomatic addition, will result in these features being inherited by the primary magma or metasomatised mantle.

9.2.2. The possible effects of carbonate addition to primary silicate liquid.

It has been suggested that carbonate liquids can act as precursor melts to silicate magmatism. What effects will this carbonate precursor have on the major element composition of the silicate magma? The answer is that in most cases the effects will be negligible, as the carbonate liquid is unlikely to constitute more than a few percent of the magma. If, however, we envisage an extreme case of the addition of 15% of carbonate liquid, some pronounced differences in composition are produced. The resulting liquid becomes:

(a) Silica-poor (undersaturated), and alumina-poor.

(b) Rich in calcium and phosphorus.

(c) Moderately to strongly alkalic.

These features are very similar to those seen in nephelinites and melilitites often seen associated with more voluminous basaltic magmatism. In Table 9.2, a hypothetical liquid has been calculated that would result from addition of 15% of carbonate liquid to primary Hawaiian basalt (Clague & Frey, 1982). This liquid shows marked compositional similarities to Oahu melilitite (Clague & Frey, 1982). The agreement in composition is poorest for titanium and potassium, both of whose concentrations are substantially higher in the melilitites than in the calculated liquid composition. This discrepancy has been attributed to smaller degrees of silicate melting in the production of the melilitite than in the production of the basalt.

Table 9.2. Possible major element effects of carbonate addition to primary silicate melt. Addition of 15% of primary carbonate liquid (estimated in Table 9.1) to the primary silicate melt believed to be parental to Hawaiian alkali basalts (Clague & Frey, 1982) produces a melt composition which shows many similarities to the Oahu nephelinites and melilitites (Clague & Frey, 1982). The only elements in the hypothetical 15% carbonate melt which do not agree well with the Oahu composition are TiO_2 and K_2O, both of which are too high in the nephelinites. Their high concentrations imply that the nephelinites must be produced by smaller degrees of silicate melting as well as addition of carbonate.

Oxides	Primary Hawaiian basalt (Clague & Frey, 1982)	Estimated primary carbonate melt	Calculated addition of 15% carbonate to primitive Hawaiian alkali basalt	Oahu Melilitite (Clague & Frey, 1982)
SiO_2	44.50	2.97	38.72	37.94
TiO_2	2.15	0.31	1.96	2.63
Al_2O_3	14.01	0.56	12.12	10.77
FeO	12.51	4.17	11.88	14.00
MnO	0.19	0.16	0.20	0.23
MgO	10.12	12.65	11.13	12.35
CaO	10.63	23.62	16.12	12.51
Na_2O	2.47	3.80	3.33	4.50
K_2O	0.53	0.53	0.61	1.52
P_2O_5	0.42	2.10	0.72	1.03

9.2.3. Differences between carbonate liquid and other fugitive agents in the mantle.

The major element composition of primary carbonate liquid is substantially different from that of any other low temperature fugitive agent in the mantle. It should therefore be possible to distinguish the action of these different agents by study of the differences in geochemical characteristics of mantle material, and mantle-derived melt.

Involvement of carbonate liquid addition will result in addition of Ca, P, Na and K. By contrast, low temperature mantle silicate melts will produce most effect on K, Ti and Fe contents . It is concluded that Fe, Ti, K enrichment seen in numerous xenolith suites (e.g. the xenolith suite from Pello Hill, Tanzania; Dawson & Smith, 1988) is the result of involvement of small-degree silicate melts.

Another proposed fugitive agent in the mantle is H_2O-rich fluid. Recent studies indicate that these fluids are unlikely to contain large quantities of most elements. The most soluble major elements in H_2O-rich fluid seem to be Si, Al and K (e.g. Odling & Randle, 1992). Relatively silicic potassic magmatism (e.g. Roman Province, Italy; Peccerillo, 1985; Peccerillo & Manetti, 1985) is therefore thought to involve H_2O-rich fluid.

One other fugitive component commonly invoked for element redistribution in the mantle is CO_2-rich fluid. Meen *et al.* (1989), and indeed experiments undertaken in this study, have shown that most elements have very low solubility in CO_2-rich fluid. It is therefore concluded that addition of CO_2-rich fluid will have little effect on major-element composition.

9.3. Trace-element characteristics.

9.3.1. Large-ion lithophile element enrichment in the carbonate liquid.

In all the experiments undertaken, the carbonate liquid was found to be relatively enriched in the whole range of LILE compared to its silicate counterpart. In general, the carbonate liquid was most strongly enriched in the alkaline earth metals (Ba and Sr). In contrast, the silicate liquid was found to be relatively enriched in HFSE.

To illustrate the extent of this LILE enrichment, Ba/Th, Ba/Zr and Ba/Hf ratios have been presented for a number of carbonate-silicate pairs in Table 9.3. Also shown are the exchange coefficients ($^{Ls/Lc}K_{D_{i/j}}$) for these ratios.

Table 9.3. Incompatible trace-element ratios in coexisting carbonate and silicate liquids. Relative LILE enrichment in the carbonate liquid. $^{Ls/Lc}K_{D_{Ba/Th}} = 0.01\text{-}0.08$. $^{Ls/Lc}K_{D_{Ba/Zr}} = 0.001\text{-}0.07$. $^{Ls/Lc}K_{D_{Ba/Hf}} \sim 0.01$. All three of these ratios are higher in the carbonate liquid by up to a factor of 1000. The variation in these ratios between experiments is believed to relate to the extent of mixing taking place in each composition.

Ratio	Composition	Ls	Lc	$^{Ls/Lc}K_D$
Ba/Th	Synthetic	0.73	26.04	0.03
	Synthetic	0.93	31.56	0.03
	BD50+CNC	56.82	7312	0.01
	BD50+CC	67.38	1667	0.04
	BD119+CNC	104.82	2138	0.05
	BD119+CC	114.88	1970	0.06
	SUN189+CNC	67.39	853	0.08
	SUN189+CC	87.08	1592	0.05
Ba/Zr	Synthetic	0.87	33.79	0.02
	Synthetic	1.00	41.79	0.02
	BD50+CNC	1.78	3062	0.001
	BD50+CC	2.20	160.83	0.01
	BD119+CNC	1.43	101.19	0.01
	BD119+CC	1.47	45.87	0.03
	SUN189+CNC	2.72	39.29	0.07
	SUN189+CC	3.17	88.96	0.04
Ba/Hf	Synthetic	0.27	20.57	0.01
	Synthetic	0.29	25.47	0.01

In all experiments, Ba/Th, Ba/Hf, and Ba/Zr are much higher in the carbonate liquid. The differences between ratios of LILE/HFSE in carbonate and silicate liquids is extreme. High LILE/HFSE ratios should therefore be a diagnostic feature of carbonate liquid involvement. Figure 9.1 shows how the recognition of carbonate liquid involvement should be possible on a graph of LILE/HFSE ratio *vs.* concentration of the HFSE. Carbonate liquids contain low concentrations of Th, Zr, Hf, etc. Addition of carbonate liquid will therefore not produce a substantial change in HFSE concentration. Variations in the concentration of elements like Th, Hf, and Zr in the same rock suite are therefore likely to be a measure of degree of partial melting. In contrast, the LILE/HFSE ratios will be greatly affected by addition of carbonate liquid. Any increase in LILE/HFSE without corresponding change in HFSE concentration may therefore be attributable to carbonate liquid involvement.

H_2O-rich fluid is also thought to be LILE enriched. It seems likely, however, that involvement of H_2O-rich fluid will result in strong enrichment in alkali metal concentrations (K, Rb, and Cs), but with less pronounced effects on Ba and Sr (Odling & Randle, 1992)). Distinction between these two styles of LILE enrichment should therefore be possible by study of the relative enrichments in Group I and Group II elements.

LILE are believed to have low solubilities in CO_2-rich fluid. LILE-enrichment in the mantle, and in mantle-derived melt, is therefore not attributable to involvement of CO_2-rich fluid.

9.3.2. LREE/HREE enrichment.

Table 3.4 shows La/Y and La/Lu ratios from a selection of experiments. In all cases, the carbonate liquid is relatively more LREE/HREE enriched than its silicate counterpart (Figure 9.2). La/Y in the carbonate liquid is 2.5-4 times larger than La/Y in the silicate liquid. La/Lu was only obtained from synthetic compositions, where it was found to be 4 times higher in the carbonate liquid than the silicate liquid. This partitioning behaviour is in agreement with the characteristics of naturally occurring carbonate magmas. Carbonatites are renowned for showing extreme LREE/HREE ratios (e.g. Cullers & Medaris; 1977, Woolley & Kempe, 1989).

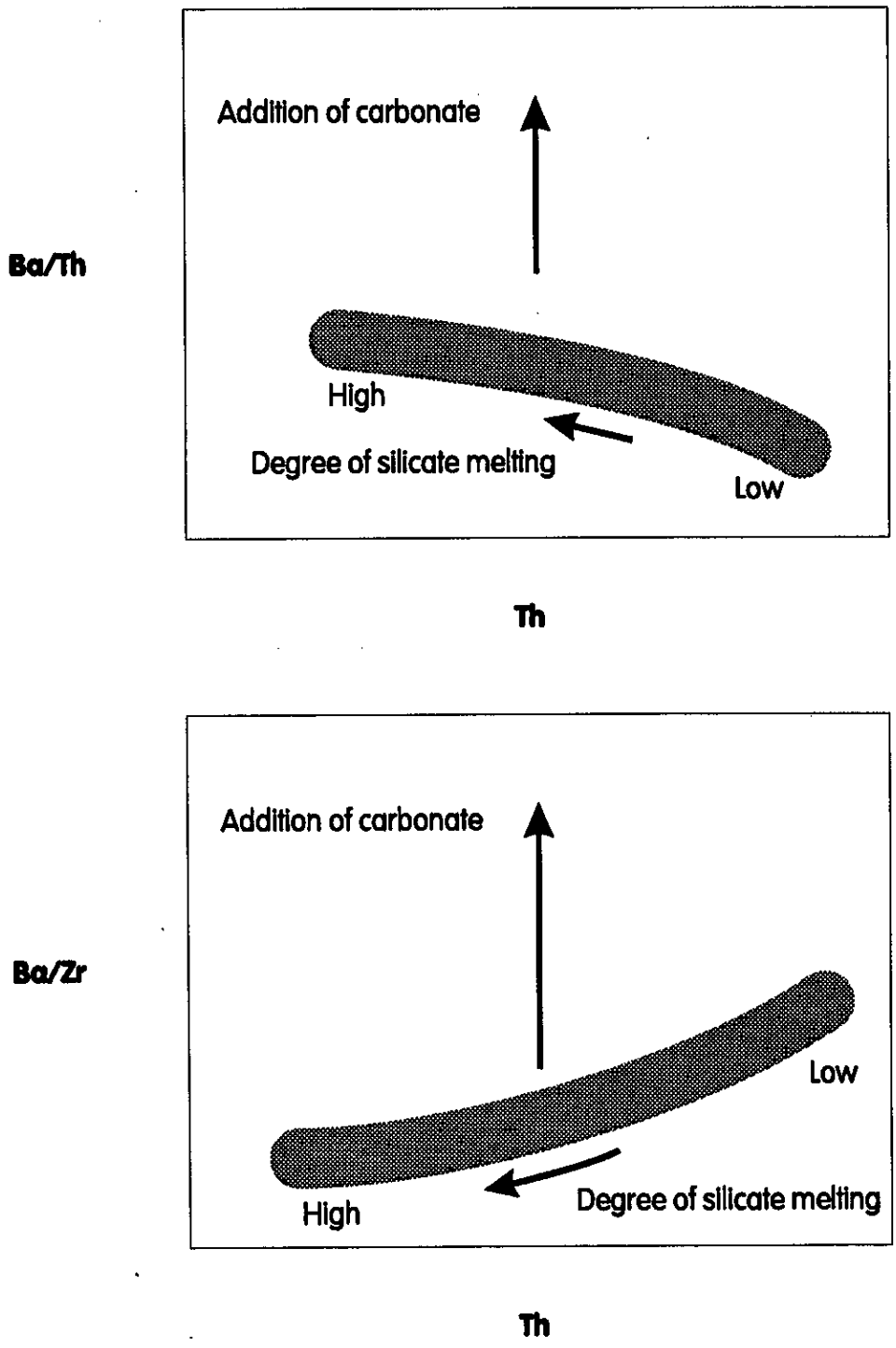

Figure 9.1. Schematic diagrams showing the likely geochemical effects of carbonate addition on ratios of LILE/HFSE. Ba/Th and Ba/Zr have been used as examples. The concentrations of Th, Zr, and Hf will be little affected by carbonate addition, and can therefore be interpreted as measures of degree of silicate partitial melting. Any ratio of incompatible elements should show a relationship with degree of melting. Deviations from this may be interpreted as addition of carbonate liquids.

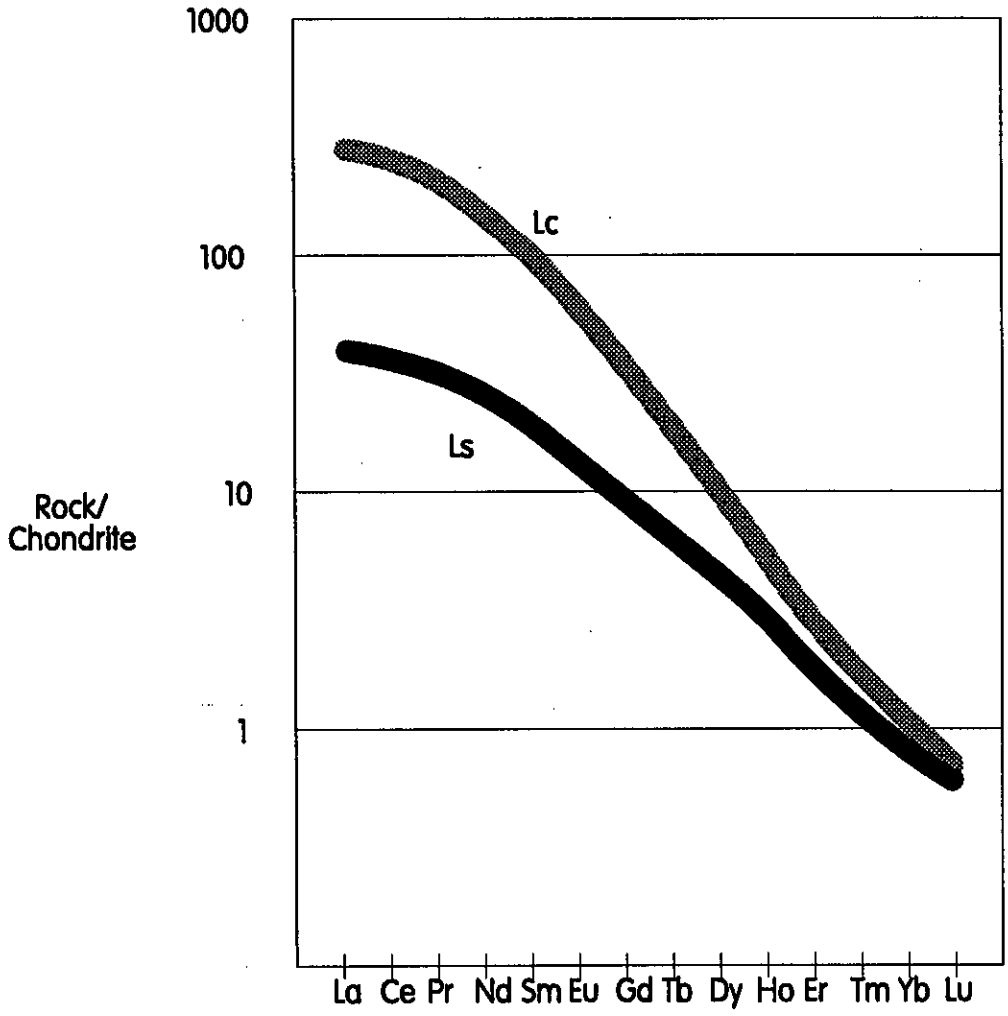

Figure 9.2. The effect of addition of carbonate liquid on REE patterns. The normalized REE concentrations are shown for coexisting carbonate and silicate liquid (BD119+CNC). Addition of carbonate liquid to natural silicate magmas will not significantly alter the concentrations of HREE, but will substantially increase the concentrations of LREE, producing a magma with more pronounced LREE/HREE enrichment.

Table 9.4. La/Y and La/Lu ratios in coexisting carbonate and silicate liquids.

Ratio	Composition	Ls	Lc	$^{Ls/Lc}K_D$
La/Y	Synthetic	0.94	3.03	0.31
	Synthetic	0.95	3.05	0.32
	BD50+CNC	3.88	15.71	0.25
	BD50+CC	3.96	8.90	0.44
	BD119+CNC	3.83	10.21	0.38
	BD119+CC	3.97	10.04	0.39
	SUN189+CNC	3.62	8.89	0.41
	SUN189+CC	3.80	10.09	0.38
La/Lu	Synthetic	0.84	3.65	0.23
	Synthetic	0.84	3.53	0.24

H_2O-rich fluid is also thought to be a possible cause of LREE/HREE enrichment. However, recent experiments have shown that the concentration of all REE in H_2O-rich fluid is low, making fluid an unlikely cause of LREE enrichment (Odling & Randle, 1992).

CO_2-rich fluid has been suggested as a possible agent of LREE enrichment (e.g. Wendlandt & Harrison, 1979). However, the experiments of Meen *et al.* (1989) suggest that REE have very low solubility in CO_2-rich fluid.

9.3.3. Fractionation of U and Th.

Th/U ratios from coexisting carbonate and silicate liquids are presented in Table 9.5. In all experiments studied, Th/U is substantially higher in the silicate liquid. $^{Ls/Lc}K_{D_{Th/U}} \sim 3$. This is perhaps surprising as U and Th are geochemically very similar, both forming +4 ions of *ca.* 108 pm in radius. One explanation for their differing behaviour is that uranium contains an extra two electrons in its outer shell, in excess to the 4 electrons lost to produce the tetravalent cation. These can be lost to produce the hexavalent uranyl ion (UO_2^{2+}) which is known to occur in many uranium minerals, and was suggested as a possible explanation of uranium behaviour in carbonates by Dawson & Gale (1970). The presence of UO_2^{2+} would imply reasonably oxidising conditions (e.g. Bäes, 1956; Adams *et al.*, 1959) similar to those

encountered in near surface weathering processes. Alternatively, the two extra electrons in the outer shell of the uranium atom can be used in the formation of tetravalent uranium complexes with carbonate and phosphate ions (e.g. McKelvey, 1956; Adams *et al.*, 1959). These complexes are stable under much more reducing conditions than UO_2^{2+}. Thorium atoms do not have the two extra electrons in the outer shell and are therefore unable to form similar complexes. For whatever reason, there is now much evidence that uranium can be included in carbonate structures, whilst thorium is rejected (e.g. Adams & Weaver, 1958). Involvement of carbonate liquid in mantle processes would therefore be expected to result in low Th/U ratios.

Table 9.5. Th/U ratios of coexisting carbonate and silicate liquids.

Ratio	Composition	Ls	Lc	$^{Ls/Lc}K_D$
Th/U	Synthetic	0.97	0.30	3.2
	Synthetic	0.76	0.32	2.4
	BD50+CNC	4.64	0.95	4.9
	BD50+CC	4.57	1.20	3.8
	BD119+CNC	2.24	0.70	3.2
	BD119+CC	2.27	0.94	2.4
	SUN189+CNC	7.26	2.41	3.0
	SUN189+CC	7.25	2.25	3.2

This partitioning behaviour is in agreement with evidence from carbonatites. Th/U ratios are only known for a few carbonatite occurrences. These include the Oldoinyo L'engai volcano (Dawson & Gale, 1970), Kaiserstuhl, Germany, (Verfaille, 1966), and the Benfontein sill, South Africa (Dawson & Hawthorne, 1973). Data from the carbonatites and associated silicate rocks are given in Table 9.6. In all cases, Th/U is lower in the carbonatites than in the associated igneous rocks. Indeed, some of the carbonatites show Th/U < 1. These are the only igneous rocks with this characteristic.

Table 9.6. Th/U in carbonatites and associated igneous rocks.

Locality	Rock type	Average Th/U ratio
Oldoinyo Lengai, Tanzania.	Phonolite	4.4
(Dawson & Gale, 1970)	Nephelinite	2.0
	Lengaiite	0.4
Kaiserstuhl, Germany.	Essexite	3.4
(Verfaille, 1966)	Phonolite	3.2
	Carbonatite (Dikes)	0.8
	Carbonatite (All)	1.8
Benfontein, South Africa.	Kimberlite	4-5
(Dawson & Hawthorne, 1973)	Carbonatite	<1

9.3.4. Fractionation of Zr and Hf.

As was mentioned in Chapter 7, Zr and Hf partitioning between carbonate and silicate liquids was expected to be identical due to similar ionic charge and size. This was not found to be the case, with Hf always being more strongly partitioned to the silicate liquid than Zr. Table 9.7 shows the Zr/Hf ratios of coexisting carbonate and silicate liquids in the synthetic experiments. Hf partitioning data from the natural experiments were considered unreliable due to low concentrations in the carbonate liquid.

Table 9.7. Zr/Hf ratios of coexisting carbonate and silicate liquids. Due to analytical difficulties in experimental charges with natural concentration levels of hafnium, the relative partitioning of Zr and Hf is only quoted from synthetic experiments.

Ratio	Composition	Ls	Lc	$^{Ls/Lc}K_D$
Zr/Hf	Synthetic	0.31	0.61	0.51
	Synthetic	0.29	0.61	0.48
	Synthetic	0.28	0.60	0.47
	Synthetic	0.29	0.61	0.47

Zr/Hf is always higher in the carbonate liquid than in the corresponding silicate liquid. $^{Ls/Lc}K_{D_{Zr/Hf}} \sim 0.5$. Although small when compared to other fractionation effects seen between immiscible carbonate and silicate melts, this effect is considered significant, since Zr and Hf are believed to behave identically in most other geological processes. Involvement of carbonate liquid is therefore one of the few processes by which variations in Zr/Hf ratio can be produced. There are several lines of evidence which support the conclusion reached from these experiments that carbonate involvement will separate Zr from Hf:

(a) High Zr/Hf ratios in zircons from alkaline complexes. Rocks believed to be associated with carbonatites often contain zircons with high Zr/Hf (Fleischer, 1955).

(b) High Zr/Hf ratios in carbonatites. Although the data is scarce, recorded Zr/Hf ratios from carbonatites are extremely high, often >100 (e.g. Gerlach *et al.*, 1988; Woolley & Kempe, 1989).

(c) Zr/Hf separation in fish debris. Although obviously referring to a different geological situation, in fish debris, Hf is found concentrated in Fe-Mn oxides, whilst Zr complexes with CO_3^{2-}, and PO_4^{2-} in carbonate-fluorapatite (Tlig, 1988).

(d) The experiments of Bedson (1983) where, although Hf values were doubted due to analytical difficulties, Zr/Hf ratios were considerably higher in the carbonate liquid of immiscible carbonate-silicate pairs.

9.3.5. Fractionation of Nb from Ta.

As with Zr and Hf, it was expected that Nb and Ta would show similar partitioning behaviour between carbonate and silicate liquids due to their similar geochemistry. Again this was found not to be the case. Table 9.8 shows Nb/Ta ratios from coexisting carbonate and silicate liquids produced in this study. In all cases Nb/Ta is higher in the carbonate liquid. $^{Ls/Lc}K_{D_{Nb/Ta}} \sim 0.4$. This is again thought to be a significant feature of carbonate involvement, as Ta and Nb behave similarly in most geochemical processes. Evidence that carbonate involvement does indeed separate Nb from Ta comes from high Nb/Ta in carbonatites (Woolley & Kempe, 1989), and from high Nb/Ta ratios in pyrochlores in carbonatites and associated igneous rocks (Parker & Fleischer, 1968). Involvement of carbonate liquid would therefore be expected to result in high Nb/Ta ratios.

Table 9.8. Nb/Ta ratios in coexisting carbonate and silicate liquids. $^{Ls/Lc}K_{D_{Nb/Ta}}$ is always less than 1. Nb is relatively enriched over Ta in the carbonate liquid.

Ratio	Composition	Ls	Lc	$^{Ls/Lc}K_D$
Nb/Ta	Synthetic	0.60	1.73	0.35
	Synthetic	0.59	1.88	0.31
	BD50+CNC	37.12	203	0.18
	BD50+CC	31.17	70	0.44
	BD119+CNC	90.64	177	0.51
	BD119+CC	100.68	228	0.44
	SUN189+CNC	17.67	45.40	0.39
	SUN189+CC	20.89	45.88	0.45

9.3.5. Enrichment of extreme high charge density ions in the carbonate liquid.

A number of extremely high charge density ions are enriched in the carbonate liquid. These include P, V, Mo and to a certain extent Nb and Ta. Table 9.9 shows that Ti/V ratios in the coexisting carbonate liquids are always lower than their silicate counterparts. Ti/V and Ti/P could also be diagnostic of carbonate involvement. It is believed that the partitioning of molybdenum may also be a diagnostic feature of carbonate liquid involvement; preliminary work suggests that nephelinites which are thought to have exsolved a carbonatitic liquid contain significantly lower Mo contents than those where the carbonate components have been retained (D. James, J.G. Fitton, Pers. Comm. 1992). Certainly, evidence exists for extreme enrichment of Mo in carbonatites, with concentrations to 100 ppm (Gold, 1963; Deans, 1966). It is expected that Mo concentrations will be good indicators of involvement of carbonate liquid in petrogenesis as more Mo data are obtained.

Table 9.9. Ti/V ratios in coexisting carbonate and silicate liquids.

Ratio	Composition	Ls	Lc	$^{Ls/Lc}K_D$
Ti/V	Synthetic	1.28	0.35	3.7
	Synthetic	1.07	0.29	3.5
	BD50+CNC	74.00	13.86	5.3
	BD50+CC	74.67	11.14	6.7
	BD119+CNC	35.47	5.99	5.9
	BD119+CC	42.55	8.78	4.9
	SUN189+CNC	64.68	12.93	5.0
	SUN189+CC	60.67	11.31	5.4

9.4. Isotopic characteristics.

Carbonate liquids have characteristic ratios of elements involved in radioactive decay series. Introduction of carbonate to mantle material will result in these ratios being inherited and this will lead, with time, to the formation of distinctive isotopic ratios in the material. Whatever processes operate subsequently, evidence of this carbonate involvement should be preserved in the form of a characteristic isotopic signature. In addition, the actual process of melting of the mantle to produce carbonate liquid, and of immiscible separation of a carbonate liquid from a silicate parent will cause fractionation of parent and daughter atoms in isotopic decay series', and will therefore result in isotopic disequilibrium. Isotopic disequilibrium studies can therefore also be influenced by carbonate liquid involvement.

9.4.1. The effect of carbonate liquid involvement on $^{87}Sr/^{86}Sr$ ratios.

In all the natural compositions studied, and in the synthetic compositions containing phosphorus, the Rb/Sr ratio of the carbonate liquid is lower than in the coexisting silicate liquid (Table 9.10).

Table 9.10. Rb/Sr ratios in coexisting carbonate and silicate liquids.
Rb/Sr ratios from synthetic compositions are taken from experiments containing 2% (*) and 8% (**) phosphorus.

Ratio	Composition	Ls	Lc	$^{Ls/Lc}K_D$
Rb/Sr	Synthetic*	0.49	0.32	1.5
	Synthetic**	0.64	0.21	3.0
	BD50+CNC	0.09	0.02	4.5
	BD50+CC	0.06	0.02	3.0
	BD119+CNC	0.05	0.03	1.7
	BD119+CC	0.05	0.03	1.7
	SUN189+CNC	0.08	0.05	1.6
	SUN189+CC	0.07	0.05	1.4

On addition of this carbonate liquid to silicate material, this characteristic low Rb/Sr will be inherited by the product. This feature will be accentuated by the fact that on solidification of the carbonate liquid, all the Sr will be added to the crystalline material in calcite, whilst much of the Rb may be lost in an H_2O-CO_2 fluid phase.

With time, as there will be less ^{87}Rb to decay to ^{87}Sr, this will lead to relatively low $^{87}Sr/^{86}Sr$ ratio compared to that caused by addition of a small volume silicate liquid. This is exactly the opposite of the effect of addition of H_2O-rich fluid to silicate material. H_2O-rich fluid is likely to contain substantial Rb, but little Sr (e.g. Odling & Randle, 1992). This will lead to a relatively high Rb/Sr ratio in the product, and thus high $^{87}Sr/^{86}Sr$ with time.

9.4.2. The effect of carbonate liquid involvement on $^{144}Nd/^{143}Nd$ ratios.

In all the experiments studied, the carbonate liquid of an immiscible liquid pair is always more LREE/HREE enriched than its conjugate silicate liquid. This implies that Sm/Nd in the carbonate liquid is lower than that in the silicate liquid. Addition of such a LREE-enriched carbonate melt to silicate material will thus result in lower Sm/Nd in the product. In time, due to the production of less ^{143}Nd from less ^{147}Sm, a low $^{143}Nd/^{144}Nd$ ratio will develop. Again, this is different to the likely effects of addition of H_2O- or CO_2-rich fluid. As has been discussed, these fluids have only low solubilities of REE, and will therefore have little effect on $^{143}Nd/^{144}Nd$ ratios.

Figure 9.3 is a Sr-Nd isotope diagram showing the likely results of addition of carbonate liquid, low-degree silicate melt, and H_2O-rich fluid to silicate material. As can be seen, the effects of each of these metasomatic agents is distinct. This type of diagram should therefore be useful in distinguishing material which has been influenced by carbonate liquid at some time in its history.

9.4.3. The effects of carbonate addition on Pb-isotope ratios.

Table 9.11 shows U/Pb, and Th/Pb ratios for coexisting carbonate and silicate liquids produced in this study. Despite the large uncertainties on the Pb data, it is clear that U/Pb, and especially Th/Pb ratios are always lower in the conjugate carbonate liquid. Addition of this carbonate liquid to mantle material will therefore result in the inheritance of these low U/Pb and Th/Pb ratios. With time, unradiogenic Pb-isotope signatures will be produced; i.e. the relative depletion in U and Th will result in the formation of less ^{208}Pb, ^{207}Pb and ^{206}Pb with time. The resulting product of enrichment by carbonate liquid would therefore have low $^{208}Pb/^{204}Pb$, $^{207}Pb/^{204}Pb$, and $^{206}Pb/^{204}Pb$ ratios (Figure 9.4).

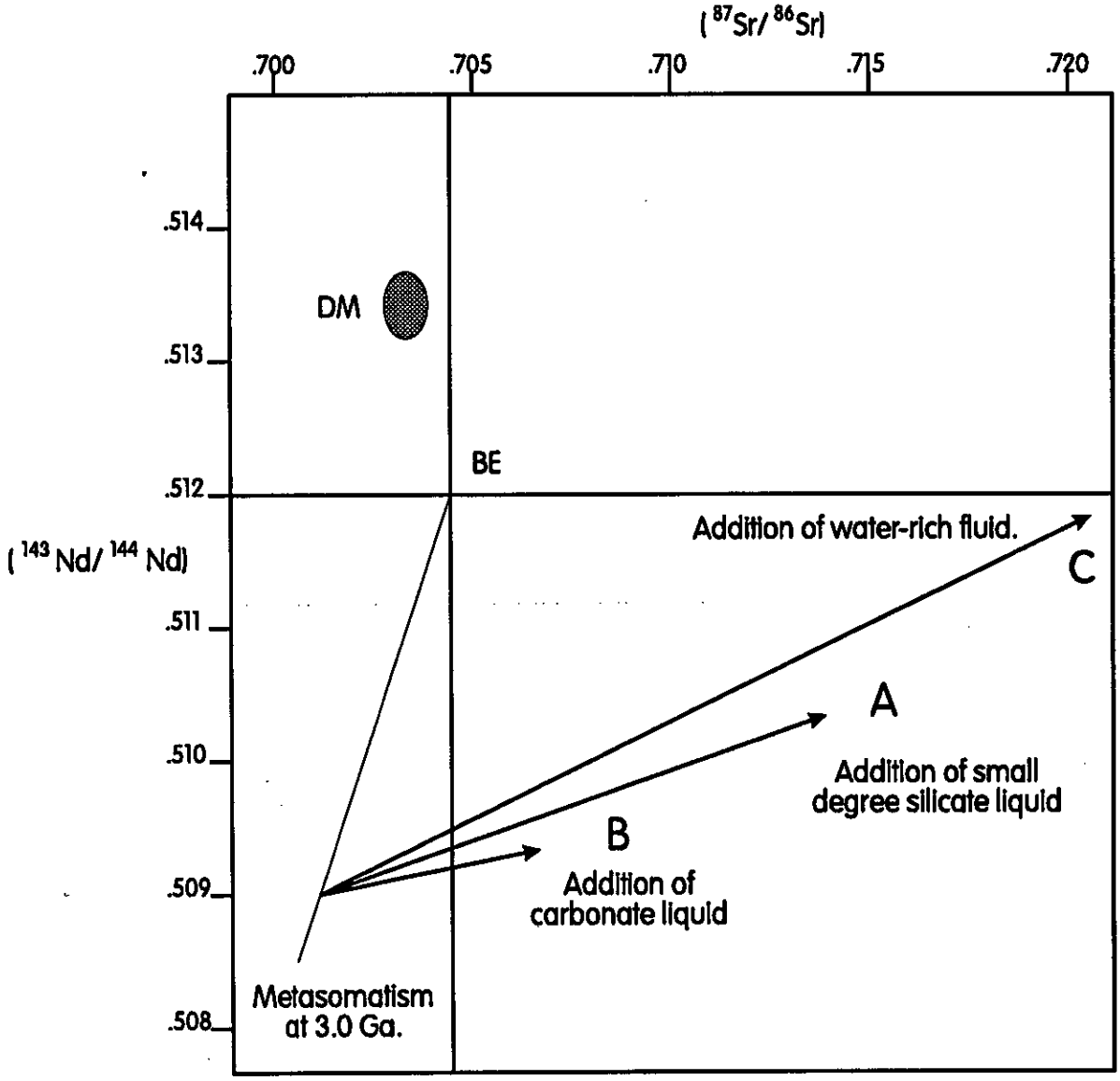

Figure 9.3. Effects of carbonate liquid addition on Sr-Nd isotope systematics. Addition of a trace-element rich fluid to mantle material results in significant changes to parent-daughter ratios. Addition of low degree mantle silicate melts is believed to lead to high Rb/Sr, and low Sm/Nd. With time, this will lead to trend A, commonly refered to as the mantle array. Addition of carbonate melt will have a profoundly different effect, resulting in less increase in Rb/Sr ratio, and even lower Sm/Nd. With time, this will give rise to trend B. In contrast, the addition of water-rich fluids will produce very high Rb/Sr, but have much less effect on Sm/Nd, resulting in trend C. Sr-Nd isotope ratio diagrams of this type should therefore be useful indicators as to the style of trace-element enrichment which has taken place. Trends A, B, and C are calculated from metasomatism of mantle of composition near Bulk Earth (BE) at 3.0 Ga. Silicate liquid has Rb/Sr = 0.3, (La/Yb)n = 20. Carbonate liquid has Rb/Sr = 0.1, (La/Yb)n = 100. Water rich fluid has Rb/Sr = 0.5, but due to low REE solubility, has little effect on Sm/Nd ratio despite being LREE/HREE enriched.

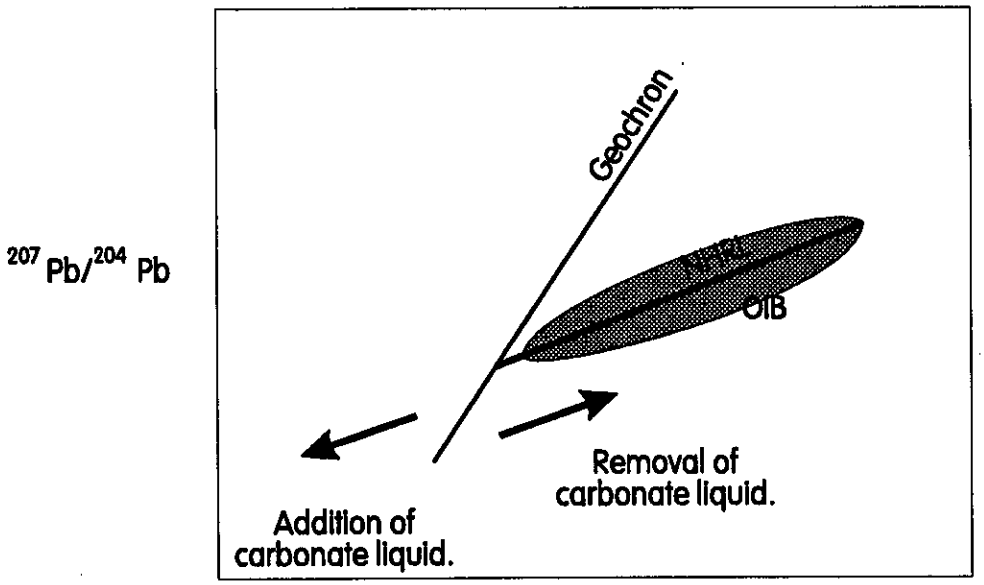

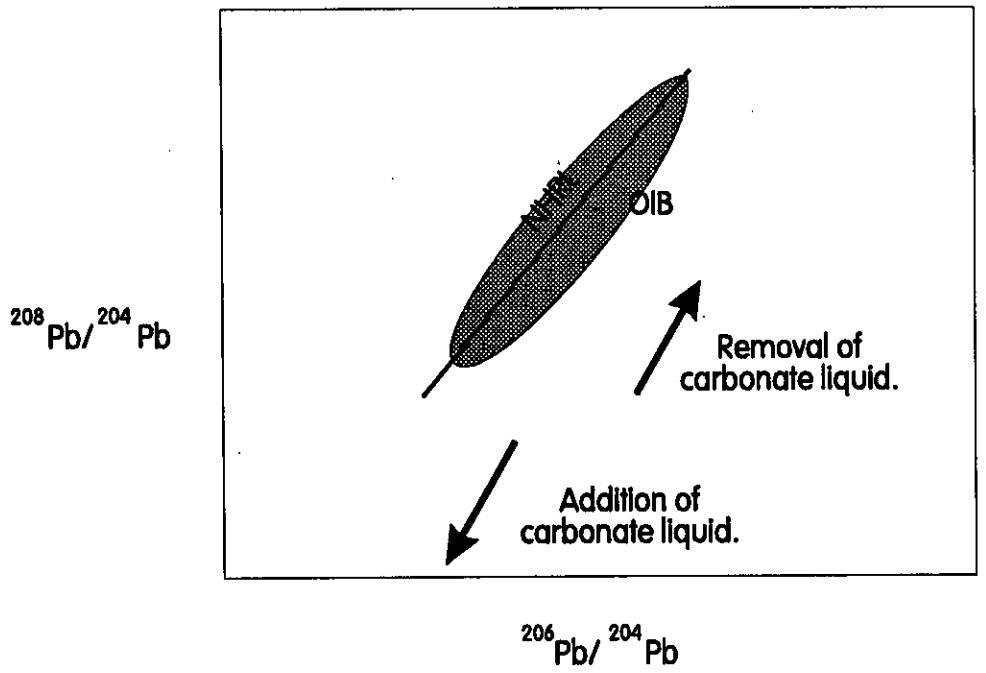

Figure 9.4. Effects of carbonate addition on lead isotope systematics. Carbonate liquid is relatively enriched in Pb, and depleted in U and Th. With time, this will lead to low $^{207}Pb/^{204}Pb$, $^{206}Pb/^{204}Pb$, and especially $^{208}Pb/^{204}Pb$.

Table 9.11. U/Pb and Th/Pb ratios in coexisting carbonate and silicate liquids.

Ratio	Composition	Ls	Lc	$^{Ls/Lc}K_D$
U/Pb	Synthetic	8.45	2.43	3.5
	Synthetic	5.97	1.89	3.2
	BD50+CNC	1.54	0.11	14.0
	BD50+CC	0.36	0.08	4.5
	BD119+CNC	0.76	0.10	7.6
	BD119+CC	0.37	0.10	3.7
	SUN189+CNC	0.20	0.07	2.9
	SUN189+CC	0.29	0.05	5.8
Th/Pb	Synthetic	8.19	0.72	11
	Synthetic	4.54	0.60	7.6
	BD50+CNC	7.06	0.11	64
	BD50+CC	1.65	0.10	17
	BD119+CNC	1.74	0.07	25
	BD119+CC	0.84	0.10	8.4
	SUN189+CNC	1.42	0.16	8.9
	SUN189+CC	2.06	0.14	15

9.4.4. The effects of carbonate liquid involvement on U-series isotopic disequilibrium studies.

On production and segregation of carbonate melt, element fractionations will occur that will produce disequilibrium between the relative amounts of nuclides in the uranium-series isotopic decay scheme. These disequilibrium features will themselves decay with time as equilibrium is re-established, the rate of decay depending on the decay constants of the isotopes involved.

Two main fractionations produced by carbonate-silicate equilibria are likely to effect U-series disequilibrium studies:

(a) Fractionation of U from Th.

Due to fractionation of U from Th during carbonate melting of the mantle, addition of a carbonate melt will lead to a relative input of unsupported ^{238}U (i.e. the ^{238}U will be added in much larger quantities than its daughter atom ^{230}Th). This will lead to samples falling to the right of the equiline on a diagram of $(^{230}Th)/(^{232}Th)$ vs. $(^{238}U)/(^{232}Th)$ (see Figure 9.5a).

In contrast, removal of a carbonate liquid will result in an excess of ^{230}Th over ^{238}U in the residual material. This will result in samples falling to the left of the equiline of Figure 9.5a

(b) Fractionation of Ra from U and Th.

Radium is likely to partition strongly to the carbonate liquid (see Chapters 7 and 8). Addition of carbonate liquid will therefore result in an excess of ^{226}Ra over both ^{230}Th and ^{238}U. Figure 9.5b shows the likely effects of carbonate addition or removal on a diagram of $(^{226}Ra)/(^{238}U)$ Vs $(^{230}Th)/(^{238}U)$. It must be pointed out that decay of ^{226}Ra is rapid, and that such disequilibrium would therefore be short-lived (less than 10,000 years, Williams & Gill, 1989).

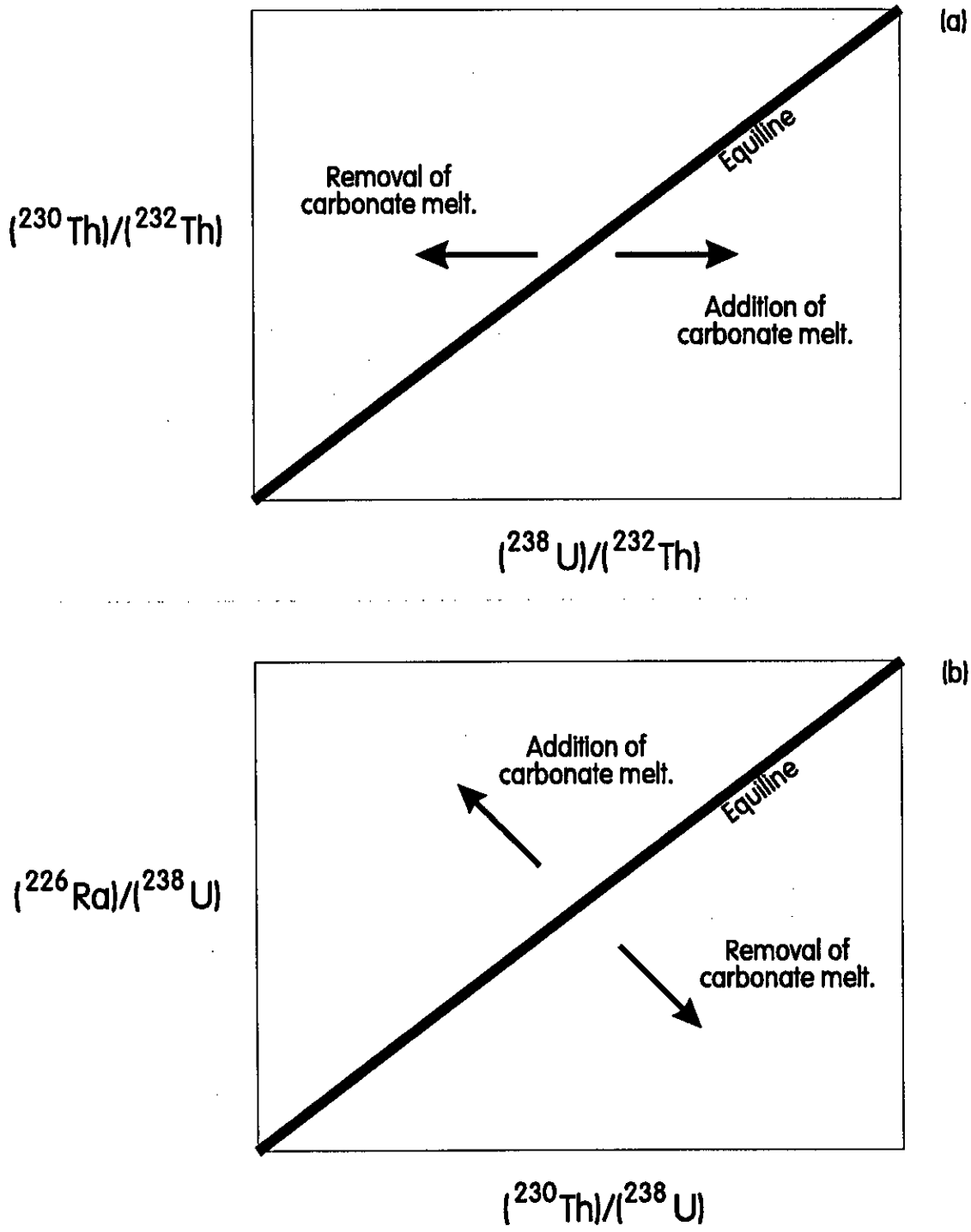

Figure 9.5. Effects of carbonate involvement on the uranium-series isotopic decay scheme.
(a) Carbonate liquid is relatively enriched in U over Th. Addition of carbonate liquid will therefore lead to unsupported ^{238}U
(b) Carbonate liquid is enriched in Ra. Addition of carbonate liquid will therefore lead to excess ^{226}Ra.

9.5. Conclusions.

The involvement of carbonate liquids in mantle processes will result in the inheritance of a number of geochemical characteristics. These include major-element, trace-element and isotopic effects. Comparison of these geochemical characteristics with those of other fugitive agents that may be present in the mantle shows that many of these features are unique to carbonate melts. These characteristics can thus be used to diagnose instances of carbonate melt involvement. This will constrain the possible extent of control of element partitioning in mantle processes by carbonate-silicate equilibria.

CHAPTER 10

IMPLICATIONS OF CARBONATE-SILICATE PARTITIONING TO CARBONATITE GENESIS AND EVOLUTION.

10.1. The origins of carbonatites.

One area where carbonate-silicate partitioning behaviour will be of considerable importance is in understanding the petrogenetic processes which lead to the formation of carbonatite magmas; carbonate-silicate equilibria are important controls in all currently held theories of carbonatite genesis.

There are many views as to the origin of carbonatites. These views are based on a wealth of petrological, experimental and geochemical evidence. This evidence will be discussed, and reassessed in the light of carbonate-silicate partitioning behaviour investigated in this study.

10.1.1. Petrological evidence for the origins of carbonatites (Figure 10.1).

Current theories of carbonatite petrogenesis which gain most attention in the literature are:

(a) Production of primary carbonatitic liquids by mantle melting followed by rapid ascent to the surface (e.g. Reid *et al.*, 1975; Bailey, 1989).

(b) Differentiation of carbonated silicate liquids, producing carbonatitic residual melts (e.g. Dawson & Hawthorne, 1973; Jones & Wyllie, 1985).

(c) Production of carbonatitic liquids by immiscible separation from carbonated silicate melt (e.g. Kjarsgaard & Peterson, 1991).

After production of the carbonatitic liquid by one of the above processes, numerous mechanisms exist for fractionating this liquid to produce the wide range of carbonatite rock compositions seen at the Earth's surface (e.g. Le Bas, 1989). There is much petrographic evidence for the operation of all three of these processes; the references cited above provide convincing examples of carbonatites formed by each process, but what of the vast majority of carbonatites, where petrographic evidence is more scarce?

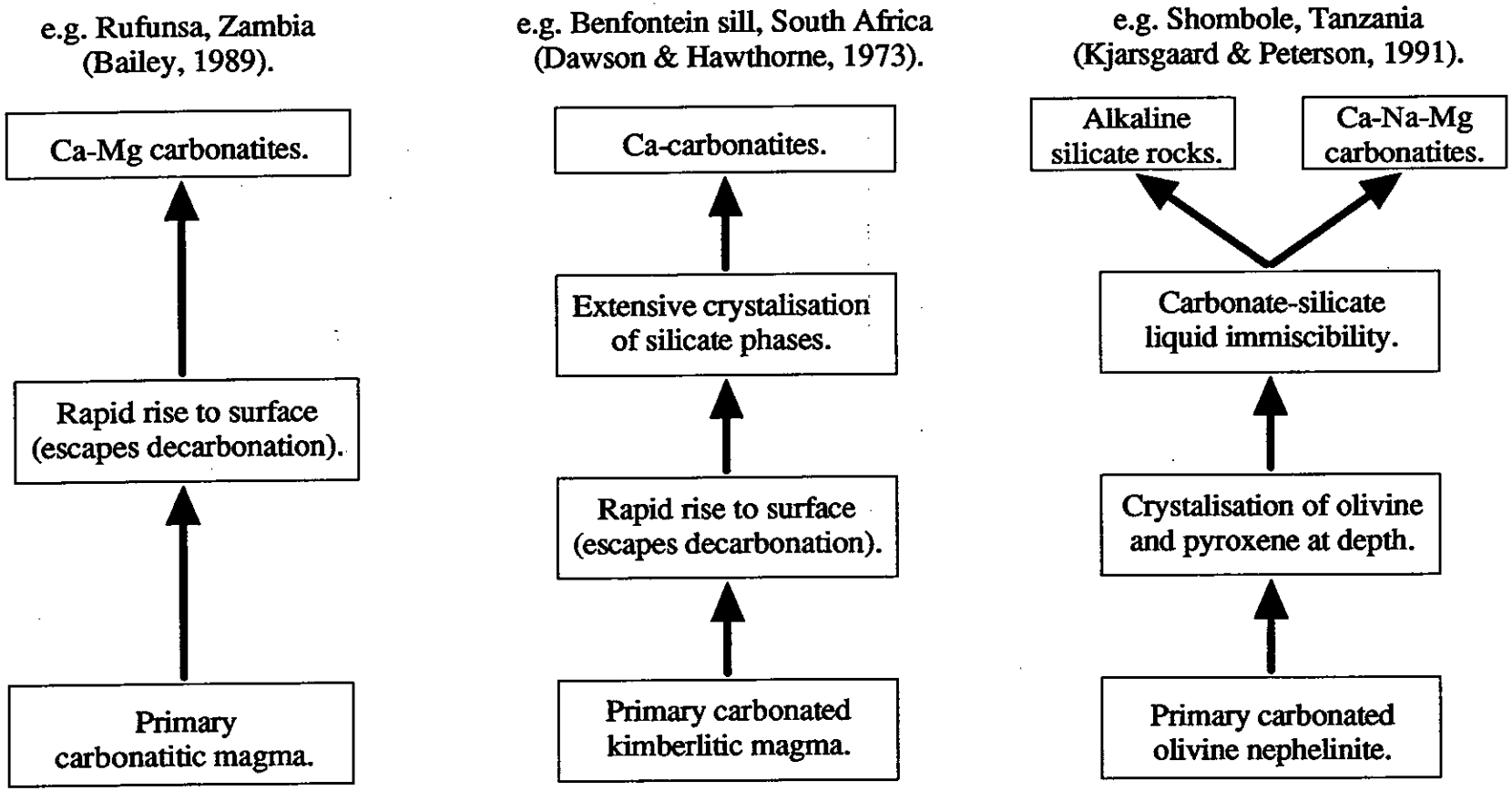

Figure 10.1. Mechanisms of carbonatite formation. From petrographic, experimental, and geochemical studies, it is becoming clear that carbonatites can be produced by a number of petrogenetic processes. Three possible methods of carbonatite genesis are mentioned here, together with suggested African examples.

(a) Production as primary mantle melts.
(b) Production by differentiation of carbonated silicate magma.
(c) Production by liquid immiscibility.

10.1.2. Experimental evidence for the origins of carbonatites.

A sizeable body of experimental evidence is also now available to aid in this discussion. Recent investigations into the phase relations of carbonated mantle peridotite have shown that carbonatitic liquids will be formed by melting of carbonated mantle at ca. 1000-1200°C, at any depth greater than 70 km (Wendlandt & Mysen, 1980; Olafsson & Eggler, 1983; Wallace & Green, 1988; Falloon & Green, 1989; Falloon & Green, 1990; Thibault *et al.*, 1992). Experimental evidence suggests that these carbonatitic liquids would be highly magnesian, and moderately alkali-rich. Fractionation of these liquids could then lead to the production of a wide range of carbonatite compositions (see Le Bas, 1989). Experimental evidence suggests that a large number of carbonatites could therefore be produced as primary melts of carbonated mantle peridotite.

A number of experiments undertaken recently have shown that high-pressure crystallisation of carbonated silicate magmas will also lead to the production of carbonatitic residual liquids. For example, experiments undertaken in this study on olivine melilitite-carbonate and olivine nephelinite-carbonate compositions between 0.25 and 3.0 GPa. produced calcium-rich carbonatitic quench as an interstitial phase. It seems unlikely that highly magnesian liquids could be produced as late-stage residual melts where the crystallising minerals are likely to be olivine, clinopyroxene etc. However, enrichment in both calcium, iron and alkalis in residual melts is to be expected. The range of Ca-Na-Fe carbonatites seen at the Earth's surface could therefore plausibly be produced by crystal fractionation of carbonated silicate melts.

Finally, experimental evidence is now accumulating which suggests that carbonate-silicate immiscibility could be a more widespread phenomenon than previously thought. Freestone & Hamilton's experiments showed that liquid immiscibility could be responsible for the production of very sodic carbonatite liquids similar to those seen at Oldoinyo Lengai, Tanzania (Freestone & Hamilton, 1980). They suggested, however, that the far more common Ca-Mg-Fe carbonatites could not be produced by this mechanism. This sparked off a number of investigations into the possibility of alkali-loss from carbonatites during crystallisation, and the belief that all carbonate liquids were originally extremely alkali-rich (e.g. Gittins & McKie, 1980). Kjarsgaard & Hamilton (1988) showed that more calcic carbonate liquids could indeed be produced by immiscibility in synthetic experiments on the joins albite-$CaCO_3$ and anorthite-$CaCO_3$. This study has reinforced that conclusion by producing

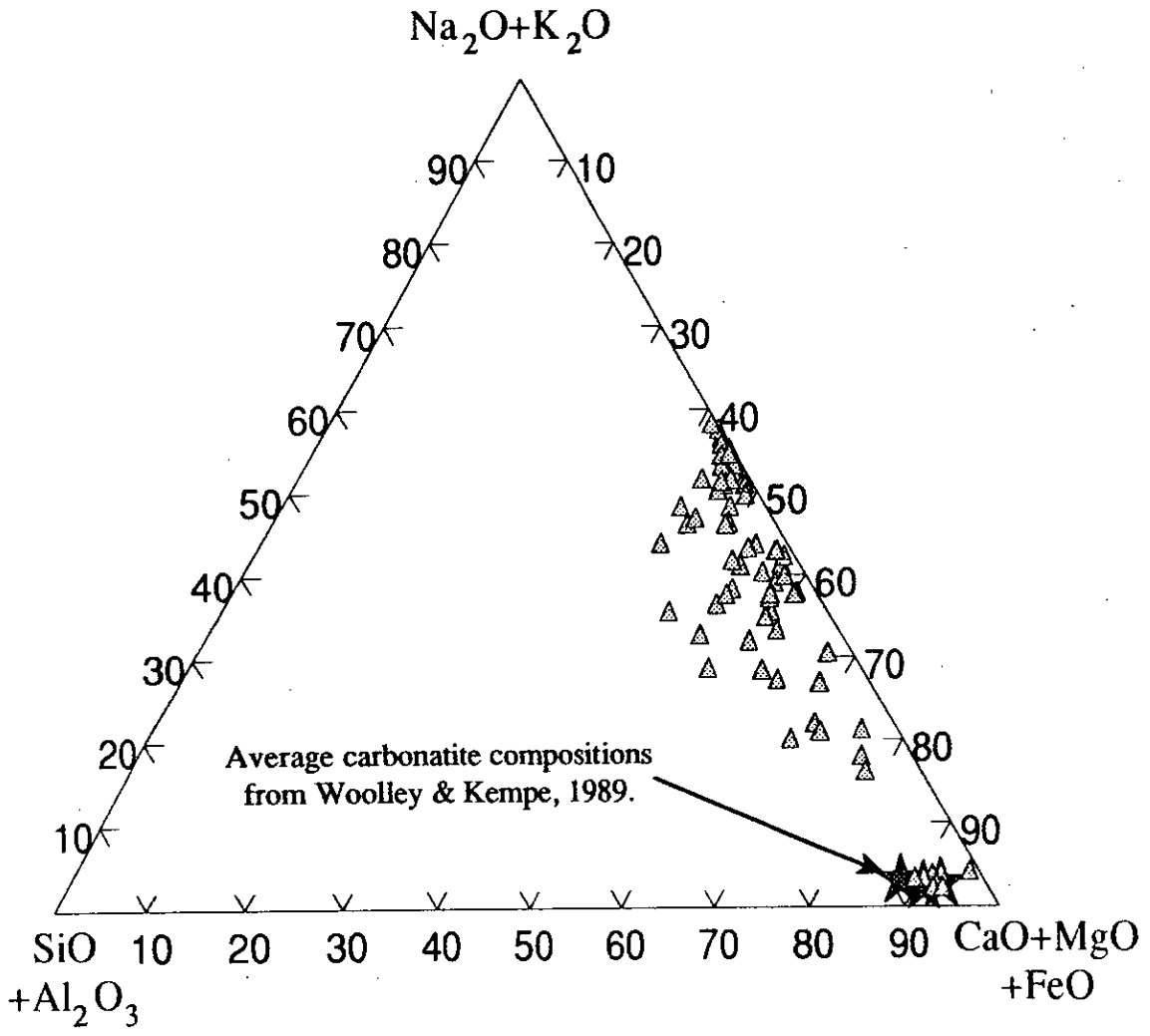

Figure 10.2. The range of compositions of carbonatites that may be produced by immiscibility. Conjugate carbonate liquids in equilibrium with natural silicate rock compositions span a very wide range of major-element composition. Only magnesian (> 5%MgO) carbonatites have yet to be produced by liquid immiscibility.

calcic carbonate liquids in equilibrium with conjugate nephelinitic liquids in *natural* systems. A number of these sodium-poor carbonatitic liquids were also found to contain sizeable contents of magnesium and iron (up to 4.5 wt. % MgO in the carbonate liquids coexisting with olivine nephelinite SUN189). Figure 10.2 shows all the compositions of carbonate liquids obtained by immiscible separation from natural olivine nephelinitic, nephelinitic and phonolitic liquids. It is clear that a very wide range of carbonatitic melt compositions can be produced by carbonate-silicate immiscibility. This range encompasses most of the bulk compositions of naturally occurring carbonatites. Again, highly magnesian carbonate liquids have yet to be produced experimentally by operation of liquid immiscibility. This may imply that many magnesiocarbonatites are not formed in this way.

In summary, it is now clear from recent experimental studies that carbonatites *can* be produced as primary melts from mantle peridotite, as differentiates from carbonated silicate melts, and by immiscible separation from carbonated silicate melt. We must now turn to geochemistry to distinguish between the actions of these three processes.

10.1.3. Geochemical evidence for the origins of carbonatites.

Clearly, carbonatites produced by primary mantle melting, immiscibility, and fractionation should have distinctly different geochemical characteristics. In this section, it is hoped that the origins of a number of carbonatite occurrences can be confirmed by investigation of these features.

(a) Oldoinyo Lengai, Tanzania:- the classic example of carbonatite formation by liquid immiscibility.

The suggestion that the carbonate and silicate lavas extruded from the Oldoinyo Lengai volcano are related by liquid immiscibility has been advocated by many authors (e.g. Freestone & Hamilton, 1980). A wealth of evidence has now been accumulated in support of this suggestion. Gerasimovskiy *et al.* (1972) investigated the REE contents of carbonate and silicate lavas at Oldoinyo Lengai. From these data, bulk rock $^{Ls/Lc}D_{REE}$ can be obtained. These are presented in Table 10.1.a, together with experimentally determined $^{Ls/Lc}D_{REE}$ from this study, and from Bedson (1983) and Hamilton *et al.* (1989). The data has been plotted against ionic size in Figure 10.3. It can be seen that liquid immiscibility adequately explains the distribution of REE seen at Oldoinyo Lengai. The agreement between partitioning data and element distribution is also good for most other elements

Table 10.1. Evidence for carbonate-silicate liquid immiscibility at Oldoinyo Lengai, Tanzania. (a) $^{La/Lc}D_{REE}$ partition coefficients between the phonolite and carbonatite lavas of Oldoinyo Lengai using the data of Gerasimovskiy *et al.* (1972). These bear close resemblance to the experimental determinations of $^{La/Lc}D_{REE}$ from both this study, and Hamilton *et al.* (1989). (b) Estimates of $^{La/Lc}D_{Pb}$, $^{La/Lc}D_{Th}$, $^{La/Lc}D_{U}$, and $^{La/Lc}D_{Ra}$ from Pyle *et al.* (1991) also bear close resemblance to partitioning seen in these experiments.

(a)

REE	$^{Ls/Lc}D_{REE}$ Gerasimovskiy *et al.*, 1972	$^{Ls/Lc}D_{REE}$ Fielding, this study (0.8 GPa, 1200°C)	$^{Ls/Lc}D_{REE}$ Hamilton *et al.* (1989) (0.3 GPa, 1050°C)
La	0.18	0.21	0.25
Ce	0.3	0.26	0.40
Pr	0.31		
Nd	0.32	0.33	0.42
Sm	0.35	0.33	0.48
Gd	0.4		
Dy	0.6		
Ho (Y)	0.8	0.98	
Yb	1.1		1.2

(b)

	Fielding (this study)			Pyle *et al.* (1991)		
$^{Ls/Lc}D_i$	Phonolite +CNC	Nephelinite +CNC	Bulk D from U-Th disequilibria	Phonolite	Phonolitic-nephelinite	Nephelinite
$^{Ls/Lc}D_{Pb}$	0.35	0.50	D(Pb)	0.27-0.36	0.31-0.41	0.25-0.33
$^{Ls/Lc}D_{Th}$	11.45	8.46	D(Th)	9-16	6-10	4-7
$^{Ls/Lc}D_{U}$	2.05	2.26	D(U)	0.6-0.9	0.5-0.7	0.8-1.2
$^{Ls/Lc}D_{Ra}$	<0.1	<0.1	D(Ra)	<0.01	<0.01	<0.01

An opportunity has recently arisen in which the origin of the Oldoinyo Lengai phonolites and carbonatites by immiscibility can be confirmed. Williams *et al.* (1986) discovered that Oldoinyo Lengai lavas showed severe U-Th isotopic disequilibrium, with extreme deficiencies in ^{230}Th in the carbonatites. This feature

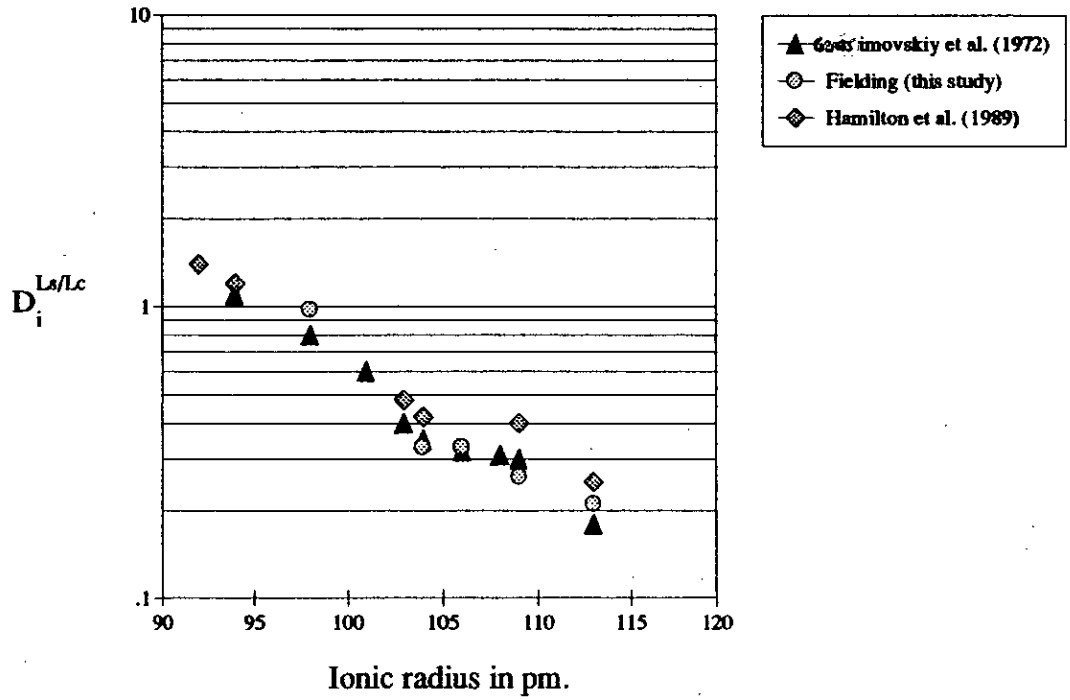

Figure 10.3. Evidence for immiscibility at Oldoinyo Lengai from REE partitioning between lengaiite and phonolite (Garasimovskiy *et al.*, 1972). $^{Ls/Lc}D_{REE}$ data from experiments reported here and by Hamilton *et al.* (1989) accurately reproduce the partitioning behaviour seen at Oldoinyo Lengai. Data from this study are taken from a run of BD50+CNC at 1200° C, 0.8 GPa. Data from Hamilton *et al.* (1989) is at 1050 °C, 0.3 GPa.

can be explained by the disparate partitioning behaviour of uranium and thorium between carbonate and silicate liquids seen in the experiments undertaken in this study. Pyle *et al.* (1991) used U-Th disequilibrium systematics in order to constrain the partitioning of U, Th, Pb, and Ra that would have had to occur during immiscible separation of the two liquids. The values he obtained are given in Table 10.1.b. The agreement with partitioning behaviour seen in these experiments is good. This agreement can be no coincidence. The specific relationships of U, Th, Pb, and Ra present in the Oldoinyo Lengai lavas cannot be easily explained by any other petrogenetic process. This is therefore considered to be the strongest evidence produced to date for generation of the Oldoinyo Lengai lavas by immiscibility.

(b) Kaiserstuhl:- a more general case of genesis of carbonatites by immiscibility.

Many authors have pointed out that Oldoinyo Lengai is a freak in terms of its rock compositions; Oldoinyo Lengai lavas are the most sodic on Earth. Convincing evidence for the formation of lengaiite by immiscibility may therefore be considered irrelevant to the origins of other carbonatites. An additional example of where it is believed immiscibility is involved in carbonatite genesis has thus been included.

Kaiserstuhl is a more "normal" alkaline igneous complex, consisting of a wide range of syenitic, nephelinitic, phonolitic, and, of course, carbonatitic rock compositions. The majority of carbonatite compositions are relatively sodium-poor, especially when compared to lengaiite (see Dawson *et al.*, 1992 for analysis of lengaiite).

The geochemistry of the rocks of Kaiserstuhl was extensively studied in the 1960s (e.g. Van Wambeke, 1966; Verfaille, 1966). Compositional data for hypabyssal phonolitic and carbonatitic rocks are given in Table 10.2. Plutonic rocks at Kaiserstuhl have in general not been included, as they are not believed to adequately represent liquid compositions. Phonolite:alvikite ratios for a range of elements have then been compared with $^{Ls/Lc}D_i$ from experiments on similar compositions (BD119+CC). The agreement between bulk-rock ratios and $^{Ls/Lc}D_i$ is good for most elements, bearing in mind that the D values have slight dependence on composition and run conditions, and that the Kaiserstuhl rocks are unlikely to have remained completely unmodified after the proposed immiscible separation. One discrepancy is noticeable; the concentrations of alkali metals (especially Rb) are lower in the Kaiserstuhl carbonatites than would be expected from their partitioning behaviour observed in the experimental work. It is proposed that this is due to the loss of alkalis to a fenitising H_2O-CO_2 fluid upon crystallisation of the carbonatitic liquids. Support for this proposal can be seen in the altered country rocks in the Kaiserstuhl area.

Table 10.2. Compositional data for phonolites and carbonatites at Kaiserstuhl, Germany. Ratios of concentrations in phonolite to those in alvikite have been compared with $^{Ls/Lc}D_i$ values obtained in this study. Many of the compositional features seen in these two closely related rock-types are best explained by liquid immiscibility (e.g. behaviour of Zr-Nb, and Ti-V). Best fit was obtained with experiment G7.3, of composition BD119+CNC run at 0.8 GPa, and 1200°C.
*Rb is thought to be lost from carbonatites in fenitising fluids.
Data from Van Wambeke (1966), Verfaille (1966), and this study.

Element	Conc. in phonolite (%)	Conc. in alvikite (%)	Phonolite / alvikite	$^{Ls/Lc}D_i$ (BD119+CNC)
Ti	0.32	0.037	9.5	8.5
V	0.0115	0.026	0.44	0.38
Fe	3.5	2.0	1.8	1.9
Mn	0.23	0.41	0.54	0.68
Rb	0.019	0	-*	0.48
Sr	0.20	0.66	0.30	0.32
Y	0.0013	0.0045	0.32	0.86
Zr	0.032	0.0034	10	14.91
Nb	0.039	0.048	0.81	0.82
Ba	0.27	0.59	0.45	0.25
La	0.013	0.08	0.16	0.33
Nd	0.0058	0.019	0.29	0.55
Th	30.7 p.p.m.	7.4 p.p.m.	4.1	3.29
U	12.3 p.p.m.	12.6 p.p.m.	1.0	1.43

(c) An example of carbonatite produced by processes other than immiscibility.

A number of carbonatite occurrences exist where relationship to associated silicate liquids by immiscibility cannot be invoked on geochemical grounds. Table 10.3 shows trace-element concentrations for carbonatite and associated rock types from the Gardar province, Greenland (Upton & Fitton, 1985).

Table 10.3. Selected trace-element concentrations from Gardar carbonatite dikes and closely associated igneous rocks. Trace-element characteristics of the carbonatites are inconsistent with an origin by immiscible separation from any of the associated silicate liquid compositions. Either the conjugate silicate liquid for these carbonatite occurrences is not exposed, or the carbonatites are produced by different means (perhaps by melting of an extremely metasomatised mantle source, or as residual liquids after extensive fractional crystallisation).
Data from Upton & Fitton (1985).

	Concentrations in p.p.m.				
Element	Carbonatite	Trachyte, Mellemlandet	Phonolite, Nunataq	Syenite, Nunataq	Giant dyke chilled margin
Sr	10540	130	45	336	922
Ba	1386	301	250	3338	1052
Th	14	4	13	1	-
La	1335	69	121	58	27
Ce	3185	147	251	144	63
Nd	1430	64	88	74	32
Y	291	40	51	52	26

The carbonatite dikes analysed by Upton and Fitton (1985) are extremely enriched in Sr, Ba, Th, and REE. It is therefore considered unlikely that they could be produced as primary mantle melts. Table 10.3 also gives representative analyses of the various silicate compositions which are closely associated with the carbonatite magmatism. If these carbonatites are related to the alkaline silicate rocks of the Gardar shown here, some extreme partitioning has to have occurred. For example, $^{Ls/Lc}D_{Sr} < 0.01$, $^{Ls/Lc}D_{La} < 0.05$, $^{Ls/Lc}D_{Y} < 0.18$, and $^{Ls/Lc}D_{Th} < 1$. This partitioning behaviour is certainly not compatible with the $^{Ls/Lc}D_i$ data produced here. This leaves us with two possibilities:

(i) The carbonatites are related by immiscibility to a silicate magma which is not exposed in the area. This is considered unlikely, as a wide spectrum of silicate rocks from the province has now been investigated.

(ii) The carbonatites are related to the silicate magmatism by extensive fractional crystallisation, as late-stage residual liquids. This is the simplest explanation of the extreme enrichment of REE and other incompatible elements in these carbonatites. This is especially true for thorium, which would not be expected to have such a high concentration in a carbonate liquid produced by immiscible separation.

(d) Is there an overall picture?

So far, only specific carbonatite occurrences have been investigated in terms of their origins. This is of little use to those who require a generalised process for carbonatite petrogenesis; a more universal analysis of the properties of carbonatites is required.

In order to investigate the possibility that most carbonatites are formed as primary mantle melts, inversion calculations of a similar nature to those of McKenzie & O'Nions (1991) have been performed, using REE concentrations and LREE/HREE enrichments seen in carbonatites (Figure 10.4). In order to give a generalised view, the average REE contents of magnesiocarbonatites, calciocarbonatites and ferrocarbonatites of Woolley & Kempe (1991) have been investigated. It is not possible to reproduce the LREE concentrations of carbonatites in simulated mantle melting using the $^{mantle/Ls}D_{REE}$ values employed by McKenzie & O'Nions (1991), even with the most extreme values of melt fraction and melt distribution. Modification of $^{mantle/Ls}D_{REE}$ by application of $^{Ls/Lc}D_{REE}$ data allows more extreme LREE/HREE patterns and higher REE concentrations to be produced. The REE distribution seen in "average magnesiocarbonatite" can be accurately reproduced by melting of the mantle using these calculated $^{mantle/Lc}D_{REE}$ partition coefficients (Figure 10.4.a). This implies that it is possible for the majority of magnesiocarbonatites to be formed as primary mantle melts, with no further enrichment processes. The REE distribution of "average calciocarbonatite" cannot be explained in this way: the concentrations of LREE are too high and the LREE/HREE ratio too extreme (Figure 10.4.b). The REE patterns can only be explained if the $^{Ls/Lc}D_{REE}$ partitioning data are applied again (i.e. that the rocks have undergone two stages of carbonate-silicate equilibration). Calciocarbonatites are therefore deemed unlikely to be primary products of mantle melting. This characteristic is also seen in ferrocarbonatites (Figure 10.4.c).

One explanation for the extreme LREE/HREE seen in calciocarbonatites and ferrocarbonatites would be the action of liquid immiscibility. The scenario is as follows. Partial melting of carbonated mantle peridotite will first produce carbonatitic liquids. These will be LREE/HREE enriched according to $^{mantle/Lc}D_{REE}$ partition coefficients. On further melting, this carbonatitic liquid will be engulfed by nephelinitic silicate melt to produce a carbonated olivine nephelinitic liquid. This liquid will inherit the carbonatitic LREE/HREE enrichment despite being of mainly silicate character. If this carbonated olivine nephelinitic liquid then undergoes liquid immiscibility, the resulting carbonatitic liquid will show a second stage of

LREE/HREE enrichment. This process would result in the extreme LREE/HREE ratios seen in calciocarbonatites and ferrocarbonatites.

It must be stated that extensive crystal fractionation could also be responsible for an increase in LREE/HREE ratio. It does however seem unlikely that the same amount of LREE/HREE enrichment would be produced by variable amounts of crystallisation: i.e. the consistent nature of the LREE enrichment seen in carbonatites militates against an origin by fractional crystallisation of carbonated silicate liquids for most carbonatite occurrences.

In summary, it is suggested that generation by immiscibility does not have to be invoked for the majority of magnesiocarbonatites, and that these could originate as primary mantle melts. In contrast, it is suggested that the majority of calciocarbonatites and ferrocarbonatites are not primary mantle melts, and must have undergone other fractionation processes. Liquid immiscibility is the most easily invoked explanation for consistently extreme LREE/HREE ratios seen in these rocks.

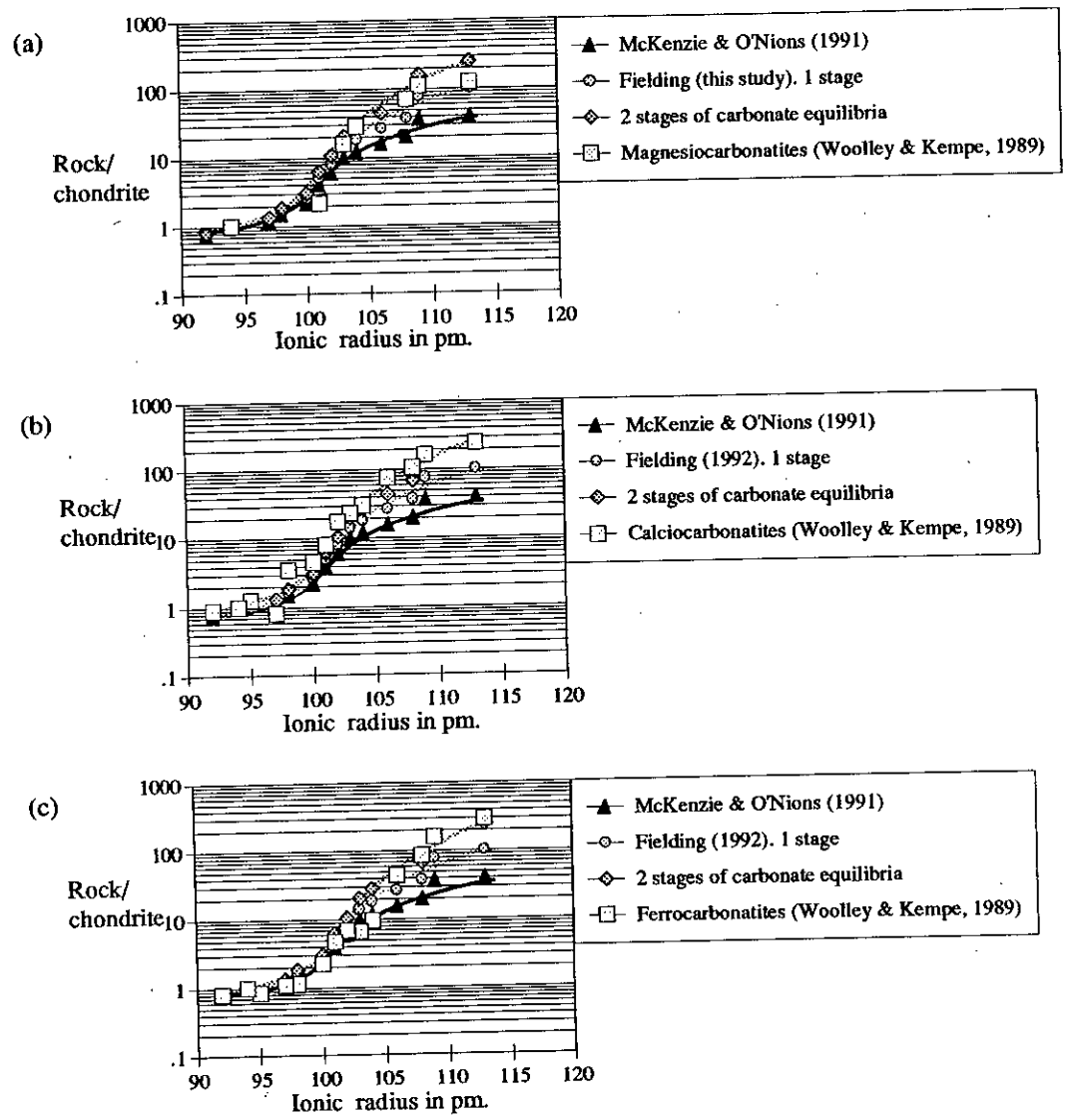

Figure 10.4. Modelling of LREE/HREE enrichment in carbonatites using inversion techniques (after Mckenzie & O'Nions, 1991). In all cases, the extreme LREE/HREE enrichment seen in carbonatites cannot be explained by single stage melting of asthenospheric mantle using silicate liquid-mantle partitioning data.

(a) The REE contents of magnesiocarbonatites can be reasonably modelled by single stage melting of the mantle using carbonate liquid-mantle partition coefficients.

(b) The REE contents of calciocarbonatites are not adequately explained in this way: two stages of carbonate-silicate equilibria are required in order to adequately reproduce the extreme LREE/HREE enrichment seen.

(c) As in (b), two stages of enrichment of LREE/HREE enrichment are required to explain REE patterns in ferrocarbonatites.

It is concluded that whilst many magnesiocarbonatites may be produced by direct melting of carbonated mantle peridotite, calciocarbonatites and ferrocarbonatites require an additional fractionation process in their history in order to produce the REE patterns seen. It is suggested that immiscible separation from a silicate liquid would result in the required LREE/HREE enrichment.

10.2. Evolution of carbonatites.

In the course of ion probe analysis of coexisting carbonate and silicate liquids, it was necessary to analyse a number of natural carbonate minerals for standardisation of the carbonate liquid concentrations. This was also seen as an opportunity to study the trace-element geochemistry of a variety of carbonate minerals for which, until recently, data have been scarce. Obviously the trace element geochemistry of the major crystallising phases in carbonatites will control their evolution. Five carbonate phases were studied in detail: A synthetic calcium carbonate mix; a calcite from the Kimsey Quarry carbonatite, Arkansas; a carbocernaite from the Samu carbonatite, India; a USNM standard dolomite (10057); and a strontianite standard (NMNH R10065). For each carbonate phase, elements were separated into three categories based on partitioning behaviour:

(a) Compatible elements. Those elements which are allowed into the carbonate structure in considerable concentrations.

(b) Moderately incompatible elements. Those elements which are present in the carbonate structure at low concentrations.

(c) Very incompatible elements. Those elements which are not accepted into the carbonate structure in any sizeable quantity (1 p.p.m. or less).

10.2.1. Element compatibility in the structure of a synthetic carbonate standard.

A synthetic carbonate powder was made up which consisted of ANALAR $CaCO_3$ spiked with a wide range of trace elements at 50-100 p.p.m. concentrations. This powder was run at 1300°C, at 0.5 GPa in an attempt to produce a calcium carbonate standard for the ion probe. In the event, the resulting charge was useless as a standard due to extreme heterogeneity. Although a failure in these terms, the experiment did show some interesting features; many of the trace-elements added were rejected from the calcite structure on crystallisation, despite being able to enter the carbonate liquid. Eight elements were not present in the calcite crystals at analysable levels (> 0.1 p.p.m.) despite original concentrations of *ca.* 100 p.p.m. This implies that extreme partitioning for these elements is also likely during crystallisation of carbonatites. Table 10.4 shows which elements were accepted into the calcite structure, which elements were concentrated in interstitial material but present at lower concentrations in the calcite, and which elements were completely excluded from the carbonate.

Table 10.4. Compatibility of elements in the carbonate structure of synthetic calcium carbonate structure. Most elements were found to be enriched in the interstitial material, with low concentrations in the carbonate. However, some elements were found to be completely rejected by the crystalline carbonate.

Compatible elements	Moderately incompatible elements	Extremely incompatible elements (1 p.p.m. or less).
Ca	Na	Ti
Mg	K	V
Sr	Rb	Zr
Ba	Cs	Nb
	Cr	Hf
	Zn	Ta
	REE	Th
	Pb	U

10.2.2. Trace-element chemistry of carbocernaite from the Samu carbonatite, India.

Carbocernaite is an orthorhombic carbonate mineral of generalised formula $(Na,Ca)(Ce,Sr,Ca,Ba)(CO_3)_2$. Structurally, it consists of (Na,Ca) and (REE,Sr) polyhedra arranged in corrugated sheets (see Miyawaki & Nakai, 1987). This open structure, combined with the varied chemistry, should make carbocernaite one of the most accommodating of natural carbonate minerals for trace elements. A sample of carbocernaite was obtained as a chip from sample C254, a carbonatite dyke at Samu, India (F.Wall, British Museum (Natural History)). In this sample, carbocernaite coexists with calcite, strontianite, barite, brithiolite (REE apatite), pyrite and magnetite (EDS spectra available for all these minerals). These minerals are believed to have crystallised from a late-stage carbonatitic liquid which was greatly enriched in a wide range of incompatible elements; especially Na, K, REE, Ba, and Sr.

The carbocernaite studied is therefore thought to represent crystallisation of the most versatile of carbonate structures under the most enriched of trace-element conditions. Incompatible trace elements which are not present in analysable quantities in Samu carbocernaite are therefore assumed unlikely to enter carbonate structures under conditions encountered during carbonatite evolution.

Table 10.5. Compatibility of elements in carbocernaite from the Samu carbonatite, India. The liquid from which the carbocernaite crystallised is believed to have been greatly enriched in all the trace elements analysed. This, combined with the complex chemistry and structure of carbocernaite, suggests that carbocernaite will have the most varied trace-element inventory of naturally occurring carbonates.

Compatible elements	Moderately incompatible elements	Extremely incompatible elements (1 p.p.m. or less).
Ca	K	Si
Mg	Rb	Ti
Mn	Cs	V
Sr	Mo	Cr
Ba	Pb	Zr
REE		Nb
Na		Hf
		Ta
		Th
		U

Rather surprisingly, all the elements that were found not to enter the calcite standard were also found not to be present in carbocernaite: these include Si, Ti, V, Cr, Zr, Nb, Hf, Ta, Th, U. The only difference about the geochemistry of carbocernaite is that it can accommodate a wider selection of elements as major components of the crystal, most notably Na, Ba and the REE.

10.2.3. Trace-element chemistry of calcite from the Kimsey Quarry carbonatite, Arkansas.

A sample of carbonatite from Kimsey Quarry, Arkansas was obtained from J.G.Fitton. This is a reasonably typical example of sövite, with REE-rich apatite needles in a matrix of crystalline calcite. Element compatibility in this calcite is shown in Table 10.6. Only Ca, Mn, Mg, Sr, and Ba are easily accepted into the structure. Low concentrations of numerous other elements were seen, with the same set of 10 trace elements being completely rejected from the carbonate.

Table 10.6. Compatibility of elements in calcite from the Kimsey Quarry carbonatite, Arkansas. Although less able to accept some elements as major components (e.g. Na and the REE), the geochemical nature of Kimsey Quarry calcite is similar to that of the carbocernaite, with the same set of trace elements rejected by the carbonate structure.

Compatible elements	Moderately incompatible elements	Extremely incompatible elements (1 p.p.m. or less).
Ca	Na	Si
Mg	K	Ti
Mn	Rb	V
Sr	Cs	Cr
Ba	Zn	Zr
	REE	Nb
	Mo	Hf
	Pb	Ta
		Th
		U

Three other calcites were also analysed on the ion probe (Norman Cross calcite, Derbyshire Iceland spar, and a departmental Iceland Spar standard). All were found to display similar chemistry, although Ba was absent from some calcites. Concentration estimates are given in Appendix B.3.

10.2.4. Trace-element chemistry of a dolomite standard.

A dolomite standard was also analysed on the ion probe to give an indication of relative ion yield for magnesium. It was from Oberdort, Austria, sample USNM 10057 (Jarosewich & Macintyre, 1983). Again similar trace-element behaviour was observed, with Si, Zr, Nb, Mo, Hf, Ta, Th, and U being rejected from the structure. Unlike the other carbonates investigated, dolomite seems to reject Ba completely from its structure, but does allow small quantities of Ti and V into the crystal lattice. It must be stated that this carbonate was precipitated from aqueous solution. Its trace-element contents will therefore be influenced by which elements were available in the fluid at the time of crystallisation.

Table 10.7. Compatibility of elements in Dolomite.
Again, similar geochemistry is seen in dolomite to that in Kimsey Quarry calcite and carbocernaite, despite the vast differences in composition and origins. Unlike the other carbonates studied, in dolomite, small quantities of Ti and V seem to be able to enter the crystalline structure.

Compatible elements	Moderately incompatible elements	Extremely incompatible elements (1 p.p.m. or less).
Mg	Na	Si
Ca	K	Zr
Mn	Rb	Nb
Sr	Cs	Mo
	Ti	Ba
	V	Hf
	Cr	Ta
	REE	Th
	Pb	U

10.2.5. Trace element chemistry of strontianite NMNH R10065.

Ion probe analysis was also undertaken for a strontianite standard to obtain strontium ion yield data. The strontianite NMNH R10065 of Jarosewich & Macintyre (1983) was employed. Trace-element behaviour is given in Table 10.8. The strontianite seems to be more specific than most of the carbonates analysed, and really only contains Sr, Ca, and Pb in any sizeable quantities.

Table 10.8. Compatibility of elements in strontianite.
Strontianite seems to have a very specific crystal lattice, and really only allows Sr, Ca, and Pb into the structure, all other elements being for the most part rejected.

Compatible elements	Moderately incompatible elements	Extremely incompatible elements (1 p.p.m. or less).	
Sr	Mg	Si	Mo
Ca	K	Ti	REE
Pb	Rb	V	Hf
	Cs	Mn	Ta
	Ba	Zr	Th
		Nb	U

Some generalisations can now be made about carbonate geochemistry in carbonatites:

(a) Ca, Mn and Mg (and presumably Fe in ankerites) behave as compatible elements in carbonate crystallisation.

(b) Na, K, Rb, Cs, Sr, Ba, Pb, and the REE are incompatible in early crystallising carbonates (e.g. calcite and dolomite), but can be incorporated into later phases (e.g. strontianite, carbocernaite).

(c) Ti, V, Zr, Nb, Hf, Ta, Th, U are unlikely to enter carbonate crystals in carbonatites and are therefore extremely enriched in the non-carbonate phases of carbonatites. This is especially important as sizeable quantities of a number of these elements have been shown to have significant solubility in carbonatitic liquids from these experiments (e.g. V, Nb, Ta and U). Crystallisation of carbonate minerals from carbonatitic liquids will therefore lead to enrichment of these elements in non-carbonate phases.

10.2.6. Separation of non-carbonate phases during carbonatite crystallisation.

The above investigation of carbonate geochemistry has shown that many of the elements present in carbonatitic liquids cannot be incorporated into carbonate crystals at any significant concentration. These elements will therefore be greatly enriched in non-carbonate minerals. Separation of these non-carbonate phases from the carbonatite magma on crystallisation provides an efficient process for the concentration of Ti, V, Cr, Mo, Zr, Hf, Nb, Ta, Th, and U.

Carbonatites have extremely low viscosities when compared to other magma types (Treiman & Schedl, 1982; Treiman, 1989; Dawson *et al.*, 1990). This implies that crystal settling will be extremely rapid if sufficient density contrasts exist. Table 10.9 shows densities for carbonatite liquid, for the likely carbonate phases separating from it, and for a selection of non-carbonate phases commonly found in carbonatites. Reid (1990) found textures in the Dicker Wilhem carbonatite, Namibia which confirm that dolomite crystals settle rapidly in calcic carbonatite melt. If this is the case, then all the non-carbonate phases listed in Table 10.9 should undergo even more rapid crystal segregation, as the density difference between them and carbonatite magma is even larger. Crystal settling is thus an extremely effective mechanism for enrichment of trace elements in specific parts of carbonatite complexes.

Table 10.9. The density of carbonate liquid in relation to phases which are believed to crystallise from carbonatite melt. Densities are given for a selection of carbonate, silicate, and accessory phases associated with carbonatites. From petrological evidence, it seems likely that any crystal with density similar to or higher than that of dolomite will be subject to rapid crystal settling in carbonate liquids.
Density data from Treiman & Schedl (1983), Treiman (1989), and Deer, Howie & Zussman, (1966).

Phase	Density (gms/cm^3)
Carbonatite liquid	~2.2
Calcite	2.72
Dolomite	2.86
Ankerite	3.0
Mg-olivine	4.1
Na-pyroxene (aegirine)	3.6
Na-amphibole	3.1
Biotite/phlogopite	3.0
Apatite	3.3
Perovskite	4.1
Pyrochlore	4.3
Magnetite	5.2

Carbonatite magmas are extremely efficient agents of element concentration. Most of the elements which are soluble in carbonatite liquid are unable to enter crystalline carbonate phases. These elements therefore become greatly enriched in the few % of non-carbonate phases present in carbonatites. At the same time, gravity settling of crystal phases in carbonatitic liquids will be a far more effective process of separation than in silicate magmas due to lower viscosities, and larger density contrasts. A combination of these features make carbonatites more susceptible to differentiation by fractional crystallisation processes than any other magma type. The diverse major, minor, and trace-element chemistry of carbonatites should therefore be no surprise.

10.3. Implications for the economic potential of carbonatites.

Processes resulting in the extreme variability in trace-element characteristics seen in carbonatites have been put forward earlier in this Chapter. These processes can be used more specifically in explaining the presence of known carbonatite economic potential, and in suggesting other economic possibilities which may be associated with carbonatites. Known economic deposits, and suggested economic possibilities will be discussed element by element, using the data presented in Mariano (1989).

10.3.1. REE mineralisation.

Carbonatite liquids formed either by direct mantle melting, or by liquid immiscibility, will be extremely enriched in LREE. Section 10.2 has shown that REE do not greatly enter calcite or dolomite, and will therefore be strongly concentrated in later mineralisation. High solubilities of REE in carbonatitic magma (e.g. Jones & Wyllie, 1986) will allow concentration to continue, resulting in REE mineralisation from late stage fluids. This is indeed found to be the case, for example at Mountain Pass, USA, where carbonatite rock is found with 7.67% REEO (Mariano, 1989).

10.3.2. Niobium (and tantalum).

Although niobium was not found to be concentrated in carbonate liquid with respect to silicate liquid, the concentrations in the carbonate liquids in these experiments were reasonably high. None of this Nb will be allowed to enter carbonate phases, and so niobium will be concentrated in specific non-carbonate phases (e.g. Pyrochlore). Gravity separation of this pyrochlore will result in further concentration of niobium. Removal of the carbonate phases by weathering will result in further enrichment of pyrochlore in lateritic deposits (e.g. Araxa, Minas Gerais, Brazil; Mariano, 1989). It is therefore not the initial concentration of niobium in carbonatites, but the subsequent segregation processes which lead to economic concentrations of niobium in carbonatites.

10.3.3. Phosphorus.

Phosphorus was found to be extremely enriched in the carbonate liquids of the experiments undertaken in this study, this affinity for carbonate liquid is unlikely to extend to carbonate crystals (for example P contents in the calcites studied are extremely low). Phosphorus will therefore be enriched in non-carbonate phases, notably apatite. Apatite cumulates are therefore the major source of phosphorus associated with carbonatites (e.g. Jacupiranga, São Paulo, Brazil; Mariano, 1989).

10.3.4. Titanium.

Although titanium does not show affinity for carbonate liquid in carbonate-silicate immiscibility experiments, it is clear that crystallisation of carbonatite liquids will cause extreme enrichment of titanium in non-carbonate phases. Further concentration by weathering has resulted in economic concentrations of titanium in laterites (e.g. Tapira, Minas Gerais, Brazil; Mariano, 1989).

10.3.5. Copper.

From the experiments of Bedson (1983) it seems likely that copper will be present in high concentrations in carbonatitic magmas. After extreme enrichment by fractional crystallisation, these concentrations may approach economic values. This has only been the case at one carbonatite occurrence, Phalaborwa, S. Africa (Mariano, 1989).

10.3.6. Fluorite.

As the immiscibility experiments have shown, fluorine is strongly enriched in carbonatites. This enrichment will become more pronounced on crystallisation as fluorine will not enter early crystallising carbonate and silicate minerals in significant quantities. It is likely that fluorine will be concentrated in H_2O-rich fluid found associated with carbonatites (e.g. Ambar Dongar, India; Mariano, 1989).

10.3.7. Other elements that may have economic potential in carbonatites.

These fall into two types:

(a) Those elements which are strongly enriched in the initial carbonate liquids. This includes Ba and Sr.

(b) Those elements which will have reasonably high initial concentrations but should be greatly enriched by processes of differentiation and fractional crystallisation. V, Mo, Pb, U, Th, and Zr fall into this category.

10.4. Conclusions.

Trace-element partitioning behaviour plays a vital rôle in our understanding of the genesis and evolution of carbonatites. Experimental investigations into immiscibility, and ion probe work on trace-element geochemistry of carbonate compositions has led to the following implications for carbonatites;

(a) The major-element compositions of the majority of carbonatites can be reproduced experimentally in conjugate immiscible carbonate melts. These carbonate liquids are in equilibrium with silicate melts ranging in composition from silica-rich phonolites to olivine melilitites.

(b) Use of trace-element partitioning behaviour investigated in this study allows us to predict the trace-element characteristics of mantle-derived primary carbonate liquid. Most carbonatites do not show these characteristics, and are therefore unlikely to have been formed as primary mantle melts. It is possible, however, that a number of magnesiocarbonatites could be formed by this process.

(c) Liquid immiscibility is seen as the most likely alternative explanation of carbonatite trace-element characteristics. In specific examples, evidence for a relationship between carbonate and silicate rock types by immiscibility is strong. In the more general case, the pronounced but consistent LREE/HREE enrichment seen in carbonatites, combined with other geochemical features, all point towards liquid immiscibility as the process resulting in the formation of most calciocarbonatites, ferrocarbonatites, and natrocarbonatites.

(d) Carbonatite examples can be found where immiscibility with silicate melt does not seem to fit the geochemical evidence. Often these are small volumes of carbonatite with highly enriched incompatible element characteristics. It is believed that these occurrences are best explained by production of carbonatite as a residual melt after extensive crystallisation of silicate phases from a carbonated silicate melt.

(e) Study of the trace-element characteristics of carbonate crystals shows that most of the trace elements present in carbonate liquid will not be incorporated into crystalline carbonate structures. These elements will be greatly concentrated in minor, non-carbonate phases which crystallise from carbonatitic liquid.

(f) The physical properties of carbonate liquids (low viscosity, low density) will cause crystal fractionation to be much more efficient at separation of crystalline phases in carbonatites than in other igneous rocks.

(g) A combination of (d) and (e) results in the wide spectrum of carbonatites seen both in terms of mineralogy, major element composition, and trace-element geochemistry.

(h) The economic potential of carbonatites can be discussed in the light of these conclusions. The presence of economic mineralisation of an element will depend on two factors:

(i) Its initial concentration in the carbonatitic liquid

(ii) How the element behaves in fractional crystallisation of the carbonatitic liquid.

Most economic deposits in carbonatites result from relatively high initial trace-element concentrations being drastically enhanced by the differentiation processes which occur during crystallisation of carbonatites.

CHAPTER 11

A WIDER ROLE FOR CARBONATE LIQUID IN MANTLE PROCESSES.

11.1. Diagnosing carbonate involvement in mantle processes.

In Chapter 1 it was suggested that carbonate liquid could be involved in a number of petrogenetic processes operating in both the lithospheric and asthenospheric upper mantle. These include:

(a) Element redistribution in the mantle and metasomatism of the lithosphere.

(b) Melting of the mantle at low temperature to produce small-volume carbonated melts, from both the lithosphere and the asthenosphere.

(c) Involvement as a precursor to more voluminous silicate melting. In this case, carbonate melt will be produced over a larger volume of mantle. Its ability to scavenge elements from the mantle will be determined by mantle-carbonate equilibria.

The geochemical characteristics of mantle carbonate liquid have been outlined in Chapter 9. These features may be inherited by the products of processes in the mantle which involve carbonate liquid, and can therefore be used in diagnosing the influence of carbonate equilibria. In this chapter, a number of specific instances of carbonate involvement will be outlined as examples of where, when, and how these processes operate. Although this approach will only confirm carbonate involvement in a few geological occurrences, it is suggested that the examples shown indicate a general involvement of carbonate liquid in mantle processes.

11.2. Metasomatism by carbonate liquids.

11.2.1. Mineralogy and major-element chemistry of selected xenolith suites.

Various authors have recently suggested that the mineralogy and major-element composition of a number of xenolith suites are best explained by metasomatism by carbonate liquid. As an example, the xenolith suite of Leura-Shadwell, Australia, comprises magnesian wehrlites, pyroxenites and lherzolites. The end member of this metasomatic process is believed to be a highly magnesian, apatite-bearing wehrlite (Yaxley *et al.*, 1991). Many features of this xenolith suite seem to indicate carbonate involvement:

(a) Lack of orthopyroxene in the metasomatised xenoliths.

Below *ca.* 70 km depth, carbonate liquid is known to react with mantle phases according to a number of equations. Equation 11.1 is a simplified end-member reaction of enstatitic orthopyroxene with dolomite component in the carbonate liquid:

$$4MgSiO_3 + CaMg(CO_3)_2 = 2Mg_2SiO_4 + (CaMg)Si_2O_6 + 2CO_2 \qquad (11.1)$$
Enstatite Dolomite Forsterite Diopside

The net effect of this reaction is to remove orthopyroxene from the assemblage and replace it with clinopyroxene and olivine.

(b) The presence of pargasitic amphibole.

Primary carbonate liquid, containing Na and H_2O can react with peridotite to form pargasite-bearing metasomatised xenoliths:

$$10MgSiO_3 + 3MgAl_2O_4 + 3CaMgSi_2O_6 + Na_2CO_3 + CaCO_3 + H_2O =$$
Enstatite Spinel Diopside Carbonate melt

$$2NaCa_2Mg_4Al_3Si_6O_{22}(OH)_2 + 4Mg_2SiO_4 + 2CO_2 \qquad (11.2)$$
Pargasite Forsterite

(c) Presence of Apatite.

Primary carbonate liquid will have a high phosphorus content. On decarbonation this phosphorus will combine with the CaO component in the carbonate liquid to form apatite.

(d) Chemically, the metasomatised xenoliths show enrichment in Ca, Na, P, and K without concomitant enrichment in Fe, Ti, etc.

(e) The xenoliths are highly magnesian, with no decrease in Mg/[Mg+Fe] with increasing metasomatism. This is to be expected from the preference of Mg over Fe in the carbonate liquid.

(f) The suite as a whole shows high Ca/Al and Na/Al ratios. Both are to be expected from addition of primary carbonate liquid.

These features are very different from the more common Fe-Ti-K-OH metasomatism seen in many other xenolith suites (e.g. Pello Hill, Tanzania; Dawson & Smith, 1988), and are all indicative of the expected effects of carbonate addition. Other examples of this form of mantle metasomatism include the recently studied West Eiffel suite (Lloyd *et al.*, 1991; Thibault *et al.*, 1992).

11.2.2. Trace-element and isotopic features of xenoliths from cratonic lithosphere.

Study of the trace-element and isotopic geochemistry of a number of on-craton xenolith and megacryst suites have resulted in the accumulation of substantial evidence for the action of carbonate liquids as metasomatising agents of cratonic lithosphere. In this section, we will concentrate on evidence from the Loch Roag (NW Scotland) xenoliths and megacrysts, although data from other cratonic areas will be mentioned where relevant.

As has been discussed previously, one of the most prominent features of mantle carbonate liquid is high LREE/HREE. Studies of clinopyroxene, apatite, mica, amphibole, garnet, and zircon megacrysts in the Loch Roag basalts have allowed estimates of the REE contents of the metasomatising melt to be calculated (Hinton & Upton, 1991; Long *et al.*, 1992). Figure 11.1 shows these calculated compositions, as well as a selection of carbonatite REE patterns. It can be seen that the calculated LREE contents of the metasomatising melt at Loch Roag resembles carbonatite.

Additional evidence exists for the action of carbonate liquid in the mantle under Loch Roag. Figure 11.2 shows $^{208}Pb/^{204}Pb$ *vs.* $^{206}Pb/^{204}Pb$, and $^{207}Pb/^{204}Pb$ *vs.* $^{206}Pb/^{204}Pb$ for Loch Roag xenoliths. In both cases, the trend to low $^{208}Pb/^{204}Pb$, $^{207}Pb/^{204}Pb$, and $^{206}Pb/^{204}Pb$ indicative of carbonate liquid addition (Chapter 9) is seen.

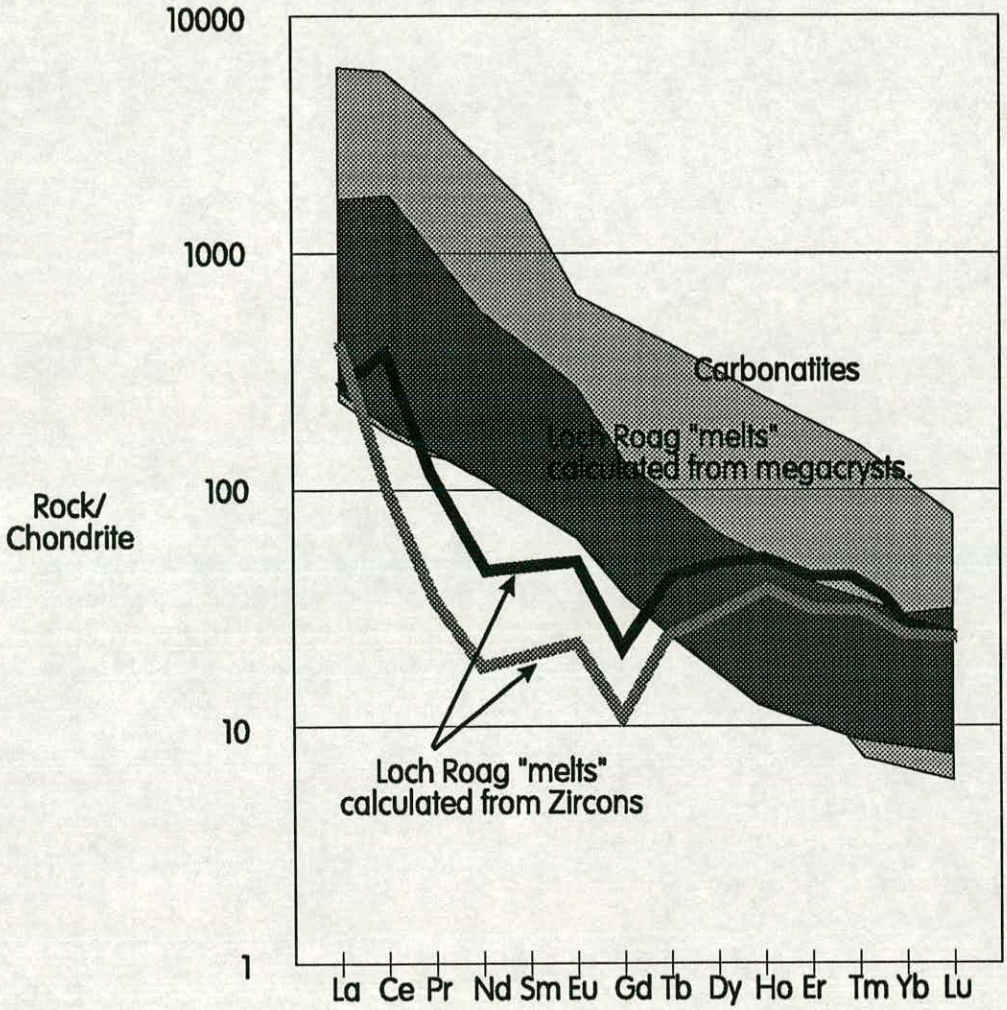

Figure 11.1. Normalized REE concentrations for melts calculated to be in equilibrium with the megacryst suite found at Loch Roag, Outer Hebrides, Scotland. These melt compositions show many features in common with carbonate liquids, represented here by a selection of carbonatites. (Data from Hinton & Upton, 1991; Long et al., 1992; Bernard-Griffiths et al., 1988, Roden et al., 1985, Nelson et al., 1988).

Carbonate-like equilibrium-melt characteristics are only produced if $^{xtal/La}D_i$ values are used in the calculation. This implies that the melt may have actually been a silicate-dominated liquid with "carbonatitic" trace-element characteristics.

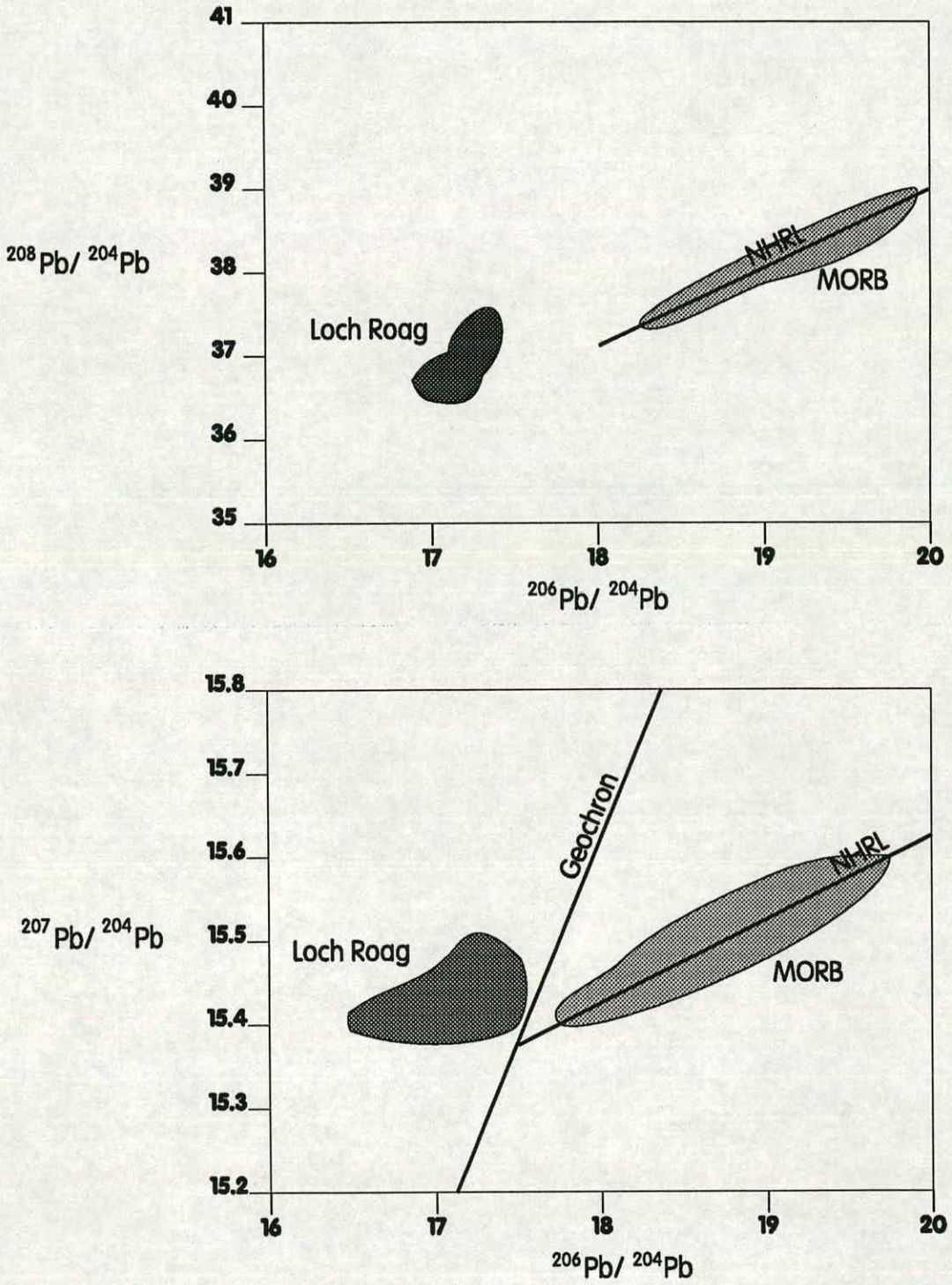

Figure 11.2. Pb-isotope systematics for Loch Roag xenolith suite (Long et al., 1992). The unradiogenic Pb-isotope signature (indicative of low time-integrated U/Pb and Th/Pb is again diagnostic of carbonate involvement. MORB data from Dupre & Allegre, 1980; Cohen & O'Nions, 1982.

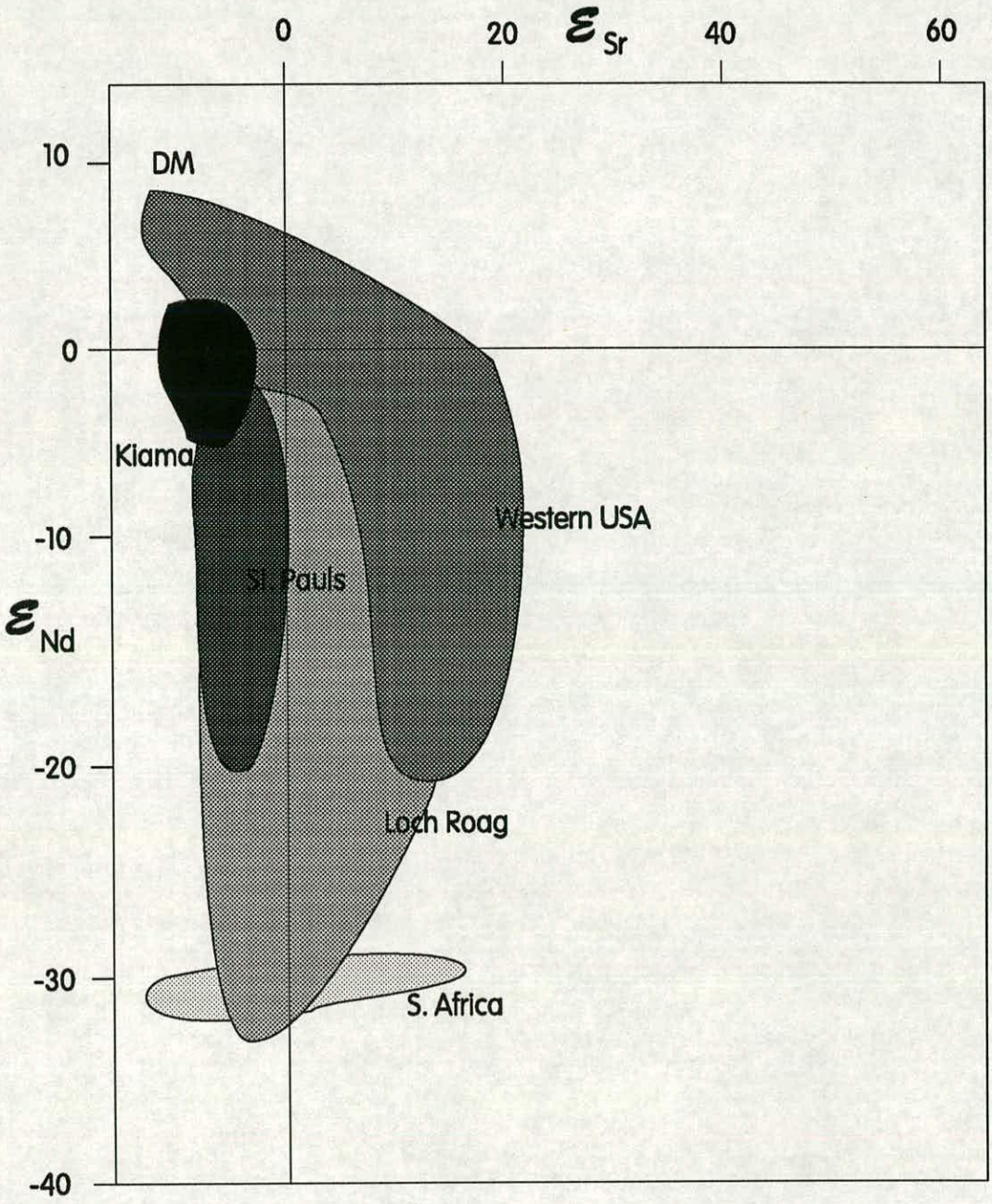

Figure 11.3. Sr-Nd isotope systematics for some cratonic lithosphere-derived mantle xenoliths and megacrysts: Examples of possible enrichment by carbonate liquids from Loch Roag, Scotland; Finsch, S.Africa; Kiama, Auastralia; and the Western USA. Data from Richardson et al. (1984), Menzies & Wass (1983), Menzies et al. (1987), Roden (1987), Menzies (1989).

Sr-Nd isotope systematics of mantle xenoliths provides further evidence for carbonate melt involvement. Figure 11.3 shows the approximate field of $(^{87}Sr/^{86}Sr)_i$ and $(^{144}Nd/^{143}Nd)_i$ for Loch Roag megacrysts. Again, the trend expected from the addition of carbonate liquid is followed, producing megacrysts with very low $(^{144}Nd/^{143}Nd)_i$ but $(^{87}Sr/^{86}Sr)_i$ near Bulk Earth values. The xenoliths and megacrysts in Loch Roag basalts are certainly not the only examples of this form of enrichment. Xenoliths from Australia (Kiama suite, Menzies & Wass, 1983; Menzies *et al.*, 1987), Africa (Finsch kimberlites, Richardson *et al.*, 1984), and North America (W. USA, Roden, 1987; Menzies, 1989) all show evidence of involvement of carbonate liquid.

11.2.3. Trace-element geochemistry and isotopic characteristics of lithosphere-derived melts.

Study of xenolith suites is not the only method for investigating the role of carbonate liquid in metasomatism of the lithosphere. Melts derived from metasomatised lithosphere may also retain geochemical evidence for earlier carbonate involvement. Certainly, if a long time gap exists between enrichment and subsequent melting, then the characteristic isotopic signatures of carbonate involvement will have had time to develop.

Lamproites are a suite of potassic igneous rocks, characterised by very coherent major-element chemistry, but widely variable trace-element concentrations and ratios (Mitchell & Bergman, 1991). They are believed to be produced by melting of depleted lithospheric mantle under reduced fO_2 conditions, and in the presence of H_2O-CH_4-F volatiles (Foley *et al.*, 1986; Foley, 1989). Lamproites contain very high concentrations of incompatible trace-elements which are not in accord with their depleted major-element chemistry; it is therefore suggested that their harzburgitic source has been enriched by "metasomatic fluid" at some unspecified time before melting (Fraser *et al.*, 1985; Hawkesworth *et al.*, 1985). This suggestion is supported by the enriched and variable isotopic signatures seen in lamproites. Harzburgitic lithosphere contains very low concentrations of incompatible trace elements, owing to previous melt removal (Taylor & Green, 1989). Melts produced from them therefore give us an opportunity to investigate the geochemical characteristics of the metasomatic agent(s) that caused enrichment prior to melting.

As discussed in Chapter 9, the characteristics of mantle carbonate melt include:

(a) High calcium contents.

(b) Enrichment in phosphorus.

(c) High ratios of LILE/HFSE (e.g. Ba/Th, Sr/Th).

(d) Extreme LREE/HREE ratio (i.e. high La/Yb).

(e) Unusually low Th/U

Table 11.1 shows data from lamproite occurrences from all over the world. It can be seen that a number of provinces show trace-element characteristics associated with carbonate liquids, most notably the lamproites at Smokey Butte, and Leucite Hills. There is very good correlation between these geochemical features, that is, lamproites which show high Ba/Th will also show extreme LREE/HREE enrichment, and will have low Th/U.

Table 11.1. Geochemical characteristics of selected lamproites and the expected effects of enrichment by carbonate liquid. Data from Mitchell *et al.* (1987), Fraser (1987), Kuehner *et al.* (1981), Mitchell & Bergman (1991), Venturelli *et al.* (1988), Nixon *et al.* (1984), Nelson *et al.* (1986)

	Smokey Butte	Leucite Hills	Francis	Murcia-Almeria	Expected effects of carbonate addition
CaO (Wt. %)	5.83	4.33	4.03	3.43	High
P_2O_5 (Wt. %)	2.49	1.64	1.23	0.90	High
Ba/Th	1514	389	147	17.2	High
Sr/Th	491	130	68	5.3	High
La/Yb	226	209	103	47	High
Th/U	1.9	3.8	7.8	5.5	Low

Figure 11.4 shows the REE characteristics of selected lithosphere-derived igneous rocks. Two trends can be seen on this diagram:

(a) a trend to very high REE concentrations without significant increase in LREE/HREE ratio. This trend is shown by most kamafugites, and a few lamproites (e.g. Murcia-Almeria). Concentration of small-degree silicate melts followed by re-melting may be responsible for the resulting REE-rich magmas.

(b) Extreme LREE/HREE enrichment with only moderate increase in REE contents. This trend is present for most lamproites, and the Toro-Ankole kamafugites. This is believed to be due to enrichment by carbonate liquid, resulting in slightly higher REE contents, but with La/Yb increased by a factor of 4-5.

The isotopic characteristics of some lamproites are also indicative of carbonate involvement. Figure 11.5 shows the Sr-Nd isotopic characteristics for a range of lamproites. Again, two trends can be identified:

(a) A trend to high $(^{87}Sr/^{86}Sr)_i$ and moderately low $(^{144}Nd/^{143}Nd)_i$. Shown by the lamproites of Western Australia and Murcia-Almeria, this is thought to be caused by addition of (possibly water-rich) silicate material.

(b) A trend to very low $(^{144}Nd/^{143}Nd)_i$ with $(^{87}Sr/^{86}Sr)_i$ remaining near bulk earth. This trend is shown by the lamproites from Smokey Butte, Leucite Hills, Sisimiut, and Prairie Creek and is attributed to the addition of carbonate liquid.

Finally, the Pb-isotope systematics of lamproites have been displayed in Figure 11.6. As mentioned in Chapter 9, the addition of carbonate liquid would be expected to lead to low $^{208}Pb/^{204}Pb$, $^{207}Pb/^{204}Pb$, and $^{206}Pb/^{204}Pb$ ratios. This trend is again seen in lamproites from Smokey Butte, Sisimiut, Prairie Creek etc. In summary, it is suggested, from geochemical and isotopic evidence, that the source areas for Smokey Butte, and many other lamproite occurrences, were metasomatised by carbonate liquids at some stage in their history.

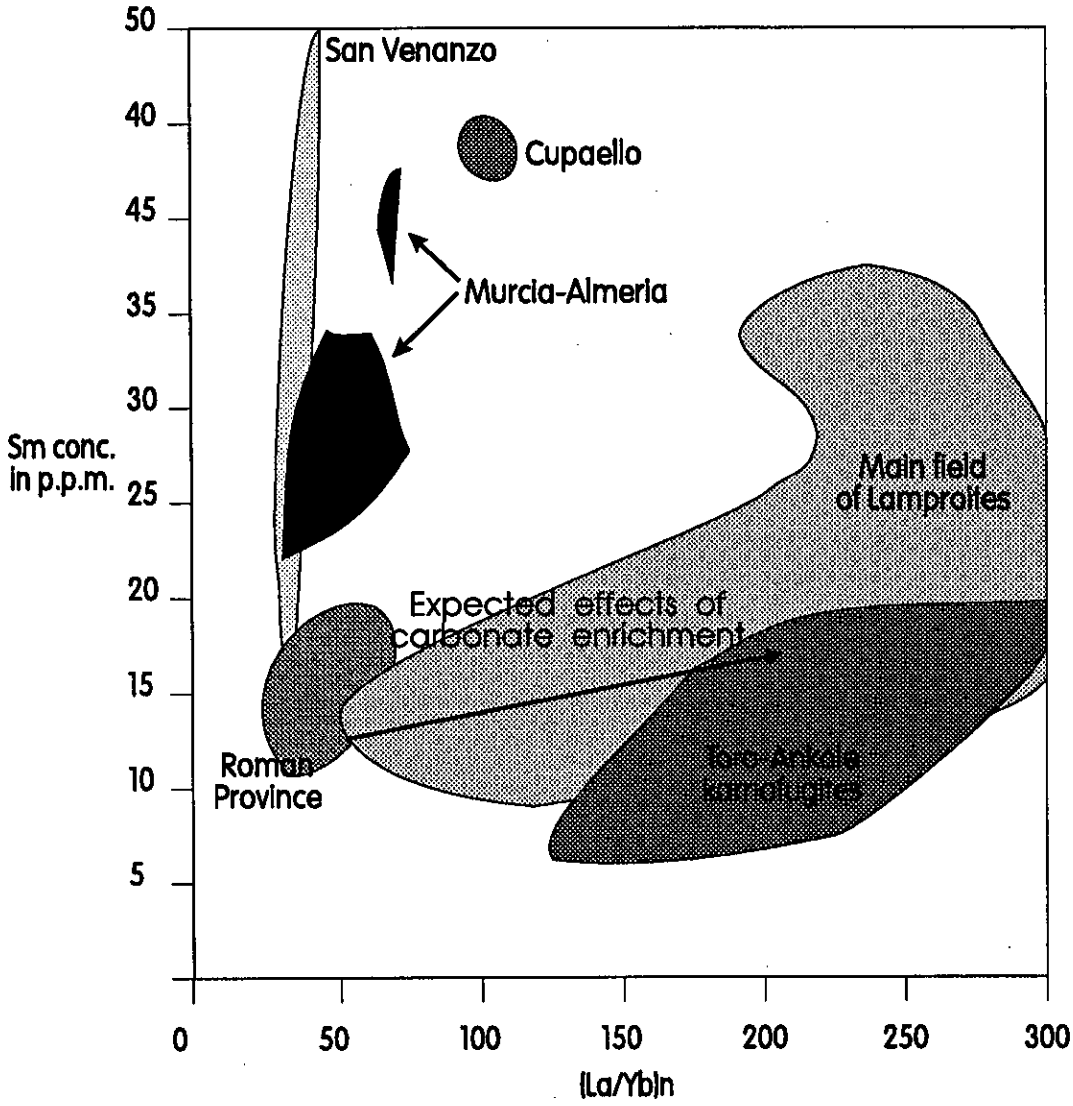

Figure TI.4. REE distributions in lithosphere-derived mantle melts. Addition of carbonate liquid will cause drastic increase in (La/Yb)n but should have less pronounced effect on Sm concentration (Sm is only slightly enriched carbonate liquid over silicate). Carbonate liquid could therefore be involved in enrichment of the source areas for some kamafugites, and most lamproites. (After Bergman, 1987; Mitchell & Bergman, 1991).

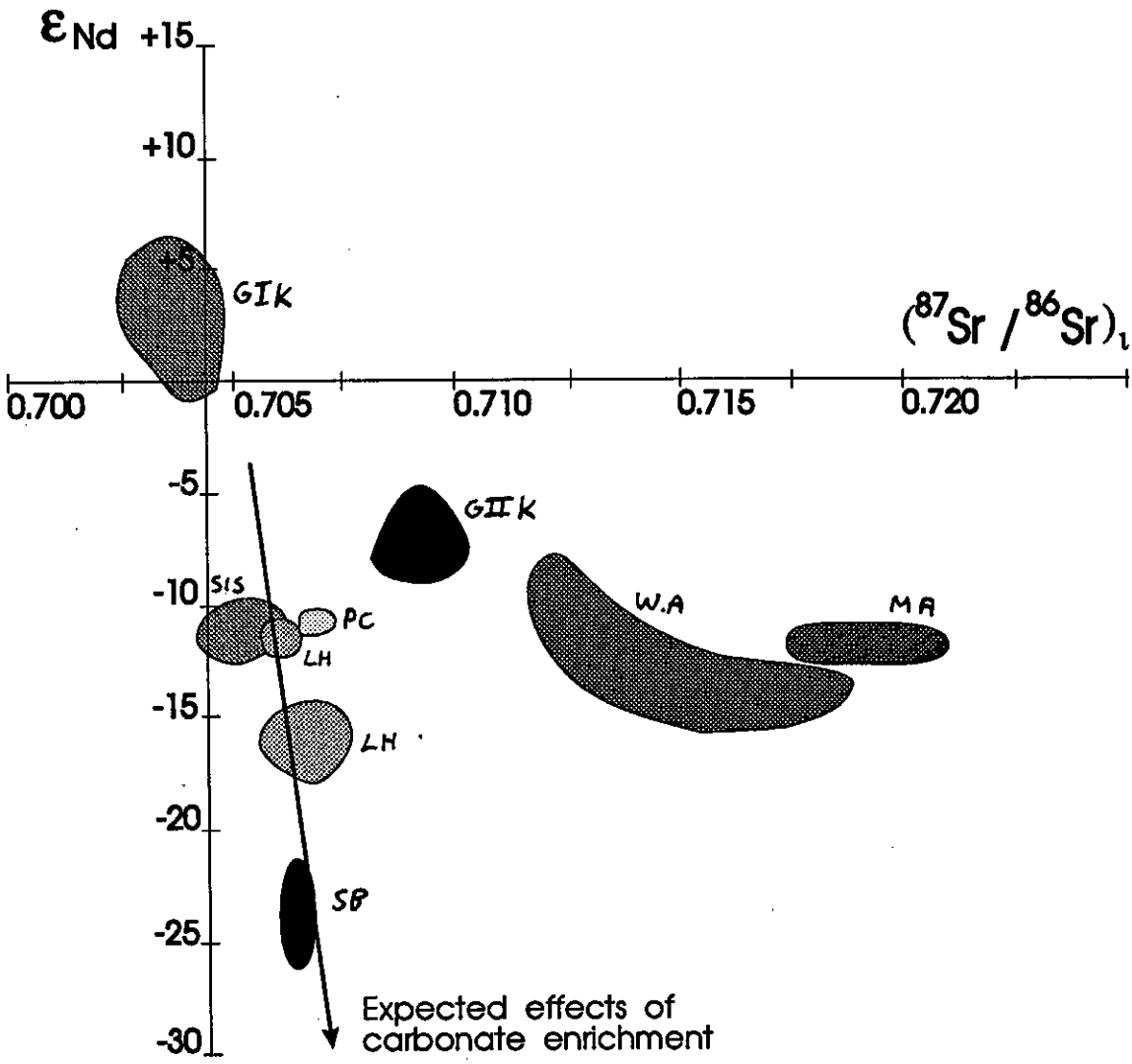

KEY

SB	■	Smokey Butte (Fraser, 1987)
LH	▩	Leucite Hills (Vollmer et al, 1984: Fraser, 1987)
SIS	▩	Sisimiut (Nelson, 1989)
PC	▩	Prairie Creek (Fraser et al, 1985)
WA	▩	Western Australia (Vollmer et al, 1984; Bolivar, 1977; Fraser et al, 1985)
M-A	▩	Murcia-Almeria (Nelson et al, 1986)
GII K	■	Group 2 Kimberlites (Smith 1983)
GI K	▩	Group 1 Kimberlites (Smith, 1983)

Figure 11.5. Sm-Nd isotope systematics for selected lamproites: Note the trend to low εNd without corresponding increase in $^{87}Sr/^{86}Sr$ seen in many lamproite occurrences. This feature is suggested as diagnostic of mantle enrichment by carbonate liquid.

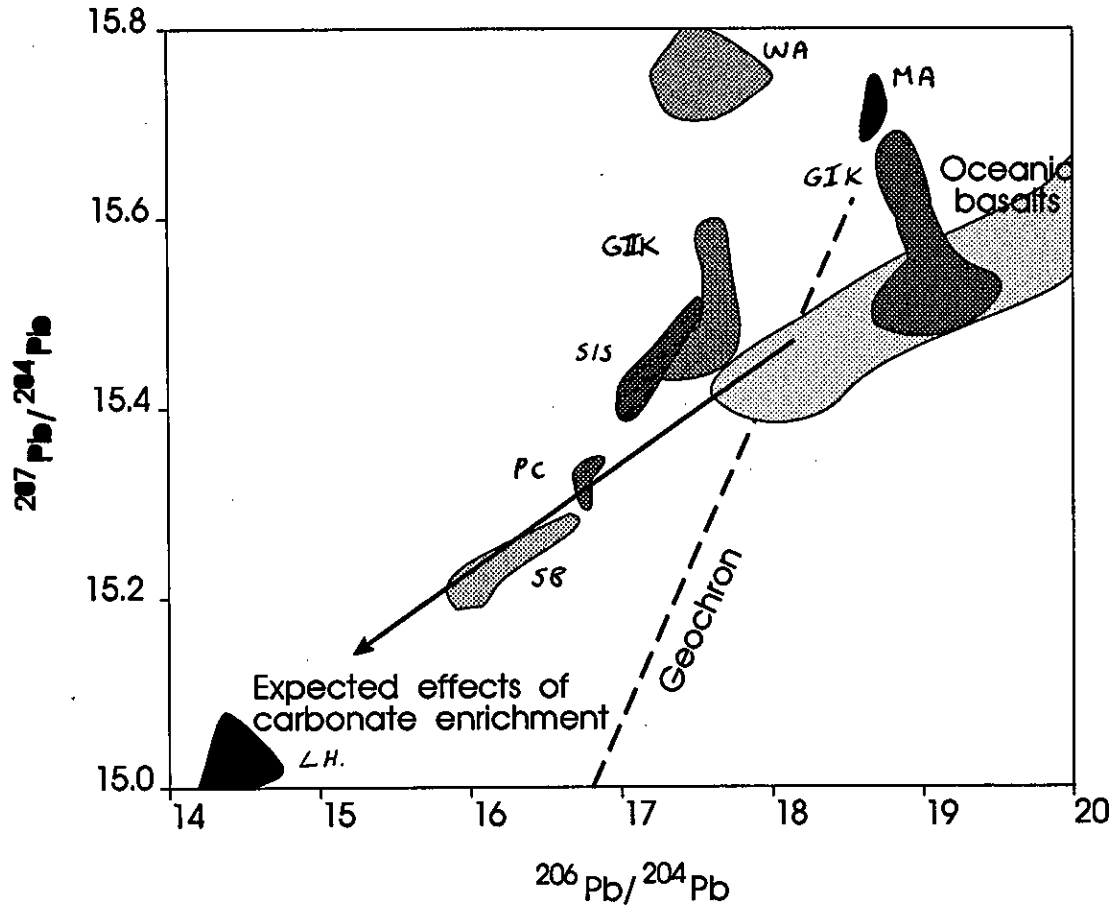

Figure 11.6. Pb-isotope systematics for selected lamproites. Note again that Smoky Butte etc. show the expected effects of source enrichment by carbonate. (Data as in Figure 11.5 with Alibert & Albarède, 1988; Nelson, 1989; Salters & Barton, 1985).

11.3. Carbonate involvement in the formation of small-volume mantle silicate melts

Many small-volume silicate melts seen at the Earth's surface have features in common with those suggested for mantle carbonate liquid. The variety in the trace-element geochemistry of small-volume melts makes it difficult to generalise about their origins and features. However, one characteristic is common to most: that of extreme LREE/HREE enrichment. As has been pointed out, this is a characteristic of carbonate liquid. There is a limit to the range of LREE/HREE enrichment which can be produced by single-stage melting of asthenospheric upper mantle (e.g. McKenzie & O'Nions, 1991). As the melt fraction tends to zero:

$$^{Liq}C_{La}/^{Mantle}C_{La} = 1/^{Mantle/Liq}D_{La}$$

And:

$$^{Liq}C_{Yb}/^{Mantle}C_{Yb} = 1/^{Mantle/Liq}D_{Yb}$$

The maximum enrichment of La over Yb can therefore be approximated as:

$$(^{Liq}C_{La}/^{Liq}C_{Yb})/(^{Mantle}C_{La}/^{Mantle}C_{Yb}) = ^{Mantle/Liq}D_{Yb}/^{Mantle/Liq}D_{La}$$

For silicate melting, $^{Mantle/Liq}D_{La} \sim 0.006$, $^{Mantle/Liq}D_{Yb} \sim 0.3$ (from McKenzie & O'Nions, 1991), the maximum $(La/Yb)_n$ ratio possible in a mantle-derived silicate should therefore be:

$$(La/Yb)_n = 0.3/0.006 = 50$$

For carbonate melting (applying $^{Ls/Lc}K_{D_{La/Yb}} = 5$, from Chapter 9), $^{Mantle/Liq}D_{La} \sim 0.0012$, whilst $^{Mantle/Liq}D_{Yb}$ will remain near 0.3. In this case, the maximum possible $(La/Yb)_n$ for a mantle-derived melt will be:

$$(La/Yb)_n = 0.3/0.0012 = 250$$

Many small-volume silicate liquids show LREE/HREE ratios outside the range possible for silicate melting (i.e. $(La/Yb)_n > 50$), but otherwise appear to be derived straight from the asthenosphere (e.g. melilitites, group I kimberlites). As Figure 11.7 shows, their LREE/HREE ratios are probably best explained by the involvement of carbonate liquid. This is not surprising as kimberlites are often carbonate-rich, and are associated with massive degassing of CO_2. The same is true for melilitites, although the degassing is usually less violent, and carbonate contents lower. In summary, small-volume silicate melts seen at the surface (e.g. melilitites and kimberlites) are thought to show considerable carbonate involvement in their genesis.

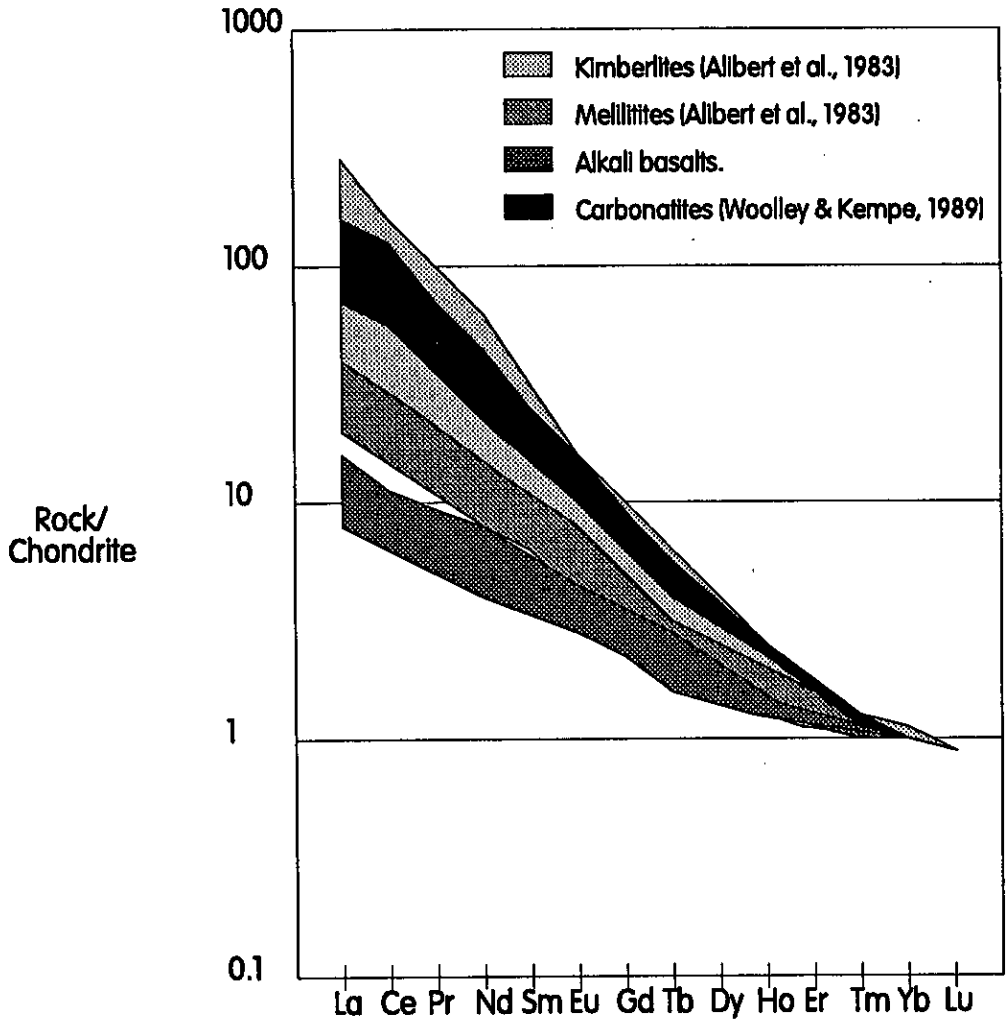

Figure 11.7. LREE/HREE enrichment in kimberlites and melilitites. REE concentrations in selected kimberlites, melilitites, alkali basalts, and carbonatites have been plotted normalized to Yb. The REE concentrations and LREE-enriched character of kimberlites and melilitites is reminiscent of that seen in carbonatites rather than the REE patterns seen in other asthenosphere-derived melts.

11.3.1. Colorado minettes (Thompson *et al.*, 1989).

The Minette dikes of NW. Colorado have been investigated as a more specific example of the influence of carbonate equilibria on the geochemistry of small-volume silicate melts. Figure 11.8 shows REE inversion modelling for these minettes based on the work of McKenzie & O'Nions (1991). McKenzie & O'Nions (1991) used the most extreme partial melt distribution possible in an attempt to explain the REE contents of the minettes using $^{mantle/La}D_{REE}$ partition coefficients. The fit for the heavy and middle REE is good; the fit for LREE is by contrast poor, with the best attempted model being outside error for La and close to error for Ce. If $^{mantle/Lc}D_{REE}$ are used, however, it is possible to reproduce all the observed REE contents. It is concluded that the REE contents of these minettes are best explained by the influence of carbonate liquid on low-degree mantle partial melt.

Many other features of these minettes are indicative of involvement of carbonate liquid in their petrogenesis. Table 11.2 shows some of the trace-element characteristics of these rocks, and relates them to other mantle-derived material. Of most note are the extremely high ratios of LILE/HFSE (e.g. Ba/Th), the low Th/U ratio, and high Zr/Hf and Nb/Ta. All these features have been ascribed to the involvement of carbonate.

Table 11.2. Trace-element characteristics of NW. Colorado minettes (Leat *et al.*, 1988, Leat *et al.*, 1991). These rocks show high ratios of LILE/HFSE, low Th/U, and high Zr/Hf and Nb/Ta. It is therefore suggested that they have been influenced by carbonate liquid.

Ratio	NW. Colorado minettes		Comparisons with other mantle derived material
	Mean	Range	
Ba/Th	344	151-1000+	(Highest from single episode of melting is *ca.* 250)
Ba/Zr	8.8	4.5-17.8	
Ba/Hf	347	251-1000+	
Sr/Th	150	98-264	
Th/U	3.4	0.9-5.9	4.2 Bulk Earth (Williams & Gill, 1990)
Zr/Hf	39.4	33.5-46.6	*Ca.* 35 in most rocks (Dupuy *et al.*, 1992)
Nb/Ta	17.3	15.3-19.9	15-17 in most rocks

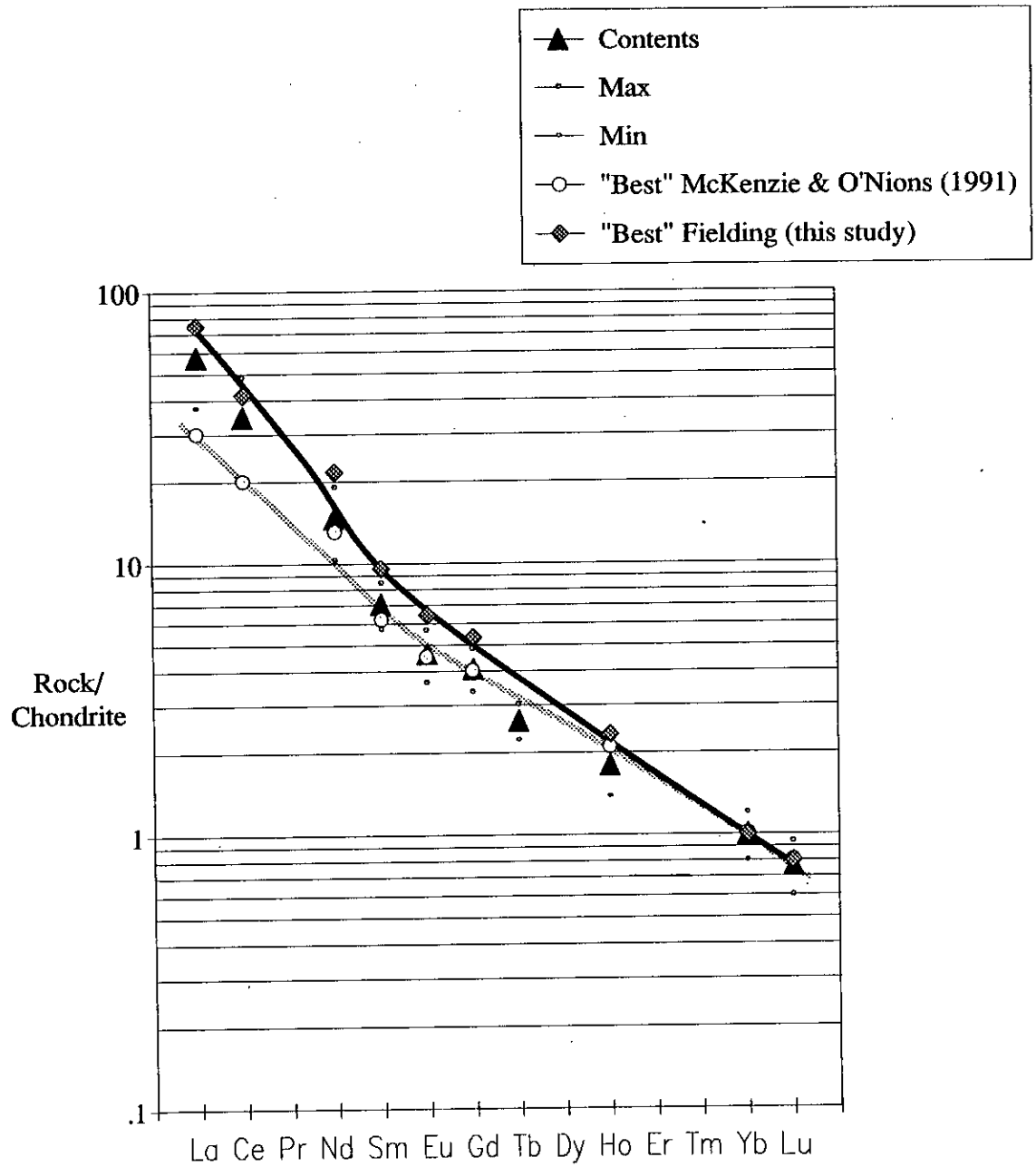

Figure 11.8. REE modelling of Minettes from NW Colorado (Thompson *et al.*, 1990). Mantle-silicate melt partition coefficients are unable to explain the LREE contents of many small volume mantle silicate melts. Application of mantle-carbonate liquid partition coefficients allows for much higher LREE contents and LREE/HREE ratios to be produced. The REE contents of most small-volume silicate melts can then be explained in terms of simple melting processes.

11.4. Carbonate liquid as a precursor to more voluminous silicate melting.

Three suites of alkaline basaltic volcanism will be discussed in an attempt to show examples of the possible effects of carbonate liquid on large-scale mantle melting episodes. Two examples are taken from continental environments (the Hessian Depression, Germany, and the Nyiragongo volcanics, Zaire), the other is an example of oceanic intraplate volcanism (Hawaiian islands).

11.4.1. Geochemistry of the alkaline lavas of the Hessian depression, Germany.

The lavas of the Hessian depression consist of a suite of basaltic rocks ranging in ciomposition from tholeiite to olivine nephelinite. Wedepohl (1985) has suggested that the source of these rocks must have had "an immediate precursor" in order to explain contents of K, P, LREE, Sr, Ba and other incompatible elements. The precursor had to have been added at the time of eruption in order to allow preservation of local disequilibrium in $^{87}Sr/^{86}Sr$. Wedepohl (1985) also noted that the basalts were saturated in CO_2 during rapid rise to the surface.

Figure 11.9 shows variations in a number of trace-element ratios in Hessian lavas. Some interesting variations occur between tholeiites and the more undersaturated rock types. In all cases, trace-element ratios show trends that would be expected by addition of carbonate liquid to the more undersaturated rocks (e.g. Ba/Th, Th/U, Rb/Sr, Ti/V all fall; P/Th, P/Zr, Zr/Hf, La/Yb, Ca/Na all rise). For Rb/Sr, P/Ta and P/Th ratios, this is the opposite trend to that expected by smaller degrees of partial melting, whilst Th/U and Zr/Hf should not be affected by partial melting.

It is concluded that the geochemical characteristics of the Hessian Depression lavas point towards the precursor melt mentioned by Wedepohl (1985) being a carbonate liquid.

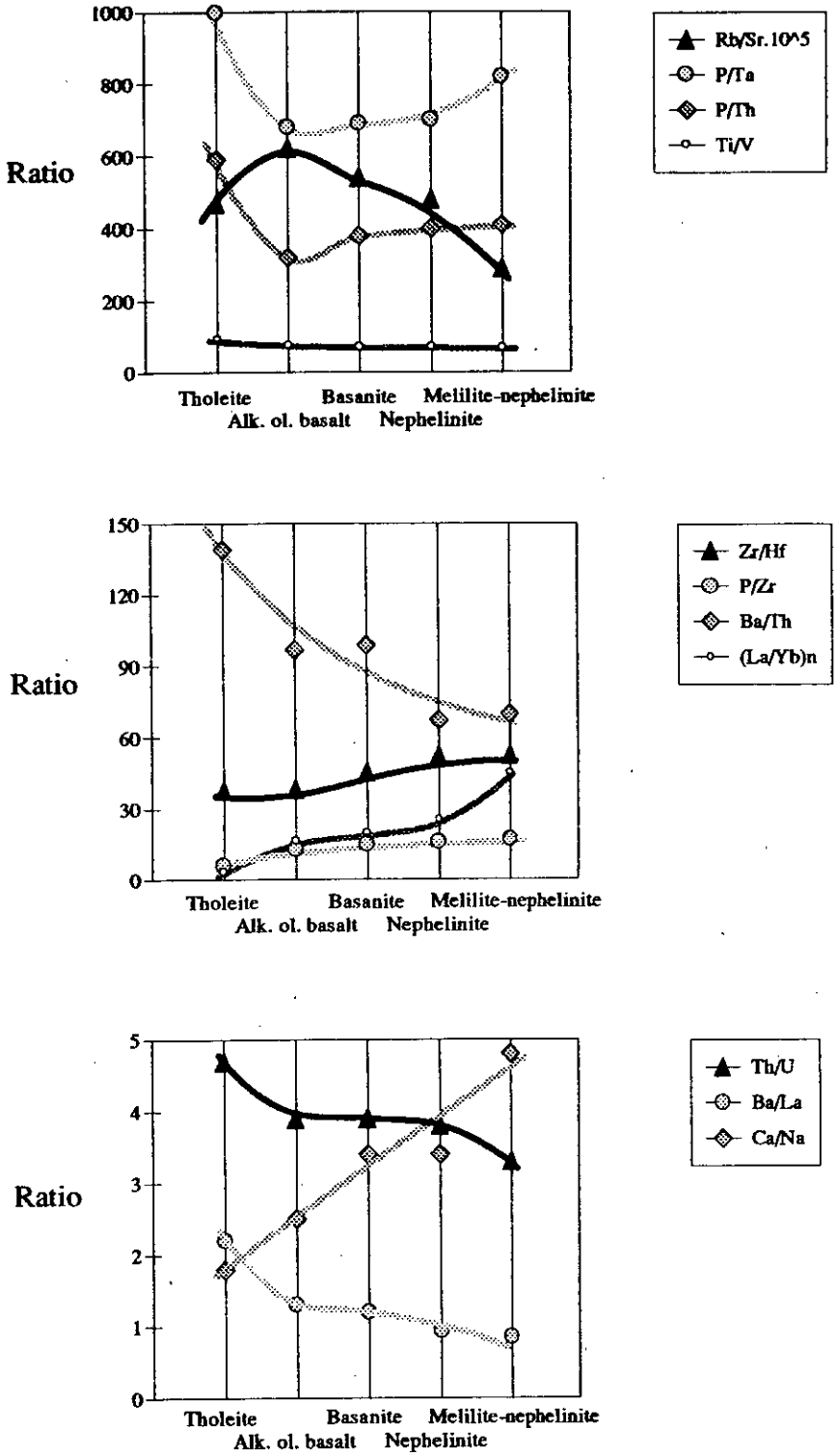

Figure 11.9. Variations in trace-element ratios with undersaturation in the lavas of the Hessian trough, Germany. In all cases, trace-element ratios show the predicted trend for increasing influence of carbonate melt with increasing undersaturation of the lavas. In the ratios plotted in the top diagram, these trends are the opposite to those expected by smaller degrees of partial melting involving silicate liquid. (Data from Wedepohl, 1986).

11.4.2. The Nyiragongo volcanics, Virunga Province, Zaire.

The Nyiragongo volcano is geochemically unusual for many reasons (Vollmer & Norry, 1983a). Many of these features are indicative of influence of carbonate liquid, the most significant of which are listed below:

(a) Very high strontium contents, and correspondingly low Rb/Sr ratios (Vollmer & Norry, 1983a).

(b) Very low ratios of Th/U. Vanlerberghe *et al.* (1987) found that Th/U ratios for lavas from Nyiragongo ranged from 1.0-4.5, with an average of *ca.* 2.6. Further evidence for low Th/U comes from Williams & Gill (1989) where Th/U ratios from samples analysed in their U-Th disequilibria studies were found to be between 1.00 and 1.24. Most basalts, and chondritic values of Th/U range between 4 and 5.

(c) Variability of Pb-isotope ratios in Nyiragongo lavas (Vollmer & Norry, 1983b). These are perhaps best explained by relatively recent fractionation of Pb, Th, and U.

(d) U-series disequilibria of Nyiragongo lavas (Williams & Gill, 1989). Nyiragongo is one of the few occurrences of large depletions of ^{230}Th relative to ^{238}U (see Figure 11.10).

11.4.3. Hawaiian volcanism.

The discussions so far have been limited to continental occurrences. In order to confirm involvement of carbonate liquids in asthenospheric processes it is necessary to constrain the role of carbonate in oceanic basaltic volcanism. The Hawaiian islands consist of some of the most volumious and also most extensively studied oceanic intraplate volcanics. They are therefore ideal as an example of carbonate involvement in the genesis of voluminous silicate magmas. This section will first concentrate on specific rock suites within the Hawaiian islands which are thought to show evidence of carbonate involvement, before making generalisations about Hawaiian volcanism as a whole.

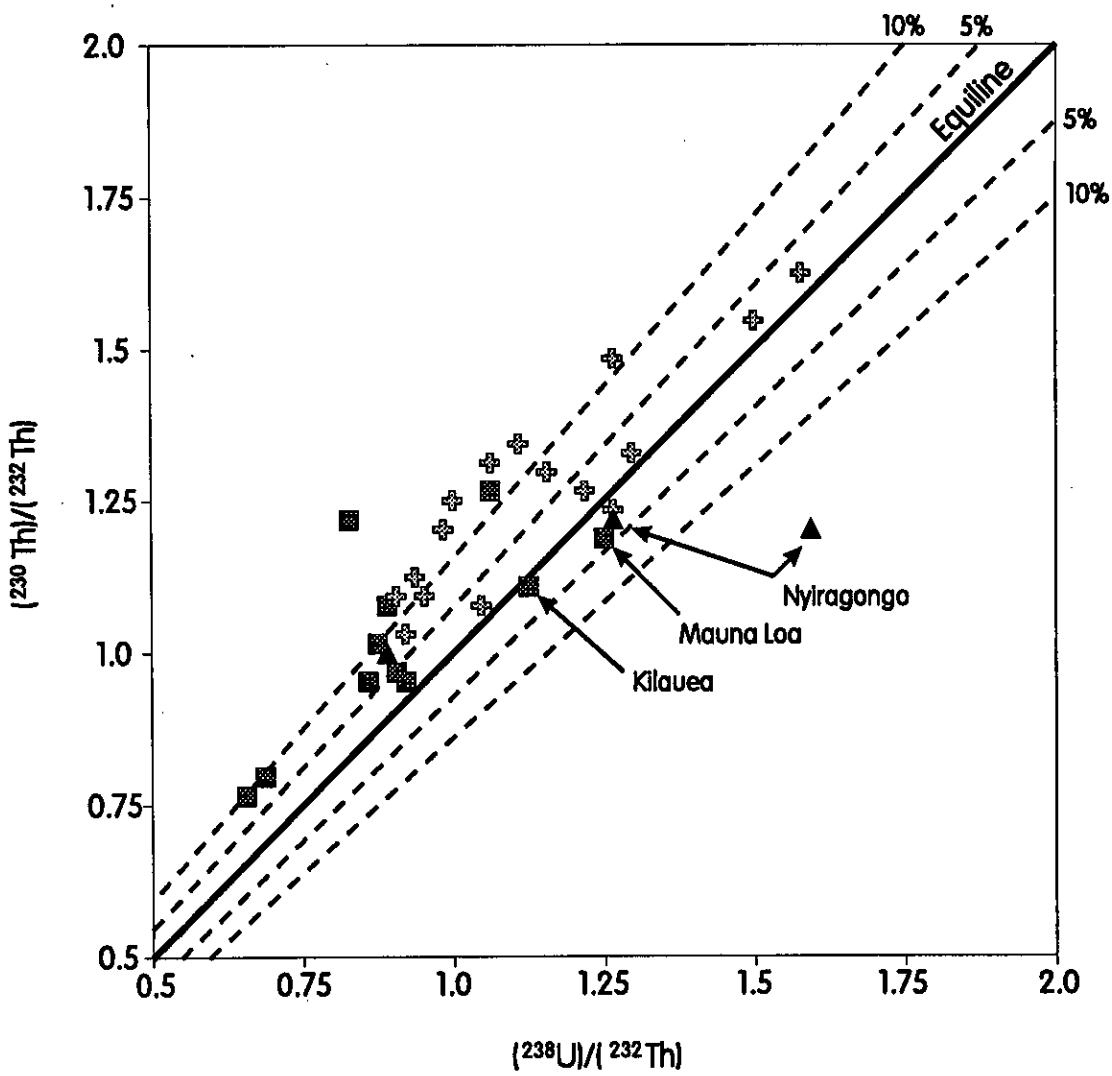

Figure 11.10. U-series disequilibrium in oceanic and continental basalts (Williams & Gill, 1989). In most basalts, certainly MORB, there seems to be an excess of ^{230}Th. This is not compatible with the effects of carbonate liquid, which will result in depletion of ^{230}Th relative to ^{238}U due to increase of U/Th. Only the rocks of Nyiragongo, Mauna Loa and Kilauea show excesses of ^{238}U over ^{230}Th. It is suggested that carbonate liquid is involved in the formation of these rocks. If partial melting is the process responsible for U-series disequilibria, then it seems likely that segregation of very small silicate-melt fractions leads to an excess of ^{230}Th over ^{238}U, i.e. thorium must be more incompatible in mantle phases than uranium.

✣ , Mid-Ocean Ridge Basalts.
■ , Ocean Island Basalts.
▲ , Continental Basalts (Nyiragongo).

(a) The Koloa volcanics, Kauai (Maaloe *et al.*, 1992).

The features which were ascribed to carbonate influence in the previous sections are also seen in this suite of alkali basalts, nephelinites and melilitites. Figure 11.11 shows that the REE distributions seen in these lavas are best explained by a single stage process of melting involving a carbonate input (after McKenzie & O'Nions, 1991). Again, as with many continental basaltic suites, the LREE contents of the Koloa volcanics cannot easily be explained using standard $^{mantle/Ls}D_{REE}$ partition coefficients.

Another method of diagnosing carbonate involvement used earlier in this chapter was comparison of elements of similar compatibility (e.g. Ba/Th, Ba/Rb, Th/U, Zr/Hf, Nb/Ta). Table 11.3 shows that the lavas of Kauai show many features diagnostic of carbonate involvement (high LILE/HFSE, low Th/U, high Zr/Hf and Nb/Ta). It is also worth noting that these features become more intense as the lavas become more undersaturated, suggesting greater carbonate involvement in the melilitites than in the alkali basalts.

Table 11.3. Geochemical features of the Koloa Volcanic Suite of Kauai, Hawaii (from Maaloe *et al.*, 1992). Note high Ba/Rb, high LILE/HFSE, high Zr/Hf, Nb/Ta, and low Th/U.

Ratios of incompatible elements	Alkali Basalt	Basanite	Nephelinite	Melilitite
Ba/Rb	22	35	40	37
Ba/Th	274	205	180	205
Ba/Hf	154	214	226	225
Ratios of elements of very similar incompatibility	**Alkali Basalt**	**Basanite**	**Nephelinite**	**Melilitite**
Zr/Hf	44	48	45	53
Nb/Ta	17	17	17	17
Th/U	2.3	2.8	4.0	3.1

(b) Other undersaturated volcanic suites (Chen & Frey, 1985; Clague & Frey, 1982).

Other alkaline suites in the Hawaiian islands also show evidence of carbonate involvement. This section will concentrate on the Haleakala volcanics, East Maui (Chen & Frey, 1985), and the Honolulu volcanics, Oahu (Clague & Frey, 1982). In both cases, ratios of LILE/HFSE have been investigated as it is here that the involvement of carbonate melt is believed to be most pronounced.

Three elements which are strongly partitioned are barium (to the carbonate) and zirconium and hafnium (to the silicate). Since the carbonate liquid should contain only minimal quantities of Hf and Zr, their concentration will be little affected by the presence of a precursor of carbonate liquid. In contrast, barium is strongly enriched in mantle carbonate liquid, and will therefore be present in extremely high concentrations. Addition of carbonate liquid will therefore result in large variations in Ba/Hf and Ba/Zr with little change in Zr and Hf concentrations (perhaps even a slight fall). This is obviously a very different effect to that produced by decreasing the degree of silicate partial melting of the mantle. In this case, the increase in Ba/Hf and Ba/Zr will be small, whilst there will be large increases in the Zr and Hf contents.

Figure 11.12 shows Ba/Hf, and Ba/Zr vs. Hf and Zr for the Haleakala lavas of East Maui. It can be seen that Ba/Hf and Ba/Zr are little related to Zr and Hf contents. Variations in these ratios are therefore not due to variations in degree of partial melting. The variations in Ba/Zr and Ba/Hf can be explained by addition of 5% carbonate liquid containing 3000 p.p.m. barium, less than 300 p.p.m. Zr, and negligible Hf.

A similar procedure has been undertaken for the lavas of the Honolulu series in Figure 11.13. Again, large variations in Ba/Hf and Ba/Zr are seen with little variation in concentration of HFSE. In this case 25% of carbonate liquid would have to be added to produce the extensive variations in Ba/Hf and Zr/Hf seen.

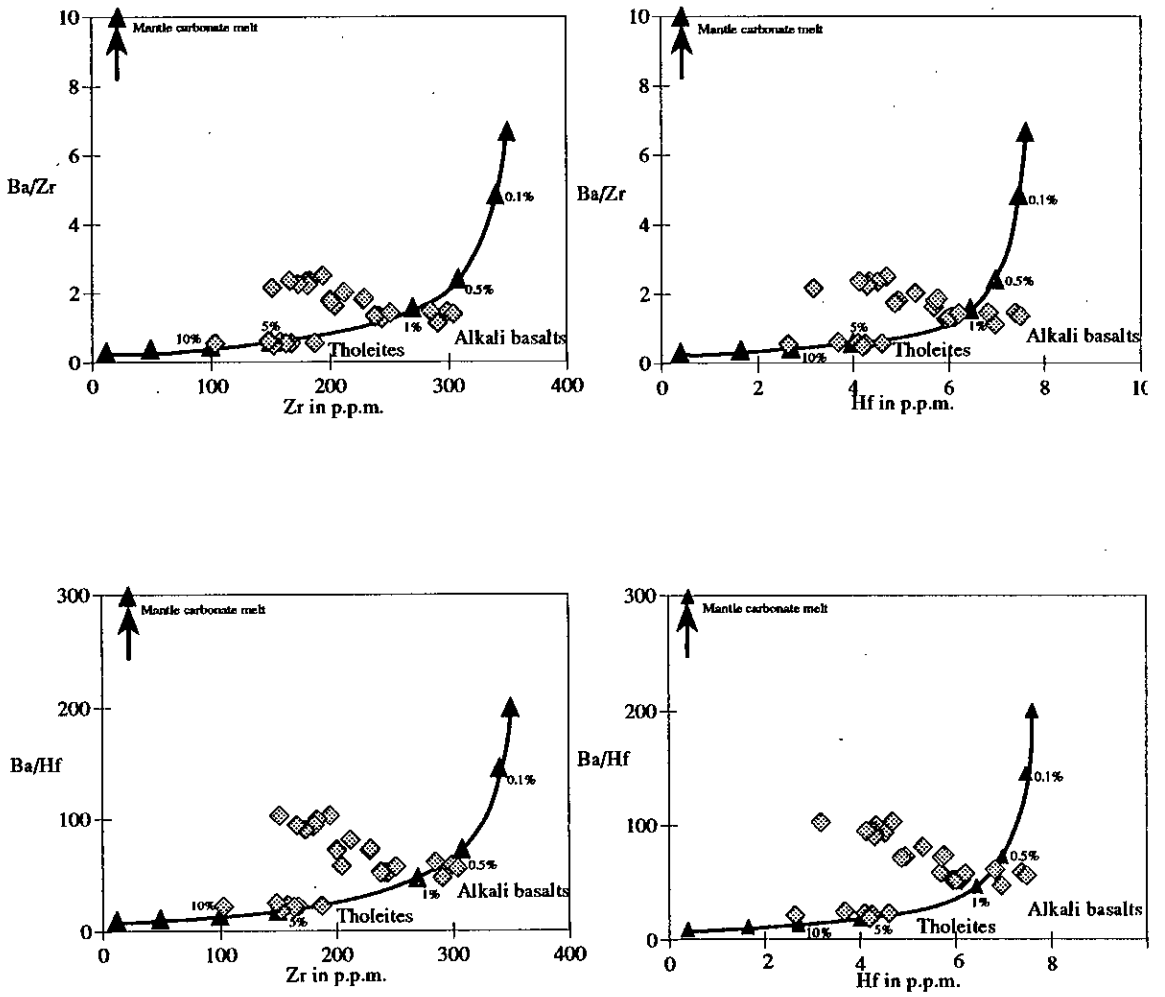

Figure 11.12. Ba/Hf and Ba/Zr ratios of the Haleakala lavas of East Maui. Variations in Ba/Hf and Ba/Th do not follow trends expected from variations in degree of silicate partial melting. The variability could however be explained by addition of *ca.* 5% of carbonate liquid. This will add over 150 p.p.m. of Ba whilst having little effect on Zr and Hf concentrations.

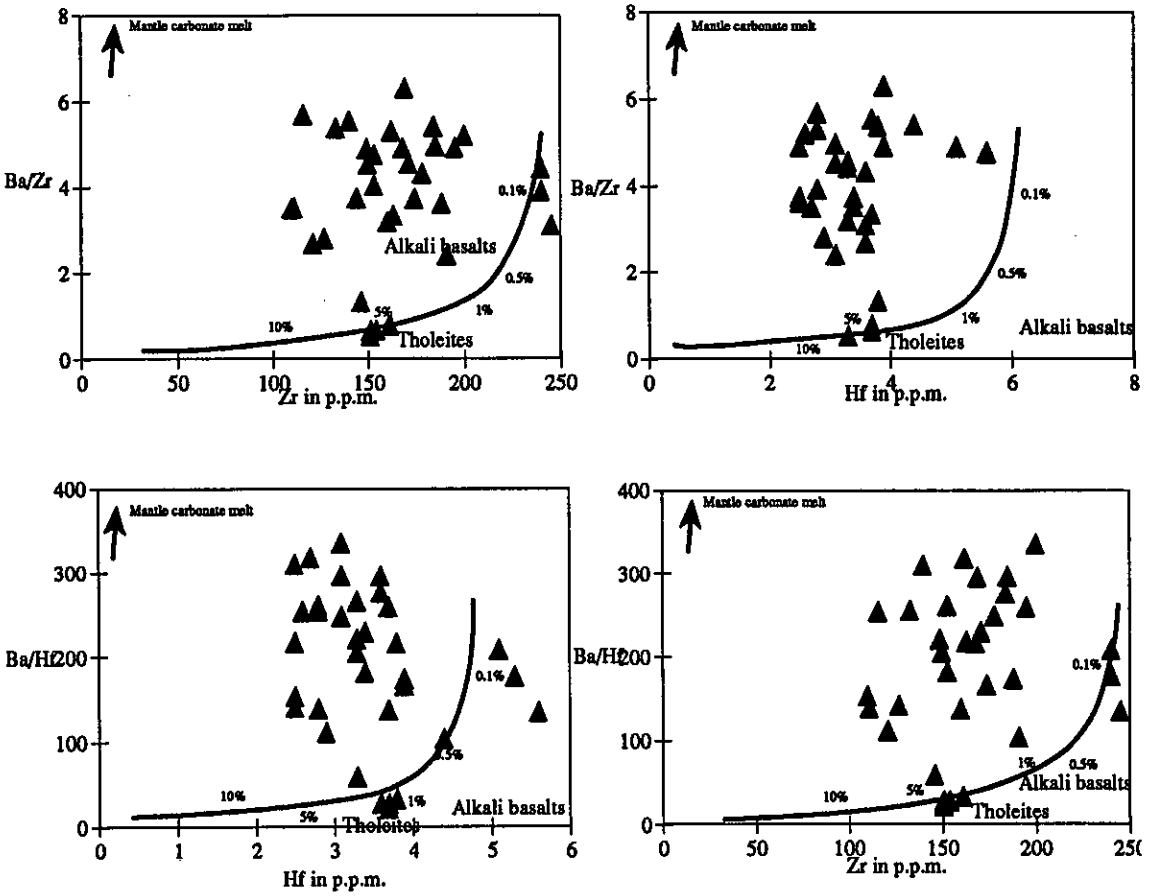

Figure 11.13. Ba/Hf and Ba/Zr ratios from the Honolulu volcanics, Oahu. The wide variability in Ba/Hf and Ba/Zr without change in Hf and Zr concentrations is best explained by addition of a carbonate liquid containing > 3000 p.p.m. Ba, but less than 300 p.p.m. Zr, and negligible Hf. Approximately 25% of this carbonate liquid would have to be added to produce the most extreme examples of Ba/Hf and Ba/Zr seen.

(c) Carbonate involvement in Hawaiian volcanism in general.

Zr/Hf and Nb/Ta ratios have been plotted for a selection of Hawaiian suites (Figure 11.14). Both are generally higher than would perhaps be expected for mantle derived melts(ca. 40 and 18 instead of 35 and 15). Also, it can be seen that both Zr/Hf and Nb/Ta rise with increasing undersaturation of the lavas. These features are consistent with addition of carbonate liquid, although the amount of carbonate necessary to produce these effects is somewhat larger than expected (at least 20% of the material).

High Zr/Hf ratios have been reported from many other undersaturated rock suites on oceanic islands (e.g. Dupuy *et al.*, 1989; Gerlach *et al.*, 1988; Liotard *et al.*, 1986; Weaver, 1990). This data, combined with data from continental intraplate volcanism, has been used by Dupuy et al. (1992) as evidence of involvement of carbonate liquid as a precursor melt in the genesis of most intraplate basaltic rocks.

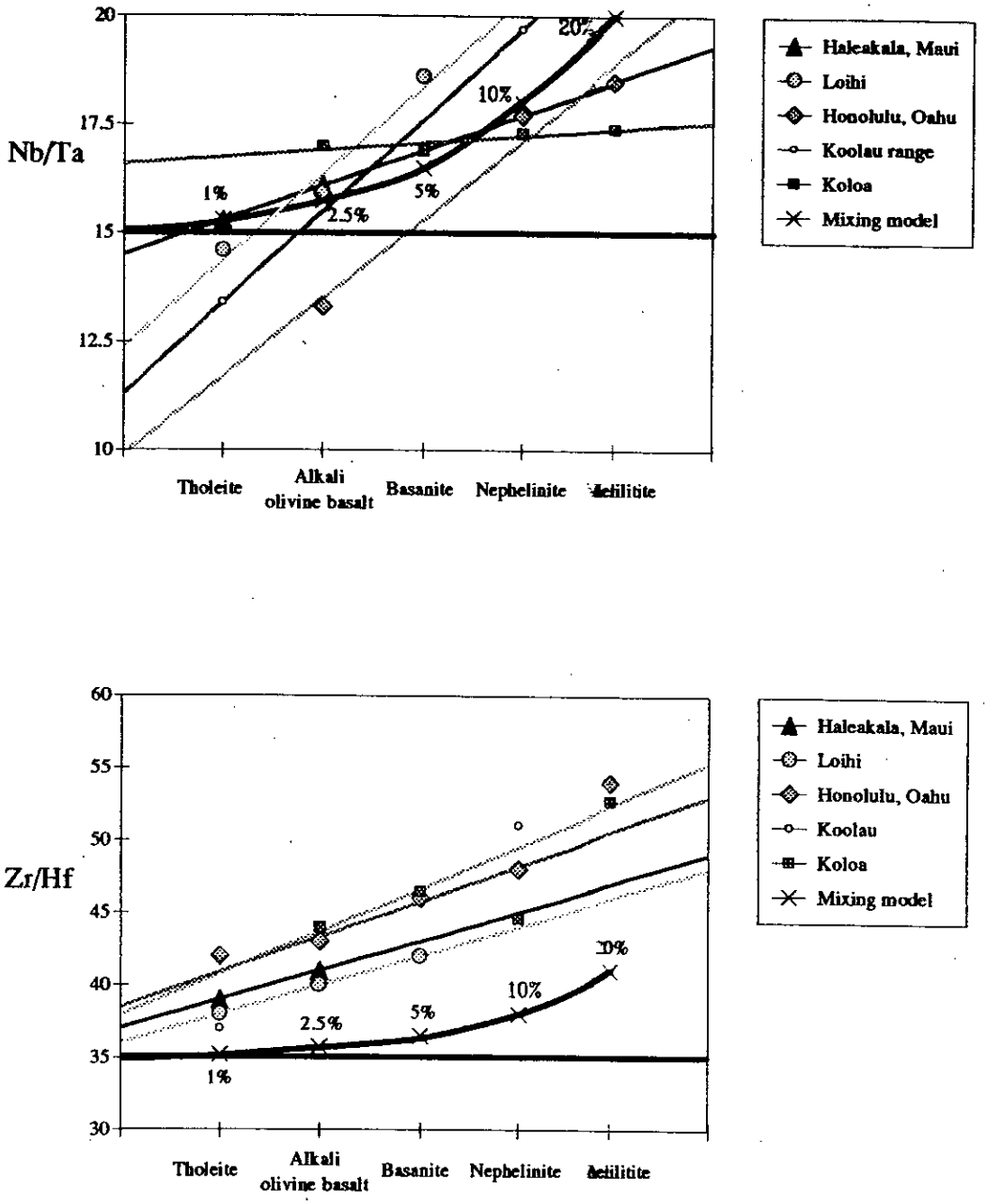

Figure 11.14. Variation in Zr/Hf and Nb/Ta in the alkaline lavas of Hawaii. Both Zr/Hf and Nb/Ta increase gradually with increasing undersaturation. For Nb/Ta these changes can be easily explained by addition of carbonate liquid. For Zr/Hf the variations are larger than would be expected from addition of reasonable quantities of carbonate. It is possible that the Zr/Hf of the mantle is actually higher than that chosen here (Zr/Hf = 35). If a higher Zr/Hf were chosen, the data would fit the mixing model more readily.

11.5. Is carbonate melt involved in MORB genesis?

McKenzie (1985b) suggested that ^{230}Th-^{238}U disequilibria seen in MORB were due to scavenging of Th by a highly-mobile small-volume carbonate melt. The partitioning behaviour observed in the experiments described in this thesis shows this suggestion is unfounded; small-volume carbonate melts will scavenge U rather than Th, and will therefore result in deficiencies in ^{230}Th rather than in the 5-10% excesses seen in MORB (see Figure 11.10). Production of ^{230}Th excesses must therefore be produced in "normal" silicate mantle melting events, presumably because Th is more incompatible than U in mantle phases. The ^{230}Th-^{238}U disequilibria that was initially attributed to the scavenging action of a carbonate melt must therefore now be viewed as evidence for the lack of a carbonate precursor in MORB genesis. This is in agreement with the work of McKenzie & O'Nions (1991), where it was shown by inversion of REE data that MORB does not contain any significant contribution of melt from the garnet-stability zone. Garnet is stable at depths below *ca.* 70 km. Similarly, carbonate liquid is only stable in the asthenospheric mantle at depths below *ca.* 75 km. MORB *cannot* therefore contain a significant carbonate component.

There is one further possibility that arises from the ^{230}Th-^{238}U disequilibria seen in MORB. Could carbonate melt have been removed from MORB source mantle shortly before decompression melting took place? This would certainly explain the disequilibrium systematics of MORB. If a ^{230}Th-depleted carbonate melt were removed from the mantle, the residue would be ^{230}Th enriched. Large-degree partial melts from this residual mantle would therefore inherit this ^{230}Th enriched character. Although this scenario fits experimental and analytical evidence, one rather major obstacle exists; where does the carbonate liquid go, and why does it not get incorporated into the MORB-generating process? Models of melt extraction (e.g. Spiegelman & McKenzie, 1987) suggest that melt produced over a wide zone (say 50 km wide) around a mid-ocean ridge would be channelled to the ridge axis by matrix corner flow. It may be possible that the depth of genesis, small melt fraction, and physical properties of carbonate melt may allow it to escape from the mid-ocean ridge plumbing system, although no explanation for this process is put forward here. In short, the cause of ^{230}Th-^{238}U disequilibria in MORB is still unknown, but it does now seem unlikely that there is significant carbonate involvement in MORB petrogenesis.

11.6. Conclusions.

The geochemical characteristics of mantle-derived melts suggest carbonate involvement in a number of petrogenetic processes:

(a) Production of carbonatites. Carbonatites may be produced directly by partial melting of carbonated peridotite, by immiscibility with mantle-derived silicate material, or as residual melts after crystallisation of dominantly silicate melts. In all cases carbonate-mantle equilibria are involved in their genesis.

(b) Metasomatism of lithospheric mantle. Evidence for carbonate involvement in mantle metasomatism comes from the major-element composition of xenolith suites (e.g. Leura-Shadwell, Australia), from trace-element and isotopic characteristics of cratonic xenoliths and xenocryst (e.g. Loch Roag, Scotland), and from the characteristics of lithosphere-derived partial melts (e.g. Smoky Butte lamproites, Wyoming, USA).

(c) Production of small-volume melts. The characteristics of many small-volume silicate melts are indicative of carbonate involvement. These include kimberlites, minettes, and melilitites.

(d) Carbonate precursors to voluminous silicate magmatism. Evidence for carbonate involvement in silicate magma genesis comes from both continental (e.g. Hessian trough, Germany), and oceanic (e.g. Hawaii) basaltic rocks. As more data become available, it is expected that involvement of carbonate melt will be invoked more frequently.

(e) Carbonate melt as a fugitive agent in the asthenospheric upper mantle. Evidence for melt movement in the asthenosphere is likely to be short-lived due to convection processes in the upper mantle. One example of evidence for carbonate melt movement may however be the ^{230}Th-^{238}U disequilibria seen in MORB, and in intraplate oceanic volcanism.

CHAPTER 12

SUMMARY, CONCLUSIONS, AND IMPLICATIONS FOR FURTHER RESEARCH

12.1. The experiments.

Four major experimental approaches were used in an attempt to constrain the geochemical properties of carbonate liquids:

(a) Experiments to find an immiscible carbonate melt in equilibrium with primary olivine melilitite (TAS 3). These proved unsuccessful, as the depolymerised melilititic melt was found to be miscible with carbonate over the range of pressures and temperatures studied. It is therefore suggested that carbonate and silicate liquids are likely to be completely miscible under mantle conditions.

(b) Experiments designed to produce carbonate-rich melts in coexistence with mantle phases (e.g. clinopyroxene). Although these experiments obtained their primary objective (production of coexisting carbonate melt and clinopyroxene), there were problems of quench heterogeneity of the carbonate liquid, modification of the liquid compositions on quenching, and in polishing the samples. These experimental charges were not considered suitable for ion probe analysis, as it was suspected that the analytical uncertainty on $^{Cpx/Lc}D_i$ values were likely to mask the true geochemical character of the carbonate melt.

(c) Experiments in the system CaO-Na_2O-Al_2O_3-SiO_2-CO_2. Immiscible carbonate and silicate liquids were obtained in the majority of experimental charges. Large-scale two-liquid textures were produced which were considered ideal for determination of partitioning behaviour. Immiscibility was obtained in both Na-rich and Na-poor charges.

(d) Experiments were performed on a number of natural rock compositions believed to be related to carbonatites by liquid immiscibility. They were mixed with Ca-rich and Ca-Na carbonates to produce coexisting carbonate liquids. Again, most of the experiments proved successful in producing coexisting carbonate and silicate liquids. A wide range of carbonate melt compositions were produced in these experiments, ranging from sodium-poor Ca-Mg-Fe carbonate melt, to sodium-rich Ca-Na carbonate melt. This range encompasses the bulk compositions of the vast majority of naturally occurring carbonatites, and dispels the suggestion that immiscibility can only occur in extremely sodic melt compositions. Again, large-scale two-liquid textures were produced, facilitating electron- and ion-probe analysis.

12.2. The data set.

Partitioning behaviour between coexisting carbonate and silicate liquids has been investigated for 30 major, minor and trace elements. Ca, Mg, Fe, Mn, Na, K, Si, Al, Ti, and P were analysed by electron probe; Mg, K, Ti, V, Mn, Fe, Rb, Sr, Y, Zr ,Nb, Mo, Cs, Ba, La , Ce, Nd, Sm, Tm, Lu, Hf, Ta, Pb, Th, and U were analysed by ion probe. Partitioning for F, Cl, and S was only determined in specially doped samples. $^{Ls/Lc}D_i$ partition coefficients are now well constrained for these elements. The exception is Pb where uncertainty on the values is large due to low concentrations and poor ion yield.

Coexisting carbonate and silicate liquids were analysed from both synthetic experimental charges and natural compositions. These melts span a wide range of composition both in terms of alkali content, and polymerisation state. $^{Ls/Lc}D_i$ have been obtained over a pressure range from 0.2 to 2.0 GPa, and a temperature range from 1100° to1300°C.

12.3. Chemical controls on partitioning.

Simple element chemistry can be used to explain partitioning behaviour, both in delineating general features, and in explaining specific relationships. Some of the physical and chemical properties believed to have most influence on partitioning behaviour are listed below.

12.3.1. Ionic radius.

Relative partitioning of elements of the same valency can be explained by variations in ionic radius; there is a simple relationship between ionic radius and $^{Ls/Lc}D_i$, with the carbonate melt preferring elements of larger ionic radius, and the silicate melt preferring smaller ions. This relationship holds for +1, +2, +3, and +5 elements. No simple relationship between ionic radius and $^{Ls/Lc}D_i$ was found for +4 elements; another factor must be influencing partitioning in this case. Overall, there is good correlation between $^{Ls/Lc}D_i$ and ionic radius for elements with R > 100 pm. In contrast. Smaller ions, however, exhibit more variable partitioning behaviour.

12.3.2. Charge density.

The majority of elements lie on a trend of increasing $^{Ls/Lc}D_i$ with increasing charge density. This trend continues until $^{Ls/Lc}D_i$ reaches a maximum at C/R ~ 0.05 (e.g. Al^{3+}, Hf^{4+}). Elements with extremely high charge density (e.g. V^{5+}, P^{5+}) are again partitioned to the carbonate liquid.

12.3.3. Complexing.

Although, in general, partitioning can be related to ionic charge and size, some discrepancies exist. For example, elements of identical charge and valency do not always partition identically (e.g. Zr^{4+}-Hf^{4+}, U^{4+}-Th^{4+}, Nb^{5+}-Ta^{5+}). It is believed that these discrepancies are related to the differences in complexing behaviour with other elements. As an example, U^{4+} has two electrons left in its outer shell (after losing the four valence electrons). It can use these electrons to form complexes with PO_4^{3-} and CO_3^{2-} ions, both of which are concentrated in the carbonate melt. Th^{4+} does not have these two electrons. Another example is thought to be REE-PO_4^{3-} complexing. REE are more strongly enriched in the carbonate liquid in the presence of P than in P-absent charges. This is best explained in terms of REE-PO_4^{3-} complex formation.

12.4. Physical controls on partitioning.

12.4.1. Structural and compositional control.

Two main compositional variables are believed to influence partitioning:

(a) Polymerisation state of the silicate liquid. Polymerisation state of the silicate melt not only controls the extent of carbonate-silicate mixing, but also causes variation in the partitioning of some trace elements. For example, the REE are more inclined to enter a depolymerised silicate melt than a polymerised silicate melt.

(b) Na-content of the carbonate melt. The main compositional variable in the carbonate melt is Ca/Na ratio. If the carbonate melt is very sodic, then sodium and the other alkali elements will be strongly enriched in the carbonate. If the melt is Ca-rich, the alkali metals are rejected from the carbonate liquid.

12.4.2. The effect of temperature.

Variations in temperature have little effect on partitioning behaviour. The sense of partitioning is unaffected by temperature, although partitioning does become less pronounced at high temperature. This is interpreted as a closure of the solvus, with more mixing of components (less structural distinction) at higher temperature.

12.4.3. The effect of pressure.

Increasing pressure has little or no effect on partitioning in the synthetic system. Variations are seen, but they are small, and rarely exceed analytical uncertainty. In contrast, quite significant variations in partitioning with pressure are seen in the natural system. Not only is the intensity of partitioning influenced, but also the sense of partitioning is reversed for some elements as pressure is increased. These variations cannot be attributed to solvus effects, and must have an alternative explanation. The only major difference between the synthetic compositions (where little pressure effect was seen) and the natural compositions (where significant variations with pressure occur) is the presence of Mg, Fe and Mn. Increasing concentrations of Mg, Fe, and Mn leads to a substantial change in the molar volume of the carbonate liquid (and therefore its density). It is this that is thought to cause the variations in partitioning seen with pressure in natural compositions.

12.5. Geochemical characteristics of mantle-derived carbonate melt.

The partitioning dataset obtained in this study has been used to determine the geochemical characteristics of mantle carbonate melt. The features thought to be most diagnostic of carbonate are given below;

(a) High LILE/HFSE ratios (e.g. Ba/Hf, Ba/Th etc.). These are often more than a factor of 100 higher in the carbonate liquid than in the corresponding silicate melt.

(b) Extreme LREE/HREE enrichment. La/Lu is 4-5 times higher in the carbonate liquid than in the coexisting silicate liquid.

(c) Low Th/U ratios. There is a tendency for U to enter the carbonate melt while Th is rejected. This leads to lower Th/U in the carbonate melt, often less than 1.

(d) High Zr/Hf ratios. Hf is more strongly rejected by the carbonate melt than is Zr. Zr/Hf, where measurable, is higher in the carbonate melt than in the corresponding silicate by a factor of *ca.* 2. There still remains the remote possibility that this is an analytical artefact rather than truly representing partitioning behaviour.

(e) High Nb/Ta ratios. As with Zr/Hf, Nb is fractionated from Ta in carbonates. Nb/Ta is usually three times higher in the carbonate liquid than in its conjugate silicate liquid. It is unlikely that such a significant difference in partitioning behaviour could be explained by analytical problems.

(f) Distinctive isotopic characteristics. Carbonate melts have low Rb/Sr, very low Sm/Nd, and low Th/Pb and U/Pb. With time, carbonate-melt influenced material will evolve distinctive isotopic characteristics.

12.6. Applications of carbonate-silicate partitioning to natural rocks.

12.6.1. Carbonatites.

The data obtained in this study have been used to test theories for the origins of carbonatites. Many magnesiocarbonatites may be produced by direct melting of mantle peridotite as primary mantle melts. However, the majority of carbonatites do not have trace-element characteristics which are in accord with this origin. Examples can be found which suggest genesis by both immiscibility, and by extreme fractional crystallisation of carbonated silicate melts.

Partitioning data obtained from analysis of carbonate standards has given an insight into the evolution of carbonatites as well as their initial concentrations. A number of elements are present in carbonate liquid at relatively high concentrations, but are unable to enter crystalline carbonate (e.g. P, Nb, Ti, V, Cu, Zr). These elements become strongly concentrated in non-carbonate phases (e.g. oxides, sulphides phosphates and silicates). It is this concentration, combined with the ease of separation of minerals by crystal settling in carbonate liquids, that leads to the wealth of economic mineralisation associated with carbonatites.

12.6.2. Metasomatism in mantle xenoliths.

The process of mantle metasomatism by carbonate liquid is recorded in the characteristics of mantle-derived xenoliths and megacrysts. Examples include the Leura-Shadwell suite, Australia and the Loch Roag suite, Scotland.

12.6.3. Source characteristics of lithosphere-derived melts.

Lithospheric melts inherit trace-element and isotopic characteristics from their source areas. In the case of a number of lithosphere-derived melts, these characteristics are indicative of mantle enrichment by carbonate melts. Examples include kamafugites from Toro-Ankole, and many lamproites (e.g. Smoky Butte, Wyoming).

12.6.4. Involvement in the generation of small-volume silicate melts.

The presence of carbonate in the mantle assemblage can lead to the production of small volumes of melt at temperatures lower than the dry peridotite solidus. Melts produced by carbonate involvement in this way show many trace-element characteristics diagnostic of carbonate melt. Examples include kimberlites, melilitites and lamprophyres.

12.6.5. Involvement of carbonate melt as a precursor to more voluminous silicate magmatism.

Certain characteristics of mantle-derived silicate magmatism have been ascribed to carbonate involvement. The alkaline lavas of the Hessian depression, Nyiragongo, and Hawaii have been used as examples of this involvement. It now seems unlikely, however, that carbonate melt is involved directly in the generation of MORB.

12.7. Avenues of further research.

Three distinct directions for further study arise from the results of this project:

(a) Experimental determination of trace-element behaviour during melting in the presence of mixed volatiles.

We now have information on the likely characteristics of the first melt produced from the mantle in the presence of pure CO_2 (as carbonate). It may now be possible to use melt-entrapment techniques (e.g. Odling & Randle, 1992) to determine trace-element partition during mantle melting in the presence of other volatile species (H_2O, CH_4, N_2, S_2, Cl_2, F_2), and indeed with mixed volatiles (e.g. H_2O-CO_2 fluid). In this way, it should be possible to constrain the role of volatiles in mantle petrogenetic processes.

(b) Applications of $^{Ls/Lc}D_i$ partitioning data to carbonatites.

From $^{Ls/Lc}D_i$ data, the likely trace-element characteristics of initial carbonatite liquids can be predicted and we can now concentrate on their evolution with fractionation processes. It should be possible to obtain data for element partition between carbonate liquid and crystalline phases found in carbonatites (e.g. carbonates, apatite, perovskite, pyrochlore etc.), either by petrographic observation, or by experimental determination. This will allow us to model the evolution of carbonatite magmas with fractional crystallisation and differentiation, and thereby gain a better understanding of carbonatite magmatism. A further area of research could involve experiments to determine trace-element partitioning between carbonate melt and alkaline, water-rich fluid. This will have obvious relevance to fenitisation processes associated with both carbonatites and alkaline silicate magmas.

(c) Applications of $^{Ls/Lc}D_i$ partitioning data to mantle-derived silicate magmatism.

The geochemical section of this project has only been able to scratch the surface of the possible involvement of carbonate liquids in the genesis of mantle-derived magma. The partitioning data now available can be used to isolate carbonate involvement in rock suites from all over the world. It is expected that, as more high-precision data become available, recognition of carbonate involvement will become more widespread. Even with the data available at present, it seems possible that application of $^{mantle/Lc}D_i$ partition coefficients will solve a number of the unanswered questions relating to mantle melting, and explain some of the surprising characteristics of mantle-derived melt.

References.

Adams JAS, Osmond JK, Rogers JJW (1959) The geochemistry of thorium and uranium. Phys. Chem. Earth 3: 298-348

Adams JAS, Weaver CE (1958) Thorium and uranium ratios as indicators of sedimentary processes: an example of geochemical facies. Am. Assoc. Petroleum Geology 42: 387-430

Alibert C, Albarede F (1988) Relationships between mineralogical, chemical, and isotopic properties of some North American kimberlites. J. Geophys. Res. 93: 7643-7671

Alibert C, Michard A, Albarede F (1983) The transition from alkali basalts to kimberlites: isotope and trace-element evidence from melilitites. Contrib. Mineral. Petrol. 82: 176-186

Allen JC, Modreski PJ, Haygood C, Boettcher AL (1972) The role of water in the mantle of the earth: the stability of amphiboles and micas. 24th Int. Geol. Congr. Rep. Sess. 231-240

Allègre CJ, Pineau F, Bernat M, Javoy M (1973) Evidence for the occurrence of carbonatite on Cape Verde and the Canary Islands. Nature (Physical Sciences) 233: 103

Allman R, Koritnig S (1971) Fluorine. In: Handbook of Geochemistry. Springer-Verlag

Amundsen HEF (1987) Evidence for liquid immiscibility in the upper mantle. Nature 327: 692-693

Arculus RJ, Delano JW (1987) Oxidation state of the upper mantle: present conditions, evolution and controls. In: Nixon PH (ed) Mantle xenoliths. John Wiley pp 589-98

Auterfage F, Couderc JJ (1980) Étude du méchanisme de la migration du sodium et du potassium au cours de leur analyse à la microsonde électronique (in French). Bull. Mineral. 103: 623-629

Baes CF Jr. (1956) The reduction of uranium (VI) by iron (II) in phosphoric acid solution. J. Phys. Chem. 60: 805-806

Bailey DK (1989) Carbonate melt from the mantle in the volcanos of S-E Zambia. Nature 338: 415-17

Baker MB, Wyllie PJ (1990) Liquid immiscibility in a nephelinite-carbonatite system at 25kb and implications for carbonatite origin. Nature 346: 168-170

Bedson P (1983) The origin of carbonatites and their relations to other rocks by liquid immiscibility. PhD thesis, University of Manchester.

Bedson P (1984) Rare-earth element distribution between immiscible silicate and carbonate liquids. Progress in experimental petrology, Sixth report NERC: 12-14

Berg GW (1986) Evidence for carbonate in the mantle. Nature 324: 50-51

Bergman SC (1987) Lamproites and other potassium-rich rocks: a review of their occurrences, mineralogy, and geochemistry. In Fitton JG, Upton BGJ (eds) Alkaline igneous rocks. Blackwell, London pp103-190

Bernard-Griffiths J, Peucat JJ, Fourcade S, Kiensast JR, Ouzegane K (1988) Origin and evolution of 2 Ga carbonatite complex (Ilouhaouene, Ahaggar, Algeria). Nd and Sr isotopic evidence. Contrib. Mineral. Petrol. 100: 339-348

Biellman C, Gillet P, Guyot F, Reynard B (1992) Stability and reactivity of carbonates at lower mantle pressures and temperatures. Terra Abstracts 4: 5

Boettcher AL, Mysen BO, Allen JC (1973) Techniques for the control of water fugacity and oxygen fugacity for experimentation in solid-media high pressure apparatus. J. Geophys. Res. 78 (26): 5898-5902

Bolivar SL (1977) Geochemisry of the Prairie Creek, Arkansas, and Elliott county, Kentucky intrusions. PhD thesis, Univ. New Mexico, Alburquerque, USA

Borum MP, Hanneman RE (1967) Local compositional changes in alkali silicate glasses during electron microprobe analysis. J. Applied Physics 38: 2406-2407

Boyd FR, England JL (1960) Apparatus for phase equilibrium measurements at pressures up to 50kb and temperatures up to 1750°C. J. Geophys. Res. 65: 741-748

Brenan JM, Watson EB (1991) Partitioning of trace elements between carbonate melt and clinopyroxene and olivine at mantle P-T conditions. Geochim. Cosmochim. Acta 55: 2203-2214

Brey GP (1976) Carbon dioxide in silica-undersaturated basaltic magmas. PhD thesis, Australian National University.

Brey GP (1978) Origin of olivine melilitites; chemical and experimental constraints. J. Volcanol. Geotherm. Res. 3: 61-88

Brey GP, Brice WR, Ellis DJ, Green DH, Harris KL, Ryabchikov ID (1983) Pyroxene-carbonate reactions in the upper mantle. Earth Planet. Sci. Letts. 62: 63-74

Brey GP, Green DH (1976) Solubility of CO_2 in olivine melilitite at high pressures and the role of CO_2 in the Earth's upper mantle. Contrib. Mineral. Petrol. 55: 217-230

Bryndzia LT, Wood BJ (1990) Oxygen thermobarometry of abyssal spinel peridotites: the redox state and C-O-H volatile composition of the Earths sub-oceanic upper mantle. Am. J. Sci. 290: 1093-1116

Byrne RH, Lee JH, Bingle LS (1991) Rare-earth element complexation by PO_4^{3-} ions in aqueous solution. Geochim. Cosmochim. Acta 55(10): 2729-2735

Canil D (1990) An experimental study bearing on the abscence of carbonate in mantle-derived xenoliths. Third international symposium of experimental mineralogy, petrology and geochemistry; Abstracts: 4

Cantrell KJ, Byrne RH (1987) Rare-earth element complexation by carbonate and oxalate ions. Geochim. Cosmochim. Acta 51: 597-605

Chang LLY (1971) Subsolidus phase relations in aragonite-type carbonates: II the systems $CaCO_3$-$SrCO_3$-$PbCO_3$ and $CaCO_3$-$BaCO_3$-$PbCO_3$. Am. Mineral. 57: 155-168

Chen C, Frey FA (1985) Trace-element and isotopic geochemistry of lavas from the Haleakala volcano, East Maui, Hawaii; implications for the origin of Hawaiian basalts. J. Geophys. Res. 90: 8743-8768

Choppin GR (1971) Structure and thermodynamics of rare-earth element complexes in solution. Pure Appl. Chem. 27: 23-41

Clague DA, Frey FA (1982) Petrology and trace-element geochemistry of the Honolulu volcanics, Oahu; implications for the oceanic mantle below Hawaii. J. Petrol. 23: 447-504

Cohen RS, O'Nions RK (1982) The lead, neodymium, and strontium isotopic structure of ocean ridge basalts. J. Petrol. 23: 299-324

Cullers RF, Medaris G (1977) Rare earth elements in carbonatites and cogenetic alkaline rocks; examples from Seabrook Lake, and Callender Bay, Ontario. Contrib. Mineral. Petrol. 65: 143-153

Daniels LRM, Gurney JJ (1991) Oxygen fugacity constraints on the Southern African lithosphere. Contrib. Mineral. Petrol. 108: 154-161

Darby Dyar M, McGuire AV, Ziegler RD, (1988) Redox equilibria and crystal chemistry of coexisting minerals from spinel lherzolite mantle xenoliths. Am. Mineral. 74: 969-980

Dawson JB, Gale NH (1970) Uranium and thorium in alkalic rocks from the active carbonatite volcano Oldoinyo Lengai. Chem. Geol. 6: 221-231

Dawson JB, Hawthorne JB (1973) Magmatic sedimentation and carbonatitic differentiation in kimberlite sills at Benfontein, South Africa. J. Geol. Soc. Lond. 129: 61-85

Dawson JB, Pinkerton H, Norton GE, Pyle, DM (1990) Physiochemical properties of alkali carbonatite lavas: data from the 1988 eruption of Oldoinyo Lengai, Tanzania. Geology 18: 260-263

Dawson JB, Smith JV, Jones AP (1985) A comparative study of bulk rock and mineral chemistry of olivine melilitites and associated rocks from East ans South Africa. Neus. Jarbuch Miner. Abh. 152 (2): 143-175

Dawson JB, Smith JV (1988) Metasomatised and veined upper mantle xenoliths from Pello Hill, Tanzania: evidence for anomalously light mantle beneath the Tanzanian sector of the East African Rift valley. Contrib. Mineral. Petrol. 100: 510-527

Dawson JB, Smith JV, Steele IM (1992) 1966 ash eruption of the carbonatite volcano Oldoinyo Lengai: mineralogy of lapilli and mixing of silicate and carbonate magmas. Mineral. Mag. 56: 1-16

Deans T (1966) Economic mineralisation in African carbonatites. In: Tuttle SD, Gittins J (eds) Carbonatites. John Wiley, New York

Deer WA, Howie RA, Zussman J (1966) Rock forming minerals. Longmans, five volumes.

Deines P, Gold DP (1983) The isotopic composition of carbonatite and kimberlite carbonates and their bearing on the isotopic composition of deep seated carbon. Geochim. Cosmochim. Acta 37: 1709-1733

Dingwell DB, Mysen BO (1985) The effect of fluorine and water on the viscosity of albite melt at high pressure: a preliminary investigation. Earth Planet. Sci. Letts. 74: 266-274

Dupré B, Allègre C (1980) Pb-Sr-Nd isotopic correlation, and the chemistry of the North Atlantic Mantle. Nature 286: 17-22

Dupuy C, Barsczus HG, Dostal J, Vidal P, Liotard JM (1989) Subducted and recycled lithosphere as the mantle source of ocean island basalts from Southern Polynesia, Central Pacific. Chem. Geol. 77: 1-18

Dupuy C, Dostal J, Liotard JM (1992) Zr/Hf fractionation in intraplate basaltic rocks: carbonate metasomatism in the mantle source. Geochim. Cosmochim. Acta 56: 2417-2423

Edgar AD (1987) The genesis of alkaline magmas with emphasis on their source regions: inferences from experimental studies. In: Fitton JG, Upton BGJ (eds) Alkaline igneous rocks. Blackwell: 29-52

Edgar AD (1989) Ba- and Sr-enriched apatites from lamproites. Am. Mineral. 74: 889-895

Eggler DH (1972) Role of CO_2 in melting processes in the mantle. Carnegie Inst. Washington Yearbook 72: 457-467

Eggler DH (1973) Effect of CO_2 on the melting of peridotite. Carnegie Inst. Washington Yearbook 73: 215-224

Eggler DH (1975) Composition of the partial melt of carbonated peridotite in the system CaO-MgO-SiO_2-CO_2. Carnegie Inst. Wash. Yearbook 75: 623-626

Eggler DH (1978) The effects of CO_2 on partial melting of peridotite in the system Na_2O-CaO-Al_2O_3-MgO-SiO_2-CO_2 to 35kb with an analysis of melting in a peridotite H_2O-CO_2 system. Am. J. Sci. 278: 305-343

Eggler DH, Kushiro I, Holloway JR (1975) Stability of carbonate minerals in a hydrous mantle. Carnegie Inst. Washington Yearbook 75: 631-636

Eggler DH, Mysen BO (1976) The role of CO_2 in the genesis of olivine melilitite: discussion. Contrib. Mineral. Petrol. 55: 231-236

Eggler DH, Mysen BO, Holloway JR, Hoering TC (1976) Fluids in the system C-O in equilibrium with graphite at high pressure: fluid species, solubilities in silicate liquid and effects on silicate phase relations. Carnegie Inst. Washington Yearbook 76: 448-454

Eggler DH, Rosenhauer M (1978) Solubilities of CO_2 and H_2O in $CaMgSi_2O_6$ (diopside) liquids and vapours at pressures to 40kb. Am. J. Sci. 178: 64-94

Falloon TJ, Green DH (1989) The solidus of carbonated fertile peridotite. Earth Planet. Sci. Letts. 94: 364-370

Falloon TJ, Green DH (1990) The solidus of carbonated fertile peridotite under fluid saturated conditions. Geology 18: 195-199

Fine G, Stolper E (1985) Dissolved CO_2 in basaltic glasses: concentrations and speciation. Earth Planet. Sci. Letts. 76: 263-279

Fleischer M (1955) Hafnium contents and hafnium-zirconium ratios in minerals and rocks. U. S. Geol. Surv. Bull. 1021-A

Foley SF (1988) The genesis of continental basaltic alkaline magmas: an interpretation in terms of redox melting. J. Petrol. Special Volume "Oceanic and continental lithosphere: similarities and differences": 139-154

Foley SF (1989) Emplacement features of lamprophyre dykes at Aillik Bay Labrador. Geol. Mag. 126(1): 29-42

Foley SF, Taylor WR, Green DH (1986) The role of fluorine and oxygen fugacity in the genesis of ultrapotassic rocks. Contrib. Mineral. Petrol. 94: 183-192

Ford CE (1978a) Platinum-iron alloy sample containers for melting experiments on iron-bearing rocks, minerals and related systems. Mineral. Mag. 42: 270-277

Ford CE (1978b) Platinum-iron alloy sample containers. NERC Progress in experimental petrology 4: 143-146

Fraser KJ (1987) Petrogenesis of kimberlites from South Africa and Lamproites from Western Australia and North America. PhD thesis, The Open Univ., Milton Keynes, UK.

Fraser KJ, Hawkesworth CJ, Erlank AJ, Mitchell RH, Scott-Simpson BH (1985) Sr, Nd, and Pb isotope and minor element geochemistry of lamproites and kimberlites. Earth Planet. Sci. Letts. 76: 57-70

Freestone IC, Hamilton DL (1980) The role of liquid immiscibility in the genesis of carbonatites: an experimental study. Contrib. Mineral. Petrol. 73: 105-117

Fuge R (1977) On the behaviour of fluorine and chlorine during magmatic differentiation. Contrib. Mineral. Petrol. 61: 245-249

Gerasimovskiy VI, Balashov VA, Karpushin A (1972) Geochemistry of REE in the extrusive rocks of East African rift zones. Geochem. Internat. 9: 305-319

Gerlach DC, Cliff RA, Davies GR, Norry M, Hodgson N (1988) Magma sources of the Cape Verdes archipelago; isotopic and trace-element constraints. Geochim. Cosmochim. Acta 52: 2979-2992

Gittins J, McKie D (1980) Oldoinyo Lengai and its wider applicability; alkalic carbonatite magmas. Lithos 3: 213-215

Gold DP (1963) Average chemical composition of carbonatites. Econ. Geol. 58: 998

Haggerty SE, Tompkins LA (1983) Redox state of the Earth's upper mantle from kimberlitic ilmenites. Nature 303: 295-300

Hamilton DL, Bedson P, Esson J (1989) The behaviour of trace elements in the evolution of carbonatites. In: Bell K (ed) Carbonatites. John Wiley: 405-427

Hamilton DH, Freestone IC, Dawson JB, Donaldson CH (1979) Origin of carbonatites by liquid immiscibility. Nature 279: 52-54

Haughton DR, Roeder PL, Skinner BJ (1974) Solubility of sulphur in mafic magmas. Economic Geology 69: 451-467

Hawkesworth CJ, Fraser KJ, Rogers NW (1985) Kimberlites and lamproites: extreme products of mantle enrichment processes. Trans. Geol. Soc. S. Africa 88: 439-447

Henderson P (1982) Inorganic Geochemistry. Pergamon Press

Hinton RW (1990) Ion microprobe trace-element analysis of multi-element glasses. Chemical Geology 83: 11-25

Hinton RW, Upton BJG (1991) The chemistry of zircon: variations within and between large crystals from syenite and alkali basalt xenoliths. Geochim. Cosmochim. Acta 55(11): 3287-3302

Holloway JR, Wood BJ (1988) Simulating the earth: experimental geochemistry. Unwin-Hyman

Hubberten HW, Katz-Lehnert K, Keller J (1988) Carbon and oxygen isotope investigations in carbonatites and related rocks from Kaiserstuhl, Germany. Chem. Geol. 70: 257-274

Hunter RH, McKenzie DP (1989) The equilibrium geometry of carbonate melts in rocks of mantle composition. Earth Planet. Sci. Letts. 92: 347-356

Irving AJ, Wyllie PJ (1975) Subsolidus and melting relationships for calcite, magnesite, and the join $CaCO_3$-$MgCO_3$ to 36kb. Geochim. Cosmochim. Acta 39: 35-53

Jarosewich E, Macintyre IG (1983) Carbonate reference samples for electron microprobe and scanning electron microscope analyses. J. Sed. Petrol. 53: 677-678

Jarosewich E, White JS (1987) Strontianite reference sample for electron microprobe and scanning electron microscope analyses. J. Sed. Petrol. 57(4): 762-763

Jones AP (1989) Upper-mantle enrichment by kimberlitic or carbonatitic magmatism. In: Bell K (ed) Carbonatites. John Wiley 18: 448-463

Jones AP, Smith JV, Dawson JB (1983) Glasses in mantle xenoliths from Olmani, Tanzania. J. Geol. 91(2): 167-178

Jones AP, Wyllie PJ (1985) Paragenetic trends of oxide minerals in carbonate-rich kimberlites, with new analyses from the Benfontein sill, South Africa. J. Petrol. 26: 210-222

Jones AP, Wyllie PJ (1986) Solubility of REE in carbonatite magmas, illustrated by the liquidus surrface in $CaCO_3$-$Ca(OH)_2$-$La(OH)_3$ at 1kbar pressure. Applied Geochem. 1: 95-102

Kjarsgaard BA, Hamilton DL (1988) Liquid immiscibility and the origin of alkali-poor carbonatites. Mineral. Mag. 52: 43-55

Kjarsgaard BA, Peterson T (1991) Nephelinite-carbonatite liquid immiscibility at the Shombole volcano, East Africa; petrology and experimental evidence. Mineralogy & Petrology 43: 293-314

Koster Van Groos AF (1975a) The effect of high CO_2 pressure on alkalic rocks and its bearing on the formation of alkaline ultrabasic rocks and associated carbonatites. Am. J. Sci. 275: 163-185

Koster Van Groos AF (1975b) The distribution of Sr between coexisting silicate nad carbonate liquids at elevated pressures and temperatures. Geochim. Cosmochim. Acta 39: 27-34

Koster Van Groos AF, Wyllie PJ (1966) Liquid immiscibility in the system Na_2O-Al_2O_3-SiO_2-CO_2 at pressures up to 1 kilobar. Am. J. Sci. 264: 234-255

Koster Van Groos AF, Wyllie PJ (1968) Liquid immiscibility in the join $NaAlSi_3O_8$-Na_2CO_3-H_2O and its bearing on the genesis of carbonatites. Am. J. Sci. 266: 932-967

Kuehner SM, Edgar AD, Arima M, Petrogenesis of ultrapotassic rocks from the Leucite Hills, Wyoming. Am. Mineral. 66: 663-677

Lancelot JR, Allègre CJ (1974) Origin of carbonatitic magma in the light of the Pb-Th-U isotope system. Earth Planet. Sci. Letts. 22: 233-238

Larsen LM, Rex DC (1992) A review of the 2500Ma span of alkaline-ultramafic, potassic, and carbonatitic magmatism in West Greenland. Lithos, in press

Leat PT, Thompson RN, Morrison MA, Hendry GL, Dickin AP (1988) Compositionally diverse miocene-recent rift-related magmatism in NW Colorado. Partial melting, mixing of mafic magmas from three different asthenospheric and lithospheric mantle sources. J. Petrol. Special Volume "Oceanic and continental lithosphere: similarities and differences": 351-375

Leat PT, Thompson RN, Morrison MA, Hendry GL, Dickin AP (1991) Alkaline hybrid mafic magmas of the Yampa area, NW Colorado, and their relationship to the Yellowstone plume and lithospheric mantle domains. Contrib. Mineral. Petrol. 107: 310-327

Le Bas MJ (1989) Diversification of carbonatite. In: Bell K (ed) Carbonatites. John Wiley. 17: 428-447

Lineweaver (1963) Oxygen outgassing caused by electron bombardment of glass. J. Applied Physics 34(6): 1786-1791

Liotard J-M, Barsczus HG, Dupuy C, Dostal J (1986) Geochemistry and origin of basaltic lavas from Marquesas archipelago, French Polynesia. Contrib. Mineral. Petrol. 92: 260-268

Lloyd FE, Edgar AD, Forsyth DM, Barnet RL (1991) The paragenesis of upper mantle xenoliths from the quaternary volcanics south east of Gees, West Eifel, Germany. Mineral. Mag. 55: 95-112

Long A, Menzies M, Thirwall M, Upton BGJ, Aspen P (1991) Carbonatite-mantle interaction, Hebridean craton, Scotland. Fifth International Kimberlite Conference: In Press.

Maaloe S, James D, Smedley P, Petersen S, Garmann LB (1992) The Koloa volcanic suite of Kauai, Hawaii. J. Petrol. 33(4): 761-784

McGetchin TR, Besançon JR (1973) Carbonate inclusions in mantle-derived pyropes. Earth Planet. Sci. Letts. 18: 408-410

McKelvey VE (1956) Uranium in phosphate rock. USGS Professional Paper 300: 477-481

McKenzie DP (1984) The generation and compaction of partially molten rocks. J. Petrol. 25: 713-765

McKenzie DP (1985a) The extraction of magma from the crust and mantle. Earth Planet. Sci. Letts. 74: 81-91

McKenzie DP (1985b) $^{230}Th/^{238}U$ disequilibrium and the melting processes beneath ridge axes. Earth Planet. Sci. Letts. 72: 149-157

McKenzie DP (1989) Some remarks on the movement of small melt fractions in the mantle. Earth Planet. Sci. Letts. 95: 53-72

McKenzie DP, Bickle MJ (1988) The volume and composition of melt generated by extension of the lithosphere. J. Petrol. 29(3): 625-679

McKenzie DP, O'Nions RK (1991) Partial melt distributions from rare-earth element inversion. J. Petrol. 32 (5): 1021-1091

Mariano AN (1989) Nature of economic mineralisation in carbonatites and related rocks. In: Bell K (ed) Carbonatites. John Wiley. 7: 149-176

Mattey DP, Taylor WR, Green DH, Pillinger CT (1990) Carbon isotope fractionation between CO_2 vapour, silicate and carbonate melts: an experimental study to 30kb. Contrib. Mineral. Petrol. 104: 492-505

Meen JK (1987) Mantle metasomatism and carbonatites: an experimental study of a complex relationship. Geol. Soc. of America, Special Paper 215: 91-100

Meen JK, Ayers JC, Fregau EJ (1989) A model for mantle metasomatism by carbonated alkaline melts: trace-element and isotopic compositions of mantle source regions of carbonatite and other continental igneous rocks. In: Bell K (ed) Carbonatites. Unwin-Hyman 1989, chapter 19: 464-499

Meen JK, Eggler DH, Ayers JC (1989) Evidence for very low solubility of REE in CO_2-rich fluids at mantle conditions. Nature 340: 301-303

Menzies MA (1989) Cratonic, circumcratonic and oceanic mantle domains beneath the Western USA. J. Geophys. Res. 94(B6): 7899-7915

Menzies MA, Halliday AN, Palacz Z, Hunter RH, Upton BGJ, Aspen P, Hawkesworth CJ (1987) Evidence from mantle xenoliths for an enriched lithospheric keel under the Outer Hebrides. Nature 325: 44-47

Menzies MA, Wass SY (1983) CO_2 and LREE-rich mantle below eastern Australia: A REE and isotopic study of alkaline magmas and apatite-rich mantle xenoliths from the Southern Highland Province, Australia. Earth Planet. Sci. Letts. 65: 287-302

Minarik WG, Watson EB (1991) Bulk iron diffusion in dunite through interstitial carbonate melts. EOS 72: 17

Mirwald PW, Getting IC, Kennedy GC (1975) Low-friction cell for piston cylinder high-pressure apparatus. J. Geophys. Res. 80: 1519-

Mitchell RH, Bergman SC (1991) Petrology of lamproites. Plenum, 1991

Mitchell RH, Platt RG, Downey M (1987) Petrology of lamproites from Smokey Butte, Montana. J. Petrol. 28: 645-77

Miyawaki R, Nakai I (1989) Crystal structures of rare-earth minerals.

Möller P (1988) The dependance of partition coefficients on differences of ionic volumes in crystal-melt systems. Contib. Mineral. Petrol. 99: 62-69

Mysen BO (1990) Relationships between silicate melt structure and petrogenetic processes. Earth-Science Reviews 27: 281-365

Mysen BO, Virgo D (1980) The solubility behaviour of CO_2 in melts on the join $NaAlSi_3O_8$-$CaAl_2Si_2O_8$-CO_2 at high pressure and temperature: a RAMAN spectroscopic study. Am. Mineral. 65: 1166-

Navon O, Hutcheson ID, Rossman GR, Wasserburg GJ (1988) Mantle-derived fluids in diamond micro-inclusions. Nature 335: 784-789

Nelson DR (1989) Isotopic characteristics and petrogenesis of the lamproites and kimberlites of central West Greenland. Lithos 22: 265-274

Nelson DR, Chirvas AR, Chappel BW, McCulloch MT (1988) Geochemical and isotopic systematics in carbonatites and implications for the evolution of ocean-island sources. Geochem. Cosmochim. Acta 52: 1-17

Nelson DR, McCulloch MT, Sun S-s (1986) The origins of ultrapotassic rocks as inferred from Sr, Nd, and Pb isotopes. Geochim. Cosmochim. Acta 50: 231-245

Newton RC, Sharp WE (1975) Stability of Forsterite + CO_2 and its bearing on the role of CO_2 in the mantle. Earth Planet. Sci. Letts. 26: 239-244

Nixon PH, Thirwall MF, Buckley F, Davies CJ (1984) Spanish and Western Australian lamproites; aspects of whole rock chemistry. In: Kornprobst J (ed) Proceedings of the third international conference. Elsevier. 1:285-296

Odling NW, Randle HA (1992) The partitioning of trace-elements between fluid and melt. Terra Abstracts 4: 32

Olaffson M, Eggler DH (1983) Phase relations of amphibole, amphibole-carbonate and phlogopite-carbonate peridotite: petrogenetic constraints on the asthenosphere. Earth Planet. Sci. Letts. 64: 305-315

Ottonello G (1983) Trace elements as monitors of magmatic processes: (i) Limits imposed by the Henry's law problem (ii) Compositional effect of silicate liquid. In: Augustithis SS (ed) The significance of trace-elements in solving petrogenetic problems. Theophrastus publications: 123-146

Parker RL, Fleischer M (1968) Geochemistry of niobium and tantalum. U. S. Geol. Surv. Prof. Paper 612

Peccerillo A (1985) Roman comagmatic province (central Italy): evidence for subduction-related magma genesis. Geology 13: 103-106

Peccerillo A, Manetti P (1985) The potassium alkaline volcanism of central-southern Italy: a review of the data relevant to petrogenesis and geodynamic significance. Trans. Geol. Soc. S. Africa 88: 379-394

Peterson TD (1990) Petrology and genesis of natrocarbonatite. Contrib. Mineral. Petrol. 105: 143-155

Pyle DM, Dawson JB, Ivanovich M (1991) Short-lived decay series disequilibria in the natrocarbonatite lavas of Oldoinyo Lengai, Tanzania: constraints on the timing of magma genesis. Earth Planet. Sci. Letts. 105: 378-396

Reid AM, Donaldson CH, Dawson JB, Brown RW, Ridley WI (1975) The Igwisi Hills extrusive "kimberlites". Phys. Chem. Earth 9: 199-219

Reid DL, Cooper AF, Rex DC, Harmer RE (1990) Timing of post-Karoo alkaline volcanism in southern Namibia. Geol. Mag. 127(5): 427-433

Richardson FD (1974) Physical chemistry of melts in metallurgy. Academic Press: 559-

Richardson SH, Gurney JJ, Erlank AJ, Harris JW (1984) Origin of diamonds in old enriched mantle. Nature 310: 198-202

Richter P, McKenzie DP (1984) Dynamic models for melt segregation from a deformable matrix. J. Geol. 92: 729-740

Roden MF (1987) Rb/Sr and Sm/Nd ratios of metasomatised mantle: implications for the rôle of metasomatised mantle in the petrogenesis of Na_2O-rich alkaline basalts. Geol. Soc. Am. Special Publication 215: 127-138

Roden MF, Murthy VR, Gaspar JC (1985) Strontium and neodymium isotopic composition of the Jacupirainga carbonatite. J. Geol. 93: 212-220

Ryerson FJ, Hess PC (1980) The role of P_2O_5 in silicate melts. Geochim Cosmochim. Acta 44: 611-624

Salters VJM, Barton M (1985) The geochemistry of ultrapotassic lavas from the Leucite Hills, Wyoming. EOS 66(46): 1109

Smith CB (1983) Pb, Sr, and Nd isotopic evidence for sources of southern African Cretaceous kimberlites. Nature 304: 51-54

Smith CS (1948) Grains, phases, and interfaces; an interpretation of microstructure. Trans. Am. Inst. Min. Metall. Engineers 175: 15-38

Smith D (1987) The genesis of carbonate in pyrope from the ultramafic diatremes on the Colorado Plateau, SW USA. Contrib. Miner. Petrol. 97: 389-396

Spera FJ, Bergman SC (1980) Carbon dioxide in igneous petrogenesis; aspects of the dissolution of CO_2 in silicate liquids. Contrib. Mineral. Petrol. 74: 55-66

Takahashi E, Kushiro I (1986) Melting of dry peridotite at high pressure and basalt magma genesis. Am. Mineral. 68: 859-879

Taylor WR, Green DH (1988) Measurement of reduced peridotite C-O-H solidus and its implications for redox melting in the mantle. Nature 332: 349-352

Taylor WR, Green DH (1989) The rôle of C-O-H fluids in mantle partial melting. In: Ross J, Jaques AL, Frerguson J, Green DH, O'Reilly SY, Danchin RV, Janse AJA (eds) Proceedings of the fourth international kimberlite conference. Geol. Soc. Australia Special Publication 14(1): 592-602

Thibault Y, Edgar AD, Lloyd FE (1992) Experimental investigation of melts from carbonated phlogopite lherzolite; implications for metasomatism in the continental lithospheric mantle. Am. Mineral. 77: 784-794

Thompson RN, Leat PT, Dickin AP, Morrison MA, Hendry GL, Gibson SA (1990) Strongly potassic mafic magmas from lithospheric mantle sources during continental extension and heating; evidence from miocene minettes of NW Colorado, USA. Earth Planet. Sci. Letts. 98: 139-153

Tlig S (1988) Fish debris as chemical scavengers of zirconium and lanthanum in oceanic environments: zirconium and hafnium fractionation in marine phosphates. Chem. Geol. 69: 59-71

Treiman AH (1989) Carbonatite magma: properties and processes. In: Bell K (ed) Carbonatites. John Wiley. 5: 89-104

Treiman AH , Schedl A (1983) Properties of carbonatite magma and processes in carbonatite magma chambers. J. Geol. 91: 437-447

Turner G, Burgess R, Bannon M (1990) Volatile-rich mantle fluids inferred from inclusions in diamond and mantle xenoliths. Nature 344: 653-655

Ulmer GC, Grandstaff DE, Weiss D, Moats MA, Buntin TJ, Gold DP, Hatton CJ, Kadik A, Koseluk RA, Rosenhauer M (1987) The mantle redox state: an unfinished story. Geol. Soc. of America, Special paper 215: 5-23

Upton BGJ, Fitton JG (1985) Gardar dykes north of the Igaliko Syenite complex Southern Greenland. Greenland Geol. Surv. Report no. 127

Vanlerberghe L, Hertogen J, McDougal JD (1986) Geochemical evolution and Th-U isotope systematics of alkaline lavas from Nyiragongo volcano. Terra cognita 7: 367

Van Wambeke (1966) La geochimie des roches du Kaiserstuhl. EUR 1827 d,f,e: 93-153

Varshneya AR, Cooper AR, Cable M (1966) Compositional changes during analysis by electron microprobe techniques. J. Applied Physics 37: 2199-

Venturelli G, Mariani ES, Foley SF, Capredi S, Crawford AJ (1988) Petrogenesis and conditions of crystallisation of Spanish lamproitic rocks. Can. Mineral. 26: 67-79

Verfaille G (1966) Dosage par spectrometrie Gamma de l'uranium et du thorium dans les roches du Kaiserstuhl. EUR 1827 d,f,e, pp154-165

Verwoerd WJ (1977) Liquid immiscibility and the carbonate-ijolite relationship: preliminary data on the join $NaFe^{3+}Si_2O_6$-$CaCO_3$ and related compositions. Carnegie Inst. Washington Yearbook 77

Vollmer R, Ogden P, Schilling J-G, Kingley RH, Waggoner DG (1984) Neodymium and strontium isotopes in ultrapotassic rocks from the Leucite Hills, Wyoming. Contrib. Mineral. Petrol. 87: 359-368

Vollmer R, Norry MJ (1983a) Possible origin of K-rich volcanic rocks from Virunga, East Africa, by metasomatism of continental crustal material: Pb, Nd, and Sr isotopic evidence. Earth Planet. Sci. Letts. 64: 374-386

Vollmer R, Norry MJ (1983b) Unusual isotopic variations in Nyiragongo nephelinites. Nature 301: 141-143

Wallace ME, Green DH (1988) An experimental determination of primary carbonatite magma composition. Nature 335: 343-345

Watson EB, Brenan JM (1987) Fluids in the lithosphere 1: experimentally determined wetting characteristics of CO_2-H_2O fluids and their implications for fluid transport, host-rock physical characteristics and fluid-inclusion formation. Earth Planet. Sci. Letts. 85: 497-515

Watson EB, Naslund HR (1976) The effect of pressure on immiscibility in the system K_2O-FeO-Al_2O_3-SiO_2-CO_2. Carnegie Inst. Wash. Yearbook 76: 410-414

Watson S, McKenzie D (1991) Melt generation by plumes: a study of Hawaiian volcanism. J. Petrol. 32 (3): 501-537

Weaver BL (1990) Geochemistry of highly-undersaturated ocean island basalt suites from the South Atlantic Ocean: Fernando de Naronha and Trindade islands. Contrib. Mineral. Petrol. 105: 502-515

Wedepohl KH (1985) Origin of the Tertiary basaltic volcanism in the Northern Hessian depression. Contrib. Mineral. Petrol. 89: 122-143

Wendlandt RF, Eggler DH (1980) The origins of potassic magmas 1 & 2. Am. J. Sci. 280: 385-458

Wendlandt RF, Harrison WJ (1979) Rare-earth partitioning between immiscible carbonate and silicate liquids and CO_2 vapour. Results and implications for the formation of LREE-enriched rocks. Contrib. Mineral. Petrol. 69: 409-419

Wendlandt RF, Mysen BO (1980) Melting phase relations of natural peridotite + CO_2 as a function of degree of partial melting at 15 and 30 kbar. Am. Mineral. 65: 37-44

Whittaker EJW, Muntus R (1970) Ionic radii for use in geochemistry. Geochim. Cosmochim. Acta 34: 945-956

Williams RW, Gill JB (1989) Effects of partial melting on the uranium decay series. Geochim. Cosmochim. Acta 53(7): 1607-1619

Williams RW, Gill JB, Bruland KW (1986) Ra-Th disequilibrium systematics. Timescale of carbonate magma formation at Oldoinyo Lengai volcano, Tanzania. Geochim. Cosmochim. Acta 50: 1249-1259

Wilshire HG (1987) A model of mantle metasomatism. Geol. Soc. of America, Special Paper 215: 47-60

Woolley AR, Kempe DCE (1989) Nomenclature and average chemical compositions of carbonatites. In: Bell K (ed) Carbonatites. John Wiley 1: 1-14

Wyllie PJ (1987) Discussion of recent papers on carbonated peridotite, bearing on mantle metasomatism and magmatism. Earth Planet. Sci. Letts. 82: 391-397

Wyllie PJ, Huang WL (1975) Peridotite, kimberlite and carbonatite explained in the system CaO-MgO-SiO_2-CO_2. Geology 46: 621-624

Wyllie PJ, Huang WL (1975) Influence of mantle CO_2 in the generation of carbonatites and kimberlites. Nature 257: 297-299

Wyllie PJ, Rutter M (1986) Experimental data on the solidus for peridotite-CO_2 with applications to alkaline magmatism and mantle metasomatism. EOS 67: 390

Yaxley GM, Crawford AJ, Green DH (1991) Evidence for carbonatite metasomatism in spinel peridotite xenoliths from Western Victoria, Australia. Earth Planet. Sci. Letts. 107: 305-317

Zyrianov VN, Volchkova NV (1987) Carbonation of Ca-rich plagioclase melt. Geochimya 5: 723-727

APPENDIX A

ELECTRON PROBE ANALYSES OF COEXISTING CARBONATE AND SILICATE LIQUIDS, AND ION PROBE STANDARDS

A.1. Carbonate and silicate liquids from experiments in the system SiO_2-Al_2O_3-CaO-Na_2O-CO_2.

These data tables show the major element compositions of coexisting carbonate and silicate liquids from synthetic experiments. There are nine tables:

SM1 experiments.
SM2 + CNC experiments.
SM2 + CC experiments.
Run duration effects: SM2 + CNC.
Run duration effects: SM2 + CC.
Experiments on the effects of minor elements.
Pressure effects: SM2 + CNC.
Reversal experiments: Major element analyses.
Repeated experiments: Major element analyses.

KEY.

G1.11 etc. = run identity.
Silicate = composition of the immiscible silicate melt.
Carbonate = composition of the immiscible carbonate melt.
(10) = number of analyses performed.
Quoted concentrations are arithmetic means of all analyses.
St. Dev. = arithmetic standard deviation on these analyses. $\sigma = [\Sigma(x-\mu)^2]^{1/2}$
St. Error = arithmetic standard error on the mean value. S.E. = $\sigma/[n]^{1/2}$
Totals = Sum of major element oxides analysed (Low due to CO_2 in melts).
KD = calculated Nernst $^{Ls/Lc}D_i$ partition coefficients.
Maximum and minimum values of $^{Ls/Lc}D_i$ are calculated as 95% confidence limits on a non-gaussian sample population (See Chapter 7 for statistical treatment).
^-Sil = values used for plotting silicate melt compositions on triangular diagrams.
^-Car = values used for plotting carbonate melt compositions on triangular diagrams.
P = approximate pressure of experimental conditions.
T = approximate temperature of experimental conditions.
Duration = length of experimental run in minutes

SM1 experiments: Major element analyses.

	G1.11	St. Dev.	St. Error	G1.12	St. Dev.	St. Error
Silicate	(10).			(10).		
SiO2	39.67	0.42	0.13	38.69	1.63	0.52
Al2O3	14.94	0.17	0.05	15.74	0.49	0.15
CaO	17.87	0.19	0.06	21.17	0.38	0.12
Na2O	22.78	0.31	0.10	15.68	0.21	0.07
Total	92.56			91.28		
Carbonate	(10).			(10).		
SiO2	1.74	0.51	0.16	4.45	0.23	0.07
Al2O3	0.17	0.07	0.02	2.29	0.03	0.01
CaO	25.09	0.32	0.10	32.06	0.25	0.08
Na2O	27.45	0.43	0.13	23.08	0.28	0.09
Total	54.45			59.81		
P	5.00			5.00		
T	1300			1300		
KD'S	Best	Max	Min	Best	Max	Min
Si	22.80	27.91	19.27	8.69	9.06	8.34
Al	87.88	115.19	71.04	6.87	7.02	6.73
Ca	0.71	0.72	0.70	0.66	0.67	0.65
Na	0.83	0.84	0.82	0.68	0.69	0.67
^-SIL						
Na	24.61			17.18		
Ca	19.31			23.19		
Si+Al	59.00			59.63		
^-CARB						
Na	50.41			38.59		
Ca	46.08			53.60		
Si+Al	3.51			11.27		
Duration	60			60		

SM2 + CNC experiments: Major element analyses.

	G6.7	St. Dev.	St. Error	G5.7	St. Dev.	St. Error	G7.7	St. Dev.	St. Error	G9.11	St. Dev.	St. Error	G28	St. Dev.	St. Error	G10.11	St. Dev.	St. Error	G27	St. Dev.	St. Error
Silicate	(10).			(10).			(10).			(10).			(10).			(10).			(10).		
SiO2	39.63	0.91	0.29	36.80	0.51	0.16	39.21	0.59	0.19	37.33	0.99	0.31	38.76	1.09	0.34	38.36	0.68	0.22	39.81	0.31	0.10
Al2O3	16.34	0.21	0.07	14.76	0.27	0.09	16.09	0.22	0.07	15.68	0.32	0.10	16.35	0.47	0.15	16.25	0.31	0.10	16.70	0.18	0.06
CaO	20.39	0.20	0.06	21.80	0.24	0.08	20.26	0.19	0.06	21.77	0.32	0.10	21.07	0.28	0.09	20.89	0.21	0.07	20.66	0.14	0.04
Na2O	16.46	0.35	0.11	17.97	0.24	0.08	16.84	0.17	0.05	17.91	0.17	0.05	17.29	0.16	0.05	17.48	0.17	0.05	16.99	0.77	0.24
Total	92.82			91.34			92.40			92.69			93.47			92.98			94.16		
Carbonate	(10).			(10).			(10).			(10).			(10).			(10).			(10).		
SiO2	2.73	0.30	0.09	3.84	0.68	0.22	4.13	0.95	0.30	3.50	0.43	0.14	4.46	1.37	0.43	4.98	1.39	0.44	5.20	3.21	1.02
Al2O3	0.08	0.04	0.01	0.22	0.13	0.04	0.22	0.06	0.02	0.16	0.03	0.01	0.30	0.09	0.03	0.39	0.38	0.12	0.34	0.27	0.09
CaO	29.01	0.24	0.08	29.10	0.76	0.24	29.47	0.61	0.19	28.21	0.47	0.15	29.72	0.46	0.15	29.52	0.26	0.08	30.23	1.12	0.35
Na2O	26.62	0.24	0.08	26.93	0.66	0.21	26.13	0.94	0.30	27.06	0.46	0.15	26.57	0.94	0.30	25.98	0.57	0.18	25.42	2.84	0.90
Total	58.44			60.29			59.94			60.29			61.05			60.88			61.20		
P	2.50			5.00			8.00			2.50			5.00			8.00			5.00		
T	1200			1200			1200			1300			1300			1300			1300		
KD'S	**Best**	Max	Min	**Best**	Max	Min	**Best**	Max	Min	**Best**	Max	Min	**Best**	Max	Min	**Best**	Max	Min	**Best**	Max	Min
Si	**14.52**	15.60	13.57	**9.58**	10.77	8.63	**9.49**	11.08	8.31	**10.67**	11.56	9.89	**8.69**	10.74	7.29	**7.70**	9.32	6.56	**7.66**	12.40	5.54
Al	**204.25**	295.99	155.91	**67.09**	105.88	49.09	**73.14**	88.03	62.55	**98.00**	110.95	87.73	**54.50**	66.99	45.91	**41.67**	105.20	25.97	**49.12**	96.73	32.91
Ca	**0.70**	0.71	0.70	**0.75**	0.76	0.74	**0.69**	0.70	0.68	**0.77**	0.78	0.76	**0.71**	0.72	0.70	**0.71**	0.71	0.70	**0.68**	0.70	0.67
Na	**0.62**	0.63	0.61	**0.67**	0.68	0.66	**0.64**	0.66	0.63	**0.66**	0.67	0.65	**0.65**	0.67	0.64	**0.67**	0.68	0.66	**0.67**	0.72	0.62
^-SIL																					
Na	17.73			19.67			18.23			19.32			18.50			18.80			18.04		
Ca	21.97			23.87			21.93			23.49			22.54			22.47			21.94		
Si+Al	60.30			56.45			59.85			57.19			58.96			58.73			60.01		
^-CARB																					
Na	45.55			44.67			43.59			44.88			43.52			42.67			41.54		
Ca	49.64			48.27			49.17			46.79			48.68			48.49			49.40		
Si+Al	4.81			6.73			7.26			6.07			7.80			8.82			9.05		
Duration	60			60			60			60			60			60			60		

SM2 + CC experiments: Major element analyses.

	G9.12	St. Dev.	St. Error	G11.2	St. Dev.	St. Error
Silicate	(10).			(10).		
SiO2	37.10	0.34	0.11	36.09	2.44	0.77
Al2O3	15.29	0.08	0.03	14.82	1.04	0.33
CaO	33.34	0.12	0.04	30.29	2.97	0.94
Na2O	10.19	0.14	0.04	9.54	0.71	0.22
Total	92.92			90.75		
Carbonate	(10).			(2).		
SiO2	4.03	0.52	0.16	4.99	2.74	1.94
Al2O3	1.70	1.29	0.41	1.04	0.80	0.57
CaO	48.44	2.64	0.83	47.28	5.12	3.62
Na2O	2.67	0.65	0.21	2.57	0.93	0.66
Total	56.84			55.88		
P	2.50			5.00		
T	1300			1300		
KD'S	Best	Max	Min	Best	Max	Min
Si	9.21	10.01	8.52	7.23	30.27	4.10
Al	8.99	16.98	6.12	14.25	215.57	6.88
Ca	0.69	0.71	0.67	0.64	0.76	0.55
Na	3.82	4.50	3.32	3.71	7.45	2.46
^-SIL						
Na	10.97			10.51		
Ca	35.88			33.38		
Si+Al	56.38			56.10		
^-CARB						
Na	4.70			4.60		
Ca	85.22			84.61		
Si+Al	10.08			10.79		
Duration	60			60		

Duration effects: SM2 + CNC.

	G8.11	St. Dev.	St. Error	G10.11	St. Dev.	St. Error	G25.6	St. Dev.	St. Error	G24.6	St. Dev.	St. Error
Sllicate	(10).			(10).			(10).			(10).		
SiO2	39.07	0.47	0.15	38.36	0.68	0.22	37.59	0.36	0.11	37.48	0.54	0.17
Al2O3	16.15	0.24	0.08	16.25	0.31	0.10	15.36	0.16	0.05	15.82	0.19	0.06
CaO	19.89	0.22	0.07	20.89	0.21	0.07	22.86	0.25	0.08	21.22	0.16	0.05
Na2O	16.77	0.11	0.03	17.48	0.17	0.05	18.08	0.27	0.09	17.86	0.13	0.04
Total	91.87			92.98			93.97			92.38		
Carbonate	(10).			(10).			(10).			(10).		
SiO2	5.52	1.38	0.44	4.98	1.39	0.44	4.17	0.71	0.22	6.31	1.43	0.45
Al2O3	0.73	0.64	0.20	0.39	0.38	0.12	0.21	0.25	0.08	0.90	0.61	0.19
CaO	29.35	0.28	0.09	29.52	0.26	0.08	30.06	0.34	0.11	29.89	0.15	0.05
Na2O	25.71	0.59	0.19	25.98	0.57	0.18	27.93	0.37	0.12	25.90	0.47	0.15
Total	61.32			60.88			62.46			63.00		
P	8.00			8.00			8.00			8.00		
T	1300			1300			1300			1300		
KD'S	**Best**	Max	Min	**Best**	Max	Min	**Best**	Max	Min	**Best**	Max	Min
Si	**7.08**	8.38	6.13	**7.70**	9.32	6.56	**9.01**	10.08	8.15	**5.94**	6.91	5.21
Al	**22.12**	48.45	14.33	**41.67**	105.20	25.97	**73.14**	279.03	42.09	**17.58**	30.31	12.38
Ca	**0.68**	0.68	0.67	**0.71**	0.71	0.70	**0.76**	0.77	0.75	**0.71**	0.71	0.71
Na	**0.65**	0.66	0.64	**0.67**	0.68	0.66	**0.65**	0.66	0.64	**0.69**	0.70	0.68
^-SIL												
Na	18.25			18.80			19.24			19.33		
Ca	21.65			22.47			24.33			22.97		
Sl+Al	60.11			58.73			56.35			57.70		
^-CARB												
Na	41.93			42.67			44.72			41.11		
Ca	47.86			48.49			48.13			47.44		
Sl+Al	10.19			8.82			7.01			11.44		
Duration	15			60			240			960		

Duration effects: SM2 + CC.

	G8.12	St. Dev.	St. Error	G10.12	St. Dev.	St. Error	G25.7	St. Dev.	St. Error	G24.7	St. Dev.	St. Error
Silicate	(10).			(10).			(10).			(10).		
SiO2	36.48	0.75	0.24	35.48	1.24	0.39	36.64	0.49	0.15	35.58	0.73	0.23
Al2O3	14.77	0.46	0.15	14.61	0.57	0.18	14.78	0.25	0.08	14.28	0.35	0.11
CaO	28.98	0.71	0.22	30.31	0.77	0.24	31.24	0.38	0.12	31.83	0.61	0.19
Na2O	8.73	0.12	0.04	9.30	0.19	0.06	9.26	0.21	0.07	8.99	0.13	0.04
Total	88.95			89.71			92.09			90.73		
Carbonate	(10).			(10).			(1).			(1).		
SiO2	13.76	1.77	0.56	7.28	2.81	0.89	7.56	-		3.97	-	
Al2O3	1.86	2.37	0.75	0.97	0.55	0.17	1.20	-		0.32	-	
CaO	40.05	4.09	1.29	43.15	6.40	2.02	42.65	-		43.61	-	
Na2O	13.76	1.77	0.56	7.09	4.05	1.28	10.29	-		15.24	-	
Total	65.87			58.50			61.70			63.17		
P	8.00			8.00			8.00			8.00		
T	1300			1300			1300			1300		
KD'S	**Best**	Max	Min	**Best**	Max	Min	**Best**	Max	Min	**Best**	Max	Min
Si	**2.65**	2.88	2.45	**4.87**	6.41	3.93	**4.85**	4.89	4.81	**8.96**	9.08	8.85
Al	**7.94**	37.77	4.43	**15.06**	23.24	11.13	**12.32**	12.45	12.19	**44.63**	45.30	43.95
Ca	**0.72**	0.77	0.68	**0.70**	0.77	0.64	**0.73**	0.74	0.73	**0.73**	0.74	0.72
Na	**0.63**	0.69	0.59	**1.31**	2.03	0.97	**0.90**	0.91	0.89	**0.59**	0.60	0.58
^-SIL												
Na	9.81			10.37			10.06			9.91		
Ca	32.58			33.79			33.92			35.08		
Si+Al	57.62			55.84			55.84			54.95		
^-CARB												
Na	20.89			12.12			16.68			24.13		
Ca	60.80			73.76			69.12			69.04		
Si+Al	23.71			14.10			14.20			6.79		
Duration	15			60			240			960		

Partitioning behaviour for minor elements: Coefficients and effects

Silicate	G29.1			G29.2			G29.3			G29.4			G29.5		
No. of Analyses	9			1			9			10			10		
	Concentration	St. Dev.	St. Error	Concentration	St. Dev.	St. Error	Concentration	St. Dev.	St. Error	Concentration	St. Dev.	St. Error	Concentration	St. Dev.	St. Error
Na2O	16.45	1.45	0.48	14.59	1.25	1.25	16.01	0.30	0.10	16.98	0.17	0.05	17.47	0.18	0.06
CaO	24.05	0.42	0.14	23.15	0.45	0.45	20.43	0.14	0.05	20.67	0.20	0.06	20.37	0.36	0.11
SiO2	37.06	0.79	0.26	41.38	0.83	0.83	40.13	0.63	0.21	40.14	0.23	0.07	38.88	0.39	0.12
Al2O3	15.40	0.35	0.12	16.99	0.53	0.53	16.38	0.24	0.08	16.54	0.16	0.05	16.03	0.09	0.03
P2O5	-	-		-	-		-	-		1.18	0.12	0.04	4.29	0.20	0.06
F2O	2.41	0.41	0.14	-	-		-	-		-	-		-	-	
Cl2O	-	-		1.58	-		-	-		-	-		-	-	
SO2	-	-		-	-		0.41	0.04	0.01	-	-		-	-	
Total	95.42			97.74			93.42			95.63			97.29		
Carbonate															
No. of Analyses	9			1			10			10			10		
	Concentration	St. Dev.	St. Error	Concentration	St. Dev.	St. Error	Concentration	St. Dev.	St. Error	Concentration	St. Dev.	St. Error	Concentration	St. Dev.	St. Error
Na2O	22.76	0.80	0.27	29.67	-		25.51	0.63	0.20	23.26	0.92	0.29	19.16	3.93	1.24
CaO	35.18	1.70	0.57	28.33	-		30.49	0.59	0.19	33.49	0.44	0.14	36.40	4.54	1.44
SiO2	9.09	3.37	1.12	3.61	-		3.14	0.96	0.30	6.34	1.67	0.53	8.29	1.57	0.50
Al2O3	1.96	1.55	0.52	0.13	-		0.22	0.20	0.06	0.70	0.44	0.14	1.61	0.58	0.18
P2O5	-	-		-	-		-	-		5.18	0.23	0.07	16.44	4.66	1.47
F2O	5.84	0.55	0.18	-	-		-	-		-	-		-	-	
Cl2O	-	-		4.27	1.89	0.60	-	-		-	-		-	-	
SO2	-	-		-	-		4.33	0.16	0.05	-	-		-	-	
Total	74.91			66.07			63.72			69.02			82.22		
D values		Max	Min		Max	Min		Max	Min		Max	Min		Max	Min
Na	0.72	0.77	0.68	0.49	0.57	0.41	0.63	0.64	0.62	0.73	0.75	0.71	0.91	1.04	0.81
Ca	0.68	0.71	0.66	0.82	0.85	0.79	0.67	0.68	0.66	0.62	0.62	0.61	0.56	0.61	0.52
Si	4.08	5.38	3.28	11.46	11.91	11.01	12.78	15.77	10.74	6.33	7.57	5.44	4.69	5.31	4.20
Al	7.86	16.26	5.18	130.69	139.68	122.70	74.45	170.56	47.62	23.63	38.71	17.00	9.96	12.82	8.14
P										0.23	0.24	0.21	0.26	0.32	0.22
F	0.41	0.47	0.36												
Cl				0.37	0.51	0.29									
S							0.09	0.10	0.09						

- = Below detection limits

Pressure effects: SM2 + CNC.

	S42	St. Dev.	St. Erro	S43	St. Dev.	St. Erro	S44	St. Dev.	St. Erro	S45	St. Dev.	St. Error
Silicate	(10).			(10).			(10).			(10).		
SiO2	39.00	0.45	0.14	39.05	0.17	0.05	40.35	0.56	0.18	39.48	0.17	0.05
Al2O3	16.05	0.27	0.09	16.08	0.09	0.03	16.61	0.16	0.05	16.24	0.11	0.03
CaO	20.44	0.31	0.10	20.22	0.16	0.05	21.07	0.16	0.05	20.85	0.19	0.06
Na2O	17.02	0.19	0.06	16.97	0.15	0.05	16.10	0.16	0.05	16.51	0.13	0.04
Total	93.02			92.83			94.61			93.59		
Carbonate	(10).			(10).			-			-		
SiO2	5.57	0.63	0.20	4.77	0.22	0.07	-	-		-	-	
Al2O3	0.82	0.25	0.08	0.61	0.08	0.03	-	-		-	-	
CaO	31.42	0.16	0.05	31.03	0.15	0.05	-	-		-	-	
Na2O	25.03	0.32	0.10	25.54	0.25	0.08	-	-		-	-	
Total	65.87			62.55			-			-		
P	15.00			15.00			20.00			11.00		
T	1300			1300			1300			1300		
KD'S	**Best**	Max	Min	**Best**	Max	Min	**Best**	Max	Min	**Best**	Max	Min
Sl	**7.00**	7.99	6.22	**8.19**	8.62	7.79						
Al	**19.57**	28.63	14.75	**26.36**	30.51	23.17						
Ca	**0.65**	0.66	0.64	**0.65**	0.66	0.64						
Na	**0.68**	0.70	0.66	**0.66**	0.68	0.65						
^-SIL												
Na	18.30			18.28			17.02			17.64		
Ca	21.97			21.78			22.27			22.28		
Sl+Al	59.18			59.39			60.21			59.54		
^-CARB												
Na	38.00			40.83			-			-		
Ca	47.70			49.61			-			-		
Sl+Al	9.70			8.60			-			-		
Duration	15			60			240			960		

Reversal experiments: Major element analyses.

	REV1	St. Dev.	St. Error	REV2	St. Dev.	St. Error	REV3	St. Dev.	St. Error	REV4	St. Dev.	St. Error
Silicate	(10).			(10).			(10).			(10).		
SiO2	40.69	0.34	0.11	38.11	0.63	0.20	49.97	0.43	0.14	33.10	0.24	0.08
Al2O3	17.35	0.15	0.05	16.15	0.24	0.08	20.32	0.11	0.03	12.78	0.11	0.03
CaO	11.66	0.09	0.03	25.56	0.36	0.11	6.39	0.08	0.03	32.90	0.24	0.08
Na2O	25.61	0.22	0.07	12.61	0.06	0.02	19.97	0.15	0.05	8.51	0.07	0.02
Total	95.31			92.43			96.64			87.29		
Carbonate	(10).			(10).			(10).			(6).		
SiO2	3.37	1.55	0.49	7.29	1.28	0.40	0.42	0.56	0.18	5.55	3.51	1.43
Al2O3	0.31	0.15	0.05	0.89	0.38	0.12	0.21	0.11	0.03	0.92	0.67	0.27
CaO	15.25	3.11	0.98	35.35	4.87	1.54	26.12	0.55	0.17	48.46	2.44	1.00
Na2O	43.00	2.98	0.94	20.30	4.36	1.38	30.28	0.93	0.29	1.10	0.53	0.22
Total	61.93			63.82			57.02			56.03		
P	5.00			5.00			5.00			5.00		
T	1200			1200			1200			1200		
KD'S	**Best**	Max	Min	**Best**	Max	Min	**Best**	Max	Min	**Best**	Max	Min
Si	**12.07**	16.89	9.40	**5.23**	5.87	4.71	**118.98**	685.38	65.14	**5.96**	12.07	3.96
Al	**55.97**	79.95	43.05	**18.15**	24.68	14.35	**96.76**	143.28	73.04	**13.89**	33.29	8.78
Ca	**0.76**	0.88	0.68	**0.72**	0.79	0.67	**0.24**	0.25	0.24	**0.68**	0.71	0.65
Na	**0.60**	0.62	0.57	**0.62**	0.72	0.55	**0.66**	0.67	0.65	**7.74**	12.59	5.58
^-SIL												
Na	26.87			13.64			20.66			9.75		
Ca	12.23			27.65			6.61			37.69		
Si+Al	60.90			58.70			72.73			52.56		
^-CARB												
Na	69.43			31.81			53.10			1.96		
Ca	24.62			55.39			45.81			86.49		
Si+Al	5.94			12.82			1.10			11.55		
Duration	60			60			60			60		

Repeated experiments: Major element analyses.

	R4	St. Dev.	St. Error	R5	St. Dev.	St. Error	R6	St. Dev.	St. Error	G5.7	St. Dev.	St. Error	G28	St. Dev.	St. Error
Silicate	(10).			(10).			(10).			(10).			(10).		
SiO2	40.20	0.50	0.16	39.92	0.30	0.09	39.89	0.63	0.20	36.80	0.51	0.16	38.76	1.09	0.34
Al2O3	16.71	0.11	0.03	16.63	0.09	0.03	16.61	0.10	0.03	14.76	0.27	0.09	16.35	0.47	0.15
CaO	20.37	0.14	0.04	20.45	0.12	0.04	20.50	0.23	0.07	21.80	0.24	0.08	21.07	0.28	0.09
Na2O	17.10	0.07	0.02	17.11	0.13	0.04	17.09	0.17	0.05	17.97	0.24	0.08	17.29	0.16	0.05
Total	94.37			94.11			94.09			91.34			93.47		
Carbonate	(10).			(10).			(10).			(10).			(10).		
SiO2	4.50	1.80	0.57	4.40	1.01	0.32	3.54	2.19	0.69	3.84	0.68	0.22	4.46	1.37	0.43
Al2O3	0.42	0.31	0.10	0.56	0.37	0.12	0.27	0.19	0.06	0.22	0.13	0.04	0.30	0.09	0.03
CaO	29.95	0.77	0.24	29.84	0.37	0.12	29.75	0.86	0.27	29.10	0.76	0.24	29.72	0.46	0.15
Na2O	25.97	1.05	0.33	26.18	0.54	0.17	26.48	1.50	0.47	26.93	0.66	0.21	26.57	0.94	0.30
Total	60.84			60.98			60.03			60.29			61.05		
P	5.00			5.00			5.00			5.00			5.00		
T	1200			1200			1200			1200			1200		
KD'S	**Best**	Max	Min	**Best**	Max	Min	**Best**	Max	Min	**Best**	Max	Min	**Best**	Max	Min
Si	**8.93**	11.88	7.16	**9.07**	10.58	7.94	**11.27**	18.28	8.14	**9.58**	10.77	8.63	**8.69**	10.74	7.29
Al	**39.79**	73.34	27.30	**29.70**	50.29	21.07	**61.52**	109.11	42.83	**67.09**	105.88	49.09	**54.50**	66.99	45.91
Ca	**0.68**	0.69	0.67	**0.69**	0.69	0.68	**0.69**	0.70	0.68	**0.75**	0.76	0.74	**0.71**	0.72	0.70
Na	**0.66**	0.68	0.64	**0.65**	0.66	0.64	**0.65**	0.67	0.62	**0.67**	0.68	0.66	**0.65**	0.67	0.64
^-SIL															
Na	18.12			18.18			18.16			19.67			18.50		
Ca	21.59			21.73			21.79			23.87			22.54		
Si+Al	60.31			60.09			60.05			56.45			58.96		
^-CARB															
Na	42.69			42.93			44.11			44.67			43.52		
Ca	49.23			48.93			49.56			48.27			48.68		
Si+Al	8.09			8.13			6.35			6.73			7.80		
Duration	60			60			60			60			60		

A.2. Coexisting carbonate and silicate liquids from experiments on natural compositions.

These tables show the major element compositions of experimentally produced carbonate and silicate liquids from runs employing natural rock powders.
There are 13 tables:

BD50 + CNC: Major element analyses.
BD50 + CC: Major element analyses.
BD119 + CNC: Major element analyses.
BD119 + CC: Major element analyses.
SUN189 + CNC: Major element analyses.
SUN189 + CC: Major element analyses.
Run duration effects: BD50 + CNC.
Run duration effects: BD119 + CNC.
Run duration effects: BD119 + CC.
Run duration effects: SUN189 + CNC.
Run duration effects: SUN189 + CC.
Pressure effects: BD119 + CNC.
Reproducibility of experiments: BD119 + CNC.

KEY.

G13.1. = run identity.
Silicate = composition of the immiscible silicate melt.
Carbonate = composition of the immiscible carbonate melt.
(10) = number of analyses performed.
Quoted concentrations are arithmetic means of all analyses.
St. Dev. = arithmetic standard deviation on these analyses. $\sigma = [\Sigma(x-\mu)^2]^{1/2}$
St. Error = arithmetic standard error on the mean value. S.E. = $\sigma/[n]^{1/2}$
Total = sum of major element oxides analysed (Low due to CO_2 in melts).
KD = calculated Nernst $^{Ls/Lc}D_i$ partition coefficients.
Maximum and minimum values of $^{Ls/Lc}D_i$ are calculated as 95% confidence limits on a non-gaussian sample population (See Chapter 7 for statistical treatment).
Total = sum of major element oxides analysed (Low due to CO_2 in melts).
^-Sil = values used for plotting silicate melt compositions on triangular diagrams.
^-Car = values used for plotting carbonate melt compositions on triangular diagrams.
P = approximate pressure of experimental conditions.
T = approximate temperature of experimental conditions.
Duration = length of experimental run in minutes

BD50 + CNC: Major element analyses.

	G13.1	St. Dev.	St. Error	G2.1	St. Dev.	St. Error	G4.1	St. Dev.	St. Error	G6.1	St. Dev.	St. Error	G5.1	St. Dev.	St. Error	G7.1	St. Dev.	St. Error	G26.1	St. Dev.	St. Error	G1.1	St. Dev.	St. Error	G10.1	St. Dev.	St. Error
SILICATE	(10).			(10).			(9).			(10).			(10).			(10).			(9).			(10).			(10).		
NA20	15.97	0.26	0.08	14.55	0.30	0.09	18.45	0.26	0.09	17.59	0.14	0.05	16.06	0.14	0.04	15.60	0.26	0.08	20.48	0.18	0.06	16.13	0.32	0.10	17.56	0.15	0.05
SIO2	49.20	0.45	0.14	51.26	0.36	0.11	48.13	0.88	0.29	45.85	0.26	0.08	49.26	0.50	0.16	51.35	0.38	0.12	45.16	0.22	0.07	45.91	0.40	0.13	44.57	0.63	0.20
K2O	3.78	0.08	0.03	3.86	0.08	0.02	4.02	0.20	0.07	3.91	0.07	0.02	3.81	0.08	0.03	3.68	0.06	0.02	4.82	0.05	0.02	3.77	0.10	0.03	3.86	0.05	0.01
FEO	1.48	0.16	0.05	2.00	0.33	0.10	2.63	0.31	0.10	1.88	0.14	0.05	2.68	0.13	0.04	2.52	0.29	0.09	1.35	0.05	0.02	1.11	0.28	0.09	1.19	0.52	0.17
MGO	0.69	0.03	0.01	0.62	0.07	0.02	0.74	0.07	0.02	0.71	0.03	0.01	0.69	0.08	0.02	0.61	0.05	0.01	0.72	0.02	0.01	0.68	0.04	0.01	0.65	0.02	0.01
AL2O3	17.93	0.26	0.08	18.91	0.54	0.17	15.62	0.66	0.22	17.17	0.01	0.00	18.28	0.41	0.13	19.21	0.26	0.08	16.82	0.10	0.03	17.05	0.11	0.03	16.09	0.26	0.08
CAO	5.76	0.27	0.09	3.53	0.25	0.08	6.40	0.96	0.32	7.05	0.15	0.05	4.83	0.47	0.15	3.72	0.13	0.04	8.15	0.09	0.03	6.94	0.18	0.06	8.00	0.49	0.15
MNO	0.15	0.03	0.01	0.13	0.03	0.01	0.15	0.06	0.02	0.15	0.04	0.01	0.13	0.04	0.01	0.12	0.04	0.01	0.13	0.02	0.01	0.14	0.05	0.01	0.13	0.02	0.01
P2O5	0.11	0.04	0.01	0.08	0.03	0.01	0.11	0.04	0.01	0.14	0.04	0.01	0.07	0.03	0.01	0.04	0.04	0.01	0.16	0.03	0.01	0.11	0.04	0.01	0.15	0.04	0.01
TIO2	0.94	0.03	0.01	0.93	0.11	0.03	0.97	0.05	0.02	0.84	0.05	0.02	0.85	0.04	0.01	0.87	0.03	0.01	0.81	0.01	0.00	0.82	0.06	0.02	0.86	0.04	0.01
TOTALS	96.10			95.91			97.31			95.40			96.73			95.77			98.71			92.75			93.18		
P	2.50			5.00			8.00			2.50			5.00			8.00			2.50			5.00			8.00		
T	1100.00			1100.00			1100.00			1200.00			1200.00			1200.00			1300.00			1300.00			1300.00		
		St. Dev.	St. Error		St. Dev.	St. Error		St. Dev.	St. Error		St. Dev.	St. Error		St. Dev.	St. Error		St. Dev.	St. Error		St. Dev.	St. Error		St. Dev.	St. Error		St. Dev.	St. Error
CARBONATE	(10).			(10).			(10).			(10).			(10).			(10).			(6).			(10).			(4).		
NA20	26.02	0.49	0.15	26.44	0.33	0.10	24.10	1.21	0.38	28.07	1.54	0.49	28.27	0.37	0.12	28.04	0.59	0.19	29.03	0.72	0.29	25.46	0.81	0.26	27.83	1.13	0.57
SIO2	0.24	0.08	0.03	0.28	0.15	0.05	0.38	0.11	0.04	0.15	0.12	0.04	0.06	0.02	0.01	0.08	0.04	0.01	0.27	0.07	0.03	0.59	0.70	0.22	0.35	0.05	0.02
K2O	3.22	0.11	0.03	3.21	0.06	0.02	4.31	0.10	0.03	5.49	2.27	0.72	3.69	0.12	0.04	4.49	0.86	0.27	3.98	0.25	0.10	3.84	0.11	0.03	3.96	0.21	0.10
FEO	0.68	0.05	0.02	1.08	0.07	0.02	0.59	0.04	0.01	0.28	0.16	0.05	0.85	0.16	0.05	1.34	0.33	0.10	0.21	0.05	0.02	0.30	0.08	0.03	0.12	0.03	0.01
MGO	0.74	0.08	0.02	1.14	0.05	0.01	0.60	0.06	0.02	0.65	0.05	0.02	0.95	0.10	0.03	1.04	0.06	0.02	0.60	0.03	0.01	0.93	0.08	0.02	0.70	0.12	0.06
AL2O3	0.23	0.08	0.02	0.03	0.01	0.00	0.06	0.02	0.01	0.21	0.20	0.06	0.04	0.05	0.02	0.07	0.03	0.01	0.07	0.03	0.01	0.46	0.46	0.15	0.16	0.13	0.06
CAO	25.39	0.33	0.10	25.67	0.27	0.09	23.63	0.33	0.10	24.90	2.40	0.76	22.01	0.45	0.14	24.18	0.22	0.07	22.81	0.36	0.15	23.82	0.67	0.21	24.25	0.56	0.28
MNO	0.13	0.04	0.01	0.17	0.02	0.01	0.12	0.07	0.02	0.11	0.03	0.01	0.15	0.06	0.02	0.19	0.04	0.01	0.09	0.05	0.02	0.14	0.05	0.02	0.11	0.04	0.02
P2O5	0.78	0.06	0.02	0.43	0.04	0.01	0.61	0.04	0.01	0.49	0.19	0.06	0.68	0.07	0.02	0.51	0.13	0.04	1.25	0.04	0.01	0.60	0.07	0.02	0.53	0.03	0.01
TIO2	0.14	0.05	0.02	0.17	0.07	0.02	0.09	0.02	0.01	0.06	0.04	0.01	0.17	0.03	0.01	0.20	0.07	0.02	0.14	0.04	0.01	0.25	0.12	0.04	0.15	0.03	0.02
TOTALS	57.96			59.00			54.85			60.39			57.18			60.50			58.76			56.85			56.90		
P	2.50			5.00			8.00			2.50			5.00			8.00			2.50			5.00			8.00		
T	1100.00			1100.00			1100.00			1200.00			1200.00			1200.00			1300.00			1300.00			1300.00		

KD'S	BEST	MAX	MIN	BEST	MAX	MIN	BEST	MAX	MIN	BEST	MAX	MIN	BEST	MAX	MIN	BEST	MAX	MIN	BEST	MAX	MIN	BEST	MAX	MIN	BEST	MAX	MIN
Na	0.61	0.62	0.60	0.55	0.56	0.54	0.77	0.79	0.74	0.63	0.65	0.61	0.57	0.57	0.56	0.56	0.57	0.55	0.71	0.72	0.69	0.63	0.65	0.62	0.63	0.66	0.61
Si	202.45	254.37	168.13	186.38	276.87	140.47	126.31	155.12	106.50	309.60	612.46	207.33	879.63	1180.08	701.07	658.27	988.03	493.53	169.78	216.72	139.55	77.43	289.65	44.68	129.18	148.63	114.21
K	1.17	1.20	1.15	1.20	1.22	1.18	0.93	0.97	0.90	0.71	0.96	0.57	1.03	1.06	1.01	0.82	0.93	0.73	1.22	1.28	1.16	0.96	0.98	0.93	0.97	1.03	0.93
Fe	2.19	2.37	2.01	1.85	2.06	1.65	4.50	4.90	4.12	6.79	10.46	5.01	3.16	3.59	2.82	1.89	2.26	1.61	6.57	8.33	5.42	3.70	4.66	2.94	10.21	14.73	6.96
Mg	0.94	1.01	0.87	0.54	0.58	0.50	1.23	1.34	1.13	1.10	1.16	1.04	0.73	0.80	0.66	0.58	0.62	0.55	1.20	1.25	1.15	0.73	0.78	0.69	0.93	1.12	0.79
Al	79.69	100.46	66.03	756.36	1158.78	561.14	251.89	327.51	204.38	80.99	199.22	50.82	456.88	1783.11	261.95	295.58	419.66	228.11	243.70	360.88	183.96	38.90	96.39	22.82	103.55	537.09	57.29
Ca	0.23	0.23	0.22	0.14	0.14	0.13	0.27	0.30	0.24	0.28	0.30	0.27	0.22	0.23	0.21	0.15	0.16	0.15	0.36	0.36	0.35	0.29	0.30	0.28	0.33	0.34	0.32
Mn	1.10	1.41	0.88	0.75	0.86	0.64	1.24	2.04	0.81	1.42	1.83	1.11	0.86	1.19	0.53	0.63	0.79	0.48	1.45	2.82	0.97	0.94	1.29	0.69	1.18	1.87	0.85
P	0.14	0.17	0.11	0.17	0.22	0.12	0.17	0.22	0.13	0.28	0.39	0.21	0.11	0.14	0.08	0.07	0.12	0.03	0.13	0.14	0.12	0.19	0.24	0.15	0.29	0.34	0.24
Ti	6.51	8.39	5.31	5.56	7.64	4.34	10.45	11.83	9.34	14.46	27.29	9.81	5.06	5.73	4.53	4.47	5.80	3.64	6.90	7.46	4.88	3.23	4.51	2.51	6.94	7.47	4.93
A-SIL	95.75			95.66			96.95			95.00			96.46			97.56			98.31			92.40			92.78		
ALKS	20.63			19.25			23.17			22.63			20.60			19.75			25.73			21.53			23.09		
CAFEMICS	8.28			6.43			10.09			10.15			8.50			7.03			10.39			9.44			10.61		
SIALTI	71.08			74.32			66.75			67.22			70.90			73.22			63.87			69.03			66.30		
A-CARB	56.66			58.01			53.76			59.80			56.03			59.43			57.07			55.75			57.50		
ALKS	51.60			51.12			52.84			56.12			57.04			54.74			57.81			52.72			55.28		
CAFEMICS	47.32			46.08			46.16			43.18			42.48			44.69			41.37			44.93			43.00		
SIALTI	45.50			0.81			1.00			0.70			0.47			0.57			0.83			2.35			1.12		
DURATION	60.00			60.00			60.00			60.00			60.00			60.00			60.00			60.00			60.00		

BD50 + CC: Major element analyses.

	G3.2	St. Dev	St. Error	G2.2	St. Dev	St. Error	G4.2	St. Dev	St. Error	G6.2	St. Dev	St. Error	G5.2	St. Dev	St. Error	G7.2	St. Dev	St. Error	G9.2	St. Dev	St. Error	G1.2	St. Dev	St. Error	G8.2	St. Dev	St. Error
SILICATE	(10).			(10).			(10).			(10).			(10).			(10).			(10).			(10).			(10).		
NA20	13.41	0.16	0.05	11.80	0.14	0.05	11.18	0.15	0 05	12.34	0.21	0 07	12.22	0.22	0.07	12.85	0.16	0.05	11 70	0.11	0.03	12.28	0.14	0.04	12.79	0.16	0 05
SIO2	44.34	0.45	0.14	43.80	0.28	0.09	41.21	0 27	0 08	44.34	0.20	0.06	46.92	0 63	0.20	44.03	0.35	0.11	45.49	0.26	0.08	44.81	0.14	0.04	44.62	0.20	0.06
K2O	4.11	0.12	0.04	4.03	0.10	0.03	3.82	0.06	0 02	4.07	0.10	0.03	3 94	0.09	0.03	3.89	0.05	0.02	4.13	0.07	0.02	4.12	0.07	0.02	3.94	0.10	0.03
FEO	2.69	0.14	0.05	3.06	0.11	0.04	3.60	0.10	0.03	2.07	0.16	0.05	2.07	0.27	0 09	2.14	0.11	0.03	1.66	0.22	0.07	2.02	0.15	0.05	2 77	0.19	0.06
MGO	0.69	0.04	0.01	0.64	0.02	0.01	0.64	0.05	0.02	0.68	0.03	0.01	0.69	0.04	0 01	0.68	0.04	0.01	0.67	0.03	0.01	0.64	0.03	0.01	0.68	0 03	0.01
AL2O3	16.09	0.34	0.11	15.62	0.22	0.07	15.14	0.18	0.06	16.30	0.24	0.08	17.33	0.27	0.09	16.20	0.19	0.06	16.35	0.11	0.03	16.43	0.10	0.03	16.39	0.16	0.05
CAO	13.31	0.44	0.14	13.65	0.22	0.07	12.51	0.23	0.07	14.18	0.20	0.06	11.98	0.43	0 13	13.84	0.20	0.06	14.83	0.29	0.09	14.26	0.14	0.05	13 55	0 21	0.07
MNO	0.12	0.02	0.01	0.14	0.03	0.01	0.14	0.03	0.01	0.13	0.04	0.01	0 12	0.04	0.01	0.15	0.03	0.01	0.15	0.02	0.01	0.12	0.04	0.01	0.13	0 04	0.01
P2O5	0.13	0.05	0.01	0.12	0.05	0.01	0.12	0.03	0.01	0.13	0.04	0.01	0.09	0.03	0.01	0.14	0.05	0.01	0.20	0.03	0.01	0.15	0.05	0.01	0.15	0.04	0.01
TIO2	0.79	0.03	0.01	0.81	0.04	0.01	0.73	0.03	0.01	0.79	0.06	0.02	0.83	0.04	0.01	0.78	0.04	0.01	0.84	0.03	0.01	0.83	0.06	0.02	0.78	0.05	0.01
TOTALS	95.88			94.08			89.26			95.25			96.37			94.90			96.26			95.87			96.01		
P	2.50			5.00			8.00						5.00			8.00			2.50			5.00			8.00		
T	1100.00			1100.00			1100.00						1200.00			1200.00			1300.00			1300.00			1300.00		
		St. Dev	St. Error		St. Dev	St. Error		St. Dev	St. Error		St. Dev	St. Error		St. Dev	St. Error		St. Dev	St. Error		St. Dev	St. Error		St. Dev	St. Error		St. Dev	St. Error
CARBONATE	(6).			(1).						(3).			(10).									(5).			(10).		
NA20	19.05	2.25	0.92	24.97			N/A			17.71	0.35	0.20	20.05	1.09	0.34	N/A			N/A			15.75	1.71	0.76	21.90	0.31	0.10
SIO2	1.14	0.65	0.27	0.50						1.96	0.55	0.32	0.72	0.18	0.06							5.59	1.16	0.52	1.45	0.28	0.09
K2O	2.89	0.30	0.12	3.77						4.72	0.08	0.05	3.32	0.25	0.08							3.70	0.27	0.12	3.81	0.03	0.01
FEO	0.31	0.07	0.03	0.04						0.67	0.24	0.14	0.72	0.11	0.03							1.15	0.29	0.13	0.56	0.05	0.01
MGO	0.48	0.07	0.03	0.33						0 63	0.05	0 03	0 47	0.13	0.04							0.41	0.11	0.05	0.43	0.02	0.01
AL2O3	0.03	0.02	0.01	0.04						0.09	0.09	0.05	0.21	0.13	0.04							0.36	0.15	0.07	0.59	0 04	0.01
CAO	34.46	2.19	0.90	27.22						31.93	0.50	0.29	33.85	0.08	0.03							33.96	1.17	0.52	30 57	0 03	0.01
MNO	0.14	0.06	0.02	0.04						0.10	0.03	0.02	0.10	0.06	0 02							0.11	0.06	0.03	0.12	0.07	0.02
P2O5	0.70	0.07	0.03	0.62						0.58	0.05	0.03	0.65	0.02	0.01							1.23	0.17	0.07	0 54	0.02	0.00
TIO2	0.11	0.05	0.02	0.07						0.18	0.05	0.03	0.18	0.02	0.01							0.21	0.06	0.03	0.07	0.03	0.01
TOTALS	59.80			57.61						59.03			59.49									62.98			60.03		
P	2.50			5.00			8.00			2.50			5.00			8.00			2.50			5.00			8.00		
T	1100.00			1100.00			1100.00			1200.00			1200.00			1200.00			1300.00			1300.00			1300.00		
KD'S	BEST	MAX	MIN	BEST	MAX	MIN	BEST	MAX	MIN	BEST	MAX	MIN	BEST	MAX	MIN	BEST	MAX	MIN	BEST	MAX	MIN	BEST	MAX	MIN	BEST	MAX	MIN
Na	0.70	0.78	0.64	0.47	0.48	0.47				0.70	0.71	0.68	0.61	0.63	0.59							0.78	0.86	0.71	0.58	0.59	0.58
Si	38.83	71.67	26.62	87.08	87.42	86.73				22.65	33.27	17.17	66.17	76.90	56.54							8.01	9.78	6.78	30.77	35.02	27.44
K	1.42	1.55	1.31	1.07	1.08	1.05				0.88	0.88	0.84	1.19	1.25	1 13							1.11	1.19	1.05	1.04	1.05	1.02
Fe	8.65	10.47	7.35	87.29	89.25	85.32				3.12	5.20	2.22	2.86	3.24	2.53							1.75	2.25	1.43	4.93	5.27	4.62
Mg	1.45	1.64	1.29	1.96	2.00	1.92				1.09	1.19	0.99	1.48	1.80	1.26							1.56	2.02	1.27	1.60	1.67	1.55
Al	575	1676.58	346.62	363	366.47	360.18				181	995.90	63.02	83	132.02	60.02							46	72.59	33.70	28	28.92	26.73
Ca	0.39	0.41	0.37	0.51	0.51	0.50				0.44	0.45	0.44	0.35	0.36	0.35							0.42	0.43	0.41	0.44	0.45	0.44
Mn	0.83	1.28	0.60	3.28	3.73	2.83				1.34	2.18	0.93	1.19	1.90	0.80							1.13	2.21	0.73	1.17	1.88	0.81
P	0.19	0.24	0.15	0.19	0.24	0.15				0.22	0.27	0.17	0.14	0.17	0.11							0.12	0.15	0.09	0.28	0.33	0.23
Ti	7.34	11.02	5.50	11.56	11.89	11.22				4.47	6.36	3.43	4.58	4.99	4.23							3.93	5.29	3.12	10.47	14.67	8.13
A-SIL	95.43			93.61			88.82			94.78			95 98			94.41			95.12			95.39			95.52		
ALKS	18.35			16.91			16 89			17.31			16.83			17.73			17.26			17.19			17.51		
CAFEMICS	17.49			18.74			18.86			17.87			15.36			17.64			17.52			17.74			17.80		
SIALTI	64.16			64.35			64.26			64.82			67.81			64.63			65.17			65.07			64.68		
A-CARB	58 46			56.94						57 88			59 61									61 13			59 37		
ALKS	37.53			50.47						38.76			39 26									31.91			43 29		
CAFEMICS	60.28			48.45						57.40			58 87									58.11			53.15		
SIALTI	2.19			1.08						3.84			1.87									10.08			3.56		
DURATION	60.00			60.00			60.00			60.00			60.00			60.00			60.00			60.00			15.00		

BD119 + CNC: Major element analyses.

	G3.3	St. Dev.	St. Error	G2.3	St. Dev.	St. Error	G4.3	St. Dev.	St. Error	G6.3	St. Dev.	St. Error	G5.3	St. Dev.	St. Error	G7.3	St. Dev.	St. Error	G9.3	St. Dev.	St. Error	G1.3	St. Dev.	St. Error	G10.3	St. Dev.	St. Error
SILICATE	(10).			(10).			(10).			(10).			(10).			(10).			(10).			(10).			(10).		
NA20	16.07	0.24	0.07	14.11	0.29	0.09	16.22	0.27	0.08	15.49	0 20	0.06	15.62	0.34	0 11	16 05	0.29	0.09	16 35	0.03	0.01	16.29	0.30	0.09	17.09	0.33	0.11
SIO2	42.93	0.30	0.10	42.91	0.57	0.18	42.27	0.38	0.12	40.09	0 59	0.19	42.61	0.66	0.21	41.19	0.70	0.22	36.50	0.94	0.30	36.82	0.76	0.24	38.08	0.45	0.14
K2O	3.56	0.09	0.03	3.52	0.08	0.03	3.60	0.09	0.03	3.59	0.08	0.03	3.66	0.18	0.06	3.49	0.07	0.02	3.51	0.10	0.03	3.76	0.06	0.02	3.72	0.15	0.05
FEO	4.45	0.31	0.10	4.18	0.44	0.14	4.92	0.16	0.05	4 04	0.35	0.11	4.26	0.80	0.25	3.42	0.16	0.05	2.71	0.10	0.03	2.90	0.05	0.02	3.31	0.55	0.17
MGO	0.95	0.05	0.01	0.91	0.06	0.02	0.93	0.03	0.01	0.94	0.03	0.01	0.91	0.04	0.01	0.92	0.05	0.01	0.92	0.03	0.01	0.93	0.06	0.02	0.94	0.02	0.01
AL2O3	13.89	0.25	0.08	14.34	0.54	0.17	13.29	0.30	0.10	13.42	0.21	0.07	14.20	0.38	0.12	13.80	0.29	0.09	11.64	0.39	0.12	12.08	0.28	0.09	12.19	0.22	0.07
CAO	11.15	0.15	0.05	10.85	0.60	0.19	10.98	0.20	0.06	13.03	0.32	0.10	10.91	0.55	0.17	11.87	0.30	0.09	14.92	0.37	0.12	14.72	0.32	0.10	14.92	0.28	0.09
MNO	0.33	0.04	0.01	0.29	0.06	0.02	0.31	0.04	0.01	0 31	0 05	0.01	0.28	0.04	0.01	0 29	0.02	0.01	0.29	0.03	0.01	0.28	0.03	0.01	0.30	0.04	0.01
P2O5	0.27	0.06	0.02	0.27	0.05	0.02	0.30	0.04	0 01	0 35	0.07	0.02	0.28	0.06	0.02	0.33	0.05	0.02	0.60	0.08	0.02	0.55	0.06	0.02	0.53	0.05	0.01
TIO2	0.98	0.04	0.01	0.97	0.06	0.02	0.97	0.04	0.01	0.93	0.05	0.02	0.99	0.05	0.02	0.92	0.04	0.01	0.91	0.03	0.01	0.85	0.04	0.01	0.95	0.06	0.02
TOTALS	94.74			92.49			93.95			92.39			93.88			92.45			88.55			89.40			92.23		
P	2.50			5.00			8.00			2.50			5.00			8.00			2.50			5.00			8.00		
T	1100.00			1100.00			1100.00			1200.00			1200.00			1200.00			1300.00			1300.00			1300.00		
		St. Dev.	St. Error		St. Dev.	St. Error		St. Dev.	St. Error		St. Dev.	St. Error		St. Dev.	St. Error		St. Dev.	St. Error		St. Dev.	St. Error		St. Dev.	St. Error		St. Dev.	St. Error
CARBONATE	(10).			(10).			(10).			(10).			(10).			(10).			(10).			(10).			(10).		
NA20	24.98	0.44	0.14	23.94	0.51	0.16	23.66	0.33	0.11	26.95	0.48	0.15	25.67	0.37	0.12	24.94	1.09	0.35	22.00	1 20	0.38	24.80	1.29	0.41	24.96	1.28	0.40
SIO2	2.08	0.96	0.30	2.79	0.98	0.31	2.96	1.81	0.57	3.24	0.26	0.08	1.87	0.25	0.08	5.01	2.54	0.80	6.72	4.17	1.32	2.16	1.54	0.49	1.38	0.94	0.30
K2O	3.62	0.08	0.02	3.90	0.09	0.03	3.90	0.07	0.02	5.82	0.54	0.17	5.43	0.11	0 03	6.13	0.19	0.06	4.33	0.33	0.10	4.12	0.38	0.12	4.65	0.16	0.05
FEO	1.17	0.58	0.18	1.14	0.40	0.13	1.30	0.43	0.14	0.41	0.15	0.05	0.81	0.09	0.03	1.24	0.52	0.16	0.38	0.22	0.07	0.52	0.38	0.12	0.50	0.27	0.08
MGO	0.70	0.27	0.08	0.74	0.21	0.07	0.73	0.09	0 03	0 39	0.11	0.04	0.68	0.07	0.02	0.75	0.40	0.13	0.62	0 10	0 03	0.56	0.19	0.06	0.60	0.23	0.07
AL2O3	0.09	0.11	0.04	0.11	0.06	0.02	0.18	0.31	0.10	0 08	0 05	0.01	0.03	0.02	0.01	0.67	0.39	0.12	1.13	0.18	0.06	0.16	0.12	0.04	0.33	0.59	0.19
CAO	26.94	0.67	0.21	27.88	0.39	0.12	27.37	0.70	0.22	27 16	0.53	0.17	27.00	0.25	0.08	25.95	0.99	0.31	25.04	0.34	0.11	25.63	1.14	0.36	24.95	0.10	0.03
MNO	0.17	0.09	0.03	0.22	0.06	0.02	0.18	0.06	0.02	0.13	0.06	0.02	0.21	0.06	0.02	0.24	0.07	0.02	0.16	0.07	0.02	0.15	0.06	0.02	0.15	0.04	0.01
P2O5	1.41	0.05	0.02	1.54	0.05	0.01	1.69	0.07	0.02	1.15	0.13	0.04	1.45	0.06	0.02	1.32	0.11	0.03	1.28	0.40	0.13	1.07	0.26	0.08	1.27	0.10	0.03
TIO2	0.20	0.09	0.03	0.19	0.07	0.02	0.18	0.11	0.04	0.04	0.03	0.01	0.12	0.03	0.01	0.28	0.13	0.04	0.32	0.13	0.04	0.13	0.08	0.03	0.10	0.06	0.02
TOTALS	61.77			62.87			62.55			62.87			63.65			66.91			62.34			59.69			59.31		
P	2.50			5.00			8.00			2.50			5.00			8.00			2.50			5.00			8.00		
T	1100.00			1100.00			1100.00			1200.00			1200.00			1200.00			1300.00			1300.00			1300.00		
KD'S	BEST	MAX	MIN	BEST	MAX	MIN	BEST	MAX	MIN	BEST	MAX	MIN	BEST	MAX	MIN	BEST	MAX	MIN	BEST	MAX	MIN	BEST	MAX	MIN	BEST	MAX	MIN
Na	0.64	0.65	0.63	0.59	0.60	0.58	0.69	0.69	0.68	0.67	0.58	0.57	0.61	0.62	0.60	0.64	0.66	0.63	0.74	0.77	0.72	0.66	0.68	0.64	0.68	0.71	0.66
Si	20.66	28.91	16.07	16.38	19.69	12.62	14.30	23.07	10.37	12.37	13.04	11.77	22.84	24.88	21.10	8.22	11.99	6.25	5.43	8.84	3.92	17.08	30.64	11.83	27.53	47.43	19.39
K	0.98	1.00	0.96	0.90	0.92	0.88	0.92	0.94	0.91	0.62	0.66	0.58	0.67	0.70	0.65	0.57	0.58	0.56	0.81	0.85	0.77	0.91	0.97	0.86	0.80	0.83	0.77
Fe	3.79	5.49	2.89	3.66	4.71	2.98	3.78	4.74	3.13	9.85	12.77	7.98	6.25	5.98	4.56	2.76	3.73	2.19	7.12	11.11	5.23	6.58	10.17	3.84	6.68	10.16	4.90
Mg	1.36	1.76	1.09	1.22	1.49	1.04	1.28	1.39	1.19	2.39	2.90	2.03	1.36	1.45	1.26	1.22	1.81	0.92	1.48	1.65	1.34	1.66	2.10	1.36	1.66	2.02	1.26
Al	149.36	621.71	84.86	136.24	201.19	101.76	73.82	908.87	35.46	166.73	255.77	122.56	417.60	697.20	297.85	20.69	32.56	15.16	10.34	11.49	9.38	77.46	142.65	53.15	36.83	-327.99	17.43
Ca	0.41	0.42	0.41	0.39	0.40	0.38	0.40	0.41	0.39	0.48	0.49	0.47	0.40	0.42	0.39	0.46	0.47	0.44	0.60	0.61	0.59	0.57	0.59	0.56	0.60	0.60	0.59
Mn	1.89	2.82	1.41	1.30	1.61	1.06	1.71	2.15	1.40	2.33	3.28	1.78	1.35	1.68	1.11	1.20	1.49	1.00	1.79	2.46	1.39	1.88	2.42	1.50	1.94	2.34	1.64
P	0.19	0.22	0.17	0.17	0.19	0.15	0.18	0.19	0.16	0.30	0.35	0.26	0.19	0.22	0.16	0.25	0.28	0.22	0.47	0.59	0.38	0.51	0.61	0.44	0.42	0.45	0.39
Ti	4.95	6.81	3.89	5.03	6.59	4.05	5.54	9.14	3.97	26.43	58.63	17.03	8.57	9.93	7.52	3.28	4.66	2.53	2.88	3.90	2.29	6.37	10.43	4.58	9.66	15.59	6.99
A-SIL	93.97			91.77			93.18			91.54			93.15			91.66			87.44			88.35			91.18		
ALKS	20.89			19.21			21.28			20.85			20.70			21.32			22.71			22.69			22.82		
CAFEMICS	17.60			17.36			18.06			19.68			17.26			17.68			21.20			20.99			21.02		
SIALTI	61.51			63.43			60.66			59.47			62.04			61.00			56.08			56.31			56.17		
A-CARB	59.78			60.69			60.27			64.09			61.59			64.96			60.53			58.08			54.27		
ALKS	47.84			45.87			45.73			51.13			50.49			47.83			43.51			49.80			50.87		
CAFEMICS	48.19			49.04			48.78			43.64			46.24			43.00			43.02			45.99			45.79		
SIALTI	3.96			5.09			5.49			5.24			3.27			9.17			13.48			4.21			3.34		
DURATION	60.00			60.00			60.00			60 00			60.00			60.00			60.00			60.00			60.00		

BD119 + CC: Major element analyses.

	G3.4	St. Dev.	St. Error	G2.4	St. Dev.	St. Error	G4.4	St. Dev.	St. Error	G6.4	St. Dev.	St. Error	G5.4	St. Dev.	St. Error	G7.4	St. Dev.	St. Error	G26 2	St. Dev.	St. Error	G1.4	St. Dev.	St. Error	G10.4	St. Dev.	St. Error
SILICATE	(10).			(10).			(10).			(10).			(10).			(10).			(10).			(10).			(10).		
NA20	11.94	0.14	0.04	10.58	0.21	0.07	11.30	0.20	0.06	11.17	0.20	0.06	10 90	0 15	0.05	11.58	0.16	0.05	13.08	0.13	0.04	12.31	0.38	0.12	11.89	0.29	0 09
SIO2	39.90	0.41	0.13	42.84	0.41	0.13	41.57	0.24	0.08	36.76	1.20	0.38	40.25	0 31	0.10	40.92	0.60	0.19	37.35	0.22	0.07	37.50	0.60	0.19	37.69	0.19	0.06
K2O	3.86	0.10	0.03	3.69	0.10	0.03	3.74	0.06	0.02	3.71	0.12	0.04	3.63	0.07	0.02	3.64	0.10	0.03	4.62	0.11	0.03	4.06	0.15	0.05	3.81	0.18	0.06
FEO	3.13	0.26	0.08	4.56	0.62	0 20	5.16	0.14	0.04	4.10	0.41	0.13	5.13	0.16	0.05	2.95	0.27	0.09	2.93	0.10	0.03	3.56	0.25	0.08	3.57	0.16	0.05
MGO	0.91	0.05	0.02	0.83	0.03	0.01	0.85	0.05	0.02	0.87	0.04	0.01	0.89	0.02	0.01	0.90	0.05	0.01	0.89	0.02	0.01	0.88	0.07	0.02	0.89	0.03	0.01
AL2O3	12.98	0.13	0.04	14.03	0.36	0.11	13.33	0.17	0.05	11.66	0.37	0.12	13.27	0.25	0.08	13.52	0.18	0.06	11 96	0.11	0.03	12.07	0.37	0.12	11.85	0.11	0.03
CAO	18.15	0.20	0.06	15.15	0.46	0.14	15.14	0.18	0.06	20.07	0.50	0.16	16.82	0 35	0.11	16.67	0 32	0.10	20.45	0.12	0 04	21.06	0.62	0.20	20.59	0.39	0.12
MNO	0.29	0.05	0.02	0.30	0.03	0.01	0.29	0.04	0.01	0.29	0.03	0.01	0 27	0.02	0.01	0.26	0.06	0.02	0 29	0.04	0.01	0.25	0.08	0 02	0.30	0.03	0 01
P2O5	0.29	0.11	0.03	0.32	0.03	0.01	0.25	0.03	0.01	0.57	0.09	0.03	0 28	0 05	0.02	0.31	0.05	0 01	0 57	0.05	0 02	0.54	0.08	0.02	0.54	0.05	0.02
TIO2	0.93	0.03	0.01	1.01	0.03	0.01	0.97	0.03	0.01	0.92	0.05	0.02	0.93	0.04	0.01	0.90	0.04	0.01	0.89	0.03	0.01	0.89	0.03	0.01	0.93	0 03	0.01
TOTALS	92.65			93.55			92.84			90.41			92.62			91.90			93.34			93.42			92.35		
P	2.50			5.00			8.00			2.50			5.00			8.00			2.50			5.00			8.00		
T	1100.00			1100.00			1100.00			1200.00			1200.00			1200.00			1300.00			1300.00			1300.00		
		St. Dev.	St. Error		St. Dev.	St. Error		St. Dev.	St. Error		St. Dev.	St. Error		St. Dev.	St. Error		St. Dev.	St. Error		St. Dev.	St. Error		St. Dev.	St. Error		St. Dev.	St. Error
CARBONATE	(10).			(10).			(10).			(10).			(10).			(10).			(10).			(3).			(10).		
NA20	19.15	1.52	0.48	13.95	0.48	0.15	13.85	0.20	0.06	17.90	0.42	0.13	16.61	0.33	0.11	16.48	1.84	0.58	19.96	1.75	0.55	21.64	1.66	0.96	16.09	1.41	0 45
SIO2	2.40	1.73	0.55	5.74	0.88	0.28	5.20	0.73	0.23	1.23	0.49	0.16	3.38	0.98	0.31	8.56	2.90	0.92	1.27	0.61	0.19	0.80	0.37	0.21	3.74	1.12	0.36
K2O	4.54	0.41	0.13	3.66	0.16	0.05	2.77	0.06	0.02	3.94	0.16	0.05	5.51	0.11	0.03	5.64	0 68	0.22	3.63	0.36	0.11	6.13	0.25	0.14	4.97	0.22	0.07
FEO	0.63	0.43	0.14	1.30	0.13	0.04	1.59	0.16	0.05	0.58	0.07	0.02	1.52	0.21	0.06	1.69	0.59	0.19	0 61	0.16	0.05	0.13	0.08	0.05	1.72	0.60	0.19
MGO	0.38	0.27	0.09	0.75	0.08	0.03	0.74	0 05	0.02	0.49	0.07	0.02	0.69	0.03	0.01	0.92	0.28	0.09	0.57	0.08	0 03	0.36	0.05	0 03	0.68	0.19	0.06
AL2O3	0.13	0.12	0.04	0.52	0.34	0.11	0.32	0.21	0.07	0.12	0.06	0.02	0.19	0.15	0.05	1.22	0.43	0.14	0 06	0.04	0 01	0.07	0.04	0.03	0.22	0.14	0.04
CAO	31.77	2.75	0.87	36.03	0.92	0.29	36.36	0.92	0.29	34.04	0.52	0.17	34.52	0.86	0.27	33.16	1.26	0.40	33.44	1.57	0.50	27.26	0.52	0 30	35.96	1.16	0.37
MNO	0.13	0.10	0.03	0.22	0.04	0.01	0.21	0.03	0.01	0 13	0.05	0.02	0.21	0.07	0.02	0.36	0.13	0.04	0.16	0.03	0.01	0.14	0.12	0.07	0.22	0.10	0.03
P2O5	2.05	0.15	0.05	1.43	0.07	0.02	1.55	0.08	0.03	1 22	0.13	0.04	1.12	0.07	0.02	1.33	0.20	0.06	0.93	0.08	0.02	0.84	0.08	0.05	1.44	0.09	0.03
TIO2	0.14	0.10	0.03	0.33	0.04	0.01	0.27	0.05	0.01	0.09	0.04	0.01	0.19	0.04	0.01	0.38	0.12	0.04	0.11	0.06	0.02	0.05	0.03	0.02	0.18	0.06	0.02
TOTALS	61.79			64.47			63.41			60.25			64.46			70.25			61.23			57.83			65.76		
P	2.50			5.00			8.00			2.50			5.00			8.00			2.50			5.00			8.00		
T	1100.00			1100.00			1100.00			1200.00			1200.00			1200.00			1300.00			1300.00			1300.00		
KD'S	BEST	MAX	MIN	BEST	MAX	MIN	BEST	MAX	MIN	BEST	MAX	MIN	BEST	MAX	MIN	BEST	MAX	MIN	BEST	MAX	MIN	BEST	MAX	MIN	BEST	MAX	MIN
Na	**0.62**	0.66	0.59	**0.76**	0.78	0.74	**0.82**	0.83	0.80	**0.62**	0.64	0.61	**0.66**	0.67	0.65	**0.70**	0.76	0.66	**0.66**	0.69	0.62	**0.57**	0.62	0.52	**0.74**	0.78	0.70
Si	**16.66**	30.18	11.51	**7.46**	8.25	6.81	**7.99**	8.75	7.35	**29.98**	39.99	23.97	**11.93**	14.55	10.11	**4.78**	6.05	3.95	**29.43**	42.04	22.64	**50.19**	96.97	30.80	**10.09**	12.41	8.51
K	**0.85**	0.90	0.80	**1.01**	1.04	0.98	**1.35**	1.37	1.33	**0.94**	0.97	0.91	**0.66**	0.67	0.65	**0.65**	0.70	0.60	**1.27**	1.36	1.20	**0.69**	0.70	0.63	**0.77**	0.80	0.74
Fe	**4.99**	8.72	3.48	**3.62**	3.90	3.16	**3.26**	3.48	3.05	**7.12**	7.87	6.45	**3.38**	3.70	3.11	**1.76**	2.24	1.42	**4.79**	5.71	4.13	**4.07**	97.27	16.48	**2.07**	2.65	1.70
Mg	**2.36**	4.23	1.63	**1.10**	1.19	1.03	**1.15**	1.22	1.09	**1.79**	1.98	1.63	**1.29**	1.34	1.25	**0.98**	1.20	0 82	**1.58**	1.74	1.44	**2.46**	2.93	2.06	**1.30**	1.57	1.10
Al	**97**	220.06	62.12	**27**	45.41	19.13	**42**	71.60	29.77	**96**	138.55	72.90	**68**	131.35	46.23	**11**	14.14	9.10	**199**	365.44	137.04	**179**	498.53	97.44	**53**	84.79	36.42
Ca	**0.57**	0.60	0.54	**0.42**	0.43	0.41	**0.42**	0.42	0.41	**0.59**	0.60	0.58	**0.49**	0.50	0.48	**0.50**	0.52	0.49	**0.61**	0.63	0.59	**0.62**	0.79	0.75	**0.57**	0.59	0.56
Mn	**2.19**	4.02	1.48	**1.36**	1.56	1.20	**1.40**	1.56	1.26	**2.20**	2.88	1.76	**1.29**	1.61	1.07	**0.72**	0.97	0.55	**1.84**	2.11	1.61	**1.94**	45.00	0.87	**1.34**	1.88	1.03
P	**0.14**	0.17	0.11	**0.22**	0 24	0.21	**0.16**	0.18	0.15	**0.46**	0.52	0.41	**0.25**	0.28	0.22	**0.23**	0.26	0.20	**0.62**	0.66	0.57	**0.64**	0.74	0.56	**0.38**	0.41	0.35
Ti	**6.60**	11.74	4.49	**3.10**	3.35	2.87	**3.60**	4.02	3.26	**9.98**	13.32	7.96	**4.92**	5.77	4.28	**2.36**	2.91	1.96	**8.38**	12.91	6.20	**19.68**	58.25	11.33	**6.13**	6.52	4.23
A-SIL	91.80			92.70			92.07			89.25			91 82			91.09			92.17			91.82			91.21		
ALKS	17.21			15.40			16.34			16.67			15.82			16.71			19.20			15.82			17.21		
CAFEMICS	24.16			22.16			22.98			28.05			24.88			22.53			26.34			24.88			27.46		
SIALTI	58.62			62.44			60.68			55.28			59.30			60.76			54.46			59.30			55.33		
A-CARB	59.14			62.28			61.10			58.39			62.61			68.06			59.64			56.44			63.56		
ALKS	40.05			28 28			27.21			37.41			35.34			32.51			39.55			49.21			33.12		
CAFEMICS	55.43			61.14			63.32			60.13			58.66			52.56			58.04			49.16			60.37		
SIALTI	4.52			10.58			9.48			2.47			6.00			14.93			2.41			1.64			6.51		
DURATION	60.00			60.00			60.00			60.00			60.00			60.00			60.00			60.00			60.00		

SUN189 + CNC: Major element analyses.

	G3.5	St. Dev.	St. Error	G2.5	St. Dev.	St. Error	G4.5	St. Dev.	St. Error	G6.5	St. Dev.	St. Error	G5.5	St. Dev.	St. Error	G7.5	St. Dev.	St. Error	G9.5	St. Dev.	St. Error	G1.5	St. Dev.	St. Error	G10.5	St. Dev.	St. Error
SILICATE	(10).			(10).			(10).			(9).			(10).			(10).			(10).			(10).			(10).		
NA20	14.55	0.22	0.07	13.20	0.28	0.09	14 66	0.31	0.10	13.85	0.35	0.12	13.77	0.25	0.08	14.33	0.25	0.08	14.454	0.163	0.05	13.95	0.32	0.10	15.04	0.277	0.09
SIO2	35.51	0.38	0.12	35.54	0.38	0.12	33.90	0.44	0 14	33.10	0.96	0.30	35.64	0 74	0.23	33.46	0.85	0.27	33.73	0.68	0.21	32.17	0.44	0 14	36.15	2.375	0.75
K2O	1.69	0.04	0.01	1.62	0.08	0.02	1.49	0.06	0.02	1.72	0.05	0.01	1.71	0.04	0.01	1.69	0.03	0.01	1.74	0.09	0.03	1.79	0.04	0 01	1.91	0.172	0.05
FEO	6.92	0.14	0.04	6.35	0.20	0.06	8.08	0.20	0.06	6.20	0.24	0.08	7.13	0.27	0.09	5.09	0.20	0.06	4.47	0.32	0.10	4.76	0.10	0.03	3.91	1.461	0.46
MGO	4.25	0.08	0.03	4.26	0.11	0.03	4.33	0.10	0.03	4.34	0.12	0.04	4.22	0.04	0.01	4.48	0.09	0.03	4.37	0.06	0.02	4.28	0.08	0.03	4.37	0 239	0.08
AL2O3	12.63	0.25	0.08	12.89	0.22	0.07	10.85	0.18	0 06	11.63	0.31	0.10	13.17	0.37	0.12	12.21	0.35	0.11	11.95	0.30	0.10	11.71	0.17	0.05	13.19	1.471	0.47
CAO	14.08	0.29	0.09	13.86	0.28	0.09	14.47	0.28	0.09	16.17	0.45	0.14	13.68	0 46	0.15	15.44	0.57	0.18	16.12	0.25	0.08	16.34	0.21	0.07	16.13	1.272	0.40
MNO	0.18	0.04	0.01	0.17	0.04	0.01	0.17	0.03	0.01	0.16	0.02	0.01	0.16	0.03	0.01	0.16	0.04	0.01	0.16	0.02	0.01	0.16	0.05	0.01	0.16	0.018	0.01
P2O5	0.45	0.04	0.01	0.42	0.06	0.02	0.51	0.07	0.02	0.71	0.08	0.03	0.49	0.05	0.01	0.59	0.07	0.02	0.68	0.06	0.02	0.69	0.04	0.01	0.64	0.057	0.02
TIO2	2.10	0.04	0.01	2.12	0.07	0.02	2.22	0.04	0.01	2.17	0.07	0.02	2.08	0.07	0.02	2.01	0.06	0.02	2.17	0.05	0.01	1.94	0.05	0.02	2.18	0.073	0.02
TOTALS	92.56			90.64			90.89			90.30			92.25			89.69			90.08			88.03			93.91		
P	2.50			5.00			8.00			2.50			5.00			8.00			2.50			5.00			8.00		
T	1100.00			1100.00			1100.00			1200.00			1200.00			1200.00			1300.00			1300.00			1300.00		
		St. Dev.	St. Error		St. Dev.	St. Error		St. Dev.	St. Error		St. Dev.	St. Error		St. Dev.	St. Error		St. Dev.	St. Error		St. Dev.	St. Error		St. Dev.	St. Error		St. Dev.	St. Error
CARBONATE	(10).			(10).			(10).			(10).			(10).			(10).			(9).			(10).			(10).		
NA20	20.27	3.99	1.26	19.30	2.62	0.83	20.87	1.94	0 61	22.24	1.78	0.56	23.78	1.80	0.57	20.67	1.41	0.45	21.52	0.92	0.31	21.31	0.89	0.28	22.93	0.16	0.05
SIO2	5.69	5.64	1.78	3.36	3.02	0.95	7.45	11.04	3.49	3.14	1.87	0.59	2.37	0.80	0.25	2.92	1.12	0.36	0.481	0.241	0.08	4.16	2.16	0.68	0.87	0.13	0.04
K2O	2.37	0.73	0.23	1.85	0.20	0.06	2.21	0.79	0 25	2.51	0.17	0.05	2.91	0.30	0.09	2.37	0.22	0.07	1.67	0.20	0.06	1.96	0.17	0.05	2.55	0.11	0.03
FEO	2.45	2.00	0.63	2.41	1.06	0.34	2.27	0.50	0.16	1.75	0.44	0.14	1.92	0.14	0.04	1.90	0.60	0.19	0.74	0.10	0.03	1.94	0.20	0.06	1.12	0.06	0.02
MGO	3.81	2.26	0.71	3.81	0.85	0.27	2.85	0.82	0.26	3.48	0.57	0.18	3.00	0.41	0.13	4.02	0.19	0.06	2.64	0.26	0.08	4.23	0.19	0.06	3.14	0.06	0.02
AL2O3	0.72	0.99	0.31	0.44	0.66	0.21	3.13	9.18	2.90	0.34	0.23	0.07	0.18	0.28	0.09	0.13	0.14	0.04	0.11	0.08	0.02	0.66	0.39	0.12	0.04	0.04	0.01
CAO	26.63	3.48	1.10	29.40	1.62	0.51	26.22	7.86	2.48	26.75	1.07	0.34	27.75	1.90	0.60	30.14	1.16	0.37	28.04	0.29	0.09	26.48	1.28	0.40	29.06	0.17	0 05
MNO	0.10	0.07	0.02	0.10	0.03	0.01	0.09	0.05	0.01	0.10	0.03	0.01	0.09	0.08	0.03	0.12	0.10	0.03	0.08	0.03	0.01	0.14	0.04	0.01	0.13	0.11	0.04
P2O5	1.61	0.28	0.09	1.76	0.43	0.14	1.64	0.59	0.19	1.87	0.22	0.07	1.47	0.15	0.05	1.55	0.09	0.03	0.88	0.07	0.02	1.07	0.09	0.03	1.26	0.05	0.01
TIO2	0.67	0.65	0.21	0.43	0.32	0.10	0.43	0.17	0.05	0.42	0.23	0.07	0.31	0.07	0.02	0.29	0.06	0.02	0.10	0.04	0.01	0.57	0.21	0.07	0.12	0.03	0.01
TOTALS	64.71			63.30			67.57			63.00			64 20			64.54			56 68			62.89			61.65		
P	2.5			5.00			8.00			2.50			5.00			8.00			2.50			5.00			8		
T	1100			1100.00			1100.00			1200.00			1200.00			1200.00			1300.00			1300.00			1300		
KD'S	BEST	MAX	MIN	BEST	MAX	MIN	BEST	MAX	MIN	BEST	MAX	MIN	BEST	MAX	MIN	BEST	MAX	MIN	BEST	MAX	MIN	BEST	MAX	MIN	BEST	MAX	MIN
Na	0.72	0.82	0.64	0.68	0.75	0.63	0.70	0.75	0.66	0.62	0.66	0.59	0.58	0.61	0.55	0.69	0.73	0.66	0.67	0.69	0.65	0.65	0.67	0.64	0.66	0.66	0.65
Si	6.24	16.18	3.87	10.58	23.82	6.80	4.55	56.00	2 37	10.55	16.72	7.70	15.02	19.00	12.42	11.47	15.08	9.26	70.12	101.72	53.49	8.57	11.41	5.86	41.79	46.27	37.98
K	0.71	0.88	0.60	0.88	0.94	0.82	0.67	0.86	0.55	0.69	0.72	0.66	0.69	0.63	0.55	0.71	0.76	0.67	1.04	1 13	0.96	0.87	0.97	0 87	0.78	0.80	0.70
Fe	2.82	5.71	1.87	2.64	3.63	2.07	3.56	4.12	3.12	3.54	4.19	3.06	3.72	3.91	3.54	2.68	3.34	2.24	6.04	6.66	5.50	3.68	2.63	2.31	3.47	4.29	2.66
Mg	1.12	1.77	0.82	1.12	1.30	0.98	1.62	1.85	1.29	1.25	1.39	1.13	1.40	1.54	1.29	1.11	1.15	1.08	1.65	1.76	1.56	1.00	1.04	0.98	1.39	1.44	1.34
Al	17.56	117.05	9.49	29.02	397.15	15.06	3.46	-4.25	1.23	34.11	58.26	24.10	72.38	1140.21	37.36	95.37	279.32	57.48	113.80	208.66	78.21	20.05	28.29	13.01	376.91	1377.13	217.13
Ca	0.53	0.58	0.49	0.47	0.49	0.45	0.55	0.68	0.47	0.50	0.62	0.59	0.49	0.52	0.47	0.51	0.53	0.50	0.57	0.58	0.57	0.52	0.64	0.60	0.56	0.58	0.53
Mn	1.73	2.91	1.20	1.76	2.21	1.41	1.87	2.77	1.39	1.71	2.09	1.42	1.69	3.65	1.09	1.27	2.64	0.81	2.13	2.99	1.64	1.14	1.50	0.88	1.21	2.60	0.78
P	0.28	0.31	0.25	0.24	0.29	0.20	0.31	0.40	0.25	0.38	0.42	0.34	0.33	0.36	0.30	0.38	0.41	0.35	0.77	0.83	0.71	0.65	0.69	0.61	0.61	0.54	0.48
Ti	3.14	7.97	1.95	4.92	9.02	3.38	5.14	6.78	4.13	5.14	7.82	3.83	6.76	7.88	5.92	7.00	8.10	6.17	22.13	29.64	17.66	3.67	4.42	2.78	18.02	20.94	15.80
A-SIL	91.73			89.84			89.99			89.19			91.40			88.72			89.00			91.40			92.87		
ALKS	17.70			16.49			17.94			17.46			16.93			18.06			18.20			16.93			18.25		
CAFEMICS	27.53			27.24			29.87			29.95			45 76			28.20			28.04			27.39			26.28		
SIALTI	54.77			56.27			52.19			52.59			55.68			53.74			53.76			55.68			55.47		
A-CARB	62.61			61.00			65.44			60 63			62.22			62.42			55.30			61.29			59.82		
ALKS	36.16			34.67			35.27			40.82			42.89			36 90			41.94			37.96			42.59		
CAFEMICS	52.54			58.39			47.89			52.75			52.51			57.76			56.82			53.26			55.70		
SIALTI	11.30			6.94			16.83			6.44			4.60			5.34			1.24			8.78			1.71		
DURATION	60.00			60.00			60.00			60.00			60.00			60.00			60.00			60.00			60.00		

SUN189 + CC: Major element analyses.

	G3.6	St. Dev.	St. Error	G2.6	St. Dev.	St. Error	G4.6	St. Dev.	St. Error	G6.6	St. Dev.	St. Error	G15	St. Dev.	St. Error	G7 6	St. Dev.	St. Error	G9 6	St. Dev.	St. Error	G1.6	St. Dev.	St. Error	G10.6	St. Dev.	St. Error
SILICATE	(10).			(10).			(10).			(10).			(10).			(10).			(10).			(10).			(10).		
NA20	9.62	0.13	0.04	8.35	0.13	0.04	10.44	0.99	0.31	9.24	0.27	0.09	8.79	0.17	0.05	9.26	0.18	0.06	8.74	0.20	0.06	8.70	0.30	0.10	8.72	0.39	0 12
SIO2	32.97	0.35	0.11	33.71	0 42	0.13	34.66	1.34	0.42	33.18	0 24	0.08	32.08	1.51	0.48	34.11	0.30	0.09	36.58	0.09	0.03	33.67	0 53	0.17	31.94	0.63	0 20
K2O	1.85	0.04	0.01	1.73	0.06	0.02	1.90	0.18	0.06	1.86	0.07	0.02	1.80	0.07	0.02	1.76	0.04	0.01	1.67	0.07	0.02	1.85	0.09	0.03	1 73	0.07	0.02
FEO	6.95	0.13	0.04	6.79	0.15	0.05	7.53	0.47	0.15	6.03	0.18	0 06	6.24	0.38	0.12	5.83	0.09	0.03	5.36	0.19	0.06	4.81	0.31	0.10	5.03	0.14	0.04
MGO	4.14	0.06	0.02	4.14	0.11	0.03	3.27	0.31	0.10	4.34	0.06	0.02	4 08	0.09	0.03	4.40	0.10	0.03	4.49	0.07	0 02	4 24	0 17	0.05	4.15	0.17	0.06
AL2O3	11.51	0.16	0.05	12.23	0.19	0.06	12.95	0.58	0.18	11.67	0.13	0.04	11 22	0.72	0.23	12.12	0.16	0.05	12.84	0.11	0.03	12.04	0.25	0.08	10.96	0.29	0.09
CAO	21.11	0.19	0.06	19.73	0.31	0.10	17.84	0.88	0.28	22.04	0.33	0.11	21.92	0.79	0.25	22.25	0.12	0.04	20.22	0.18	0.06	21.46	0.77	0.24	21.94	0.55	0.17
MNO	0.17	0.03	0.01	0.16	0.04	0.01	0.21	0.03	0.01	0.16	0.04	0.01	0.16	0.02	0.01	0.16	0.06	0.02	0.18	0.02	0.01	0.16	0.03	0.01	0.16	0.04	0.01
P2O5	0.59	0.06	0.02	0.49	0.04	0.01	0.49	0.07	0.02	0.56	0.06	0.02	0.69	0.14	0.04	0.58	0.06	0.02	0.49	0.04	0.01	0.59	0 08	0.02	0.72	0.07	0.02
TIO2	1.97	0.05	0.01	1.97	0.05	0.02	2.08	0.06	0.02	2.01	0.06	0.02	2.01	0.06	0.02	2.01	0.08	0.02	2.31	0.03	0.01	2.01	0.06	0.02	2.08	0.06	0.02
TOTALS	91.20			89.60			91.43			91.41			89 31			92.82			93.17			89 84			87.75		
P	2.50			5.00			8.00			2.50			5.00			8.00			2.50			5.00			8.00		
T	1100.00			1100.00			1100.00			1200.00			1200.00			1200.00			1300.00			1300.00			1300.00		
		St. Dev.	St. Error		St. Dev.	St. Error		St. Dev.	St. Error		St. Dev.	St. Error		St. Dev.	St. Error		St. Dev.	St. Error		St. Dev.	St. Error		St. Dev.	St. Error		St. Dev.	St. Error
CARBONATE	(4).			(10).			(10).			(6).			(9).			(10).			(10).			(12).			(10).		
NA20	2.01	0.72	0.36	10.65	1.95	0.62	12.28	4.36	1.38	1.39	0.45	0.18	5.68	0.95	0.32	15.69	0.31	0.10	1.05	0.19	0.06	8.98	3.75	1.08	7 92	2.64	0 83
SIO2	0.27	0.14	0.07	5.89	3.33	1.05	4.01	3.32	1.05	1.88	2.02	0.82	1.45	1.59	0.53	1.38	0.34	0.11	2.10	0.85	0.27	2.55	1.52	0.44	2.68	1.73	0.55
K2O	0.19	0.08	0.04	1.86	0.48	0.15	1.23	0.43	0.14	0.69	0.34	0.14	0.82	0.26	0.09	2.52	0.10	0.03	0.28	0.10	0.03	1.37	0.34	0.10	1.18	0.33	0.10
FEO	1.67	0.11	0.06	3.14	1.39	0.44	2.33	1.72	0.54	1.62	0.12	0.05	1.95	0.15	0.05	1.40	0.17	0.05	1.36	0.19	0.06	1.18	0.08	0.02	1.86	0.33	0.10
MGO	2.92	0 09	0.05	3.93	1.23	0.39	2.08	1.39	0.44	3.18	0.08	0.03	3 38	0.20	0 07	2.89	0.14	0.04	3.27	0.08	0.02	3.23	0.11	0.03	3.86	0.72	0.23
AL2O3	0.17	0.07	0.03	0.75	0.54	0.17	0.64	0 61	0.19	0.76	0.45	0.18	0.13	1.51	0.50	0.05	0.05	0.02	0.16	1.18	0.37	0.30	0.29	0.08	0.37	0.38	0.12
CAO	44.72	1 85	0.93	35.48	3.00	0.95	38.58	4.52	1.43	45.29	1.60	0.65	40.84	0.13	0.04	35.96	0.31	0.10	40.48	0.16	0.05	39.58	2.39	0 69	38.23	2.07	0 65
MNO	0.11	0.04	0.02	0.14	0.04	0.01	0.12	0.05	0.02	0.12	0.06	0.02	0.08	0.05	0.02	0.11	0.05	0.02	0.11	0.04	0.01	0.12	0.04	0 01	0.13	0.06	0.02
P2O5	0.49	0.07	0.03	1.80	0.34	0.11	1.77	1.07	0.34	0.46	0.14	0.06	0.93	0.21	0.07	0.94	0.09	0.03	0.29	0.08	0.02	1.03	0.17	0.05	1.44	0.34	0.11
TIO2	0.10	0.03	0.02	0.66	0.34	0.11	0.43	0.43	0.13	0.22	0.11	0.05	0.25	0.17	0.06	0.15	0.06	0.02	0.32	0.11	0.04	0.32	0.11	0.03	0.31	0.13	0.04
TOTALS	53.31			64.83			64.05			56.28			56.12			61.79			50.02			59.23			58.56		
P	2.50			5.00			8.00			2.50			5.00			8.00			2.50			5.00			8.00		
T	1100.00			1100.00			1100.00			1200 00			1200.00			1200.00			1300.00			1300.00			1300.00		

KD'S	BEST	MAX	MIN	BEST	MAX	MIN	BEST	MAX	MIN	BEST	MAX	MIN	BEST	MAX	MIN	BEST	MAX	MIN	BEST	MAX	MIN	BEST	MAX	MIN	BEST	MAX	MIN
Na	4.79	7.38	3.55	0.78	0.88	0.70	0.86	1.10	0.69	6.66	8.95	5.29	1.56	1.74	1.39	0.59	0.60	0.58	8.29	9.33	7.46	0.98	1.27	0.78	1.10	1.39	0.91
Si	123.03	250.20	81.56	5.73	8.82	4.24	8.66	17.82	5.71	17.63	124.16	9.49	22.12	77.66	12.89	24.68	29.11	21.42	17.45	23.29	13.95	12.68	19.89	9.87	11.93	19.91	8 51
K	0.61	16.18	6.83	0.93	1.11	0.80	1.54	1 98	1.25	2.69	4.44	1.93	2.20	2.79	1.82	0.70	0.72	0.68	6.02	7.70	4.94	1.31	1.57	1.17	1.47	1.78	1 25
Fe	4.15	4.45	3.89	2.17	2.99	1.70	3.22	5.95	2.21	3.72	3.96	3.50	3.20	3.40	3.00	4.17	4.50	3.88	3.93	4.32	3.61	5.30	4.31	3.87	2.71	3.05	2.44
Mg	1.42	1.47	1.37	1.05	1.31	0.88	1.57	2.69	1.11	1.36	1.39	1.33	1.21	1.26	1.16	1.62	1.58	1.47	1.37	1.40	1.35	1.27	1.36	1.28	1.08	1.22	0.96
Al	68.94	114.72	49.27	16.24	29.36	11.22	20.20	48.80	12.72	18.42	29.46	10.44	86.96	648.00	10.04	262.46	687.38	154.61	82.83	659.00	14.54	37.77	89.82	26.17	29.63	80.14	18.09
Ca	0.47	0.49	0.45	0.56	0.59	0.53	0.46	0.50	0.43	0.49	0.50	0.47	0.54	0.55	0.52	0.62	0.62	0.61	0.60	0.50	0.50	0.55	0.57	0.52	0.57	0.60	0.55
Mn	1.56	2.35	1.15	1.14	1.43	0.91	1.83	2.58	1.39	1.32	2.14	0.93	2.06	3.33	1.47	1.49	2.29	1.00	1.69	2.02	1.30	1.37	1.78	1.07	1.21	1.74	0.89
P	1.21	1.41	1.05	0.27	0.31	0.24	0.27	0.44	0.20	1.21	1.61	0.96	0.74	0.90	0.61	0.61	0.67	0.56	1.71	2.05	1.46	0.57	0.65	0.51	0.50	0.59	0.43
Ti	19.31	27.89	14.77	2.99	4.38	2.26	4.82	12.40	2.99	9.28	15.81	6.56	8.06	14.76	5.54	13.57	18.14	10.83	7.20	9.21	5.91	6.25	7.74	5.20	6.67	8.92	5.32
A-SIL	90.13			88.65			90 67			90.36			88 13			91.72			92.20			88.13			86.55		
ALKS	12.73			11.37			13.60			12.28			12.02			12.01			11.28			12.02			12.07		
CAFEMICS	35.73			34.59			31.59			35.86			36.57			35.40			32.61			36.57			35.96		
SIALTI	51.54			54.04			54.81			51.87			51.41			52.58			56.11			51.41			51.97		
A-CARB	52.05			62.35			61 59			55.03			54.49			60 04			49 02			57.50			56.41		
ALKS	4.23			20.06			21.95			3.78			3.82			30.33			2.72			18.00			16.13		
CAFEMICS	94.74			68.23			69.81			91.03			91.92			67.04			92 04			76.49			77.91		
SIALTI	1.03			11.70			8.25			5.19			5.24			2.63			5.25			5.51			5.96		
DURATION	60.00			60.00			60.00			60.00			60.00			60.00			60.00			60.00			60.00		

Duration effects: BD50 + CNC.

	G8.1	St. Dev.	St. Error	G10.1	St. Dev.	St. Error	G25.1	St. Dev.	St. Error	G24.1	St. Dev.	St. Error
SILICATE	(10).			(10).			(10).			(10).		
NA20	15.99	0.21	0.07	17.56	0.15	0.05	16.29	0.17	0.05	17.94	0.51	0.16
SIO2	48.97	0.48	0.15	44.57	0.63	0.20	49.40	0.46	0.15	50.19	1.09	0.35
K2O	3.70	0.06	0.02	3.86	0.05	0.01	4.08	0.06	0.02	4.64	0.23	0.07
FEO	2.48	0.16	0.05	1.19	0.52	0.17	0.42	0.18	0.06	0.31	0.03	0.01
MGO	0.62	0.05	0.02	0.65	0.02	0.01	0.62	0.03	0.01	0.64	0.05	0.01
AL2O3	18.30	0.40	0.13	16.09	0.26	0.08	18.07	0.18	0.06	18.77	0.26	0.08
CAO	4.78	0.25	0.08	8.00	0.49	0.15	5.48	0.15	0.05	5.15	0.73	0.23
MNO	0.11	0.05	0.02	0.13	0.02	0.01	0.13	0.03	0.01	0.12	0.02	0.01
P2O5	0.11	0.04	0.01	0.15	0.04	0.01	0.09	0.04	0.01	0.09	0.03	0.01
TIO2	0.86	0.03	0.01	0.86	0.04	0.01	0.84	0.03	0.01	0.86	0.03	0.01
TOTALS	95.98			93.18			95.50			98.80		
P	8.00			8.00			8.00			8.00		
T	1300.00			1300.00			1300.00			1300.00		
		St. Dev.	St. Error		St. Dev.	St. Error		St. Dev.	St. Error		St. Dev.	St. Error
CARBONATE	(10).			(4).			(10).			(9).		
NA20	29.14	0.31	0.10	27.83	1.13	0.57	27.43	0.59	0.19	28.68	0.62	0.21
SIO2	0.06	0.02	0.01	0.35	0.05	0.02	0.49	0.69	0.22	0.27	0.27	0.09
K2O	3.57	0.06	0.02	3.96	0.21	0.10	3.91	0.29	0.09	2.30	0.12	0.04
FEO	0.92	0.07	0.02	0.12	0.03	0.01	0.43	0.13	0.04	0.05	0.04	0.01
MGO	1.26	0.10	0.03	0.70	0.12	0.06	1.13	0.15	0.05	0.99	0.09	0.03
AL2O3	0.04	0.03	0.01	0.16	0.13	0.06	0.15	0.10	0.03	0.08	0.07	0.02
CAO	24.69	0.28	0.09	24.25	0.56	0.28	24.08	1.13	0.36	24.69	0.75	0.25
MNO	0.21	0.04	0.01	0.11	0.04	0.02	0.19	0.02	0.01	0.15	0.02	0.01
P2O5	0.53	0.05	0.02	0.53	0.03	0.01	0.50	0.15	0.05	0.44	0.09	0.03
TIO2	0.22	0.03	0.01	0.15	0.03	0.02	0.35	0.27	0.09	0.16	0.11	0.04
TOTALS	58.00			56.90			59.02			58.17		
P	8.00			8.00			8.00			8.00		
T	1300.00			1300.00			1300.00			1300.00		

KD'S	BEST	MAX	MIN	BEST	MAX	MIN	BEST	MAX	MIN	BEST	MAX	MIN
Na	**0.55**	0.55	0.54	**0.63**	0.66	0.61	**0.59**	0.60	0.59	**0.63**	0.64	0.61
Si	**790**	987.31	658.17	**129**	148.63	114.21	**101**	750.59	53.91	**188**	553.97	113.16
K	**1.04**	1.05	1.02	**0.97**	1.03	0.93	**1.04**	1.09	1.00	**2.02**	2.11	1.93
Fe	**2.71**	2.88	2.55	**10.21**	14.73	6.96	**0.97**	1.32	0.69	**6.27**	11.77	4.25
Mg	**0.49**	0.53	0.46	**0.93**	1.12	0.79	**0.55**	0.60	0.50	**0.65**	0.70	0.60
Al	**426**	749.79	296.97	**104**	537.09	57.29	**121**	210.70	85.16	**244**	543.61	157.12
Ca	**0.19**	0.20	0.19	**0.33**	0.34	0.32	**0.23**	0.24	0.22	**0.21**	0.23	0.19
Mn	**0.53**	0.69	0.38	**1.18**	1.87	0.85	**0.67**	0.77	0.57	**0.85**	0.97	0.75
P	**0.20**	0.25	0.15	**0.29**	0.34	0.24	**0.19**	0.25	0.14	**0.20**	0.26	0.15
Ti	**3.97**	4.41	3.61	**5.94**	7.47	4.93	**2.38**	4.55	1.61	**5.53**	10.59	3.74

A-SIL	95.69			92.78			95.19			98.51		
ALKS	20.57			23.09			21.39			22.93		
CAFEMICS	8.24			10.61			6.85			6.19		
SIALTI	71.20			66.30			71.76			70.88		
A-CARB	59.89			57.50			57.97			57.21		
ALKS	54.61			55.28			54.05			54.15		
CAFEMICS	44.85			43.60			44.24			44.97		
SIALTI	0.54			1.12			1.71			0.87		
DURATION	15.00			60.00			240.00			960.00		

Duration effects: BD119 + CNC.

	G8.3	St. Dev.	St. Error	G10.3	St. Dev.	St. Error	G25.2	St. Dev.	St. Error	G24.2	St. Dev.	St. Error
SILICATE	(10).			(10).			(11).			(9).		
NA2O	15.33	0.25	0.08	17.09	0.33	0.11	15.92	0.29	0.09	17.80	0.15	0.05
SIO2	41.67	0.44	0.14	38.08	0.45	0.14	40.94	0.68	0.20	41.95	0.65	0.22
K2O	3.46	0.11	0.03	3.72	0.15	0.05	3.90	0.09	0.03	4.45	0.05	0.02
FEO	5.80	0.21	0.07	3.31	0.55	0.17	2.63	0.17	0.05	0.99	0.04	0.01
MGO	0.88	0.05	0.02	0.94	0.02	0.01	0.85	0.04	0.01	0.90	0.02	0.01
AL2O3	14.02	0.29	0.09	12.19	0.22	0.07	13.33	0.21	0.06	14.04	0.24	0.08
CAO	11.39	0.28	0.09	14.92	0.28	0.09	12.40	0.32	0.10	12.36	0.30	0.10
MNO	0.28	0.06	0.02	0.30	0.04	0.01	0.28	0.04	0.01	0.27	0.03	0.01
P2O5	0.29	0.06	0.02	0.53	0.05	0.01	0.40	0.07	0.02	0.40	0.04	0.01
TIO2	0.91	0.04	0.01	0.95	0.06	0.02	0.93	0.04	0.01	0.94	0.02	0.01
TOTALS	94.20			92.23			91.75			94.28		
P	8.00			8.00			8.00			8.00		
T	1300.00			1300.00			1300.00			1300.00		
		St. Dev.	St. Error		St. Dev.	St. Error		St. Dev.	St. Error		St. Dev.	St. Error
CARBONATE	(10).			(10).			(9).			(10).		
NA2O	26.28	0.16	0.05	24.96	1.28	0.40	24.00	0.20	0.07	24.62	0.75	0.24
SIO2	1.27	0.13	0.04	1.38	0.94	0.30	5.08	1.49	0.50	4.38	2.22	0.70
K2O	5.22	0.11	0.03	4.65	0.16	0.05	4.66	0.09	0.03	4.14	0.07	0.02
FEO	0.77	0.06	0.02	0.50	0.27	0.08	1.00	0.21	0.07	0.33	0.09	0.03
MGO	0.67	0.06	0.02	0.60	0.23	0.07	0.83	0.13	0.04	0.78	0.13	0.04
AL2O3	0.04	0.04	0.01	0.33	0.59	0.19	0.56	0.32	0.11	0.48	0.60	0.19
CAO	27.35	0.17	0.05	24.95	0.10	0.03	26.17	0.71	0.24	26.92	0.89	0.28
MNO	0.18	0.11	0.04	0.15	0.04	0.01	0.20	0.05	0.02	0.20	0.05	0.02
P2O5	1.46	0.05	0.01	1.27	0.10	0.03	1.43	0.08	0.03	1.40	0.11	0.03
TIO2	0.08	0.03	0.01	0.10	0.06	0.02	0.31	0.09	0.03	0.28	0.09	0.03
TOTALS	63.74			59.31			64.63			63.93		
P	8.00			8.00			8.00			8.00		
T	1300.00			1300.00			1300.00			1300.00		

KD'S	BEST	MAX	MIN	BEST	MAX	MIN	BEST	MAX	MIN	BEST	MAX	MIN
Na	**0.58**	0.59	0.58	**0.68**	0.71	0.66	**0.66**	0.67	0.66	**0.72**	0.74	0.71
Si	**33**	34.90	30.87	**28**	47.43	19.39	**8**	9.96	6.76	**10**	13.99	7.29
K	**0.66**	0.68	0.65	**0.80**	0.83	0.77	**0.84**	0.85	0.82	**1.07**	1.09	1.06
Fe	**7.56**	8.00	7.16	**6.68**	10.16	4.90	**2.64**	3.07	2.31	**3.00**	3.65	2.55
Mg	**1.30**	1.39	1.22	**1.55**	2.02	1.26	**1.01**	1.13	0.91	**1.15**	1.28	1.04
Al	**326**	796.96	204.83	**37**	328.00	17.43	**24**	38.34	17.34	**29**	131.50	16.52
Ca	**0.42**	0.42	0.41	**0.60**	0.60	0.59	**0.47**	0.48	0.46	**0.46**	0.47	0.45
Mn	**1.54**	2.52	1.08	**1.94**	2.34	1.64	**1.40**	1.69	1.18	**1.35**	1.64	1.14
P	**0.20**	0.22	0.17	**0.42**	0.45	0.39	**0.28**	0.31	0.25	**0.29**	0.31	0.27
Ti	**11.43**	14.47	9.43	**9.66**	15.59	6.99	**3.02**	3.69	2.55	**3.38**	4.23	2.82

A-SIL	93.46			91.18			90.88			93.42		
ALKS	20.11			22.82			21.80			23.81		
CAFEMICS	19.33			21.02			17.47			15.25		
SIALTI	60.56			56.17			60.73			60.94		
A-CARB	61.68			54.27			62.61			61.93		
ALKS	51.06			50.87			45.77			46.45		
CAFEMICS	46.67			45.79			44.72			45.26		
SIALTI	2.26			3.34			9.51			8.29		
DURATION	15.00			60.00			240.00			960.00		

Duration effects: BD119 + CC.

	G8.4	St. Dev.	St. Error	G10.4	St. Dev.	St. Error	G25.3	St. Dev.	St. Error	G24.3	St. Dev.	St. Error
SILICATE	(10).			(10).			(10).			(10).		
NA20	10.90	0.20	0.06	11.89	0.29	0.09	11.00	0.17	0.05	13.93	0.17	0.05
SIO2	40.00	0.86	0.27	37.69	0.19	0.06	39.56	0.28	0.09	37.54	0.21	0.07
K2O	3.57	0.10	0.03	3.81	0.18	0.06	4.02	0.07	0.02	4.99	0.08	0.03
FEO	5.28	0.46	0.14	3.57	0.16	0.05	2.69	0.12	0.04	1.11	0.04	0.01
MGO	0.85	0.05	0.02	0.89	0.03	0.01	0.82	0.04	0.01	0.90	0.04	0.01
AL2O3	13.50	0.66	0.21	11.85	0.11	0.03	12.80	0.12	0.04	11.97	0.06	0.02
CAO	16.65	0.71	0.23	20.59	0.39	0.12	17.76	0.22	0.07	21.56	0.12	0.04
MNO	0.30	0.07	0.02	0.30	0.03	0.01	0.29	0.02	0.00	0.30	0.02	0.01
P2O5	0.35	0.09	0.03	0.54	0.05	0.02	0.42	0.04	0.01	0.60	0.03	0.01
TIO2	0.89	0.04	0.01	0.93	0.03	0.01	0.90	0.03	0.01	0.88	0.02	0.01
TOTALS	92.54			92.35			90.54			94.09		
P	8.00			8.00			8.00			8.00		
T	1300.00			1300.00			1300.00			1300.00		
		St. Dev.	St. Error		St. Dev.	St. Error		St. Dev.	St. Error		St. Dev.	St. Error
CARBONATE	(10).			(10).			(10).			(3).		
NA20	16.09	1.41	0.45	16.09	1.41	0.45	14.44	0.62	0.20	20.83	1.62	0.94
SIO2	3.74	1.12	0.36	3.74	1.12	0.36	8.45	2.89	0.91	3.82	0.91	0.53
K2O	4.97	0.22	0.07	4.97	0.22	0.07	3.93	0.22	0.07	4.03	0.12	0.07
FEO	1.72	0.60	0.19	1.72	0.60	0.19	1.32	0.29	0.09	0.14	0.04	0.02
MGO	0.68	0.19	0.06	0.68	0.19	0.06	0.80	0.11	0.04	0.32	0.06	0.04
AL2O3	0.22	0.14	0.04	0.22	0.14	0.04	1.47	0.90	0.29	0.24	0.16	0.09
CAO	35.96	1.16	0.37	35.96	1.16	0.37	33.59	2.17	0.69	30.56	1.42	0.82
MNO	0.22	0.10	0.03	0.22	0.10	0.03	0.25	0.03	0.01	0.12	0.08	0.05
P2O5	1.44	0.09	0.03	1.44	0.09	0.03	1.32	0.25	0.08	1.12	0.05	0.03
TIO2	0.18	0.06	0.02	0.18	0.06	0.02	0.44	0.09	0.03	0.17	0.07	0.04
TOTALS	65.76			65.76			66.50			61.80		
P	8.00			8.00			8.00			8.00		
T	1300.00			1300.00			1300.00			1300.00		

KD'S	BEST	MAX	MIN	BEST	MAX	MIN	BEST	MAX	MIN	BEST	MAX	MIN
Na	**0.72**	0.72	0.64	**0.74**	0.78	0.70	**0.76**	0.78	0.74	**0.67**	0.73	0.61
Si	**11**	13.17	9.02	**10**	12.41	8.51	**5**	5.94	3.86	**10**	13.48	7.73
K	**0.73**	0.74	0.70	**0.77**	0.80	0.74	**1.02**	1.06	0.99	**1.24**	1.28	1.20
Fe	**1.71**	3.93	2.50	**2.07**	2.65	1.70	**2.04**	2.36	1.79	**7.93**	11.72	5.99
Mg	**1.32**	1.50	1.05	**1.30**	1.57	1.10	**1.03**	1.13	0.94	**2.83**	3.66	2.31
Al	**60**	96.71	43.72	**53**	84.79	38.42	**9**	14.11	6.31	**51**	231.56	28.61
Ca	**0.46**	0.48	0.45	**0.57**	0.59	0.56	**0.53**	0.55	0.51	**0.71**	0.74	0.67
Mn	**1.16**	1.92	0.98	**1.34**	1.88	1.03	**1.19**	1.30	1.09	**2.57**	12.10	1.44
P	**0.24**	0.29	0.20	**0.38**	0.41	0.35	**0.32**	0.36	0.28	**0.54**	0.57	0.51
Ti	**4.98**	6.24	4.04	**5.13**	6.52	4.23	**2.06**	2.34	1.83	**5.06**	9.30	3.48

Λ-SIL	91.64			91.21			89.56			92.86		
ALKS	15.79			17.21			16.77			20.37		
CAFEMICS	24.86			27.46			23.76			25.37		
SIALTI	59.35			55.33			59.47			54.26		
Λ-CARB	63.56			63.56			64.43			60.11		
ALKS	33.12			33.12			28.51			41.36		
CAFEMICS	60.37			60.37			55.42			51.60		
SIALTI	6.51			6.51			16.07			7.03		

Duration effects: SUN189 + CNC.

	G8.5	St. Dev.	St. Error	G10.5	St. Dev.	St. Error	G25.4	St. Dev.	St. Error	G24.4	St. Dev.	St. Error
SILICATE	(10).			(10).			(10).			(10).		
NA20	14.95	0.61	0.19	15.04	0.277	0.09	13.93	0.40	0.13	14.29	0.131	0.04
SIO2	34.90	0.99	0.31	36.15	2.375	0.75	34.49	3.13	0.99	32.67	0.366	0.12
K2O	1.69	0.09	0.03	1.91	0.172	0.05	1.80	0.03	0.01	1.98	0.031	0.01
FEO	6.44	1.33	0.42	3.91	1.461	0.46	3.63	0.64	0.20	2.25	0.146	0.05
MGO	4.18	0.13	0.04	4.37	0.239	0.08	4.29	0.10	0.03	4.23	0.067	0.02
AL2O3	12.92	0.44	0.14	13.19	1.471	0.47	12.34	1.36	0.43	11.53	0.134	0.04
CAO	14.31	0.69	0.22	16.13	1.272	0.40	15.71	1.23	0.39	16.48	0.291	0.09
MNO	0.15	0.07	0.02	0.16	0.018	0.01	0.16	0.02	0.01	0.16	0.023	0.01
P2O5	0.46	0.08	0.03	0.64	0.057	0.02	0.55	0.18	0.06	0.66	0.063	0.02
TIO2	2.01	0.09	0.03	2.18	0.073	0.02	2.08	0.15	0.05	2.01	0.043	0.01
TOTALS	92.02			93.91			89.07			86.51		
P	8.00			8.00			8.00			8.00		
T	1300.00			1300.00			1300.00			1300.00		
		St. Dev.	St. Error		St. Dev.	St. Error		St. Dev.	St. Error		St. Dev.	St. Error
CARBONATE	(10).			(10).			(8).			(6).		
NA20	22.93	0.16	0.05	22.93	0.16	0.05	20.73	2.73	0.97	20.72	1.785	0.73
SIO2	0.87	0.13	0.04	0.87	0.13	0.04	2.35	1.53	0.54	4.35	6.684	2.73
K2O	2.55	0.11	0.03	2.55	0.11	0.03	1.74	0.26	0.09	1.54	0.432	0.18
FEO	1.12	0.06	0.02	1.12	0.06	0.02	1.27	0.43	0.15	0.86	0.063	0.03
MGO	3.14	0.06	0.02	3.14	0.06	0.02	3.95	0.91	0.32	4.07	0.413	0.17
AL2O3	0.14	0.04	0.01	0.04	0.04	0.01	0.33	0.45	0.16	0.96	1.41	0.58
CAO	29.06	0.17	0.05	29.06	0.17	0.05	29.41	2.15	0.76	26.68	2.633	1.07
MNO	0.13	0.11	0.04	0.13	0.11	0.04	0.14	0.04	0.01	0.15	0.029	0.01
P2O5	1.26	0.05	0.01	1.26	0.05	0.01	1.87	0.50	0.18	0.85	0.053	0.02
TIO2	0.12	0.03	0.01	0.12	0.03	0.01	0.34	0.14	0.05	0.46	0.308	0.13
TOTALS	61.65			61.65			62.60			60.63		
P	8.00			8			8.00			8		
T	1300.00			1300			1300.00			1300		

KD'S	BEST	MAX	MIN	BEST	MAX	MIN	BEST	MAX	MIN	BEST	MAX	MIN
Na	**0.65**	0.67	0.64	**0.66**	0.66	0.65	**0.67**	0.74	0.61	**0.69**	0.74	0.65
SI	**40**	44.38	36.96	**42**	46.27	37.98	**15**	26.76	10.06	**8**	32.66	3.37
K	**0.66**	0.69	0.64	**0.75**	0.80	0.70	**1.03**	1.15	0.93	**1.28**	1.66	1.05
Fe	**5.73**	6.50	4.97	**3.47**	4.29	2.66	**2.85**	3.78	2.24	**2.60**	2.80	2.43
Mg	**1.33**	1.36	1.30	**1.39**	1.44	1.34	**1.09**	1.29	0.94	**1.04**	1.13	0.96
Al	**96**	117.99	80.42	**.377**	1377.13	217.13	**37**	621.43	19.12	**12**	67.72	5.53
Ca	**0.49**	0.51	0.48	**0.56**	0.58	0.53	**0.53**	0.57	0.50	**0.62**	0.67	0.57
Mn	**1.12**	2.50	0.64	**1.21**	2.60	0.78	**1.14**	1.42	0.94	**1.05**	1.27	0.88
P	**0.36**	0.41	0.32	**0.51**	0.54	0.48	**0.29**	0.39	0.22	**0.78**	0.84	0.72
Ti	**16.62**	19.34	14.55	**18.02**	20.94	15.80	**6.07**	8.59	4.68	**4.40**	9.54	2.86

A-SIL	91.38			92.87			88.26			85.44		
ALKS	18.21			18.25			17.82			19.05		
CAFEMICS	27.27			26.28			26.77			26.87		
SIALTI	54.52			55.47			55.41			54.08		
A-CARB	59.92			59.82			60.14			59.63		
ALKS	42.52			42.59			37.37			37.33		
CAFEMICS	55.61			55.70			57.60			53.00		
SIALTI	1.87			1.71			5.03			9.66		

Duration effects: SUN189 + CC.

	G8.6	St. Dev.	St. Error	G10.6	St. Dev.	St. Error	G25.5	St. Dev.	St. Error	G24.5	St. Dev.	St. Error
SILICATE	(10).			(10).			(10).			(10).		
NA20	9.40	0.61	0.19	8.72	0.39	0.12	8.84	0.16	0.05	8.74	0.14	0.04
SIO2	29.29	0.99	0.31	31.94	0.63	0.20	32.06	0.12	0.04	32.79	0.19	0.06
K2O	1.80	0.09	0.03	1.73	0.07	0.02	1.87	0.06	0.02	1.98	0.04	0.01
FEO	6.78	1.33	0.42	5.03	0.14	0.04	4.85	0.10	0.03	2.87	0.10	0.03
MGO	4.14	0.13	0.04	4.15	0.17	0.06	4.12	0.07	0.02	4.22	0.06	0.02
AL2O3	10.26	0.44	0.14	10.96	0.29	0.09	11.14	0.11	0.04	11.35	0.14	0.04
CAO	22.53	0.69	0.22	21.94	0.55	0.17	21.91	0.18	0.06	22.29	0.12	0.04
MNO	0.15	0.07	0.02	0.16	0.04	0.01	0.16	0.02	0.01	0.16	0.03	0.01
P2O5	0.75	0.08	0.03	0.72	0.07	0.02	0.70	0.03	0.01	0.69	0.04	0.01
TIO2	1.80	0.09	0.03	2.08	0.06	0.02	1.95	0.06	0.02	1.99	0.05	0.02
TOTALS	87.24			87.75			87.91			87.43		
P	8.00			8.00			8.00			8.00		
T	1300.00			1300.00			1300.00			1300.00		
		St. Dev.	St. Error		St. Dev.	St. Error		St. Dev.	St. Error		St. Dev.	St. Error
CARBONATE	(10).			(10).			(9).			(9).		
NA20	13.67	2.73	0.86	7.92	2.64	0.83	11.02	2.27	0.76	11.91	2.33	0.78
SIO2	2.72	2.17	0.69	2.68	1.73	0.55	1.72	1.01	0.34	3.91	2.49	0.83
K2O	2.90	0.63	0.20	1.18	0.33	0.10	1.29	0.19	0.06	0.93	0.31	0.10
FEO	2.32	1.38	0.44	1.86	0.33	0.10	1.82	0.73	0.24	0.95	0.50	0.17
MGO	3.88	1.48	0.47	3.86	0.72	0.23	4.10	1.10	0.37	3.13	1.55	0.52
AL2O3	0.19	0.08	0.03	0.37	0.38	0.12	0.13	0.09	0.03	0.64	0.48	0.16
CAO	35.89	3.77	1.19	38.23	2.07	0.65	37.74	2.67	0.89	39.35	1.24	0.41
MNO	0.12	0.04	0.01	0.13	0.06	0.02	0.14	0.05	0.02	0.16	0.05	0.02
P2O5	1.57	0.38	0.12	1.44	0.34	0.11	1.29	0.50	0.17	1.15	0.43	0.14
TIO2	0.34	0.25	0.08	0.31	0.13	0.04	0.38	0.23	0.08	0.45	0.27	0.09
TOTALS	64.16			58.56			60.17			63.18		
P	8.00			8.00			8.00			8.00		
T	1300.00			1300.00			1300.00			1300.00		

KD'S	BEST	MAX	MIN	BEST	MAX	MIN	BEST	MAX	MIN	BEST	MAX	MIN
Na	**0.69**	0.79	0.61	**1.10**	1.39	0.91	**0.80**	0.93	0.71	**0.73**	0.84	0.65
Si	**11**	21.27	7.19	**12**	19.91	8.51	**19**	30.13	13.47	**8**	14.34	5.92
K	**0.62**	0.72	0.54	**1.47**	1.78	1.25	**1.45**	1.60	1.32	**2.13**	2.71	1.75
Fe	**2.92**	4.70	2.08	**2.71**	3.05	2.44	**2.67**	3.63	2.11	**3.02**	4.61	2.24
Mg	**1.07**	1.40	0.86	**1.08**	1.22	0.96	**1.01**	1.22	0.86	**1.35**	1.99	1.02
Al	**53**	72.57	41.92	**30**	80.14	18.09	**88**	167.39	60.06	**18**	34.56	11.83
Ca	**0.63**	0.67	0.59	**0.57**	0.60	0.55	**0.58**	0.61	0.55	**0.57**	0.58	0.55
Mn	**1.23**	1.76	0.82	**1.21**	1.74	0.89	**1.16**	1.52	0.93	**1.01**	1.28	0.81
P	**0.48**	0.57	0.41	**0.50**	0.59	0.43	**0.54**	0.73	0.43	**0.60**	0.80	0.48
Ti	**5.25**	9.67	3.60	**6.67**	8.92	5.32	**5.14**	8.44	3.69	**4.39**	7.20	3.16

A-SIL	86.00			86.55			86.72			86.25		
ALKS	13.02			12.07			12.34			12.44		
CAFEMICS	38.90			35.96			35.60			34.08		
SIALTI	48.08			51.97			52.05			53.49		
A-CARB	61.92			56.41			58.18			61.28		
ALKS	26.77			16.13			21.15			20.95		
CAFEMICS	67.96			77.91			75.02			70.87		
SIALTI	5.26			5.96			3.83			8.17		
DURATION	15.00			60.00			240.00			960.00		

Pressure effects: BD119 + CNC.

SILICATE	G9.3 (10).	St. Dev.	St. Error	G1.3 (10).	St. Dev.	St. Error	G10.3 (10).	St. Dev.	St. Error	S40 (10).	St. Dev.	St. Error	S39 (10).	St. Dev.	St. Error	S41 (10).	St. Dev.	St. Error
NA20	16.35	0.03	0.01	16.29	0.30	0.09	17.09	0.33	0.11	15.56	0.22	0.07	15.65	0.16	0.05	14.10	0.24	0.08
SIO2	36.50	0.94	0.30	36.82	0.76	0.24	38.08	0.45	0.14	40.13	1.17	0.37	41.99	0.46	0.14	44.17	1.31	0.42
K2O	3.51	0.10	0.03	3.76	0.06	0.02	3.72	0.15	0.05	3.58	0.10	0.03	3.52	0.10	0.03	2.99	0.05	0.02
FEO	2.71	0.10	0.03	2.90	0.05	0.02	3.31	0.55	0.17	4.33	0.34	0.11	4.50	0.18	0.06	2.12	0.08	0.02
MGO	0.92	0.03	0.01	0.93	0.06	0.02	0.94	0.02	0.01	0.88	0.05	0.01	0.87	0.05	0.02	0.64	0.03	0.01
AL2O3	11.64	0.39	0.12	12.08	0.28	0.09	12.19	0.22	0.07	13.33	0.35	0.11	13.34	0.14	0.04	15.18	0.66	0.21
CAO	14.92	0.37	0.12	14.72	0.32	0.10	14.92	0.28	0.09	12.17	0.49	0.15	11.68	0.20	0.06	9.23	0.21	0.07
MNO	0.29	0.03	0.01	0.28	0.03	0.01	0.30	0.04	0.01	0.29	0.04	0.01	0.28	0.05	0.01	0.20	0.03	0.01
P2O5	0.60	0.08	0.02	0.55	0.06	0.02	0.53	0.05	0.01	0.38	0.05	0.02	0.35	0.05	0.02	0.34	0.04	0.01
TIO2	0.91	0.03	0.01	0.85	0.04	0.01	0.95	0.06	0.02	0.89	0.04	0.01	0.94	0.04	0.01	0.69	0.04	0.01
TOTALS	88.55			89.40			92.23			91.72			93.28			89.81		
P	2.50			5.00			8.00			11.00			15.00			20.00		
T	1300.00			1300.00			1300.00			1300.00			1300.00			1300.00		

CARBONATE	(10).	St. Dev.	St. Error	(10).	St. Dev.	St. Error	(10).	St. Dev.	St. Error	(3).	St. Dev.	St. Error	(5).	St. Dev.	St. Error	(10).	St. Dev.	St. Error
NA20	22.00	1.20	0.38	24.80	1.29	0.41	24.96	1.28	0.40	22.00	0.86	0.50	24.44	1.75	0.78	19.20	0.33	0.10
SIO2	6.72	4.17	1.32	2.16	1.54	0.49	1.38	0.94	0.30	5.31	0.59	0.34	1.41	0.21	0.10	3.05	0.88	0.28
K2O	4.33	0.33	0.10	4.12	0.38	0.12	4.65	0.16	0.05	4.19	0.14	0.08	3.62	0.13	0.06	2.73	0.11	0.03
FEO	0.38	0.22	0.07	0.52	0.38	0.12	0.50	0.27	0.08	1.07	0.08	0.05	0.80	0.06	0.03	1.12	0.07	0.02
MGO	0.62	0.10	0.03	0.56	0.19	0.06	0.60	0.23	0.07	0.80	0.02	0.01	0.80	0.09	0.04	1.00	0.05	0.02
AL2O3	1.13	0.18	0.06	0.16	0.12	0.04	0.33	0.59	0.19	0.89	0.13	0.08	0.08	0.08	0.03	0.51	0.23	0.07
CAO	25.04	0.34	0.11	25.63	1.14	0.36	24.95	0.10	0.03	26.42	0.44	0.25	27.83	0.25	0.11	31.64	0.65	0.21
MNO	0.16	0.07	0.02	0.15	0.06	0.02	0.15	0.04	0.01	0.27	0.06	0.04	0.14	0.06	0.02	0.29	0.04	0.01
P2O5	1.17	0.40	0.13	1.07	0.26	0.08	1.27	0.10	0.03	1.05	0.03	0.02	1.44	0.09	0.04	1.63	0.11	0.03
TIO2	0.32	0.13	0.04	0.13	0.08	0.03	0.10	0.06	0.02	0.37	0.09	0.05	0.13	0.05	0.02	0.28	0.03	0.01
TOTALS	62.34			59.69			59.31			64.63			0.61			61.92		
P	2.50			5.00			8.00			11.00			15.00			20.00		
T	1300.00			1300.00			1300.00			1300.00			1300.00			1300.00		

KD'S	BEST	MAX	MIN	BEST	MAX	MIN	BEST	MAX	MIN	BEST	MAX	MIN	BEST	MAX	MIN	BEST	MAX	MIN
Na	0.74	0.77	0.72	0.66	0.68	0.64	0.68	0.71	0.66	0.71	0.74	0.68	0.64	0.68	0.60	0.73	0.75	0.72
Si	5.43	8.84	3.92	17.08	30.64	11.83	27.53	47.43	19.39	7.55	8.64	6.71	29.83	34.39	26.33	14.47	17.65	12.26
K	0.81	0.85	0.77	0.91	0.97	0.86	0.90	0.83	0.77	0.86	0.89	0.82	0.97	1.01	0.94	1.09	1.12	1.07
Fe	7.12	11.11	5.23	5.68	10.17	3.84	6.68	10.16	4.90	4.05	4.49	3.67	5.64	6.04	5.29	1.89	1.98	1.81
Mg	1.48	1.65	1.34	1.65	2.10	1.36	1.55	2.02	1.26	1.10	1.14	1.05	1.09	1.22	0.98	0.64	0.67	0.61
Al	10.34	11.49	9.38	77.46	142.65	53.15	36.83	327.99	17.43	14.93	17.89	12.81	160.72	911.83	88.12	29.65	41.34	23.09
Ca	0.60	0.61	0.59	0.57	0.59	0.56	0.60	0.60	0.59	0.46	0.48	0.45	0.42	0.43	0.41	0.29	0.30	0.29
Mn	1.79	2.46	1.39	1.96	2.42	1.50	1.94	2.34	1.64	1.11	1.53	0.86	1.94	2.97	1.42	0.69	0.79	0.60
P	0.51	0.65	0.41	0.51	0.61	0.44	0.42	0.45	0.39	0.37	0.40	0.33	0.24	0.27	0.21	0.21	0.23	0.19
Ti	2.88	3.90	2.28	6.37	10.43	4.58	9.68	15.59	6.99	2.39	3.24	1.90	7.16	10.35	5.47	2.61	2.71	2.34
A-SIL	87.44			88.35			91.18			90.86			92.49			89.13		
ALKS	22.71			22.69			22.82			21.07			20.72			19.18		
CAFEMICS	21.20			20.99			21.02			19.12			18.43			13.45		
SIALTI	56.08			56.31			56.17			59.82			60.84			67.37		
A-CARB	60.53			58.08			54.27			61.05			59.10			59.53		
ALKS	43.51			49.80			50.87			42.90			47.47			36.84		
CAFEMICS	43.02			45.99			45.79			46.33			49.78			56.71		
SIALTI	13.48			4.21			3.34			10.77			2.74			6.45		
DURATION	60.00			60.00			60.00			75.00			75.00			75.00		

Reproducibility of experiments: BD119 + CNC.

	G5.3	St. Dev.	St. Error	R1	St. Dev.	St. Error	R2	St. Dev.	St. Error	R3	St. Dev.	St. Error
SILICATE	(10).			(10).			(10).			(10).		
NA20	15.62	0.34	0.11	16.91	0.21	0.07	16.83	0.16	0.05	17.09	0.09	0.03
SIO2	42.61	0.66	0.21	41.64	0.29	0.09	41.64	0.69	0.22	42.13	0.23	0.07
K2O	3.66	0.18	0.06	4.31	0.06	0.02	4.40	0.17	0.05	4.29	0.05	0.02
FEO	4.26	0.80	0.25	4.30	0.13	0.04	4.72	0.33	0.10	4.35	0.47	0.15
MGO	0.91	0.04	0.01	0.90	0.04	0.01	0.94	0.03	0.01	0.92	0.03	0.01
AL2O3	14.20	0.38	0.12	13.85	0.14	0.04	13.80	0.30	0.10	13.96	0.17	0.05
CAO	10.91	0.55	0.17	11.75	0.15	0.05	11.48	0.30	0.10	11.52	0.17	0.06
MNO	0.28	0.04	0.01	0.29	0.16	0.05	0.30	0.02	0.01	0.30	0.02	0.01
P2O5	0.28	0.06	0.02	0.36	0.19	0.06	0.36	0.05	0.02	0.33	0.03	0.01
TIO2	0.99	0.05	0.02	0.96	0.02	0.01	0.97	0.02	0.00	0.97	0.02	0.01
TOTALS	93.88			95.45			95.61			96.03		
P	5.00			5.00			5.00			5.00		
T	1200			1200			1200			1200		
		St. Dev.	St. Error		St. Dev.	St. Error		St. Dev.	St. Error		St. Dev.	St. Error
CARBONATE	(10).			(10).			(10).			(10).		
NA20	25.67	0.37	0.12	25.73	0.20	0.06	25.77	0.24	0.08	25.33	0.39	0.12
SIO2	1.87	0.25	0.08	2.44	0.86	0.27	2.31	1.10	0.35	2.47	0.73	0.23
K2O	5.43	0.11	0.03	3.90	0.06	0.02	4.32	0.11	0.04	4.13	0.11	0.04
FEO	0.81	0.09	0.03	1.00	0.19	0.06	1.10	0.21	0.07	0.73	0.11	0.03
MGO	0.68	0.07	0.02	0.70	0.07	0.02	0.71	0.07	0.02	0.71	0.07	0.02
AL2O3	0.03	0.02	0.01	0.16	0.21	0.07	0.11	0.20	0.06	0.12	0.15	0.05
CAO	27.00	0.25	0.08	27.21	0.46	0.15	26.79	0.58	0.18	27.21	0.43	0.14
MNO	0.21	0.06	0.02	0.18	0.07	0.02	0.16	0.07	0.02	0.17	0.05	0.01
P2O5	1.45	0.06	0.02	1.55	0.09	0.03	1.50	0.08	0.02	1.56	0.09	0.03
TIO2	0.12	0.03	0.01	0.17	0.07	0.02	0.17	0.11	0.03	0.17	0.06	0.02
TOTALS	63.65			63.46			63.32			63.00		
P	5.00			5.00			5.00			5.00		
T	1200			1200			1200			1200		

KD'S	BEST	MAX	MIN	BEST	MAX	MIN	BEST	MAX	MIN	BEST	MAX	MIN
Na	**0.61**	0.62	0.60	**0.66**	0.66	0.65	**0.65**	0.66	0.65	**0.67**	0.68	0.67
Si	**22.84**	24.88	21.10	**17.10**	21.88	14.03	**18.02**	25.61	13.90	**17.07**	20.88	14.43
K	**0.67**	0.70	0.65	**1.11**	1.12	1.09	**1.02**	1.05	0.99	**1.04**	1.06	1.02
Fe	**5.25**	5.98	4.56	**4.28**	4.84	3.83	**4.29**	4.90	3.81	**5.93**	6.64	5.31
Mg	**1.35**	1.45	1.26	**1.28**	1.37	1.20	**1.33**	1.42	1.25	**1.29**	1.38	1.21
Al	**417.50**	697.20	297.85	**85.48**	426.61	47.50	**124.28**	1242.57	59.17	**118.31**	619.12	65.40
Ca	**0.40**	0.42	0.39	**0.43**	0.44	0.43	**0.43**	0.44	0.42	**0.42**	0.43	0.42
Mn	**1.35**	1.68	1.11	**1.61**	2.37	1.02	**1.95**	2.70	1.53	**1.80**	2.17	1.54
P	**0.19**	0.22	0.16	**0.23**	0.31	0.16	**0.24**	0.26	0.22	**0.21**	0.22	0.20
Ti	**8.57**	9.93	7.52	**5.77**	7.88	4.55	**5.76**	9.64	4.11	**5.61**	7.02	4.67

Λ-SIL	93.15	94.62	94.78	95.24
ALKS	20.70	22.42	22.40	22.45
CAFEMICS	17.26	17.91	18.09	17.63
SIALTI	62.04	59.67	59.51	59.92
Λ-CARB	61.59	61.31	61.27	60.87
ALKS	50.49	48.32	49.10	48.39
CAFEMICS	46.24	47.17	46.67	47.08
SIALTI	3.27	4.51	4.23	4.53
DURATION	60.00	60.00	60.00	60.00

A.3. Electron probe analyses of natural and synthetic carbonates for ion probe standardization.

In order to enable quantitive analysis for trace-element concentrations on the ion probe, adequate standard materials are needed that have well constrained trace-element concentrations. The following tables are an attempt to constrain trace-element concentrations in a number of carbonate materials using the electron probe. There are three tables:

Mineral chemistry of Samu carbonatite, India. (mounted crystalline intergrowth of at least 7 minerals).
Mineral chemistry of Kimsey Quarry carbonatite. (mounted whole crystal of calcite with large included apatites).
Synthetic carbonate standards. (Per-cent levels of Ba, Sr, and Pb in experimentally produced carbonate matrix).

Tables are self-explanatory.

Mineral chemistry of carbonatite C254, Samu, India.

Mineral	Sr-Calcite		Sr-Calcite		Strontianite		Strontianite		Carbocernaite(18/2/92)		Carbocernaite(22/2/92)		Carbocernaite(All)		Carbocernaite	
Analyser	KDF		F. Wall		KDF		F. Wall		KDF		KDF		KDF		F. Wall	
No. of analyses	6	Error	1	Error	5	Error	1	Error	14	Error	15	Error	29	Error	1	Error
Na2O	-	-	-	-	**0.30**	0.03	**0.30**	-	**4.23**	0.11	**4.18**	0.14	**4.20**	0.13	**4.26**	-
CaO	**41.58**	1.72	**45.44**	-	**17.05**	0.25	**19.09**	-	**14.03**	0.25	**13.79**	0.86	**13.91**	0.57	**16.36**	-
MgO	**0.55**	0.03	**0.41**	-	-	-	-	-	-	-	-	-	-	-	-	-
MnO	**2.90**	0.26	**3.15**	-	-	-	-	-	**0.13**	0.08	**0.21**	0.15	**0.17**	0.12	**0.37**	-
BaO	**0.30**	0.09	**0.93**	-	**0.87**	0.13	**0.22**	-	**0.86**	0.12	**0.90**	0.09	**0.88**	0.10	**1.26**	-
SrO	**10.47**	2.30	**9.49**	-	**44.69**	0.45	**47.76**	-	**20.56**	0.61	**19.78**	0.70	**20.16**	0.66	**21.60**	-
La2O3	**0.13**	0.08	-	-	**0.48**	0.09	**0.14**	-	**10.44**	0.32	**10.53**	0.40	**10.49**	0.36	**9.69**	-
Ce2O3	**0.27**	0.14	-	-	**1.02**	0.14	**0.24**	-	**12.20**	0.46	**12.28**	0.66	**12.24**	0.56	**11.85**	-
Nd2O3	**0.12**	0.06	-	-	**0.35**	0.06	-	-	**1.78**	0.12	**1.78**	0.15	**1.78**	0.14	**0.80**	-
Pr2O3	-	-	-	-	-	-	-	-	**0.56**	0.10	**0.55**	0.13	**0.55**	0.12	**1.87**	-
Total	**56.64**		**59.42**		**64.90**		**67.75**		**64.86**		**65.05**		**64.96**		**68.22**	

Other minerals present include:

Barite
Britholite (Apatite)
Pyrite
Magnetite

EDS spectra available

FeO* = Total iron as FeO

- = Below detection limits

Analysis by electron microprobe at Edinburgh and the British Museum (Natural History)

Mineral chemistry of Kimsey quarry carbonatite.

Standard	Calcite		Apatite	
Analyser	KDF		KDF	
No. of analyses	5	Error	3	Error
Na2O	0.03	0.01	0.10	0.01
CaO	55.58	0.46	53.98	0.10
BaO	0.09	0.06	0.02	0.02
FeO	-	-	-	-
MgO	0.05	0.03	0.03	0.02
P2O5	0.04	0.02	36.05	0.71
SrO	0.67	0.01	0.09	0.03
La2O3	-	-	0.38	0.02
Ce2O3	-	-	0.44	0.21
Nd2O3	-	-	0.10	0.06
Total	56.666		91.28	

- = Below detection limits

Analysis by electron microprobe at Edinburgh University

Synthetic carbonate standards for the Ion microprobe.

Standard	Sr-standard		Ba-standard		Pb-standard	
Analyser	KDF		KDF		KDF	
No. of analyses	10	Error	10	Error	20	Error
CaO	52.66	1.33	50.32	0.81	49.46	0.57
MgO	0.03	0.01	0.03	0.01	0.03	0.01
BaO	-	-	1.12	0.31	-	-
SrO	1.21	0.35	-	-	-	-
PbO	-	-	-	-	1.40	0.46
Total	54.75		52.38		50.86	

- = Below detection limits

Analysis by electron microprobe at Edinburgh University

APPENDIX B

ION MICROPROBE ANALYSES OF COEXISTING CARBONATE AND SILICATE LIQUIDS AND CARBONATE STANDARDS.

B.1. Trace-element concentrations in coexisting carbonate and silicate liquids in the system SiO_2-Al_2O_3-CaO-Na_2O-CO_2.

For each experiment, concentrations for both carbonate and silicate liquids are given for all elements analysed. 22-24 elements were analysed, including examples of LILE, HFSE, and REE. In some tables, two values have been quoted for Ti. The first is calculated from ^{47}Ti analysis and the second from ^{50}Ti. ^{47}Ti is thought to suffer from an interference problem, therefore the second Ti value should be used.

There are six tables:

Liquids from SM2+CNC compositions at 1200°C.
Run duration effects: SM2+CNC.
Pressure effects: SM2+CNC.
Effects of minor elements.
Reversal experiments.
Compositional effects: SM2+CNC vs. SM2+CC.

Mean values are quoted (with number of analyses in brackets), togethor with the standard deviation of the sample population, and the standard error on the mean value ($\sigma/n^{1/2}$).

SM2+CNC: Partitioning at 1200 C

	G5.7.			G7.7.		
	Mean(4)	St. Dev.	St. Error.	Mean(4)	St. Dev.	St. Error.
Mg	48	4.68	2.34	50	1.22	0.61
K	103	4.27	2.13	133	7.34	3.67
Ca	95708	1106	553.06	106670	2149	1074.59
Ti	46	0.28	0.14	50	1.45	0.73
V	36	0.51	0.26	47	1.06	0.53
Rb	22	0.14	0.07	30	0.93	0.46
Sr	61	0.66	0.33	72	2.39	1.20
Y	45	0.26	0.13	51	0.75	0.38
Zr	46	0.91	0.46	51	0.64	0.32
Nb	69	1.21	0.60	85	1.84	0.92
Ce	47	1.34	0.67	65	2.70	1.35
Ba	40	0.50	0.25	51	2.82	1.41
La	61	1.11	0.55	71	1.77	0.89
Ce	66	1.22	0.61	86	1.48	0.74
Nd	55	1.17	0.59	64	1.78	0.89
Sm	52	0.36	0.18	59	1.51	0.75
Tm	70	1.13	0.57	80	1.48	0.74
Lu	73	1.54	0.77	84	1.45	0.72
Hf	146	4.70	2.35	176	3.86	1.93
Ta	114	2.29	1.15	144	2.29	1.15
Pb	6.68	1.43	0.71	12	1.33	0.66
Th	55	6.89	3.44	66	0.15	0.08
U	56	1.25	0.62	72	2.27	1.13

Carbonate	Mean(12)	St. Dev.	St. Error.	Mean(11)	St. Dev.	St. Error.
Mg	106	31	8.95	85	15	4.67
Si	26911	11487	3316.00	22218	5782	1743.41
K	569	48	13.82	588	29	8.70
Ti	32	12	3.45	25	4.17	1.26
V	111	17	4.94	72	8.13	2.45
Rb	143	6.65	1.92	154	8.59	2.59
Sr	259	6.82	1.97	289	15	4.52
Y	25	7.05	2.03	29	4.18	1.26
Zr	6.07	4.89	1.41	5.76	4.10	1.23
Nb	104	21	6.03	81	5.52	1.66
Ce	363	30	8.69	375	30	9.01
Ba	205	17	5.02	241	33	9.81
La	101	18	5.28	124	7.79	2.35
Ce	103	19	5.49	133	7.76	2.34
Nd	57	11	3.14	72	4.50	1.36
Sm	49	6.95	2.01	62	5.82	1.75
Tm	32	10	2.83	40	6.90	2.08
Lu	28	10	2.87	35	7.50	2.26
Hf	10	8.06	2.33	9.45	8.68	2.62
Ta	60	23	6.67	43	10	2.95
Pb	11	3.29	0.95	13	1.77	0.53
Th	7.88	4.40	1.27	7.62	3.16	0.95
U	26	1[illegible]	2.96	24	4.78	1.44

Run duration effects: SM2+CNC.

	G8.11.			G10.11			G25.6			G24.6.	
Mean(4)	St. Dev.	St. Error.	Mean (6)	St. Dev.	St. Error.	Mean (5)	St. Dev.	St. Error.	Mean (6)	St. Dev.	St. Error.
53	2.06	1.03	47	1.79	0.73	50	2.16	0.96	48	1.08	0.44
			179032			175440			174902		
126	2.40	1.20	171	16	6.34	163	6.06	2.71	166	7.01	2.86
102357	725	363	144184	2084	851	182871	2724	1218	145839	1138	465
50	0.97	0.48	32	1.81	0.74	34	1.28	0.57	34	1.45	0.59
		0.00	290	13.55	5.53	311	14	6.34	293	7.18	2.93
45	1.52	0.76	56	2.18	0.89	66	2.96	1.32	59	0.76	0.31
28	0.54	0.27	31	1.93	0.79	36	1.65	0.74	33	1.24	0.51
69	0.73	0.37	100	2.31	0.94	117	4.53	2.02	103	1.49	0.61
49	1.07	0.53	71	1.02	0.42	74	1.81	0.81	72	1.86	0.76
50	0.74	0.37	65	1.96	0.80	64	1.47	0.66	68	2.50	1.02
85	1.88	0.94	120	4.20	1.71	124	5.39	2.41	122	3.99	1.63
61	1.42	0.71	74	4.77	1.95	89	7.37	3.30	81	4.81	1.96
47	0.99	0.49	63	2.90	1.18	73	4.29	1.92	65	1.45	0.59
68	1.77	0.88	100	3.46	1.41	106	4.20	1.88	100	2.65	1.04
75	1.41	0.70	109	3.50	1.43	117	4.77	2.14	110	3.37	1.38
61	0.69	0.35	70	0.80	0.33	72	3.70	1.65	75	3.99	1.63
57	1.21	0.60	59	3.65	1.49	64	2.96	1.32	64	2.15	0.88
78	1.54	0.77	163	5.94	2.43	166	7.57	3.38	163	5.23	2.14
83	1.31	0.65	185	7.17	2.93	186	9.29	4.16	185	7.16	2.92
172	4.03	2.02	200	10.21	4.17	192	11	5.08	204	11	4.34
141	2.46	1.23	151	9.79	4.00	142	12	5.50	151	8.51	3.47
14	1.02	0.51	10	2.29	0.93	13	5.63	2.52	25	3.08	1.26
52	9.80	4.90	82	3.95	1.61	71	4.96	2.22	73	2.00	0.81
71	0.84	0.42	81	7.24	2.95	80	6.65	3.07	84	5.58	2.28

Mean(8)	St.Dev.	St. Error.	Mean (12)	St. Dev.	St. Error.	Mean (12)	St. Dev.	St. Error.	Mean (12)	St. Dev.	St. Error.
202	74	26.09	63	10	2.94	63	10	2.94	69	7.58	2.19
25845	10920	3861	42574	10344	2986	42574	10344	2986	42377	7502	2166
662	71	25.13	471	101	29.30	471	101	29.30	393	12	3.55
			210864			210864	0	0.00	260000	0	0.00
71	31	10.96	15.48	3.44	0.99	15.48	3.44	0.99	14	1.69	0.49
		0.00	35.27	14	4.01	35.27	14	4.01	42	13	3.71
113	15	5.28	96	6.88	1.99	96	6.88	1.99	132	2.97	0.86
147	12	4.12	96	1.80	0.52	86	1.80	0.52	104	3.01	0.87
266	7.62	2.69	208	3.37	0.97	208	3.37	0.97	256	1.78	0.51
35	8.37	2.96	40	6.29	1.81	40	6.29	1.81	37	5.49	1.58
5	1.92	0.68	8.50	4.41	1.27	8.50	4.41	1.27	7.27	3.04	0.88
106	19	6.80	118	13	3.80	118	13	3.80	111	7.80	2.25
387	22	7.65	290	11	3.20	290	11	3.20	339	7.13	2.06
241	10	3.58	181	8.75	2.53	181	8.75	2.53	215	14	4.08
148	21	7.52	136	5.84	1.68	136	5.84	1.68	138	8.51	2.46
149	21	7.33	139	8.80	2.54	139	8.80	2.54	139	10.27	2.97
84	12	4.21	62	3.84	1.11	62	3.84	1.11	51	5.53	1.60
72	9.71	3.43	45	3.63	1.05	45	3.63	1.05	49	5.12	1.48
45	11	3.79	71	15	4.23	71	15	4.23	64	12	3.37
38	10	3.61	70	18	5.14	70	18	5.14	52	12	3.37
7	3.78	1.34	17	8.60	2.48	17	8.60	2.48	14	6.38	1.84
56	19	6.57	56	16	4.52	56	16	4.52	46	8.30	2.40
23	4.81	1.70	12	4.63	1.34	12	4.63	1.34	19	14	3.92
7	3.14	1.11	14	5.67	1.64	14	5.67	1.64	9.42	2.78	0.80
30	8.52	3.01	32	6.94	2.00	32	6.94	2.00	33	6.34	1.83

Pressure effects: SM2+CNC.

	G10.11			S42			S43		
	Mean (6)	St. Dev.	St. Error.	Mean (6)	St. Dev.	St. Error.	Mean (2)	St. Dev.	St. Error.
Mg	47	1.79	0.73	52	2.31	0.94	56	0.65	0.46
Si	179022	0.00	0.00	182000	0	0.00	182243	0	0.00
K	171	16	6.34	140	1.53	0.62	145	2.40	1.70
Ca	144184	2084	851	140537	1443	589	147258	950	672
Ti	32	1.81	0.74	33	0.77	0.31	35	0.96	0.68
Tl	290	13.55	5.53	268	7.81	3.19	280	14.09	9.92
V	56	2.18	0.89	43	1.38	0.56	48	0.49	0.35
Rb	31	1.93	0.79	29	0.33	0.13	28	0.60	0.43
Sr	100	2.31	0.94	95	1.15	0.47	103	1.75	1.24
Y	71	1.02	0.42	69	1.47	0.60	73	1.64	1.16
Zr	65	1.96	0.80	61	1.64	0.67	67	0.52	0.37
Nb	120	4.20	1.71	112	1.82	0.74	120	2.59	1.83
Cs	74	4.77	1.95	66	3.00	1.22	71	3.05	2.16
Ba	63	2.90	1.18	57	2.86	1.17	55	5.18	3.66
La	100	3.46	1.41	94	2.97	1.21	107	0.36	0.25
Ce	109	3.50	1.43	103	3.73	1.52	111	1.31	0.93
Nd	70	0.80	0.33	67	2.38	0.97	71	0.39	0.28
Sm	59	3.65	1.49	57	1.59	0.65	61	1.06	0.77
Tm	163	5.94	2.43	151	4.85	1.98	164	4.48	3.16
Lu	185	7.17	2.93	174	4.75	1.94	190	7.89	5.58
Hf	200	10.21	4.17	188	2.43	0.99	205	11	7.54
Ta	151	9.79	4.00	142	3.32	1.36	149	3.65	2.58
Pb	10	2.29	0.93	15	6.16	2.51	13	6.17	4.36
Th	82	3.95	1.61	83	1.82	0.74	125	5.66	4.00
U	81	7	2.95	74	4.37	1.78	84	3.96	2.80

Carbonate	Mean (12)	St. Dev.	St. Error.	Mean (3)	St. Dev.	St. Error.	Mean (3)	St. Dev.	St. Error.
Mg	63	10	2.94	62	8	4.62	80	10.90	6.29
Si	42574	10344	2986.19	29648	822	474.48	28975	2189	1263.90
K	471	101	29.30	355	7	3.76	354	10	5.73
Ca	210864	0	0.00	221657	0	0.00	224464	0	0.00
Ti	15.48	3.44	0.99	11.19	0.76	0.44	11	2.11	1.22
Tl	35.27	14	4.01	20.08	2	1.19	27	1	0.60
V	96	6.88	1.99	44	1.35	0.78	36	1.75	1.01
Rb	96	1.80	0.52	93	3.06	1.76	96	3.86	2.23
Sr	208	3.37	0.97	216	2.56	1.48	223	1.60	0.92
Y	40	6.29	1.81	25	0.82	0.48	25	1.18	0.68
Zr	8.50	4.41	1.27	3.88	0.34	0.20	5.38	0.39	0.22
Nb	118	13	3.80	69	2	1.35	55	2.36	1.36
Cs	290	11	3.20	286	3	1.83	304	12.87	7.43
Ba	181	8.75	2.53	171	5.56	3.21	172	2	1.15
La	136	5.84	1.68	104	3.95	2.28	100	5.69	3.29
Ce	139	8.80	2.54	102	3.06	1.76	101	4.06	2.35
Nd	62	3.84	1.11	46	2.82	1.63	45	2.43	1.41
Sm	45	3.63	1.05	35	2.54	1.47	35	0.57	0.33
Tm	71	15	4.23	44	4	2.33	47	1	0.83
Lu	70	18	5.14	40	2	1.00	46	1	0.58
Hf	17	8.60	2.48	8	1.88	1.08	11	1.98	1.14
Ta	56	16	4.52	26	2	1.04	31	1.73	1.00
Pb	12	4.63	1.34	6	4.74	2.74	15	3	1.52
Th	14	5.67	1.64	7	0.41	0.24	5.04	0.67	0.38
U	32	6.94	2.00	16	1.08	0.62	18	0.92	0.53

Effects of minor elements.

	G291			G292			G293			G294			G295		
	Mean (6)	St. Dev.	St. Error.	Mean (6)	St. Dev.	St. Error.	Mean (6)	St. Dev.	St. Error.	Mean (6)	St. Dev.	St. Error.	Mean (6)	St. Dev.	St. Error.
Mg	49	0.68	0.28	55	2.86	1.17	53	1.31	0.54	45	1.90	0.77	44	1.46	0.59
Si	172950	0.00	0.00	193100			187270			187320			181440		
K	146	2.97	1.21	106	1.90	0.78	139	1.94	0.79	148	2.06	0.84	170	19	7.79
Ca	166083	2607	1064	162206	1510	617	140758	1189	485	134331	3014	1230	124832	1215	496
Ti	69	2	0.84	38	3.35	1.37	35	0.71	0.29	65	1.30	0.53	155	6.80	2.78
Tl	269	2	0.72	237	10	3.95	286	11	4.62	274	10	4.14	274	8.10	3.31
V	54	1	0.34	56	3.08	1.26	56	0.83	0.34	54	1.18	0.48	52	0.35	0.14
Rb	34	2	0.69	20	1.46	0.59	29	1.27	0.52	31	1.71	0.70	32	0.50	0.20
Sr	126	2	0.95	97	1.97	0.80	97	1.87	0.76	92	2.95	1.20	89	1.23	0.50
Y	69	1	0.48	77	1.08	0.44	75	1.38	0.56	70	1.06	0.43	63	1.22	0.50
Zr	64	3	1.25	73	1.51	0.62	71	1.93	0.79	66	1.68	0.68	62	1.41	0.58
Nb	116	3	1.21	128	3.51	1.43	125	2.17	0.88	118	2.27	0.93	109	0.92	0.38
Cs	82	5	2.03	44	3.50	1.43	68	3.46	1.41	74	4.08	1.67	72	3.30	1.35
Ba	65	2	0.73	56	1.99	0.81	61	1.20	0.49	57	1.66	0.68	58	1.91	0.78
La	101	2	0.88	108	2.66	1.09	103	1.89	0.77	92	1.96	0.80	82	1.38	0.57
Ce	105	3	1.20	120	2.18	0.89	115	2.72	1.11	104	2.95	1.20	91	2.05	0.84
Nd	70	2	0.65	86	4.16	1.70	76	4.09	1.67	66	2.97	1.21	61	2.88	1.18
Sm	57	3	1.22	69	3.86	1.58	66	0.87	0.36	57	2.39	0.98	50	2.19	0.89
Tm	154	4	1.77	181	13	5.20	172	5.64	2.30	156	4.83	1.97	140	3.72	1.52
Lu	175	5	2.15	204	6.84	2.79	198	6.46	2.64	179	6.07	2.48	162	5.54	2.26
Hf	192	12	4.71	235	12	4.97	230	13	5.32	210	12	5.10	197	8.84	3.61
Ta	146	8	3.39	168	11	4.66	167	5.98	2.44	152	8.63	3.53	142	4.39	1.79
Pb	14	5	1.93	17	6.11	2.50	28	7.75	3.16	17	0.86	0.35	20	6.39	2.61
Th	77	2	0.87	73	3.28	1.34	85	2.97	1.21	85	3.13	1.28	57	2.04	0.83
U	74	5	1.94	90	6.25	2.55	85	5.63	2.30	78	4.64	1.89	75	2.98	1.22

	Mean (6)	St. Dev.	St. Error.	Mean (12)	St. Dev.	St. Error.	Mean (12)	St. Dev.	St. Error.	Mean (9)	St. Dev.	St. Error.	Mean (9)	St. Dev.	
Mg	46	7.60	3.10	35	21	6.06	43	14	4.14	58	7.24	2.41	84	16	6.02
Si	36881	11285	4607	10230	8524	2461	19071	11369	3282	33835	7339	2446	53203	9891	3297
K	204	58	24	496	110	32	329	16	4.60	285	10	3.35	230	49	16
Ca	189405	43008	17558	202357			218776			239214			260000		
Ti	47	13	5.30	8.74	4.74	1.37	8.85	3.21	0.93	121	17	5.54	685	135	45
Tl	39	14	5.64	14	11	3.06	24	13	3.76	33	12	3.84	51	12	4.15
V	64	11	4.56	68	30	8.66	89	16	4.74	84	4.22	1.41	88	16	5.23
Rb	55	13	5.51	152	44	13	98	4.95	1.43	74	2.41	0.80	45	12	3.98
Sr	178	34	13.82	190	3.25	0.94	215	2.44	0.71	225	4.04	1.35	210	17	5.59
Y	29	8.22	3.36	13	9.06	2.62	22	10	2.89	32	5.59	1.86	53	5.45	1.82
Zr	9.02	3.74	1.53	1.79	1.36	0.39	4.13	1.36	0.39	7.95	1.36	0.45	13	3.14	1.05
Nb	74	18	7.32	59	36	11	65	22	6.39	90	7.50	2.50	121	29	10
Cs	172	42	17	462	142	41	320	8.09	2.33	237	16	5.24	117	35	12
Ba	112	19	7.86	152	41	12	173	17	4.97	168	18	5.93	141	38	13
La	82	4.31	1.76	60	23	6.58	94	23	6.71	109	17	5.77	157	20	6.52
Ce	82	4.69	1.91	59	26	7.40	94	26	7.59	114	14	4.51	177	19	6.32
Nd	38	3.58	1.46	28	12	3.54	42	11	3.04	53	5.99	2.00	80	4.67	1.56
Sm	33	7.84	3.20	21	9.36	2.70	31	8.96	2.59	40	5.73	1.91	60	5.26	1.75
Tm	53	15	6.24	23	19	5.62	40	22	6.29	59	15	4.86	101	12	3.95
Lu	53	16	6.73	22	21	5.93	39	24	6.92	58	17	5.70	99	15	4.96
Hf	22	9.37	3.83	4.20	3.21	0.93	10	3.21	0.93	19	3.21	1.07	30	7.08	2.36
Ta	47	14	5.77	25	12	3.46	27	12	3.46	42	12	4.00	78	18	5.87
Pb	7.49	5.80	2.37	7.43	2.84	0.82	15	6.94	2.00	6.48	5.12	1.71	13	6.80	2.27
Th	12	4.74	1.93	2.62	1.97	0.57	6.01	1.97	0.57	12	1.97	0.66	17	3.11	1.04
U	22	8.16	3.33	17	13	3.76	21	11	3.29	28	6.49	2.16	48	12	4.12

Reversal experiment (contains different concentrations).

	G10.11			REV3		
	Mean (6)	St. Dev.	St. Error.	Mean (6)	St. Dev.	St. Error.
Mg	47	1.79	0.73	55	1.39	0.57
Sl	179032	0.00	0.00	233200	0	0.00
K	171	16	6.34	50	3.12	1.28
Ca	144184	2084.20	851	40703	976	399
Tl	32	1.81	0.74	21	0.69	0.28
Tl	290	13.55	5.53	306	7.97	3.26
V	56	2.18	0.89	29	1.02	0.41
Rb	31	1.93	0.79	15	0.58	0.24
Sr	100	2.31	0.94	19	0.77	0.31
Y	71	1.02	0.42	16	0.52	0.21
Zr	65	1.96	0.80	30	0.90	0.37
Nb	120	4.20	1.71	19	0.45	0.18
Ce	74	4.77	1.95	6	0.85	0.35
Ba	63	2.90	1.18	10	0.22	0.09
La	100	3.46	1.41	10	0.53	0.22
Ce	109	3.50	1.43	12	0.21	0.09
Nd	70	0.80	0.33	9	0.49	0.20
Sm	59	3.65	1.49	10	0.91	0.37
Tm	163	5.94	2.43	20	0.75	0.31
Lu	185	7.17	2.93	0	0.02	0.01
Hf	200	10.21	4.17	15	1.28	0.52
Ta	151	9.79	4.00	14	1.06	0.43
Pb	10	2.29	0.93	4	3.77	1.54
Th	82	3.95	1.61	6	0.39	0.16
U	81	7	2.95	14	0.83	0.34

Carbonate	Mean (12)	St. Dev.	St. Error	Mean (12)	St. Dev.	St. Error.
Mg	63	10	4.15	67	18	7.17
Sl	42574	10344	4223	24205	25071	10235
K	471	101	41.43	82	21	8.75
Ca	210864	0	0.00	185557	0	0.00
Tl	15.48	3.44	1.40	12.54	10.81	4.41
Tl	35.27	14	5.68	15.80	14	5.56
V	96	6.88	2.81	42	18.00	7.35
Rb	86	1.80	0.73	33	16.19	6.61
Sr	208	3.37	1.37	137	1.70	0.69
Y	40	6.29	2.57	8	1.66	0.68
Zr	8.50	4.41	1.80	2.02	1.36	0.56
Nb	116	13	5.37	35	15	6.12
Ce	290	11	4.59	17	13	5.50
Ba	181	8.75	3.57	50	3.94	1.61
La	136	5.84	2.38	28	5.75	2.35
Ce	139	8.80	3.59	28	4.37	1.78
Nd	62	3.84	1.57	16	2.84	1.16
Sm	45	3.63	1.48	18	1.95	0.80
Tm	71	15	5.98	10	3	1.32
Lu	70	18	7.27	0	0	0.00
Hf	17	8.60	3.51	1	1.00	0.41
Ta	56	16	6.39	9	6	2.45
Pb	12	4.63	1.89	7	4.77	1.95
Th	14	5.67	2.32	1	1.97	0.80
U	32	6.94	2.83	12	9.00	3.67

Compositional effects: SM2+CNC and SM2+CC.

	G8.11			G8.12		
	Mean(4)	St. Dev.	St. Error.	**Mean (4)**	St. Dev.	St. Error.
Mg	**53**	2.06	1.03	**85**	1.25	0.63
K	**126**	2.40	1.20	**125**	5	2.36
Ca	**102357**	725	363	**145256**	5876	2938
Tl	**50**	0.97	0.48	**45**	1.04	0.52
V	**46**	1.52	0.76	**42**	0.98	0.49
Rb	**28**	0.54	0.27	**31**	1.10	0.55
Sr	**69**	0.73	0.37	**84**	4.38	2.19
Y	**49**	1.07	0.53	**47**	0.39	0.20
Zr	**50**	0.74	0.37	**47**	0.83	0.42
Nb	**85**	1.88	0.94	**78**	2.88	1.44
Cs	**61**	1.42	0.71	**68**	3.07	1.54
Ba	**47**	0.99	0.49	**50**	2.80	1.40
La	**68**	1.77	0.88	**75**	2.87	1.44
Ce	**75**	1.41	0.70	**72**	2.07	1.04
Nd	**61**	0.69	0.35	**59**	2.48	1.24
Sm	**57**	1.21	0.60	**56**	1.59	0.80
Tm	**78**	1.54	0.77	**74**	0.75	0.38
Lu	**83**	1.31	0.65	**77**	1.13	0.57
Hf	**172**	4.03	2.02	**155**	2.55	1.28
Ta	**141**	2.46	1.23	**125**	3.30	1.65
Pb	**14**	1.02	0.51	**18**	2.04	1.02
Th	**62**	9.80	4.90	**44**	1.21	0.61
U	**71**	0.84	0.42	**61**	0.23	0.12

Carbonate	**Mean(8)**	St.Dev.	St. Error	**Mean(8)**	St. Dev.	St. Error.
Mg	**202**	74	26.09	**221**	50	17.63
Ca	**26846**	10920	3860.92	**48961**	15289	5405.63
K	**662**	71	25.13	**620**	344	121.58
Ti	**7**	3	1.08	**40**	12	4.21
V	**113.43**	14.93	5.28	**86.63**	18.31	6.47
Rb	**147.28**	12	4.12	**104.20**	26	9.02
Sr	**286**	7.62	2.69	**303**	6.46	2.28
Y	**35**	8.37	2.96	**44**	10.98	3.88
Zr	**5**	1.92	0.68	**16**	7.56	2.67
Nb	**106**	19.22	6.80	**108**	24.34	8.61
Cs	**387.28**	21.62	7.65	**265.40**	61.61	21.78
Ba	**241**	10	3.58	**231**	36	12.72
La	**148**	21	7.52	**140**	14	4.91
Ce	**149**	20.72	7.33	**144**	17.67	6.25
Nd	**84**	11.92	4.21	**85**	10.93	3.86
Sm	**72**	9.71	3.43	**77**	12.73	4.50
Tm	**45**	10.73	3.79	**60**	16.72	5.91
Lu	**38**	10.20	3.61	**55**	15.97	5.64
Hf	**7**	4	1.34	**31**	18	6.53
Ta	**56**	19	6.57	**72**	24	8.42
Pb	**23**	4.81	1.70	**18**	3.80	1.34
Th	**7**	3	1.11	**32**	14	4.85
U	**30**	8.52	3.01	**38**	13.19	4.66

B.2. Trace-element concentrations in carbonate and silicate melts of natural compositions.

23 trace elements were analysed in most charges, including examples of LILE, HFSE, and REE. Molybdenum was analysed as an extra element in a number of the later analyses.

There are 11 tables:

BD50+CNC: Trace-element concentrations.
BD50+CC: Trace-element concentrations.
BD119+CNC: Trace-element concentrations. Two tables.
BD119+CC: Trace-element concentrations. Two tables.
SUN189+CNC: Trace-element concentrations. Two tables.
SUN189+CC: Trace-element concentrations.
Pressure effects: BD119+CNC.
Run duration effects: BD119+CNC.
Molybdenum results: all compositions.

Mean values are quoted (with number of analyses in brackets), togethor with the standard deviation of the sample population, and the standard error on the mean value ($\sigma/n^{1/2}$).

BD50+CNC: Trace-element concentrations.

	G1.1			G2.1			G5.1			G16.1			G7.1	
Silicate	Mean(4)	St. Dev.	St. Error	Mean(4)	St. Dev.	St. Error	Mean(10)	St. Dev.	St. Error	Mean (6)	St. Dev.	St. Error	Mean(4)	St. Dev.	St. Error
Mg	4307	36	18	3951	147	73	3763	104	33	4077	110	45	3366	182	91
K	36981	1131	565	34601	1183	591	29979	433	137	29695	264	108	36131	502	251
Ca	54025	724	362	28265	528	264	34944	532	168	49699	2807	1146	27584	585	292
Ti	5021	126	63	5618	228	114	4793	54	17	4595	51	21	5086	274	137
V	76	1.56	0.78	69	2.43	1.22	63	2.49	0.79	62	1.09	0.45	70	4.05	2.02
Cr	43	1.68	0.84	46	7.19	3.59	46	3.75	1.18	30	0.96	0.39	40	2.02	1.01
Fe	8338	195	98	14053	1632	816	21707	853	270				13368	1027	514
Mn	1164	24	12	1111	28	14	1135	26	8.19	1156	57	23	967	8.13	4.06
Rb	81	2.26	1.13	74	1.86	0.93	82	1.65	0.52	58	1.90	0.78	76	1.16	0.58
Sr	1140	18	8.96	624	39	20	724	34	11	1066	69	28	593	18	9.05
Y	20	0.34	0.17	21	0.17	0.09	19	0.33	0.11	17	0.51	0.21	17	1.14	0.57
Zr	559	4.82	2.41	655	15	7.29	523	11	3.61	504	4.59	1.88	600	29	15
Nb	168	4.66	2.33	177	11	5.34	137	5.56	1.76	144	2.63	1.07	162	5	2.70
Cs	1.73	0.08	0.04	1.88	0.22	0.11	1.47	0.17	0.05	0.91	0.22	0.09	1.89	0.11	0.05
Ba	1293	18	8.93	817	58	29	842	50	16	1219	86	35	789	20	10
La	89	0.15	0.07	68	1.03	0.51	69	1.84	0.58	85	1.59	0.65	57	4.51	2.26
Ce	154	2.30	1.15	126	2.28	1.14	119	2.57	0.81	153	2.28	0.93	105	6.46	3.23
Nd	50	1.41	0.71	43	0.61	0.30	40	0.95	0.30	38	2.81	1.15	36	3.06	1.53
Sm	8.32	0.18	0.09	6.96	0.32	0.16	6.62	0.49	0.15	4.38	0.48	0.19	5.79	0.40	0.20
Hf	10	0.19	0.09	12	1.12	0.56	9.10	0.47	0.15	5.98	0.51	0.21	11	0.74	0.37
Ta	5.22	0.18	0.09	6.35	0.79	0.39	4.64	0.40	0.13	2.10	0.18	0.07	5.54	0.09	0.05
Pb	2.58	1.00	0.50	1.85	0.16	0.08	9.35	3.92	1.24	1.69	1.10	0.45	3.92	2.07	1.03
Th	21	1.88	0.94	23	1.46	0.73	18	1.04	0.33	12	0.58	0.24	22	1.07	0.53
U	4.81	0.32	0.16	5.27	0.32	0.16	3.91	0.32	0.10	2.10	0.19	0.08	5.11	0.21	0.10

Carbonate	Mean(8)	St. Dev.	St. Error	Mean (10)	St. Dev.	St. Error	Mean(17)	St.Dev.	St. Error	Mean (12)	St. Dev.	St. Error	Mean(4)	St. Dev.	St. Error
Mg	2900	372	132	3856	446	141	3845	537	162	2559	236	68	3684	68	34
Si	1346	352	124	5871	5134	1623	3259	2297	693	3596	1536	444	2301	2076	1038
K	69343	6566	2322	58218	6901	2182	47634	10146	3059	73978	3126	902	60130	1086	543
Ti	1205	283	100	2026	749	237	1677	977	295	1368	399	115	1200	260	130
V	77	11	3.75	127	29	9.06	156	86	26	320	69	20	53	7.02	3.51
Cr	12	2.68	0.95	29	10	3.07	24	12	3.51	10	1.78	0.52	17	1.92	0.96
Fe	757	80	28	3894	1184	374	5792	2700	814				3110	159	80
Mn	522	32	11	710	46	15	608	40	12	426	20	5.90	720	5.74	2.87
Rb	132	12	4.31	114	16	5.17	96	24	7.31	144	5.60	1.67	111	2.79	1.40
Sr	5112	171	61	4676	205	65	3846	201	60	4770	140	41	4820	25	12
Y	12	0.54	0.19	16	1.87	0.59	12	1.32	0.40	7.43	0.99	0.29	18	1.00	0.50
Zr	0.68	0.33	0.12	2.62	1.49	0.47	2.63	2.02	0.61	8.55	3.80	1.10	3.13	1.29	0.65
Nb	93	29	10	124	61	19	108	63	19	144	53	15	80	16	8.17
Cs	3.95	1.91	0.67	3.20	0.73	0.23	2.95	0.66	0.20	2.63	0.31	0.09	2.77	0.23	0.12
Ba	6165	416	147	5309	458	148	4056	539	163	6005	281	81	5773	156	78
La	174	9.30	3.29	245	16	5.18	169	17	5.16	135	4.79	1.38	267	5.05	2.53
Ce	257	14	5.08	368	27	8.65	252	23	6.89	189	5.38	1.55	406	7.99	3.99
Nd	76	4.86	1.72	95	7.20	2.28	64	5.76	1.74	37	1.22	0.35	110	1.05	0.53
Sm	14	1.27	0.45	16	1.89	0.60	11	1.02	0.31	4.61	0.60	0.17	17	0.29	0.14
Hf	1.28	0.07	0.02	1.87	0.28	0.09	1.85	0.46	0.14	10.07	1.46	0.42	1.68	0.27	0.14
Ta	0.53	0.16	0.06	1.00	0.84	0.27	1.07	0.43	0.13	0.30	0.13	0.04	0.67	0.27	0.14
Pb	20	7.16	2.53	5.24	2.26	0.71	20	2.98	0.90	23	7.57	2.19	51	11	5.46
Th	0.86	0.10	0.04	2.05	1.44	0.46	1.53	0.73	0.22	0.30	0.09	0.03	1.48	0.23	0.11
U	1.11	0.21	0.07	1.87	1.07	0.34	1.92	1.06	0.32	1.09	0.33	0.10	0.81	0.28	0.14

BD50+CC: Trace-element concentrations.

		G5.2	
Silicate	Mean(12)	St. Dev.	St. Error
Mg	4146	34	10
K	29854	427	123
Ca	87718	1949	563
Ti	4323	51	15
V	58	1.34	0.39
Cr	47	1.83	0.53
Fe	21259	568	164
Mn	1246	24	7.03
Rb	63	1.88	0.54
Sr	1008	17	4.78
Y	20	0.62	0.18
Zr	475	8.37	2.42
Nb	123	2.63	0.76
Cs	1.68	0.32	0.09
Ba	1043	23	6.71
La	78	2.90	0.84
Ce	129	4.34	1.25
Nd	45	2.41	0.69
Sm	7.25	0.41	0.12
Hf	8.29	0.86	0.25
Ta	3.93	0.35	0.10
Pb	9.36	6.90	1.99
Th	15	0.67	0.19
U	3.39	0.19	0.05

Carbons	Mean(15)	St. Dev.	St. Error
Mg	6061	1303	337
Si	16682	5053	1305
K	40044	2898	748
Ti	1561	367	95
V	140	22	5.70
Cr	25	5.57	1.44
Fe	7808	1607	415
Mn	768	250	65
Rb	81	6.52	1.68
Sr	3597	113	29
Y	16	2.89	0.75
Zr	24	13	3.45
Nb	106	21	5.48
Cs	2.47	0.46	0.12
Ba	3781	286	74
La	138	7.49	1.93
Ce	198	10	2.68
Nd	51	3.91	1.01
Sm	8.19	1.02	0.26
Hf	2.18	0.61	0.16
Ta	1.52	0.57	0.15
Pb	23	11	2.90
Th	2.27	0.64	0.17
U	1.88	0.38	0.10

BD119+CNC: Trace-element concentrations.

		G1.3			G2.3			G3.3			G4.3			G5.3	
Silicate	Mean(4)	St. Dev.	St. Error.	Mean(4)	St. Dev.	St. Error.	Mean	St. Dev.	St. Error.	Mean(12)	St. Dev.	St. Error.	Mean(12)	St. Dev.	St. Error.
Mg	6284	88	44	6080	256	128	6064	12	5.85	6057	67	33	5795	226	113
K	43645	1564	782	30600	325	163	32775	708	354	32881	1767	883	29449	873	436
Ca	130490	1009	504	89656	3330	1665	91435	279	139	94244	2067	1034	89588	2841	1420
Ti	5502	59	29	5532	206	103	5643	58	29	5895	190	95	5449	201	101
V	189	2.91	1.45	149	6.85	3.43	146	2.15	1.07	161	5.26	2.63	140	6.03	3.01
Cr	46	1.40	0.70	27	1.64	0.82	27	1.79	0.89	43	23.12	11.56	46	4.70	2.35
Fe	29189	828	414	39791	634	317	35830	298	149	42665	3459	1730	40960	3562	1781
Mn	2964	29	14	2935	98	49	3040	21	10	3095	76	38	2927	78	39
Rb	113	5.91	2.96	78	0.67	0.34	82	2.51	1.25	85	4.72	2.36	73	2.57	1.29
Sr	2227	57	29	1363	48	24	1406	13	6.50	1466	42	21	1348	42	21
Y	42	0.72	0.36	40	1.30	0.65	42	0.62	0.31	43	1.36	0.68	38	0.93	0.46
Zr	874	19	10	913	48	24	944	14	7.16	1007	34	17	892	29	15
Nb	294	6.90	3.45	266	11	5.64	274	5.78	2.89	310	41	20	257	7.76	3.88
Cs	2.27	0.08	0.04	1.78	0.18	0.09	1.49	0.08	0.04	1.64	0.26	0.13	1.70	0.18	0.09
Ba	1819	70	35	1031	31	16	1092	20	10	1173	48	24	1023	33	17
La	174	2.01	1.00	139	6.82	3.41	146	2.27	1.14	157	7.22	3.61	138	5.26	2.63
Ce	260	5.71	2.85	212	13	6.48	227	3.47	1.73	242	9.33	4.67	211	8.68	4.34
Nd	87	2.48	1.24	72	3.54	1.77	75	0.75	0.38	81	2.70	1.35	72	3.34	1.67
Sm	15	0.36	0.18	13	0.50	0.25	13	0.48	0.24	14	0.88	0.44	13	0.85	0.43
Hf	12	0.31	0.15	11	0.89	0.45	13	0.81	0.41	13	1.16	0.58	12	0.81	0.40
Ta	3.96	0.18	0.09	3.71	0.30	0.15	4.00	0.31	0.16	4.14	0.40	0.20	4.18	0.28	0.14
Pb	14	1.55	0.78	14	1.69	0.84	1.96	2.75	1.37	11	1.24	0.62	23	4.20	2.10
Th	15	0.72	0.36	14	1.00	0.50	15	0.87	0.43	16	1.74	0.87	14	0.77	0.38
U	7.21	0.27	0.14	6.48	0.77	0.39	6.44	0.32	0.16	7.41	0.75	0.37	6.31	0.36	0.18

Carbonate	Mean(9)	St. Dev.	St. Error.	Mean(12)	St. Dev.	St. Error.	Mean(2)	St. Dev.	St. Error.	Mean(10)	St. Dev.	St. Error.	Mean(15)	St. Dev.	St. Error.
Mg	4271	1110	370	10600	1731	500	10073	233	165	9019	1546	489	8415	842	217
Si	11978	6242	2081	20989	8005	2311	17090	398	281	19275	9059	2865	14539	3739	965
K	64094	6448	2149	50771	3760	1085	45590	2101	1485	46225	3477	1099	47104	3015	778
Ti	985	332	111	1981	555	160	1755	154	109	1834	815	258	1444	321	83
V	356	150	50	294	63	18	371	34	24	258	22	7.06	314	49	13
Cr	13	3.17	1.06	17	2.34	0.68	20	0.45	0.32	16	5.06	1.60	20	3.62	0.94
Fe	6187	2374	791	15792	3166	914	16269	2434	1721	18557	5565	1760	9644	1769	457
Mn	855	171	57	2362	448	129	2491	492	348	1968	451	143	1876	76	20
Rb	133	14	4.75	127	11	3.07	129	0.19	0.13	121	8.11	2.56	119	9.06	2.34
Sr	4469	207	69	3809	132	38	3532	90	63	3779	78	25	3915	73	19
Y	15	3.03	1.01	31	5.28	1.53	26	6.92	4.89	23	6.74	2.13	24	2.66	0.69
Zr	30	15	5.00	77	58	17	47	6.99	4.94	67	59	19	29	27	7.08
Nb	130	43	14	202	41	12	234	55	39	165	54	17	171	18	4.61
Cs	2.73	0.46	0.15	3.45	0.35	0.10	9.22	0.91	0.64	3.19	0.48	0.15	3.91	0.40	0.10
Ba	4264	637	212	3463	394	114	3508	504	356	3381	230	73	3421	183	47
La	171	22	7.38	261	59	17	281	81	57	230	25	8.06	242	13	3.38
Ce	218	25	8.22	365	78	22	379	112	79	316	42	13	323	18	4.70
Nd	58	5.80	1.93	91	17	4.94	207	56	40	72	9.91	3.13	75	3.68	0.95
Sm	10	1.09	0.36	14	2.50	0.72	33	7.86	5.56	12	2.27	0.72	13	1.22	0.32
Hf	1.49	0.75	0.25	1.89	0.51	0.15	5.09	2.25	1.59	1.83	0.63	0.20	2.78	0.47	0.12
Ta	0.63	0.39	0.13	1.24	0.35	0.10	3.89	0.91	0.64	1.18	0.54	0.17	1.55	0.34	0.09
Pb	17	4.08	1.36	36	11	3.05	60	19	14	23	4.71	1.49	38	4.49	1.16
Th	1.23	1.31	0.44	1.86	0.75	0.22	4.81	1.12	0.80	1.80	1.10	0.35	1.53	0.75	0.19
U	2.27	0.87	0.29	2.45	0.41	0.12	8.62	3.21	2.27	1.97	0.81	0.26	2.74	0.42	0.11

BD119+CNC: Trace-element concentrations.

Silicate	G6.3 Mean(12)	St. Dev.	St. Error	G7.3 Mean(4)	St. Dev.	St. Error	G8.3 Mean (6)	St. Dev.	St. Error	G10.3 Mean (6)	St. Dev.	St. Error
Mg	5874	299	86	4958	28	14	5621	92	38	5539	130	53
K	31466	902	260	29258	478	239	30036	689	281	40171	1961	800
Ca	99293	8795	2539	78735	1044	522	86582	1753	716	141128	1610	657
Ti	5229	138	40	4771	28	14	5407	106	43	5616	95	39
V	143	5.79	1.67	144	2.29	1.14	138	5.43	2.22	185	4.45	1.82
Cr	35	5.32	1.54	32	1.04	0.52	16	2.59	1.06	26	1.14	0.46
Fe	41282	3440	993	27395	416	208						
Mn	2789	167	48	2412	11	5.47	2709	80	33	3029	63	26
Rb	77	3.18	0.92	75	0.39	0.20	72	2.28	0.93	96	4.06	1.66
Sr	1490	129	37	1251	24	12	1508	42	17	2560	36	15
Y	38	1.94	0.56	34	0.35	0.18	37	0.95	0.39	42	0.37	0.15
Zr	840	19	5.42	794	18	9.02	933	33	14	919	21	8.44
Nb	245	8.27	2.39	244	3.48	1.74	305	12	5.04	317	8.61	3.52
Cs	1.66	0.19	0.06	1.42	0.07	0.04	0.91	0.05	0.02	1.41	0.28	0.12
Ba	1084	100	29	1003	18	8.79	1256	46	19	2081	59	24
La	132	12	3.51	123	1.69	0.84	152	5.45	2.22	199	8.14	3.32
Ce	197	18	5.05	190	1.46	0.73	236	9.45	3.86	299	11	4.29
Nd	66	5.85	1.69	65	2.84	1.42	58	2.32	0.95	81	4.73	1.93
Sm	12	1.26	0.36	11	0.28	0.14	7.08	0.43	0.18	10	0.52	0.21
Hf	9.43	1.14	0.33	10	0.34	0.17	7.34	0.94	0.38	8.83	0.53	0.22
Ta	3.46	0.29	0.08	3.46	0.10	0.05	2.02	0.20	0.08	1.84	0.15	0.06
Pb	18	5.01	1.45	6.18	1.52	0.76	17	4.67	1.91	18	1.40	0.57
Th	11	1.99	0.57	13	0.48	0.24	9.27	0.87	0.35	10	0.53	0.22
U	5.35	0.50	0.14	5.90	0.20	0.10	3.58	0.27	0.11	4.03	0.35	0.14

Carbonate	Mean(17)	St. Dev.	St. Error	Mean(12)	St. Dev.	St. Error	Mean (12)	St. Dev.	St. Error	Mean (12)	St. Dev.	St. Error
Mg	9479	1744	423	16360	2890	834	8265	2791	806	7046	3112	898
Si	36133	19789	4800	43771	5000	1443	24188	16066	4638	10360	3652	1054
K	68373	11284	2737	60671	4149	1198	55418	7955	2296	68479	3488	1007
Ti	2149	579	140	3522	395	114	2153	1212	350	1857	593	171
V	416	92	22	379	76	22	268	49	14	323	145	42
Cr	24	4.82	1.17	33	5.09	1.47	7.88	4.16	1.20	12	7.60	2.19
Fe	16341	2985	724	25092	4837	1396						
Mn	1751	343	83	3535	546	158	1814	687	198	1328	565	163
Rb	176	37	8.91	158	10	2.86	143	27	7.92	145	12	3.42
Sr	3808	285	69	3853	133	38	4430	33	9.49	4452	135	39
Y	19	4.70	1.14	39	4.80	1.38	20	8.36	2.41	19	5.96	1.72
Zr	17	3.07	0.75	162	16	4.75	44	34	10	28	12	3.37
Nb	246	50	12	298	40	11	229	109	31	224	78	22
Cs	5.22	1.18	0.29	3.97	0.41	0.12	2.56	0.41	0.12	2.04	0.54	0.16
Ba	3496	717	174	3949	440	127	3975	241	70	4466	276	80
La	163	44	11	370	52	15	211	36	10	244	75	22
Ce	217	54	13	526	73	21	304	63	18	321	101	29
Nd	56	13	3.11	119	14	4.14	50	12	3.39	63	13	3.88
Sm	11	2.72	0.66	18	2.12	0.61	6.95	1.05	0.30	7.85	1.55	0.45
Hf	3.11	1.17	0.28	3.02	0.32	0.09	6.97	0.84	0.24	6.36	1.01	0.29
Ta	2.18	0.56	0.14	1.94	0.12	0.04	0.74	0.42	0.12	0.68	0.30	0.09
Pb	66	25	6.10	21	5.23	1.51	41	19	5.38	35	17	4.92
Th	2.59	1.19	0.29	3.97	0.30	0.09	1.27	0.86	0.25	1.24	0.54	0.15
U	3.84	1.26	0.31	4.13	0.73	0.21	1.64	0.68	0.20	2.33	0.78	0.23

BD119+CC:Trace-element concentrations.

		G3.4			G4.4			G5.4			G7.4	
Silicate	Mean(4)	St. Dev.	St. Error	Mean(4)	St. Dev.	St. Error	Mean(16)	St. Dev.	St. Error	Mean(4)	St. Dev.	St. Error
Mg	6137	77	39	5958	117	58	5984	100	26	5600	132	66
K	34337	634	317	32974	2032	1016	30986	844	218	38456	2411	1206
Ca	152009	1215	607	125672	1965	982	137870	2879	743	132459	1442	721
Ti	17530	24294	12147	5529	127	64	5213	106	27	5505	91	45
V	161	1.40	0.70	156	5.45	2.73	141	4.36	1.13	167	5.05	2.53
Cr	34	1.16	0.58	27	0.63	0.31	28	3.88	1.00	36	0.74	0.37
Fe	43005	297	149	43614	1445	723	56126	5837	1507	29297	930	465
Mn	3058	17	8.32	2927	42	21	2998	194	50	2823	34	17
Rb	90	1.81	0.91	85	6.24	3.12	79	2.76	0.71	98	5.27	2.64
Sr	1773	16	7.89	1405	36	18	1520	34	8.65	1580	26	13
Y	41	0.30	0.15	40	1.01	0.51	40	0.85	0.22	39	1.12	0.56
Zr	925	8.66	4.33	961	22	11	874	22	5.68	948	27	13
Nb	270	3.65	1.82	282	12	5.86	255	8.87	2.29	291	12	6.21
Cs	2.03	0.14	0.07	1.81	0.13	0.07	2.35	0.51	0.13	2.07	0.14	0.07
Ba	1406	16	7.83	1090	41	21	1124	43	11	1266	50	25
La	166	2.51	1.26	141	4.36	2.18	143	4.69	1.21	146	3.09	1.54
Ce	248	2.47	1.24	219	8.34	4.17	213	8.17	2.11	222	7.01	3.50
Nd	93	1.57	0.78	73	1.57	0.78	73	8.63	2.23	74	1.16	0.58
Sm	14	0.75	0.38	13	0.39	0.19	14	1.69	0.42	13	0.58	0.29
Hf	12	0.34	0.17	12	0.31	0.16	12	1.52	0.39	13	0.74	0.37
Ta	3.81	0.11	0.05	3.93	0.28	0.14	4.00	0.65	0.17	4.11	0.54	0.27
Pb	14	3.22	1.61	17	1.80	0.90	56	22	5.73	11	0.97	0.48
Th	15	0.15	0.08	15	0.57	0.28	13	2.88	0.74	16	0.28	0.14
U	6.79	0.28	0.14	6.68	0.52	0.26	6.04	1.51	0.39	7.06	0.47	0.24

Carbonate	Mean(12)	St. Dev.	St. Error	Mean(11)	St. Dev.	St. Error	Mean(17)	St. Dev.	St. Error	Mean(4)	St. Dev.	St. Error
Mg	12458	3982	664	6601	1472	444	9469	1814	440	9052	401	201
Si	39305	22399	3733	22695	8519	2568	30877	8836	2143	29874	1539	769
K	59103	19911	3319	36314	2666	804	54420	4701	1140	54734	13141	6570
Ti	2866	1272	212	1710	409	123	3324	605	147	2265	162	81
V	550	166	28	200	28	8.40	383	136	33	228	12	6.10
Cr	26	11	1.75	16	5.63	1.70	18	4.40	1.07	21	1.75	0.88
Fe	21452	8922	1487	11583	2132	643	25852	4975	1207	13840	614	307
Mn	2868	995	166	1580	396	120	2201	418	101	2256	119	60
Rb	148	36	6.01	83	5.89	1.77	140	16	3.98	133	26	13
Sr	3723	145	24	3766	192	58	3658	96	23	3821	97	48
Y	28	10	1.62	23	3.04	0.92	26	4.74	1.15	29	2.40	1.20
Zr	88	84	14	90	51	15	98	30	7.30	129	6.48	3.24
Nb	326	142	24	141	29	8.69	228	45	11	193	16	7.90
Cs	3.67	1.04	0.17	2.45	0.20	0.06	4.64	0.71	0.17	3.32	0.29	0.14
Ba	4260	679	113	3074	395	119	3371	351	85	3573	106	53
La	248	63	10	226	27	8.18	208	39	10	265	22	11
Ce	349	94	16	316	41	12	287	61	15	377	32	16
Nd	79	20	3.26	78	8.79	2.65	70	15	3.59	91	7.49	3.74
Sm	12	2.94	0.49	13	1.32	0.40	13	2.12	0.52	15	0.87	0.43
Hf	2.25	0.97	0.16	1.89	0.37	0.11	3.90	1.58	0.38	2.42	0.59	0.30
Ta	1.64	0.90	0.15	0.97	0.30	0.09	2.76	0.76	0.18	1.38	0.21	0.10
Pb	33	11	1.87	15	3.13	0.95	55	30	7.38	26	4.13	2.07
Th	2.66	1.73	0.29	2.36	0.78	0.24	3.00	0.85	0.21	3.39	0.29	0.14
U	4.10	1.92	0.32	1.98	0.65	0.20	2.40	0.73	0.18	2.91	0.31	0.16

BD119+CC: Trace-element concentrations.

		G11.2			G12			G16.2	
Silicate	Mean (4)	St. Dev.	St. Error	Mean (5)	St. Dev.	St. Error	Mean (6)	St. Dev.	St. Error
Mg	5974	17	8.42	5778	169	76	6215	32	13
Si	175000			200000			171546		
K	34693	692	346	30677	302	135	35831	829	338
Ca	156800	1807	904	116910	4493	2009	171938	4084	1667
Ti	5102	48	24	5450	105	47	5124	59	24
V	148	1.45	0.73	133	8.50	3.80	152	2.35	0.96
Cr	16	0.33	0.17	16	1.34	0.60	16	0.49	0.20
Mn	2740	14	6.98	2724	94	42	2897	63	26
Rb	83	4.05	2.03	72	2.60	1.16	85	2.15	0.88
Sr	2016	34	17	1457	56	25	2198	72	29
Y	38	0.37	0.19	38	1.71	0.77	40	1.76	0.72
Zr	867	17	8.37	980	18	8.01	878	20	8.09
Nb	299	2.76	1.38	302	10	4.39	298	11	4.32
Cs	1.28	0.32	0.16	1.19	0.12	0.05	1.17	0.19	0.08
Ba	1642	29	15	1205	41	18	1787	82	33
La	170	2.55	1.27	150	7.73	3.46	183	5.55	2.27
Ce	262	4.14	2.07	238	12	5.39	275	6.91	2.82
Nd	64	0.78	0.39	58	6.27	2.80	69	3.70	1.51
Sm	8.60	0.94	0.47	7.80	0.85	0.38	8.63	0.78	0.32
Hf	6.32	0.39	0.20	8.26	0.46	0.21	6.80	1.15	0.47
Ta	1.82	0.50	0.25	2.40	0.28	0.13	1.79	0.18	0.07
Pb	12	2.12	1.06	20	5.37	2.40	19	4.60	1.88
Th	9.07	1.15	0.58	10.00	0.45	0.20	8.73	0.64	0.26
U	3.82	0.67	0.34	4.29	0.37	0.17	3.66	0.38	0.15

Carbonate	Mean (12)	St. Dev.	St. Error	Mean (12)	St. Dev.	St. Error	Mean (12)	St. Dev.	St. Error
Mg	5037	1304	376	11414	421	122	6931	2994	864
Si	34752	23808	6873	33324	1378	398	23205	8487	2450
K	46068	7769	2243	40316	893	258	63163	6933	2001
Ca	237286			257364			243171		
Ti	2192	1305	377	2450	105	30	1501	338	98
V	337	201	58	319	16	4.48	464	132	38
Cr	6.28	2.03	0.59	12	1.34	0.39	8.13	2.39	0.69
Mn	1098	196	56	2682	112	32	1316	520	150
Rb	96	31	9.04	88	4.73	1.37	160	20	5.87
Sr	3891	249	72	4187	59	17	4166	98	28
Y	12	1.89	0.55	29	1.01	0.29	12	3.46	1.00
Zr	46	34	10	69	23	6.65	46	30	8.66
Nb	238	107	31	259	13	3.65	232	45	13
Cs	1.15	0.61	0.18	1.70	0.31	0.09	2.42	0.58	0.17
Ba	2793	510	147	4098	150	43	4031	648	187
La	145	26	7.40	329	17	4.84	148	36	10
Ce	204	33	9.39	478	18	5.27	205	51	15
Nd	43	5.55	1.60	83	8.71	2.51	35	7.12	2.05
Sm	6.13	1.06	0.30	9.99	1.24	0.36	5.69	1.48	0.43
Hf	4.47	1.14	0.33	3.71	0.75	0.22	5.98	1.52	0.44
Ta	0.91	0.45	0.13	0.76	0.32	0.09	0.45	0.25	0.07
Pb	12	7.78	2.25	26	8.28	2.39	29	14	4.03
Th	1.55	0.68	0.20	1.60	0.32	0.09	0.77	0.29	0.08
U	1.93	0.85	0.25	2.04	0.31	0.09	1.38	0.35	0.10

SUN189+CNC: Trace-element concentrations.

		G1.5			G2.5			G3.5			G5.5			G7.5			G16.3	
Silicate	Mean(4)	St. Dev.	St. Error	Mean(4)	St. Dev.	St. Error	Mean(4)	St. Dev.	St. Error	Mean(12)	St. Dev.	St. Error	Mean(12)	St. Dev.	St. Error	Mean (6)	St. Dev.	St. Error
Mg	29816	120	60	30444	215	108	31626	306	153	29754	424	122	28529	285	82	31629	325	133
K	20254	1403	701	16522	664	332	16169	189	95	16120	943	272	17814	1415	409	19193	582	237
Ca	129646	3331	1665	116064	2544	1272	128066	850	425	119286	837	242	116987	4838	1397	136893	2030	829
Ti	12456	242	121	13110	190	95	12937	103	52	13008	160	46	12459	243	70	12891	156	64
V	211	6.76	3.38	198	5.51	2.76	192	0.61	0.30	186	4.01	1.16	208	9.15	2.64	199	2.43	0.99
Cr	66	3.12	1.56	71	2.41	1.21	81	5.46	2.73	69	4.68	1.35	61	4.52	1.30	47	6.01	2.45
Fe	53465	1229	614	77722	1935	968	58774	318	159	57337	4604	1329	58745	2841	820			
Mn	1701	19	10	1772	40	20	1826	11	5.52	1789	36	10	1678	37	11	1753	20	8.35
Rb	58	3.81	1.91	48	1.72	0.86	48	2.09	1.04	48	2.01	0.58	51	4.28	1.23	47	0.91	0.37
Sr	661	27	13	543	21	10	612	6.14	3.07	576	13	3.76	580	43	12	733	12	4.92
Y	19	0.25	0.13	19	0.42	0.21	21	0.47	0.23	20	0.43	0.12	19	0.41	0.12	18	0.29	0.12
Zr	161	2.55	1.27	174	4.05	2.03	174	3.98	1.99	176	4.49	1.29	165	4.46	1.29	143	3.67	1.50
Nb	76	3.32	1.66	73	2.58	1.29	70	1.33	0.66	72	2.48	0.72	74	4.22	1.22	76	1.89	0.77
Cs	0.80	0.10	0.05	0.60	0.09	0.04	0.77	0.11	0.06	0.88	0.10	0.03	0.70	0.08	0.02	0.32	0.11	0.05
Ba	484	23	12	377	22	11.09	428	3.33	1.66	406	19	5.61	414	43	13	556	15	5.99
La	70	2.47	1.24	64	1.67	0.84	71	1.40	0.70	67	1.98	0.57	64	3.31	0.96	78	1.75	0.72
Ce	134	5.09	2.55	124	2.87	1.43	135	1.88	0.94	131	4.53	1.31	125	7.20	2.08	168	4.61	1.88
Nd	59	1.12	0.56	56	2.69	1.34	59	0.92	0.46	58	1.89	0.55	55	3.14	0.91	83	2.13	0.87
Sm	10	0.72	0.36	10	0.35	0.17	10	0.32	0.16	11	0.68	0.20	10	0.87	0.25	6.78	0.14	0.06
Hf	4.19	0.11	0.05	5.03	0.33	0.17	4.69	0.34	0.17	5.24	0.30	0.09	4.55	0.42	0.12	3.19	0.65	0.26
Ta	4.67	0.24	0.12	4.50	0.42	0.21	4.15	0.70	0.35	5.16	0.37	0.11	4.55	0.30	0.09	2.87	0.17	0.07
Pb	3.30	0.38	0.19	3.73	1.48	0.74	5.55	1.61	0.81	10.87	3.38	0.98	5.23	2.55	0.74	4.11	3.91	1.59
Th	7.06	0.40	0.20	6.94	0.46	0.23	7.11	0.16	0.08	7.61	0.55	0.16	6.85	0.71	0.20	5.18	0.40	0.16
U	1.08	0.12	0.06	0.91	0.07	0.03	0.96	0.03	0.02	1.20	0.18	0.05	1.01	0.22	0.06	0.59	0.21	0.08

Carbonate	Mean(12)	St. Dev.	St. Error	Mean(12)	St. Dev.	St. Error	Mean(11)	St. Dev.	St. Error	Mean(3)	St. Dev.	St. Error	Mean(12)	St. Dev.	St. Error	Mean (12)	St. Dev.	St. Error
Mg	28634	12350	3565	59193	13834	3993	64108	22678	6838	40425	5907	1705	67268	10661	3078	52723	11882	3430
Si	63536	49401	14261	35847	13282	3834	40962	19933	6010	20420	4981	1438	54091	18800	5427	38538	5565	1607
K	42335	16671	4812	33661	4509	1302	34947	6836	2061	26872	3404	983	31362	3601	1039	38341	2059	594
Ti	8276	5884	1699	6093	1936	559	6963	2980	899	3918	650	188	7853	2119	612	6980	1289	372
V	524	234	67	681	122	35	572	189	57	334	128	37	430	73	21	805	171	49
Cr	22	15	4.27	52	14	3.97	65	26	7.81	36	6.66	1.92	67	15	4.41	26	8.40	2.42
Fe	20532	13541	3909	46229	14391	4154	41848	17938	5409	32618	9184	2651	47112	10683	3084			
Mn	663	243	70	1173	359	104	1090	472	142	841	30	8.72	1570	446	129	686	59	17
Rb	135	76	22	104	15	4	109	24	7.25	80	17	4.83	93	12	3.39	120	12	3.57
Sr	1227	85	24	1342	57	16	1169	52	16	1253	19	5.36	1335	114	33	1352	48	14
Y	8.39	2.34	0.68	11	2.69	0.78	8.79	3.36	1.01	8.85	0.16	0.05	14	3.71	1.07	4.44	0.21	0.06
Zr	62	40	12	19	12	3.56	24	17	5.17	11	1.84	0.53	37	20	5.81	29	4.26	1.23
Nb	91	62	18	76	23	6.69	81	32	10	50	14	4.09	69	17	4.91	96	20	5.74
Cs	2.32	1.66	0.48	1.60	0.36	0.10	1.70	0.46	0.14	1.76	0.39	0.11	1.25	0.25	0.07	1.16	0.21	0.06
Ba	948	113	33	1294	195	56	1097	236	71	1069	71	20	1088	156	45	1209	114	33
La	75	8.17	2.36	95	18	5.09	67	21	6.35	88	7.10	2.05	94	17	4.91	59	5.09	1.47
Ce	131	13	3.78	156	20	5.71	117	36	11	147	11	3.26	174	35	10	102	8.33	2.40
Nd	44	3.78	1.09	50	6.22	1.80	39	11	3.26	50	2.73	0.79	56	13	3.75	25	1.11	0.32
Sm	7.75	0.92	0.27	8.95	0.91	0.26	7.18	1.81	0.55	9.40	0.37	0.11	9.30	2.26	0.65	3.98	0.49	0.14
Hf	1.49	0.54	0.16	1.33	0.50	0.14	1.43	0.52	0.16	2.10	0.16	0.05	1.64	0.87	0.25	1.81	0.69	0.20
Ta	2.29	1.34	0.39	1.73	0.76	0.22	2.09	0.99	0.30	1.49	0.35	0.10	2.14	1.26	0.36	1.11	0.29	0.08
Pb	7.24	1.49	0.43	4.81	1.74	0.50	10	3.06	0.92	19	1.74	0.50	22	16	5	11	4.61	1.33
Th	1.91	1.37	0.39	1.44	0.59	0.17	1.37	0.67	0.20	1.30	0.19	0.05	1.81	1.23	0.36	0.68	0.19	0.06
U	0.79	0.38	0.11	0.64	0.20	0.06	0.60	0.26	0.08	0.78	0.08	0.02	0.61	0.25	0.07	0.34	0.21	0.06

SUN189+CC: Trace-element concentrations.

		G1.6			G2.6			G150	
Silicate	Mean(4)	St. Dev.	St. Error	Mean(4)	St. Dev.	St. Error	Mean (6)	St. Dev.	St. Error
Mg	33328	110	55	30579	182	91	30039	149	61
K	19251	380	190	17342	441	220	18070	510	208
Ca	207561	2422	1211	170184	2924	1462	181642	2971	1213
Ti	12537	199	100	12297	104	52	11964	110	45
V	225	5.60	2.80	200	2.00	1.00	185	3.75	1.53
Cr	81	1.52	0.76	75	1.91	0.95	45	4.03	1.64
Fe	58962	1896	948	76178	385	193			
Mn	1811	32	16	1705	34	17	1682	21	8.54
Rb	56	1.99	0.99	52	1.43	0.72	48	1.88	0.77
Sr	753	20	10	615	25	13	743	24	10
Y	20	0.39	0.19	20	0.41	0.20	18	0.24	0.10
Zr	166	4.97	2.49	165	4.00	2.00	146	4.37	1.78
Nb	72	3.39	1.69	72	1.93	0.97	70	1.88	0.77
Cs	0.79	0.11	0.05	0.60	0.10	0.05	0.47	0.05	0.02
Ba	508	23	11	431	19	10	561	20	8
La	76	2.87	1.44	69	2.77	1.39	74	2.79	1.14
Ce	144	5.40	2.70	132	4.71	2.35	150	4.71	1.92
Nd	64	3.25	1.63	59	2.83	1.42	48	0.85	0.35
Sm	11	0.58	0.29	10	0.62	0.31	6.43	0.51	0.21
Hf	4.46	0.48	0.24	4.27	0.22	0.11	2.65	0.45	0.18
Ta	4.34	0.64	0.32	4.54	0.20	0.10	2.32	0.25	0.10
Pb	4.14	1.41	0.71	2.71	0.85	0.42	2.23	1.82	0.74
Th	7.14	0.72	0.36	6.70	0.88	0.44	4.46	0.31	0.13
U	0.91	0.06	0.03	1.09	0.24	0.12	0.67	0.15	0.06

Carbonate	Mean(12)	St.Dev.	St. Error	Mean(10)	St. Dev.	St. Error	Mean (12)	St. Dev.	St. Error
Mg	25959	11401	3291	69108	14454	4571	20138	886	256
Si	29267	11409	3293	49361	11973	3786	18102	11424	3298
K	22884	9482	2737	35457	5744	1816	13308	3210	927
Ti	3781	2000	577	7297	1634	517	2611	896	259
V	365	233	67	563	87	28	246	45	13
Cr	19	10	3.01	71	16	5.18	5.00	1.48	0.43
Fe	10824	6431	1857	54496	13094	4141			
Mn	502	91	26	1333	350	111	554	25	7.33
Rb	73	34	10	107	19	5.91	24	9.38	2.71
Sr	1429	78	23	1240	46	15	1544	23	6.64
Y	6.90	0.75	0.22	11	2.12	0.67	6.03	0.35	0.10
Zr	13	5.94	1.72	29	10	3.03	8.52	4.33	1.25
Nb	40	19	5.51	74	17	5.33	30	11	3.07
Cs	1.11	0.49	0.14	1.54	0.34	0.11	0.49	0.32	0.09
Ba	1115	215	62	1196	184	58	1169	40	11
La	7.7	11	3.24	30	11	3.53	72	1.54	0.45
Ce	125	20	5.77	142	21	6.54	129	3.00	0.87
Nd	36	6.04	1.74	46	5.47	1.73	32	3.44	0.99
Sm	6.57	1.13	0.33	8.41	1.01	0.32	4.41	0.56	0.16
Hf	1.00	0.44	0.13	1.58	0.47	0.15	0.93	0.34	0.10
Ta	1.11	0.40	0.12	2.04	0.54	0.17	0.46	0.33	0.10
Pb	9.06	1.92	0.55	5.98	1.64	0.52	20	12	3.60
Th	1.01	0.41	0.12	1.70	0.51	0.16	0.39	0.24	0.07
U	0.41	0.18	0.05	0.57	0.15	0.05	0.30	0.16	0.05

Pressure effects: BD119+CNC.

		G1.3			G10.3			S39			S40			S41	
Silicate	Mean(4)	St. Dev.	St. Error	Mean (6)	St. Dev.	St. Error	Mean (6)	St. Dev.	St. Error	Mean (6)	St. Dev.	St. Error	Mean (6)	St. Dev.	St. Error
Mg	6284	88	44	6539	130	53	5851	56	23	5907	52	21	3846	54	22
K	43645	1564	782	40171	1961	800	30223	304	124	32235	403	165	23774	140	57
Ca	130490	1009	504	141128	1610	657	90647	394	161	91588	608	248	61221	1115	455
Ti	5502	59	29	5616	95	39	5597	16	6.36	5437	34	14	3841	22	8.92
V	189	2.91	1.45	185	4.45	1.82	151	1.17	0.48	146	1.43	0.58	152	1.47	0.60
Cr	46	1.40	0.70	26	1.14	0.46	19	1.14	0.47	17	0.78	0.32	36	1.70	0.69
Fe	29189	828	414												
Mn	2964	29	14	3028	63	26	2732	66	27	2725	52	21	1617	45	18
Rb	113	5.91	2.96	96	4.06	1.66	72	2.01	0.82	79	1.93	0.79	51	0.41	0.17
Sr	2227	57	29	2560	36	15	1517	12	4.87	1510	21	8.70	1052	27	11
Y	42	0.72	0.36	42	0.37	0.15	38	0.06	0.03	38	0.52	0.21	21	0.43	0.18
Zr	874	19	10	919	21	8.44	957	4.60	1.88	952	21	8.40	862	11	4.62
Nb	294	6.90	3.45	317	8.61	3.52	316	4.62	1.88	310	5.13	2.09	228	3.08	1.26
Cs	2.27	0.08	0.04	1.41	0.28	0.12	0.84	0.07	0.03	0.94	0.08	0.03	0.63	0.14	0.06
Ba	1819	70	35	2081	59	24	1257	6.73	2.75	1209	24	9.86	895	20	8.31
La	174	2.01	1.00	199	8.14	3.32	157	2.24	0.91	149	3.24	1.32	84	1.00	0.41
Ce	260	5.71	2.85	299	11	4.29	247	4.74	1.94	234	3.69	1.51	137	4.30	1.76
Nd	87	2.48	1.24	81	4.73	1.93	60	1.83	0.75	62	1.10	0.45	32	1.71	0.70
Sm	15	0.36	0.18	10	0.52	0.21	8.47	0.84	0.34	8.08	0.92	0.38	4.32	0.36	0.15
Hf	12	0.31	0.15	9	0.53	0.22	8.36	0.86	0.35	8.16	1.18	0.48	9.46	0.97	0.40
Ta	3.95	0.18	0.09	1.84	0.15	0.06	2.35	0.15	0.06	2.41	0.36	0.15	1.66	0.22	0.09
Pb	14	1.55	0.78	18	1.40	0.57	26	4.04	1.65	17	7.16	2.92	8.56	3.34	1.36
Th	15	0.72	0.36	10	0.53	0.22	10	0.04	0.02	10	0.21	0.09	5.93	0.51	0.21
U	7.21	0.27	0.14	4.03	0.35	0.14	3.90	0.53	0.22	3.91	0.21	0.08	2.80	0.26	0.11

Carbonate	Mean(9)	St. Dev.	St. Error	Mean (12)	St. Dev.	St. Error	Mean (6)	St. Dev.	St. Error	Mean (9)	St. Dev.	St. Error	Mean (11)	St. Dev.	St. Error
Mg	4271	1110	370	7046	3112	898	5978	912	372	9630	1206	402	6860	323	97
Si	11978	6242	2081	10360	3652	1054	61843	22808	9311	27930	12048	4016	26182	3643	1098
K	64094	6448	2149	68479	3488	1007	51685	1575	643	58596	5566	1855	35226	1690	509
Ti	985	332	111	1857	593	171	2263	623	254	2372	712	237	1793	145	44
V	386	150	50	323	145	42	172	13	5.21	245	18	5.89	142	7.35	2.22
Cr	13	3.17	1.06	12	7.60	2.19	8.74	3.06	1.25	10	1.52	0.51	20	2.53	0.76
Fe	6187	2374	791												
Mn	965	171	57	1328	565	163	1462	272	111	1978	243	81	1641	48	15
Rb	133	14	4.75	145	12	3.42	121	8.24	3.36	153	20	6.82	76	3.04	0.92
Sr	4469	207	69	4452	135	39	4337	61	25	4017	74	25	4675	86	26
Y	15	3.03	1.01	19	5.96	1.72	19	3.29	1.35	26	3.70	1.23	23	1.13	0.34
Zr	30	15	5.00	28	12	3.37	224	99	40	125	76	25	133	21	6.46
Nb	130	43	14	224	78	22	176	35	14	229	52	17	134	12	3.61
Cs	2.73	0.46	0.15	2.04	0.54	0.16	2.07	0.37	0.15	2.52	0.65	0.22	1.34	0.17	0.05
Ba	4264	637	212	4466	276	80	3555	102	42	3605	148	49	3596	121	36
La	171	22	7.38	244	75	22	230	45	18	263	8.83	2.94	282	11	3.32
Ce	218	25	8.22	321	101	29	314	35	14	377	15	4.86	396	15	4.59
Nd	58	5.80	1.93	63	13	3.88	55	7.99	3.26	70	5.90	1.97	77	3.91	1.18
Sm	10	1.09	0.36	7.85	1.55	0.45	7.42	0.76	0.31	10	0.28	0.09	10	0.90	0.27
Hf	1.49	0.75	0.25	6.36	1.01	0.29	8.11	1.19	0.48	6.08	0.77	0.26	5.86	1.37	0.41
Ta	0.63	0.39	0.13	0.68	0.30	0.09	1.23	0.45	0.19	1.07	0.45	0.15	0.69	0.17	0.05
Pb	17	4.08	1.36	35	17	4.92	20	12	4.86	25	4.75	1.58	19	10	2.97
Th	1.23	1.31	0.44	1.24	0.54	0.15	2.51	0.97	0.40	1.73	0.96	0.32	1.68	0.32	0.10
U	2.27	0.87	0.29	2.33	0.78	0.23	1.74	0.38	0.15	2.62	0.66	0.22	1.36	0.14	0.04

Run duration effects: BD119+CNC.

		G8.3			G10.3			G25.2			G24.2	
Silicate	Mean (6)	St. Dev.	St. Error.	Mean (6)	St. Dev.	St. Error.	Mean (6)	St. Dev.	St. Error.	Mean (4)	St. Dev.	St. Error.
Mg	5621	92	38	6539	130	53	5409	51	21	5440	57	23
K	30036	689	281	40171	1961	800	30737	667	272	30756	1218	497
Ca	86582	1753	716	141128	1610	657	84047	978	399	82111	1693	691
Ti	5407	106	43	5616	95	39	5311	40	16	5303	113	46
V	138	5.43	2.22	185	4.45	1.82	140	2.68	1.09	141	3.60	1.47
Cr	16	2.59	1.06	26	1.14	0.46	15	1.37	0.56	16	0.96	0.39
Fe												
Mn	2709	80	33	3028	63	26	2540	55	23	2303	69	28
Rb	72	2.28	0.93	96	4.06	1.66	73	2.89	1.18	68	2.92	1.19
Sr	1508	42	17	2560	36	15	1448	18	7.38	1395	40	16
Y	37	0.95	0.39	42	0.37	0.15	35	0.23	0.09	33	1.19	0.48
Zr	933	33	14	919	21	8.44	925	22	8.92	908	20	7.96
Nb	305	12	5.04	317	8.61	3.52	299	8.06	3.29	304	10	4.12
Ce	0.91	0.05	0.02	1.41	0.28	0.12	0.91	0.21	0.09	1.18	0.10	0.04
Ba	1256	46	19	2081	59	24	1245	24	9.92	1179	46	19
La	152	5.45	2.22	199	8	3.32	147	4.53	1.85	137	5.25	2.14
Ce	236	9.45	3.86	299	11	4.29	196	86	34.96	218	8.81	3.60
Nd	58	2.32	0.95	81	4.73	1.93	60	2.92	1.19	55	4.85	1.98
Sm	7.08	0.43	0.18	10	0.52	0.21	7.65	0.83	0.34	7.63	0.52	0.21
Hf	7.34	0.94	0.38	8.83	0.53	0.22	21	31	12.52	8.69	1.67	0.68
Ta	2.02	0.20	0.08	1.84	0.15	0.06	1.96	0.21	0.09	2.00	0.30	0.12
Pb	17	4.67	1.91	18	1.40	0.57	12	4.50	1.84	6.77	3.55	1.45
Th	9.27	0.87	0.35	10	0.53	0.22	10	0.54	0.22	9.38	0.30	0.12
U	3.58	0.27	0.11	4.03	0.35	0.14	3.99	0.40	0.16	4.41	0.47	0.19

Carbonate	Mean (12)	St. Dev.	St. Error.	Mean (12)	St. Dev.	St. Error.	Mean (12)	St. Dev.	St. Error.	Mean (12)	St. Dev.	St. Error.
Mg	9265	2791	806	7046	3114	899	16880	2333	673	11735	2765	798
Si	24188	16066	4638	10360	3652	1054	49273	10718	3094	22117	6147	1775
K	55418	7955	2296	58479	3488	1007	60129	2070	598	43478	4534	1309
Ti	2153	1212	350	1857	593	171	3721	733	212	1998	516	149
V	268	49	14	323	145	42	425	38	11	351	74	21
Cr	7.88	4.16	1.20	12	7.60	2.19	17	3.82	1.10	13	4.13	1.19
Fe												
Mn	1814	687	198	1328	577	167	3572	419	121	2481	542	157
Rb	143	27	7.92	148	12	3.42	155	12	3.40	92	12	3.45
Sr	4430	33	9.49	4452	135	39	4400	785	227	4239	79	23
Y	20	8.36	2.41	19	6.20	1.79	36	5.54	1.60	26	6.76	1.95
Zr	44	34	10	28	12	3.37	179	66	19	27	15	4.30
Nb	229	109	31	224	78	22	365	57	17	223	61	18
Cs	2.56	0.41	0.12	2.04	0.54	0.16	2.43	0.24	0.07	1.89	0.22	0.06
Ba	3975	241	70	4466	276	80	4368	185	53	3947	415	120
La	211	36	10	244	75	22	383	20	5.74	365	81	23
Ce	304	63	18	321	101	29	560	33	9.39	519	114	33
Nd	50	12	3.39	63	13	3.88	89	7.63	2.20	86	18	5.18
Sm	6.95	1.05	0.30	7.85	1.55	0.45	11	1.24	0.36	10	2.38	0.69
Hf	5.97	0.84	0.24	6.36	1.01	0.29	7.16	1.09	0.31	5.49	2.08	0.60
Ta	0.74	0.42	0.12	0.68	0.30	0.09	1.06	0.39	0.11	0.68	0.31	0.09
Pb	41	19	5.38	35	17	4.92	32	8.02	2.32	21	8.47	2.44
Th	1.27	0.86	0.25	1.24	0.54	0.16	2.82	0.95	0.27	1.27	0.55	0.16
U	1.64	0.68	0.20	2.33	0.78	0.23	3.43	0.71	0.21	2.30	0.86	0.25

B.3. Carbonate and silicate standards for the ion probe, and the trace-element geochemistry of carbonate minerals.

A similar range of trace-element concentrations was determined as were used to obtain partitioning data. Tables included here are:

Synthetic calcium carbonate standard.
Synthetic sodium carbonate standard.
Trace-element concentrations in carbocernaiite, Samu carbonatite, India.
Trace-element concentrations in calcite, Kimsey Quarry, Arkansas, USA.
Trace-element concentrations in Norman Cross calcite.
Trace-element concentrations in Derbyshire Iceland Spar.
Trace-element concentrations in Department Iceland Spar standard.
Trace-element concentrations in Striontianite.
Trace-element chemistry of Dolomite.

Tables are self-explanatory

Trace-element concentrations in calcium carbonate standard.

	Concentrations added.		Concentrations inquench	
Elements	Estimate	Error	Mean	Std. Dev.
Na	300 max		20.57	0.93
Mg	450	10	458.45	37.28
K	100	10	16.58	0.25
Ti	100	10	1.05	0.46
V	100	10	2.94	0.19
Cr	100	10	9.27	2.68
Zn	100	10	8.49	0.40
Rb	100	10	13.43	0.44
Sr	108	5	105.07	0.76
Y	100	10	22.48	0.11
Zr	100	10	0.61	0.05
Nb	100	10	0.09	0.02
Cs	100	10	1.97	0.08
Ba	72	5	59.48	0.32
La	100	10	35.41	0.64
Ce	100	10	32.28	0.02
Nd	100	10	36.26	0.72
Sm	100	10	45.26	0.09
Tm	100	10	24.03	0.80
Yb	100	10	11.24	0.28
Hf	100	10	0.14	0.00
Ta	100	10	0.17	0.09
Pb	100	10	5.43	0.71
Th	100	10	0.09	0.09
U	100	10	0.10	0.03

Trace-element concentrations in sodium carbonate standard.

	Concentrations inquench	
Elements	Mean	Std. Dev.
Mg	768.62	31.37
K	164.70	36.73
Ti	31.83	3.12
V	21.38	2.58
Cr	0	0
Zn	0.73	0.13
Rb	145.68	43.10
Sr	79.38	12.40
Y	7.11	2.21
Zr	0.57	0.32
Nb	37.30	1.65
Cs	47.45	9.89
Ba	53.13	4.25
La	6.18	3.26
Ce	5.80	2.62
Nd	6.03	1.71
Sm	7.98	0.69
Tm	3.82	0.57
Yb	1.57	0.32
Hf	0.23	0.08
Ta	5.80	0.77
Pb	2.57	2.82
Th	0	0
U	2.21	1.63

Trace-element chemistry of carbocernaiite, Samu carbonatite, India.

	Concentrations in ppm.									Mean (9)	St. Dev.
Mg	87	82	85	110	104	107	129	127	128	106	19
Si	273	29	30	175	61	118	66	28	47	92	84
K	731	770	750	588	618	603	462	480	471	608	122
Ca	99357	99357	99357	99357	99357	99357	99357	99357	99357	99357	0
Ti	0	0	0	1	0	1	0	0	0	0	0
V	0	0	0	0	0	0	0	0	0	0	0
Cr	1	1	1	1	1	1	1	1	1	1	0
Mn	1556	1562	1559	1784	1766	1775	1962	1951	1956	1763	172
Rb	5	5	5	3	4	4	3	4	4	4	1
Sr	162600	165992	164140	156087	158064	157086	162621	163349	162975	161435	3460
Y	270	262	266	188	187	188	195	188	192	215	38
Zr	0	0	0	0	0	0	0	0	0	0	0
Nb	0	0	0	0	0	0	0	0	0	0	0
Mo	15	14	15	15	15	15	15	15	15	15	0
Cs	0	0	0	0	0	0	0	0	0	0	0
Ba	10229	10634	10429	9829	10146	9988	9229	9376	9300	9907	510
La	67074	67751	67413	68730	69483	69106	63084	63272	63197	66568	2654
Ce	69248	70056	69652	74140	74858	74499	70325	70505	70415	71522	2274
Nd	13909	14063	13986	14980	15008	15025	15086	15208	15147	14712	551
Sm	496	511	503	492	510	501	588	592	590	532	44
Hf	283	267	275	7	5	6	5	5	5	95	135
Ta	4	3	4	3	3	3	3	2	3	3	1
Pb	87	107	97	93	71	82	111	99	105	95	13
Th	1	1	1	1	1	1	1	1	1	1	0
U	0	0	0	0	0	0	0	0	0	0	0

Trace-element chemistry of calcite, Kimsey Quarry carbonatite, Arkansa

	Concentrations in ppm.						Mean (6)	St. Dev.
Mg	201	190	196	197	186	191	194	5.44
Si	8	5	2	13	4	9	7	3.97
K	7	2	1	5	1	3	3	2.33
Ca	397740	397740	397740	397740	397740	397740	397740	0
Ti	0	0	0	0	0	0	0	0
V	0	0	0	0	0	0	0	0
Cr	6	5	5	6	5	6	5	0.50
Mn	56	53	54	53	52	52	53	1.44
Rb	0	0	0	0	0	0	0	0
Sr	6834	6896	6865	6697	6813	6755	6810	73
Y	12	10	11	8	8	8	9	1.74
Zr	0	0	0	0	0	0	0	0
Nb	0	0	0	0	0	0	0	0
Mo	2	1	1	2	2	2	2	0.45
Cs	0	0	0	0	0	0	0	0
Ba	667	695	681	658	692	675	678	14
La	78	81	79	74	76	75	77	2.61
Ce	56	59	58	56	56	56	57	1.44
Nd	13	11	12	11	13	12	12	1.18
Sm	3	3	3	1	2	1	2	0.82
Hf	1	1	1	0	0	0	1	0.56
Ta	0	0	0	0	0	0	0	0
Pb	8	0	4	9	0	4	4	3.81
Th	0	0	0	0	0	0	0	0
U	0	0	0	0	0	0	0	0

Trace-element chemistry of Norman Cross calcite.

	Concentrations in ppm.		Mean (2)	St. Dev.
Mg	1681	1623	1652	41
Si	3	1	2	1.27
K	7	2	4	3.45
Ca	400000	400000	400000	0
Ti	0	0	0	0
V	0	0	0	0
Cr	3	3	3	0.25
Mn	1305	1286	1295	14
Rb	0	0	0	0
Sr	811	790	801	15
Y	2	2	2	0.04
Zr	0	0	0	0
Nb	0	0	0	0
Mo	22	18	20	2.79
Cs	0	0	0	0
Ba	2	3	2.57	0.33
La	2	2	1.99	0.15
Ce	2	3	2.33	0.51
Nd	1	1	1.01	0.45
Sm	0	0	0.38	0.01
Hf	0	0	0	0
Ta	0	0	0	0
Pb	0	11	5	7.71
Th	0	0	0	0
U	0	0	0	0

Trace-element chemistry of Derbyshire Iceland Spar.

	Concentrations in ppm.		Mean (2)	St. Dev.
Mg	418	401	409	12
Si	0	0	0	0.35
K	5	1	3	2.67
Ca	400000	400000	400000	0
Ti	0	0	0	0
V	1	1	1	0
Cr	1	5	3	3.07
Mn	700	702	701	1
Rb	0	0	0	0
Sr	50	47	49	2
Y	0	0	0	0
Zr	0	0	0	0
Nb	0	0	0	0
Mo	23	20	21	2.04
Cs	0	0	0	0
Ba	0	0	0	0
La	0	0	0	0
Ce	0	0	0	0
Nd	0	0	0	0
Sm	0	0	0	0
Hf	0	0	0	0
Ta	0	0	0	0
Pb	8	0	4	5.41
Th	0	0	0	0
U	0	0	0	0

Trace-element chemistry of Department Iceland Spar standard.

	Concentrations in ppm.		Mean (2)	St. Dev.
Mg	0.39	0.39	0.39	0.00
Si	2	1	1	0.36
K	5	1	3	2.27
Ca	400000	400000	400000	0
Ti	0	0	0	0
V	0	0	0	0
Cr	3.81	5.22	4.51	0.99
Mn	22	22	22	0
Rb	0	0	0	0
Sr	271	263	267	6
Y	0	0	0	0
Zr	0	0	0	0
Nb	0	0	0	0
Mo	1.32	0.80	1.06	0.37
Cs	0	0	0	0
Ba	0	0	0	0
La	0.51	0.51	0.51	0.00
Ce	0.65	0.61	0.63	0.03
Nd	0	0	0	0
Sm	0	0	0	0
Hf	0	0	0	0
Ta	0	0	0	0
Pb	0	0	0	0
Th	0	0	0	0
U	0	0	0	0

Trace-element chemistry of Strontianite.

	Concentrations in ppm.		Mean (3)	St. Dev.
Mg	4	2	3	1
Si	2	1	2	1
K	17	6	12	8
Ca	12271	12512	12391	171
Ti	0	0	0	0
V	0	0	0	0
Cr	0	1	0	0
Mn	0	0	0	0
Rb	30	22	26	6
Sr	572210	572210	572210	0
Y	1157	874	1016	200
Zr	0	0	0	0
Nb	0	0	0	0
Mo	0	0	0	0
Cs	0	0	0	0
Ba	88	91	89	2
La	1	1	1	0
Ce	1	1	1	0
Nd	17	16	16	1
Sm	0	0	0	0
Hf	4	3	4	1
Ta	0	0	0	0
Pb	1299	1208	1253	64
Th	0	0	0	0
U	0	0	0	0

Trace-element chemistry of Dolomite.

	Concentrations in ppm.		Mean (2)	St. Dev.
Mg	71248	70851	71049	281.12
Si	4	0	2	2.59
K	14	5	9	6.29
Ca	218290	218290	218290	0
Ti	432	407	420	18
V	3.89	3.66	3.77	0.16
Cr	2.40	3.15	2.77	0.53
Mn	47	47	47	0.24
Rb	0	0	0	0
Sr	330	329	329	0.84
Y	40	41	41	0.54
Zr	0	0	0	0
Nb	0	0	0	0
Mo	0.24	1.17	0.70	0.66
Cs	0	0	0	0
Ba	0	0	0	0
La	4.92	5.29	5.10	0.26
Ce	16.66	14.74	16	1.36
Nd	18	17	18	0.42
Sm	7	7	7.19	0.06
Hf	1	0	0	0
Ta	0	0	0	0
Pb	7	7	7.21	0.02
Th	0	0	0	0
U	0	0	0	0

APPENDIX C

ION MICROPROBE DATA: TRACE ELEMENT PARTITION COEFFICIENTS

C.1. Trace-element partition coefficients between coexisting carbonate and silicate liquids in the system SiO_2-Al_2O_3-CaO-Na_2O-CO_2.

$^{Ls/Lc}D_i$ values calculated from ion probe concentrations as:

$$^{Ls/Lc}D_i = \frac{\text{Concentration of element } i \text{ in the silicate melt}}{\text{Concentration of element } i \text{ in the carbonate melt}}$$

22-24 elements were analysed, including examples of LILE, HFSE, and REE. In some tables, two values have been quoted for Ti. The first is calculated from ^{47}Ti analysis and the second from ^{50}Ti. ^{47}Ti is thought to suffer from an interference problem, therefore the second Ti value should be used.

There are six tables:

SM2+CNC: Partitioning at 1200°C.
Run duration effects: SM2+CNC.
Pressure effects: SM2+CNC.
Effects of minor elements.
Reversal experiments.
Compositional effects: SM2+CNC vs. SM2+CC.

Maximum and minimum values quoted are assymetric 95% confidence limits based on standard errors of ion probe concentrations.

SM2+CNC: Partitioning at 1200C

Element	G5.7. Best	Max.	Min.	G7.7. Best	Max.	Min.
Mg	0.45	0.55	0.37	0.59	0.66	0.53
K	0.18	0.19	0.16	0.23	0.24	0.21
Ti	1.43	1.82	1.18	1.97	2.18	1.78
V	0.32	0.35	0.30	0.66	0.70	0.61
Rb	0.16	0.16	0.15	0.19	0.20	0.18
Sr	0.23	0.23	0.22	0.25	0.26	0.24
Y	1.77	2.10	1.53	1.73	1.89	1.59
Zr	7.53	13.84	5.17	8.82	15.23	6.21
Nb	0.66	0.75	0.60	1.05	1.10	1.00
Cs	0.13	0.14	0.12	0.17	0.18	0.16
Ba	0.19	0.20	0.19	0.21	0.23	0.19
La	0.60	0.67	0.54	0.57	0.60	0.55
Ce	0.64	0.72	0.58	0.65	0.67	0.62
Nd	0.96	1.07	0.86	0.89	0.93	0.85
Sm	1.05	1.14	0.97	0.95	1.01	0.90
Tm	2.20	2.66	1.87	1.99	2.22	1.81
Lu	2.62	3.29	2.17	2.40	2.75	2.13
Hf	14.67	27.06	10.05	18.60	40.73	12.05
Ta	1.90	2.43	1.56	3.33	3.84	2.93
Pb	0.61	0.80	0.46	0.95	1.09	0.83
Th	6.95	10.31	5.12	7.18	9.51	5.77
U	2.14	2.74	1.75	3.01	3.42	2.68

Pressure (GPa)	0.5	0.8
Temperature (C)	1200	1200
Duration (mins)	60	60

Duration effects: SM2+CNC

	G8.11			G10.11			G25.6			G24.6		
Elements	Best	Max.	Min.	Best	Max.	Min.	Best	Max.	Min.	Best	Max.	Min.
Mg	0.26	0.35	0.18	0.74	0.82	0.68	0.78	0.87	0.71	0.70	0.75	0.66
Si				4.21	4.88	3.70	4.12	4.78	3.62	4.13	4.59	3.75
K	0.19	0.21	0.17	0.36	0.42	0.32	0.35	0.39	0.31	0.42	0.44	0.41
Ca				0.68	0.69	0.68	0.77	0.78	0.76	0.56	0.56	0.56
Ti		1.01		2.09	2.40	1.84	2.20	2.53	1.94	2.44	2.64	2.26
Ti				8.21	10.59	6.69	8.81	11.37	7.17	6.91	8.35	5.90
V	0.41	0.45	0.37	0.59	0.62	0.56	0.69	0.73	0.65	0.45	0.46	0.44
Rb	0.19	0.20	0.18	0.37	0.38	0.35	0.42	0.43	0.40	0.32	0.33	0.31
Sr	0.24	0.25	0.24	0.48	0.49	0.47	0.56	0.58	0.54	0.40	0.41	0.40
Y	1.42	1.70	1.21	1.80	1.98	1.65	1.86	2.05	1.70	1.96	2.14	1.80
Zr	11.00	15.55	8.51	7.59	10.76	5.86	7.50	10.62	5.79	9.37	12.29	7.56
Nb	0.80	0.91	0.71	1.02	1.09	0.95	1.05	1.13	0.97	1.10	1.16	1.05
Cs	0.16	0.16	0.15	0.25	0.27	0.24	0.31	0.33	0.29	0.24	0.25	0.23
Ba	0.20	0.20	0.19	0.35	0.36	0.33	0.41	0.43	0.38	0.30	0.31	0.29
La	0.46	0.51	0.41	0.73	0.76	0.71	0.78	0.81	0.74	0.73	0.76	0.70
Ce	0.50	0.56	0.46	0.78	0.81	0.75	0.84	0.88	0.80	0.79	0.83	0.76
Nd	0.72	0.80	0.66	1.12	1.17	1.08	1.16	1.23	1.10	1.23	1.32	1.15
Sm	0.78	0.87	0.72	1.33	1.42	1.24	1.44	1.53	1.36	1.31	1.40	1.23
Tm	1.74	2.08	1.49	2.29	2.60	2.04	2.33	2.66	2.07	2.53	2.83	2.29
Lu	2.20	2.71	1.85	2.63	3.08	2.29	2.65	3.11	2.30	2.99	3.36	2.69
Hf	24.66	39.48	17.91	12.08	17.13	9.30	11.59	16.46	8.91	14.20	19.03	11.30
Ta	2.52	3.28	2.05	2.68	3.21	2.30	2.53	3.04	2.14	3.29	3.70	2.96
Pb	0.63	0.75	0.54	0.81	1.09	0.60	1.11	1.66	0.67	1.31	2.20	0.92
Th	7.90	12.15	5.57	6.03	7.93	4.86	5.28	6.97	4.23	7.75	9.32	6.63
U	2.36	2.94	1.97	2.54	2.94	2.22	2.48	2.88	2.16	2.53	2.88	2.25

Pressure (GPa)	0.8	0.8	0.8	0.8
Temperature (C)	1300	1300	1300	1300
Duration (mins)	15	60	360	960

Pressure effects: SM2+CNC

Dsil/car	G10.11			S42			S43		
Elements	Best	Max.	Min.	Best	Max.	Min.	Best	Max.	Min.
Mg	0.74	0.82	0.68	0.83	0.98	0.72	0.70	0.82	0.60
Si	4.21	4.88	3.70	6.83	7.08	6.60	6.29	6.88	5.79
K	0.36	0.42	0.32	0.40	0.40	0.39	0.41	0.43	0.39
Ca	0.68	0.69	0.68	0.63	0.64	0.63	0.66	0.66	0.65
Ti	2.09	2.40	1.84	2.93	3.18	2.71	3.28	4.22	2.68
Ti	8.21	10.59	6.69	13.33	15.11	11.91	10.36	11.23	9.53
V	0.59	0.62	0.56	0.98	1.02	0.94	1.33	1.40	1.25
Rb	0.37	0.38	0.35	0.31	0.32	0.29	0.30	0.31	0.28
Sr	0.48	0.49	0.47	0.44	0.45	0.43	0.46	0.47	0.45
Y	1.80	1.98	1.65	2.72	2.84	2.62	2.90	3.08	2.73
Zr	7.59	10.76	5.86	15.89	17.71	14.39	12.37	13.48	11.43
Nb	1.02	1.09	0.95	1.63	1.70	1.57	1.83	1.93	1.74
Cs	0.25	0.27	0.24	0.23	0.24	0.22	0.23	0.25	0.21
Ba	0.35	0.36	0.33	0.33	0.35	0.32	0.32	0.36	0.28
La	0.73	0.76	0.71	0.90	0.95	0.86	1.07	1.15	1.01
Ce	0.78	0.81	0.75	1.02	1.06	0.97	1.11	1.16	1.06
Nd	1.12	1.17	1.08	1.45	1.56	1.35	1.58	1.68	1.48
Sm	1.33	1.42	1.24	1.60	1.75	1.48	1.76	1.81	1.70
Tm	2.29	2.60	2.04	3.43	3.83	3.10	3.50	3.69	3.33
Lu	2.63	3.08	2.29	4.33	4.57	4.11	4.15	4.41	3.89
Hf	12.08	17.13	9.30	23.75	32.49	18.72	19.18	24.48	15.63
Ta	2.68	3.21	2.30	5.40	5.87	5.00	4.86	5.23	4.53
Pb	0.81	1.09	0.60	2.46	26.81	1.14	0.85	1.47	0.28
Th	6.03	7.93	4.86	12.33	13.27	11.50	20.70	23.96	18.10
U	2.54	2.94	2.22	4.68	5.13	4.28	4.69	5.11	4.29

Pressure (GPa)	0.8	1.5	1.5
Temperature (C)	1300	1300	1300
Duration (mins)	60	>5	75

Effects of minor elements: SM2+CNC.

D values.	Fluorine			Chlorine			Sulphur			Phosphorus			Phosphorus		
	G29.1			G29.2			G29.3			G29.4			G29.5		
	Best	Max.	Min.	Best	Max.	Min.	Best	Max.	Min.	Best	Max.	Min.	Best	Max.	Min.
Mg	1.06	1.22	0.93	1.58	2.41	1.17	1.21	1.49	1.02	0.78	0.86	0.72	0.52	0.68	0.45
Si	4.69	6.22	3.77	18.88	35.72	12.83	9.82	14.82	7.34	5.54	6.45	4.85	3.41	4.19	3.04
K	0.72	0.93	0.59	0.22	0.25	0.20	0.42	0.44	0.41	0.52	0.53	0.50	0.74	1.05	0.63
Ca	0.88	1.07	0.74	0.80	0.81	0.80	0.64	0.65	0.64	0.56	0.57	0.55	0.48	0.48	0.48
Ti	1.47	1.89	1.20	4.32	6.28	3.27	3.92	4.93	3.25	0.54	0.59	0.50	0.24	0.31	0.21
Ti	6.89	9.62	5.37	17.41	31.18	12.06	11.99	17.39	9.14	8.24	10.66	6.70	5.38	7.34	4.63
V	0.84	0.98	0.74	0.82	1.09	0.65	0.63	0.70	0.57	0.63	0.66	0.61	0.59	0.72	0.53
Rb	0.62	0.77	0.51	0.13	0.16	0.11	0.30	0.31	0.28	0.42	0.45	0.40	0.71	0.99	0.61
Sr	0.70	0.83	0.61	0.51	0.52	0.50	0.45	0.46	0.44	0.41	0.42	0.40	0.42	0.46	0.40
Y	2.35	3.03	1.92	6.09	10.29	4.33	3.34	4.47	2.67	2.18	2.46	1.95	1.19	1.36	1.12
Zr	7.05	10.57	5.28	40.66	71.46	28.41	17.27	21.24	14.53	8.36	9.43	7.51	4.76	6.43	4.11
Nb	1.57	1.95	1.31	2.18	3.37	1.61	1.91	2.36	1.60	1.30	1.38	1.23	0.89	1.19	0.77
Cs	0.47	0.59	0.39	0.10	0.12	0.08	0.21	0.22	0.20	0.31	0.33	0.29	0.62	0.93	0.51
Ba	0.58	0.67	0.51	0.37	0.43	0.32	0.35	0.37	0.33	0.34	0.37	0.32	0.41	0.59	0.35
La	1.24	1.30	1.19	1.80	2.30	1.48	1.10	1.28	0.96	0.84	0.94	0.76	0.49	0.57	0.46
Ce	1.27	1.34	1.21	2.03	2.69	1.63	1.22	1.45	1.05	0.91	0.98	0.84	0.51	0.59	0.48
Nd	1.84	1.99	1.71	3.06	4.06	2.44	1.82	2.14	1.59	1.25	1.36	1.15	0.77	0.86	0.73
Sm	1.72	2.12	1.44	3.30	4.42	2.62	2.14	2.56	1.84	1.42	1.57	1.29	0.83	0.95	0.78
Tm	2.90	3.77	2.35	7.72	14.55	5.23	4.34	6.30	3.30	2.63	3.14	2.26	1.39	1.61	1.28
Lu	3.28	4.37	2.63	9.21	19.40	6.03	5.24	8.18	3.85	3.08	3.82	2.58	1.64	2.00	1.49
Hf	8.81	13.47	6.52	56.04	98.87	39.01	23.47	28.95	19.67	11.21	12.73	9.97	6.66	9.14	5.73
Ta	3.14	4.16	2.51	6.76	9.32	5.27	6.21	8.32	4.95	3.58	4.42	3.00	1.83	2.44	1.59
Pb	1.90	5.09	1.07	2.28	3.24	1.54	1.87	2.68	1.33	2.68	5.55	1.76	1.61	4.66	1.06
Th	6.39	9.34	4.85	27.82	48.43	19.48	14.33	17.61	12.06	7.05	7.92	6.34	3.36	4.27	2.99
U	3.32	4.71	2.55	5.16	9.00	3.60	3.97	5.70	3.03	2.76	3.26	2.38	1.56	2.18	1.33

Pressure (GPa)	All at	0.5
Temperature (C)		1300
Duration (mins)		60

Reversal experiments.

Dsil/car	G10.11			REV3		
Element	Best	Max.	Min.	Best	Max.	Min.
Mg	0.74	0.86	0.66	0.83	1.05	0.68
Si	4.21	5.22	3.52	9.63	56.28	5.27
K	0.36	0.44	0.30	0.61	0.77	0.50
Ca	0.68	0.69	0.68	0.22	0.22	0.21
Ti	8.21	12.01	6.22	19.35	62.50	11.44
V	0.59	0.63	0.55	0.69	1.05	0.51
Rb	0.37	0.38	0.35	0.46	0.76	0.33
Sr	0.48	0.49	0.47	0.14	0.14	0.13
Y	1.80	2.07	1.60	2.00	2.39	1.72
Zr	7.59	13.00	5.36	14.97	32.54	9.72
Nb	1.02	1.12	0.93	0.55	0.85	0.41
Cs	0.25	0.27	0.24	0.36	0.98	0.22
Ba	0.35	0.36	0.33	0.16	0.17	0.15
La	0.73	0.77	0.70	0.35	0.42	0.30
Ce	0.78	0.83	0.74	0.43	0.49	0.38
Nd	1.12	1.18	1.07	0.54	0.63	0.47
Sm	1.33	1.44	1.23	0.54	0.61	0.49
Tm	2.29	2.75	1.96	1.91	2.56	1.52
Lu	2.63	3.31	2.18	-	-	-
Hf	12.08	20.68	8.51	30.35	50.51	11.63
Ta	2.68	3.47	2.18	1.61	3.69	1.03
Pb	0.81	1.21	0.57	0.63	1.63	0.18
Th	6.03	9.10	4.50	4.90	14.74	2.10
U	2.54	3.11	2.13	1.18	2.85	0.74

Pressure (GPa)	0.8	0.8
Temperature (C)	1300	1300
Duration (mins)	60	60

Compositional effects: SM2+CNC vs SM2+CC

Dsil/car	G8.11			G8.12		
Element	Best	Max.	Min.	Best	Max.	Min.
Mg	0.26	0.35	0.21	0.38	0.46	0.33
K	0.19	0.21	0.18	0.20	0.33	0.15
Ti	7.11	10.17	5.46	1.13	1.43	0.94
V	0.41	0.45	0.37	0.49	0.58	0.43
Rb	0.19	0.20	0.18	0.29	0.35	0.25
Sr	0.24	0.25	0.24	0.28	0.29	0.26
Y	1.42	1.70	1.21	1.07	1.29	0.91
Zr	11.00	15.55	8.51	2.95	4.40	2.21
Nb	0.80	0.91	0.71	0.72	0.86	0.62
Cs	0.16	0.16	0.15	0.26	0.31	0.22
Ba	0.20	0.20	0.19	0.22	0.25	0.19
La	0.46	0.51	0.41	0.54	0.58	0.50
Ce	0.50	0.56	0.46	0.50	0.55	0.46
Nd	0.72	0.80	0.66	0.70	0.77	0.63
Sm	0.78	0.87	0.72	0.72	0.82	0.65
Tm	1.74	2.08	1.49	1.24	1.53	1.04
Lu	2.20	2.71	1.85	1.40	1.75	1.16
Hf	24.66	39.48	17.91	4.96	8.42	3.52
Ta	2.52	3.28	2.05	1.73	2.25	1.41
Pb	0.63	0.75	0.54	1.03	1.25	0.86
Th	7.90	12.15	5.57	1.40	2.00	1.07
U	2.36	2.94	1.97	1.58	2.08	1.28

Pressure (GPa)	0.8	0.8
Temperature (C)	1300	1300
Duration (mins)	15	15

C.2. Trace-element partition coefficients between carbonate and silicate melts of natural compositions.

$^{Ls/Lc}D_i$ values are calculated from ion probe concentrations as:

$$^{Ls/Lc}D_i = \frac{\text{Concentration of element } i \text{ in the silicate melt}}{\text{Concentration of element } i \text{ in the carbonate melt}}$$

23 trace elements were analysed in most charges, including examples of LILE, HFSE, and REE. Molybdenum was analysed as an extra element in a number of the later analyses.

There are 11 tables:

BD50+CNC: Trace-element partitioning.
BD50+CC: Trace-element partitioning.
BD119+CNC: Trace-element partitioning. Two tables.
BD119+CC: Trace-element partitioning. Two tables.
SUN189+CNC: Trace-element partitioning. Two tables.
SUN189+CC: Trace-element partitioning.
Pressure effects: BD119+CNC.
Run duration effects: BD119+CNC.
Molybdenum results: all compositions.

Maximum and minimum values quoted are assymetric 95% confidence limits based on standard errors of ion probe concentrations.

BD50+CNC: Trace-element partitioning.

D values	G1.1			G2.1			G5.1			G16.1			G7.1		
Elements	**Best**	Max.	Min.	**Best**	Max.	Min.	**Best**	Max.	Min.	**Best**	Max.	Min.	**Best**	Max.	Min.
Mg	**1.49**	1.72	1.31	**1.02**	1.20	0.88	**0.98**	1.17	0.83	**1.59**	1.80	1.42	**0.91**	0.98	0.85
K	**0.53**	0.61	0.47	**0.59**	0.70	0.51	**0.63**	0.81	0.51	**0.40**	0.42	0.38	**0.60**	0.62	0.58
Ti	**4.17**	5.58	3.29	**2.77**	4.58	1.94	**2.86**	6.93	1.79	**3.36**	4.79	2.57	**4.24**	5.70	3.29
V	**0.99**	1.17	0.85	**0.54**	0.72	0.42	**0.40**	0.93	0.25	**0.19**	0.25	0.16	**1.33**	1.62	1.11
Cr	**3.55**	4.75	2.79	**1.58**	2.73	1.00	**1.93**	4.02	1.19	**2.90**	3.60	2.40	**2.37**	2.81	2.02
Fe	**11.01**	12.60	9.73	**3.61**	5.79	2.45	**3.75**	7.30	2.46	**-**	-	-	**4.30**	4.88	3.78
Mn	**2.23**	2.42	2.06	**1.56**	1.71	1.43	**1.87**	2.04	1.71	**2.74**	3.02	2.49	**1.34**	1.37	1.32
Rb	**0.61**	0.69	0.54	**0.65**	0.78	0.56	**0.65**	0.89	0.50	**0.41**	0.44	0.38	**0.68**	0.71	0.65
Sr	**0.22**	0.23	0.21	**0.13**	0.15	0.12	**0.19**	0.21	0.17	**0.22**	0.25	0.20	**0.12**	0.13	0.12
Y	**1.76**	1.88	1.65	**1.38**	1.59	1.22	**1.57**	1.79	1.39	**2.35**	2.79	2.02	**0.98**	1.11	0.87
Zr	**827**	1621	552	**251**	594	156	**207**	1059	113	**59**	107	40	**192**	343	129
Nb	**1.70**	2.56	1.26	**1.43**	2.96	0.90	**1.27**	3.19	0.77	**1.00**	1.62	0.72	**2.02**	2.62	1.62
Cs	**0.44**	0.89	0.28	**0.59**	0.85	0.42	**0.50**	0.72	0.36	**0.32**	0.45	0.22	**0.68**	0.79	0.59
Ba	**0.21**	0.23	0.19	**0.15**	0.18	0.13	**0.21**	0.25	0.17	**0.20**	0.23	0.18	**0.14**	0.14	0.13
La	**0.52**	0.55	0.49	**0.28**	0.30	0.26	**0.41**	0.46	0.36	**0.63**	0.66	0.59	**0.21**	0.23	0.19
Ce	**0.60**	0.64	0.56	**0.34**	0.38	0.31	**0.47**	0.53	0.42	**0.81**	0.84	0.77	**0.26**	0.28	0.24
Nd	**0.67**	0.73	0.61	**0.45**	0.50	0.42	**0.63**	0.70	0.56	**1.04**	1.15	0.93	**0.33**	0.36	0.30
Sm	**0.61**	0.68	0.54	**0.45**	0.54	0.38	**0.61**	0.72	0.51	**0.95**	1.21	0.75	**0.33**	0.36	0.30
Hf	**8.01**	8.61	7.47	**6.60**	8.48	5.21	**4.92**	6.88	3.73	**0.59**	0.75	0.47	**6.57**	8.39	5.27
Ta	**9.91**	14.90	7.29	**6.37**	45.57	3.03	**4.35**	7.91	2.83	**6.92**	13.12	4.44	**9.64**	18.63	6.43
Pb	**0.13**	0.28	0.06	**0.35**	0.68	0.23	**0.46**	0.77	0.23	**0.07**	0.18	0.02	**0.08**	0.15	0.03
Th	**24.85**	30.79	20.21	**11.45**	41.00	6.31	**11.48**	23.31	7.31	**39.35**	58.99	28.77	**14.64**	18.12	12.07
U	**4.32**	5.66	3.40	**2.82**	6.97	1.68	**2.03**	4.91	1.20	**1.94**	3.06	1.35	**6.28**	9.93	4.50

Pressure (GPa)	**0.5**			**0.5**			**0.5**			**0.25**			**0.8**		
Temperature (C)	**1300**			**1100**			**1200**			**1200**			**1200**		
Duration (mins)	**60**			**60**			**60**			**60**			**60**		

BD50+CC: Trace-element partitioning.

D values	G5.2. Best	Max.	Min.
Mg	0.68	0.77	0.62
K	0.75	0.77	0.72
Ti	2.77	3.15	2.48
V	0.41	0.45	0.38
Cr	1.90	2.15	1.70
Fe	2.72	3.04	2.46
Mn	1.62	1.94	1.39
Rb	0.78	0.82	0.75
Sr	0.28	0.29	0.28
Y	1.27	1.41	1.16
Zr	20.22	28.38	15.70
Nb	1.16	1.29	1.05
Cs	0.68	0.78	0.59
Ba	0.28	0.29	0.27
La	0.57	0.59	0.55
Ce	0.65	0.67	0.63
Nd	0.88	0.93	0.84
Sm	0.89	0.95	0.83
Hf	3.80	4.47	3.28
Ta	2.59	3.22	2.16
Pb	0.41	0.65	0.23
Th	6.83	7.99	5.96
U	1.80	2.01	1.62

Pressure (GPa)	0.5
Temperature (C)	1200
Duration (mins)	60

BD119+CNC: Trace-element partitioning.

D values	G1.3			G2.3			G3.3			G4.3			G5.3		
	Best	Max.	Min.	**Best**	Max.	Min.	**Best**	Max.	Min.	**Best**	Max.	Min.	**Best**	Max.	Min.
Mg	**1.47**	1.77	1.26	**0.57**	0.64	0.52	**0.60**	0.62	0.58	**0.67**	0.75	0.61	**0.69**	0.73	0.65
K	**0.68**	0.73	0.63	**0.60**	0.63	0.58	**0.72**	0.77	0.67	**0.71**	0.76	0.66	**0.63**	0.65	0.60
Ti	**5.59**	7.17	4.58	**2.79**	3.33	2.40	**3.22**	3.66	2.87	**3.21**	4.44	2.51	**3.77**	4.27	3.37
V	**0.49**	0.66	0.39	**0.51**	0.58	0.45	**0.39**	0.45	0.35	**0.63**	0.67	0.59	**0.45**	0.49	0.41
Cr	**3.53**	4.22	3.03	**1.61**	1.78	1.46	**1.35**	1.46	1.26	**2.65**	4.27	1.23	**2.32**	2.65	2.02
Fe	**4.72**	6.30	3.76	**2.52**	2.84	2.26	**2.26**	2.86	1.87	**2.30**	2.86	1.90	**4.25**	4.82	3.75
Mn	**3.43**	3.94	3.03	**1.24**	1.40	1.12	**1.22**	1.68	0.96	**1.57**	1.84	1.37	**1.51**	1.56	1.46
Rb	**0.85**	0.93	0.78	**0.62**	0.65	0.59	**0.63**	0.65	0.61	**0.70**	0.75	0.65	**0.61**	0.65	0.58
Sr	**0.50**	0.52	0.48	**0.36**	0.37	0.34	**0.40**	0.41	0.38	**0.39**	0.40	0.38	**0.34**	0.36	0.33
Y	**2.78**	3.21	2.45	**1.30**	1.45	1.18	**1.60**	2.53	1.17	**1.83**	2.24	1.55	**1.60**	1.70	1.50
Zr	**29**	42.79	21.81	**12**	20.66	8.26	**20**	25.58	16.76	**15**	33.17	9.75	**32**	63.17	21.27
Nb	**2.25**	2.88	1.85	**1.32**	1.50	1.17	**1.17**	1.73	0.88	**1.88**	2.43	1.49	**1.50**	1.59	1.41
Cs	**0.83**	0.94	0.74	**0.51**	0.58	0.46	**0.16**	0.19	0.14	**0.51**	0.61	0.42	**0.43**	0.49	0.39
Ba	**0.43**	0.48	0.39	**0.30**	0.32	0.28	**0.31**	0.39	0.26	**0.35**	0.37	0.33	**0.30**	0.31	0.29
La	**1.02**	1.12	0.94	**0.53**	0.62	0.47	**0.52**	0.87	0.37	**0.68**	0.74	0.63	**0.57**	0.60	0.55
Ce	**1.19**	1.29	1.10	**0.58**	0.67	0.51	**0.60**	1.01	0.43	**0.76**	0.84	0.70	**0.65**	0.69	0.62
Nd	**1.50**	1.61	1.40	**0.79**	0.89	0.71	**0.36**	0.58	0.26	**1.12**	1.23	1.03	**0.96**	1.02	0.92
Sm	**1.49**	1.62	1.39	**0.91**	1.02	0.82	**0.39**	0.58	0.29	**1.17**	1.34	1.03	**1.02**	1.10	0.94
Hf	**7.93**	11.86	5.95	**5.80**	6.95	4.92	**2.54**	6.56	1.57	**7.03**	9.07	5.66	**4.30**	4.79	3.86
Ta	**6.23**	10.39	4.44	**2.99**	3.61	2.52	**1.11**	1.73	0.81	**3.51**	4.98	2.68	**2.70**	3.09	2.38
Pb	**0.82**	1.00	0.69	**0.39**	0.48	0.32	**0.03**	0.09	-0.01	**0.49**	0.58	0.42	**0.61**	0.73	0.50
Th	**11.95**	39.42	7.03	**7.33**	9.58	5.89	**3.19**	4.74	2.40	**9.16**	14.93	6.50	**9.08**	12.12	7.22
U	**3.17**	4.23	2.53	**2.65**	3.08	2.27	**0.75**	1.55	0.49	**3.76**	5.12	2.93	**2.30**	2.53	2.09

Pressure (GPa)	**0.5**			**0.5**			**0.25**			**0.8**			**0.5**		
Temperature (C)	**1300**			**1100**			**1100**			**1100**			**1200**		
Duration (mins)	**60**			**60**			**60**			**60**			**60**		

BD119+CNC: Trace-element partitioning.

D values	G6.3			G7.3			G8.3					
	Best	Max.	Min.	Best	Max.	Min.	Best	Max.	Min.	Best	Max.	Min.
Mg	0.62	0.68	0.57	0.30	0.34	0.28	0.68	0.84	0.57	0.93	1.24	0.74
K	0.46	0.50	0.43	0.48	0.50	0.46	0.54	0.59	0.50	0.59	0.62	0.56
Ti	2.43	2.79	2.16	1.35	1.45	1.27	2.51	3.69	1.90	3.02	3.69	2.56
V	0.34	0.38	0.31	0.38	0.43	0.34	0.52	0.58	0.47	0.57	0.77	0.46
Cr	1.43	1.63	1.26	0.98	1.08	0.90	2.03	2.95	1.51	2.17	3.40	1.59
Fe	2.69	3.00	2.43	1.09	1.23	0.98	-	-	-	-	-	-
Mn	1.59	1.77	1.45	0.68	0.75	0.63	1.49	1.90	1.23	2.28	3.00	1.84
Rb	0.44	0.49	0.40	0.48	0.49	0.46	0.50	0.56	0.45	0.67	0.71	0.63
Sr	0.39	0.42	0.37	0.32	0.33	0.32	0.34	0.35	0.33	0.57	0.59	0.56
Y	2.00	2.28	1.78	0.86	0.92	0.80	1.80	2.34	1.46	2.22	2.70	1.89
Zr	48.17	52.62	44.41	4.91	5.23	4.62	21.04	36.80	14.71	33.39	43.96	26.91
Nb	0.99	1.10	0.90	0.82	0.89	0.76	1.33	1.83	1.05	1.41	1.76	1.18
Cs	0.32	0.36	0.28	0.36	0.39	0.33	0.35	0.39	0.32	0.69	0.86	0.55
Ba	0.31	0.35	0.28	0.25	0.27	0.24	0.32	0.33	0.30	0.47	0.49	0.45
La	0.81	0.94	0.71	0.33	0.36	0.31	0.72	0.80	0.65	0.82	0.99	0.69
Ce	0.91	1.04	0.80	0.36	0.39	0.33	0.78	0.88	0.69	0.93	1.13	0.79
Nd	1.18	1.34	1.06	0.55	0.59	0.51	1.14	1.32	1.01	1.28	1.47	1.13
Sm	1.17	1.35	1.03	0.62	0.66	0.58	1.02	1.13	0.93	1.29	1.46	1.15
Hf	3.03	3.73	2.53	3.41	3.65	3.19	1.05	1.19	0.93	1.39	1.54	1.26
Ta	1.59	1.82	1.40	1.79	1.87	1.71	2.74	4.07	2.04	2.70	3.63	2.14
Pb	0.27	0.35	0.21	0.30	0.39	0.22	0.42	0.60	0.30	0.51	0.71	0.39
Th	4.14	5.40	3.30	3.29	3.49	3.11	7.28	11.81	5.22	7.81	10.37	6.25
U	1.39	1.66	1.19	1.43	1.59	1.29	2.19	2.88	1.75	1.73	2.15	1.43

Pressure (GPa)	0.25	0.8	0.8	0.8
Temperature (C)	1200	1200	1300	1300
Duration (mins)	60	60	15	60

BD119+CC: Trace-element partitioning.

D values	G3.4			G4.4			G5.4			G7.4		
	Best	Max.	Min.	Best	Max.	Min.	Best	Max.	Min.	Best	Max.	Min.
Mg	0.49	0.55	0.45	0.90	1.04	0.80	0.63	0.70	0.58	0.62	0.65	0.59
K	0.58	0.65	0.52	0.91	0.98	0.84	0.57	0.60	0.55	0.70	0.92	0.56
Ti	6.12	14.69	2.20	3.23	3.77	2.83	1.57	1.72	1.44	2.43	2.62	2.27
V	0.27	0.30	0.25	0.78	0.85	0.71	0.37	0.44	0.31	0.73	0.78	0.69
Cr	1.32	1.53	1.16	1.81	2.35	1.47	1.57	1.81	1.37	1.68	1.83	1.55
Fe	2.00	2.32	1.76	3.77	4.24	3.38	2.17	2.42	1.96	2.12	2.23	2.01
Mn	1.07	1.20	0.96	1.85	2.18	1.61	1.36	1.51	1.24	1.25	1.32	1.18
Rb	0.61	0.67	0.57	1.01	1.10	0.93	0.56	0.59	0.53	0.74	0.92	0.62
Sr	0.48	0.48	0.47	0.37	0.39	0.36	0.42	0.42	0.41	0.41	0.43	0.40
Y	1.45	1.64	1.31	1.71	1.86	1.58	1.55	1.70	1.43	1.34	1.47	1.23
Zr	10.51	15.28	8.00	10.64	15.99	7.97	8.96	10.50	7.81	7.34	7.77	6.94
Nb	0.83	0.97	0.73	2.01	2.30	1.78	1.12	1.23	1.02	1.51	1.66	1.38
Cs	0.55	0.62	0.49	0.74	0.80	0.67	0.51	0.58	0.44	0.62	0.70	0.56
Ba	0.33	0.35	0.31	0.35	0.39	0.33	0.33	0.35	0.32	0.35	0.37	0.34
La	0.67	0.73	0.62	0.62	0.68	0.58	0.69	0.75	0.63	0.55	0.60	0.51
Ce	0.71	0.78	0.65	0.69	0.76	0.64	0.74	0.83	0.67	0.59	0.65	0.54
Nd	1.04	1.14	0.96	0.94	1.01	0.88	1.05	1.18	0.94	0.81	0.89	0.75
Sm	1.14	1.26	1.04	1.03	1.11	0.97	1.07	1.18	0.97	0.89	0.96	0.83
Hf	5.23	6.10	4.57	6.49	7.36	5.81	3.16	3.95	2.62	5.20	6.87	4.16
Ta	2.32	2.82	1.96	4.05	5.00	3.37	1.45	1.70	1.25	3.03	3.71	2.49
Pb	0.42	0.53	0.31	1.07	1.26	0.91	1.03	1.46	0.74	0.43	0.52	0.36
Th	5.70	7.24	4.70	6.54	8.15	5.45	4.33	5.19	3.64	4.59	5.02	4.22
U	1.66	1.96	1.43	3.38	4.25	2.78	2.52	3.06	2.08	2.42	2.75	2.14

BD119+CC: Trace-element partitioning.

	G11.2			G12			G16.2		
D values	Best	Max.	Min.	Best	Max.	Min.	Best	Max.	Min.
Mg	1.19	1.39	1.03	0.51	0.52	0.49	0.90	1.19	0.72
Si	5.04	8.22	3.63	6.00	6.15	5.86	7.39	9.32	6.13
K	0.75	0.83	0.69	0.76	0.77	0.75	0.57	0.61	0.53
Ca	0.66	0.67	0.65	0.45	0.47	0.44	0.71	0.72	0.69
Ti	2.33	3.51	1.74	2.22	2.29	2.16	3.41	3.91	3.03
V	0.44	0.66	0.33	0.42	0.44	0.39	0.33	0.39	0.28
Cr	2.49	3.05	2.11	1.33	1.47	1.21	1.91	2.29	1.63
Mn	2.52	2.80	2.29	1.02	1.06	0.98	2.20	2.84	1.80
Rb	0.86	1.06	0.72	0.81	0.85	0.78	0.57	0.62	0.53
Sr	0.52	0.54	0.50	0.35	0.36	0.34	0.53	0.54	0.51
Y	3.05	3.34	2.81	1.30	1.36	1.24	3.33	4.00	2.85
Zr	18.97	32.65	13.36	10.99	12.88	9.58	19.15	30.40	13.97
Nb	1.26	1.68	1.00	1.17	1.22	1.12	1.28	1.45	1.15
Cs	1.12	1.70	0.76	0.70	0.80	0.61	0.48	0.58	0.40
Ba	0.59	0.66	0.53	0.29	0.30	0.28	0.44	0.49	0.40
La	1.17	1.30	1.06	0.46	0.48	0.43	1.23	1.43	1.08
Ce	1.28	1.41	1.18	0.50	0.52	0.47	1.34	1.56	1.17
Nd	1.51	1.63	1.40	0.70	0.78	0.62	1.96	2.22	1.74
Sm	1.40	1.62	1.21	0.78	0.88	0.69	1.54	1.84	1.32
Hf	1.41	1.67	1.22	2.23	2.54	1.98	1.14	1.39	0.93
Ta	2.00	2.99	1.34	3.18	4.26	2.50	3.96	5.80	2.98
Pb	0.98	1.56	0.68	0.77	1.03	0.57	0.69	1.00	0.49
Th	5.87	7.97	4.53	6.24	7.08	5.56	11.41	14.64	9.30
U	1.98	2.75	1.48	2.10	2.36	1.88	2.65	3.15	2.27

SUN189+CNC: Trace-element partitioning.

D values	G1.5			G2.5			G3.5			G5.5			G7.5			G16.3		
	Best	Max.	Min.	**Best**	Max.	Min.	**Best**	Max.	Min.	**Best**	Max.	Min.	**Best**	Max.	Min.	**Best**	Max.	Min.
Mg	**1.04**	1.38	0.84	**0.51**	0.59	0.45	**0.49**	0.62	0.41	**0.74**	0.80	0.68	**0.42**	0.47	0.39	**0.60**	0.69	0.53
K	**0.48**	0.62	0.39	**0.49**	0.54	0.45	**0.46**	0.52	0.41	**0.60**	0.65	0.56	**0.57**	0.62	0.53	**0.47**	0.49	0.46
Ti	**1.51**	2.52	1.07	**2.15**	2.62	1.82	**1.86**	2.49	1.48	**3.32**	3.66	3.03	**1.59**	1.87	1.38	**1.85**	2.06	1.67
V	**0.40**	0.54	0.32	**0.29**	0.32	0.26	**0.34**	0.42	0.28	**0.55**	0.71	0.46	**0.48**	0.53	0.44	**0.25**	0.28	0.22
Cr	**3.08**	5.04	2.21	**1.36**	1.60	1.18	**1.24**	1.63	0.99	**1.93**	2.16	1.73	**0.91**	1.05	0.80	**1.79**	2.24	1.47
Fe	**2.59**	4.12	1.89	**1.68**	2.04	1.43	**1.64**	2.20	1.31	**2.68**	3.19	2.30	**1.25**	1.43	1.10	-	-	-
Mn	**2.57**	3.24	2.12	**1.51**	1.83	1.29	**1.68**	2.25	1.33	**2.13**	2.18	2.08	**1.07**	1.27	0.92	**2.56**	2.69	2.44
Rb	**0.43**	0.63	0.32	**0.46**	0.51	0.42	**0.44**	0.51	0.39	**0.60**	0.69	0.54	**0.55**	0.60	0.51	**0.39**	0.41	0.37
Sr	**0.54**	0.57	0.51	**0.40**	0.42	0.39	**0.52**	0.54	0.51	**0.46**	0.47	0.45	**0.43**	0.46	0.41	**0.54**	0.56	0.53
Y	**2.25**	2.68	1.94	**1.72**	2.00	1.51	**2.35**	3.03	1.91	**2.25**	2.29	2.21	**1.37**	1.62	1.19	**3.98**	4.10	3.86
Zr	**2.62**	4.14	1.91	**9.06**	14.24	6.64	**7.27**	12.58	5.11	**16.22**	17.96	14.78	**4.40**	6.33	3.37	**4.89**	5.34	4.51
Nb	**0.84**	1.37	0.60	**0.96**	1.16	0.81	**0.87**	1.14	0.70	**1.43**	1.70	1.23	**1.06**	1.23	0.93	**0.79**	0.90	0.71
Cs	**0.34**	0.58	0.24	**0.37**	0.45	0.31	**0.45**	0.56	0.37	**0.50**	0.57	0.43	**0.56**	0.64	0.49	**0.27**	0.36	0.19
Ba	**0.51**	0.55	0.47	**0.29**	0.32	0.26	**0.39**	0.45	0.35	**0.38**	0.40	0.36	**0.38**	0.42	0.34	**0.46**	0.49	0.43
La	**0.93**	1.00	0.87	**0.66**	0.74	0.60	**1.07**	1.31	0.90	**0.76**	0.80	0.73	**0.68**	0.76	0.61	**1.33**	1.40	1.26
Ce	**1.02**	1.10	0.96	**0.80**	0.86	0.74	**1.16**	1.42	0.98	**0.89**	0.94	0.85	**0.72**	0.81	0.64	**1.54**	1.62	1.46
Nd	**1.33**	1.41	1.27	**1.10**	1.20	1.02	**1.50**	1.79	1.29	**1.16**	1.20	1.12	**0.99**	1.15	0.87	**2.12**	2.20	2.03
Sm	**1.34**	1.47	1.22	**1.11**	1.19	1.04	**1.43**	1.69	1.24	**1.13**	1.18	1.09	**1.05**	1.23	0.92	**1.70**	1.84	1.59
Hf	**2.81**	3.55	2.33	**3.79**	4.85	3.08	**3.29**	4.23	2.67	**2.49**	2.63	2.36	**2.77**	3.98	2.12	**1.76**	2.34	1.35
Ta	**2.04**	3.05	1.52	**2.60**	3.50	2.04	**1.99**	2.85	1.46	**3.46**	4.01	3.04	**2.12**	3.18	1.59	**2.58**	3.04	2.23
Pb	**0.46**	0.54	0.39	**0.77**	1.16	0.46	**0.56**	0.78	0.39	**0.57**	0.68	0.47	**0.24**	0.45	0.15	**0.36**	0.68	0.09
Th	**3.69**	6.20	2.61	**4.81**	6.29	3.87	**5.20**	7.34	4.02	**5.87**	6.46	5.37	**3.78**	6.15	2.71	**7.66**	9.25	6.50
U	**1.37**	1.90	1.05	**1.42**	1.74	1.18	**1.60**	2.17	1.27	**1.53**	1.70	1.38	**1.96**	2.76	1.49	**1.70**	2.80	1.09

SUN189+CC: Trace-element partitioning.

D values	G1.6			G2.6			G150		
	Best	Max.	Min.	Best	Max.	Min.	Best	Max.	Min.
Mg	1.28	1.71	1.03	0.44	0.51	0.39	1.49	1.53	1.45
K	0.84	1.10	0.68	0.49	0.55	0.44	1.36	1.57	1.19
Ti	3.32	4.73	2.55	1.69	1.96	1.48	4.58	5.69	3.84
V	0.62	0.96	0.45	0.36	0.39	0.32	0.75	0.84	0.68
Cr	4.25	6.14	3.25	1.06	1.24	0.93	9.07	11.02	7.64
Fe	5.17	7.80	3.86	1.40	1.64	1.22	-	-	-
Mn	3.61	4.02	3.27	1.28	1.53	1.10	3.04	3.12	2.96
Rb	0.76	1.04	0.60	0.49	0.55	0.44	1.96	2.51	1.61
Sr	0.53	0.55	0.51	0.50	0.52	0.47	0.48	0.49	0.47
Y	2.94	3.14	2.76	1.84	2.11	1.64	2.91	3.01	2.81
Zr	13.24	18.09	10.42	5.66	7.12	4.70	17.09	24.01	13.25
Nb	1.81	2.48	1.41	0.98	1.14	0.85	2.34	2.94	1.95
Cs	0.72	0.98	0.55	0.52	0.62	0.43	0.98	1.58	0.70
Ba	0.46	0.51	0.41	0.36	0.40	0.33	0.48	0.50	0.46
La	1.01	1.11	0.92	0.86	0.94	0.78	1.03	1.06	0.99
Ce	1.15	1.28	1.05	0.93	1.03	0.85	1.17	1.20	1.13
Nd	1.75	1.96	1.58	1.29	1.41	1.18	1.48	1.58	1.40
Sm	1.68	1.88	1.51	1.23	1.35	1.12	1.46	1.61	1.33
Hf	4.45	6.02	3.47	2.70	3.32	2.27	2.84	3.69	2.24
Ta	3.91	5.10	3.07	2.22	2.68	1.90	5.08	8.62	3.56
Pb	0.51	0.71	0.34	0.45	0.63	0.30	0.11	0.22	0.04
Th	7.07	9.33	5.61	3.94	5.00	3.16	11.32	17.26	8.38
U	2.21	2.94	1.76	1.93	2.52	1.45	1.90	2.84	1.33

Pressure effects: BD119+CNC.

D values	G1.3			G10.3			S39			S40			S41		
	Best	Max.	Min.	**Best**	Max.	Min.	**Best**	Max.	Min.	**Best**	Max.	Min.	**Best**	Max.	Min.
Mg	**1.47**	1.77	1.26	**0.93**	1.24	0.74	**0.98**	1.12	0.87	**0.61**	0.67	0.57	**0.56**	0.58	0.54
K	**0.68**	0.73	0.63	**0.59**	0.62	0.56	**0.58**	0.60	0.57	**0.55**	0.59	0.52	**0.67**	0.69	0.66
Ti	**5.59**	7.17	4.58	**3.02**	3.69	2.56	**2.47**	3.17	2.03	**2.29**	2.85	1.92	**2.14**	2.25	2.04
V	**0.49**	0.66	0.39	**0.57**	0.77	0.46	**0.88**	0.94	0.83	**0.60**	0.63	0.57	**1.07**	1.10	1.03
Cr	**3.53**	4.22	3.03	**2.17**	3.40	1.59	**2.15**	3.00	1.67	**1.60**	1.77	1.45	**1.80**	1.96	1.65
Fe	**4.72**	6.30	3.76	-	-	-	-	-	-	-	-	-	-	-	-
Mn	**3.43**	3.94	3.03	**2.28**	3.00	1.84	**1.87**	2.20	1.62	**1.38**	1.50	1.27	**1.05**	1.08	1.02
Rb	**0.85**	0.93	0.78	**0.67**	0.71	0.63	**0.59**	0.63	0.56	**0.52**	0.57	0.47	**0.67**	0.69	0.66
Sr	**0.50**	0.52	0.48	**0.57**	0.59	0.56	**0.35**	0.35	0.35	**0.38**	0.38	0.37	**0.22**	0.23	0.22
Y	**2.78**	3.21	2.45	**2.22**	2.70	1.89	**2.08**	2.42	1.82	**1.46**	1.61	1.33	**0.95**	0.98	0.91
Zr	**28.91**	42.79	21.81	**33.39**	43.96	26.91	**4.27**	6.59	3.16	**7.62**	12.62	5.46	**6.49**	7.17	5.92
Nb	**2.25**	2.88	1.85	**1.41**	1.76	1.18	**1.79**	2.13	1.55	**1.35**	1.59	1.18	**1.70**	1.80	1.62
Cs	**0.83**	0.94	0.74	**0.69**	0.86	0.55	**0.41**	0.48	0.35	**0.37**	0.45	0.31	**0.47**	0.57	0.38
Ba	**0.43**	0.48	0.39	**0.47**	0.49	0.45	**0.35**	0.36	0.35	**0.34**	0.35	0.33	**0.25**	0.26	0.24
La	**1.02**	1.12	0.94	**0.82**	0.99	0.69	**0.68**	0.81	0.59	**0.57**	0.58	0.55	**0.30**	0.30	0.29
Ce	**1.19**	1.29	1.10	**0.93**	1.13	0.79	**0.79**	0.87	0.72	**0.62**	0.64	0.60	**0.35**	0.36	0.33
Nd	**1.50**	1.61	1.40	**1.28**	1.47	1.13	**1.08**	1.23	0.97	**0.88**	0.93	0.83	**0.42**	0.44	0.40
Sm	**1.49**	1.62	1.39	**1.29**	1.46	1.15	**1.14**	1.28	1.02	**0.83**	0.91	0.75	**0.44**	0.48	0.40
Hf	**7.93**	11.86	5.95	**1.39**	1.54	1.26	**1.03**	1.19	0.90	**1.34**	1.54	1.16	**1.62**	1.91	1.38
Ta	**6.23**	10.39	4.44	**2.70**	3.63	2.14	**1.91**	2.72	1.47	**2.26**	3.17	1.72	**2.40**	2.88	2.01
Pb	**0.82**	1.00	0.69	**0.51**	0.71	0.39	**1.31**	2.53	0.86	**0.69**	0.95	0.45	**0.44**	0.69	0.28
Th	**11.95**	39.42	7.03	**7.81**	10.37	6.25	**4.10**	5.93	3.13	**5.51**	8.63	4.05	**3.53**	4.05	3.11
U	**3.17**	4.23	2.53	**1.73**	2.15	1.43	**2.25**	2.79	1.85	**1.49**	1.79	1.27	**2.06**	2.27	1.87

Pressure (GPa)	**0.5**	**0.8**	**1.1**	**1.5**	**2**
Temperature (C)	**1300**	**1300**	**1300**	**1300**	**1300**
Duration (mins)	**60**	**60**	**75**	**75**	**75**

Duration effects: BD119+CNC.

D values	G8.3			G10.3			G25.2			G24.2		
	Best	Max.	Min.	Best	Max.	Min.	Best	Max.	Min.	Best	Max.	Min.
Mg	0.68	0.81	0.55	0.93	1.24	0.74	0.32	0.35	0.30	0.46	0.53	0.40
K	0.54	0.59	0.50	0.59	0.62	0.56	0.51	0.52	0.50	0.71	0.75	0.66
Ti	2.51	3.31	1.71	3.02	3.69	2.56	1.43	1.59	1.27	2.65	3.04	2.26
V	0.52	0.57	0.46	0.57	0.77	0.46	0.33	0.35	0.31	0.40	0.45	0.35
Cr	2.03	2.90	1.48	2.17	3.40	1.59	0.91	1.06	0.79	1.26	1.53	1.05
Fe	-	-	-	-	-	-	-	-	-	-	-	-
Mn	1.49	1.82	1.17	2.28	3.02	1.83	0.71	0.76	0.66	0.93	1.04	0.81
Rb	0.50	0.56	0.45	0.67	0.71	0.63	0.47	0.49	0.44	0.73	0.79	0.67
Sr	0.34	0.35	0.33	0.57	0.59	0.56	0.33	0.36	0.30	0.33	0.34	0.32
Y	1.80	2.27	1.41	2.22	2.72	1.87	0.98	1.07	0.90	1.24	1.44	1.07
Zr	21.04	30.64	12.25	33.39	43.96	26.91	5.18	6.28	4.10	34.19	46.15	23.88
Nb	1.33	1.70	0.97	1.41	1.76	1.18	0.82	0.89	0.74	1.36	1.58	1.15
Cs	0.35	0.42	0.34	0.69	0.86	0.55	0.37	0.47	0.31	0.62	0.73	0.61
Ba	0.32	0.33	0.30	0.47	0.49	0.45	0.29	0.29	0.28	0.30	0.32	0.28
La	0.72	0.79	0.65	0.82	0.99	0.69	0.38	0.40	0.37	0.38	0.42	0.33
Ce	0.78	0.87	0.68	0.93	1.13	0.79	0.35	0.47	0.23	0.42	0.47	0.37
Nd	1.14	1.30	0.99	1.28	1.47	1.13	0.67	0.71	0.63	0.64	0.73	0.55
Sm	1.02	1.15	0.94	1.29	1.46	1.15	0.71	0.80	0.64	0.76	0.89	0.67
Hf	1.05	1.21	0.94	1.39	1.54	1.26	2.90	6.48	0.53	1.58	2.16	1.27
Ta	2.74	25.86	12.96	2.70	3.63	2.14	1.85	3.72	2.35	2.93	14.22	7.98
Pb	0.42	0.57	0.29	0.51	0.71	0.39	0.37	0.50	0.25	0.32	0.49	0.18
Th	7.28	24.42	10.78	7.81	10.37	6.25	3.39	4.67	3.14	7.41	14.86	8.99
U	2.19	3.79	2.31	1.73	2.15	1.43	1.16	1.42	1.07	1.92	2.87	1.81

Pressure (GPa)	0.8	0.8	0.8	0.8
Temperature (GPa)	1300	1300	1300	1300
Duration (mins)	15	60	360	960

Partitioning behaviour of Molybdenum between carbonate and silicate liquids.

Run identity.	Composition	Pressure (GPa.)	Temperature (C)	Ls	St. Dev.	Lc	St. Dev.	Dsil/car	Max.	Min.
G16.1	BD50+CNC	0.25	1200	4.4	1.2	34	5	**0.13**	0.19	0.08
G8.3	BD119+CNC	0.8	1300	9	1.6	34	5	**0.26**	0.37	0.19
G10.3	BD119+CNC	0.8	1300	8	1	56	14	**0.14**	0.21	0.10
G24.2	BD119+CNC	0.8	1300	6.2	1.2	38	11	**0.16**	0.27	0.10
G25.2	BD119+CNC	0.8	1300	8.2	1.8	45	6	**0.18**	0.26	0.13
S39	BD119+CNC	1.5	1300	6.2	0.6	27	3	**0.23**	0.28	0.19
S40	BD119+CNC	2	1300	8.7	1	33	1.5	**0.26**	0.31	0.22
S41	BD119+CNC	1.1	1300	5.8	0.5	39	3	**0.15**	0.18	0.13
G11.2	BD119+CC	0.5	1300	14	3	24	3	**0.58**	0.81	0.41
G12	BD119+CC	0.5	1100	11	2	54	7	**0.20**	0.28	0.15
G16.2	BD119+CC	0.25	1200	13	3	82	51	**0.16**	0.52	0.08
G16.3	SUN189+CNC	0.25	1200	8	1	78	15	**0.10**	0.14	0.08
G15	SUN189+CC	0.5	1200	12	2	23	5	**0.52**	0.78	0.36